FUNGAL BIOLOGY AND RELATED DISEASES

EDITED BY: Marcos Dias Pereira, Allan J. Guimaraes and Lívia Kmetzsch
PUBLISHED IN: Frontiers in Microbiology

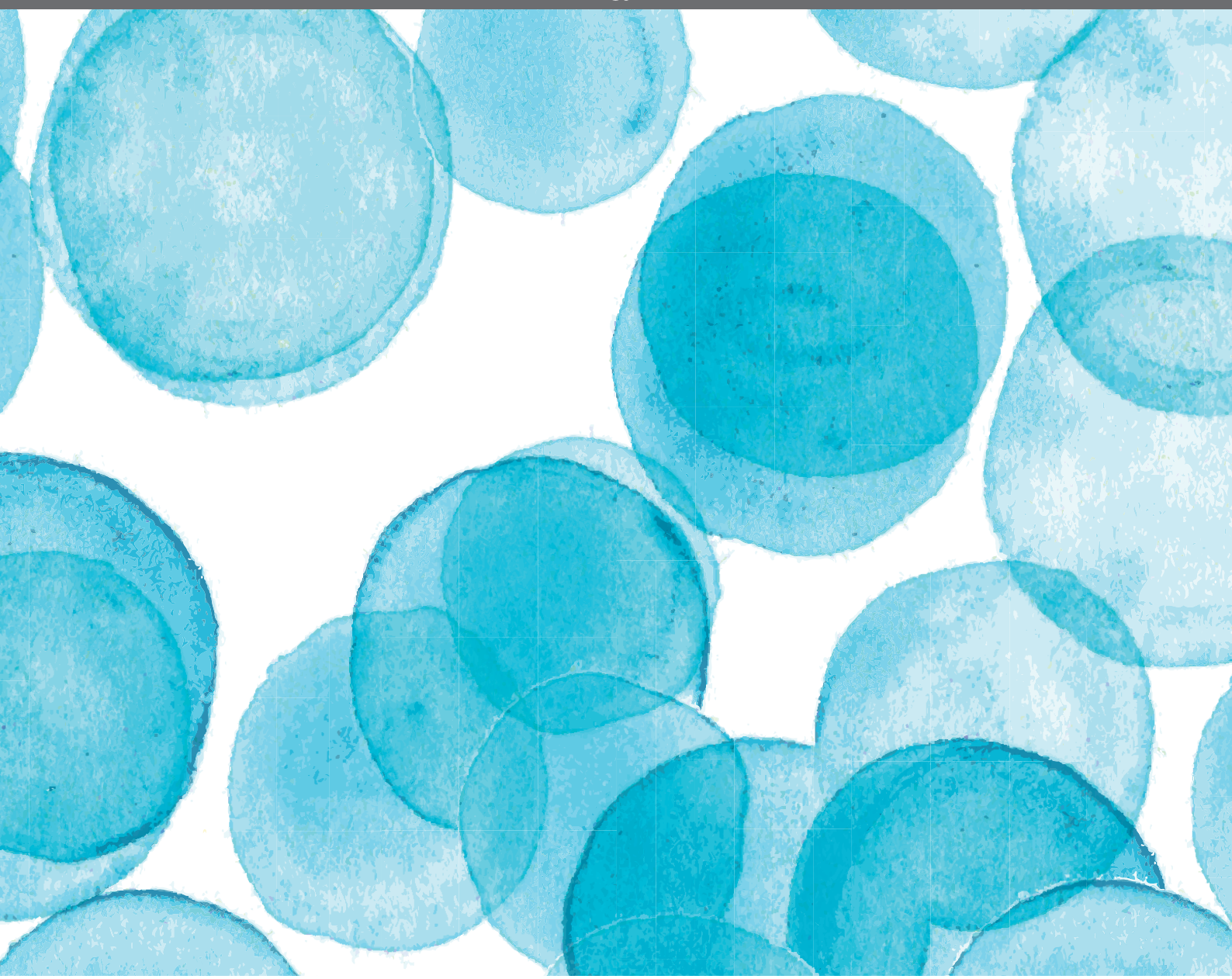

frontiers Research Topics

ISSN 1664-8714
ISBN 978-2-88974-994-2
DOI 10.3389/978-2-88974-994-2

About Frontiers

Frontiers is more than just an open-access publisher of scholarly articles: it is a pioneering approach to the world of academia, radically improving the way scholarly research is managed. The grand vision of Frontiers is a world where all people have an equal opportunity to seek, share and generate knowledge. Frontiers provides immediate and permanent online open access to all its publications, but this alone is not enough to realize our grand goals.

Frontiers Journal Series

The Frontiers Journal Series is a multi-tier and interdisciplinary set of open-access, online journals, promising a paradigm shift from the current review, selection and dissemination processes in academic publishing. All Frontiers journals are driven by researchers for researchers; therefore, they constitute a service to the scholarly community. At the same time, the Frontiers Journal Series operates on a revolutionary invention, the tiered publishing system, initially addressing specific communities of scholars, and gradually climbing up to broader public understanding, thus serving the interests of the lay society, too.

Dedication to Quality

Each Frontiers article is a landmark of the highest quality, thanks to genuinely collaborative interactions between authors and review editors, who include some of the world's best academicians. Research must be certified by peers before entering a stream of knowledge that may eventually reach the public - and shape society; therefore, Frontiers only applies the most rigorous and unbiased reviews.
Frontiers revolutionizes research publishing by freely delivering the most outstanding research, evaluated with no bias from both the academic and social point of view. By applying the most advanced information technologies, Frontiers is catapulting scholarly publishing into a new generation.

What are Frontiers Research Topics?

Frontiers Research Topics are very popular trademarks of the Frontiers Journals Series: they are collections of at least ten articles, all centered on a particular subject. With their unique mix of varied contributions from Original Research to Review Articles, Frontiers Research Topics unify the most influential researchers, the latest key findings and historical advances in a hot research area! Find out more on how to host your own Frontiers Research Topic or contribute to one as an author by contacting the Frontiers Editorial Office: frontiersin.org/about/contact

FUNGAL BIOLOGY AND RELATED DISEASES

Topic Editors:
Marcos Dias Pereira, Federal University of Rio de Janeiro, Brazil
Allan J. Guimaraes, Fluminense Federal University, Brazil
Lívia Kmetzsch, Federal University of Rio Grande do Sul, Brazil

Citation: M. D., Pereira, A. J., Guimaraes, L., Kmetzsch, eds. (2022). Fungal Biology and Related Diseases. Lausanne: Frontiers Media SA. doi: 10.3389/978-2-88974-994-2

Table of Contents

frontiers | Frontiers in Microbiology

TYPE Editorial
PUBLISHED 21 October 2022
DOI 10.3389/fmicb.2022.1037329

OPEN ACCESS

EDITED AND REVIEWED BY
Biswarup Mukhopadhyay,
Virginia Tech, United States

*CORRESPONDENCE
Allan J. Guimarães
allanguimaraes@id.uff.br
Lívia Kmetzsch
livia.kmetzsch@ufrgs.br
Marcos Dias Pereira
marcosdp@iq.ufrj.br

SPECIALTY SECTION
This article was submitted to Microbial Physiology and Metabolism, a section of the journal Frontiers in Microbiology

RECEIVED 05 September 2022
ACCEPTED 04 October 2022
PUBLISHED 21 October 2022

CITATION
Guimarães AJ, Kmetzsch L and Pereira MD (2022) Editorial: Fungal biology and related diseases. *Front. Microbiol.* 13:1037329. doi: 10.3389/fmicb.2022.1037329

Editorial: Fungal biology and related diseases

Allan J. Guimarães[1,2]*, Lívia Kmetzsch[3]* and Marcos Dias Pereira[2,4]*

[1]Department of Microbiology and Parasitology, Biomedical Institute, Fluminense Federal University, Niterói, Brazil, [2]Rede Micologia RJ - Fundação de Amparo à Pesquisa do Estado do Rio de Janeiro (FAPERJ), Rio de Janeiro, Brazil, [3]Biosciences Institute, Federal University of Rio Grande do Sul, Porto Alegre, Brazil, [4]Biochemistry Department, Federal University of Rio de Janeiro, Rio de Janeiro, Brazil

KEYWORDS

fungal biology, fungal metabolism, virulence, fungal gene expression, new antifungal strategies

Editorial on the Research Topic
Fungal biology and related diseases

The worldwide increasing incidence and mortality of fungal infections, including those by classical or (re-)emergent pathogens poses a serious public health problem. There is an urgent need for the implementation of compulsory notification of these neglected fungal diseases, besides a solid and strong investment on new efficient diagnostic and therapeutic alternatives to improve the control of mycoses. In this scenario, scientists have lately focused on decoding several aspects of fungal cells, including energy metabolism, cell cycle, gene expression, proteostasis, mitochondrial function, response to stress, secretory pathways and intrinsic or acquired resistance mechanisms. Therefore, for this Research Topic, we invited experts to share their latest findings on fungal biology: (i) metabolism and response to environmental changes; (ii) *in vivo* models of infection and virulence; (iii) gene expression and regulation; (iv) metagenomics and diagnosis and (v) strategies for the control of fungal infections.

As multifaceted organisms, fungi adapt to their environment, undergoing metabolic and morphological changes. Fabri et al. described pathways involved in the heat shock (HS) response linked to cell wall ultrastructural modifications and control of cell wall integrity (CWI) in *Aspergillus fumigatus*. In fact, expression of the HsfA and hsp90 is required for fungal adaptation to stress in *Aspergillus* biofilms. HsfA in turn, regulated the HS response gene expression and cell wall and lipid homeostasis, demonstrating its central role in the interplay of HS and the CWI cross-pathway regulation for *A. fumigatus* thermophily.

Adaptation to temperature was also explored by Almeida et al., on the thermally dimorphic fungus *Histoplasma capsulatum*. Comparative proteomics revealed that mycelia abundantly express glycolytic pathway and alcoholic fermentation enzymes, indicating the preferential utilization of anaerobic pathways for energy production, whereas yeast

cells expressed tricarboxylic acid cycle and HS response proteins. Additionally, distinct expression of oxidative stress response or cell wall metabolism enzymes, differentially regulated the composition of this structure in the two morphologies of *H. capsulatum*.

Fungal metabolic adaptation, specifically lower funneling catabolism pathways of *Scedosporium* species, including the degradation of conserved aromatic intermediate compounds, were investigated by Poirier et al. The authors predicted several ring-cleaving dioxygenases in the *Scedosporium* genome, which were validated by the determination of expression levels of the gentisic acid cluster genes, overexpressed in the presence of lignin (or gentisic acid) and granting fungal environmental adaptation.

A key aspect of environmental adaptation and propagation of filamentous fungi is the proper spore formation. The mycopathogenic fungi *Trichoderma* produces chlamydospores, with enormous advantages over conidia regarding biotechnological applications. Peng et al. reported a time course transcriptomic analysis and differential gene expression during chlamydospore formation in *Trichoderma virens*, with emphasis on proper chitin synthesis for the cellular differentiation.

The characterization of fungal virulence and the host response to infection are necessary for the description of new therapeutics against fungi. Cryptococcal infection is dependent on the expression of several virulence determinants. Despite being well characterized, experimental murine cryptococcosis models do not mimic the human disease and relatively little is known when human infection is considered. de Sousa et al. reviewed the current procedures used to study Cryptococcus sp. virulence in humans, association and correlation of clinical patient data and characterization of fungal virulence and host-pathogen interactions, pointing out to the importance of international collaboration and data integration to overcome the difficulties and impulse the human cryptococcosis knowledge.

Considering fungal pathogens and plant models, species from *Fusarium* genera are known to infect a myriad of hosts, in which the associated diseases are hard to control. Damodaran et al. evaluate the application of the mycopathogen *Trichoderma reesei* to control *Fusarium* wilt in bananas, showing a high decrease in severity of the disease. This effect is possibly associated with increased production of antifungal compounds, and decreased production of *Fusarium* toxins.

Regarding the characterization of the expression of fungal virulence, agglutinin-like sequence (ALS) gene family of *Candida* species, including *Candida parapsilosis,* comprehends an important class of virulence determinants. However, due to the high sequence identity and the proportion of tandem repeats, correct assembly of these loci using high-throughput sequencing are generally unreachable. Oh et al. performed a mixed approach employing Oxford Nanopore MinION, Illumina MiSeq, and Sanger sequencing to fully uncover the ALS gene family in *C. parapsilosis*. Also, qRT-PCR assays were performed to evaluate expression of each ALS gene in *C. albicans*, *C. dubliniensis*, as well as *C. parapsilosis*, revealing a complex pattern of gene expression of the ALS gene family.

For the establishment of effective therapies to fungal infections, the correct identification of the etiological agent is necessary. Classical methodologies rely on culture and microscopical evaluations, which are time consuming and often non-specific and lack sensitivity. The description of new generation sequencing methodologies, including long-reads, at lower cost can accelerate the specific identification of pathogens in clinical samples. Hoang et al. discuss the pros and cons for the implementation of these techniques in the routine diagnosis of mycosis.

At last, understanding host responses and the proposal of new therapeutic strategies could help to control fungal infections more efficiently. Araújo et al. described how the administration of glucocorticoids impacted *C. neoformans* proliferation and its capsular structure, resulting in worst infections outcome in animal models, including higher organ fungal loads and shortened survival times, and could additionally explain the clinical failures in the setting of immunocompromised individuals. In the other hand, Granato et al. characterize the antifungal effects of 1,10-phenanthroline-5,6-dione (phendione) and its metal-based complexes against *Phialophora verrucosa*. While demonstrating additive effects to amphotericin B, their prominent effects on *P. verrucose* biofilms and their capacity to reduce infections to macrophages and fungal burden in *Galleria mellonella* models corroborate to their promising therapeutic potential.

In summary, the manuscripts in this collection cover many unexplored aspects of fungal biology being targeted for the development of new therapeutics and diagnosis, including new gene silencing and sequencing methodologies, omics and drug development approaches.

Author contributions

All authors listed have made a substantial, direct, and intellectual contribution to the work and approved it for publication.

Funding

AG was supported by FAPERJ (E-26/202.696/2018) and Conselho Nacional de Desenvolvimento Científico e Tecnológico (CNPq grant 309736/2021-8). LK was supported by Conselho Nacional de Desenvolvimento Científico e Tecnológico (CNPq. grant 312797/2021-4). MP was supported by Fundação Carlos Chagas Filho de Amparo à Pesquisa do Estado do Rio de Janeiro (FAPERJ, E-26/010001697/2019)

and Conselho Nacional de Desenvolvimento Científico e Tecnológico (CNPq, grant 313783/2018-7).

Conflict of interest

The authors declare that the research was conducted in the absence of any commercial or financial relationships that could be construed as a potential conflict of interest.

Publisher's note

frontiers in Microbiology

ORIGINAL RESEARCH
published: 16 December 2020
doi: 10.3389/fmicb.2020.595845

Biological Management of Banana Fusarium Wilt Caused by *Fusarium oxysporum* f. sp. *cubense* Tropical Race 4 Using Antagonistic Fungal Isolate CSR-T-3 (*Trichoderma reesei*)

Thukkaram Damodaran[1], Shailendra Rajan[2], Muthukumar Manoharan[2]*, Ram Gopal[1], Kavita Yadav[1], Sandeep Kumar[2], Israr Ahmad[2], Nidhi Kumari[2], Vinay K. Mishra[1] and Sunil K. Jha[1]*

[1] Indian Council of Agricultural Research-Central Soil Salinity Research Institute, Regional Research Station, Lucknow, India, [2] Indian Council of Agricultural Research-Central Institute for Subtropical Horticulture, Lucknow, India

OPEN ACCESS

Edited by:
Lívia Kmetzsch, Federal University of Rio Grande do Sul, Brazil

Reviewed by:
Chetan Keswani, Banaras Hindu University, India
M. Carmen Limon, Sevilla University, Spain

***Correspondence:**
Muthukumar Manoharan
muthukumarbt@gmail.com
Thukkaram Damodaran
damhort73@gmail.com

Specialty section:
This article was submitted to Fungi and Their Interactions, a section of the journal Frontiers in Microbiology

Received: *17 August 2020*
Accepted: *26 October 2020*
Published: *16 December 2020*

Citation:
Damodaran T, Rajan S, Muthukumar M, Ram Gopal, Yadav K, Kumar S, Ahmad I, Kumari N, Mishra VK and Jha SK (2020) Biological Management of Banana Fusarium Wilt Caused by Fusarium oxysporum f. sp. cubense Tropical Race 4 Using Antagonistic Fungal Isolate CSR-T-3 (Trichoderma reesei). Front. Microbiol. 11:595845. doi: 10.3389/fmicb.2020.595845

Fusarium wilt in bananas is one of the most devastating diseases that poses a serious threat to the banana industry globally. With no effective control measures available to date, biological control has been explored to restrict the spread and manage the outbreak. We studied the effective biological control potential of different *Trichoderma* spp. in the management of *Fusarium oxysporum* f. sp. *cubense* tropical race 4 (Foc TR4). Expression of the defense related genes and metabolites in banana plants inoculated with Foc TR4 and treated with effective *Trichoderma* sp interactions were also studied. The *in vitro* growth inhibition of Foc TR4 by *Trichoderma reesei* isolate CSR-T-3 was 85.19% indicating a higher antagonistic potential than other *Trichoderma* isolates used in the study. Further, in *in vivo* assays, the banana plants treated with the isolate CSR-T-3 *T. reesei* had a significant reduction in the disease severity index (0.75) and also had increased phenological indices with respect to Foc TR4 treated plants. Enhanced activity of defense enzymes, such as β-1, 3-glucanase, peroxidase, chitinase, polyphenol oxidase, and phenylalanine ammonia lyase with higher phenol contents were found in the *Trichoderma* isolate CSR-T-3 treated banana plants challenge-inoculated with Foc TR4. Fusarium toxins, such as fusaristatin A, fusarin C, chlamydosporal, and beauveric acid were identified by LC-MS in Foc TR4-infected banana plants while high intensity production of antifungal compounds, such as ß-caryophyllene, catechin-o-gallate, soyasapogenol rhamnosyl glucoronide, peptaibols, fenigycin, iturin C19, anthocyanin, and gallocatechin-o-gallate were detected in *T. reesei* isolate CSR-T-3 treated plants previously inoculated with Foc TR4. Gene expression analysis indicated the upregulation of *TrCBH1*/*TrCBH2*, *TrXYL1*, *TrEGL1*, *TrTMK1*, *TrTGA1*, and *TrVEL1* genes in CSR-T-3 treatment. LC-MS and gene expression analysis could ascertain the upregulation of genes involved in mycoparasitism and the signal transduction pathway leading to secondary metabolite production under CSR-T-3 treatment. The plants in the field study

showed a reduced disease severity index (1.14) with high phenological growth and yield indices when treated with *T. reesei* isolate CSR-T-3 formulation. We report here an effective biocontrol-based management technological transformation from lab to the field for successful control of *Fusarium* wilt disease caused by Foc TR4 in bananas.

Keywords: *Trichoderma reesei*, banana, Fusarium wilt TR4, antifungal, LC-MS, gene expression, field evaluation

INTRODUCTION

Fusarium wilt caused by *Fusarium oxysporum* f. sp. *cubense* tropical race 4 (Foc TR4) is considered to be one of the most devastating diseases of bananas limiting banana production worldwide (Ploetz and Pegg, 2000; Dita et al., 2018). The pathogen was first reported in South East Asia during the early 1990s and toward the end of the century, endemic outbreak of Foc TR4 was realized over large areas in the northern territory of Australia, China, Indonesia, Malaysia, and Taiwan (Ploetz, 2006a,b). Most recently, severe outbreak of Foc TR4 in the northern region in India covering the states of Uttar Pradesh and Bihar threatening banana cultivation in the region were reported, which is the largest producer of bananas (Damodaran, 2018). The polycyclic nature of the disease suggests that its multiple cycle of infection in bananas is causing devastating losses over a period of time (Buddenhagen, 2009). Different types of toxins are produced by Fusarium which are involved in pathogenesis and disease development. The major toxins that are reported from Fusarium species include; nivalenol, zearalenone, fumonisins, trichothecene, fusarins, and Fusaric acid (Niehaus et al., 2014; Dong et al., 2017; López-Díaz et al., 2017; Perincherry et al., 2019; Qiu et al., 2019). Differential colonization patterns of Foc race 4 from race 1 were identified and explained by upregulation of pathogenicity-associated genes, such as *Fga1*, *Fhk1*, *Fow2,* and *Ste12* that allowed faster colonization in the xylem with higher virulence (Guo et al., 2015). The discrimination of Foc TR4 from Foc race 1 proved very efficient with the PCR-based detection employed for secreted in xylem (*SIX*) genes (Carvalhais et al., 2019) and comparative analysis of various specific primers has also ascertained the efficiency of *SIX* gene-specific primers in the molecular detection of Foc TR4 (Magdama et al., 2019). These advances have now paved the way for a reliable dependable confirmatory assay for the early detection/diagnosis of Foc TR4.

Management and control of Foc TR4 is a matter of serious concern and different approaches, such as chemical and biological control, manipulation of cultural practices, and resistant breeding have been attempted by different research groups. The ability of Foc TR4 to survive in the absence of its host is a significant factor limiting the successful management of this disease through agronomic practices like crop rotation (Brandes, 1919). Besides this, use of chemical control measures involving corm injection and soil drenching of carbendazim fungicide failed to provide sustainable management of the disease but their repeated use has raised environmental concerns (Getha and Vikineswary, 2002). Application of soil fumigants, field sanitation, and flood fallowing provided limited control over a large area (Ploetz et al., 1990). In another approach using resistance breeding, some advances were reported for evolving resistant varieties and hybrids against Foc race 1 (Damodaran et al., 2009) but to date no successful reports are available for Foc TR4 (de Matos et al., 2011; Amorim et al., 2013; Garcez et al., 2016; Rebouças et al., 2018; Ribeiro et al., 2018; Gonçalves et al., 2019). Moreover, the selection of resistant cultivars seems to be an effective control strategy against the disease, however, the existence of poor fertility in the Cavendish group (AAA) limited its improvement programs through conventional breeding (Aguilar Moran, 2013). Thus, the only alternative approach for management is by exploring antagonistic and growth promoting fungi or bacteria which have earlier been successfully demonstrated in biological control of soil borne pathogens in different crop plants (Tan et al., 2015, Khan et al., 2018). Rhizospheric existence and endophytic colonization of the potential antagonist are known to not only suppress the pathogen but also incite systemic-induced host plant resistance (Ting et al., 2009, Sood et al., 2020).

Trichoderma (Teleomorph: *Hypocrea*) is a fast-growing soil inhabitant fungus known for the production of a large numbers of spores and has been reported to have biocontrol potentials (Monfil and Casas-Flores, 2014). The antagonism of *Trichoderma* against phytopathogens is achieved by mycoparasitism (Papavizas, 1985) through the production of enzymes (chitinases, glucanases, and proteases) that degrade the fungal cell wall which is mainly composed of chitin (Qian et al., 2019) as well as antibiosis (Harman and Kubicek, 1998); through production of secondary metabolites and antimicrobial compounds active against a wide array of phytopathogens (Speckbacher and Zeilinger, 2018). Additionally, when the plant encounters the pathogen it induces a host defense mechanism while on interaction with a non-pathogenic organism the mechanism for induced systemic resistance (ISR) gets activated (Hermosa et al., 2013; Mukherjee et al., 2013). A plethora of studies suggest that *Trichoderma* spp. induce systemic resistance to the subsequent attack by the pathogens in the host plants (Martínez-Medina et al., 2013). Elevated production of antioxidants like polyphenols, cell wall degrading enzymes like glucanases, chitinases, etc. by Trichoderma probably induced the host defense mechanism against the invading pathogens including Fusarium (Kavino et al., 2009). Though, long term efficacy of biocontrol agents in field studies have seldom come up with repeatability at a field level (Ploetz, 2004), yet, repeated application of biocontrol agents has resulted in the suppression of soil borne pathogens. These discoveries showed promise for exploring antagonistic biocontrol agents and developing a package for the management of the Foc TR4 pathogen causing Fusarium wilt in bananas. The prime focus of the study was

to identify an elite antagonistic fungus by screening different *Trichoderma* isolates from diverse biotic and abiotic stressed environments that has the potential to inhibit the Foc TR4 pathogen, assess its efficacy in the management of the disease under pot culture and sick field experiments, and to decipher its antifungal mode of action/mechanism in disease suppression through gene expression and LC-MS analysis. We report here a systematic development of a technological innovation involving a *Trichoderma* isolate and its field transformation as a biocontrol agent toward successful management of banana wilt caused by *Fusarium oxysporum* f. sp. *cubense* tropical race 4.

MATERIALS AND METHODS

Collections of *Trichoderma* spp. and *Fusarium oxysporum* f. sp. *cubense* Tropical Race 4

The virulent strain of the *Fusarium oxysporum* f. sp. *cubense* tropical race 4 was collected from the culture collections of the Soil Microbiology Laboratory, ICAR-Central Soil Salinity Research Institute, Regional Research Station, Lucknow, India that had submitted the first report on the outbreak of the disease in India (Damodaran et al., 2018). The three *Trichoderma* isolates used in the study are described as follows; (i) *Trichoderma reesei* (CSR-T-3, MK050013) isolated from the rhizosphere soil of banana cultivar G-9 grown in salt affected soil, (ii) *Trichoderma asperellum* (CSR-T-4, MN227242) isolated from the disease suppressive rhizosphere of banana cultivar G-9 grown in the Foc TR4 affected region of Uttar Pradesh, India, and (iii) *Trichoderma koningiopsis* (CSR-T-2, KJ812401) obtained from the rhizosphere of *Saccharam spontaneum* in the barren sodic soil of Uttar Pradesh, India. These isolates were identified and submitted to the culture collections (NBIMCC-SF-0030) at the ICAR-National Bureau of Agriculturally Important Microorganisms (ICAR-NBAIM), Mau, India and have been reported in our earlier studies (Damodaran et al., 2019c; Yadav et al., 2020).

In vitro Antagonistic Assays

The three isolates of the *Trichoderma* species were evaluated for their *in vitro* antagonistic potential against CSR-F-1 (the virulent strain of Foc TR4) through a dual culture test as described by Tian et al. (2016). Mycelial disks of Foc TR4 and *Trichoderma* spp. from actively growing colonies were placed on a 9 cm diameter petri dish filled with potato dextrose medium (PDA) in combinations. The isolates were placed at 5.5 cm apart on the same plate and were incubated for 72 h at 22°C. Foc TR4 isolate CSR-F-1 was also placed without disks of *Trichoderma* isolates as control. The growth of the isolates was monitored and observations were recorded at an interval of every 24 h from which the percentage of pathogen growth inhibition was calculated. The inhibition efficacy of *Trichoderma* isolates on the mycelia growth of Foc TR4 and the radius of the Foc colony in each plate were measured, and a standard growth curve was derived as described by Matarese et al. (2012). The distance between the Foc TR4 inoculating point and furthest point of the colony in control plates (r1) and the distance between the Foc TR4 sowing point and the edge of the colony where the mycelia came in contact with *Trichoderma* spp. in the treatment plates was taken at an interval of 24 h for calculating the inhibition percentage (IP) using the formula; IP = ((r1 – r2)/r1)*100. This *in vitro* dual culture assay was carried out in five replicates and the data was statistically analyzed by analysis of variance (ANOVA) using Duncan's multiple range tests using the SAS 9.0 software.

SEM Analysis of Dual Culture Interaction to Ascertain Antagonism of the Best Performing Isolate

Scanning electron microscopy of the dual culture regions was carried out for establishing and observing the CSR-T-3 antagonism against Foc TR4 (CSR-F-1) as described in protocol given by Kumar et al. (2018). Pieces of agar from the interaction zones of the dual culture plates at their early stage of interaction were fixed in 3% glutaraldehyde dissolved in 0.1 M phosphate buffer (pH 7.0). The specimens were dehydrated using acetone at a series of concentration (30, 50, 60, 70, 80, 90, and 95%) for 20 min. The samples were dried for 30 min and mounted on a steel stub with double sided carbon tape. The samples were finally coated with a film of gold-palladium alloy under vacuum and observed with a scanning electron microscope (SEM, Fei Quanta 200) at Bhaba Bhimrao Ambedkar University, Lucknow, India. The control plates involving the individual plates of *T. reesei* (CSR-T-3) and Foc TR4 (CSR-F-1) were also maintained for comparison.

In vivo Assay of Antifungal Potential Using Pot Culture

The *in vivo* assays were performed with the best performing *Trichoderma* isolate from the *in vitro* dual culture assay. A systematic pot culture experiment was carried out in June-July 2017 and June-July 2018 at the ICAR-Central Soil Salinity Research Institute, Regional Research Station, Lucknow, India by following a completely randomized design (CRD) with three replicates. The temperature of the green house during the experimental period ranged from 29 to 32°C with 70% humidity. The fungal culture was prepared by inoculating the 5-days-old culture of the best performing *Trichoderma* isolate in potato dextrose broth (PDB) with subsequent incubation for 5 days at 28°C in an incubated shaker. The spore suspension was obtained by filtering the broth through double-layered cheese cloth. The filtrate thus obtained was diluted 50 times and the spore number was adjusted from 10^7 to 10^8 using a hemocytometer. About 100 ml of the diluted filtrate was added in sterile soil. Likewise, the pathogen inoculum was prepared using the same procedure and the spore count was adjusted from 10^5 to 10^6. For sterilizing the soil, normal clayey loam soil (pH 7.45, E.C. 0.32 dS/m, organic carbon content of 3.0 g/kg) was collected from the research farm of the Institute, passed through a 20 mm mesh sieve and sterilized in an autoclave at 121°C for 30 min for 3 consecutive days.

Secondary hardened tissue cultured banana plantlets of the Grand Naine variety (susceptible) of uniform height were selected to conduct the experiment. The plants were inoculated with the pathogen by dipping them in the pathogen spore

suspension containing 10^6 conidia/ml for 30 min as described by Pérez-Vicente et al. (2014) before planting. Three treatments viz, TC: uninoculated plants, TF: plants inoculated with CSR-F-1 (Foc TR4) at the time of planting and TFTR: plants inoculated with CSR-F-1 (Foc TR4) along with soil drenching with suspension of the best performing *Trichoderma* isolate were included in the pot experiment with five replicates for each treatment. The experiment was repeated three times.

The phenological indices of banana seedlings like plant height (cm), girth (cm), and number of leaves was noted at 0, 30, 60, and 90 days after planting. The morphological growth-related parameters like root biomass and shoot biomass were recorded at the end of the experiment. The wilt disease was scored by adopting the following disease scale as followed by Pérez-Vicente et al. (2014).

Grade 1	No symptoms
Grade 2	10–20% initial corm discoloration
Grade 3	20–40% slight discoloration of the corm
Grade 4	40–60% discoloration of the corm
Grade 5	60–80% complete discoloration of the corm

$$\text{Disease index} = \frac{£\left(\text{Number of diseased plants in each grade} \times \text{value of relative grade}\right)}{\text{Total number inspected} \times 5}$$

Besides this, the chlorophyll content was also estimated at the end of the experiment. Chlorophyll a, b, and total chlorophyll contents were estimated by following the method of Sadasivam and Manickam (1996) using 80% acetone and magnesium carbonate. The data were statistically analyzed by subjecting them to analysis of variance (ANOVA) and means were compared by a Duncan's multiple range test ($p < 0.05$) (Rangaswamy, 1995).

Liquid Chromatography Coupled With Mass Spectrometric (LC-MS) Analysis

LC-MS analysis was performed in the plant samples of treatments TC (treatment negative control), TF (treatment Foc-TR4), and TFTR (treatment Foc-TR4 and *Trichoderma reesei* isolate CSR-T-3) of the pot experiment to identify important organic compounds and their role in inducing host tolerance. The whole plant was uprooted, washed with sterile distilled water, and then shade-dried for 30 days. Further the protocol for sample preparation was as prescribed by the Sophisticated Analytical Instrumentation Facility (SAIF), Central Drug Research Institute (CDRI), Lucknow, Uttar Pradesh, India.

A total of 250 g of dry weight plant material was used for the preparation of plant extracts consisting of root, leaves, and stem. Ethanol crude extract was obtained by crushing the plants in 70% ethanol which was further purified by using ethanol acetate. A small fraction of the solvent free plant extract was collected in Eppendorf for further analysis. The extract residue was stored at 4°C until used for the antimicrobial assay.

The ESI-LC–MS of the TLC purified sample was analyzed using a MICROMASS QUATTRO II triple quadrupole mass spectrometer with a JASCO PU-980 HPLC pump at the Sophisticated Analytical Instrumentation Facility, CSIR-Central Drug Research Institute, Lucknow, India. The WATER SPHERISORB ODS 2 (250 _ 4.6 mm _ 5 l) column was used with acetonitrile: water +0.1% formic acid solvent system. Gradient elution was performed at 1.0 ml/min. The photodiode array was monitored at 200–650 nm and recorded at 220 nm. The mass spectra were scanned in the range 80–1,000 DA in 2.5 s. The ESI capillary was set at 3.5 kV and the cone voltage at 40 V. The m/z spectral chromatographs were analyzed, key metabolites were predicted based on already published reports and tabulated for comparative analysis between the TC, TF, and TFTR samples.

Biocontrol Mechanism of *Trichoderma reesei* Against Foc Through Gene Expression Analysis

To study the basis of resistance achieved in banana plants against Foc TR4 through drenching the soil with the best performing *Trichoderma* isolate at the time of planting, the expression levels of the genes of *T. reesei* and Foc TR4 were studied using a real time-polymerase chain reaction (RT-PCR) assay. Genomic sequence information for the genes involved in mycoparasitism *viz*., *TrCBH1*/*TrCBH2*, *TrXYL1*, and *TrEGL1* encoding cellobiohydrolase, xylanase, and endoglucanase, respectively and few genes involved in the signaling transduction pathway leading to secondary metabolite production in *T. reesei*, i.e., *TrTMK1*, *TrTGA1*, and *TrVEL1* genes encoding mitogen activated protein kinase (MAPK), G-protein alpha subunit, and VELVET1 protein, respectively were mined from the whole genome sequence of *T. reesei* QM6a as reported by Martínez-Hidalgo et al. (2015) (Bioproject: PRJNA15571) available at NCBI database. Similarly, the genes involved in Fusaric acid biosynthesis were mined from the whole genome information of *F. oxysporum* f. sp. *cubense* (Foc TR4) in the NCBI database (Bioproject: PRJNA529756). The selection of these genes was based on the well-established antagonistic biocontrol potential evincing molecular mechanism of *Trichoderma* sp. against *Fusarium* species earlier reported by Druzhinina et al. (2012) and Zeilinger et al. (2016). The primers for the genes used in RT-PCR analysis were designed for exonic segments contributing to the functional domains based on protein structural domain analysis and exon predictions (phylogenetic analysis of genes and structural predictions are presented in **Supplementary Figures 1, 2**) using the primer3 software and were synthesized from Xcelris Labs Pvt. Ltd, Ahmedabad, India (**Table 1**). The root samples of healthy banana plants (negative control), banana plants inoculated with CSR-F-1 (Foc TR4), banana plants challenged with CSR-F-1 (Foc TR4) followed by subsequent treatment with the best performing *Trichoderma* isolate (Foc-TR4 + CSR-T-3), and banana plants treated with the best performing *Trichoderma* isolate alone were collected at 30 days after treatment. Total RNA was isolated from the root samples of all four treatments using the Spectrum™ Plant Total RNA Kit (Sigma USA) following the manufacturer's instructions. The quality of total RNA was checked on 1% agarose gel and quantified using a QIAxpert spectrophotometer (Qiagen Germany). The RNA (3 μg) was subjected to cDNA synthesis

TABLE 1 | Description of primers used for gene expression analysis through RT-PCR.

Gene	Forward primer (5′-3′)	Reverse primer (5′-3′)	Product size (bp)
MaRPM1	TACACCATTCTCGGCGGCGG	TGCCTCGCCATCACCACCAG	150
TrACT	CACCTTCTCCACCACCGCAG	GAGGAGCACGGAATCGGTCG	179
FocACT	TCGCCCCCGTCATCATGGTA	GGTTGATGGGAGCCTCGGTG	227
TrTGA1	TCCACGAGGGCGGCTACTCT	ACTCCTGCACGCCGTGATCC	249
TrTMK	GCCCGATCTGCTGCTTCCCA	AGCCAGGATGCAGCCCACAG	147
TrVEL	CGGCACCCTACTCTGCACCC	TGGCGGAGGAGGAAGAGGCT	149
TrTAC1	ACCCTCGCTGTTGGAAGCCC	GCTGTTGCGCCAGTTCGACG	127
TrCBHI	ACCTTATGGCGAACGGCGAC	TCACAGTACCCCGTGCCGTA	193
TrCBH2	AGCAGCCTACCGGACAGCAA	CCGGTTGCAAGGCATCTGGG	204
TrEGL1	CCACCACTGGCTCTGGCTCC	AAGTGGCAACAGGAGCGGCA	210
TrXYN1	CGAGCCTTCCATCGTCGGCA	TCCTCCCCACCCCTCCACAG	172
FocFUB3	GTGCAGAAGCCGTGGGGTCA	ATCGTGCTCGGCCAGGATGG	243
FocFUB8	ACAGGTGTCGAGATGCGCCC	CGGGGTGTTTCGGGTGTCGT	157
FocFUB7	GGTTCTCTGGCCAGGCTCCG	TGGCATCACCCACGTTGGCA	173
FocFUB6	CCAGAGCCCGGCGTCCATAC	GGGGATCGAGACCAGCCGTG	103
FocFUB9	TGCCATTGAGCGGGGTGTTGA	GCAATGCGCGTCTTGCCCTT	129

using a Maxima First Strand cDNA Synthesis Kit. RT-PCR was performed using 10 ng cDNA as the template, forward and reverse primers (5 picomoles each), and the SYBR master mix (ABI, NY, USA) in Applied Biosystems™ 7500 Real-Time PCR Systems (ABI, NY, USA). PCR amplification was programmed with a pre PCR read at 60°C for 30 s, a holding stage at 95°C for 10 min, and a cycling stage at 95°C for 15 s and at 60°C for 1 min. Data were normalized twice, once with banana housekeeping gene encoding disease resistance protein RPM (*MaRPM*) and then with actin genes of *Fusarium* and *Trichoderma* (*FocACT*, *TrACT*) for assessing the relative abundance of the transcripts related with Fusaric acid biosynthesis and *Trichoderma* related genes, respectively. The differential expression of the genes was expressed in terms of 2-fold change using the formula, Fold Change (FC) $= 2^{(-\Delta\Delta Ct)}$.

Biochemical Analysis of Defense-Related Enzymes and Phenol Content

Leaf samples of 1 g (three samples from each replicate) were homogenized with 2 ml of 0.1 M sodium citrate buffer (pH 5.0) at 48°C and centrifuged for 20 min at 10,000 rpm. The supernatant crude enzyme extract was used for assaying 1, 3-glucanase (Pan et al., 1991) and chitinase (Boller and Mauch, 1988) activity. Enzyme extracted in 0.1 M sodium phosphate buffer (pH 7.0) was used for the estimation of peroxidase (PO) (Hammerschmidt et al., 1982), polyphenol oxidase (PPO) (Mayer et al., 1965), and phenylalanine ammonia lyase (PAL) (Ross and Sederoff, 1992). The phenol content was estimated following the procedure of Zieslin and Ben-Zaken (1993) and expressed as catechol equivalents g^{-1} of protein. The assays were carried out for the TC, TF, and TFTR samples and the data were statistically analyzed using the SAS 9.2 statistical software.

Preparation of Bioformulation of CSR-T-3 and Application Techniques

A 2 mm disc of the best performing *Trichoderma* isolate was inoculated into the CSR patent protected culture media (Rai et al., 2012) and incubated in a rotary shaker at 150 rpm for 72 h at room temperature (28 ± 2°C). After 72 h of incubation, the formulation containing 6×10^7 spores ml^{-1} was used for drenching the plants. The plants were drenched with 500 ml/plant with 1% of the formulation prepared using the best performing *Trichoderma* isolate CSR-T-3 at 2, 4, 6, and 8 months after planting (Damodaran et al., 2019a). The untreated control plants were drenched with the plain culture at the same quantity used in treatment. The incidence of wilt disease in the treatments was scored based on a 1–5 disease scale (Ploetz et al., 1999). Besides disease incidence, observations of growth parameters, such as the girth and height of the pseudo stem, leaf area, yield, and number of hands were recorded according to the guidelines of the International Network for the Improvement of Banana and Plantain (INIBAP).

Field Evaluation of CSR-T-3 on Disease Affected Hotspot of Uttar Pradesh (India)

A field experiment was performed in the Sohawal block (26° 46′ 3.3852″ N latitude; 81° 59′ 42.7992″ E longitude) of the Faizabad district (Uttar Pradesh, India) during 2018–2019 wherein there was an extensive outbreak reported in 2017 (Damodaran et al., 2018) to evaluate the effectiveness of bioformulation in Fusarium wilt management at field level. The fields (clayey loam soil, pH-7.2) that were reported to have 60–80% *Fusarium* wilt incidence over the past 2 years (2017 and 2018) were selected. Average annual rainfall at the experimentation fields was in the range of 800–900 mm. Disease free banana plantlets of cv. Grand Naine (G-9) produced in the tissue culture laboratory of the ICAR-Central Soil Salinity Research Institute, Regional Research Station, Lucknow, Uttar Pradesh were planted and 50 plants per replication were used for each treatment. The experiment was laid out in a completely randomized block design with two treatments (one treatment included G-9 banana plantlets planted in a Foc infested field while the other treatment included banana G-9 plantlets planted in a Foc infested field and treated with the CSR-T-3 *Trichoderma* isolate formulation). The plants under the treatment were drenched with 500 ml/plant with 3% of the formulation at 2, 4, 6, and 8 months after planting replicated three times with 50 plants in each replication. The fertilizers and farm yard manure (FYM with nitrogen 0.5–1.5, phosphorus 0.4–0.8, and potassium 0.5–1.9) were applied as per the recommended dosage (Crop Production Guide, 2017). The data on growth and yield were recorded and the data on field experiment were subjected to a paired *t*-test ($p < 0.05$) for each parameter and were statistically analyzed using the SAS 9.2 statistical software. The percentage values of the disease index were arcsine transformed (Rangaswamy, 1995).

RESULTS

In vitro Bioassay of the *Trichoderma* Isolates for Selecting an Elite Antagonistic Isolate Against Foc TR4

Three *Trichoderma* isolates *viz*., *T. reesei* (CSR-T-3), *T. koningiopsis* (CSR-T-2), and *T. asperellum* (CSR-T-4) were assessed for their *in vitro* efficacy by a dual co-culture technique

on PDA medium. All of the three isolates utilized the nutrient source and showed a significant increase in the inhibition percentage between 48 and 72 h after inoculation by inhibiting the mycelia growth of Foc TR4 (CSR-F-1). The maximum reduction of the mycelia growth of the pathogen was elicited by the isolate CSR-T-3 that showed the highest inhibition percentage of 85.19% (**Figure 1**) at 120 h after inoculation, whereas CSR-T-1 showed the least inhibition (50.00%). The inhibition percentage of CSR-T-2 (*T. koningiopsis*) was 62.65%. Based on these results, it is evident that CSR-T-3 (*T. reesei*) is the most effective *Trichoderma* isolate with a tremendous antagonistic ability against Foc TR4.

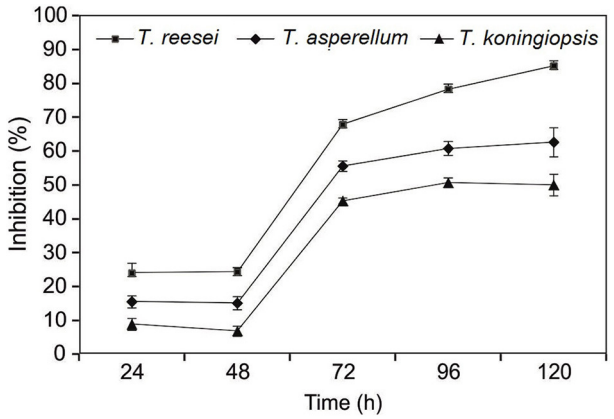

FIGURE 1 | Inhibitory effect of CSR-T-3 (*Trichoderma reesei*) against pathogenic isolate CSR-F-1 of *Foc* TR4. Percentage inhibition of *Foc* TR4 was found to be highest in CSR-T-3 (*Trichoderma reesei*) over a period of time in comparison with *T. asperellum* and *T. koningiopsis*.

SEM Analysis of Dual Culture Interaction to Ascertain CSR-T-3 Antagonism

SEM analysis of the dual culture interaction zones between the CSR-T-3 (*T. reesei* isolate) and CSR-F-1 Foc TR4 isolates revealed considerable changes in the morphology including collapse, deformation, and broken cells (**Figures 2A–C**) leading to the loss of integrity of the Foc TR4 hyphae while the spores and mycelium in the control plates were intact and undisturbed leading to normal spore formation. This morphological microscopic identification indicates the mycoparasitism exhibited by CSR-T-3 which is identified as *T. reesei* (NAIMCC-SF-0030; NCBI No. MH997668).

Green House Evaluation of CSR-T-3 (*Trichoderma reesei*) on *Fusarium* Disease Control

From the *in vitro* antifungal assay of the *Trichoderma* isolates against CSR-F-1 (Foc TR4), *Trichoderma* isolate CSR-T-3 with a significantly high inhibition percentage was used for *in vivo* pot culture studies. The disease spread was rapid and the symptoms of yellowing of older leaves started appearing in the

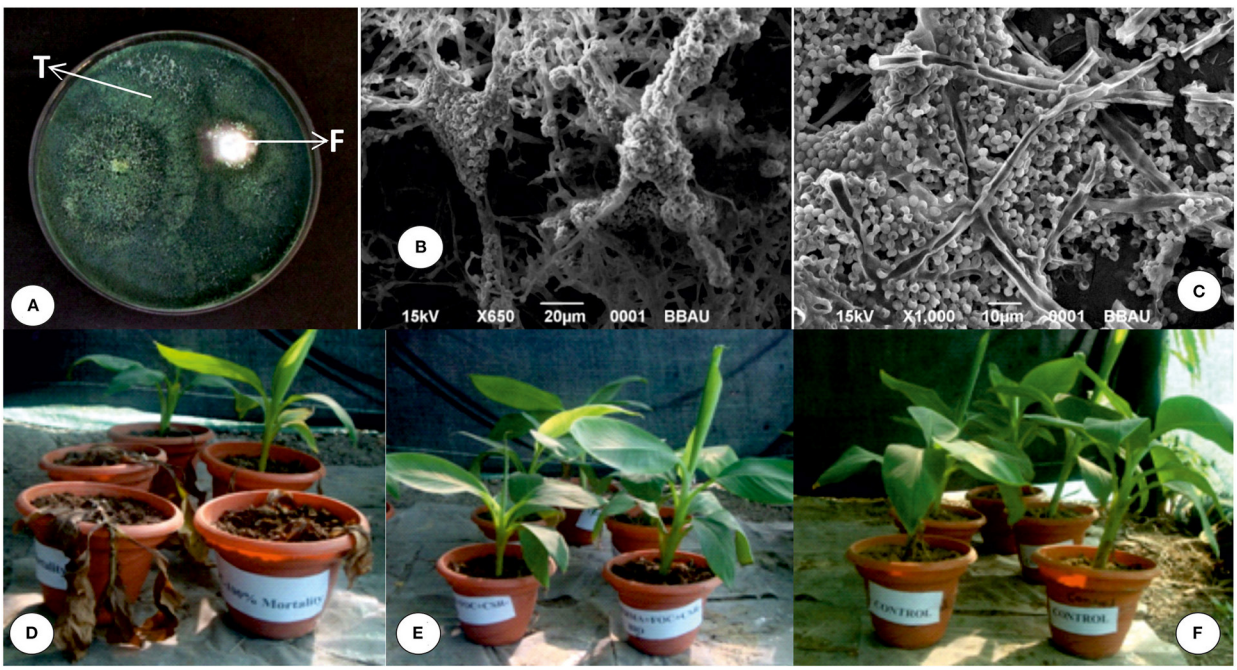

FIGURE 2 | Characterization and evaluation of CSR-T-3 as a biocontrol agent for the management of banana wilt caused by *Fusarium oxysporum* f. sp. *cubense* tropical race 4 (Foc TR4). **(A)** *in vitro* dual culture assay showing inhibition of *Foc* TR4 (F) by the CSR-T-3 *Trichoderma reesei* isolate (T). Scanning electron micrograph showing **(B,C)** mycoparasitism of the *Trichoderma reesei* CSR-T-3 isolate on *Foc* TR-4 mycelium. Pot culture experiment of banana plants for testing the biocontrol potential of the formulation of CSR-T-3 showing **(D)** TF (treatment with *Foc* TR4), **(E)** TFTR (treatment with *Foc* TR4 + CSR-T-3), and **(F)** TC (treatment negative control). Characteristic wilting symptoms manifested in TF **(D)** where the pathogen was challenge-inoculated whereas, the plants treated with CSR-T-3 and challenged with *Foc* TR4 showed healthy growth indicating the protection offered by CSR-T-3 as a biocontrol agent.

TABLE 2 | Effect of *Trichoderma reesei* (CSR-T-3) on *Fusarium* wilt incidence and growth of banana plantlets under greenhouse pot experiment.

Treatment	Plant height			Plant girth			No. of leaves	Disease severity index
	Initial	Final	Increment	Initial	Final	Increment		
TF	17.15[b] (±1.63)	26.5[a] (±4.40)	33.83[a] (±13.17)	3.35[a] (±0.17)	3.62[a] (±0.17)	7.51[a] (±4.51)	1.75[a] (±1.25)	3.75[b] (±1.50)
TFTR	14.9[b] (±2.01)	33.75[b] (±1.49)	55.79[b] (±6.29)	3.50[a] (±0.40)	5.47[b] (±0.55)	35.82[b] (±7.44)	4.50[b] (±0.57)	0.75[a] (±0.50)
TC	13.12[a] (±1.51)	35.47[b] (±1.94)	62.89[b] (±5.14)	3.80[a] (±0.35)	5.55[b] (± 0.17)	31.63[b] (±4.35)	5.00[b] (±0.00)	0.00[a] (±0.00)

TF, treatment with Fusarium; TFTR, treatment with Fusarium and Trichoderma; TC, treatment control.

Values are the means of five replicates with the sample size n = 5.

Means in the columns followed by the same letter (either a or b) are not significantly different according to Duncan's multiple range test at P = 0.05. Values in the parentheses indicate the standard deviation of the mean.

Foc TR4 inoculated plants from 24 days after planting in control plants (**Figure 2D**; additional root morphological differences in **Supplementary Figure 3**). As time went on the plants in the Foc TR4 alone treatment began to show mortality between 60 and 90 days. At 90 days after planting when the experiment was completed, the plants that had been treated with Foc TR4 showed a significantly high mean disease severity index of 3.75 while the plants treated with TFTR recorded significantly lower DSI (0.75) that was similar to the plants of control that were not inoculated with the pathogen (**Table 2**). None of the plants treated with TFTR showed mortality until the end of the experiment (**Figure 2E**).

Plant height and girth in the TFTR-treated plants were recorded to be 33.75 and 5.47 cm, respectively which were significantly higher than the TF-treated plants (Foc TR4 alone treated banana plants). Interestingly, there were no significant difference in height and girth observed in the TFTR-treated plants (*T. reesei* isolate CSR-T-3 treated banana plants with challenge inoculation of Foc TR4 strain) as well as in the case of TC (untreated negative control). About a 55.79% increase in plant height was noticed in plants with TFTR treatment which also exhibited increased stem girth by 35.82% in comparison with plants with Foc TR4 alone treatment (TF) (**Figures 2E,F**). The results suggest that the treatment of the fungi *T. reesei* (CSR-T-3) significantly reduced the incidence of the disease and also promoted the growth of the seedlings on par with that of healthy plants.

Effect of *Trichoderma reesei* CSR-T-3 on Biomass and Chlorophyll Content of Bananas

Although, there was no improvement in plant height and pseudo stem girth in CSR-T-3 treatment, significant differences were recorded for growth parameters like weight of the pseudo stem and root. The mean fresh (**Figure 3A**) and dry (**Figure 3B**) weight of the plantlets treated with the *T. reseei* CSR-T-3 isolate were higher compared to those in the other treatments including control without any microbial inoculations (CSR-T-3, antagonistic biocontrol agent and CSR-F-1, Foc TR4 pathogen). The fresh root and shoot weight for the TFTR treatment (14.20 and 56.30 g, respectively) inoculated with CSR-T-3 *T. reesei* isolate along with Foc TR4 was significantly higher than the TC control and TF treatment. However, there was no significant difference between root and shoot dry weights in the TFTR treatment (1.11 and 2.60 g, respectively) and TC which were significantly higher than the TF treatment (0.96 and 2.60, respectively). Thus, treatment with the *T. reesei* CSR-T-3 isolate had a growth promoting effect on banana plants. Similarly, total chlorophyll content 0.60 mg/g was recorded in the TFTR treatment, which was significantly higher than the TF treatment (value). The total chlorophyll content in the untreated control TC treatment (0.72 mg/g) and TFTR treatment showed non-significant differences indicating the effect of the treatment in reducing the stress of the plants due to the inoculation of the pathogen (**Figure 3C**). Overall, it was observed that there was additional growth improvement noticed in the CSR-T-3 treatment apart from disease suppression, despite the stress imposed by the inoculation of Foc TR4. The growth attributes were found to be on par with the healthy plants.

Metabolite Profiling of CSR-T-3 Efficacy Using LC-MS Analysis

The crude metabolites of plants treated with Foc TR4 (TF), Foc TR4, and CSR-T-3 (TFTR), and untreated negative control (TC) were analyzed by LC-MS to detect the production of antimicrobial compounds by CSR-T-3 as well as Fusarium toxins. LC-MS spectral profiles with different retention times and relative intensity (%) facilitated the identification of the compound showing distinct peak values by comparing their identity using similar molecular mass (m/z) values reported for distinct compounds (**Figure 4**). The compounds identified from LC-MS analysis could be broadly categorized as phenolic esters, antioxidants, fatty acids, fungal toxins, and compounds with antifungal and antibacterial principles. The extracts from the treatment control (TC) showed distinct peaks for fatty acid compound 20-methyl spirolide G (MeG) and soyasapogenol e-3-*o*-rhamnosyl glucosyl glucuronide (**Table 3**). The compounds in the crude extract of TFTR treatment with relative abundance was identified as ß-caryophyllene (1,429.9), catechin-o-gallate, soyasapogenol rhamnosyl glucoronide (729), peptaibols (1,788.2), fenigycin (1,462.2), iturin C19 (1,134.9), anthocyanin (1,191.7), and gallocatechin-o-gallate (913.5)

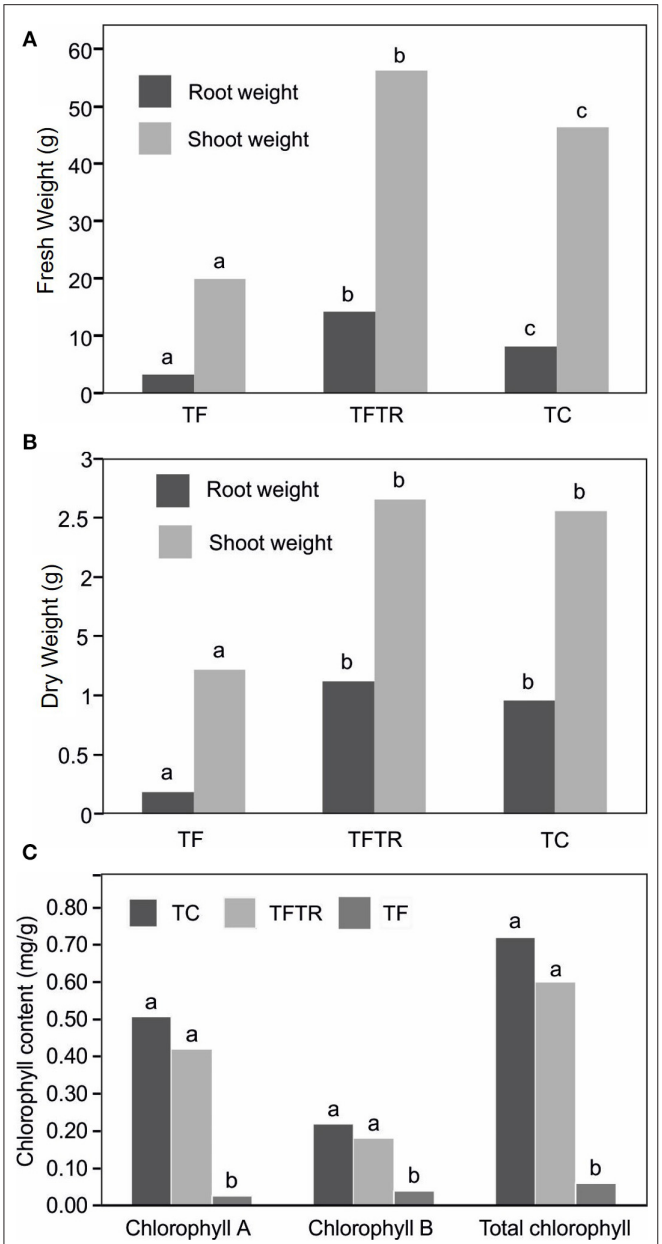

FIGURE 3 | Effect of CSR-T-3 (*Trichoderma reesei*) on banana root and shoot tissues, **(A)** fresh weight in "g" and **(B)** dry weight in "g" under greenhouse pot experiment while **(C)** shows variations in chlorophyll content. Both fresh and dry weights of shoot and root tissues were found to be enhanced in TFTR indicating growth promotion aided by the treatment in comparison with control. Quite contrarily, the TF plants showed reduced shoot and root weights (fresh and dry) which could be attributed to the wilting and senescence of the tissues. Chlorophyll a and b as well as total chlorophyll content reduced in TFTR and TF over the control TC.

(**Figures 4C–F**). Fungal toxins and metabolites produced by *Fusarium* spp. like enniatin A, fusarin C, chlamydosporal, etc. were also identified in TFTR treatment with low peak intensity (**Figures 4C,D**). The extracts of treatment Foc TR4 showed distinct compounds like fusaristatin A, fusarin C, chlamydosporal, and beauveric acid with high peak intensity (**Figures 4A,B**).

Gene Expression Profiling of Banana Plants With CSR-T-3 Treatment

Gene expression profiling revealed that the expression levels of *Fusarium*-related genes indicated a clear pattern of upregulation of the Fusaric acid biosynthesis genes in only *Fusarium* treatments (TF and TFTR) evident from the heat map presented in **Figure 5**. In the case of *Trichoderma* mycoparasitism genes (*TrCBH1*, *TrCBH2*, *TrEGL1*, *TrXYN1*) and signal transduction pathway genes for secondary metabolite production (*TrTGA1*, *TrTMK1*, and *TrVEL1*) a distinct pattern of upregulation was recorded in only the *Trichoderma* treatments (TFTR and TTR) (**Figure 5**). The significant upregulation of the Fusaric acid biosynthetic genes in TF and their corresponding downregulation in TFTR confirmed the suppression of Fusarium toxin production by *T. reesei*. An exception was recorded in the expression levels of the *FUB3* gene which showed a trend toward no change in TFTR (Z score-0). Contrarily, the significant downregulation in TTR (i.e., almost no expression) also strongly affirms the absence of the pathogen Foc TR4 and thereby toxin pathway gene expressions are being curtailed. On the other hand, the mycoparasitism-related genes, such as *TrCBH1*, *TrCBH2*, *TrEGL1*, *TrXYN1* were found to be significantly upregulated in TFTR and these genes were involved in the breakdown of the Foc cell wall and their components and are being produced by CSR-T-3. Interestingly, the *TrCBH1* gene seems to be an inducible gene upon pathogen invasion as seen in the change from Z-score 0 (no change) in TTR toward +1 (significant upregulation) in TFTR. But other genes seemed to exhibit constitutive expression as both TFTR and TTR showed similar levels of upregulation. Some signal transduction pathway genes, such as *TrVEL1* and *TrTMK1* were found to be significantly upregulated in TFTR which was similar to the pattern exhibited by TTR even though an upstream gene *TrTGA1* showed downregulation in TFTR which was observed to be upregulated in TTR.

Possible Biocontrol Mechanism Elucidated From Gene Expression and LC-MS Analysis

LC-MS and gene expression studies have provided some insights on the probable mode of action which is proposed as a probable mechanism of biocontrol exhibited by the CSR-T-3 *Trichoderma reesei* isolate against Foc TR4 (**Figure 6**). The role of Fusaric acid was confirmed from gene expression analysis but was not evident from LC-MS analysis. Fusaric acid is the major toxin reported in many Fusarium species. Fusaric acid biosynthesis involves several enzymes polyketide synthase (*FUB1*), aminoacid kinase (*FUB3*), hydrolase (*FUB4*), acetyl transferase (*FUB5*), dehydrogenase (*FUB8*), and proteins of unknown function (*FUB2*, *FUB6s*, and *FUB9*). But in the present study, from the LC-MS analysis, the role of other toxins, such as fusaristatin A, fusarin C, chlamydosporal, and beauveric acid could be established to be present in infected plants. Based on the time and location of the sampling for LC-MS analysis, it is evident that Fusarium-related toxins are accumulated in the Foc TR4-infected

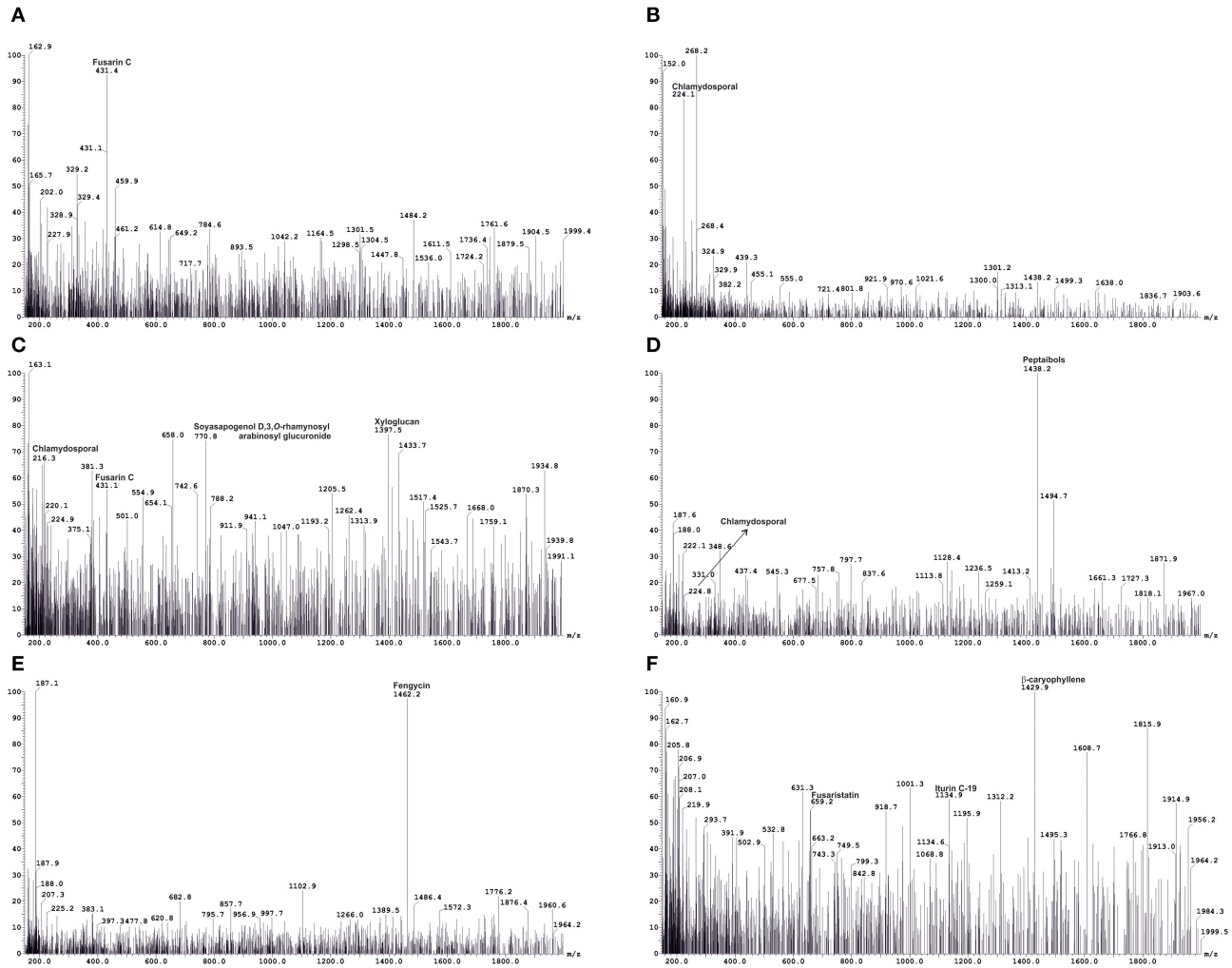

FIGURE 4 | A representation of liquid chromatography-mass spectrometry (LC-MS) analysis used for identification of key metabolites produced by host-pathogen interactions. Metabolite profiling using LC-MS indicating the production of pathogen-related toxins, such as fusarin C and chlamydosporal **(A,B)** in *Foc* TR4-infected wilted plants (TF) and detection of antifungal compounds **(C–F)**, such as ß caryophyllene, soyasapogenol D, 3-*O*-rhamnosyl arabinosyl glucuronide, peptaibols, and fengycinin CSR-T-3 treated banana plants challenged with *Foc* TR4 (TFTR). Simultaneous detection of pathogen-related toxins at low intensity **(C,D)** indicating a reduction of toxins and increase in antifungal metabolites under CSR-T-3 TFTR treatment.

plants which are responsible for the discoloration (**Figure 6A**). The mycelial growth of the pathogen and establishment in the plant tissues caused vascular clogging thereby blocking nutrient-water movement and eventually resulting in the sudden wilting of the plants. The counteracting mechanism of biocontrol agent CSR-T-3 by mycoparasitism and production of antifungal metabolites was established by the results observed in gene expression and LC-MS analysis. The typical signal transduction pathway, especially the genes upstream to the production of secondary metabolites induction, as well as those associated with the antifungal properties were upregulated in both TFTR and TTR. This was supported by the downregulation of Fusarium-related toxins and the upregulation of antifungal compounds in the LC-MS data. Thus, a possible mechanism of biocontrol potential of the CSR-T-3 *T. reesei* isolate against Foc TR4 has mycoparasitism and antifungal metabolites as key contributors (**Figure 6B**).

Biochemical Analysis of Defense-Related Enzymes and Phenol Content

Stress conditions are known to induce reactive oxygen species (ROS) production thereby resulting in oxidative damage in the cells. This effect can be recorded by assaying and quantifying the ROS scavenging enzymes which may be produced by the host banana plants upon infection with Foc TR4. Sometimes, the biocontrol agents also facilitate production and induction of host defense enzymes. Assaying the defense enzymes in different treatments was completed with the aim of assessing the host response in combination with the CSR-T-3 treatment (**Table 4**). The accumulation of defense enzymes and phenols

TABLE 3 | Key metabolites identified from LC-MS analysis of crude extracts of the banana root samples under various treatments.

Treatments	Compound	Peak value	RT (min)[a]	Intensity (%)	Activity	References
*TC	Methyl esters of 20-methyl spirolide G (MeG)	887.6	24.96	100	Fatty acid	Aasen et al., 2006
	6″-p-coumaroylglucoside	609.0	9.21	100		Trikas et al., 2016
	Soyasapogenol E-3-*O*-rhamnosyl glucosyl glucuronide	793.5	26.64	100	Antifungal, antibacterial	Sagratini et al., 2009; Pollier et al., 2011
**TFTR	Catechin-*o*-gallate	729	29.03	44	Antioxidant	Tala et al., 2013
	ß caryophyllene	1429.9	2.22	100	Antifungal	Qi et al., 2017
	Enniatin A	687.3	21.56	25	Secondary metabolite *Fusarium* sp.	Sorensen and Giese, 2013
	Soyasapogenol E-3-*O*-rhamnosyl glucosyl glucuronide	793.6	21.56	100	Antifungal, antibacterial	Sagratini et al., 2009; Pollier et al., 2011
	Peptaibols	1438.2	7.13	100	Antifungal	Mukherjee and Kenerley, 2010
	Xyloglucan	1397.5	5.08	80	Antifungal	Vinueza et al., 2013
	Soyasapogenol D-3-*O*-rhamnosyl Arabinosyl glucuronide	770.8	5.08	75	Antifungal	Jin et al., 2006, 2007; Tava et al., 2009, 2011
	Fenigycin	1462.2	7.40	100	Antifungal	Pathak and Keharia, 2014
	Iturin C19	1134.9	2.22	60	Antifungal	Pathak and Keharia, 2014
	Anthocyanin	1191.7	7.98	70	Antioxidant	Hwang et al., 2017
	(Epi)gallocatechin-O-gallate	913.5	13.58	100	Antioxidant	Tala et al., 2013
***TF	1-Palmitoyl-2-10-hydroxy-5,8,11-tridecatrienoic acid	732.6	17.25	100	Host defense	Reis et al., 2005
	Gallocatechin-O-gallate	913.5	13.61	100	Antioxidant	Tala et al., 2013
	Beauveric acid	801.7	27.33	25	Fungal toxin	Li et al., 2013
	Fusaristatin A	659.8	1.81	20	Fungal toxin	Hegge et al., 2015
	Fusarin C	431.4	10.27	100	Fungal toxin	Sorensen and Giese, 2013
	Chlamydosporal	224.1	1.48	85	Secondary metabolite of *Fusarium* sp.	Sorensen and Giese, 2013

**TC, treatment control; **TFTR, treatment with Foc TR4 and Trichoderma reesei isolate CSR-T-3; ***TF, treatment with Foc TR4 alone.*

was significantly higher in the TFTR treatment (where plants were treated with the pathogenic isolate of Foc TR4 and the *T. reesei* CSR-T-3 isolate) in comparison with TF (Foc TR4-treated) and TC (negative control with no treatments). The treatments involving *T. reesei* isolate CSR-T-3 invariably had a higher induction of peroxidase (POD), polyphenol oxidase (PPO), phenylalanine ammonia lyase (PAL), and ß-1, 3-glucanase activity than the TF and TC treatments. Significant induction of chitinase activity (3.160-fold increase in nmol of GlcNAc g^{-1}fw min^{-1}) was observed in *T. reesei* isolate CSR-T-3 inoculated TFTR treatment while Foc TR4 alone inoculated TF treatment recorded induction but at low levels. The treatments involving *T. reesei* isolate CSR-T-3 had nearly 1.382 times higher phenolic content than the control plants.

Development of Bioformulation and Field Evaluation of CSR-T-3 (*T. reesei*) Bioformulation

Bioformulation developed using the *T. reesei* CSR-T-3 isolate that showed promising results in pot culture studies under greenhouse conditions (**Figure 2**) in terms of disease suppression was taken to the field level evaluation in the hotspot region of the wilt disease. Efficacy of CSR-T-3 formulation was tested on sick plots in the hot spot area of Sohawal (26° 46′ 3.3852″ N latitude; 81° 59′ 42.7992″ E longitude) where there were severe disease incidences during 2017 and 2018 (Damodaran et al., 2019c). The CSR-T-3 *T. reesei* isolate was formulated in the form of bioformulation using a loopful of a 2 mm disc in the CSR patent protected bio-media and incubated for 72 h. After 72 h, the plants under the treatment were drenched with 500 ml/plant with 3% of the formulation at 2, 4, 6, and 8 months after planting.

Typical wilting symptoms of yellowing in the older leaves started in the untreated control plants from the 4th month (November) after planting followed by pseudo stem splitting at the 6th month (January) after planting with the disease spreading rapidly over 12–14 months after planting (July-August) corresponding with the flowering and fruiting stages. High disease incidence percentage (46.50%) (**Table 5**) was recorded in the plants that were not treated with CSR-T-3 *T. reesei*. However, there was a significant reduction in the disease incidence percentage (10.58%) of the plants treated with *Trichoderma* isolate CSR-T-3. At harvest, the disease severity index of the *Trichoderma*-treated plants were significantly lower (1.14) compared with those that were not treated (3.46).

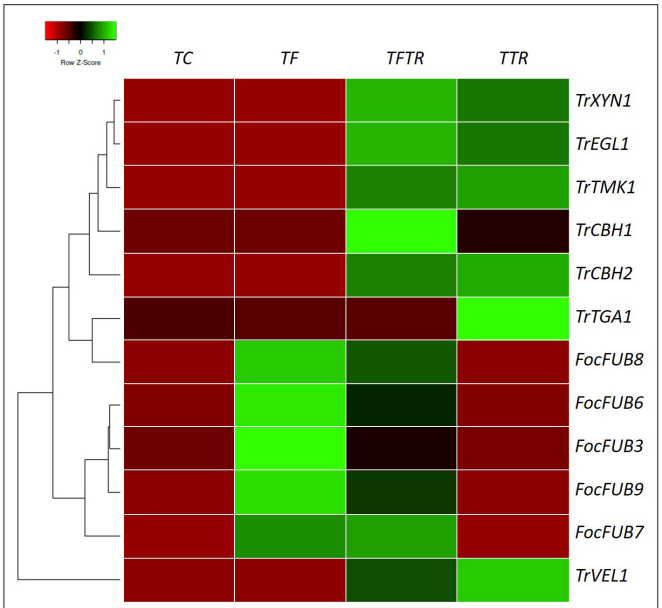

FIGURE 5 | Heat map showing gene expression patterns of key genes involved in fusaric acid biosynthesis by *Foc* TR4, mycoparasitism, and secondary metabolite production inducing signal transduction pathway genes of *Trichoderma reesei* in various treatments for establishing the biocontrol mechanism of CSR-T-3. Fusaric acid biosynthesis involves a series of genes, such as *FUB3*, *FUB6*, *FUB7*, *FUB8*, and *FUB9*. Fusaric acid is one of the major toxins produced by *Fusarium oxysporum* f. sp. *cubense* tropical race 4 and the upregulation of these genes in banana plants challenge-inoculated with Foc TR4 (TF) while downregulation of the same was recorded in TFTR (CSR-T-3-treated banana plants challenge-inoculated with *Foc* TR4) and TTR (CSR-T-3-treated banana plants without pathogen). Similarly, the genes involved in mycoparasitism (*TrCBH1*, *TrCBH2*, *TrEGL1*, *TrXYN1*) and those involved in the signal transduction pathway inducing secondary metabolite production (*TrVEL1*, *TrTGA1*, *TrTMK1*) were found to be significantly upregulated in TTR and TFTR. Green color code represents upregulation and red color code indicates downregulation. TC indicates negative control (no pathogen, no biocontrol), TF represents *Foc* TR4-challenged banana plants, TFTR indicates CSR-T-3-treated banana plants challenged with *Foc* TR4 and TTR indicates positive control (banana plants with CSR-T-3 (*Trichoderma reesei* isolate).

The plant height (230.73 cm), girth (43.9 cm), and leaf area (73.13 cm^2) of the treated plant group were significantly higher than the other untreated control group. The mean yield (30.57 kg/plant) of the treated plants were significantly higher compared to the untreated plants (7.71 kg). However, there was no significant difference in the number of leaves and number of hands between the treated and untreated plants. There was a significant increase in bunch size and finger size that was attributed to enhanced yield over the diseased plant. The yield under treatment was found to be on par with the average yield of the locality that ranged from 25 to 30 kg/plant. Thus, the drenching of *T. reesei* isolate CSR-T-3 not only had an antifungal effect in the control of the disease but also had a growth promoting effect in increasing certain growth parameters, such as plant vigor, finger, and bunch size besides yield (bunch weight) which increased 2-fold over untreated control plants.

DISCUSSION

The global banana production system has been exposed to serious threats in the mid-twentieth century by the devastating wilt disease caused by *F. oxysporum* f. sp. *cubense* (Stover, 1962). Popularly known as Panama disease it wiped out the Gros Micheal cultivation in Central America (Ploetz, 1992). The banana industry was sustained with the identification of the Cavendish (AAA) cultivar as a resistant source for the Foc race 1 pathogen. However, the choice varieties of the Indian subcontinent comprising of Pisang Awak (ABB), Rasthali/Amritpani (AAB), and Malbhog (AAB) still remained highly susceptible to the Foc race 1 and are threatened with extinction (Thangavelu et al., 2001). In the early 1990s, a new race was identified in the tropics, in a much more virulent form, devastating the Cavendish cultivars and designated as tropical race 4 (TR4) that causes 70–100% loss (Ploetz and Churchill, 2011) and also economic loss amounting to US$ 388.1 million (FAO, 2017). The perennial nature of the pathosystem complicated the development of sustainable control measures (Ploetz, 2007). The chance of obtaining a tolerant variety was very difficult due to the existence of extremely poor fertility in the Cavendish cultivars (Ortiz, 2013). However, the utilization of antagonistic microorganisms from suppressive soils, such as *Pseudomonas*, *Bacillus*, and *Trichoderma* species can aid in the curtailment of the growth and development of the pathogen (Deng et al., 2013). Even among the antagonistic microbes, *Trichoderma* has been widely exploited as the potential biocontrol agent owing to their distinct properties in the control of soil borne disease and non-eco-toxic nature of the genus (Benitez et al., 2004). The fast growing and mycoparasitism ability of the *Trichoderma* isolates place them as potential antagonistic microbes (Monfil and Casas-Flores, 2014; Sellamani et al., 2016). Prominent inhibitory effects of different *Trichoderma* isolates against Fusarium diseases by mycotoxin production were established and indicated the further need of their ability through field validation (Tian et al., 2018).

Success of biological control in the field depends on the correct identification of potential strains and application in the field (Chaves et al., 2011). Therefore, isolation and screening of the highly efficient microorganisms form the base of biocontrol. An attempt was made to assess the efficacy of three *Trichoderma* isolates that were isolated from the rhizosphere of biotic (banana wilt suppressive) and abiotic (banana salt stressed) stress ecosystem (Damodaran and Mishra, 2016; Damodaran et al., 2019c). These antagonists exert differential inhibition potential to the pathogen growth that was evident from the *in vitro* assay and the dominating role of disease suppression with isolate CSR-T-3 was successfully demonstrated in the *in vivo* pot culture study. PGPR strains, such as *Pseudomonas fluorescens* PF-1 and *Trichoderma* species TRC-54 were earlier reported to have controlled the mycelia growth of Foc race 1 of banana under a dual culture study through the direct action of enzymes and metabolites produced by PGPR (O'Sullivan et al., 1992; Nagarajkumar et al., 2004). CSR-T-3 was the first strain of *Trichoderma reesei* isolated from the salt affected rhizosphere to show disease suppression against the banana Foc TR4. The antifungal property was further demonstrated in this study using a pot and field experiment.

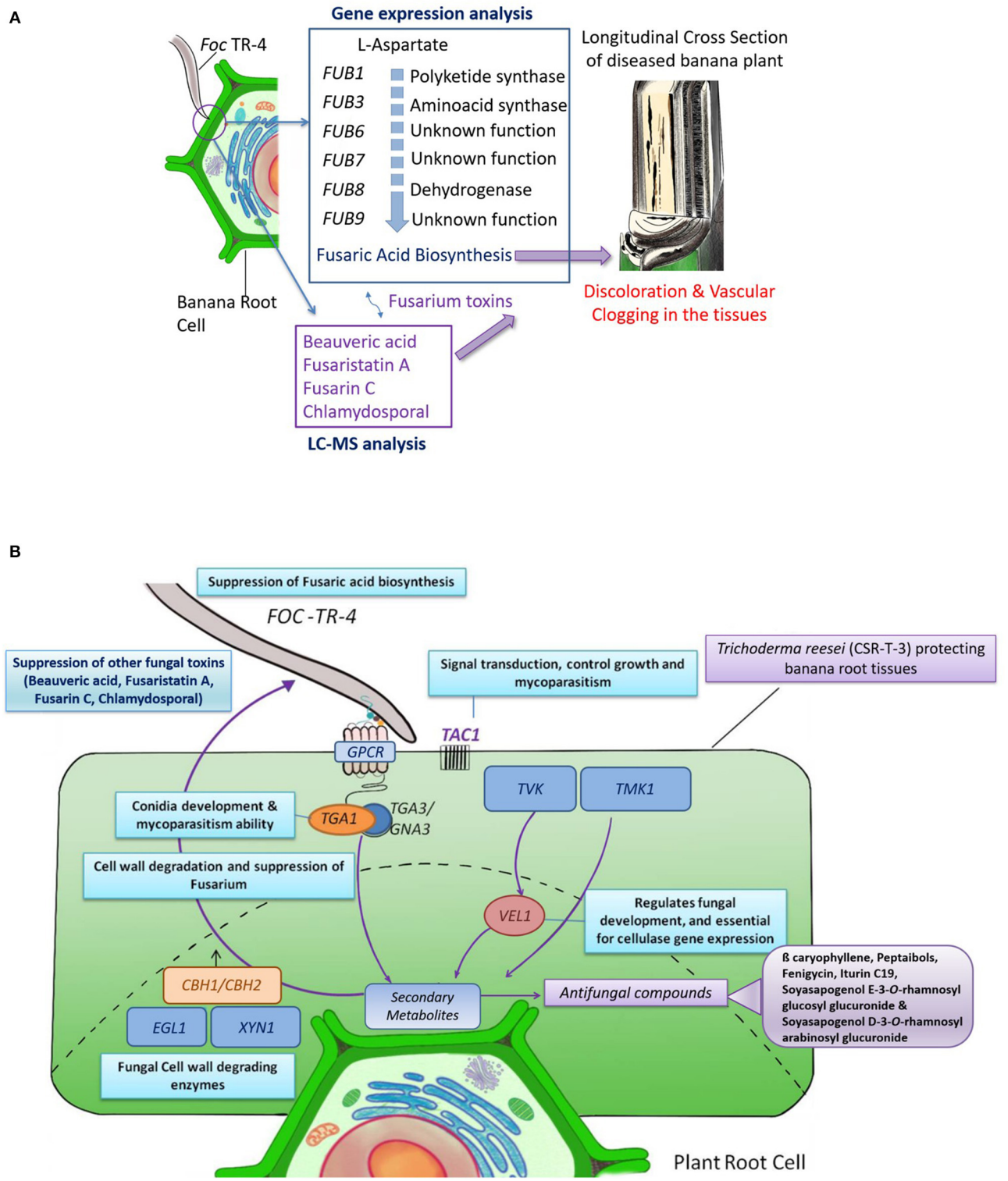

FIGURE 6 | Possible mechanism of CSR-T-3 (*Trichoderma reesei*) in providing protection against Foc TR4 pathogen in bananas. **(A)** Mode of infection in the banana plants are induced by the toxins produced by *Fusarium oxysporum* f. sp. *cubense* tropical race 4 (*Foc* TR4) which was evident from the gene expression analysis and LC-MS profiling. The toxins and the mycelial mats results in discoloration and vascular clogging of the plant tissues, the most characteristic symptom of *Foc* TR4. **(B)** Mechanism of CSR-T-3 through the expression of mycoparasitism-related genes cellobiohydrolase (*CBH1*/*CBH2*), endoglucanse (*EGL1*), and xylanase (*XYL1*) genes and the signal pathway that are induced by *TMK1* and *VEL1* genes are evident from the gene expression studies. Expression of these genes also triggers the production of secondary metabolites especially antifungal compounds, such as ß-caryophyllene, catechin-o-gallate, soya sapogenol rhamnosyl glucoronide, peptaibols, fenigycin, iturin C19, anthocyanin, and gallocatechin-o-gallate. Co-suppression of fusaric acid and other toxins, such as beauveric acid, fusarastatin A, fusarin C, and chlamydosporal during the same time results in conferring tolerance in the banana plants.

TABLE 4 | Profiling changes in activities of defense enzymes in *Trichoderma reesei* (CSR-T-3)-inoculated banana plantlets challenged with pathogenic isolate CSR-F-1 of Foc TR-4.

Treatment	Peroxidase ($ng^{-1}fw\ min^{-1}$)	PPO* ($ng^{-1}fw\ min^{-1}$)	PAL** (nmol of trans-cinnamic acid $g^{-1}fw\ min^{-1}$)	β-1, 3-glucanase (mg of glucose $g^{-1}fw\ min^{-1}$)	Chitinase (nmol of GlcNAc $g^{-1}fw\ min^{-1}$)	Phenols (μg/g fresh weight)
TC	19.463[a] (±0.61)	0.136[a] (±0.61)	1386.570[a] (±42.23)	198.800[a] (±11.14)	25.560[a] (±8.57)	378.400[a] (±25.11)
TF	20.154[a] (±0.57)	0.176[a] (±0.01)	2020.630[b] (±59.71)	225.600[b] (±14.14)	33.290[b] (±2.22)	463.600[b] (±16.15)
TFTR	25.526[b] (±0.74)	0.187[a] (±0.01)	2688.030[c] (±81.33)	316.560[c] (±5.15)	80.778[c] (±3.16)	523.000[c] (±26.02)

TF, treatment with Fusarium; TFTR, treatment with Fusarium and Trichoderma; TC, treatment control; PPO, Polyphenol oxidase; PAL*, Phenylalanine ammonia lyase.*
Values are the means of five replicates with the sample size n = 5.
Means in the columns followed by the same letter (a, b, or c) are not significantly different according to Duncan's multiple range test at P = 0.05. Values in the parentheses indicate the standard deviation of the mean.

TABLE 5 | Effect of *Trichoderma reesei* (CSR-T-3) on *Fusarium* wilt and the growth of banana plantlets under field experiment in sick fields.

Treatment	Plant height (cm)	Girth (cm)	No. of leaves	Leaf area (cm^2)	Yield (kg/plant)	No. of hands	Disease incidence (%)	Disease severity index
CSR-T-3	230.73[a] (±4.70)	43.9[a] (±7.33)	7.86[a] (±0.38)	73.13[a] (±7.14)	30.57[a] (±3.60)	8.14[a] (±0.69)	10.58[a] (±4.64)	1.14[a] (±0.69)
Control	214.76[b] (±2.73)	36.1[a] (±9.72)	6.71[b] (±0.76)	51.84[b] (±6.40)	16.29[b] (±6.13)	7.71[a] (±1.11)	46.50[b] (±18.33)	3.46[b] (±0.51)

Values are the means of ten replicates.
Means in the columns followed by the same letter are not significantly different according to paired t-test at P = 0.05. Values in the parentheses indicate the standard deviation of the mean.

Application of the isolate successfully reduced the disease severity index significantly when compared to Foc TR4-infected plants and also promoted the growth of the banana crop successfully. Earlier, there were successful reports on the biological control of Fusarium wilt disease in bananas using bacterial strains like bacterial isolate ITBB B5 1 (Tan et al., 2015), *Streptomyces* strain CB75 (Chen et al., 2018), and *Bacillus flexus* strain Typr1 (Thangavelu and Gopi, 2015) under pot experiments. But none of these reports have indicated field level application and validation of these strains for commercial use. We report here the first successful report of a fungal strain CSR-T-3 controlling Foc TR4 causing wilt disease in bananas at a field level besides pot culture studies.

Trichoderma spp. are known to produce a wide range of bioactive secondary metabolites that are known to have antifungal, antibacterial, and toxic properties to control a wide range of phytopathogens, such as *Alternaria alternata*, *Botrytis cinerea*, *Fusarium* spp., *Pythium* spp., *Rhizoctonia solani*, *Sclerotinia sclerotiorum*, and *Ustilago maydis* (Hyder et al., 2017; Sood et al., 2020). *Trichoderma* spp. is reported as an inexhaustible source of antibiotic derivatives (from the acetaldehydes to alpha-pyrones) terpenes, polyketides, isocyanide derivatives, piperacines, and complex families of peptaibols (Keszler et al., 2000; Sood et al., 2020). Therefore, in order to characterize and profile the metabolites, LCMS analysis was performed which aided in the identification of microbial metabolites who were produced by both the pathogen (CSR-F-1) and the biocontrol agent (CSR-T-3). The treatment involving Foc TR4 challenge inoculation and *T. reesei* isolate CSRT-3 showed the production of a wide range of bioactive antifungal and antioxidant metabolites with high intensity m/z peaks. They include peptaibols, fenigycin, xyloglucan, soyasapanogenol rhamnosyl glucuronide, iturin C, ß-caryophyllene, and antioxidants like catechin-O-galate. The presence of *Fusarium* related metabolites like fusaristatin, fusarin C, chlamydosporal, enniatin C, etc. were also observed but the intensity of the m/z peaks were comparatively lower than the antifungal and antioxidant metabolites in this treatment. However, significant production of *Fusarium*-related metabolites like Fusarin C with a high intensity m/z peak was observed in the TF treatment where only the Foc TR4 isolate was inoculated. This implies that there is a suppression of toxins produced by Foc TR4 in the presence of the antifungal metabolites produced by *T. reesei* isolate CSR-T-3 in this present study. Peptaibols are small peptides of α-aminoisobutyric acid (Aib) produced by the genus *Trichoderma* that are economically important for their anti-microbial and anti-cancer properties as well as their ability to induce systemic resistance in plants against microbial invasion (Mukherjee et al., 2013). The involvement of these compounds in mycoparasitism established with their role in induced systemic resistance in plants by both apoptosis and autophagy suggest their capability in preventing the invasion of root-invading fungi (Schuster and Schmoll, 2010). The intensity of mass peaks assigned for iturin C and fengycin in the TFTR

treatment in our study explicitly show the high antifungal potency of the *T. reseei* CSR-T-3 isolate. The cyclic heptapeptide iturin with ß-amino fatty acid was known to have high hemolytic and antifungal properties while fengycin, a cyclic depsipeptide with 10 amino acids and a ß-hydroxy fatty acid tail, is known for its excellent antifungal potential against filamentous fungi (Winkelmann et al., 1983; Vanittanakom et al., 1986). Pathak and Keharia (2014), reported iturin C and fengycin as an antifungal compound produced by *Bacillus subtilis*. Phenolic compounds have crucial roles in inducing the plant defense mechanism through free radical termination by providing hydrogen to reduce free radicals. The presence of phenolic compounds, such as gallocatechin-o-gallate in our LCMS fractions in TFTR and TF treatment signifies the activities of plant defense systems when exposed to biotic stress. The bacterization of tomato plants with beneficial strains showed antifungal activity through the deposition of phenolic compounds and restricting the growth of *F. oxysporum* f. sp. *lycopersici* (M'Piga et al., 1997).

Our study has demonstrated the possibility of the increase in the plant defense system through an increase in the activities of phenols and enzymes like peroxidase (POD) and phenylalanine ammonia lyase (PAL). Peroxidase is a defense enzyme implicated in the last enzymatic step of lignin biosynthesis that oxidizes the hydroxyl cinnamyl alcohols into free radicals that are later coupled with lignin polymer (Gross, 1980). POD is known to inhibit the spore germination and mycelia growth of some pathogenic fungi like *Pseudocercospora abelmoschi* and *Pseudocercospora cruenta* (Joseph et al., 1998). Enhanced POD and PAL activities were reported by Kavino et al. (2007) in bacterial strain-treated banana plantlets that showed tolerance to *Banana bunchy top virus*. PAL is an enzyme that plays an important role in the biosynthesis of defense chemicals in phenyl propanoid metabolism (Daayf et al., 1997). Another prominent group of enzymes and compounds that are commonly correlated with the tolerance mechanism exhibited by the *Trichoderma* spp. are ß-glucanase and chitinase (Chet, 1987). ß-glucans are polysaccharides that stimulate the host immune response on interaction (Garfoot et al., 2014). The higher activity of ß-glucanase and chitinase in the *T. reesei*-treated plants was observed in biochemical assays of our study which could be another additional mechanism attributing to increasing the host immune response to the pathogen. Radjacommare et al. (2004) assessed the chitinoyltic enzyme against *Rhizoctonia solani* in rhizobacteria-treated rice which induced a defense response in the host by bacterial co-inoculants of *Pseudomonas* sp. Higher activity of ß-glucanase and chitinase was present in *F. oxysporum* f. sp. *cubense* race 1 tolerant cultivars and hybrids of bananas (Kavino et al., 2009). Previous reports by Migheli et al. (1996) on the biocontrol of *P. debaryanum* by *Arthrobacter* spp. elucidated the role of glucanase and protease in the lysis of mycelium.

The genome of *T. reesei* has been reported to possess genes encoding for 2 cellobiohydrolases, 5 endo-ß-1,4-glucanases, and different isoforms of ß-glucosidases, hemicellulases, and accessory enzymes (Martinez et al., 2008; Hakkinen et al., 2012; Dita et al., 2018). *CBH* encodes for exo-cellobiohydrolases or exoglucanases which are involved in the hydrolysis of 1,4-beta-D-glucosidic bonds in the external structure of cellulose and aid in cell wall degradation (Antonieto et al., 2014; Nogueira et al., 2015). CBH1 is reported to be an inducible gene in the presence of inducers, such as cellulose, sephorose, lactose, and cellobiose (Dos Santos et al., 2014; Nogueira et al., 2015); which was confirmed in the present study as pathogen interaction with CSR-T-3 induced the expression. On the contrary, endo-β-1,6-glucanase is one of the important genes for mycoparastic activity of *Trichoderma* sp which catalyzes cell wall degradation by breaking β-1,6 linkages internally (De la Cruz et al., 1995; Gruber and Seidl-Seiboth, 2011). In the present study, the upregulation of *CBH1*/*CBH2*, *EGL1*, and *XYN1* genes in TFTR have ascertained the mycoparasitism activity of CSR-T-3. Other signal transduction pathway genes were also found to be upregulated in the treatments involving CSR-T-3. The *TGA1* gene encodes for a G protein α subunit, which is involved in mycoparasitic coiling, conidiation (Rocha-Ramirez et al., 2002), formation of chitinase, and the production of antifungal metabolites (Reithner et al., 2005). *VEL1* controls the regulation of the pheromone system, mating partner sensing, and sexual and asexual development (Bazafkan et al., 2015). The *VEL1* gene encodes for velvet protein 1, a part of the VELVET complex composed of *LAE1*, *VEL1*/*VELA*, and *VEL2*/*VELB* proteins. This *VEL1* protein is also responsible for morphogenetic traits, is a key regulator of biocontrol in *T. virens*, and is highly conserved in different species of *Trichoderma* (**Supplementary Figure 2**) (Mukherjee and Kenerley, 2010). It is also reported to have a role in the induction of cellulase gene family expression which includes cellobiohydrolases, glucanases, chitinases, and xylanases (Karimi Aghcheh et al., 2016). The *TMK*1 gene encodes for a mitogen activated protein kinase (MAPK) which plays an important role in mycoparasitism by the regulation of mycoparasitic host attack, formation of aerial hyphae, and conidiation (Reithner et al., 2007; Schmoll, 2008; Swain and Mukherjee, 2020). Generally, MAPK are involved in signal transduction pathways that converge into the accumulation of secondary metabolites. Earlier, Reithner et al. (2007) reported that tmk1 deletion caused reduced mycoparasitic activity against *Rhizoctonia solani* and *Botrytis cinerea* and were also associated with the regulation of production 6-pentyl-a-pyrone and peptaibol antibiotics. The upregulation of the *TGA1*, *TMK1*, and *VEL1* genes indicate the possibility of enhanced chitinase activity. This information also supports the result of high chitinase and phenol activities in TFTR and TTR treatments in the study.

Biocontrol mechanisms of CSR-T-3 (*T. reesei*) against Fusarium wilt pathogen Foc TR4 (CSR-F-1) are considered to be mainly because of mycoparasitism, the production of antifungal metabolites, such as iturin C, ß-carophyllene etc., and a reduction in the fungal toxins like fusaristatin A, fusarin C, beauveric acid, and chlamydosporal production (**Figure 6**). This well-established concept of biocontrol reported to occur in *Trichoderma* species was confirmed by gene expression profiling of the fusaric acid biosynthesis and cellulolytic enzymes of *Fusarium* species and *T. reesei*, respectively. *Trichoderma* species colonize the epidermal root surface and also induce the plant to produce secondary metabolites that include compounds with low molecular weight inducing the expression of genes involved

in the defense response against the pathogen (Hermosa et al., 2012; Malmierca et al., 2014; Sood et al., 2020). Earlier whole genome transcriptome analysis indicated that defense genes associated with CEBiP, BAK1, NB-LRR proteins, PR proteins, transcription factor, and cell wall lignification were expressed strongly in resistant variety Yueyoukang 1 indicating that these genes play important roles against Foc TR4 infection in bananas (Bai et al., 2013).

Developing a bioformulation using the CSR-T-3 *T. reesei* isolate based on the antagonistic effect on the pathogen and the epidemiology of the disease in the hotspot region, we standardized the application schedule and mode of application. A field evaluation of CSR-T-3 bioformulation in the sick plots of a hot spot area has clearly demonstrated the successful control of the pathogen which is evident from the reduced disease incidence at the same time contributed to the successful management of the disease. Earlier, Damodaran et al. (2019b) demonstrated successful control of Foc TR4 using ICAR-FUSICONT. To date, no product is available in India for biological control of Fusarium wilt disease Foc TR4 and this study is the first of its kind to find evidence for successful management.

CONCLUSION

The current gaps in devising management schedules for Fusarium wilt disease include the scarcity of resistant varieties, no effective chemical control measure, the lack of a virulent biological control agent that could work at field level, and also their clear mode of action. Our study has been a solution to the latter category of biological control of Fusarium wilt disease of bananas caused by Foc TR4. We report here an effective virulent CSR-T-3 isolate of *T. reesei* that was successfully proven in a pot culture experiment and field evaluation in sick fields of hot spot areas of plants affected by Foc TR4. This biocontrol agent has been proven to have a good effect on the fruit yield and weight besides the suppression of the pathogen. The mechanism of mycoparasitism and reduction in toxin accumulation was also elucidated using gene expression and LC-MS analysis which has established the role of cell wall degrading enzymes. Signal transduction pathways inducing secondary metabolites with antifungal properties in *Trichoderma* has resulted in the suppression of toxins produced by Foc TR4 and thus conferred induced tolerance to banana plants. Field evaluation of the CSR-T-3 showed the potential of this bioagent in the management of the banana Fusarium wilt disease on a large scale. This study is a holistic approach to the technological advancement of *T. reesei* from lab to field in the management of Fusarium disease in bananas.

DATA AVAILABILITY STATEMENT

All raw data analyzed supporting this article will be made available by the authors. Public domain genome sequence data sets were used for primer designing and the accession numbers are provided in the article.

AUTHOR CONTRIBUTIONS

TD conceived, planned, and designed the experiments. SR designed the statistical methodology and analyzed the data. MM designed the gene expression studies, designed primers for expression analysis, and contributed equally to the manuscript preparation with TD. RG and KY performed the experiments of dual culture, pot, and field experiment. SK performed the molecular wet lab studies. IA performed the molecular identification of isolates. NK assisted in the disease screening experiments. SKJ and VKM performed the soil analysis of the pot soil used in the screening trial. All authors contributed to the article and approved the submitted version.

FUNDING

This work has been initially supported from Application of Microorganisms in Agriculture and Allied Sectors (AMAAS) project operated at ICAR-Central Institute of Soil Salinity Research, Regional Research Station, Lucknow and Flagship project of Indian Council of Agricultural Research operated at ICAR Central Institute for Subtropical Horticulture, Lucknow and then further supported by financial aid from Extra mural fund (EMF).

ACKNOWLEDGMENTS

The Director General, ICAR was acknowledged for critically evaluating the entire program and guiding us toward perfection. The authors thank Dr. A. K. Singh, Deputy Director General, Indian Council of Agricultural Research (ICAR) for providing financial support under the ICAR Extramural Project for taking up the research work and also for motivating the execution of the work. Thanks are due to the Director, ICAR-Central Soil Salinity Research Institute, Karnal, India for providing all logistic support in conducting the experiment. The Director, ICAR-National Institute of Agriculturally Important Micro-organism, Mau, Uttar Pradesh, India, was acknowledged for partial funding under the AMAAS network scheme for the execution of the initial microbiological studies. We thank Dr. N. K. Krishnakumar, Bioversity International, Dr. B. K. Pandey, ADG in-charge (Horticultural Sciences-II), ICAR, and Dr. S. Uma, Director, ICAR-National Research Centre of Banana for their guidance and motivation in the execution of the program. Also, we thank Dr. P. Chakrabarthy, ADG (Plant Protection) for providing critical input into the characterization of *Trichoderma reesei*. We dedicate the work in memory of the late Dr. R. B. Rai who was the inspiring force for this work.

SUPPLEMENTARY MATERIAL

The Supplementary Material for this article can be found online at: https://www.frontiersin.org/articles/10.3389/fmicb.2020.595845/full#supplementary-material

REFERENCES

Aasen, J. A. B., Hardstaff, W., Aune, T., and Quilliam, M. A. (2006). Discovery of fatty acid ester metabolites of spirolide toxins in mussels from Norway using liquid chromatography/tandem mass spectrometry. *Rapid Commun. Mass Spectrom.* 20, 1531–1537. doi: 10.1002/rcm.2501

Aguilar Moran, J. F. (2013). Improvement of Cavendish Banana Cultivars through conventional breeding. *Acta Hortic.* 986, 205–208. doi: 10.17660/ActaHortic.2013.986.21

Amorim, E. P., dos Santos-Serejo, J. A., Amorim, V. B. O., Ferreira, C. F., and Silva, S. O. (2013). Banana breeding at Embrapa cassava and fruits. *Acta Hortic*. 986, 171–176. doi: 10.17660/ActaHortic.2013.986.18

Antonieto, A. C. C., dos Santos Castro, L., Silva-Rocha, R., Persinoti, G. F., and Silva, R. N. (2014). Defining the genome-wide role of CRE1 during carbon catabolite repression in *Trichoderma reesei* using RNA-Seq analysis. *Fungal Genet. Biol.* 73, 93–103. doi: 10.1016/j.fgb.2014.10.009

Bai, T. T., Xie, W. B., Zhou, P. P., Wu, Z. L., and Xiao, W. C. (2013). Transcriptome and expression profile analysis of highly resistant and susceptible banana roots challenged with *Fusarium oxysporum* f. sp. *cubense* tropical race 4. *PLoS ONE* 8:e73945. doi: 10.1371/journal.pone.0073945

Bazafkan, H., Dattenböck, C., Böhmdorfer, S., Tisch, D., Stappler, E., and Schmoll, M. (2015). Mating type-dependent partner sensing as mediated by *VEL1* in *Trichoderma reesei*. *Mol. Microbiol.* 96, 1103–1118. doi: 10.1111/mmi.12993

Benitez, T., Rincon, A. M., Limon, M. C., and Codon, A. C. (2004). Biocontrol mechanism of *Trichoderma* strains. *Int. Microbiol.* 7, 249–260.

Boller, T., and Mauch, F. (1988). Colorimetric assay for chitinase. *Methods Enzymol*. 161, 430–435. doi: 10.1016/0076-6879(88)61052-4

Brandes, E. W. (1919). Banana wilt. *Phytopathology* 9,339–389. doi: 10.5962/bhl.title.36913

Buddenhagen, I. (2009). Understanding strain diversity in *Fusarium oxysporum* f. sp. *cubense* and history of introduction of 'tropical race 4' to better manage banana production. *Acta Hortic.* 828, 193–204. doi: 10.17660/ActaHortic.2009.828.19

Carvalhais, L. C., Henderson, J., Rincon-Florez, V. A., O'Dwyer, C., Czislowski, E., Aitken, E. A. B., et al. (2019). Diagnostics of banana Fusarium wilt targeting secreted-in-xylem genes. *Front. Plant Sci.* 10:547. doi: 10.3389/fpls.2019.00547

Chaves, J. Q., Pires, E. S., and Vivoni, A. M. (2011). Genetic diversity, antimicrobial resistance and toxigenic profiles of *Bacillus cereus* isolated from food in Brazil over three decades. *Int. Food Microbiol*. 147, 12–16. doi: 10.1016/j.ijfoodmicro.2011.02.029

Chen, Y., Zhou, D., Qi, D., Gao, Z., Xie, J., and Luo, Y. (2018). Growth promotion and disease suppression ability of a *Streptomyces* sp. CB-75 from banana rhizosphere soil. *Front. Microbiol.* 8:2704. *doi: 10.3389/fmicb.2017.02704*

Chet, I. (1987). "*Trichoderma*-application, mode of action, and potential as biocontrol agent of soil borne plant pathogenic fungi." in *Innovative Approaches to Plant Disease Control*, ed I. Chet (New York, NY: John Wiley & Sons), 137–160.

Crop Production Guide (2017). *Department of Agriculture*. Chennai: Government of Tamil Nadu.

Daayf, F., Schmitt, A., and Belenger, R. R. (1997). Evidence of phytoalexins in cucumber leaves infected with powdery mildew following treatment with leaf extracts of *Reynoutria sachalinesis*. *Plant Physiol.* 113:719727. doi: 10.1104/pp.113.3.719

Damodaran, T. (2018). "Banana production in subtropics–strategies, challenges and research initiatives." in *National Conference on Strategies and Challenges in Doubling Farmer's Income Through Horticultural Technologies in Subtropics* (ICAR-Central Institute for Sub-tropical Horticulture) (Lucknow), 99–101.

Damodaran, T., Gopal, R., Yadav, K., Mishra, V. K., and Jha, S. K. (2019c). "CSR-T-3 (*Trichoderma reesei*)–a potential cellulolytic and proteolytic isolate used for inducing tolerance to biotic and abiotic stress in commercial agri-horticulture crops," in *Souvenir on A Golden Jubilee International Salinity Conference: Resilient Agriculture in Saline Environment Under Changing Climate: Challenges and Opportunities* (Karnal), 86–87.

Damodaran, T., Kumar, N., and Kavino, M. (2009). Breeding and evaluation of Musa hybrids resistant to *Fusarium oxysporum* f. sp. *cubense* race 1. *Fruits* 64, 1–16. doi: 10.1051/fruits/2008044

Damodaran, T., and Mishra, V. K. (2016). "Rhizosphere engineering: an innovative approach for sustainable crop production in sodic soils," in *Innovative Saline Agriculture*, eds J. Dagar, P. Sharma, D. Sharma, and A. Singh (New Delhi: Springer Publications), 105–117. doi: 10.1007/978-81-322-2770-0_5

Damodaran, T., Rajan, S., Gopal, R., Yadav, A., Yadav, K., Shukla, P. K., et al. (2019b). Successful community based management of banana wilt caused by *Fusarium oxysporum* f. sp. *cubense* Tropical race-4 through ICAR- FUSICONT. *J. Appl. Hortic.* 21, 37–41. doi: 10.37855/jah.2019.v21i01.06

Damodaran, T., Rajan, S., Mishra, V. K., Jha, S. K., Gopal, R., and Ahmad, I. (2018). First report of Fusarium wilt in banana caused by *Fusarium oxysporum* f. sp. *cubense* tropical race 4 in India. *Plant Dis.* 103:1022. doi: 10.1094/PDIS-07-18-1263-PDN

Damodaran, T., Rajan, S., Mishra, V. K., Jha, S. K., Gopal, R., and Sharma, P. C. (2019a). "ICAR-FUSICONT–an innovative technology for the control of Fusarium wilt (TR4) of banana var. Grand Naine in normal and reclaimed sodic soils," in *Souvenir on A Golden Jubilee International Salinity Conference: Resilient Agriculture in Saline Environment Under Changing Climate: Challenges and Opportunities* (Karnal), 153.

De la Cruz, J., Pintor-Toro, J. A., Benítez, T., and Llobell, A. (1995). Purification and characterization of an endo-beta-1, 6-glucanase from *Trichoderma harzianum* that is related to its mycoparasitism. *J. Bacteriol.* 177, 1864–1871. doi: 10.1128/JB.177.7.1864-1871.1995

de Matos, A. P., Cordeiro, Z. J. M., de Oliveira e Silva, S., Amorim, E. P., and Ferreira, D. M. V. (2011). Reaction of diploid (AA) and tetraploid (AAAB) banana hybrids to *Fusarium* wilt under field conditions. *Acta Hortic.* 897, 387–390. doi: 10.17660/ActaHortic.2011.897.53

Deng, X., Li, Q. F., Hou, X. W., and Wu, C. Y. (2013). Soil microbial functional diversity from different infection grades of banana Fusarium wilt (*Fusarium oxysporum* f. sp. *cubense*). *Appl. Mech. Mater.* 2301, 2274–2280. doi: 10.4028/www.scientific.net/AMM.295-298.2274

Dita, M., Barquero, M., Heck, D., Mizubuti, E. S. G., and Staver, C. P. (2018). *Fusarium* wilt of Banana: current knowledge on epidemiology and research needs toward sustainable disease management. *Front. Plant Sci.* 9:1468. doi: 10.3389/fpls.2018.01468

Dong, F., Wang, S., Yu, M., Sun, Y., Xu, J., and Shi, J. (2017). Natural occurrence of deoxynivalenol and deoxynivalenol-3-glucoside in various wheat cultivars grown in Jiangsu Province, China. *World Mycotoxin J.* 10, 285–293. doi: 10.3920/WMJ2016.2158

Dos Santos, C. L., Pedersoli, W. R., Antonieto, A. C. C., Steindorff, A. S., Silva-Rocha, R., Martinez-Rossi, N. M., Rossi, A., et al. (2014). Comparative metabolism of cellulose, sophorose and glucose in *Trichoderma reesei* using high-throughput genomic and proteomic analyses. *Biotechnol. Biofuels* 7:41. doi: 10.1186/1754-6834-7-41

Druzhinina, I. S., Shelest, E., and Kubicek, C. P. (2012). Novel traits of *Trichoderma* predicted through the analysis of its secretome. *FEMS Microbiol. Lett.* 337, 1–9. doi: 10.1111/j.1574-6968.2012.02665.x

FAO (2017). *Banana Market Review*. Rome: FAO.

Garcez, M., Santos Martins, J. A., and Rodrigues, E. J. R. (2016). Evaluation of different banana genotypes for resistance to panama disease. *Biosci. J.* 32, 431–435. doi: 10.14393/BJ-v32n2a2016-29818

Garfoot, A. L., Dearing, K. L., VanSchoiak, A. D., Wysocki, V. H., and Rappleye, C. A. (2014). Eng1 and Exg8 are the major β-Glucanases secreted by the fungal pathogen *Histoplasma capsulatum*. *J. Biol. Chem.* 292, 4801–4810. doi: 10.1074/jbc.M116.762104

Getha, K., and Vikineswary, S. (2002). Antagonistic effects of *Streptomyces violaceusniger* strain G10 on *Fusarium oxysporum* f. sp. *cubense* race 4: indirect evidence for the role of antibiosis in the antagonistic process. *J. Ind. Microbiol. Biot*. 28, 303–310. doi: 10.1038/sj.jim.7000247

Gonçalves, Z. S., Haddad, F., de Oliveira Amorim, V. B, Ferreira, C., F., de Oliveira, S., and Amorim, E. P. (2019). Agronomic characterization and identification of banana genotypes resistant to *Fusarium* wilt race 1. *Eur. J. Plant Pathol.* 155, 1093–1103. doi: 10.1007/s10658-019-01837-5

Gross, G. G. (1980). The biochemistry of lignification. *Adv. Bot. Res.* 8, 25–63. doi: 10.1016/S0065-2296(08)60032-4

Gruber, S., and Seidl-Seiboth, V. (2011). Self versus non-self: fungal cell wall degradation in Trichoderma. *Microbiology* 158, 26–34. doi: 10.1099/mic.0.052613-0

Guo, L., Yang, L., Liang, C., Wang, G., Dai, Q., and Huang, J. (2015). Differential colonization patterns of Bananas (*Musa* spp.) by physiological Race 1 and Race

4 isolates of *Fusarium oxysporum* f. sp. *cubense*. *J. Phytopathol.* 163, 807–817. doi: 10.1111/jph.12378

Hakkinen, M., Arvas, M., Oja, M., Aro, N., Penttila, M., Saloheimo, M., et al. (2012). Re-annotation of the *CAZy* genes of *Trichoderma reesei* and transcription in the presence of lignocellulosic substrates. *Microb. Cell Fact.* 11:134. doi: 10.1186/1475-2859-11-134

Hammerschmidt, R., Nuckles, E. M., and Kuc, J. (1982). Association of enhanced peroxidase activity with induced systemic resistance of cucumber of *Colletotrichum lagenarium*. *Physiol. Plant Pathol.* 20, 73–82. doi: 10.1016/0048-4059(82)90025-X

Harman, G. E., and Kubicek, C. P. (1998). *Trichoderma and Gliocladium: Enzymes, Biological Control and Commercial Applications*. Vol. 2. London: CRC Press.

Hegge, A., Lonborg, R., Nielsen, D. M., and Sorensen, J. L. (2015). Factors influencing production of Fusaristatin A in *Fusarium graminearum*. *Metabolites* 5, 184–191. doi: 10.3390/metabo5020184

Hermosa, R., Belén Rubio, M., Cardoza, R. E., Nicolás, C., Monte, E., and Gutiérrez, S. (2013). The contribution of *Trichoderma* to balancing the costs of plant growth and defense. *Int. Microbiol.* 16, 69–80. doi: 10.2436/20.1501.01.181

Hermosa, R., Viterbo, A., Chet, I., and Monte, E. (2012). Plant-beneficial effects of Trichoderma and of its genes. *Microbiology* 158, 17–25. doi: 10.1099/mic.0.052274-0

Hwang, J. W., Natarajan, S. B., Kim, Y. S., Kim, E. K., Lee, J. W., Moon, S. H., et al. (2017). Biosynthesis of oligomeric anthocyanins from grape skin extracts. *Molecules* 22:497. doi: 10.3390/molecules22030497

Hyder, S., Inam-ul-Haq, M., Bibi, S., Malik, A., Ghuffar, S., and Iqbal, S. (2017). Novel potential of *Trichoderma* Spp. as biocontrol agent. *J. Entomol. Zool. Stud.* 5, 214–222.

Jin, M. C., Yang, Y. W., Su, B. G., and Ren, Q. L. (2006). Rapid quantification and characterization of soyasaponins by high-performance liquid chromatography coupled with electrospray mass spectrometry. *J. Chromatogr.* 1108, 31–37. doi: 10.1016/j.chroma.2005.12.099

Jin, M. C., Yang, Y. W., Su, B. G., and Ren, Q. L. (2007). Determination of soyasaponins Ba and Bb in human serum by high performance liquid chromatography coupled with electrospray ionization tandem mass spectrometry. *J. Chromatogr.* 846, 169–175. doi: 10.1016/j.jchromb.2006.08.043

Joseph, L. M., Koon, T. K., and Man, W. S. (1998). Antifungal effects of hydrogen peroxide and peroxidase on spore germination and mycelial growth of *Pseudocercospora* species. *Can. J. Bot.* 76, 2119–2124. doi: 10.1139/b98-166

Karimi Aghcheh, R., Németh, Z., Atanasova, L., Fekete, E., Paholcsek, M., Sándor, E., et al. (2016). The *VELVET* an orthologue *VEL1* of *Trichoderma reesei* regulates fungal development and is essential for cellulase gene expression. *PLoS ONE* 9:e112799. doi: 10.1371/journal.pone.0112799

Kavino, M., Harish, S., Kumar, N., Saravanakumar, D., Damodaran, T., Soorianathasundaram, K., and Samiyappan, R. (2007). Rhizosphere and endophytic bacteria for induction of systemic resistance of banana plantlets against bunchy top virus. *Soil Biol. Biochem.* 39, 1087–1098. doi: 10.1016/j.soilbio.2006.11.020

Kavino, M., Kumar, N., Damodaran, T., Harish, S., and Saravanakumar, D. (2009). Biochemical markers as a useful tool for the early identification of *Fusarium oxysporum*f. sp. *cubense*, race 1 resistance banana clones. *Arch. Phytopathol. Pflanzenschutz.* 42, 1069–1078. doi: 10.1080/03235400701622089

Keszler, A., Forgacs, E., Kotai, L., Vizcaíno, J. A., Monte, E., and García-Acha, I. (2000). Separation and identification of volatile components in the fermentation broth of *Trichoderma atroviride* by solid-phase extraction and gas chromatography-mass spectroscopy. *J. Chromatogr. Sci.* 38, 421–424. doi: 10.1093/chromsci/38.10.421

Khan, N., Hidalgo, P. M., Ice, T. A., Maymon, M., Humm, E. A., Nejat, N., et al. (2018). Antifungal activity of *Bacillus* species against *Fusarium* and analysis of the potential mechanisms used in biocontrol. *Front. Microbiol.* 9:2363. doi: 10.3389/fmicb.2018.02363

Kumar, V., Lee, J. D., Clark, R. J., and Woodruff, T. M. (2018). Development and validation of a LC-MS/MS assay for pharmacokinetic studies of complement C5a receptor antagonists PMX53 and PMX205 in mice. *Sci. Rep.* 8:8101. doi: 10.1038/s41598-018-26387-4

Li, C., Zuo, C., Deng, G., Kuang, R., Yang, Q., Hu, C., et al. (2013). Contamination of bananas with beauvericin and fusaric acid produced by *Fusarium oxysporum* f. sp. *cubense*. *PLoS ONE* 8:e70226. doi: 10.1371/journal.pone.0070226

López-Díaz, C., Rahjoo, V., Sulyok, M., Ghionna, V., Martín-Vicente, A., Capilla, J., et al. (2017). Fusaric acid contributes to virulence of *Fusarium oxysporum* on plant and mammalian hosts. *Mol. Plant Pathol.* 19, 440–453. doi: 10.1111/mpp.12536

Magdama, F., Monserrate-Maggi, L., Serrano, L., Sosa, D., Geiser, D. M., Jiménez-Gasco, M., et al. (2019). Comparative analysis uncovers the limitations of current molecular detection methods for *Fusarium oxysporum* f. sp. *cubense* race 4 strains. *PLoS ONE* 14:e0222727. doi: 10.1371/journal.pone.0222727

Malmierca, M. G., Barua, J., Mccormick, S. P., Izquierdo-Bueno, I., Cardoza, R. E., Alexander, N. J., et al. (2014). Novel aspinolide production by *Trichoderma arundinaceum* with a potential role in *Botrytis cinerea* antagonistic activity and plant defence priming. *Environ. Microbiol.* 17, 1103–1118. doi: 10.1111/1462-2920.12514

Martinez, D., Berka, R. M., Henrissat, B., Saloheimo, M., Arvas, M., Baker, S. E., et al. (2008). Genome sequencing and analysis of the biomass-degrading fungus *Trichoderma reesei* (syn. *Hypocrea jecorina*). *Nat. Biotech.* 26, 553–560. doi: 10.1038/nbt1403

Martínez-Hidalgo, P., García, J. M., and Pozo, M. J. (2015). Induced systemic resistance against *Botrytis cinerea* by *Micromonospora* strains isolated from root nodules. *Front. Microbiol.* 6:922. doi: 10.3389/fmicb.2015.00922

Martínez-Medina, A., Fernandez, I., Sánchez-Guzmán, M. J., Jung, S. C., Pascual, J. A., and Pozo, M. J. (2013). Deciphering the hormonal signaling network behind the systemic resistance induced by *Trichoderma harzianum* in tomato. *Front. Plant Sci.* 4:206. doi: 10.3389/fpls.2013.00206

Matarese, F., Sarrocco, S., Gruber, S., Seidl-Seiboth, V., and Vannacci, G. (2012). Biocontrol of Fusarium head blight: interactions between Trichoderma and mycotoxigenic Fusarium. *Microbiology* 158, 98–106. doi: 10.1099/mic.0.052639-0

Mayer, A. M., Harel, E., and Shaul, R. B. (1965). Assay of catechol oxidase, a critical comparison of methods. *Phytochemistry* 5, 783–789. doi: 10.1016/S0031-9422(00)83660-2

Migheli, Q., Friard, O., Del Tedesco, D., Musso, M. R., and Gullino, M. L. (1996). Stability of transformed antagonistic *Fusarium oxysporum* strains *in vitro* and in soil microcosms. *Mol. Ecol.* 5, 641–649. doi: 10.1111/j.1365-294X.1996.tb00359.x

Monfil, V. O., and Casas-Flores, S. (2014). "Molecular mechanisms of biocontrol in *Trichoderma* spp. and their applications in agriculture," in *Biotechnology and Biology of Trichoderma*, eds V. K. Gupta, M. Schmoll, A. Herrera-Estrella, R. S. Upadhyay, I. Druzhinina, and M. G. Tuohy (Dordrecht: Elsevier), 429–453. doi: 10.1016/B978-0-444-59576-8.00032-1

M'Piga, P., Bélanger, R. R., Paulitz, T. C., and Benhamou, N. (1997). Increased resistance to *Fusarium oxysporum* f. sp. *radicis-lycopersiciin* tomato plants treated with the endophytic bacterium *Pseudomonas fluorescens* strain 63-28. *Physiol. Mol. Plant Pathol.* 50, 301–320. doi: 10.1006/pmpp.1997.0088

Mukherjee, P. K., Horwitz, B. A., Herrera-Estrella, A., Schmoll, M., and Kenerley, C. M. (2013). *Trichoderma* research in the genome era. *Annu. Rev. Phytopathol.* 51, 105–129. doi: 10.1146/annurev-phyto-082712-102353

Mukherjee, P. K., and Kenerley, C. M. (2010). Regulation of morphogenesis and biocontrol properties in *Trichoderma virens* by a VELVET protein, Vel1. *Appl. Environ. Microbiol.* 76, 2345–2352. doi: 10.1128/AEM.02391-09

Nagarajkumar, M., Bhaaskaran, R., and Velazhahan, R. (2004). Involvement of secondary metabolites and extracellularlytic enzymes produced by *Pseudomonas fluorescens* in inhibition of *Rhizoctonia solani*, the rice sheath of blight pathogen. *Microbiol. Res.* 159, 73–81. doi: 10.1016/j.micres.2004.01.005

Niehaus, E. M., Díaz-Sánchez, V., von Bargen, K. W., Kleigrewe, K., Humpf, H. U., Limón, M. C., et al. (2014). "Fusarins and fusaric acid in fusaria," in *Biosynthesis and Molecular Genetics of Fungal Secondary Metabolites*, Fungal Biology, eds Martín J. F., García-Estrada C., and Zeilinger S (New York, NY: Springer), 239–262. doi: 10.1007/978-1-4939-1191-2_11

Nogueira, K. M. V., Costa, M. d. N., de Paula, R. G., Mendonça-Natividade, F. C., Ricci-Azevedo, R., and Silva, R. N. (2015). Evidence of cAMP involvement in cellobiohydrolase expression and secretion by *Trichoderma reesei* in presence of the inducer sophorose. *BMC Microbiol.* 15:195. doi: 10.1186/s12866-015-0536-z,

Ortiz, R. (2013). Conventional banana and plantain breeding. *Acta Hortic.* 986, 177–194. doi: 10.17660/ActaHortic.2013.986.19

O'Sullivan, M., Stephens, P. M., and O'Gara, F. (1992). Extracellular protease production by fluorescent *Pseudomonas* spp. and the

colonization of sugar beet roots and soil. *Soil Biol. Biochem.* 23, 623–627. doi: 10.1016/0038-0717(91)90074-T

Pan, S. Q., Ye, X. S., and Kuc, J. (1991). Association of β-1,3-glucanase activity and isoform pattern with systemic resistance to blue mold in tobacco induced by stem injection with *Peronospora tabacina* or leaf inoculation with tobacco mosaic virus. *Physiol. Mol. Plant Pathol.* 39, 25–39. doi: 10.1016/0885-5765(91)90029-H

Papavizas, G. (1985). *Trichoderma and Gliocladium*: biology, ecology, and potential for biocontrol. *Annu. Rev. Phytopathol.* 23, 23–54. doi: 10.1146/annurev.py.23.090185.000323

Pathak, K. V., and Keharia, H. (2014). Application of extracellular lipopeptide biosurfactant produced by endophytic *Bacillus subtilis* K1 isolated from aerial roots of banyan (*Ficus benghalensis*) in microbially enhanced oil recovery (MEOR). *3 Biotech.* 4, 41–48. doi: 10.1007/s13205-013-0119-3

Pérez-Vicente, L., Dita, M. A., and Martínez-De La, P. E. (2014). *Technical Manual: Prevention and Diagnostic of Fusarium Wilt (Panama disease) of Banana Caused by Fusarium oxysporum f.sp.Cubense Tropical Race 4 (TR4)*. Roma: FAO, 75.

Perincherry, L., Lalak-Kańczugowska, J., and Stepień, L. (2019). *Fusarium*-produced mycotoxins in plant-pathogen interactions. *Toxins (Basel)* 11:664. doi: 10.3390/toxins11110664

Ploetz, R. C. (1992). "Fusarium wilt of banana (Panama disease)," in *Plant Diseases of International Importance*, Vol. III, eds A. N. Mukhopadhyay, H. S. Chaube, J. Kumar, and U. S. Singh (Upper Saddle River, NJ: Prentice Hall), 270–282.

Ploetz, R. C. (2004). "Biological control of Fusarium wilt: a review and an evaluation," in *Abstract Booklet, International Congress on Musa: Harnessing Research to Improve Livelihoods* (Penang: INIBAP Bioversity International), 141.

Ploetz, R. C. (2006a). Fusarium wilt of banana is caused by several pathogens referred to as *Fusarium oxysporum* f. sp. *cubense*. *Phytopathology* 96, 653–656. doi: 10.1094/PHYTO-96-0653

Ploetz, R. C. (2006b). Panama disease: an old nemesis rears its ugly head. Part 2. The Cavendish era and beyond. *Plant Health Prog.* 7:36. doi: 10.1094/APSnetFeature-2005-1005

Ploetz, R. C. (2007). Diseases of tropical perennial crops: challenging problems in diverse environments. *Plant Dis.* 91, 644–663. doi: 10.1094/PDIS-91-6-0644

Ploetz, R. C., and Churchill, A. C. L. (2011). Fusarium wilt: the banana disease that refuses to go away. *Acta Hortic.* 897, 519–526. doi: 10.17660/ActaHortic.2011.897.73

Ploetz, R. C., Haynes, J. L., and Vazquez, A. (1999). Responses of new banana accessions in South Florida to Panama disease. *Crop Protec.* 18, 445–449. doi: 10.1016/S0261-2194(99)00043-5

Ploetz, R. C., Herbert, J., Sebasigari, K., Hernandez, J. H., Pegg, K. G., Ventura, J. A., et al. (1990). "Importance of Fusarium wilt in different banana-growing regions," in *Fusarium Wilt of Banana*, ed R. C. Ploetz (St. Paul, MN: APS Press), 9–26.

Ploetz, R. C., and Pegg, K. G. (2000). "Fusarium wilt." in *Diseases of banana, Abaca and Enset*, ed R. Jones (Wallingford: CABI Publishing), 1–34.

Pollier, J., Morreel, K., and Geelen, D. (2011). Metabolite profiling of triterpene saponins in medicago truncatula hairy roots by liquid chromatography fourier transform ion cyclotron resonance mass spectrometry. *J. Nat. Products* 74, 1462–1476. doi: 10.1021/np200218r

Qi, D., Zou, L., Zhou, D., Feng, R., Gao, Z., and Zhang, X. (2017). Isolation, identification of strain GA1-2 and its antifungal activity against Fusarium oxysporum f. sp. cubense. *J. Plant Prot*. 44, 809–816.

Qian, Y., Zhong, L., Sun, Y., Sun, N., Zhang, L., Liu, W., et al. (2019). Enhancement of cellulase production in *Trichoderma reesei* via disruption of multiple protease genes identified by comparative secretomics. *Front. Microbiol.* 10:2784. doi: 10.3389/fmicb.2019.02784

Qiu, J., Xu, J., and Shi, J. (2019). *Fusarium* toxins in Chinese wheat since the 1980s. *Toxins (Basel)* 11:248. doi: 10.3390/toxins11050248

Radjacommare, R., Kandan, A., Nandakumar, R., and Samiyapan, R. (2004). Association of the hydrolytic enzyme chitinase against *Rhizoctonia solani* in rhizobacteria treated rice plants. *J. Phytopathol.* 152, 365–370. doi: 10.1111/j.1439-0434.2004.00857.x

Rai, R. B., Damodaran, T., Kannan, R., Rathore, A. P., Sharma, D. K., Mishra, V. K., et al. (2012). Low cost multiplication technology of salt tolerant bio-growth enhancers (*Bacillus*, *Pseudomonads* and *Trichoderma*) for increasing productivity of agri-horti crops in normal and sodic soils. *J. Plant Interact*. 9, 577–584. doi: 10.1080/17429145.2013.873958

Rangaswamy, R. (1995). *A Textbook Book of Agricultural Statistics*. New Delhi: New Age International (P) Ltd.

Rebouças, T. A., Haddad, F., Ferreira, C. F., de Oliveira, S. A. S., da Silva Ledo, C. A., and Amorim, E. P. (2018). Identification of banana genotypes resistant to *Fusarium* wilt race 1 under field and greenhouse conditions. *Sci Hortic.* 239, 308–313. doi: 10.1016/j.scienta.2018.04.037

Reis, A., Domingues, M. R. M., Amado, F. M. L., Ferrer-Correia, A. J. V., and Domingues, P. (2005). Separation of peroxidation products of diacyl-phosphatidylcholines by reversed-phase liquid chromatography–mass spectrometry. *Biomed. Chromatogr.* 19, 129–137. doi: 10.1002/bmc.429

Reithner, B., Brunner, K., Schuhmacher, R., Peissl, I., Seidl, V., Krska, R., et al. (2005). The G protein α subunit *Tga1* of *Trichoderma atroviride* is involved in chitinase formation and differential production of antifungal metabolites. *Fungal Genet. Biol.* 42, 749–760. doi: 10.1016/j.fgb.2005.04.009

Reithner, B., Schuhmacher, R., Stoppacher, N., Pucher, M., Brunner, K., and Zeilinger, S. (2007). Signaling via the Trichoderma atroviride mitogen-activated protein kinase *Tmk1 d*ifferentially affects mycoparasitism and plant protection. *Fungal Genet Biol*. 44, 1123–1133. doi: 10.1016/j.fgb.2007.04.001

Ribeiro, L. R., Silva, S. d. O., Oliveira, S. A. S. d., Amorim, E. P., Serejo, J. A. S. S., and Haddad, F. (2018). Sources of resistance to *Fusarium oxysporum* f. sp. *cubense* in banana germplasm. *Rev. Brasil. Fruticult.* 40:e-202. doi: 10.1590/0100-29452018202

Rocha-Ramirez, V., Omero, C., Chet, I., Horwitz, B. A., and Herrera-Estrella, A. (2002). *Trichoderma atroviride* G-protein alpha-subunit gene *tga1* is involved in mycoparasitic coiling and conidiation. *Eukaryot. Cell* 1, 594–605. doi: 10.1128/EC.1.4.594-605.2002

Ross, W. W., and Sederoff, R. R. (1992). Phenylalanine ammonia-lyase from Loblolly Pine. *Plant Physiol.* 98, 380–386. doi: 10.1104/pp.98.1.380

Sadasivam, S., and Manickam, A. (1996). *Biochemical Methods. 2nd Edn.* New Delhi: New Age International (P) Ltd.

Sagratini, G., Zuo, Y., Caprioli, G., Cristalli, G., Giardina, D., Maggi, F., et al. (2009). Quantification of soyasaponins I and βg in Italian lentil seeds by solid-phase extraction (SPE) and high-performance liquid chromatography-mass spectrometry (HPLC-MS). *J. Agric. Food Chem.* 57, 11226–11233. doi: 10.1021/jf901707z

Schmoll, M. (2008). The information highways of a biotechnological workhorse-signal transduction in *Hypocrea jecorina*. *BMC Genomics.* 9:430. doi: 10.1186/1471-2164-9-430

Schuster, A., and Schmoll, M. (2010). Biology and biotechnology of Trichoderma. *Appl. Microbiol. Biot.* 87, 787–799. doi: 10.1007/s00253-010-2632-1

Sellamani, M., Kalagatur, N. K., Siddaiah, C., Mudili, V., Krishna, K., Natarajan, G., et al. (2016). Antifungal and zearalenone inhibitory activity of *Pediococcus pentosaceus* isolated from dairy products on *Fusarium graminearum*. *Front. Microbiol.* 7:890. doi: 10.3389/fmicb.2016.00890

Sood, M., Kapoor, D., Kumar, V., Sheteiwy, M. S., Ramakrishnan, M., Landi, M., et al. (2020). *Trichoderma*: the "Secrets" of a multitalented biocontrol agent. *Plants* 9:762. doi: 10.3390/plants9060762

Sorensen, J. L., and Giese, H. (2013). Influence of carbohydrates on secondary metabolism in *Fusarium avenaceum*. *Toxins* 5, 1655–1663. doi: 10.3390/toxins5091655

Speckbacher, V., and Zeilinger, S. (2018). "Secondary metabolites of mycoparasitic fungi," in *Secondary Metabolites–Sources and Applications*, ed R. Vijayakumar, and S. S. S. Raja (London: Intechopen). doi: 10.5772/intechopen.75133

Stover, R. H. (1962). *Fusarium Wilt (Panama disease) of Bananas and Other Musa Species*. London: Common wealth Mycological Institute.

Swain, H., and Mukherjee, A. K. (2020). "Host–pathogen–trichoderma interaction," in *Trichoderma, Rhizosphere Biology*, eds A. Sharma and P. Sharma (Singapore: Springer). doi: 10.1007/978-981-15-3321-1_8

Tala, V. R. S., Silva, V. C., Rodrigues, C. M., Nkengfack, A. E., Santos, L. C., and Vilegas, W. (2013). Characterization of proanthocyanidins from *Parkia biglobosa* (Jacq.) G. Don. (Fabaceae) by flow injection analysis-electrospray ionization ion trap tandem mass spectrometry and liquid chromatography/electrospray ionization mass spectrometry. *Molecules* 18, 2803–2820. doi: 10.3390/molecules18032803

Tan, D., Fu, L., Han, B., Sun, X., Zheng, P., and Zhang, J. (2015). Identification of an endophytic antifungal bacterial strain isolated from the rubber tree and its application in the biological control of banana Fusarium wilt. *Plos ONE* 10:e0131974. doi: 10.1371/journal.pone.0131974

Tava, A., Mella, M., Avato, P., Biazzi, E., Pecetti, L., Bialy, Z., et al. (2009). New triterpenic saponins from the aerial parts of *Medicago arabica* (L.) huds. *J. Agric. Food Chem.* 57, 2826–2835. doi: 10.1021/jf8036984

Tava, A., Pecetti, L., Romani, M., Mella, M., and Avato, P. (2011). Triterpenoid glycosides from the leaves of two cultivars of *Medicago polymorpha* L. *J. Agric. Food Chem.* 59, 6142–6149. doi: 10.1021/jf2005854

Thangavelu, R., and Gopi, M. (2015). Field suppression of Fusarium wilt disease in banana by the combined application of native endophytic and rhizospheric bacterial isolates possessing multiple functions. *Phytopathol. Mediter.* 54, 241–252. doi: 10.14601/Phytopathol_Mediterr-15160

Thangavelu, R., Palaniswami, A., Ramakrishnan, G., Doraiswamy, S., Muthukrishnan, S., and Velazhahan, R. (2001). Involvement of fusaric acid detoxification by *Pseudomonas fluorescens* strain Pf10 in the biological control of Fusarium wilt of banana caused by *Fusarium oxysporum* f. sp *cubense. J. Plant Dis. Prot.* 108, 433–445.

Tian, Y., Tan, Y., Liu, N., Yan, Z., Liao, Y., Chen, J., et al. (2016). Detoxification of deoxynivalenol via glycosylation represents novel insights on antagonistic activities of Trichoderma when confronted with *Fusarium graminearum*. *Toxins* 8:335. doi: 10.3390/toxins8110335

Tian, Y., Tan, Y., Yan, Z., Liao, Y., Chen, J., Boevre, M. D., Saeger, S. D. and Wu, A. (2018). Antagonistic and detoxification potentials of Trichoderma isolates for control of Zearalenone (ZEN) producing Fusarium graminearum. *Front. Microbiol.* 8:2710. doi: 10.3389/fmicb.2017.02710

Ting, A. S. Y., Meon, S., Kadir, J., Radu, S., and Singh, G. (2009). Induced host resistance by non-pathogenic Fusarium endophyte as a potential defense mechanism in Fusarium wilt management of banana. *Pest Technol.* 3, 67–72.

Trikas, E. D., Papi, R. M., Kyriakidis, D. A., and Zachariadi, G. A. (2016). A sensitive LC-MS method for anthocyanins and comparison of by products and equivalent wine content. *Separations* 3:18. doi: 10.3390/separations3020018

Vanittanakom, N., Loeffler, W., Koch, U., and Jung, G. (1986). Fengycin-a novel antifungal lipopeptide antibiotic produced by *Bacillus subtilis* F-29-3. *J. Antibiot.* 39, 888–901. doi: 10.7164/antibiotics.39.888

Vinueza, N. R., Gallardo, V. A., Klimek, J. F., Carpita, N. C., and Kenttamaa, H. I. (2013). Analysis of xyloglucans by ambient chloride attachment ionization tandem mass spectrometry. *Carbohydr. Polym.* 98, 1203–13. doi: 10.1016/j.carbpol.2013.06.070

Winkelmann, G., Allgaier, H., Lupp, R., and Jung, G. (1983). Iturin A_L-a NEW long chain iturin a possessing an unusual high content of C16-β-amino acids. *J. Antibiot.* 36, 1451–1457. doi: 10.7164/antibiotics.36.1451

Yadav, K., Damodaran, T., Kumari, N., Dutt, K., Gopal, R., and Muthukumar, M. (2020). Characterization of Trichoderma isolates and assessment of antagonistic potential against *Fusarium oxysporum* f. sp. *cumini. J. Appl. Hortic.* 22, 38–44. doi: 10.37855/jah.2020.v22i01.08

Zeilinger, S., Gruber, S., Bansal, R., and Mukherjee, P. K. (2016). Secondary metabolism in *Trichoderma*–chemistry meets genomics. *Fungal Biol. Rev.* 30, 74–90. doi: 10.1016/j.fbr.2016.05.001

Zieslin, N., and Ben-Zaken, R. (1993). Peroxidase activity and presence of phenolic substances in peduncles of rose flowers. *Plant Physiol. Biochem.* 31, 333–339.

Conflict of Interest: The authors declare that the research was conducted in the absence of any commercial or financial relationships that could be construed as a potential conflict of interest.

frontiers in Microbiology

ORIGINAL RESEARCH
published: 20 January 2021
doi: 10.3389/fmicb.2020.594531

Pursuing Advances in DNA Sequencing Technology to Solve a Complex Genomic Jigsaw Puzzle: The Agglutinin-Like Sequence (*ALS*) Genes of *Candida tropicalis*

*Soon-Hwan Oh[1], Allyson Isenhower[2], Rubi Rodriguez-Bobadilla[2], Brooke Smith[2], Jillian Jones[2], Vit Hubka[3,4], Christopher Fields[5], Alvaro Hernandez[5] and Lois L. Hoyer[1]**

[1] Department of Pathobiology, College of Veterinary Medicine, University of Illinois at Urbana-Champaign, Urbana, IL, United States, [2] Department of Biology, Millikin University, Decatur, IL, United States, [3] Department of Botany, Faculty of Science, Charles University, Prague, Czechia, [4] Laboratory of Fungal Genetics and Metabolism, Institute of Microbiology, Czech Academy of Sciences, Prague, Czechia, [5] Roy J. Carver Biotechnology Center, University of Illinois at Urbana-Champaign, Urbana, IL, United States

OPEN ACCESS

Edited by:
Lívia Kmetzsch, Federal University of Rio Grande do Sul, Brazil

Reviewed by:
Eugenio Mancera, Unidad Irapuato (CINVESTAV), Mexico
Bruno César Feltes, Federal University of Rio Grande do Sul, Brazil

***Correspondence:**
Lois L. Hoyer
lhoyer@illinois.edu

Specialty section:
This article was submitted to Fungi and Their Interactions, a section of the journal Frontiers in Microbiology

Received: *13 August 2020*
Accepted: *17 November 2020*
Published: *20 January 2021*

Citation:
Oh S-H, Isenhower A, Rodriguez-Bobadilla R, Smith B, Jones J, Hubka V, Fields C, Hernandez A and Hoyer LL (2021) Pursuing Advances in DNA Sequencing Technology to Solve a Complex Genomic Jigsaw Puzzle: The Agglutinin-Like Sequence (ALS) Genes of Candida tropicalis. Front. Microbiol. 11:594531. doi: 10.3389/fmicb.2020.594531

The agglutinin-like sequence (*ALS*) gene family encodes cell-surface adhesins that interact with host and abiotic surfaces, promoting colonization by opportunistic fungal pathogens such as *Candida tropicalis*. Studies of Als protein contribution to *C. tropicalis* adhesion would benefit from an accurate catalog of *ALS* gene sequences as well as insight into relative gene expression levels. Even in the genomics era, this information has been elusive: genome assemblies are often broken within *ALS* genes because of their extensive regions of highly conserved, repeated DNA sequences and because there are many similar *ALS* genes at different chromosomal locations. Here, we describe the benefit of long-read DNA sequencing technology to facilitate characterization of *C. tropicalis ALS* loci. Thirteen *ALS* loci in *C. tropicalis* strain MYA-3404 were deduced from a genome assembly constructed from Illumina MiSeq and Oxford Nanopore MinION data. Although the MinION data were valuable, PCR amplification and Sanger sequencing of *ALS* loci were still required to complete and verify the gene sequences. Each predicted Als protein featured an N-terminal binding domain, a central domain of tandemly repeated sequences, and a C-terminal domain rich in Ser and Thr. The presence of a secretory signal peptide and consensus sequence for addition of a glycosylphosphatidylinositol (GPI) anchor was consistent with predicted protein localization to the cell surface. TaqMan assays were designed to recognize each *ALS* gene, as well as both alleles at the divergent *CtrALS3882* locus. *C. tropicalis* cells grown in five different *in vitro* conditions showed differential expression of various *ALS* genes. To place the *C. tropicalis* data into a larger context, TaqMan assays were also designed and validated for analysis of *ALS* gene expression in *Candida albicans* and *Candida dubliniensis*. These comparisons identified the subset of highly expressed *C. tropicalis*

ALS genes that were predicted to encode proteins with the most abundant cell-surface presence, prioritizing them for subsequent functional analysis. Data presented here provide a solid foundation for future experimentation to deduce *ALS* family contributions to *C. tropicalis* adhesion and pathogenesis.

Keywords: genome, *Candida tropicalis*, *ALS* genes, gene expression, fungal adhesion

INTRODUCTION

Adhesion and subsequent colonization provide the opportunity for microbial pathogens to cause disease. Identification of adhesin-encoding genes is facilitated by the availability of genome sequences. An accurate catalog of potential adhesins focuses efforts to characterize protein function and develop therapeutic approaches that could be effective against multiple microbial species. Anti-adhesion therapies have been hailed as superior to traditional antimicrobials because their mechanism of action does not promote antimicrobial resistance (Krachler and Orth, 2013). This report describes characterization of genes encoding the agglutinin-like sequence (Als) family of adhesins in the fungal pathogen *Candida tropicalis*. The work highlights how emerging advances in DNA sequencing technology were used to fill key knowledge gaps that have persisted for many years.

Agglutinin-like sequence (*ALS*) genes encode cell-surface adhesins that recognize a broad variety of peptide ligands (Lin et al., 2014). The gene family was characterized initially in *Candida albicans* with investigations into protein structure and activity also focused on this species (reviewed in Hoyer and Cota, 2016). Starting in the pre-genome era and extending over a period of approximately 20 years, projects moved from identification of the first *ALS* gene, to the recognition that the gene was part of a larger family, to characterization of the family, and the relative abundance of specific Als proteins on the cell surface under a variety of growth conditions. More recently, the structure of the N-terminal Als protein adhesive domain was solved (NT-Als; reviewed in Hoyer and Cota, 2016). Experimental progress to define the *C. albicans ALS* family was slow because detection of additional *ALS* genes relied on techniques such as the Southern blotting of genomic DNA (Hoyer et al., 1995, 1998a,b). Locating *ALS* genes in draft genome sequences would accelerate progress substantially.

As emerging genome sequencing technologies were applied to pathogenic fungal species, the *C. albicans ALS* sequences were used to recognize potential *ALS* genes in draft genomes (Butler et al., 2009). *ALS* gene hallmarks such as the 5′ end sequences that encode the adhesive domain, central regions of a conserved 108-bp tandemly repeated sequence, and the 3′ end sequences that include a glycosylphosphatidylinositol (GPI) anchor addition site were clues for identifying possible *ALS* loci. While these techniques could quickly identify potential *ALS* genes, the large *ALS* gene size and considerable sequence identity across multiple physical loci in the same species complicated accurate assembly. Computational assemblies broke within the conserved tandemly repeated sequences in the middle of the coding region, or mistakenly placed the 5′ end of one gene onto the 3′ end of another. The research community was left without accurate knowledge of the *ALS* gene number or sequence in common fungal pathogens.

Like *C. albicans*, *C. tropicalis* causes superficial mucosal infections, as well as disseminated and deep-seated infections; the rising incidence of azole-resistant *C. tropicalis* is causing clinical concern (reviewed in de Oliveira et al., 2020). Previous reports about *C. tropicalis ALS* genes suggested that the family is larger in this species than in other common fungal pathogens (Butler et al., 2009; Jackson et al., 2009), representing perhaps the most challenging *ALS* family puzzle to solve. Short-read sequence technologies were not helpful in this regard because the read lengths often did not include unique information that could place *ALS* sequences in the correct physical location.

One key technological development that appeared at the start of this project was the ability to derive long-read DNA sequences. Here, we describe combining short-read (Illumina MiSeq) and long-read (Oxford Nanopore MinION) datasets to develop a *C. tropicalis* genome assembly that served as the foundation for characterization of the 13 *ALS* loci in strain MYA-3404. Accurate gene sequences facilitated design of a specific TaqMan assay for each *ALS* gene. The assays were used to assess relative gene expression under a variety of growth conditions to reveal which *ALS* genes were likely to produce the most abundant Als cell-surface proteins, thereby prioritizing them for further functional analysis toward the development of anti-adhesion therapies.

MATERIALS AND METHODS

Fungal Strains

Table 1 shows the fungal strains used in this study. *C. tropicalis* strains were authenticated using several methods (data not shown). First, each isolate was streaked on CHROMagar *Candida* medium (Becton Dickinson) to ensure that it produced the expected blue colony color. Molecular verification of strain identification used PCR primers ITS4 (5′ TCCTCCGCTTATTGATATGC 3′) and ITS5 (5′ GGAAGTAAAAGTCGTAACAAGG 3′; White et al., 1990). PCR products were Sanger sequenced at the Roy J. Carver Biotechnology Center, University of Illinois at Urbana-Champaign. DNA sequences were confirmed as *C. tropicalis* by comparison to the non-redundant nucleotide database at the National Center for Biotechnology Information using the blastn algorithm[1]. Karyotypes for the *C. tropicalis* strains were also investigated using contour-clamped homogeneous electrical field (CHEF) gels and found to

[1]https://blast.ncbi.nlm.nih.gov/Blast.cgi

TABLE 1 | Fungal strains and sources.

Species	Strain	Source
Candida tropicalis	951 (CAPG-3)	Pat Kammeyer, Loyola University Medical Center
	952 (T60700)	Pat Kammeyer, Loyola University Medical Center
	1019 (ATCC 13803)	American Type Culture Collection
	1020 (ATCC 201380)	American Type Culture Collection
	1021 (ATCC 201381)	American Type Culture Collection
	3242 (NRRL Y-5716)	Agricultural Research Service Culture Collection
	3528 (MYA-3404)	David Soll, University of Iowa
Candida albicans	SC5314	American Type Culture Collection
Candida dubliniensis	CD36	David Coleman, Trinity College Dublin

be similar across the isolates; methods for the karyotype analysis and examples of the results were published previously (Hoyer et al., 2001).

C. tropicalis Genome Sequences

A previously published *C. tropicalis* genome sequence was used as the basis for initial identification of putative *ALS* genes (strain MYA-3404; ASM633v3; GCA_000006335.3; Butler et al., 2009). A new genome sequence was generated for *C. tropicalis* strain MYA-3404. Methods for this effort were similar to the methods for generating a genomic sequence for *Candida metapsilosis* (Oh et al., 2019) and were reproduced here for the reader's convenience.

Cells were grown in YPD (per liter: 10 g yeast extract, 20 g Bacto peptone, 20 g dextrose) to saturation (approximately 16 h at 37°C and 200 r/min shaking). Genomic DNA was isolated according to Sherman et al. (1986). The method involved zymolyase spheroplasting of cells, sodium dodecyl sulfate lysis, phenol extraction, DNA precipitation with isoproposal, and Proteinase K treatment of the final preparation. Gentle mixing and pipetting with wide-bore tips were used to minimize DNA shearing. High-molecular-weight DNA was visualized by agarose gel electrophoresis and ethidium-bromide staining prior to further processing.

Strain MYA-3404 libraries were constructed and sequenced at the Roy J. Carver Biotechnology Center, University of Illinois at Urbana-Champaign. Data were derived using Illumina (short-read) and Oxford Nanopore (long-read) methods. MiSeq shotgun libraries were prepared with the Hyper Library construction kit (Kapa Biosystems). The library was quantitated by qPCR and sequenced on one MiSeq flowcell for 151 cycles from each end of the fragment using a MiSeq 300-cycle sequencing kit (version 2). FASTQ files were generated and demultiplexed with the bclfastq Conversion Software (Illumina, version 2.17.1.14). MiSeq reads were quality trimmed using Trimmomatic (Bolger et al., 2014) with the parameters "LEADING:30 TRAILING:30" prior to assembly.

For Oxford Nanopore long-read sequencing, 1 μg of genomic DNA was sheared in a gTube (Covaris, Woburn, MA, United States) for 1 min at 6,000 r/min in a MiniSpin plus microfuge (Eppendorf, Hauppauge, NY, United States). The sheared DNA was converted to a shotgun library with the LSK-108 kit from Oxford Nanopore, following the manufacturer's instructions. The library was sequenced on a SpotON R9.4 flowcell for 48 h using a MinION MK 1B sequencer.

Basecalling and demultiplexing were performed in real time with the Metrichor Agent V2.45.3 using the 1D BaseCalling plus Barcoding for FLO-MIN_106_450bp workflow. Removed from both ends of each Oxford Nanopore read were 60 nt, followed by additional trimming using a Github checkout (commit 92c0b65f) of Porechop (Wick et al., 2017) to remove reads with potential internal barcodes which were likely chimeric. Only reads longer than 800 nt were used in the final assembly. Canu v1.4 (Koren et al., 2017) was used for assembly with the following parameters: "canu -p asm -d C_trop_default genomeSize = 14m useGrid = false -nanopore-raw c_tropicalis.qualtrim.clean.fastq.gz."

Oxford Nanopore reads were then aligned against the assembly using bwa mem (Li, 2018) with parameters "bwa mem -x ont2d C_tropicalisCanuAsm.fasta reads.fa", and the alignment was then used to polish the assembly using nanopolish v 0.6.0 (Senol Cali et al., 2018). Quality-trimmed MiSeq data were used to polish the assembly using Pilon v1.21 for error correction (Walker et al., 2014). **Supplementary File S1** includes details regarding the computational analyses and characteristics of the resulting *C. tropicalis* MYA-3404 genome sequence. The sequence was deposited in the NCBI database (ASM694213v1; GCA_006942135.1).

Ambiguities in the genome sequence data were resolved by PCR amplification of the region and Sanger sequencing of the product. Primer design was aided by the PrimerQuest Tool (Integrated DNA Technologies). **Supplementary Table S1** lists PCR primer sequences that were used for amplification and/or Sanger sequencing for the various *ALS* loci.

During finalization of this manuscript, a new *C. tropicalis* MYA-3404 genome sequence was noted in the NCBI database (ASM1317755v1; GCA_013177555.1; Guin et al., 2020). The sequence was generated with a combination Illumina HiSeq and PacBio Sequel technology and had the same number of contigs as *C. tropicalis* has chromosomes. This sequence was used for comparative analysis of *ALS* sequences derived from ASM694213v1.

Identification of *ALS* Genes and Predicted Als Protein Features

Methods for identifying *C. tropicalis ALS* genes and deducing predicted protein features were identical to those reported for analysis of *C. metapsilosis* (Oh et al., 2019). Details were reproduced here for the reader's convenience. BLAST[2] was used to identify potential *ALS* genes and Als proteins in the genome sequences. Query sequences included all *C. albicans ALS* genes as reported by Oh et al. (2019). As new *ALS*/Als sequences were identified, they were also used as BLAST queries until

[2]https://blast.ncbi.nlm.nih.gov/Blast.cgi

search reports failed to reveal new sequences. SignalP Server[3] (Nielsen, 2017) was used to locate putative secretory signal peptides. The big-PI Predictor[4] (Eisenhaber et al., 1999) identified potential GPI anchor addition sites. European Bioinformatics Institute (EMBL-EBI) tools were used for translating nucleotide sequences, sequence alignment, and other general processes[5] (Cook et al., 2017).

Phylogenetics Analysis

Phylogeny of the *ALS* family was estimated using sequences from the 5′ domain that is present in each gene (see **Supplementary File S2**). Because of the large sequence divergences within the 5′ domain, nucleotide sequences were translated using the alternative yeast nuclear code and the resulting amino acid sequences aligned with PROMALS3D (Pei et al., 2008). Poorly aligned regions were eliminated using Gblocks v 0.91b with default settings (Castresana, 2000). There were 227 positions in the final alignment. Model selection was performed using ModelFinder (Kalyaanamoorthy et al., 2017) implemented in IQ-TREE (Nguyen et al., 2015); LG+I+G4 was chosen as a best-fit model according to the Bayesian information criterion. The maximum likelihood tree was constructed with IQ-TREE v. 1.6.12 with nodal support determined by non-parametric bootstrapping with 500 replicates. Bayesian posterior probabilities were calculated using MrBayes 3.2.6 (Ronquist et al., 2012). The analysis ran for 3×10^6 generations. Two parallel runs were used with four chains each, sample frequency of 100 generations, and 25% burn-in.

Fungal Growth Conditions for Gene Expression Analysis

C. tropicalis, *C. albicans*, and *Candida dubliniensis* isolates were grown using the same methods except where noted below. All fungal isolates were stored as 30% glycerol stocks at −80°C and streaked to a YPD plate prior to use in an experiment. YPD stock plates were incubated for approximately 24 h at 37°C and then kept at 4°C for no more than 1 week. A starter culture was prepared by inoculating one representative colony from the YPD plate into 20 ml of liquid YPD in a 50-ml flask. The flask was incubated at 30°C and 200 r/min shaking for 16 h. All cells were collected by centrifugation and washed twice in sterile MilliQ water. Cell number was calculated using a hemacytometer. A small portion of the 16 h culture was flash frozen in dry ice/ethanol and duplicate samples stored at −80°C for RNA extraction to measure relative gene expression in a saturated culture.

Growth conditions were selected from previous analyses of *ALS* gene expression and Als protein production in cultured *C. albicans* cells. Growth in RPMI 1640 medium (Gibco; 11875-135) induces *C. albicans* germ tube formation and its associated differential Als protein production (Coleman et al., 2009). For growth in RPMI 1640, washed cells from the starter culture were used to inoculate 20 ml of the medium at a density of 5×10^7 cells/ml in a 50-ml flask. Flasks were incubated at 37°C and 200 r/min shaking for 1 h. The culture was divided into two equal portions, and cells were collected by filtration over a sterile 0.45-μm pore-size membrane (GVS Life Sciences; 1213776). Filters were flash frozen in dry ice/ethanol and stored at −80°C.

Analysis of *ALS* gene expression in cells from an early-growth-stage culture used YPD (rich) medium. Two identical 250-ml flasks were filled with 100 ml of YPD and inoculated at a cell density of 1×10^6 per ml. Flasks were incubated for 1 h at either 37°C (*C. tropicalis*) or 30°C (*C. albicans* and *C. dubliniensis*) and 200 r/min shaking. Cells were collected by filtration as detailed above and filters flash frozen and stored at −80°C for RNA extraction.

Additional growth conditions for *C. tropicalis* were intended to examine *ALS* gene expression during morphological change. Lackey et al. (2013) described growth in synthetic defined medium [SD; 6.7 g/l yeast nitrogen base without amino acids (BD Biosciences)] supplemented with 50% fetal bovine serum (FBS) for this purpose. Early (2 h) and late (24 h) time points were evaluated to assess differential gene expression over the course of a growth curve. Washed cells from the 16-h YPD starter culture were resuspended in 15 ml of SD medium at an OD_{600} of approximately 1.7. Ten milliliters of the SD culture were added to 10 ml of 100% FBS and incubated at 30°C and 200 r/min shaking for 2 h. The culture was divided in half, cells collected by centrifugation, flash frozen in dry ice/ethanol, and stored at −80°C. The remaining 5 ml of the 15 ml SD starter culture was combined with 5 ml of 100% FBS and incubated for 24 h at 30°C and 200 r/min shaking. Cells were collected and stored as described above.

Cultures were prepared on three different days. Each experimental day had daily replication by creating two unique cultures from two different colonies on the original agar plate.

TaqMan Assays for Analysis of *ALS* Gene Expression

TaqMan assays were designed to specifically detect each of the *C. tropicalis ALS* genes, as well as to differentiate between alleles of *CtrALS3882*. To place *C. tropicalis* gene expression data into a larger context, TaqMan assays were also designed and validated for each *ALS* gene in *C. albicans*. TaqMan assays were also designed for *C. dubliniensis ALS* genes because the literature lacked information about *ALS* gene expression in this species. Methods for designing and validating TaqMan assays were detailed by Oh et al. (2019). Although an amplicon size of 140 bp was targeted, some assays required a shorter or longer product to ensure specificity of detection. Amplicon sizes ranged from 106 to 213 bp; PCR efficiencies ranged from 95 to 102% (**Supplementary Table S2**).

TaqMan assay specificity was validated carefully using cloned control gene fragments (DNA templates; **Supplementary Table S3**). Detailed methods and examples of acceptable results were described previously (Oh et al., 2019). TaqMan control reactions targeted *ACT1* and *TEF1* using primer/probe sets capable of recognizing all species in the study (**Supplementary Table S2**).

[3]http://www.cbs.dtu.dk/services/SignalP

[4]https://mendel.imp.ac.at/gpi/gpi_server.html

[5]https://www.ebi.ac.uk/services

Methods for RNA extraction, genomic DNA removal, cDNA synthesis, and TaqMan assays were described previously (Oh et al., 2019). Experiments in this report were completed entirely on a QuantStudio 3 Real-Time PCR System. Statistical significance was assessed using a mixed-model analysis of variance (PROC MIXED in SAS 9.4; SAS Institute Inc., Cary, NC, United States). LSMEANS was used for separation of means.

RESULTS

Generation of a Novel Genome Sequence for *C. tropicalis* MYA-3404

The major goal of this work was to define the *ALS* gene family in *C. tropicalis*. At the time the project began, the best genome assembly available was accession ASM633v3, initially deposited in 2005. The dataset had 128 contigs, assembled into 24 scaffolds that, in places, were spliced together by strings of "NNN" to indicate sequence ambiguity. Putative *ALS* loci were located using BLAST. The fragmented loci were documented in **Supplementary Figure S1** and the predicted partial proteins in **Supplementary Figure S2**.

Long-read sequencing using the Oxford Nanopore MinION technology was just emerging at the start of this project in 2017. The potential for long-read sequencing to span sometimes-lengthy repeated regions within *ALS* open reading frames led to the development of a new genome assembly that used Illumina MiSeq and Oxford Nanopore MinION data (ASM694213v1; GCA_006942135.1). The accurate Illumina data were included to correct the MinION data, which were already recognized as error prone (de Lannoy et al., 2017). The assembly included 29 contigs and no Ns (**Supplementary File S1**). Although the long-read data provided an improved assembly compared to ASM633v3, completion of the *ALS* loci still required additional considerable effort.

The overall strategy for accurate assembly of the *C. tropicalis ALS* family involved identifying unique genomic landmarks to anchor specific *ALS* loci in their proper physical location. PCR primers were designed to amplify regions that required improvement. Sanger sequencing was used to generate the final data. **Figures 1**, **2** display the assembled *ALS* loci and predicted proteins, respectively. **Table 2** lists the assembled *ALS* genes and places them into the context of the original MYA-3404 genome assembly (ASM633v3) as well as previous publications that mentioned the *C. tropicalis ALS* family.

In May 2020, a new *C. tropicalis* MYA-3404 genome assembly became available in the NCBI database (ASM1317755v1; GCA_01317755.1; Guin et al., 2020). This assembly was generated using PacBio Sequel and Illumina HiSeq data. It was notable because the number of contigs equaled the number of *C. tropicalis* chromosomes, signaling the highest-quality assembly available to date. A comparison between our carefully curated *ALS* genes and the new assembly is presented in **Table 3**. Overall, the new Sequel assembly had the correct number of *ALS* genes, placed in the proper physical locations. Some of the Sequel *ALS* ORFs were identical in length to our hand-curated data, although many were longer. Nucleotide polymorphisms existed between our gene sequences and those in the Sequel assembly. For three genes, these polymorphisms resulted in frameshifts

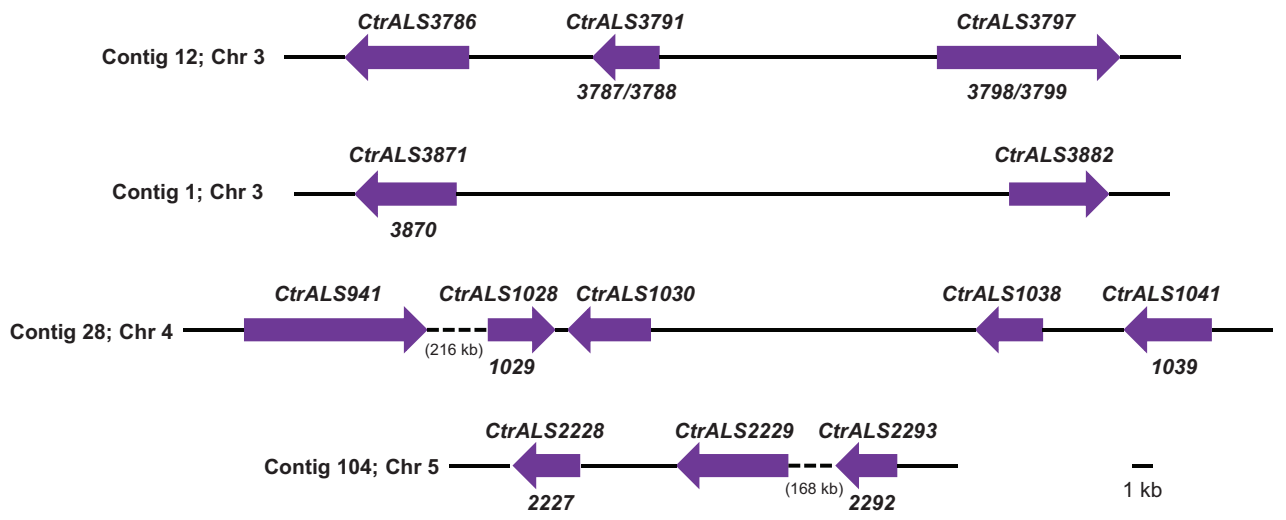

FIGURE 1 | Schematic of *ALS* loci in *Candida tropicalis* MYA-3404 as deduced using assembly ASM694213v1, PCR amplification, and Sanger sequencing. Contig numbers from assembly ASM694213v1 were noted at the left of each diagram; chromosome assignments included in assembly ASM1317755v1 (Guin et al., 2020) were also noted. Arrows were drawn to scale and represent the size of one allele at each *ALS* locus. Because *ALS* sequences were finalized using PCR amplification for Sanger sequencing, the alleles shown here were likely biased toward the smaller allele when one existed. Final gene names were indicated above each locus; ASM633v3 open reading frames (ORFs) that were combined into the final gene were designated below. Intergenic distances were drawn to scale except where quite large and then indicated by a dashed line and approximate length (in kb). Sequences were deposited in GenBank and accession numbers listed in **Table 2**. In some cases where the number of copies of the tandem repeat sequence was exceptionally large, unique primers for PCR amplification and Sanger sequencing could not be designed. Instead, the reported sequence was the consensus from the 105× coverage of the Illumina MiSeq/Oxford Nanopore MinION data.

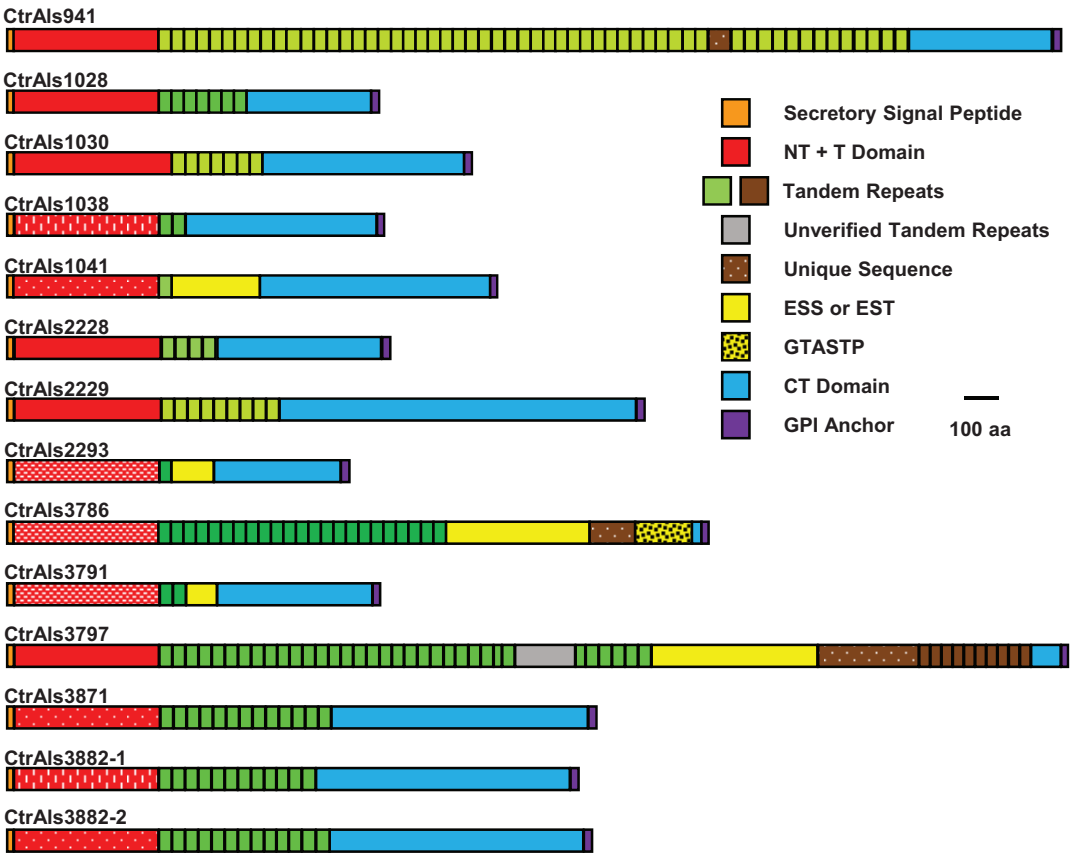

FIGURE 2 | Schematic of predicted *C. tropicalis* MYA-3404 Als proteins drawn to scale. Protein sequences showed common Als features (reviewed in Hoyer and Cota, 2016) including a secretory signal sequence, NT + T domain, copies of tandemly repeated sequences, and a C-terminal (CT) domain that was rich in Ser/Thr. *C. tropicalis* Als proteins had some novel repeated sequences such as those rich in ESS or EST, or the GTASTP motif. Protein features were color coded to recognize similarity across the family. Red blocks that represent NT + T domains were further modified to denote similarity between sequences (e.g., speckles or dashed lines as reflected by percent identity values in **Figure 3**). Blocks denoting tandemly repeated sequences were in different shades of green to indicate sequences with greater similarity to each other. CtrAls2293 was drawn to include a predicted GPI anchor domain, although the putative signal is much weaker in this sequence than others in the family. Extremely long tandem-repeat domains (e.g., *CtrALS941* and *CtrALS3797*) could not be verified by PCR amplification and Sanger sequencing because highly conserved repeated units did not permit the design of unique primers. The reported sequence relied on the 105× coverage from assembly ASM694213v1, which for *CtrALS3797* required insertion of "XXX" (gray color) to make the size of the gene match the fragment sizes generated by PCR.

and/or premature stop codons, thus an incomplete *ALS* ORF in the Sequel data.

The *C. tropicalis ALS*/Als Family

The 13 distinct physical loci in the *C. tropicalis ALS* family (**Figure 1**) predicted proteins (**Figure 2**) with Als features including a secretory signal peptide and a GPI anchor addition site that target the mature protein toward linkage to β-1,6-glucan in the fungal cell wall (Lu et al., 1994). Each predicted protein had a domain structure characteristic of Als proteins (Hoyer and Cota, 2016) including an NT-Als adhesive domain (Lin et al., 2014), followed by a Thr-rich (T) sequence and at least one copy of a sequence that resembled an Als tandem repeat. Like previously characterized Als sequences, those in *C. tropicalis* were increasingly rich in Ser and Thr residues toward the C-terminal end (reviewed in Hoyer et al., 2008; Lombardi et al., 2019; Oh et al., 2019).

Closer examination of these features suggested that the predicted NT-Als adhesive domain of each *C. tropicalis* Als protein was only approximately 50% identical to *C. albicans* NT-Als3 for which the molecular structure is known (Lin et al., 2014; **Figure 3**). Percent sequence identity among the predicted NT-Als domains in *C. tropicalis* was also in the 30–50% range for most comparisons, even between proteins encoded by the *CtrALS3882* alleles, which were only 52% identical (**Figure 4**). A high degree of sequence conservation was noted among some NT-Als domains including CtrAls2293/CtrAls3786/CtrAls3791, which were 88–93% identical (**Figure 3**). CtrAls3882-2 NT-Als was 88% identical to CtrAls3871, while CtrAls3882-1 NT-Als more closely resembled CtrAls1038 (73%). CtrAls1041 NT-Als was 80% identical to the same region in CtrAls3871. Nearly all NT-Als domains predicted from DNA sequence data encoded eight conserved Cys residues that direct folding of the adhesive domain (Lin et al., 2014); CtrAls1030 had only six Cys residues and CtrAls3871 had 10.

TABLE 2 | *C. tropicalis* MYA-3404 *ALS* genes from ASM694213v1 and their corresponding open reading frames (ORFs) in previously published work.

Gene Name	Size (bp)	GenBank Accession Number	NCBI ORFs Included in Final ORF*	*ALS* ORFs from Butler et al. (2009)	*ALS* ORFs from Jackson et al. (2009)
CtrALS941	8,865	MH753531	CTRG_00941	00941	00941.3
CtrALS1028	3,192	MH753521	CTRG_01028[b,c], CTRG_01029[a]	01028	1028.3
CtrALS1030†	3,963	MH753522	CTRG_01030	01030	1030.3
CtrALS1038	3,204	MK128125	CTRG_01038[b,c]	01038	1038.3
CtrALS1041	4,200	MK128127	CTRG_01041[b,c], CTRG_01039[c]	01041	1041.3
CtrALS2228‡	3,255	MT863732	CTRG_02228[b,c], CTRG_02227[a,c]	02228	02228.3
CtrALS2229	5,406	MH753523	CTRG_02229[a]	02229	02229.3
CtrALS2293†	2,925	MK182724	CTRG_02293[b], CTRG_02292[c]	02293	02293.3
CtrALS3786	6,030	MK332912	CTRG_03786[b,c]	03786	03786.3
	N/A	N/A	Incorporated into *CtrALS3791*	03787	
CtrALS3791	3,171	MK170233	CTRG_03791[c], CTRG_03788[a,c], CTRG_03787[a,c]	03791	03791.3
CtrALS3797†	8,850	MN224675	CTRG_03797[b], CTRG_03798[a], CTRG_03799[c]	03797	03797.3
CtrALS3871	4,968	MH753524	CTRG_03871[b,c]	03871	03871.3
CtrALS3882-1	4,833	MH753525	CTRG_03882	03882	03882.3
CtrALS3882-2	4,440	MN893367	N/A	N/A	N/A

**Superscripts in the NCBI ORFs column denote defects in the ASM633v3 assembly of ALS genes. a = lack of a secretory signal peptide. b = lack of a GPI anchor addition signal. c = lack of sequence features expected for the ALS family or not recognized as a potential ALS gene fragment in the original annotation. †Partial ALS sequences were deduced from PCR amplification of C. tropicalis genomic DNA using consensus primers developed from alignment of C. albicans ALS sequences (Hoyer et al., 2001). These gene fragments can now be assigned to a complete ORF. In the original manuscript, the gene fragments were named ALST1 (GenBank accession AF201686.1; now recognized as CtrALS3797), ALST2 (AF211865.1; CtrALS1030), and ALST3 (AF211866.1; CtrALS2293). ‡The larger allele of CtrALS2228 was also deposited into GenBank (accession number MK128126; 4,872 bp). The larger allele encoded more copies of the tandemly repeated sequence than the smaller allele and, in assembly ASM694213v1, included frameshifts within the tandem repeat domain.*

The divergent sequences in the 5′ domain of *CtrALS3882-1* and *CtrALS3882-2* complicated the assembly and definition of the *C. tropicalis ALS* family. The presence of divergent sequences was first noted during attempts to amplify the 5′ domain of *CtrALS3882* for Sanger sequencing. Resulting chromatograms yielded overlapping peaks that suggested a diploid sequence (data not shown). Subsequent efforts focused on designing PCR primers that anchored *CtrALS3882* to an exact physical location, then demonstrating that both alleles occupied the same location, presumably on sister chromosomes (**Figure 4**). The effort was made more difficult by additional sequence conservation in the region, including the closely related genes *CTRG_03872* and *CTRG_03881*, which were 97% identical. DNA fragments were amplified, cloned, and Sanger sequenced to reveal unique areas to which additional primers could be designed. For example, primers 12-62F and 12-58R were used with Q5 polymerase (New England Biolabs) to specifically amplify *CtrALS3882-2*. The physical location of each allele was validated by amplifying upstream and downstream fragments for Sanger sequence analysis. Examples include the use of primers 12-33F/12-36R and 12-31F/12-58R that amplified the regions upstream and downstream of *CtrALS3882-2*, respectively, amplification of the region upstream of *CtrALS3882-1* with primers 12-33F/12-19R, and amplification of the region upstream of *CtrALS3871* with primers 11-26F/11-25R. Sequence polymorphisms unique to each physical location were deduced by comparison among the PCR products and available genome assemblies. Each *CtrALS3882* allele was detected in all six *C. tropicalis* isolates studied suggesting that heterozygosity at this locus is reasonably common within the species. DNA sequences for each allele in the various isolates are included in **Supplementary File S3**.

Tandem repeat copy number in some *C. tropicalis* MYA-3404 *ALS* alleles was large (e.g., *CtrALS941* and *CtrALS3797*) and in others was limited to a single unit (*CtrALS1041* and *CtrALS2293*). The consensus sequence derived from the main, central domain of tandem repeats was similar to those found in previously characterized Als proteins (**Figure 5A**). Repeat unit length generally was 36 amino acids, although CtrAls1030 contained multiple copies of a 37-amino-acid repeated sequence, and other alleles contained irregular repeat lengths (i.e., individual units of 35 or 40 amino acids). Novel repeat sequences were present such as short motifs (ESS, EST, GTASTP) or a 30-amino acid tandem motif in CtrAls3797 (**Figure 5B**).

Phylogenetic analysis was conducted using the amino acid sequences from the NT-Als adhesive (functional) domain from each Als protein in *C. albicans* (Ca), *C. dubliniensis* (Cd), *C. tropicalis* (Ctr), *Candida parapsilosis* (Cp), *Candida orthopsilosis* (Co), and *C. metapsilosis* (Cm; **Figure 6**). Sequences beyond this region could not be included because of their high level of divergence. Nucleotide sequences encoding NT-Als were also too divergent, so amino acid sequences were aligned and variable regions extracted as described in Section "Materials and Methods." Results showed three phylogenetically distant groups: Ca/Cd, Cp/Co/Cm, and Ctr. Orthologs were apparent in the Ca/Cd group (e.g., CaAls9/CdAls64220, CaAls4/CdAls64610, CaAls6/CdAls86290, and CaAls7/CdAls86150). A previous publication (Jackson et al., 2009) offered evidence to support the orthology of CaAls1/CdAls64210. Within the Cp/Co/Cm

TABLE 3 | Comparison between *ALS* sequences in *C. tropicalis* MYA-3404 genome assemblies ASM694213v1 (MiSeq/MinION) and ASM1317755v1 (HiSeq/Sequel).

Gene	MinION (aa)	Sequel (aa)*	Identity (%)†
CtrALS941	2,954	2,954	99.1
CtrALS1028	1,063	1,063	97.0
CtrALS1030	1,320	**1,356**	99.7
CtrALS1038	1,069	**1,356**	98.5
CtrALS1041	1,399	**2,803**	99.6
CtrALS2228	1,084	**1,696**	99.7
CtrALS2229	1,801	1,801	100
CtrALS2293	974	**1,639**	96.9
CtrALS3786	2,009	**2,469**‡	—§
CtrALS3791	1,056	**2,264**‡	—§
CtrALS3797	2,949	**3,109**‡	—§
CtrALS3871	1,655	**2,015**	99.6
CtrALS3882-1	1,610	1,610	99.5
CtrALS3882-2	1,479	1,610	82.8

**Bold type indicates predicted protein lengths that were larger than the sequences from MinION/MiSeq/Sanger sequencing. Smaller size for the MinION alleles was likely due to PCR amplification of target regions which biases for smaller fragments.* †*Percent identity was calculated using Clustal Omega alignment of the sequences (Cook et al., 2017).* ‡*Predicted size was estimated by reading past the broken gene sequence and locating a putative GPI anchor signal and stop codon.* §*Percent identity could not be calculated because genes in the Sequel assembly were incomplete. In the Sequel assembly, CtrALS3786 had two frameshifts, then two premature stop codons. CtrALS3791 had a frameshift. CtrALS3797 had two premature stop codons.*

group, orthologs CpAls660/CoAls800/CmAls800 were evident. Paralogous sequences, most likely resulting from duplication events and generating contiguous genes within a species included CoAls4210/CoAls4220 and CpAls4770/CpAls4780/CpAls4800. The NT-Als sequences from *C. tropicalis* were relatively distant phylogenetically. The larger number of *ALS* genes in *C. tropicalis* compared to the other species likely arose from gene duplication. Potential paralogs included CtrAls1041/CtrAls3871/CtrAls3882-2, CtrAls1038/CtrAls3882-1, and CtrAls3791/CtrAls2293/CtrALS3786. CtrAls3797 grouped more closely to the Cp/Co/Cm sequences. This trend was also apparent for CpAls4790/CmAls4220 that grouped more closely with the Ca/Cd sequences suggesting a potential ortholog within that group. Functional information for each protein would aid interpretation of these distinctions.

Relative Expression Levels of *Candida tropicalis ALS* Genes

Real-time RT-PCR analysis of *ALS* gene expression was pursued to determine if the family was differentially expressed by growth condition and cellular morphology. High gene expression levels might also predict which Als proteins were present in the greatest abundance on the *C. tropicalis* cell surface, thereby positioned to contribute most to the adhesive function. A unique TaqMan assay was designed for each *ALS* gene and to differentiate between the alleles of *CtrALS3882*. Assay primers and probe sequences were placed at a similar location within the 5′ domain for each gene. *C. tropicalis* MYA-3404 cells were harvested from five different culture conditions, RNA extracted, and cDNA synthesized for TaqMan analysis.

Color coding in **Figure 7** denotes high (red) and low (purple) expression levels based on the threshold (ΔC_t) values relative to the *ACT1* and *TEF1* control genes. With C_t values that lagged only one to two cycles behind the control gene expression, *CtrALS1028* showed high expression levels in RPMI medium and from a 2-h culture of SD + FBS. These expression levels were not significantly different from each other ($p = 0.1276$). Expression levels were lower in cells from a 16-h YPD culture and the 24-h SD + FBS condition; these values were not significantly different from each other either ($p = 0.1245$). All other comparisons were significantly different suggesting differential expression of *CtrALS1028* by stage of culture growth (1 vs. 16 h in YPD; $p < 0.0001$; 2 h vs. 24 h in SD + FBS; $p < 0.0001$) with higher expression levels in cells that were more recently transferred to fresh growth medium. In contrast, *CtrALS941* expression was lower at early stages of culture growth and significantly higher as the culture reached saturation (16 h vs. 1 h in YPD; $p = 0.0007$; 24 vs. 2 h in SD + FBS; $p < 0.0001$). *CtrALS3791* showed yet another type of differential expression pattern with its highest expression in the 1 h YPD culture and significantly lower values in the early-stage growth in other media ($p < 0.0001$). Many genes had an expression pattern like *CtrALS1030*, expressed at only moderate levels in all five growth conditions. For *CtrALS1030*, none of the statistical comparisons were significant ($p > 0.05$) suggesting lack of differential expression for the growth conditions tested.

The examples above provided a context for statistical significance for differences between the gene expression values. Coupled with the color coding in **Figure 7**, many other comparisons can be made visually and quickly evaluated for their potential statistical significance. However, the data did not provide a biological context for the relationship between TaqMan ΔC_t values and detectable Als protein on the *C. tropicalis* cell surface. A potential context was provided by designing TaqMan assays for *C. albicans ALS* genes (**Supplementary Table S2**) and using them to assess gene expression in growth conditions for which the association between differential gene expression and protein abundance on the fungal cell surface was known. The rationale for this approach was that use of monoclonal antibodies specific for individual Als proteins demonstrated that CaAls1, CaAls3, and CaAls4 can be visualized readily by immunofluorescent labeling on the *C. albicans* surface, while CaAls5 and CaAls6 cannot (Coleman et al., 2009, 2010, 2012). CaAls5 could be detected in Western blots of *C. albicans* cell wall extracts, while the CaAls6 signal remained negative (Zhao et al., 2011). These previous observations corresponded well with the TaqMan ΔC_t values (**Figure 8A**) and suggested that a ΔC_t value of approximately 7 might serve as a potential cutoff between detectable and non-detectable cell-surface protein.

Revisiting **Figure 7** with this insight suggested that although most comparisons between TaqMan ΔC_t values for *CtrALS2228* and *CtrALS2229* were statistically significant, neither gene was transcribed at a level that was likely to produce detectable protein on the *C. tropicalis* cell surface. In each growth condition assayed, several other genes were transcribed at a level that was

	941	1028	1030	1038	1041	2228	2229	2293	3786	3791	3797	3871	3882-1	3882-2	*ALS3*
941	-----	59	56	53	56	56	49	58	57	58	56	54	53	54	58
1028	49	-----	62	65	68	59	55	61	61	61	61	65	65	67	64
1030	43	49	-----	58	58	55	50	54	55	55	54	57	57	59	59
1038	42	54	44	-----	64	56	49	56	55	55	56	61	77	63	58
1041	47	57	45	55	-----	56	51	60	60	60	58	85	62	88	60
2228	48	49	41	46	49	-----	47	59	60	60	55	55	56	56	58
2229	34	41	30	32	35	33	-----	49	50	50	49	49	50	51	50
2293	51	51	44	49	52	54	38	-----	90	92	59	59	56	59	61
3786	50	50	43	47	53	55	37	88	-----	95	59	59	56	59	61
3791	50	51	44	49	53	54	37	91	93	-----	59	59	56	59	62
3797	46	48	43	45	45	46	34	52	53	52	-----	57	56	57	60
3871	44	52	42	53	80	46	32	49	49	50	45	-----	62	92	61
3882-1	40	54	43	73	54	44	32	46	45	46	44	53	-----	62	56
3882-2	45	55	45	54	85	47	34	49	50	51	47	88	52	-----	61
Als3	48	52	48	46	51	50	35	54	54	55	52	50	47	50	-----

FIGURE 3 | Percent identity values between the nucleotide sequences for the 5′ domain of the *C. tropicalis ALS* genes (upper diagonal) and their predicted amino acid sequences (lower diagonal). The region used for comparisons corresponds to the NT-Als domain of each protein. *C. albicans* Als3 (GenBank AY223552.1) was included for comparison. Boxes were shaded to indicate overall percent identity with hotter colors (red, yellow) used for higher percent identity than cooler colors (green, blue, and gray). Both alleles of *CtrALS3882* were included in the diagram to highlight lack of identity to each other, but high sequence conservation with other loci.

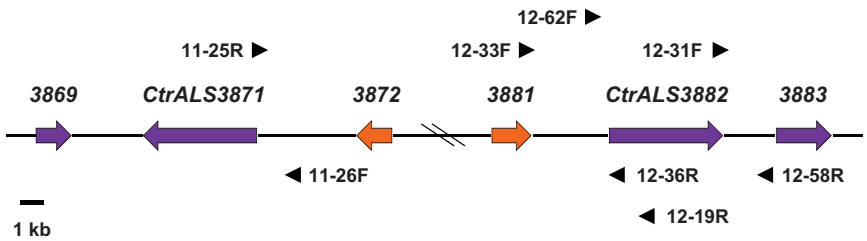

FIGURE 4 | Schematic of the *CtrALS3882* locus to support the conclusion that *CtrALS3882-1* and *CtrALS3882-2* occupied the same relative physical location on the diploid chromosomes of *C. tropicalis* MYA-3404. Hash marks in the diagram indicated an approximate distance; an accurate distance was shown in **Figure 1**. *CtrALS3882-1* and *CtrALS3882-2* were only 52% identical in the 5′ domain of the ORF (**Figure 3**). ORFs were represented by arrows that indicate the orientation of each gene. Orange arrows indicate *CTRG_03872* and *CTRG_03881*, which were 97% identical. Primers used to demonstrate the physical location of each ORF are shown; primer sequences are recorded in **Supplementary Table S1** to indicate whether they recognized both alleles or were specific for *CtrALS3882-1* or *CtrALS3882-2*.

also unlikely to produce detectable protein (i.e., *CtrALS1030*, *CtrALS1038*, *CtrALS1041*, and *CtrALS3871*). Some genes were differentially expressed at a sufficient level to produce detectable protein in specific growth conditions (e.g., *CtrALS3791* in 1 h YPD), while others appeared to produce the proteins that might have the greatest cell-surface presence. For example, *CtrALS2293* was transcribed highly in all growth conditions tested. In a 24-h SD + FBS culture, it was likely that CtrAls2293 and CtrAls3882-1 would dominate the cell surface. In each growth condition tested, *CtrALS3882-1* was more highly expressed than its allele *CtrALS3882-2* ($p < 0.0001$).

One larger goal of our work was to understand the cell-surface Als presence on various fungal species that cause candidiasis. In this regard, little attention has been given to the expression of *C. dubliniensis ALS* genes. *C. dubliniensis* and *C. albicans* are closely related species in which *ALS* genes occupy similar physical loci (Jackson et al., 2009). However, *C. dubliniensis* does not encode an *ALS3* ortholog, and sequences for two of the *C. dubliniensis ALS* loci (*Cd64800* and *Cd65010*) are 100% identical within the 5′ domain of the gene. TaqMan assays were designed and used to analyze *ALS* gene expression in cells from strain CD36 grown using the same conditions applied to *C. tropicalis* and *C. albicans*; a single assay detected transcription from *Cd64800* and *Cd65010* (**Figure 8B**). Some *C. dubliniensis ALS* genes were capable of high expression levels (e.g., *Cd64610*, *Cd64800/Cd65010*), while others were barely transcribed (*Cd86150*). Differential expression was observed among the growth conditions tested (*Cd64210*, *Cd86290*).

The newly validated TaqMan assays were a tool that others may use to explore various hypotheses regarding the *C. tropicalis ALS* family. One potential experimental question was whether *ALS* expression patterns varied across *C. tropicalis* clinical isolates. DNA sequences were derived for the 5′ domain of each *ALS* gene in the six *C. tropicalis* isolates in our laboratory collection (**Supplementary File S3**). While many sequences showed a perfect match to TaqMan assay primers and probes, sequence variation was noted in some instances. These target sequences were cloned and verified; dilutions of purified DNA were used as the TaqMan assay template. **Figure 9** shows an array of these examples, selected to titrate the degree of sequence mismatch that might result in underestimated or false-negative assay results. For example, one nucleotide mismatch in the middle of one primer was not sufficient to interfere with assay function (**Figure 9A**); however, accumulation of more mismatches, especially in key primer or probe positions led to falsely low estimates of transcript abundance (**Figures 9B,C**).

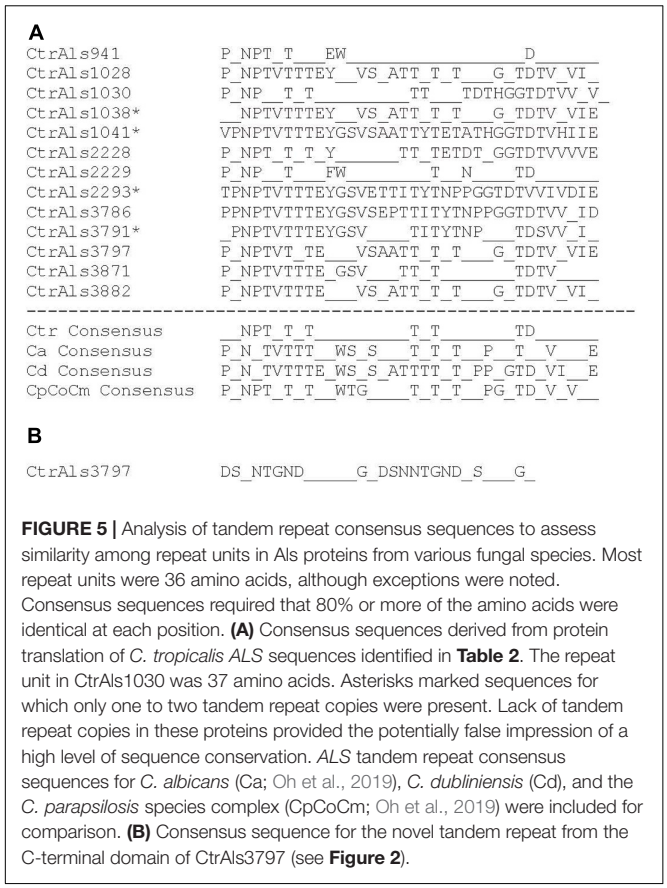

FIGURE 5 | Analysis of tandem repeat consensus sequences to assess similarity among repeat units in Als proteins from various fungal species. Most repeat units were 36 amino acids, although exceptions were noted. Consensus sequences required that 80% or more of the amino acids were identical at each position. **(A)** Consensus sequences derived from protein translation of *C. tropicalis ALS* sequences identified in **Table 2**. The repeat unit in CtrAls1030 was 37 amino acids. Asterisks marked sequences for which only one to two tandem repeat copies were present. Lack of tandem repeat copies in these proteins provided the potentially false impression of a high level of sequence conservation. *ALS* tandem repeat consensus sequences for *C. albicans* (Ca; Oh et al., 2019), *C. dubliniensis* (Cd), and the *C. parapsilosis* species complex (CpCoCm; Oh et al., 2019) were included for comparison. **(B)** Consensus sequence for the novel tandem repeat from the C-terminal domain of CtrAls3797 (see **Figure 2**).

Some mismatches between the TaqMan primers/probe and target sequences were so extensive that the assay was unable to detect the sequence (**Figure 9D**). Examination of the sequence data for the collection of six *C. tropicalis* isolates (**Supplementary File S3**) suggested that the TaqMan assays matched target sequences in nearly all instances. Strain 951 was the most divergent with three genes at risk of falsely low estimates of expression level (*CtrALS1038*, *CtrALS3797*, and *CtrALS3882-2*); sequence mismatches for *CtrALS3797* in three additional strains (1019, 1020, 3242) suggested the potential for redesign of that TaqMan assay depending on the strains and biological questions addressed.

DISCUSSION

Advances in DNA sequencing technology are providing long-sought information about the composition of the *ALS* family in fungal species. The availability of Oxford Nanopore MinION technology provided the initial opportunity to incorporate long-read DNA sequence data to resolve the *C. tropicalis ALS* genes. Despite the insights added by these long-read data, assembling accurate *ALS* sequences required considerable additional effort. The more recently released PacBio Sequel-based assembly (Guin et al., 2020) leverages technological improvements in DNA sequence accuracy that will continue to reduce the tedium associated with solving genomic puzzles that involve complex genes like those in the *ALS* family. The accurate list of *C. tropicalis ALS* loci provides an essential foundation for subsequent investigations into adhesion and pathogenesis of the species.

The *C. tropicalis* gene list (**Table 2**) also provides a standard set of names that can be used to derive and communicate unambiguous experimental results. Two published studies attempted to characterize *C. tropicalis ALS* gene expression without the benefit of a complete gene list (Yu et al., 2016; Galán-Ladero et al., 2019). **Supplementary Table S4** shows that some of the PCR primers used in these studies are likely to amplify more than one *C. tropicalis ALS* gene, potentially complicating interpretation of results.

ALS gene names across publications can also be confusing. This confusion seems to originate from misinterpretation of Supplementary Table 23 from Butler et al. (2009). The Als family portion of the table is reproduced in **Supplementary Table S5**. Protein names in the left column match the entries in the *C. albicans* column but do not necessarily correspond to protein names in the other species. For example, the Candida Gene Order Browser[6] (Fitzpatrick et al., 2010; Maguire et al., 2013) indicates that there is no positional ortholog for *C. albicans ALS1* (orf19.5714) in *C. tropicalis*, so *C. tropicalis* CTRG_02293 is not "*C. tropicalis ALS1*" and is definitely not *ALST1* as described by Hoyer et al. (2001; **Table 2**). This disambiguation of gene names is offered to assist readers with interpreting published information about the *C. tropicalis ALS* family.

The current literature is limited to two papers that examine *C. tropicalis ALS* gene expression (Yu et al., 2016; Galán-Ladero et al., 2019). The analyses in both papers compared *C. tropicalis ALS* gene expression in planktonic and sessile cells. Yu et al. (2016) grew sessile *C. tropicalis* on either a polystyrene surface or a human urinary bladder epithelial cell line. Nine clinical isolates and ATCC 750 were studied. Although results varied by strain, *ALST1* (*CtrALS3797*) expression increased in sessile cells. *ALST3* (which likely combines readings from *CtrALS2293*, *CtrALS3786*, and *CtrALS3791*) had the highest expression across the three experimental conditions, perhaps consistent with the high level of *CtrALS2293* expression demonstrated here (**Figure 7**). Galán-Ladero et al. (2019) studied similar *C. tropicalis* properties, also using multiple clinical isolates. Although there was considerable strain variation, *ALS* gene expression generally increased in biofilm-grown cells. Interest in the role of *ALS* genes in *C. tropicalis* biofilm formation is stimulated by the key role that Als proteins play in *C. albicans* biofilms (reviewed in Lohse et al., 2018).

Gene expression patterns investigated here focus on the potential for differential *ALS* expression with growth stage or cellular morphology. Growth conditions (e.g., use of YPD and RPMI media) were selected deliberately to place *C. tropicalis* results into a well-characterized context that was developed for studies of *ALS* gene expression in *C. albicans* (reviewed in Hoyer et al., 2008). The ability of *C. tropicalis* to grow in a filamentous form (Lackey et al., 2013; **Figure 7**) was also leveraged to assess *ALS* gene expression changes associated with morphology. Comparative analyses were furthered by developing TaqMan

[6]http://cgob.ucd.ie/

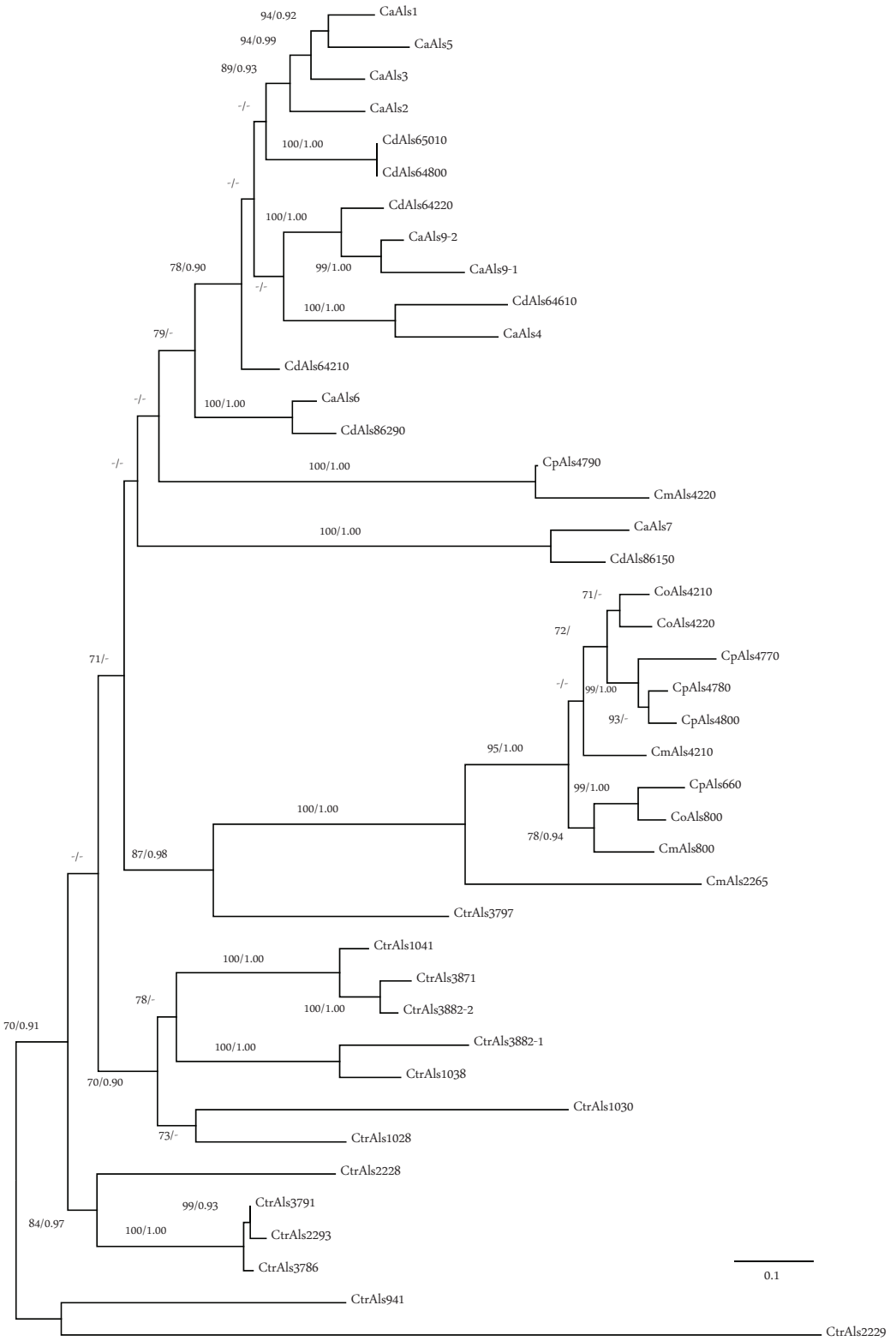

FIGURE 6 | Phylogeny of Als N-terminal domain sequences from *C. albicans* (Ca), *C. dubliniensis* (Cd), *C. tropicalis* (Ctr), *C. parapsilosis* (Cp), *C. orthopsilosis* (Co), and *C. metapsilosis* (Cm). The best-scoring Maximum likelihood tree is shown with maximum likelihood bootstrap values and Bayesian posterior probabilities at each node; only support values greater than 70% and 0.90, respectively, were shown. Branch lengths were proportional to evolutionary change and measured in substitutions per site.

C. tropicalis MYA-3404	*CtrALS941*	*CtrALS1028*	*CtrALS1030*	*CtrALS1038*	*CtrALS1041*	*CtrALS2228*	*CtrALS2229*
Allele size (bp)	8865	3192	3963	3204	4200	4872	5406
YPD; 30°C; 16 h	5.8± 0.5	6.9 ± 0.5	7.1 ± 0.5	7.6 ± 0.5	8.1 ± 0.5	14.0 ± 0.5	10.9 ± 0.5
YPD; 37°C; 1 h	8.1 ± 0.5	3.5 ± 0.5	8.0 ± 0.5	6.9 ± 0.5	7.8 ± 0.5	10.9 ± 0.5	14.1 ± 0.5
RPMI; 37°C; 1 h	7.0 ± 0.5	2.2 ± 0.5	7.6 ± 0.5	6.4 ± 0.5	7.5 ± 0.5	13.1 ± 0.5	13.3 ± 0.5
SD + 50%FBS; 30°C; 2 h	8.7 ± 0.5	1.2 ± 0.5	7.5 ± 0.5	7.0 ± 0.5	7.9 ± 0.5	16.6 ± 0.5	16.6 ± 0.5
SD + 50%FBS; 30°C; 24 h	4.5 ± 0.5	5.9 ± 0.5	6.8 ± 0.5	6.9± 0.5	6.5 ± 0.5	15.7 ± 0.5	13.0 ± 0.5

	CtrALS2293	*CtrALS3786*	*CtrALS3791*	*CtrALS3797*	*CtrALS3871*	*CtrALS3882-1*	*CtrALS3882-2*
Allele size (bp)	2925	6030	3171	8850	4968	4833	4440
YPD; 30°C; 16 h	3.7 ± 0.5	8.1 ± 0.5	6.0 ± 0.5	4.4 ± 0.5	8.6 ± 0.5	3.2 ± 0.5	6.8 ± 0.5
YPD; 37°C; 1 h	-0.5 ± 0.5	8.8 ± 0.5	4.0 ± 0.5	3.0 ± 0.5	7.5 ± 0.5	5.4 ± 0.5	8.8 ± 0.5
RPMI; 37°C; 1 h	2.3 ± 0.5	7.3 ± 0.5	7.3 ± 0.5	4.3 ± 0.5	7.8 ± 0.5	3.8 ± 0.5	7.2 ± 0.5
SD + 50%FBS; 30°C; 2 h	4.5 ± 0.5	9.7 ± 0.5	12.0 ± 0.5	6.3 ± 0.5	8.1 ± 0.5	4.9 ± 0.5	8.2 ± 0.5
SD + 50%FBS; 30°C; 24 h	2.9 ± 0.5	5.5 ± 0.5	8.6 ± 0.5	3.9 ± 0.5	6.5 ± 0.5	2.2 ± 0.5	5.1 ± 0.5

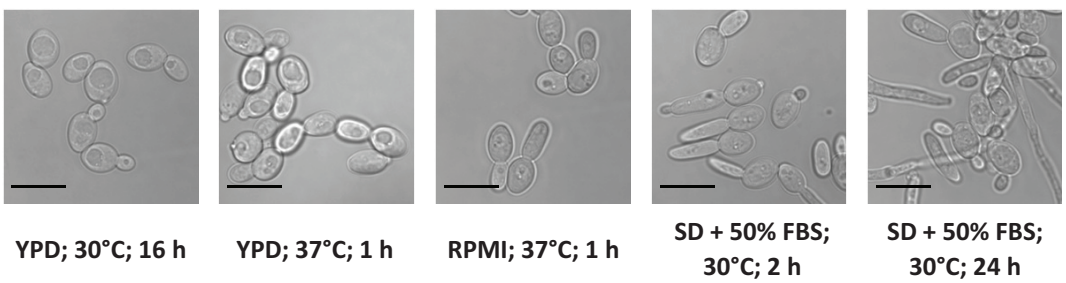

FIGURE 7 | Relative expression of *C. tropicalis ALS* genes as measured by TaqMan assays. Expression of the 13 *C. tropicalis ALS* genes was measured for strain MYA-3404 grown in five different culture conditions. Micrographs of representative cells from each culture condition were captured to show cellular morphology that corresponded to the gene expression data (scale bar = 10 μm). ΔC_t values and standard errors of the mean were reported. The color bar below the data tables was shaded to represent high (red) to low (purple) expression levels.

assays for *C. albicans* and *C. dubliniensis ALS* genes. TaqMan assays correctly identified *C. albicans ALS* genes that were capable of high expression levels (*CaALS1*, *CaALS3*, and *CaALS4*) and those that were not (*CaALS6*, *CaALS7*; reviewed in Hoyer et al., 2008). Differential expression patterns such as upregulation of *CaALS3* in growth conditions that promote germ tube and hyphal formation were also observed (Hoyer et al., 1998a). High levels of *CaALS4* expression in saturated cultures were also noted using the TaqMan assay, as were the residual high level of mRNA in cells that were early in the growth stage in fresh medium that had been previously documented using Northern blots (Hoyer et al., 1998b). TaqMan-assessed expression of *CaALS1* showed high levels in cells transferred to fresh medium and in cells transitioning to hyphal growth (Zhao et al., 2004). However, the *CaALS1* expression level in saturated culture conditions was higher than anticipated.

Some of these *C. albicans ALS* gene expression themes were noted in *C. tropicalis* such as *CtrALS1028* increased expression in cells placed into fresh growth medium and *CtrALS941* increased expression in saturated cultures (**Figure 7**). None of the *CtrALS* genes showed increased expression in filamentous growth morphologies. Other genes, particularly *CtrALS2293* and *CtrAls3882-1*, were highly expressed regardless of growth condition. The highly abundant CtrAls proteins are the strongest candidates for contributing to adhesive function *in vitro*. However, the *C. albicans ALS* gene expression is known to differ *in vitro* and *in vivo* (Coleman et al., 2012), so assaying *in vivo*-grown *C. tropicalis* would better predict the display of Als proteins on cells in the host environment. Understanding which Als proteins are prominent on the fungal cell surface is the first step toward developing adhesion inhibitors that will function across pathogenic fungal species.

Although strain differences in *CtrALS* gene expression were not systematically examined here, the works of Yu et al. (2016) and Galán-Ladero et al. (2019) suggest that they exist. Strain differences in *ALS* gene expression were also noted for *C. parapsilosis* and *C. metapsilosis* (Oh et al., 2019). Although there was some strain variation in *C. orthopsilosis ALS* gene expression, *ALS* expression increases in cells that are transferred to fresh culture media compared to saturated cultures

A

C. albicans SC5314	*CaALS1*	*CaALS2*	*CaALS3*	*CaALS4*	*CaALS5*	*CaALS6*	*CaALS7*	*CaALS9*
YPD; 30°C; 16 h	-1.4 ± 0.3	4.0 ± 0.3	4.3 ± 0.3	1.1 ± 0.3	5.8 ± 0.3	11.6 ± 0.3	7.4 ± 0.3	3.6 ± 0.3
YPD; 30°C; 1 h	-0.7 ± 0.3	6.1 ± 0.3	6.1 ± 0.3	2.6 ± 0.3	5.9 ± 0.3	8.2 ± 0.3	9.9 ± 0.3	5.5 ± 0.3
RPMI; 37°C; 1 h	1.4 ± 0.3	6.5 ± 0.3	-3.2 ± 0.3	7.0 ± 0.3	6.3 ± 0.3	12.5 ± 0.3	13.8 ± 0.3	6.6 ± 0.3

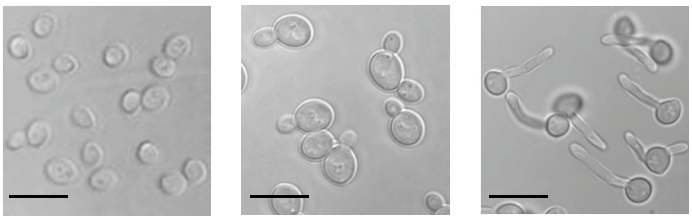

YPD; 30°C; 16 h YPD; 30°C; 1 h RPMI; 37°C; 1 h

B

C. dubliniensis CD36	*Cd64210*	*Cd64220*	*Cd64610*	*Cd64800 Cd65010*	*Cd86150*	*Cd86290*
Ortholog; alias	*CaALS1; ALSD2*	*CaALS9*	*CaALS4; ALSD3*	*CaALS2*	*CaALS7*	*CaALS6; ALSD1*
YPD; 30°C; 16 h	5.1 ± 0.2	6.2 ± 0.2	0.4 ± 0.2	-0.3 ± 0.2	9.3 ± 0.2	12.1 ± 0.2
YPD; 30°C; 1 h	3.9 ± 0.2	6.8 ± 0.2	3.3 ± 0.2	2.5 ± 0.2	11.8 ± 0.2	3.3 ± 0.2
RPMI; 37°C; 1 h	-0.6 ± 0.2	8.0 ± 0.2	1.7 ± 0.2	2.8 ± 0.2	11.3 ± 0.2	11.7 ± 0.2

YPD; 30°C; 16 h YPD; 30°C; 1 h RPMI; 37°C; 1 h

FIGURE 8 | TaqMan measurement of *ALS* gene expression in *C. albicans* **(A)** and *C. dubliniensis* **(B)**. *C. albicans* SC5314 and *C. dubliniensis* CD36 were grown in various culture conditions known to display differential expression of *C. albicans ALS* genes. Images were captured for representative cells from each culture (scale bar = 10 μm). ΔC_t values and standard errors of the mean were reported. The color-coded scale bar ranged from high expression (red) to low (purple). Two *C. dubliniensis ALS* loci had identical sequences and were detected by the same TaqMan assay (*CdALS64800* and *CdALS65010*). *C. dubliniensis ALS* genes were orthologous to *C. albicans ALS* loci as designated in **(B)**. Prior to availability of a *C. dubliniensis* genome sequence, *ALS* genes were identified using consensus PCR primers derived from *C. albicans ALS* sequences (Hoyer et al., 2001). These were designated *ALSD1* (now recognized as *CdALS86290*), *ALSD2* (*CdALS64210*), and *ALSD3* (*CdALS64610*).

(Lombardi et al., 2019). *C. orthopsilosis ALS* gene transcription also showed a reliable hierarchy of expression level with *CoALS4220* > *CoALS4210* > *CoALS800* (Lombardi et al., 2019).

ALS genes in other species are known to have considerable allelic variation, even within the same strain (Zhang et al., 2003; reviewed in Hoyer et al., 2008). *C. tropicalis* genes likely have this large degree of allelic variation, as well. For example, examination of *CtrALS1030* (called "*ALS2*" in the manuscript) in 68 *C. tropicalis* isolates revealed considerable sequence variation in the coding region, localized primarily to the central tandem repeat domain (Zhang et al., 2019). The present work with strain MYA-3404 resulted in two distinct *CtrALS2228* sequences

A

>*CtrALS3791* MYA-3404

AACTACCCAACTTCAGCGGATTCCTTTTCTTATACCCAAACTTGTACT
TCCAAAAGTTTTCAAATAACATTCAATAATATTCCAGCCGGCTATCGT
CCATATATTGCTGCATTGGTTCAAGCTCCATCTTCGGATTATAAAATT
GATTATACTGCAAAATATCAATGTGCTGGATCTTCCCAAAAAGATGCT
TCGAAATCGGTCACTTGGTCAGG

>*CtrALS3791* 1020

AACTACCCAACTTCAGCGGATTCCTTTTCTTATACCCAAACTTGTACT
TCCAAAAGTTTTCAAATAACATTCAATAATATTCCAGCCGGCTATCGT
CCATATATTGCTGCATTGGTTCAAGCTCCATCTTCGGATTATAAAATT
GATTATACTGCAAAATATCAATGTGCTGGATCTTCCCAAAAAGATGCT
TCAAAATCGGTCACTTGGTCAGG

CtrALS3791	5 pg	0.5 pg	0.05 pg	0.005 pg
MYA-3404	19.6	23.1	26.6	30.1
1020	19.6	22.9	26.4	29.9
Difference	**0.0**	**-0.2**	**-0.2**	**-0.2**

B

>*CtrALS1028* MYA-3404

GATTAATGCTGCTACTGATTATACTTTTACTATTAGTTACATTTCCAA
GTACACATGTGCTACCGGTGATTATCATGATAAATCTATTACTAAAAA
TTGGGCTCCATATAAAAATGGTCTTGCTGATAGTGATGGTGCTGTTGT
TTTTGTTACAACTAGTACTTATCTTGAATCAACTACTG

>*CtrALS1028* 951

GATTAATGCTGCTACTGATTATACTTTTACTATCAGTTATATTTCCAA
GTACACATGCGCTACTGGTGATTATCATGATAAATCTATTACTAAAAA
TTGGGCTCCATATAAAAATGGTCTTGCCGATAGTGATGGAGCTGTTGT
TTTTGTTACAACTAGTACTTATCTTGAATCCACTACTG

CtrALS1028	5 pg	0.5 pg	0.05 pg	0.005 pg
MYA-3404	20.0	23.5	26.8	30.2
951	20.6	24.2	27.3	30.9
Difference	**0.6**	**0.7**	**0.5**	**0.7**

C

>*CtrALS3797* MYA-3404

TGATGCCTATATTAAAACACCTACTTCCACATATGCGGTGACATACAC
TTTCAAATATGTTTGTGCCGATGGAAAATCATATAATAGTAATCGAAG
TTTGAATTGGTCCGGATATGTTAACGGTGATGCAGATTCTGAAGGTAT

>*CtrALS3797* 951

TGATGCTTATATTAAAGCACCTACTTCCACATACCCCATGACATACAC
TTACAAATATGTTTGTTCCGATGGAAAATCATATAATGGCAATACAAA
ATTGAATTGGTCGGGATATGTTAACAGTGATGCAGATTCTGAAGGTAT

CtrALS3797	5 pg	0.5 pg	0.05 pg	0.005 pg
MYA-3404	18.8	22.1	25.4	28.8
951	20.5	24.0	27.4	30.6
Difference	**1.7**	**1.9**	**2.0**	**1.8**

D

>*CtrALS1038* MYA-3404

AGGGAAAATGGGTTTTGACTACAAGTATAGTGTTGTCTGTGCAGATGG
TGAATCTCTTGAGCATCCTACTCACTATGACTGGGGTACTTATAACAC
TCAAACAGCCGATAGTAATGGGGCTAT

>*CtrALS1038* 951

AAGGGGATATGGGGTTTGACTATAAGTATAGTGTTGTTTGCGCTGACG
GTGAGTCTCGTGAGCATCCTACTCACTATAACTGGGGTACTTATAACA
CGCAGACAGCTGATAGTAATGGTGCTGT

CtrALS1038	5 pg	0.5 pg	0.05 pg	0.005 pg
MYA-3404	19.4	22.7	25.7	29.6
951	U/D	U/D	U/D	U/D
Difference	**N/A**	**N/A**	**N/A**	**N/A**

FIGURE 9 | Effect of nucleotide sequence mismatch on TaqMan assay measurement of nucleic acid abundance. TaqMan assays were designed using gene sequences from *C. tropicalis* strain MYA-3404. Selection of unique target regions that distinguished among genes in the *ALS* family was the primary consideration in assay design. Sequencing of the 5′ domain of each *(Continued)*

FIGURE 9 | Continued

ALS gene in six other *C. tropicalis* isolates revealed some mismatches in the TaqMan primer and/or probe sequences. Examples were selected to titrate the effect of an increasing number of mismatches, some in key primer/probe positions. Sequences in each panel were taken from **Supplementary File S3**. The forward primer was highlighted in green, reverse primer in blue, and probe in gray. Mismatches were noted with yellow color. Target sequences in each strain examined were PCR amplified, cloned, and Sanger sequence verified to ensure the mismatches were present. Cloned DNA was purified, diluted, and used in the assays reported here. **(A)** The sequence of the 5′ domain of *CtrALS3791* in strain 1020 showed a single nucleotide mismatch in the middle of the reverse primer. C_t values from TaqMan assays with 10-fold dilutions of cloned construct showed almost an equal ability for the assay to detect each strain (e.g., no difference for 5 pg DNA and negligible differences for subsequent dilutions). **(B)** *C. tropicalis* strain 951 showed one to two mismatches each in the primer and probe sequences for gene *CtrALS1028*. C_t values suggested that detection of strain 951 lagged approximately 0.6 cycle behind detection of strain MYA-3404, providing an underestimate of DNA abundance. **(C)** Increasing numbers of mismatches between primer and probe sequences resulted in greater underestimates of DNA abundance for strain 951, this time in *CtrALS3797* where nearly a two-cycle difference in C_t was observed. **(D)** Mismatches for *CtrALS1038* in strain 951 were so marked that the TaqMan assay was unable to detect genomic DNA, even at the highest concentration. These data provide the foundation necessary to adapt use of the TaqMan assays to *C. tropicalis* isolates in which primer and probe mismatches may exist.

deposited in GenBank (**Table 2**) that primarily varied in the number of copies of the repeated sequence in the tandem repeat domain. DNA sequences in **Supplementary File S3** document diploid nucleotide sequences and variation between strains within the 5′ domain of each *C. tropicalis ALS* gene reported here. Comparison between the MinION *C. tropicalis ALS* sequences and those derived from the Sequel assembly (Guin et al., 2020) reveals length variations that are probably the diploid alleles in strain MYA-3404. MinION data were validated by PCR amplification and Sanger sequencing, techniques that would preferentially amplify the shorter allele where one exists.

All six *C. tropicalis* strains examined encode the 13 *ALS* loci described here (**Supplementary File S3**). Genome sequencing would be helpful to determine if the strains encode additional *ALS* loci. The number of *ALS* loci varies among strains in some species. For example, examination of draft *C. parapsilosis* genome sequences available in GenBank revealed variable *ALS* gene numbers with some strains encoding only two and others having five (Oh et al., 2019). Intergenic recombination between the contiguous *C. albicans ALS5* and *ALS1* loci resulted in a reduction in the *ALS* gene number in approximately 5% of isolates tested (Zhao et al., 2011); heterozygosity at the locus was observed with some strains revealing recombination on one chromosome but not the other. In *C. tropicalis*, the recombination events that created the divergent 5′ domains of *CtrALS3882-1* and *CtrALS3882-2* are found in the six isolates examined. Divergent 5′ domain sequences were also noted for *CaALS9*, although the sequences were 89% identical compared to the 52% identity at the *CtrALS3882* locus (Zhao et al., 2007). Analysis of the adhesive phenotype of strains in which *C. albicans ALS9* was deleted and individual alleles reintegrated revealed the ability of *CaALS9-2*, but not *CaALS9-1*, to rescue the adhesion defect. It is possible

that alleles of *CtrALS3882* may make different contributions to *C. tropicalis* adhesion because of their sequence differences but also because of the greater representation of *CtrALS3882-1* on the cell surface as predicted from the higher transcriptional activity from this allele (**Figure 7**).

Compared to discovery of the *ALS* family in *C. albicans* where genes were introduced into the literature over the period of a decade or more as they were detected using Southern blots (reviewed in Hoyer et al., 2008), advances in genome sequencing technology make it possible to detect all genes in the family at one time. Because of the complexity of the *ALS* genes in *C. tropicalis*, however, accurate assembly of the sequences was not attempted until the availability of long-read sequence technology. The Illumina MiSeq/Oxford Nanopore genome assembly (ASM694213v1) was completed during 2017 yet the large number of *C. tropicalis ALS* genes, lengthy tandem repeat regions, and unexpected allelic variation at the *CtrALS3882* locus required considerably more effort to resolve. The recent PacBio Sequel/Illumina HiSeq assembly (ASM1317755v1; Guin et al., 2020) would have provided a great time savings and suggests that other fungal genomes should be re-sequenced as newer, more accurate, long-read technologies emerge. The relatively low cost of generating accurate long-read sequence data would more than pay for itself in savings of human effort to assemble the complex jigsaw puzzle for *ALS* sequences and other gene families that contain conserved, repeated sequences.

DATA AVAILABILITY STATEMENT

The genome assembly for *Candida tropicalis* strain MYA-3404, generated using Illumina MiSeq and Oxford Nanopore MinION data, is available in GenBank under BioProject accession number PRJNA432250, BioSample accession number SAMN08439037, and Genome accession number PQTP00000000. Version 01 of the project has the accession number PQTP01000000 and consists of sequences PQTP01000001–PQTP01000029. All individual *ALS* gene sequences were deposited in GenBank. Accession numbers are noted throughout the manuscript.

AUTHOR CONTRIBUTIONS

LLH conceptualized the study, acquired funding, and was in charge of project administration. VH, CF, and AH conducted formal analysis. S-HO, AI, RR-B, BS, JJ, CF, AH, and LLH performed the investigation. VH, CF, AH, and LLH developed the study methodology. S-HO, AI, RR-B, JJ, VH, CF, AH, and LLH wrote the original draft. All authors contributed to the article and approved the submitted version.

FUNDING

This work was funded by R15 DE026401 from the National Institute of Dental and Craniofacial Research, National Institutes of Health.

ACKNOWLEDGMENTS

AI, RR-B, BS, and JJ were part of the Undergraduate Program in Fungal Genomics, which is a collaboration between the University of Illinois at Urbana-Champaign and Millikin University. Other students who contributed to this effort included Kaia Ball, Madeline Batek, Anton Bershanskiy, Stephen DeMartini, Erica Forbes, Zeidy Garcia, Jessie Kirk, Mariah McNamer, Deniz Namik, and Quinn Nguyen. The authors thank Drs. Travis Wilcoxen and Laura Zimmerman, Millikin University Department of Biology, for coordinating student participation and supervising research credit for students in the program. The authors thank Pat Kammeyer (Loyola University Medical Center), David Coleman (Trinity College Dublin), and David Soll (University of Iowa) for providing the fungal isolates.

SUPPLEMENTARY MATERIAL

The Supplementary Material for this article can be found online at: https://www.frontiersin.org/articles/10.3389/fmicb.2020.594531/full#supplementary-material

REFERENCES

Bolger, A. M., Lohse, M., and Usadel, B. (2014). Trimmomatic: a flexible trimmer for Illumina sequence data. *Bioinformatics* 30, 2114–2120. doi: 10.1093/bioinformatics/btu170

Butler, G., Rasmussen, M. D., Lin, M. F., Santos, M. A. S., Sakthikumar, S., Munro, C. A., et al. (2009). Evolution of pathogenicity and sexual reproduction in eight *Candida* genomes. *Nature* 459, 657–662. doi: 10.1038/nature08064

Castresana, J. (2000). Selection of conserved blocks from multiple alignments for their use in phylogenetic analysis. *Mol. Biol. Evol.* 17, 540–542. doi: 10.1093/oxfordjournals.molbev.a026334

Coleman, D. A., Oh, S.-H., Manfra-Maretta, S. L., and Hoyer, L. L. (2012). A monoclonal antibody specific for *Candida albicans* Als4 demonstrates overlapping localization of Als family proteins on the fungal cell surface and highlights differences between Als localization in vitro and in vivo. *FEMS Immunol. Med. Micobiol.* 64, 321–333. doi: 10.1111/j.1574-695X.2011.00914.x

Coleman, D. A., Oh, S.-H., Zhao, X., and Hoyer, L. L. (2010). Heterogeneous distribution of *Candida albicans* cell-surface antigens demonstrated with an Als1-specific monoclonal antibody. *Microbiology* 156, 3645–3659. doi: 10.1099/mic.0.043851-0

Coleman, D. A., Oh, S.-H., Zhao, X., Zhao, H., Hutchins, J. T., Vernachio, J. H., et al. (2009). Monoclonal antibodies specific for *Candida albicans* Als3 that immunolabel fungal cells in vitro and in vivo and block adhesion to host surfaces. *J. Microbiol. Methods* 78, 71–78. doi: 10.1016/j.mimet.2009.05.002

Cook, C. E., Bergman, M. T., Cochrane, G., Apweiler, R., and Birney, E. (2017). The European Bioinformatics Institute in 2017: data coordination and integration. *Nucleic Acids Res.* 46, D21–D29. doi: 10.1093/nar/gkx1154

de Lannoy, C., de Ridder, D., and Risse, J. (2017). The long reads ahead: *de novo* genome assembly using the MinION. *F1000Res.* 6:1083. doi: 10.12688/f1000research.12012.2

de Oliveira, J. S., Pereira, V. S., Castelo-Branco, D. S. C. M., Cordeiro, R. A., Sidrim, J. J. C., Brilhante, R. S. N., et al. (2020). The yeast, the antifungal, and the wardrobe: a journey into the antifungal resistance mechanisms of *Candida tropicalis*. *Can. J. Microbiol.* 66, 377–388. doi: 10.1139/cjm-2019-0531

Eisenhaber, B., Bork, P., and Eisenhaber, F. (1999). Prediction of potential GPI-modification sites in proprotein sequences. *Mol. Cell Biol.* 292, 741–758. doi: 10.1006/jmbi.1999.3069

Fitzpatrick, D. A., O'Gaora, P., Byrne, K. P., and Butler, G. (2010). Analysis of gene evolution and metabolic pathways using the Candida Gene Order Browser. *BMC Genomics* 11:290. doi: 10.1186/1471-2164-11-290

Galán-Ladero, M. A., Blanco-Blanco, M. T., Fernández-Calderón, M. C., Lucio, L., Gutiérrez-Martín, Y., Blanco, M. T., et al. (2019). *Candida tropicalis* biofiom formation and expression levels of the *CTRG ALS*-like genes in sessile cells. *Yeast* 36, 107–115. doi: 10.1002/yea.3370

Guin, K., Chen, Y., Mishra, R., Muzaki, S. R. B., Thimmappa, B. C., O'Brien, C. E., et al. (2020). Spatial inter-centromeric interactions facilitated the emergence of evolutionary new centromeres. *Elife* 9:e58556. doi: 10.7554/eLife.58556

Hoyer, L. L., and Cota, E. (2016). *Candida albicans* agglutinin-like sequence (Als) family vignettes: a review of Als protein structure and function. *Front. Microbiol.* 7:280. doi: 10.3389/fmicb.2016.00280

Hoyer, L. L., Fundyga, R., Hecht, J. E., Kapteyn, J. C., Klis, F. M., and Arnold, J. (2001). Characterization of agglutinin-like sequence genes from non-*albicans Candida* and phylogenetic analysis of the *ALS* family. *Genetics* 157, 1555–1567.

Hoyer, L. L., Green, C. B., Oh, S.-H., and Hoyer, L. L. (2008). Discovering the secrets of the *Candida albicans* agglutinin-like sequence (*ALS*) gene family – a sticky pursuit. *Med. Mycol.* 46, 1–15. doi: 10.1080/13693780701435317

Hoyer, L. L., Payne, T. L., Bell, M., Myers, A. M., and Scherer, S. (1998a). *Candida albicans ALS3* and insights into the nature of the *ALS* gene family. *Curr. Genet.* 33, 451–459. doi: 10.1007/s002940050359

Hoyer, L. L., Payne, T. L., and Hecht, J. E. (1998b). Identification of *Candida albicans ALS2* and *ALS4* and localization of Als proteins to the fungal cell surface. *J. Bacteriol.* 180, 5334–5343. doi: 10.1128/JB.180.20.5334-5343.1998

Hoyer, L. L., Scherer, S., Shatzman, A. R., and Livi, G. P. (1995). *Candida albicans* ALS1: domains related to a *Saccharomyces cerevisiae* sexual agglutinin separated by a repeating motif. *Mol. Microbiol.* 15, 39–54. doi: 10.1111/j.1365-2958.1995.tb02219.x

Jackson, A. P., Gamble, J. A., Yeomans, T., Moran, G. P., Saunders, D., Harris, D., et al. (2009). Comparative genomics of the fungal pathogens *Candida dubliniensis* and *Candida albicans*. *Genome Res.* 19, 2231–2244. doi: 10.1101/gr.097501.109

Kalyaanamoorthy, S., Minh, B. Q., Wong, T. K. F., von Haeseler, A., and Jermiin, L. S. (2017). ModelFinder: fast model selection for accurate phylogenetic estimates. *Nat. Methods* 14, 587–589. doi: 10.1038/nmeth.4285

Koren, S., Walenz, B. P., Berlin, K., Miller, J. R., Bergman, N. H., and Phillippy, A. M. (2017). Canu: scalable and accurate long-read assembly via adaptive k-mer weighting and repeat separation. *Genome Res.* 27, 722–736. doi: 10.1101/gr.215087.116

Krachler, K. M., and Orth, K. (2013). Targeting the bacteria-host interface: strategies in anti-adhesion therapy. *Virulence* 4, 284–294. doi: 10.4161/viru.24606

Lackey, E., Vipulanandan, G., Childers, D. S., and Kadosh, D. (2013). Comparative evolution of morphological regulatory functions in *Candida* species. *Eukaryot. Cell* 12, 1356–1368. doi: 10.1128/EC.00164-13

Li, H. (2018). Minimap2: pairwise alignment for nucleotide sequences. *Bioinformatics* 34, 3094–3100. doi: 10.1093/bioinformatics/bty191

Lin, J., Oh, S.-H., Jones, R., Garnett, J. A., Salgado, P. S., Rushnakova, S., et al. (2014). The peptide-binding cavity is essential for Als3-mediated adhesion of *Candida albicans* to human cells. *J. Biol. Chem.* 289, 18401–18412. doi: 10.1074/jbc.M114.547877

Lohse, M. B., Gulati, M., Johnson, A. D., and Nobile, C. J. (2018). Development and regulation of single- and multi-species *Candida albicans* biofilms. *Nat. Rev. Microbiol.* 16, 19–31. doi: 10.1038/nrmicro/2017.107

Lombardi, L., Zoppo, M., Rizzato, C., Bottai, D., Hernandez, A. G., Hoyer, L. L., et al. (2019). Characterization of the *Candida orthopsilosis* agglutinin-like sequence (*ALS*) genes. *PLoS One* 14:e0215912. doi: 10.1371/journal.pone.0215912

Lu, C. F., Kurjan, J., and Lipke, P. N. (1994). A pathway for cell wall anchorage of *Saccharomyces cerevisiae* alpha-agglutinin. *Mol. Cell. Biol.* 14, 4825–4833. doi: 10.1128/MCB.14.7.4825

Maguire, S. L., ÓhÉigeartaigh, S. S., Byrne, K. P., Schröder, M. S., O'Gaora, P., Wolfe, K. H., et al. (2013). Comparative genome analysis, and gene finding in *Candida* species using CGOB. *Mol. Biol. Evol.* 30, 1281–1291. doi: 10.1093/molbev/mst042

Nguyen, L.-T., Schmidt, H. A., von Haeseler, A., and Minh, B. Q. (2015). IQ-TREE: a fast and effective stochastic algorithm for estimating maximum-likelihood phylogenies. *Mol. Biol. Evol.* 32, 268–274. doi: 10.1093/molbev/msu300

Nielsen, H. (2017). "Predicting secretory proteins with SignalP," in *Protein Function Prediction, Methods in Molecular Biology*, Vol. 1611, ed. D. Kihara (New York, NY: Humana Press), 59–73. doi: 10.1007/978-1-4939-7015-5_6

Oh, S.-H., Smith, B., Miller, A. N., Staker, B., Fields, C., Hernandez, A., et al. (2019). Agglutinin-like sequence (*ALS*) genes in the *Candida parapsilosis* species complex: blurring the boundaries between gene families that encode cell-wall proteins. *Front. Microbiol.* 10:781. doi: 10.3389/fmicb.2019.00781

Pei, J., Kim, B.-H., and Grishin, N. V. (2008). PROMALS3D: a tool for multiple protein sequence and structure alignments. *Nucleic Acids Res.* 36, 2295–2300. doi: 10.1093/nar/gkn072

Ronquist, F., Teslenko, M., van der Mark, P., Ayres, D. L., Darling, A., Höhna, S., et al. (2012). MrBayes 3.2*:* efficient Bayesian phylogenetic inference and model choice across a large model space. *Syst. Biol.* 61, 539–542. doi: 10.1093/sysbio/sys029

Senol Cali, D., Kim, J. S., Ghose, S., Alkan, C., and Mutlu, O. (2018). Nanopore sequencing technology and tools for genome assembly: computational analysis of the current state, bottlenecks and future directions. *Brief. Bioinform.* 20, 1542–1559. doi: 10.1093/bib/bby017

Sherman, F., Fink, G. R., and Hicks, J. B. (1986). *Laboratory Course Manual for Methods in Yeast Genetics*. Cold Spring Harbor, NY: Cold Spring Harbor Press.

Walker, B. J., Abeel, T., Shea, T., Priest, M., Abouelliel, A., Sakthikumar, S., et al. (2014). Pilon: an integrated tool for comprehensive microbial variant detection and genome assembly improvement. *PLoS One* 9:e112963. doi: 10.1371/journal.pone.0112963

White, T. J., Bruns, T., Lee, S., and Taylor, J. (1990). "Amplification and direct sequencing of fungi ribosomal RNA genes for phylogenetics," in *PCR Protocols. A Guide to Methods and Applications*, eds M. A. Innis, D. H. Gelfand, J. J. Sninsky, and T. J. White (San Diego, CA: Academic Press), 315–322. doi: 10.1016/b978-0-12-372180-8.50042-1

Wick, R. R., Judd, L. M., Gorrie, C. L., and Holt, K. E. (2017). Completing bacterial genome assemblies with multiplex MinION sequencing. *Microb. Genom.* 3:e000132. doi: 10.1099/mgen.0.000132

Yu, S., Li, W., Liu, X., Che, J., Wu, Y., and Lu, J. (2016). Distinct expression levels of *ALS*, *LIP*, and *SAP* genes in *Candida tropicalis* with diverse virulent activities. *Front. Microbiol.* 7:1175. doi: 10.3389/fmicb.2016.01175

Zhang, L.-J., Yu, S.-B., Li, W.-G., Zhang, W.-Z., Wu, Y., and Lu, J.-X. (2019). Polymorphism analysis of virulence-related genes among *Candida tropicalis* isolates. *Chinese Med. J.* 132, 446–453. doi: 10.1097/CM9.0000000000000069

Zhang, N., Harrex, A. L., Holland, B. R., Fenton, L., Cannon, R. D., and Schmid, J. (2003). Sixty alleles of the *ALS7* open reading frame in *Candida albicans*: *ALS7* is a hypermutable contingency locus. *Genome Res.* 13, 2005–2017. doi: 10.1101/gr.1024903

Zhao, X., Oh, S.-H., Cheng, G., Green, C. B., Nuessen, J. A., Yeater, K., et al. (2004). *ALS3* and *ALS8* represent a single locus that encodes a *Candida albicans* adhesin; functional comparisons between Als3p and Als1p. *Microbiology* 150, 2415–2428. doi: 10.1099/mic.0.26943-0

Zhao, X., Oh, S.-H., Coleman, D. A., and Hoyer, L. L. (2011). *ALS51*, a newly discovered gene in the *Candida albicans ALS* family, created by intergenic recombination: analysis of the gene and protein, and implications for evolution of microbial gene families. *FEMS Immunol. Med. Microbiol.* 61, 245–257. doi: 10.1111/j.1574-695X.2010.00769.x

Zhao, X., Oh, S.-H., and Hoyer, L. L. (2007). Unequal contributions of *ALS9* alleles to adhesion between *Candida albicans* and human vascular endothelial cells. *Microbiology* 153, 2342–2350. doi: 10.1099/mic.0.2006/005017-0

Conflict of Interest: The authors declare that the research was conducted in the absence of any commercial or financial relationships that could be construed as a potential conflict of interest.

frontiers in Fungal Biology

ORIGINAL RESEARCH
published: 10 February 2021
doi: 10.3389/ffunb.2021.643537

Dexamethasone and Methylprednisolone Promote Cell Proliferation, Capsule Enlargement, and *in vivo* Dissemination of *C. neoformans*

*Glauber R. de S. Araújo [1,2], Vinicius Alves [1,2], Pedro H. Martins-de-Souza [1,2], Allan J. Guimarães [3], Leandro Honorato [4], Leonardo Nimrichter [4], Christina Maeda Takiya [5], Bruno Pontes [6,7] and Susana Frases [1,2]**

[1] Laboratório de Ultraestrutura Cellular Hertha Meyer, Instituto de Biofísica Carlos Chagas Filho, Universidade Federal Do Rio de Janeiro, Rio de Janeiro, Brazil, [2] Laboratório de Biofísica de Fungos, Instituto de Biofísica Carlos Chagas Filho, Universidade Federal Do Rio de Janeiro, Rio de Janeiro, Brazil, [3] Laboratório de Bioquímica e Imunologia das Micoses, Depto. de Microbiologia e Parasitologia, Instituto Biomédico, Universidade Federal Fluminense, Niterói, Brazil, [4] Instituto de Microbiologia Paulo de Góes, Universidade Federal Do Rio de Janeiro, Rio de Janeiro, Brazil, [5] Laboratório de Imunopatologia. Instituto de Biofísica Carlos Chagas Filho, Universidade Federal Do Rio de Janeiro, Rio de Janeiro, Brazil, [6] Instituto de Ciências Biomédicas, Universidade Federal Do Rio de Janeiro, Rio de Janeiro, Brazil, [7] Centro Nacional de Biologia Estrutural e Bioimagem (CENABIO), Universidade Federal Do Rio de Janeiro, Rio de Janeiro, Brazil

OPEN ACCESS

Edited by:
Marcos Sergio Toledo, Federal University of São Paulo, Brazil

Reviewed by:
José Ascención Martínez-Álvarez, University of Guanajuato, Mexico
Kevin K. Fuller, University of Oklahoma Health Sciences Center, United States

***Correspondence:**
Susana Frases
susanafrases@biof.ufrj.br

Specialty section:
This article was submitted to Fungal Physiology and Metabolism, a section of the journal Frontiers in Fungal Biology

Received: *18 December 2020*
Accepted: *19 January 2021*
Published: *10 February 2021*

Citation:
Araújo GRS, Alves V, Martins-de-Souza PH, Guimarães AJ, Honorato L, Nimrichter L, Takiya CM, Pontes B and Frases S (2021) Dexamethasone and Methylprednisolone Promote Cell Proliferation, Capsule Enlargement, and in vivo Dissemination of C. neoformans. Front. Fungal Biol. 2:643537. doi: 10.3389/ffunb.2021.643537

Cryptococcus neoformans is a fungal pathogen that causes life-threatening infections in immunocompromised individuals, who often have some inflammatory condition and, therefore, end up using glucocorticoids, such as dexamethasone and methylprednisolone. Although the effects of this class of molecules during cryptococcosis have been investigated, their consequences for the biology of *C. neoformans* is less explored. Here, we studied the effects of dexamethasone and methylprednisolone on the metabolism and on the induction of virulence factors in *C. neoformans*. Our results showed that both glucocorticoids increased fungal cell proliferation and surface electronegativity but reduced capsule and secreted polysaccharide sizes, as well as capsule compaction, by decreasing the density of polysaccharide fibers. We also tested whether glucocorticoids could affect the fungal virulence in *Galleria mellonella* and mice. Although the survival rate of *Galleria* larvae increased, those from mice showed a tendency to decrease, with infected animals dying earlier after glucocorticoid treatments. The pathogenesis of spread of cryptococcosis and the interleukin secretion pattern were also assessed for lungs and brains of infected mice. While increases in the spread of the fungus to lungs were observed after treatment with glucocorticoids, a significant difference in brain was observed only for methylprednisolone, although a trend toward increasing was also observed for dexamethasone. Moreover, increases in both pulmonary and cerebral IL-10 production, reduction of IL-6 production but no changes in IL-4, IL-17, and INF-γ were also observed after glucocorticoid treatments. Finally, histopathological analysis confirmed the increase in number of fungal cells in lung and brain tissues of mice previously subjected to dexamethasone or methylprednisolone treatments. Together, our results provide compelling evidence for the effects of

dexamethasone and methylprednisolone on the biology of *C. neoformans* and may have important implications for future clinical treatments, calling attention to the risks of using these glucocorticoids against cryptococcosis or in immunocompromised individuals.

Keywords: *Cryptococcus neoformans*, glucocorticosteroids, methylprednisolone, dexamethasone, immune reconstitution inflammatory syndrome (IRIS), fungal virulence, capsule, polysaccharide

INTRODUCTION

Fungal infections that cause systemic mycoses have become a major threat since the end of the 20th century. Although fungal infections are underreported or undetected due to limitations in the differential diagnosis (Perfect, 2013), the rise in number of fungal infections is closely associated with a significant increase in immunocompromised patients due to glucocorticoid therapy, immunotherapy, oncological and hematological diseases, transplants, surgical procedures and acquired immunodeficiency syndrome (AIDS), among others (Singh et al., 2008; Henao-Martínez and Beckham, 2015; Liao et al., 2016). In addition, factors such as extremes of age and prolonged exposure to antimicrobial therapies are also associated with high rates of human fungal infections. An epidemiological study carried out in the United States revealed that in the period between 1979 and 2000, there was a striking 207% annual increase in sepsis caused by fungi (Martin et al., 2003).

Currently, emerging viruses like the pandemic SARS-CoV-2, which causes Coronavirus Disease 2019 (COVID-19), alert doctors to the possibility of increased co-infections associated with the physiological impairment of COVID-19 patients and its clinical management (Segrelles-Calvo et al., 2020c). The SARS-CoV-2 infection is characterized by an increase in pro-inflammatory cytokines and a decrease in anti-inflammatory cytokines, resulting in a state of cytokine storm syndrome. Recent studies have shown that the use of dexamethasone has reduced inflammation and the period of invasive mechanical ventilation and hospital mortality in severe COVID-19 patients (Sterne et al., 2020). However, the use of corticosteroids is a risk factor widely studied for the development of invasive mycoses in critically ill patients (Sinha et al., 2020). Although there is still not enough published statistical data, fungal co-infections in COVID-19 patients are present in a significant number of hospitalized individuals, leading to serious complications or even death. Co-infections have been described for *Aspergillus* spp. (Segrelles-Calvo et al., 2020b), *Trichosporon asahii* (Segrelles-Calvo et al., 2020a), *Candida* spp. (Al-Hatmi et al., 2020), and *Cryptococcus* spp. (Passerini et al., 2020).

Among the vast fungal species that cause systemic mycoses in humans, *Cryptococcus* spp., of which *Cryptococcus neoformans* and *Cryptococcus gattii* are the main representative of the genus, is capable of causing cryptococcosis, a disease with 223,100 clinical cases per year and approximately 181,000 deaths (Rajasingham et al., 2017; Williamson et al., 2017). The high rates of incidence and mortality caused by fungal infections, especially cryptococcosis, associated with the absence of an efficient therapy, have led to the search for novel diagnostic and therapeutic alternatives to control these diseases (Prado et al., 2009; Kronstad et al., 2012; Chen et al., 2014).

Cryptococcus spp. is a basidiomycete that presents itself as a haploid and spherical yeast surrounded by a polysaccharide (PS) capsule, a unique feature among eukaryotes (McFadden et al., 2006). Infection with *Cryptococcus* spp. is acquired through inhalation of dried spores or yeasts (Ellis and Pfeiffer, 1990). The lungs, therefore, acts as the primary site of infection (Barbosa et al., 2006). After the fungus enters the host's alveolar epithelium, the infection can take the latent form or manifest itself as the acute form of the disease (Goldman et al., 2010). The successful spread of the pathogen is due to the evasion capacity of the host's immune system, benefited by several mechanisms of adaptation, such as the production of a capsule, titan cells, melanin and urease, among others (Kronstad et al., 2012; Zaragoza, 2019).

Cryptococcus spp. manages to easily deceive the immune system in a human host with some degree of immunosuppression. After the establishment of pulmonary infection, the fungus reaches the lung parenchyma and subsequently the bloodstream, causing systemic infections with damage to various anatomical sites, such as skin, bones, eyes, prostate and/or genitourinary tract (Casadevall and Perfect, 1998). However, the main scenario of cryptococcosis is the colonization of the Central Nervous System (CNS) (Mitchell and Perfect, 1995; Mitchell et al., 1995), considered the most advanced and lethal manifestation of the disease.

The Willis polygon, a set of cerebral arteries that vascularizes the CNS, plays a crucial role in the spread of the fungus. The medium-sized cerebral arteries branch into smaller pial and arterioles arteries that run along the surface of the brain. The pial arteries are surrounded by smooth muscle, a layer of endothelial cells and an outer layer of leptomeningeal cells (Chang et al., 2004; Franco-Paredes et al., 2017). The Virchow-Robin space surrounds the walls of arteries, arterioles, veins, and venules as they flow from the subarachnoid space and, when penetrating the cerebral parenchyma, plays an important role in draining interstitial fluid (Zhang et al., 1990). *Cryptococcus* spp. colonizes the cerebrospinal fluid (CSF), in the perivascular spaces and in the brain parenchyma via transcellular crossing of the endothelial cells of the blood-brain barrier (BBB), but without affecting the integrity of the latter. Other strategies used by *Cryptococcus* spp. to enter the CNS is the use of mononuclear cells in the process known as "Trojan horse" where fungi pass through the BBB within infected phagocytes or cause the endothelial cell junctions in the BBB to rupture, allowing the passage of free fungi (Chen et al., 2003; Chang et al., 2004; Jong et al., 2008; Charlier et al., 2009; Casadevall, 2010; Dromer and Levitz, 2010; Vu et al., 2013; Santiago-Tirado et al., 2017; Zaragoza, 2019).

After reaching the CNS, *Cryptococcus* spp. can promote two distinct clinical manifestations and both are potentially fatal: (I) cryptococcal meningoencephalitis or parenchymal presentations in the context of advanced immunosuppression, the most common infection of the CNS, and (II) *cryptococcus*-related Immune Reconstitution Inflammatory Syndrome (IRIS), that occurs after the initiation of highly active antiretroviral therapies (Del Valle and Piña-Oviedo, 2006).

Cryptococcal IRIS is well-characterized in HIV-infected patients and is associated with significant rates of morbidity and mortality. In addition, Cryptococcal IRIS is estimated to occur between 5 and 11% in patients who received organ transplantation with cryptococcal infection and is associated with the increased risks of allograft failure (Morrison et al., 1994; Patterson, 1999). The clinical characteristics of cryptococcal IRIS are similar to the active cryptococcal infection itself, occurring more commonly as a CNS disease, with meningeal disease as the most serious presentation. Furthermore, lymphadenitis, pneumonitis, soft tissue involvement and, mediastinitis have also been reported. A differential diagnosis is the appearance of necrotic granulomatous inflammation with the presence of yeasts in histopathological analysis. Despite changes in inflammatory markers, there are no specific reliable tests for cryptococcal IRIS thus, establishing the diagnosis is a considerable clinical challenge, especially because of atypical presentations (Maziarz and Perfect, 2016).

Given the high frequency of glucocorticoid use in the clinic, when the patient has an inflammatory condition without a proper microbiological diagnosis, it becomes necessary to better evaluate the effects of this class of molecules during fungal infections. Glucocorticoids have shown short-term improvement in quality of life for patients with Cryptococcal IRIS due to their anti-inflammatory activity, thus apparently decreasing the need for hospitalization. However, they should not be used to prevent IRIS or to control intracranial pressure, since studies have associated their use with patients' death, although the causes of high mortality are not yet fully understood (Kuwahara et al., 2014; Beardsley et al., 2016). Some immunosuppressive characteristics induced by glucocorticoids are already known in cryptococcosis. For example, cortisone acetate has been shown to decrease the ability of alveolar macrophages to phagocytize *C. neoformans*, potentially leading to the spread of fungi in the bloodstream (Gross et al., 1996). Likewise, it substantially reduces the chemotactic activity of polymorphonuclear cells (PMNs) and monocytes in the cerebrospinal fluid, thus contributing to the subsequent inability to eradicate fungi with tropism to the CNS (Granger et al., 1985; Perfect and Durack, 1985a). Perfect and collaborators (Perfect et al., 1983) showed that glucocorticoids represent a high risk of cryptococcemia. Although some of the effects of these drugs on the host's immune system have been studied, little is known about the effect of corticosteroids on the metabolism and on the induction of virulence factors in *Cryptococcus* spp.

In the present work, we combined morphological and physicochemical characterization of *C. neoformans* capsular and its secreted PS together with histopathological analysis, survival curves, and interleukin modulation, to investigate the effects of dexamethasone (DX) or methylprednisolone (MP) on the metabolism and on the induction of virulence factors in *C. neoformans*. Our aim was to collect experimental evidence that provide a basis for future clinical administration of glucocorticoids in patients with cryptococcosis.

RESULTS

Dexamethasone and Methylprednisolone Increase *C. neoformans* Proliferation and Surface Electronegativity but Reduce Capsule and Secreted PS Sizes

To analyze the effects of glucocorticoids on *C. neoformans*, yeast cells were allowed to grow in minimal media supplemented with different concentrations (10, 20, 50, and 100 μg/mL) of DX or MP for 3, 5, and 7 days (**Figure 1**). Cell proliferation, capsule size and electronegativity of the cell surface were evaluated.

The analyses of yeast cells grown in minimal media supplemented with different DX or MP concentrations showed an increase in *C. neoformans* proliferation when compared to control conditions, without the glucocorticoids (**Figures 1A,D**, respectively). This effect was more pronounced for DX. On day 3 of culture with DX, there was a significant increase in the number of cells for all tested concentrations (**Figure 1A**). For MP, the effect was slower, and the differences only began to be visualized after 5 days of treatment (**Figure 1D**).

Both DX and MP treatments induced a reduction in *C. neoformans* capsule size when compared to the controls, without glucocorticoids (**Figures 1B,E**). However, DX again showed stronger effects when compared to MP. A significant reduction in capsule size was observed at the day 3 with concentrations higher than 20 μg/mL of DX and became more pronounced as the length of treatment and DX concentration increased (**Figure 1B**). On the other hand, MP effects occurred more smoothly and upon 5 days of culture, where reductions in capsule size for all concentrations of glucocorticoids were observed (**Figure 1E**). It is worth mentioning that there was a slight increase in capsule size on day 3 and with 50 and 100 μg/mL of MP; however, this increase was reversed after day 5 onwards.

Changes in electronegativity of the cell surface were evaluated through Zeta potential analysis. Again, both DX and MP treatments showed increases in the surface electronegativity when compared to their respective controls (**Figures 1C,F**). For DX treatments, the Zeta potentials were more negative than the control from day 5 onwards and became more pronounced as the DX continued up to day 7 (**Figure 1C**). For MP treatments, the effects on Zeta potential slightly changed from the third day of cultivation; however, it became more pronounced on day 7 (**Figure 1F**).

In order to evaluate the effect of both DX and MP glucocorticoids on *C. neoformans* secreted PS, we next decided to limit our observations on the concentrations of 50 μg/mL (**Figure 2**). We first measured the rate of PS production (total amount of secreted PS divided by the number of cells in culture). Control cells showed a production rate of 1.8 ng/cell. However, rates of 0.58 ng/cell and 1.1 ng/cell

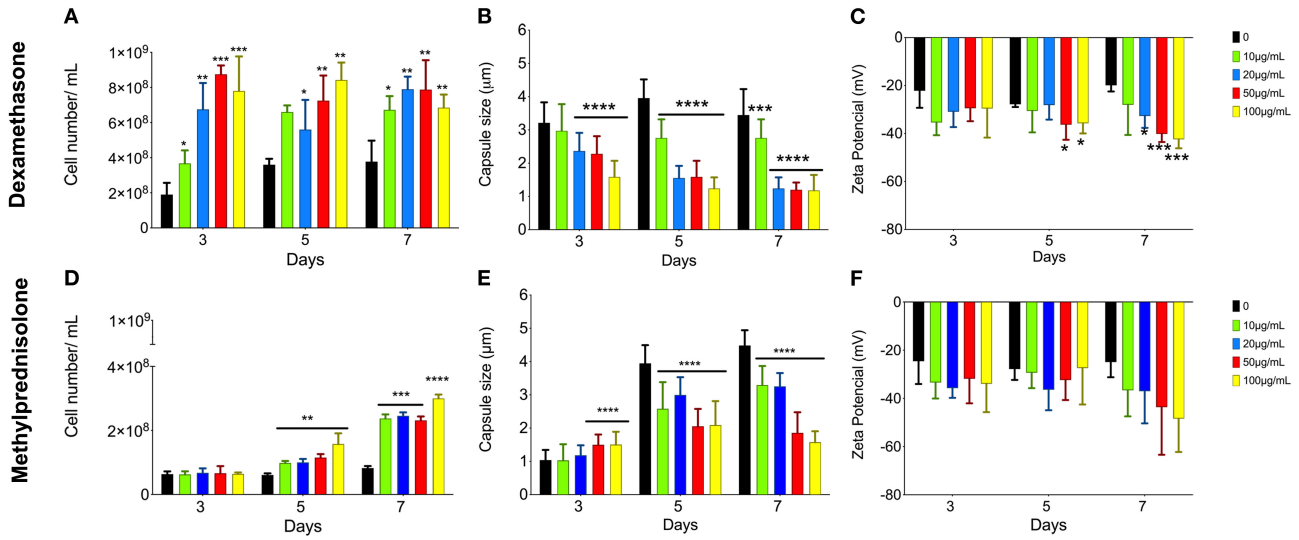

FIGURE 1 | Effect of glucocorticoids on *C. neoformans* in growth, capsule size and Zeta potential (ξ). Yeast cells were grown in minimal media with 10 (green bars), 20 (blue bars), 50 (red bars), and 100 (yellow bars) μg/mL of dexamethasone **(A–C)** or methylprednisolone **(D–F)** for 3, 5, and 7 days. *$p < 0.1$; **$p < 0.01$; ***$p < 0.001$; ****$p < 0.0001$.

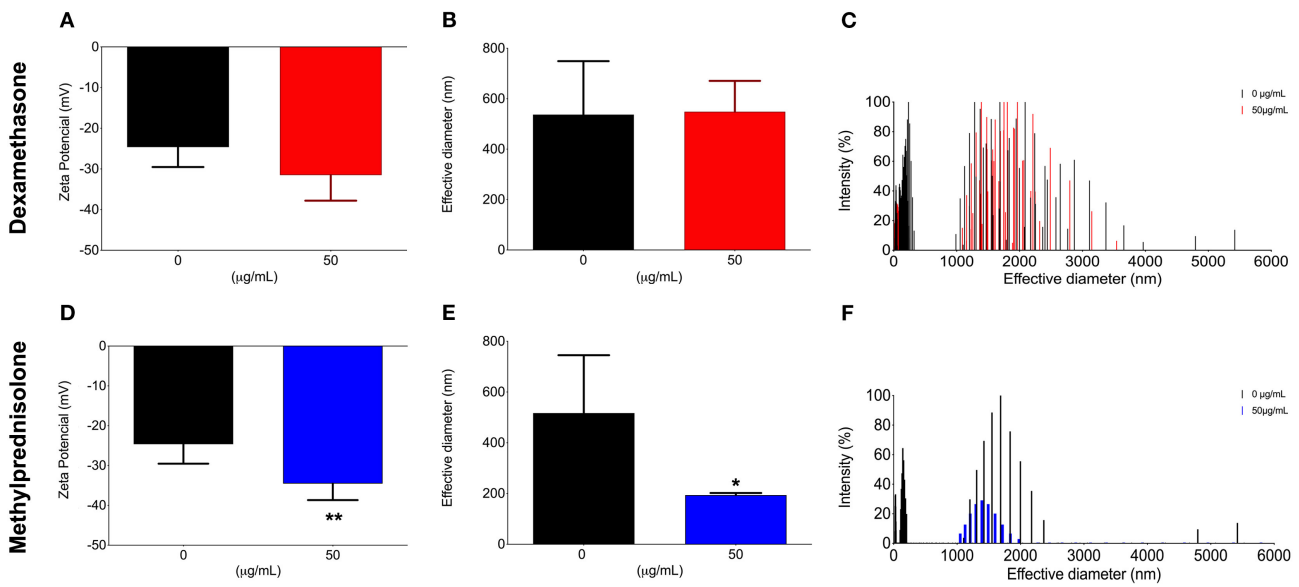

FIGURE 2 | Effect of glucocorticoids on *C. neoformans* secreted polysaccharide I. Yeast cells were grown in medium minimum without corticoids (black bars, control) or 50 μg/mL of dexamethasone (**A–C**—red bars) or methylprednisolone (**D–F**—blue bars) for 3, 5, and, 7 days. *$p < 0.1$; **$p < 0.01$.

were obtained after treatments with 50 μg/mL of DX and MP, respectively. Surprisingly, the secreted PSs did not undergo significant changes in their electronegativities or in their sizes after treatment with DX (**Figures 2A–C**). In contrast, MP produced a significant change in the electronegativity of PS fibers (**Figure 2D**) and presented fibers with sizes 2.6-times smaller in terms of effective diameter than the secreted PS from control condition (**Figures 2E,F**).

Dexamethasone and Methylprednisolone Decrease the Compactness of PS Fibers of *C. neoformans* Capsule

Next, to observe possible changes in the ultrastructure of *C. neoformans* PS capsule, control cells or those treated with either DX or MP were processed and visualized by scanning electron microscopy (SEM) (**Figure 3**). Control cells presented more compact capsules, with a denser network of polysaccharides.

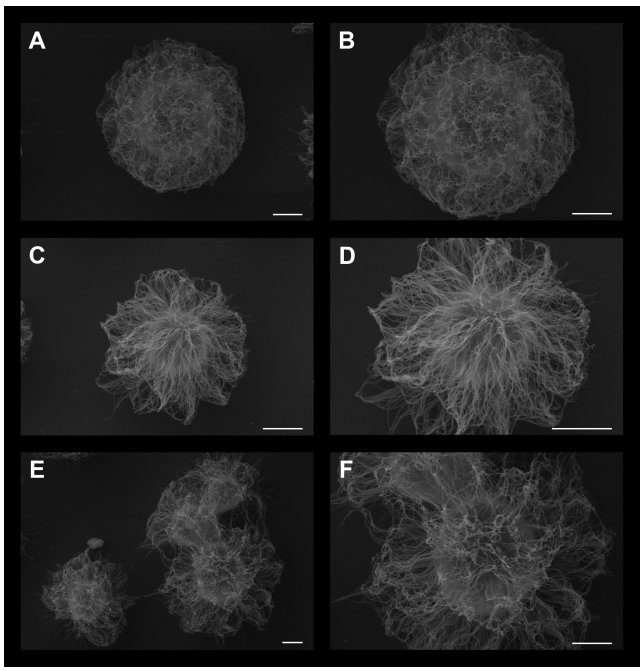

FIGURE 3 | Scanning electron microscopy of *C. neoformans* grown in the presence of 50 μg/mL dexamethasone **(C,D)** or 50 μg/mL methylprednisolone (E and F panel). Control cells without treatment are presented in **(A,B)**. Scale bar: **(A,C,E)** 2 μm; **(B,D,F)** 1 μm.

Conversely, cells treated with DX (**Figures 3C,D**) or MP (**Figures 3E,F**) showed a loosened arrangement of the polysaccharide chains. This different feature allows the India ink to better penetrate in-between the empty spaces surrounding the PS fibers of both DX and MP conditions when compared to the control, thus explaining the apparent differences in capsule sizes shown in **Figure 1**.

Dexamethasone and Methylprednisolone Increase the Survival Rate of *Galleria mellonella* Larvae Infected With *C. neoformans*

To assess possible influences on the virulence of *C. neoformans* after treatments with either DX or MP, we utilized the invertebrate host *G. mellonella*. This model has been used to study not only *C. neoformans* virulence but also the action of antifungals against this pathogen (Araujo et al., 2012; Araújo et al., 2017). All infected and untreated larvae died by day 8 upon infection (**Figure 4**). However, infected larvae previously injected with either DX or MP showed an overall prolongation on survival, with all subjects dying at day 10 and day 9, respectively, for DX (Square pictograms in red) and MP (Blue triangles pictograms), with significant differences in survival rates between treated groups and their respective controls.

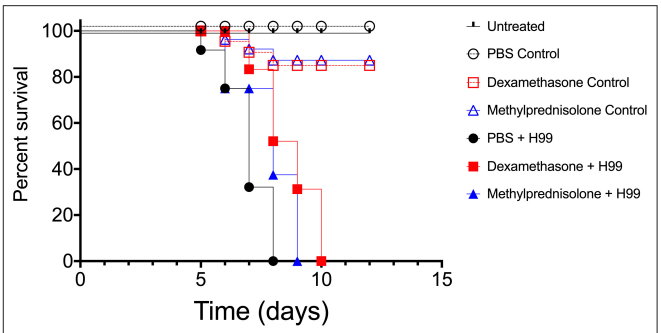

FIGURE 4 | Infection model of *Galleria mellonella*. Survival curves of *G. mellonella* larvae infected with *C. neoformans* and treated with dexamethasone (DX–red square pictogram) our methylprednisolone (MP–blue triangle pictogram). Logrank and Gehan-Breslow-Wilcoxon tests $p < 0.1$ between filled black circles and filled blue triangles groups. $p < 0.01$ between filled black circles and filled red squares groups.

Effects of Dexamethasone and Methylprednisolone on the Survival, Spread, and on Changes in the Pattern of Cytokines in Mice Infected With *C. neoformans*

Given the high frequency of glucocorticoid use in the clinic, when the patient has an inflammatory condition without a proper microbiological diagnosis, we next decided to investigate the pattern of *C. neoformans* infection in mice by following infected animals undergoing treatment with either DX or MP without any administration of associated antifungals. First, we tested whether DX or MP treatments could provide protection against infection by *C. neoformans*. Balb/C mice were treated with either DX or MP to later be infected with *C. neoformans* or treated with PBS, as a control. We observed that control mice (PBS, MP, and DX) maintained 100% survival after day 60 (**Figure 5**). Infection with *C. neoformans* (without DX or MP) led to the death of all animals on day 39 after infection (**Figure 5**). For infected mice that were treated with either DX or MP, the death of all animals occurred on days 38 and 37, respectively (**Figure 5**). Although statistical analysis did not show significant differences between the groups, infected animals treated with either DX or MP started to die earlier than the untreated animals, especially DX, indicating a possible change in the modulation of the infection.

Subsequently, we tested whether the *in vivo* administration of either DX or MP could alter the pathogenesis of the spread of cryptococcosis. In our model, the fungus spread was evaluated after 5 and 7 days of infection. On day 5, mice that received the DX treatment showed similar numbers of lung colony forming units (CFUs) as those from the control (**Figure 6A**, $4.3 \pm 2.5 \times 10^5$ vs. $7.9 \pm 4.4 \times 10^5$ CFUxg^{-1}, respectively). A similar behavior was observed for cerebral CFUs and its control (**Figure 6B**, 0.0 ± 0.0; 4.0 ± 7.5 CFUxg^{-1}, respectively). However, infected mice that received the MP treatment presented lung CFUs significantly different from its control (**Figure 6A**, $1.4 \pm 0.4 \times 10^6$ vs. $7.9 \pm 4.4 \times 10^5$ CFUxg^{-1}, respectively—p= 0.0342) but no difference was observed between the cerebral CFU

of MP treatment and its control (**Figure 6B**, 13.6 ± 21.5; 4.0 ± 7.5 $CFUxg^{-1}$, respectively).

On day 7 after infection, the mice that received the DX treatment showed lung CFUs significantly larger than its control (**Figure 6C**, $5.5 \pm 1.6 \times 10^6$ vs. $1.3 \pm 0.5 \times 10^6$ CFU/g^{-1}, respectively) but no significant difference between cerebral CFUs and its control (**Figure 6D**, $1.2 \pm 0.8 \times 10^3$ vs. $1.2 \pm 0.1 \times 10^3$ $CFUxg^{-1}$, respectively). In turn, mice that received MP treatment demonstrated lung CFUs significantly higher than control (**Figure 6C**, $5.1 \pm 1.9 \times 10^6$ vs. $1.3 \pm 0.5 \times 10^6$ $CFUxg^{-1}$, respectively). MP treatment also significantly increased cerebral CFUs compared to its control, (**Figure 6D**, $5.4 \pm 3.3 \times 10^4$ vs. $1.2 \pm 0.1 \times 10^3$ $CFUxg^{-1}$, respectively).

To investigate the secretion pattern of different immune system modulators (IL-10, IL-4, INF-γ; IL-6 and IL-17), the lungs and brain homogenates of either control or infected mice were analyzed after 7 days of infection (**Figure 7**). The mice that received the selected doses of DX or MP showed a statistically significant increase in pulmonary and cerebral IL-10 production when compared to the controls (**Figure 7**), whereas the IL-4 and IL-17 levels in either lungs and brains did not show significant differences among groups. Moreover, when the anti-inflammatory IL-6 was followed, we observed that both DX and MP treatments induced a drastic reduction in its pulmonary and cerebral levels (**Figure 7**). For the pro-inflammatory INF-γ however, no significant differences were noticed among controls, DX or MP treatments in lungs and brains (**Figure 7**).

To corroborate and also to better visualize the inflammatory changes and the presence of fungal cells in the lung and brain after 7 days of infection, samples of these organs were preserved and stained with mucicarmine (**Figure 8**). The presence of inflammatory cells was visualized in lung tissues of mice infected with *C. neoformans* cells, with presence of few yeasts (**Figure 8A**). Contrarily, the mice treated with either DX or MP showed a reduction of inflammatory cells but a strong increase in the number of encapsulated fungal cells (**Figures 8B,C**, respectively).

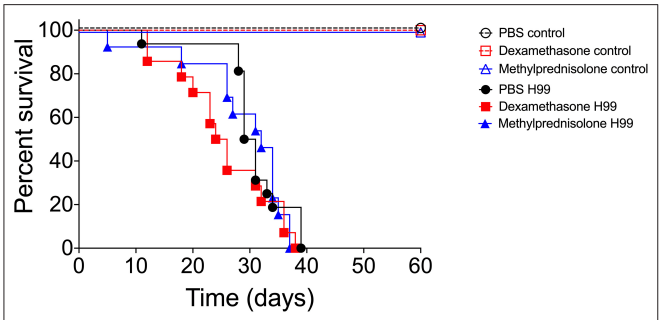

FIGURE 5 | Infection model of Balb/c mice. Pictograms: black opened circle, red opened square, and blue opened triangle lines are controls. Black closed circle lines represented mice infected with *C. neoformans*; red closed square lines are mice infected with *C. neoformans* and treated with DX; blue closed triangle lines are mice infected with *C. neoformans* and treated with MP.

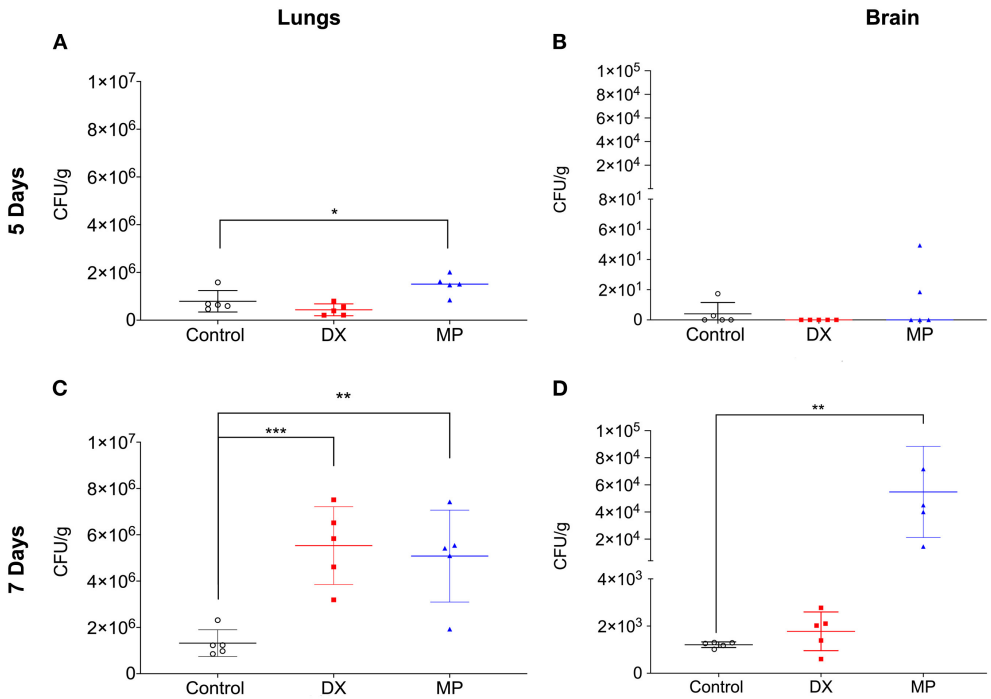

FIGURE 6 | Colony-forming units (CFU) in the lungs **(A,C)** and brain **(B,D)** of Balb/c mice. DX represented mice infected with *C. neoformans* and treated with dexamethasone (DX; MP are mice infected with *C. neoformans* and treated with methylprednisolone (MP). CFU were analyzed after five **(A,B)** and seven **(C,D)** days of infection. *$p < 0.1$; **$p < 0.01$; ***$p < 0.001$.

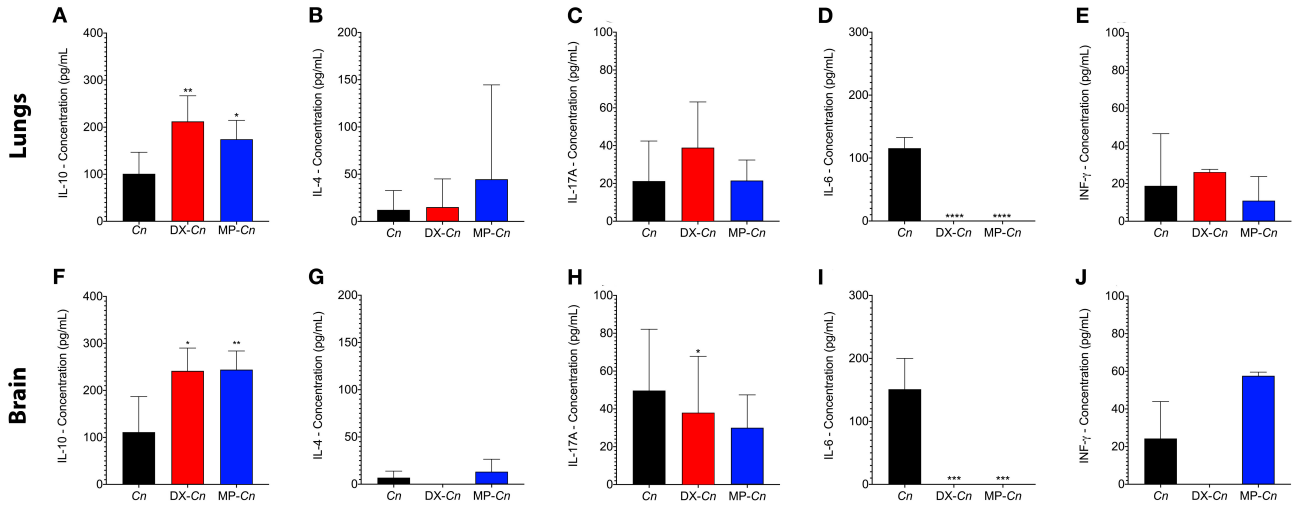

FIGURE 7 | Comparisons of expressions of IL-4, IL-10, IL-17A, IL6, and INF- γ in lungs and brain of animals treated with dexamethasone (DX) and methylprednisolone (MP) at 7-days post infection. Cn: *C. neoformans* control; DX-CN: *C. neoformans* treated with DX; MP-Cn: *C. neoformans* treated with MP. $^{*}p < 0.1$, $^{**}p < 0.01$, $^{***}p < 0.001$, and $^{****}p < 0.0001$.

For brain tissues, both the control group and those mice treated with DX presented a great number of inflammatory cells and few yeast elements (**Figures 8D,E**). However, the mice treated with MP showed a fair reduction in the number of inflammatory cells and an intense increase in number of fungal cells (**Figure 8F**).

DISCUSSION

Cryptococcosis is an important systemic fungal disease, threatening the lives of humans and other animals, predominantly due to pulmonary and CNS alterations. It usually affects immunocompromised individuals, mainly those with HIV, presenting itself as an opportunistic infection, although other predisposing conditions have been described, including treatment with immunosuppressants, organ transplants, lymphoproliferative disorders and, neoplasms (Mitchell and Perfect, 1995; Perfect and Casadevall, 2002). Estimates show that almost 45% of seropositive individuals in advanced immunosuppression stages succumb as a result of cryptococcosis (Clumeck et al., 1984; Van De Perre et al., 1984; Park et al., 2009; Rajasingham et al., 2017). In a recent demographic study among the population of South Africa, individuals who received antiretroviral treatment had rates of Cryptococcus infection of 95 cases/100,000 inhabitants while individuals with advanced immunosuppression had about a 10 times higher prevalence (McCarthy et al., 2006).

The main manifestations of cryptococcosis include respiratory infections, since the lungs are the agent's first entrance into the host, through the inhalation of propagules present in the environment in the form of dehydrated yeasts, while the CNS is the destination due to the fungus neurotropism (Galanis et al., 2010). In lungs, cryptococcosis varies from a simple colonization of the airways in asymptomatic patients to an acute respiratory distress syndrome with severe respiratory failure, in patients with deficiency in cellular immunity (Henson and Ross Hill, 1984; Vilchez et al., 2001). In the CNS, cryptococcosis shows well-known manifestations of meningitis and meningoencephalitis, and its evolution is generally subacute or chronic (Graybill et al., 2000). Although some HIV patients present minor symptoms due to a high degree of immunosuppression; this does not reduce the high morbidity and mortality of the disease (Perfect and Casadevall, 2002).

Moreover, when a patient has an inflammatory condition, without a known infection, the administration of glucocorticoids is quite common. However, the effects of these molecules during cryptococcosis have been investigated. For example, cortisone acetate has been shown to decrease the ability of alveolar macrophages to bind and ingest *C. neoformans*, potentially leading to the spread of fungi in the bloodstream (Gross et al., 1996). Previous clinical work has shown that glucocorticoids represent a high risk of cryptococcemia. In addition, glucocorticoids predispose patients with cancer or sarcoidosis and recipients of allogeneic bone marrow and solid organ transplants to cryptococcosis. The administration of glucocorticoids reduces the chemotactic activity of cerebrospinal fluid in relation to polymorphonuclear leukocytes (PMNs) and monocytes (Perfect and Durack, 1985b). This factor may contribute to the significant lack of influx of PMN into the cerebrospinal fluid and subsequent inability to eradicate fungi with tropism in the CNS, such as *C neoformans*. Such attenuation is further intensified by abnormalities induced by glucocorticoids in microglial cells. Glucocorticoids are also a critical factor for the outcome of this infection. Diamond and Bennet reported that recurrences of cryptococcal meningitis were associated with the maintenance of glucocorticoid treatment, in addition to the termination of antifungal therapy (Diamond, 1974).

Although some effects of glucocorticoids on the clinic are already known, their effects on the metabolism and induction of

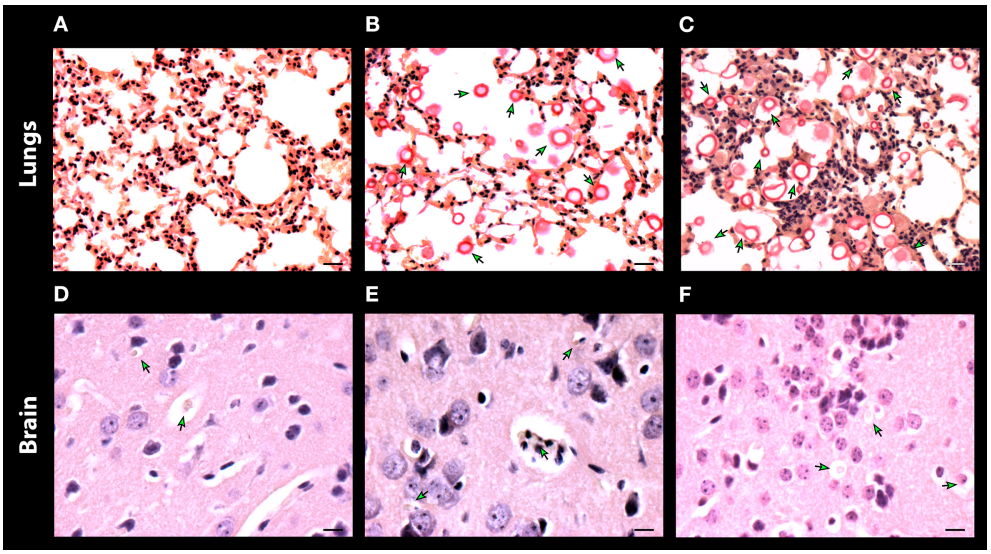

FIGURE 8 | Histopathology of lungs **(A–C)** and, brain **(D–F)** of mice infected with *C. neoformans*. Control without treatment **(A,D)** and treated with dexamethasone **(B,E)** and methylprednisolone **(C,F)**. Scale bar 10 μm.

virulence factors in *Cryptococcus neoformans* were less studied. Herein, we observed how *C. neoformans* cells behave after being in contact with either DX or MP, particularly focusing on the biological aspects of this fungus. We demonstrated that all the used concentrations of either DX and MP induced an increase in cell proliferation of *C. neoformans*, but the effect was more prominent for DX than for MP. In addition, either DX and MP treatments induced an apparent reduction in *C. neoformans* capsule size when compared to the control. Deeper observations using scanning electron microscopy showed that these reductions were probably correlated to modifications in PS fiber morphology, that changed from denser and more compacted capsules in control condition, to capsules with more sparse PS fibers under DX and MP treatments, therefore possibly allowing greater penetration of India ink, which gave the apparent impression of smaller capsule size. Indeed, differences in capsule ultrastructural morphology were recently described using scanning electron microscopy (Lopes et al., 2020). Although the study from Lopes et al. showed that several capsule morphologies are present in the same population, we conjecture that a global change in phenotype, tending to one of the morphologies could occur after a population is confronted with a specific external agent, for example, the glucocorticoids used in our present study. However, it remains to be investigated how these possible variations affect *C. neoformans* virulence as well as the clinical symptoms.

We also observed a reduction in *C. neoformans* PS production, from 1.8 ng/cell in control to 0.58 ng/cell after DX treatment. Surprisingly, these secreted PSs did not undergo significant changes in electronegativity and the polysaccharide fibers dimension remained unaltered. In contrast, the MP treatment did not induce a significant change in PS production but showed significant alterations in the electronegativity of secreted PS, with more negative Zeta potentials compared to control cells, and size of fragments, with values 2.6-times smaller in terms of effective diameter. Previous results from our group have demonstrated that the biological properties of PSs are greatly influenced by their size and physicochemical properties, implying that structural parameters can not only alter their biological functions but can also induce different host responses (Frases et al., 2009a,b; Albuquerque et al., 2014; Pontes and Frases, 2015; Araújo et al., 2016, 2017, 2019). Overall, our results suggest that changes in the size, morphology, and electronegativity of the capsule and secreted PSs can affect the fungal pathogenesis, producing different dissemination patterns due to the influence of corticosteroids in these structures. Our results also argue in favor of the general assumption that corticosteroids, while helping during the inflammation process, can also compromise the patient's prognosis by increasing the fungal load and reshaping the PS structure to possibly more active forms.

Moreover, it is already known that glucocorticoids decrease the number of macrophages, their phagocytic capacity and antigen processing as well as their recruitment to sites of inflammation (Balow and Rosenthal, 1973; Keil et al., 1995; Xie et al., 2019). In addition to the effects that these drugs have on the host's phagocytic cells, we are showing in the present study that DX and MP also influence the secreted capsule and polysaccharide sizes and electronegativity. Changes in capsule size, flexibility and electronegativity have been described as capable of influencing the capacity of macrophages to phagocytize *C. neoformans* (Frases et al., 2011; Albuquerque et al., 2014; Pontes and Frases, 2015; Ding et al., 2016; Araújo et al., 2017). Thus, we conjecture that the effects of DX and MP would probably reduce the ability of macrophages to phagocytize *C. neoformans*, not only due to the direct effects of these drugs on macrophages (Balow and Rosenthal, 1973; Keil et al., 1995; Xie

et al., 2019), but also because the alterations in the fungus surface would probably lead to a decrease in phagocytosis if compared to the changes already reported in the literature (Frases et al., 2011; Albuquerque et al., 2014; Pontes and Frases, 2015; Ding et al., 2016; Araújo et al., 2017). Nevertheless, future studies would be essential to confirm this hypothesis.

Our results also warn that the "indiscriminate" use of corticosteroids, without consolidating the correct antifungal treatment, can lead to the death of patients in a similar or even faster than in their absences, since we observed no significant differences with regards to the overall survival between both untreated and treated mice groups, but also a trend of increasing mortality in the first days. We conjecture that the 5-day corticosteroid treatment window concomitant with *C. neoformans* infection, was probably responsible for causing the initial death acceleration in mice observed at the beginning of the survival curves (Dexamethasone H99 and Methylprednisolone H99), when compared to that of control (PBS H99). However, as the corticosteroid treatment was interrupted in the following days, the survival curves show a tendency to approach that of control. Altogether, the survival curves in mice indicate a possible change in the modulation of infection, probably due to the increase in fungal proliferation in the first days caused by the corticosteroid treatment, and this increase in proliferation allows a faster dissemination through the hematological route (Wilson et al., 1970).

In contrast, the *G. mellonella* model shows an opposite behavior. *G. mellonella* larvae have been used extensively to investigate virulence properties of fungi and the relevance of the innate immune response during fungal infections (Mylonakis et al., 2005; Jemel et al., 2020; Wojda et al., 2020). Although this result could be considered unexpected, this is not the first report showing that *C. neoformans* virulence attributes have a distinct profile when comparing mice and insect models. Eisenman and colleagues (Eisenman et al., 2014) have shown that larvae of *G. mellonella* infected with melanized yeasts of *C. neoformans* lived longer than that infected with non-melanized fungi. Thus, it is possible that the modified capsule and GXM could promote a higher activation of innate immune cells, increasing the insect resistance. Further studies are required to confirm this hypothesis.

We also analyzed whether DX or MP could alter the pathogenesis of the spread of cryptococcosis. We observed that in the acute phase, mice that received treatment with DX presented a similar fungal load to control in lungs and brain. For MP, mice that received the treatment had pulmonary CFUs significantly higher than controls but showed no differences in their CNS. However, the described scenario completely changed during the chronic phase. The mice that received treatment with DX started to present pulmonary CFUs significantly higher than their controls, whereas cerebral CFUs displayed similar levels. For MP, the mice that received treatment had pulmonary and cerebral CFUs significantly greater than their respective controls.

Finally, we also analyzed the pattern of cytokine expression for mice who received treatments with either DX or MP. A statistically significant increase in the production of IL-10 was observed for both treatments, when compared to the control, indicating a possible Th2 response, despite the unchanged levels of anti-inflammatory IL-4. In turn, the production of IL-17 did not show significant differences between the treated groups (DX or MP) and organs (lungs and brain). A striking observation was that animals treated with DX or MP prior to infection suffered a drastic reduction in the lungs and the brain levels of IL-6 when compared to the control, despite its role as pro-inflammatory cytokine and antagonist to regulatory T cells and regulating the production of IL-1 and TNF-α. In the case of INF-γ, no significant differences were observed between the control mice and those treated with DX and MP. The immunosuppressive response to the increase in IL-10, together with a reduction in IL-6 levels, supports the spread of *C. neoformans* infection. IL-6 is a cytokine that influences the blood-brain barrier integrity by reducing the blood-brain barrier permeability during *Cryptococcus* meningitis (Li et al., 2015). Our results show a decrease in the presence of IL-6 in the treated mice, which may provide an explanation for the higher values of dissemination in these groups.

CONCLUSIONS

Several studies have demonstrated the role of glucocorticoids in microbial infection focusing on their role in the host. However, the present study demonstrated that changes in the ultrastructure and polysaccharide architecture, influenced by glucocorticoids, may further support the spread and severity of the infection.

Nowadays the use of glucocorticoids, such as hydrocortisone, dexamethasone and methylprednisolone, in the treatment of inflammatory diseases such as COVID-19, has reduced mortality by almost one third among patients who need respirators and in about one fifth among patients who require only oxygen therapy. However, the number of fungal infections associated with COVID-19 is increasing. Our results bring a medical alert to the indiscriminate use of glucocorticoids that may trigger physiological impairment in patients at risk for cryptococcosis.

METHODS

Cryptococcus Strain

C. neoformans var. grubii H99 (ATCC 208821, clinical isolate), donated by Prof. Arturo Casadevall (Johns Hopkins Bloomberg School of Public Health, Baltimore, Maryland, USA) was used for all the experiments of this work. Yeasts were maintained in glycerol stocks at −80°C and grown on Sabouraud media at 30°C.

Glucocorticosteroids and Growth Conditions

Yeasts were grown in minimal medium (15 mM glucose, 10 mM $MgSO_47H_2O$, 29 mM KH_2PO_4, 13 mM glycine, and 3 μM thiamine, pH 5.5) supplemented with 10, 20, 50, and 100 μg/mL of methylprednisolone sodium succinate (CAS Number:83-43-2, Sigma Aldrich) or dexamethasone acetate (CAS Number: 50-02-2, Sigma Aldrich), at 37°C, for 3, 5, and 7 days. Cells grown in minimal media without drugs were used as controls. After growth, the cells were obtained by centrifugation (6,708

× *g* for 5 min), with subsequent determination of growth rates performed by CFUs counting in Sabouraud media.

Capsule Size

To measure capsule thickness, cells from all experimental conditions used in this study were centrifuged at 6708 x *g* for 5 min, negatively stained with India ink and then imaged in an AXIO Lab.A1 light microscope (ZEISS, Germany). The capsule thickness (i.e., the distance between the cell wall and the outer limit of the capsule) was measured from a minimum of 100 cells, using the ImageJ software 1.8.0g (http://rsb.info.nih.gov/ij/. National Institutes of Health (NIH), Bethesda, MD).

Scanning Electron Microscopy (SEM)

In brief, *C. neoformans* cells grown for 7 days at 50 μg/mL were washed three times in PBS pH 7.4 and fixed in 2.5% glutaraldehyde solution grade I (Electron Microscopy Sciences, Hatfield, PA, USA) in sodium cacodylate buffer 0.1 M pH 7.2 for 1 h at room temperature. Then, the cells were washed three times in 0.1 M sodium cacodylate buffer pH 7.2 containing 0.2 M sucrose and 2 mM $MgCl_2$ (Merck Millipore Darmstadt, Germany), and adhered to 12 mm diameter round glass coverslips (Paul Marienfeld GmbH Co. KG, Germany) previously coated with 0.01% poly-L-lysine (Sigma-Aldrich, Darmstadt, Germany) for 20 min. Adhered cells were then gradually dehydrated in an ethanol (Merck Millipore, Darmstadt, Germany) series (30, 50, and, 70% for 5 min and 95 and 100% twice for 10 min). The coverslips were then critical-point-dried using an EM DPC 300 critical point drier (Leica, Germany) and mounted on specimen stubs using a conductive carbon adhesive (Pelco Tabs™, Stansted, Essex, UK). Next, the samples were coated with a thin layer of gold-palladium (10-15 nm) using the sputter method (Balzers Union FL−9496, Balzers, FL) (Carl Zeiss Evo LS or FEI Quanta 250), operating at 10–20 kV.

Purification of Secreted Polysaccharides

Secreted capsule polysaccharides (secreted PS) from cells grown for 7 days at 50 μg/mL of MP or DX were purified by ultrafiltration using an Amicon® (Merck KGaA, Darmstadt, Germany) system with a cutoff of 10 kDa (Millipore, Danvers, MA), as described previously (Nimrichter et al., 2007). The concentration of polysaccharides in filtered solutions was determined by the phenol-sulfuric method (Dubois et al., 1951). Glucose solutions were used as a standard. Cells grown for 7 days in the absence of glucocorticoids were used as controls.

Calculation of the Effective Diameter and Hydrodynamic Radius of the Secreted PS Samples by Dynamic Light Scattering (DLS)

The effective diameter and polydispersity of the PS from cells grown for 7 days at 50 μg/mL of MP or DX were determined by dynamic light scattering on a NanoBrook Omni particle equipment (Brookhaven Instruments Corporation, Holtsville, NY) from a 1 mg/mL solution (Araujo et al., 2012; Araújo et al., 2016, 2017, 2019). Cells grown for 7 days in the absence of glucocorticoids were used as controls.

Zeta Potential Measures (ξ)

The Zeta potential of PS samples at 1 mg/mL, from cells grown for 7 days at 50 μg/mL of MP or DX, were calculated on a Zeta potential analyzer (NanoBrook Omni particle, Brookhaven Instruments Corporation, Holtsville, NY) (Araujo et al., 2012; Araújo et al., 2016, 2017, 2019).

Galleria mellonella Infections

G. mellonella larvae were selected according to size, mass, and the absence of any pigmentation marks for reproducible results. First, infection area was cleaned with 70% ethanol using a cotton swab. Larvae with initial mass of 300 ± 3 mg was previously treated with MP (30 mg/kg), DX (2 mg/kg) or PBS control for 2 days before infection. Subsequently, animals were inoculated with 10 μL of a yeast suspension prepared with 10^5 cells (10^7 cells/mL) through an injection in the last left proleg using a 26G gauge needle with Hamilton syringes. Ensuing to infection, larvae continued to receive daily doses of DX, MP or PBS for 5 days. In order to mitigate possible damage caused by successive injections, pharmacological administration was alternated between the last prolegs (right and left), the same occurred with non-pharmacological groups.

After the injection, the caterpillars were placed in 90 mm glass plates and incubated at 37°C. The number of dead caterpillars was monitored daily. The groups evaluated were: **(I)** Sham (without any treatment or manipulation); **(II)** PBS—Negative control (manipulative effect); **(III)** DX control (pharmacological control group without infection); (IV) MP control (pharmacological control group without infection); **(V)** Treated with DX and subsequently infected with *C. neoformans*; **(VI)** Treated with MP and subsequently infected with *C. neoformans* and **(VII)** Infected with *C. neoformans* alone (infection control without treatment with glucocorticoid). Survival curves were plotted using GraphPad Prism 9.0.0 (La Jolla, CA, USA). Each experiment was repeated at least twice.

Mice Infections

Female Balb/c mice (*Mus musculus*) aged 6–8 weeks, with a mass of 20–25 grams, were previously treated with MP [30 mg/kg, intraperitoneally (IP)], DX (2 mg/Kg, IP) or PBS control for 2 days prior to infection. The infection with *C. neoformans* occurred at the third day upon treatment with the respective glucocorticoids. *C. neoformans* were injected intratracheally with 50 μL of an initial inoculum at 10^6 cells/mL. Further treatment for an additional 5 days with MP (30 mg/kg, IP) or DX (2 mg/kg, IP) were administrated to evaluate the survival rate. In parallel, mice were also evaluated for fungal load, cytokine profile, and histopathology of the main organs (lungs and brain) affected during the infection.

The groups evaluated were: **(I)** Sham (without any treatment or manipulation); **(II)** PBS–Negative control; **(III)** DX control (pharmacological control group without infection); **(IV)** MP control (pharmacological control group without infection); **(V)** Treated with DX and subsequently infected with *C. neoformans*; **(VI)** Treated with MP and subsequent infected with *C. neoformans* and **(VII)** infected with *C. neoformans* alone (infection control without glucocorticoid treatment). All animals

were maintained under optimal conditions. For survival tests, the death of animals was assessed daily, as well as the signs and symptoms of the disease. For the dissemination tests and impact of treatment on organ fungal load, after 5 and 7 days of infection, the animals were euthanized, and the lungs and brain were removed. A small fragment was separated for histopathological analysis upon fixation and staining with hematoxylin-eosin and mucicarmine stain. The remaining organ was homogenized and plated on Sabouraud media plates for CFU enumeration. For the analysis of selected cytokines, organs were centrifuged at 5,000 *g*, the supernatants from lungs and brains were collected and the presence of cytokines determined using the "RayBio® Mouse Cytokine Antibody Array" kit (RayBiotech, Inc), following the manufacturer's instructions. Positive reactions were quantified using the Scion Image software (2000 Scion Corporation, NIH).

Statistical Analysis

All the data, except those from the survival curves, are presented as mean ± standard deviation. Data were analyzed using GraphPad Prism 9.0.0 (GraphPad Software, San Diego, California USA, www.graphpad.com). Student's *t*-test were used for comparisons between each situation and the respective control. Survival curves were analyzed using the Logrank and Gehan-Breslow-Wilcoxon tests. $^{*}p < 0.05$; $^{**}p < 0.01$; $^{***}p < 0.001$, and $^{****}p < 0.0001$. The *p-values* and other numbers for all experiments are provided in the figure legends.

DATA AVAILABILITY STATEMENT

The raw data supporting the conclusions of this article will be made available by the authors, without undue reservation.

ETHICS STATEMENT

The animal study was reviewed and approved by the Ethics Committee on the Use of Animals in Scientific Experimentation (CEUA) at the Health Sciences Center of the Federal University of Rio de Janeiro, registered with the National Council for the Control of Animal Experimentation (CONCEA) under the protocol number 01200.001568/2013-87 (112/17).

AUTHOR CONTRIBUTIONS

GA: conceptualization, methodology, investigation, visualization, data curation, formal analysis, writing—original draft, and writing—review & editing. VA, PM-d-S, HL, and CT: methodology and writing—review & editing. AG and LN: conceptualization, methodology, investigation, visualization, data curation, resources, supervision, formal analysis, writing—original draft, and writing—review & editing. BP and SF: conceptualization, methodology, investigation, visualization, data curation, resources, supervision, funding acquisition, formal analysis, writing—original draft, and writing—review & editing. All authors contributed to the article and approved the submitted version.

FUNDING

This work was supported by the Brazilian agencies Conselho Nacional de Desenvolvimento Científico e Tecnológico (CNPq), Coordenação de Aperfeiçoamento de Pessoal de Nível Superior (CAPES)—Finance code 001 and Fundação de Amparo à Pesquisa do Estado do Rio de Janeiro (FAPERJ).

REFERENCES

Albuquerque, P. C., Fonseca, F. L., Dutra, F. F., Bozza, M. T., Frases, S., Casadevall, A., et al. (2014). *Cryptococcus neoformans* glucuronoxylomannan fractions of different molecular masses are functionally distinct. *Future Microbiol.* 9, 147–161. doi: 10.2217/fmb.13.163

Al-Hatmi, A. M. S., Mohsin, J., Al-Huraizi, A., and Khamis, F. (2020). COVID-19 associated invasive candidiasis. *J. Infect.* doi: 10.1016/j.jinf.2020.08.005

Araújo, G. R., de, S., Freitas, G. J. C., Fonseca, F. L., Leite, P. E. C., Rocha, G. M., et al. (2017). The environmental yeast *Cryptococcus liquefaciens* produces capsular and secreted polysaccharides with similar pathogenic properties to those of C. *neoformans*. *Sci. Rep.* 7:46768. doi: 10.1038/srep46768

Araújo, G. R., Fontes, G. N., Leão, D., Rocha, G. M., Pontes, B., Sant'Anna, C., et al. (2016). *Cryptococcus neoformans* capsular polysaccharides form branched and complex filamentous networks viewed by high-resolution microscopy. *J. Struct. Biol.* 193, 75–82. doi: 10.1016/j.jsb.2015.11.010

Araújo, G. R. D., de, S., Viana, N. B., Pontes, B., and Frases, S. (2019). Rheological properties of cryptococcal polysaccharide change with fiber size, antibody binding and temperature. *Future Microbiol.* 14, 867–884. doi: 10.2217/fmb-2018-0320

Araujo, G. S., Fonseca, F. L., Pontes, B., Torres, A., Cordero, R. J. B., Zancopé-Oliveira, R. M., et al. (2012). Capsules from pathogenic and non-pathogenic *Cryptococcus* spp. manifest significant differences in structure and ability to protect against phagocytic cells. *PLoS ONE* 7:e29561. doi: 10.1371/journal.pone.0029561

Balow, J. E., and Rosenthal, A. S. (1973). Glucocorticoid suppression of macrophage migration inhibitory factor. *J. Exp. Med.* 137, 1031–1041. doi: 10.1084/jem.137.4.1031

Barbosa, A. T. F., Colares, F. A., Gusmão, E., da, S., Barros, A. A., Cordeiro, C. G., et al. (2006). Criptococose pulmonar isolada em paciente imunocompetente. *J. Bras. Pneumol.* 32, 476–480. doi: 10.1590/S1806-37132006000500016

Beardsley, J., Wolbers, M., Kibengo, F. M., Ggayi, A.-B. M., Kamali, A., Cuc, N. T. K., et al. (2016). Adjunctive dexamethasone in HIV-associated cryptococcal meningitis. *N. Engl. J. Med.* 374, 542–554. doi: 10.1056/NEJMoa1509024

Casadevall, A. (2010). Cryptococci at the brain gate: break and enter or use a Trojan horse? *J. Clin. Invest.* 120, 1389–1392. doi: 10.1172/JCI42949

Casadevall, A., and Perfect, J. R. (1998). *Cryptococcus neoformans, 1st Edn*. Washington, DC: ASM Press. doi: 10.1111/j.1365-280X.1999.00238.x

Chang, Y. C., Stins, M. F., McCaffery, M. J., Miller, G. F., Pare, D. R., Dam, T., et al. (2004). Cryptococcal yeast cells invade the central nervous system via transcellular penetration of the blood-brain barrier. *Infect. Immun.* 72, 4985–4995. doi: 10.1128/IAI.72.9.4985-4995.2004

Charlier, C., Nielsen, K., Daou, S., Brigitte, M., Chretien, F., and Dromer, F. (2009). Evidence of a role for monocytes in dissemination and brain invasion by *Cryptococcus neoformans*. *Infect. Immun.* 77, 120–127. doi: 10.1128/IAI.01065-08

Chen, S. H. M., Stins, M. F., Huang, S.-H., Chen, Y. H., Kwon-Chung, K. J., Chang, Y., et al. (2003). *Cryptococcus neoformans* induces alterations in the cytoskeleton of human brain microvascular endothelial cells. *J. Med. Microbiol.* 52, 961–970. doi: 10.1099/jmm.0.05230-0

Chen, Y., van der Mei, H. C., Busscher, H. J., and Norde, W. (2014). Viscous nature of the bond between adhering bacteria and substratum surfaces probed by atomic force microscopy. *Langmuir* 30, 3165–3169. doi: 10.1021/la404874x

Clumeck, N., Sonnet, J., Taelman, H., Mascart-Lemone, F., De Bruyere, M., Vandeperre, P., et al. (1984). Acquired Immunodeficiency Syndrome in African Patients. *N. Engl. J. Med.* 310, 492–497. doi: 10.1056/NEJM198402233100804

Del Valle, L., and Piña-Oviedo, S. (2006). HIV disorders of the brain: pathology and pathogenesis. *Front. Biosci.* 11, 718–732. doi: 10.2741/1830

Diamond, R. D. (1974). Prognostic factors in *Cryptococcal Meningitis*. *Ann. Intern. Med.* 80, 176. doi: 10.7326/0003-4819-80-2-176

Ding, H., Mayer, F. L., Sánchez-León, E., de, S., Araújo, G. R., Frases, S., et al. (2016). Networks of fibers and factors: regulation of capsule formation in *Cryptococcus neoformans*. *F1000Research* 5:1786. doi: 10.12688/f1000research.8854.1

Dromer, F., and Levitz, S. M. (2010). *Invasion of Cryptococcus Into the Central Nervous System. Cryptococcus: From Human Pathogen to Model Yeast, 1st Edn*. eds J. Heitman, T. R. Kozel, K. J. Kwon, Chung, J. R. Perfect, and A. Casadevall. Washington, DC: ASM Press. doi: 10.1128/9781555816858.ch34

Dubois, M., Gilles, K., Hamilton, J. K., Rebers, P. A., and Smith, F. (1951). A colorimetric method for the determination of sugars. *Nature* 168, 167–167. doi: 10.1038/168167a0

Eisenman, H. C., Duong, R., Chan, H., Tsue, R., and McClelland, E. E. (2014). Reduced virulence of melanized *Cryptococcus neoformans* in *Galleria mellonella*. *Virulence* 5, 611–618. doi: 10.4161/viru.29234

Ellis, D. H., and Pfeiffer, T. J. (1990). Ecology, life cycle, and infectious propagule of *Cryptococcus neoformans*. *Lancet* 336, 923–925. doi: 10.1016/0140-6736(90)92283-n

Franco-Paredes, C., Chastain, D. B., Rodriguez-Morales, A. J., and Marcos, L. A. (2017). Cryptococcal meningoencephalitis in HIV/AIDS: when to start antiretroviral therapy? *Ann. Clin. Microbiol. Antimicrob.* 16:9. doi: 10.1186/s12941-017-0184-2

Frases, S., Pontes, B., Nimrichter, L., Rodrigues, M. L., Viana, N. B., and Casadevall, A. (2009a). The elastic properties of the *Cryptococcus neoformans* capsule. *Biophys. J.* 97, 937–945. doi: 10.1016/j.bpj.2009.04.043

Frases, S., Pontes, B., Nimrichter, L., Viana, N. B., Rodrigues, M. L., and Casadevall, A. (2009b). Capsule of *Cryptococcus neoformans* grows by enlargement of polysaccharide molecules. *Proc. Natl. Acad. Sci. U.S.A.* 106, 1228–1233. doi: 10.1073/pnas.0808995106

Frases, S., Viana, N. B., and Casadevall, A. (2011). Biophysical methods for the study of microbial surfaces. *Front. Microbiol.* 2:207. doi: 10.3389/fmicb.2011.00207

Galanis, E., MacDougall, L., Kidd, S., and Morshed, M. (2010). Epidemiology of *Cryptococcus gattii*, British Columbia, Canada, 1999–2007. *Emerg. Infect. Dis.* 16, 251–257. doi: 10.3201/eid1602.090900

Goldman, J. D., Vollmer, M. E., and Luks, A. M. (2010). Cryptococcosis in the immunocompetent patient. *Respir. Care* 55, 1499–503.

Granger, D. L., Perfect, J. R., and Durack, D. T. (1985). Virulence of *Cryptococcus neoformans*. Regulation of capsule synthesis by carbon dioxide. *J. Clin. Invest.* 76, 508–516. doi: 10.1172/JCI112000

Graybill, J. R., Sobel, J., Saag, M., van der Horst, C., Powderly, W., Cloud, G., et al. (2000). Diagnosis and management of increased intracranial pressure in patients with AIDS and Cryptococcal Meningitis. *Clin. Infect. Dis.* 30, 47–54. doi: 10.1086/313603

Gross, N. T., Chinchilla, M., Camner, P., and Jarstrand, C. (1996). Anticryptococcal activity by alveolar macrophages from rats treated with cortisone acetate during different periods of time. *Mycopathologia* 136, 1–8. doi: 10.1007/BF00436653

Henao-Martínez, A. F., and Beckham, J. D. (2015). Cryptococcosis in solid organ transplant recipients. *Curr. Opin. Infect. Dis.* 28, 300–307. doi: 10.1097/QCO.0000000000000171

Henson, D. J., and Ross Hill, A. (1984). Cryptococcal pneumonia: a fulminant presentation. *Am. J. Med. Sci.* 288, 221–222. doi: 10.1097/00000441-198412000-00006

Jemel, S., Guillot, J., Kallel, K., Botterel, F., and Dannaoui, E. (2020). *Galleria mellonella* for the evaluation of antifungal efficacy against medically important fungi, a narrative review. *Microorganisms* 8:390. doi: 10.3390/microorganisms8030390

Jong, A., Wu, C.-H., Shackleford, G. M., Kwon-Chung, K. J., Chang, Y. C., Chen, H.-M., et al. (2008). Involvement of human CD44 during *Cryptococcus neoformans* infection of brain microvascular endothelial cells. *Cell. Microbiol.* 10, 1313–1326. doi: 10.1111/j.1462-5822.2008.01128.x

Keil, D. E., Luebke, R. W., and Pruett, S. B. (1995). Differences in the effects of dexamethasone on macrophage nitrite production: dependence on exposure regimen (*in vivo* or *in vitro*) and activation stimuli. *Int. J. Immunopharmacol.* 17, 157–166. doi: 10.1016/0192-0561(95)00008-P

Kronstad, J., Saikia, S., Nielson, E. D., Kretschmer, M., Jung, W., Hu, G., et al. (2012). Adaptation of *Cryptococcus neoformans* to mammalian hosts: integrated regulation of metabolism and virulence. *Eukaryot. Cell* 11, 109–118. doi: 10.1128/EC.05273-11

Kuwahara, H., Tsuchiya, K., Kobayashi, Z., Inaba, A., Akiyama, H., and Mizusawa, H. (2014). Cryptococcal meningitis accompanying lymphocytic inflammation predominantly in cerebral deep white matter: a possible manifestation of immune reconstitution inflammatory syndrome. *Neuropathology* 34, 45–48. doi: 10.1111/neup.12046

Li, X., Liu, G., Ma, J., Zhou, L., Zhang, Q., and Gao, L. (2015). Lack of IL-6 increases blood–brain barrier permeability in fungal meningitis. *J. Biosci.* 40, 7–12. doi: 10.1007/s12038-014-9496-y

Liao, T.-L., Chen, Y.-M., and Chen, D.-Y. (2016). Risk factors for cryptococcal infection among patients with rheumatoid arthritis receiving different immunosuppressive medications. *Clin. Microbiol. Infect. 22*, 815.e1–815.e3. doi: 10.1016/j.cmi.2016.05.030

Lopes, W., Cruz, G. N. F., Rodrigues, M. L., Vainstein, M. H., Kmetzsch, L., Staats, C. C., et al. (2020). Scanning electron microscopy and machine learning reveal heterogeneity in capsular morphotypes of the human pathogen *Cryptococcus* spp. *Sci. Rep.* 10:2362. doi: 10.1038/s41598-020-59276-w

Martin, G. S., Mannino, D. M., Eaton, S., and Moss, M. (2003). The epidemiology of sepsis in the United States from 1979 through 2000. *N. Engl. J. Med.* 348, 1546–1554. doi: 10.1056/NEJMoa022139

Maziarz, E. K., and Perfect, J. R. (2016). Cryptococcosis. *Infect. Dis. Clin. North Am.* 30, 179–206. doi: 10.1016/j.idc.2015.10.006

McCarthy, K. M., Morgan, J., Wannemuehler, K. A., Mirza, S. A., Gould, S. M., Mhlongo, N., et al. (2006). Population-based surveillance for cryptococcosis in an antiretroviral-naive South African province with a high HIV seroprevalence. *AIDS* 20, 2199–2206. doi: 10.1097/QAD.0b013e3280106d6a

McFadden, D., Zaragoza, O., and Casadevall, A. (2006). The capsular dynamics of *Cryptococcus neoformans*. *Trends Microbiol.* 14, 497–505. doi: 10.1016/j.tim.2006.09.003

Mitchell, D. H., Sorrell, T. C., Allworth, A. M., Heath, C. H., McGregor, A. R., Papanaoum, K., et al. (1995). Cryptococcal disease of the CNS in immunocompetent hosts: influence of cryptococcal variety on clinical manifestations and outcome. *Clin. Infect. Dis.* 20, 611–616. doi: 10.1093/clinids/20.3.611

Mitchell, T. G., and Perfect, J. R. (1995). Cryptococcosis in the era of AIDS - 100 years after the discovery of *Cryptococcus neoformans*. *Clin. Microbiol. Rev.* 8, 515–548.

Morrison, V. A., Haake, R. J., and Weisdorf, D. J. (1994). Non-Candida fungal infections after bone marrow transplantation: risk factors and outcome. *Am. J. Med.* 96, 497–503. doi: 10.1016/0002-9343(94)90088-4

Mylonakis, E., Moreno, R., El Khoury, J. B., Idnurm, A., Heitman, J., Calderwood, S. B., et al. (2005). *Galleria mellonella* as a model system to study *Cryptococcus neoformans* pathogenesis. *Infect. Immun.* 73, 3842–3850. doi: 10.1128/IAI.73.7.3842-3850.2005

Nimrichter, L., Frases, S., Cinelli, L. P., Viana, N. B., Nakouzi, A., Travassos, L. R., et al. (2007). Self-aggregation of *Cryptococcus neoformans* capsular glucuronoxylomannan is dependent on divalent cations. *Eukaryot. Cell* 6, 1400–1410. doi: 10.1128/EC.00122-07

Park, B. J., Wannemuehler, K. A., Marston, B. J., Govender, N., Pappas, P. G., and Chiller, T. M. (2009). Estimation of the current global burden of cryptococcal meningitis among persons living with HIV/AIDS. *AIDS* 23, 525–530. doi: 10.1097/QAD.0b013e328322ffac

Passerini, M., Terzi, R., Piscaglia, M., Passerini, S., and Piconi, S. (2020). Disseminated cryptococcosis in a patient with metastatic prostate cancer who died in the Coronavirus Disease 2019 (COVID-19) outbreak. *Cureus* 12:e8254. doi: 10.7759/cureus.8254

Patterson, J. E. (1999). Epidemiology of fungal infections in solid organ transplant patients. *Transpl. Infect. Dis.* 1, 229–236. doi: 10.1034/j.1399-3062.1999.010402.x

Perfect, J. R. (2013). Fungal diagnosis: how do we do it and can we do better? *Curr. Med. Res. Opin.* 29 (Suppl. 4), 3–11. doi: 10.1185/03007995.2012.761134

Perfect, J. R., and Casadevall, A. (2002). Cryptococcosis. *Infect. Dis. Clin. North Am.* 16, 837–874. doi: 10.1016/S0891-5520(02)00036-3

Perfect, J. R., and Durack, D. T. (1985a). Chemotactic activity of cerebrospinal fluid in experimental cryptococcal meningitis. *Sabouraudia* 23, 37–45. doi: 10.1080/00362178585380071

Perfect, J. R., and Durack, D. T. (1985b). Effects of cyclosporine in experimental cryptococcal meningitis. *Infect. Immun.* 50, 22–26. doi: 10.1128/IAI.50.1.22-26.1985

Perfect, J. R., Durack, D. T., and Gallis, H. A. (1983). Cryptococcemia. *Medicine (Baltimore).* 62, 98–109. doi: 10.1097/00005792-198303000-00003

Pontes, B., and Frases, S. (2015). The *Cryptococcus neoformans* capsule: Lessons from the use of optical tweezers and other biophysical tools. *Front. Microbiol.* 6:640. doi: 10.3389/fmicb.2015.00640

Prado, M., Silva, M. B., da, Laurenti, R., Travassos, L. R., and Taborda, C. P. (2009). Mortality due to systemic mycoses as a primary cause of death or in association with AIDS in Brazil: a review from 1996 to 2006. *Mem. Inst. Oswaldo Cruz* 104, 513–521. doi: 10.1590/s0074-02762009000300019

Rajasingham, R., Smith, R. M., Park, B. J., Jarvis, J. N., Govender, N. P., Chiller, T. M., et al. (2017). Global burden of disease of HIV-associated cryptococcal meningitis: an updated analysis. *Lancet Infect. Dis.* 17, 873–881. doi: 10.1016/S1473-3099(17)30243-8

Santiago-Tirado, F. H., Onken, M. D., Cooper, J. A., Klein, R. S., and Doering, T. L. (2017). Trojan horse transit contributes to blood-brain barrier crossing of a eukaryotic pathogen. *MBio* 8:e02183–16. doi: 10.1128/mBio.02183-16

Segrelles-Calvo, G., Araújo, G. R. D. S., Llopis-Pastor, E., and Frasés, S. (2020a). *Trichosporon asahii* as cause of nosocomial pneumonia in patient with COVID-19: a triple co-infection. *Arch. Bronconeumol.* S0300–2896(20)30527–5. doi: 10.1016/j.arbres.2020.11.007

Segrelles-Calvo, G., Araújo, G. R. S., Llopis-Pastor, E., Carrillo, J., Hernández-Hernández, M., Rey, L., et al. (2020b). Prevalence of opportunistic invasive aspergillosis in COVID-19 patients with severe pneumonia. *Mycoses.* 64, 144–151. doi: 10.1111/myc.13219

Segrelles-Calvo, G., de, S., Araújo, G. R., and Frases, S. (2020c). Systemic mycoses: a potential alert for complications in COVID-19 patients. *Future Microbiol.* 15, 1405–1413. doi: 10.2217/fmb-2020-0156

Singh, N., Dromer, F., Perfect, J. R., and Lortholary, O. (2008). Cryptococcosis in solid organ transplant recipients: current state of the science. *Clin. Infect. Dis.* 47, 1321–1327. doi: 10.1086/592690

Sinha, P., Matthay, M. A., and Calfee, C. S. (2020). Is a "Cytokine Storm" Relevant to COVID-19? *JAMA Intern. Med.* 180:1152. doi: 10.1001/jamainternmed.2020.3313

Sterne, J. A. C., Murthy, S., Diaz, J. V., Slutsky, A. S., Villar, J., Angus, D. C., et al. (2020). Association between administration of systemic corticosteroids and mortality among critically Ill patients with COVID-19. *JAMA* 324:1330. doi: 10.1001/jama.2020.17023

Van De Perre, P., Lepage, P., Kestelyn, P., Hekker, A., Rouvroy, D., Bogaerts, J., et al. (1984). Acquired immunodeficiency syndrome in Rwanda. *Lancet* 324, 62–65. doi: 10.1016/S0140-6736(84)90240-X

Vilchez, R. A., Linden, P., Lacomis, J., Costello, P., Fung, J., and Kusne, S. (2001). Acute respiratory failure associated with pulmonary Cryptococcosis in non-AIDS patients. *Chest* 119, 1865–1869. doi: 10.1378/chest.119.6.1865

Vu, K., Eigenheer, R. A., Phinney, B. S., and Gelli, A. (2013). *Cryptococcus neoformans* promotes its transmigration into the central nervous system by inducing molecular and cellular changes in brain endothelial cells. *Infect. Immun.* 81, 3139–3147. doi: 10.1128/IAI.00554-13

Williamson, P. R., Jarvis, J. N., Panackal, A. A., Fisher, M. C., Molloy, S. F., Loyse, A., et al. (2017). Cryptococcal meningitis: epidemiology, immunology, diagnosis and therapy. *Nat. Rev. Neurol.* 13, 13–24. doi: 10.1038/nrneurol.2016.167

Wilson, T. S., Fleming, W. A., Robinson, F. L. J., and Nicholl, B. (1970). Cryptococcal meningitis associated with steroid therapy. *J. Clin. Pathol.* 23, 657–663. doi: 10.1136/jcp.23.8.657

Wojda, I., Staniec, B., Sułek, M., and Kordaczuk, J. (2020). The greater wax moth *Galleria mellonella* : biology and use in immune studies. *Pathog. Dis.* 78:ftaa057. doi: 10.1093/femspd/ftaa057

Xie, Y., Tolmeijer, S., Oskam, J. M., Tonkens, T., Meijer, A. H., and Schaaf, M. J. M. (2019). Glucocorticoids inhibit macrophage differentiation towards a pro-inflammatory phenotype upon wounding without affecting their migration. *Dis. Model. Mech.* 12:dmm037887. doi: 10.1242/dmm.037887

Zaragoza, O. (2019). Basic principles of the virulence of *Cryptococcus*. *Virulence* 10, 490–501. doi: 10.1080/21505594.2019.1614383

Zhang, E. T., Inman, C. B., and Weller, R. O. (1990). Interrelationships of the pia mater and the perivascular (Virchow-Robin) spaces in the human cerebrum. *J. Anat.* 170, 111–23.

Conflict of Interest: The authors declare that the research was conducted in the absence of any commercial or financial relationships that could be construed as a potential conflict of interest.

frontiers in Microbiology

ORIGINAL RESEARCH
published: 09 April 2021
doi: 10.3389/fmicb.2021.656548

The Heat Shock Transcription Factor HsfA Is Essential for Thermotolerance and Regulates Cell Wall Integrity in *Aspergillus fumigatus*

*João Henrique Tadini Marilhano Fabri[1], Marina Campos Rocha[1], Caroline Mota Fernandes[2], Gabriela Felix Persinoti[3], Laure Nicolas Annick Ries[4], Anderson Ferreira da Cunha[1], Gustavo Henrique Goldman[5], Maurizio Del Poeta[2,6,7,8] and Iran Malavazi[1]**

[1] Departamento de Genética e Evolução, Centro de Ciências Biológicas e da Saúde, Universidade Federal de São Carlos, São Carlos, Brazil, [2] Department of Microbiology and Immunology, Stony Brook University, Stony Brook, NY, United States, [3] Laboratório Nacional de Biorrenováveis (LNBR), Centro Nacional de Pesquisa em Energia e Materiais (CNPEM), Campinas, São Paulo, Brazil, [4] MRC Centre for Medical Mycology, University of Exeter, Exeter, United Kingdom, [5] Faculdade de Ciências Farmacêuticas de Ribeirão Preto, Universidade de São Paulo, São Paulo, Brazil, [6] Division of Infectious Diseases, School of Medicine, Stony Brook University, Stony Brook, NY, United States, [7] Institute of Chemical Biology and Drug Discovery, Stony Brook University, Stony Brook, NY, United States, [8] Veterans Administration Medical Center, Northport, NY, United States

OPEN ACCESS

Edited by:
Allan J. Guimaraes, Fluminense Federal University, Brazil

Reviewed by:
Louise Walker, University of Aberdeen, United Kingdom
Nir Osherov, Tel Aviv University, Israel

***Correspondence:**
Iran Malavazi
imalavazi@ufscar.br

Specialty section:
This article was submitted to Microbial Physiology and Metabolism, a section of the journal Frontiers in Microbiology

Received: *21 January 2021*
Accepted: *11 March 2021*
Published: *09 April 2021*

Citation:
Fabri JHTM, Rocha MC, Fernandes CM, Persinoti GF, Ries LNA, Cunha AF, Goldman GH, Del Poeta M and Malavazi I (2021) The Heat Shock Transcription Factor HsfA Is Essential for Thermotolerance and Regulates Cell Wall Integrity in Aspergillus fumigatus. Front. Microbiol. 12:656548. doi: 10.3389/fmicb.2021.656548

The deleterious effects of human-induced climate change have long been predicted. However, the imminent emergence and spread of new diseases, including fungal infections through the rise of thermotolerant strains, is still neglected, despite being a potential consequence of global warming. Thermotolerance is a remarkable virulence attribute of the mold *Aspergillus fumigatus*. Under high-temperature stress, opportunistic fungal pathogens deploy an adaptive mechanism known as heat shock (HS) response controlled by heat shock transcription factors (HSFs). In eukaryotes, HSFs regulate the expression of several heat shock proteins (HSPs), such as the chaperone Hsp90, which is part of the cellular program for heat adaptation and a direct target of HSFs. We recently observed that the perturbation in cell wall integrity (CWI) causes concomitant susceptibility to elevated temperatures in *A. fumigatus*, although the mechanisms underpinning the HS response and CWI cross talking are not elucidated. Here, we aim at further deciphering the interplay between HS and CWI. Our results show that cell wall ultrastructure is severely modified when *A. fumigatus* is exposed to HS. We identify the transcription factor HsfA as essential for *A. fumigatus* viability, thermotolerance, and CWI. Indeed, HS and cell wall stress trigger the coordinated expression of both *hsfA* and *hsp90*. Furthermore, the CWI signaling pathway components PkcA and MpkA were shown to be important for HsfA and Hsp90 expression in the *A. fumigatus* biofilms. Lastly, RNA-sequencing confirmed that *hsfA* regulates the expression of genes related to the HS response,

cell wall biosynthesis and remodeling, and lipid homeostasis. Our studies collectively demonstrate the connection between the HS and the CWI pathway, with HsfA playing a crucial role in this cross-pathway regulation, reinforcing the importance of the cell wall in *A. fumigatus* thermophily.

Keywords: *Aspergillus fumigatus*, HsfA, thermotolerance, heat shock (HS), transcription factor, cell wall integrity (CWI)

INTRODUCTION

Fungal human diseases and their impacts on human health and world economy have frequently been overlooked (Brown et al., 2012). It is believed that fungal infections kill more than 1.5 million people worldwide per year (Benedict et al., 2019), and prospects are even worse if the last decades' environmental changes are considered. For instance, it has been proposed that global warming may significantly enhance the adaptation of fungal populations to higher temperatures, which may cause the emergence of new fungal diseases associated with difficult treatment (Garcia-Solache and Casadevall, 2010; Casadevall et al., 2019).

In this worrisome scenario, the saprophytic mold and opportunistic human pathogen *Aspergillus fumigatus* stands out for its intrinsic thermophilic and thermotolerance traits and the rise of resistant isolates to available antifungal drugs (van Paassen et al., 2016). Unlike other *Aspergillus* species, *A. fumigatus* can germinate under temperatures above 40°C, and its conidia remain viable up to 70°C (Araujo and Rodrigues, 2004). These attributes of *A. fumigatus* biology help to explain its high prevalence in the environment and support the thermotolerance as an essential determinant for its pathogenicity since it allows the adaptation of the fungus to temperatures found before and after the infection of mammalian host and favors the persistence of this fungus inside the human lungs (Albrecht et al., 2010; Haas et al., 2016).

Living organisms continuously monitor the environmental temperature to survive (Leach and Cowen, 2013). In response to temperature rise, gene expression is adjusted, allowing the cells to synthesize a specific group of proteins called heat shock proteins (HSPs) that deal with this stressing condition (Parsell and Lindquist, 1993). During heat shock (HS), these molecular chaperones prevent the aggregation of denatured proteins and restore their native conformations and function (Hartl, 1996). To allow this orchestrated response, an influential group of conserved DNA binding proteins, the heat shock transcription factors (HSFs), regulate gene transcription during HS and other stress sources (Albrecht et al., 2010; Sueiro-Olivares et al., 2015; Gomez-Pastor et al., 2018). One member of this family, the heat shock transcription factor 1 (Hsf1), is a key player in mediating the cell transcriptional response to HS and has been widely studied in humans, *Saccharomyces cerevisiae*, and *Candida albicans* (Sarge et al., 1993; Eastmond and Nelson, 2006; Nicholls et al., 2009; Leach et al., 2016). Hsf1 is essential for viability and it is hyperphosphorylated in both fungal organisms in response to HS (Wiederrecht et al., 1988; Hashikawa and Sakurai, 2004; Nicholls et al., 2009, 2011). Under stressing conditions, Hsf1 homotrimers bind to specific DNA motifs named HS elements (HSE) located in target gene promoters, inducing the expression of molecular chaperones and other genes related to thermal adaptation (Sorger and Pelham, 1988; Sorger and Nelson, 1989; Yamamoto et al., 2005; Leach et al., 2016). Concomitantly, chaperones such as Hsp70 and Hsp90 are known regulators of Hsf1 activity via a well-described feedback regulatory loop in which Hsp90 binds to Hsf1 to keep it in an inactive state (Leach et al., 2012a; Schopf et al., 2017; Kijima et al., 2018; Krakowiak et al., 2018). In conditions where the chaperones are required for other functions and are no longer available for Hsf1 inhibition, the transcription of target HS genes increases (Veri et al., 2018). In *A. fumigatus*, putative HSEs were found in genes encoding HSPs and enzymes involved in the oxidative stress response, protein translation, carbohydrate and nitrogen metabolism, and signal transduction (Albrecht et al., 2010).

Thermoadaptation has also been directly associated with the activation of signaling pathways that govern cellular processes such as fungal morphogenesis and dimorphism, plasma membrane fluidity, and cell wall integrity (CWI) [reviewed in Brown et al. (2010); Leach and Cowen (2013); Fabri et al. (2020)]. The CWI pathway, which comprises the apical kinase PkcA, the three-component mitogen-activated protein kinases (MAPKs) Bck1, Mkk2, and MpkA, and the transcription factor RlmA (Valiante et al., 2009; Rocha et al., 2015, 2016), is one of the signaling cascades responsible for the regulation of cell wall biosynthesis and maintenance (Valiante et al., 2015). This signaling pathway also sustains the fungal cell wall viability during heat stress (Kamada et al., 1995; Fuchs and Mylonakis, 2009; Rocha et al., 2020b). However, despite the significance of the interplay between thermotolerance and CWI, little is known about the molecular events that reciprocally govern these two essential *A. fumigatus* virulence attributes.

Precedent exists indicating that the Hsf1-Hsp90 circuit is a connecting point between thermotolerance and the fungal CWI pathway (LaFayette et al., 2010; Lamoth et al., 2012; Leach et al., 2012a). For instance, without the proper expression of Hsp90 driven by Hsf1 in *S. cerevisiae* and *C. albicans*, CWI is compromised, leading to deficient expression of genes that promote CWI during exposure to high temperatures (Truman et al., 2007; Nicholls et al., 2009; Leach et al., 2012a). Also, Hsp90 potentiates the resistance to echinocandins in different fungal pathogens, including *A. fumigatus*, since depletion of this chaperone increases the susceptibility to these antifungals (Cowen, 2009; LaFayette et al., 2010; Lamoth et al., 2013, 2015; Chatterjee and Tatu, 2017). We have previously demonstrated that three critical components of the *A. fumigatus* CWI pathway (PkcA, MpkA, and RlmA) are Hsp90 clients (Rocha et al., 2020b),

suggesting an involvement of the Hsf1-Hsp90 regulatory function over the *A. fumigatus* CWI pathway. However, it remained unclear how $hsfA^{HSF1}$ contributes to thermal adaptation and the disturbed cell wall homeostasis observed in the CWI pathway mutants. This is a follow-up study to our previous work (Rocha et al., 2020b), and our results show that cell wall ultrastructure is severely modified when cells are exposed to HS. We observe that *hsfA* is essential for thermotolerance, impacts the expression of genes related to the cell wall biosynthesis, and genetically interacts with the main players of the CWI and HOG pathway. We show a clear link between the HS and cell wall stress modulated by HsfA and the CWI pathway in *A. fumigatus* biofilms *in vitro* by following the fluctuations in HsfA expression. Our results also show that cell integrity genes are modulated when *hsfA* expression is repressed.

MATERIALS AND METHODS

Strains and Culture Conditions

The *A. fumigatus* strains used in this study are described in **Supplementary Table 1**. Strains were maintained in complete medium [YG; glucose 2% (w/w), 0.5% yeast extract (w/w), 1 × trace elements)] or minimal medium [MM; glucose 1% (w/w), 1 × high-nitrate salts, and 1 × trace elements (pH 6.5)]. Trace elements and high nitrate salt compositions were as described previously (Malavazi and Goldman, 2012). For solid media, agar 2% (w/w) was added. To grow the ΔKU80 *pyrG1* strain, the media was supplemented with 1.2 g/L of uridine and uracil. When required, pyrithiamine (Sigma) or hygromycin B (Merck) was added to a final concentration of 0.2 μg/ml or 200 μg/ml, respectively. Different xylose concentrations were used depending on the experiment to induce *hsfA* expression in the *xylP::hsfA* conditional strain.

The wild-type and *xylP::hsfA* strains were grown and analyzed by DIC (Differential Interference Contrast) microscopy to analyze hyphal growth. Accordingly, 1×10^5 conidia of each strain were inoculated in glass-bottom dishes (MatTek Corporation) containing 2 ml of MM supplemented with different xylose concentrations at 37°C for 12 h. Images were captured with an AxioCam MRm camera (Zeiss) and processed using ZEN software.

Construction of the *A. fumigatus* Mutants

For the *xylP::hsfA* cassette construction, two fragments spanning the 5′ UTR region of *hsfA* (Afu5g01900) gene were PCR-amplified from genomic DNA of the CEA17 strain, according to **Supplementary Figure 1A**. The primers used are listed in **Supplementary Table 2**. The opposite sites of the 5′ regions contained a short sequence homologous to the multiple cloning site of the pRS426 plasmid (the small bold letters indicated in **Supplementary Table 2**). The *pyrG* gene inserted into the cassette was amplified from pCDA21 plasmid (Chaveroche et al., 2000) and used as a prototrophy marker. The pYES-hph-pXyl devR vector was used to amplify the *Penicillium chrysogenum* xylose reductase gene promoter (*xylP*), which is activated in the presence of xylose and repressed in the presence of glucose (Zadra et al., 2000). The substitution cassette was generated by *in vivo* recombination in *S. cerevisiae*, as reported previously (Malavazi and Goldman, 2012). All the PCR amplifications were performed using Phusion High-Fidelity DNA Polymerase (Thermo Scientific). The cassette was transformed into protoplasts of the *A. fumigatus* ΔKU80 pyrG1 according to previously described procedures (Malavazi and Goldman, 2012). Transformants were carefully tested by PCR (**Supplementary Figure 1B**) and Southern blot analysis, using the 5′ flanking region as a probe (**Supplementary Figure 1C**). An endogenous *hsfA* promoter region spanning 467 bp was maintained before the *hsfA* gene because we previously observed that complete replacement of the native *hsfA* promoter resulted in transformants with growth defects and inconsistent control of *hsfA* transcription (data not shown).

To generate the double mutant Δ*mpkA xylP::hsfA*, the *mpkA* deletion cassette was amplified from the genomic DNA of the Δ*mpkA* strain (Valiante et al., 2009) using primers MpkA 5F and MpkA 3′ REV and transformed into the *xylP::hsfA* strain selected for pyrithiamine resistance. The *hsfA* locus in this strain was checked using the primers HsfA 600 ups and HsfA 2 5UTR REV pRS426 (**Supplementary Figure 1D**), while the *mpkA* replacement was checked by using the primers MpkA FW and MpkA REV (**Supplementary Table 2** and **Supplementary Figure 1E**). Likewise, to construct the double mutant $pkcA^{G579R}$ *xylP::hsfA*, the *xylP::hsfA* cassette was transformed into the $pkcA^{G579R}$ *pyrG-* strain (Rocha et al., 2020b). The *xylP::hsfA* replacement in this mutant was checked using the primers HsfA 5 FW and xylP REV (**Supplementary Figure 1F**), while the primers pkcA GC FW and Afu5g11970 3R (**Supplementary Figure 1G**) were used to check the mutated *pkcA* locus. The $pkcA^{G579R}$ mutation is a Gly579Arg substitution in the PkcA protein, and the strain carrying this mutation is defective in the activation of MpkA and consequently the activation of the CWI pathway, resulting in altered expression of genes encoding cell wall-related proteins (Rocha et al., 2015). To construct the double mutant Δ*sakA xylP::hsfA*, the *sakA* deletion cassette was amplified from the genomic DNA of the Δ*sakA* strain (Altwasser et al., 2015) using primers sakA yes FW and sakA yes REV and transformed into the *xylP::hsfA* strain selected for hygromycin resistance. The *xylP::hsfA* locus in this mutant was checked using the primers HsfA 5 FW and xylP REV (**Supplementary Figure 1H**), while the primers IM-563 and IM-566 (**Supplementary Figure 1I**) were used to check the *sakA* locus.

To generate HsfA fusion with the luciferase gene (*luc*), a substitution cassette was constructed in which the *hsfA* genomic sequence without stop codon was cloned in-frame with the *luc* gene in a C-terminal fusion (**Supplementary Figure 1J**). The *luc* gene (1665 bp) without spacer was PCR-amplified from the pUC57 plasmid (Jacobsen et al., 2014) using the primers Luc FW and Luc REV. The *pyrG* gene was also used as a marker for prototrophy. The cassette was constructed *in vivo* in *S. cerevisiae* and transformed in *A. fumigatus* wild-type (**Supplementary Figures 1K,L**) and $pkcA^{G579R}$ *pyrG-* (**Supplementary Figures 1M,N**) strains. The Δ*mpkA* cassette

was also used to transform the *hsfA::luc* strain to obtain the double mutant (**Supplementary Figures 1O,P**).

To generate the reporter strain in which the *hsp90* promoter (*hsp90P*) was fused with the luciferase gene (*luc*), a substitution cassette was constructed by cloning the *hsp90P* (975 bp) in-frame with the *luc* gene (**Supplementary Figure 1Q**) flanked by 5′ UTR (0.833 kb) and 3′ UTR (0.573 kb) regions of the *pyrG* gene to allow integration of the construct at the *pyrG* locus. *hsp90P* was amplified from the genomic DNA of the CEA17 strain using the primers Hsp90P pyrG FW and Hsp90P RV luc, and the 5' UTR of *pyrG* was amplified by the primers pRS426 5UTR pyrG FW and 5UTR pyrG RV. The fragment containing the *luc* gene, the hygromycin resistance marker gene, and the 3′ UTR region of *pyrG* was amplified from the pNB04 plasmid (Rocha et al., 2016) using primers luc 2 FW and pyrG 3UTR pRS426 RV. The *hsp90P::luc* cassette was generated by recombination in *S. cerevisiae* and transformed into the *A. fumigatus* wild-type (**Supplementary Figures 1R,S**), $pkcA^{G579R}$ (**Supplementary Figures 1T,U**), Δ*rlmA* (**Supplementary Figures 1T,V**), and Δ*mpkA* (**Supplementary Figures 1T,W**) strains to obtain relevant single and double mutants.

DNA Manipulation and Southern Blot Analysis

Southern blot analysis was used to confirm that the *xylP::hsfA* cassette integrated homologously at the targeted locus. Genomic DNA from *A. fumigatus* was extracted as previously described (Malavazi and Goldman, 2012). For Southern blot analysis, *Xho*I-restricted chromosomal DNA fragments were separated on a 1% agarose gel and blotted onto Hybond N^+ nylon membranes (GE Healthcare), following standard techniques. Probe labeling was performed using AlkPhos Direct Labelling and Detection System (GE Healthcare) according to the manufacturer's description. Labeled membranes were exposed to ChemiDoc XRS gel imaging system (BioRad) to generate the images.

Transmission Electron Microscopy (TEM) Analysis

A total of 1×10^7 conidia of the wild-type strain were statically grown in 10 ml of liquid YG for 36 h at 30°C. HS was induced by transferring the mycelia to fresh pre-heated YG (48°C) for 5, 10, 15, 30, and 60 min of incubation at 48°C. The control was left at 30°C. To analyze the cell wall organization in the conditional *hsfA* mutant, wild-type and *xylP::hsfA* strains were statically grown in liquid MM supplemented with xylose 1% for 36 h at 30°C. The mycelia were collected by centrifugation, washed twice with fresh MM, and further incubated in MM (repression) or MM lacking glucose but supplemented with xylose 0.06% (induction) for 4 h at 30°C. Finally, the repressed samples were heat-shocked at 48°C for 15, 30, and 60 min or treated with 2 μg/ml of caspofungin (CASP) for 1 h to induce cell wall stress. The untreated control remained at 30°C. Next, the mycelia were fixed in 3% EM grade glutaraldehyde in 0.1 M sodium cacodylate buffer, pH 7.4, for 24 h at 4°C. Cells were processed as described previously (Munshi et al., 2018), and TEM image acquisition was achieved using a FEI TeCnai12 BioTwinG2 microscope at an acceleration voltage of 120 kV. Digital images were acquired with an AMT XR-60 CCD Digital Camera system. Cell wall thicknesses of 50 sections of different germlings were measured using ImageJ software.

Phenotypic Assays

The radial growth of the wild-type and *xylP::hsfA* strains at different temperatures was analyzed by spotting 1×10^4 conidia of each strain onto the center of 90 mm Petri dishes containing solid MM supplemented with different concentrations of xylose. The plates were incubated for 72 h at 30°C, 37°C, or 48°C and analyzed. Similarly, to investigate the susceptibility of the strains to agents that impair cell wall maintenance or cell membrane [caffeine (CAF), calcofluor white (CFW), congo red (CR), caspofungin (CASP), and sodium dodecyl sulfate (SDS), respectively], 1×10^4 conidia of each strain were inoculated on solid MM supplemented with xylose 0.06% and increasing concentrations of the drugs. The same procedures were employed to test susceptibility to osmotic stress caused by sorbitol and oxidative stress induced by paraquat and menadione. All the Petri dishes were incubated at 37°C for 72 h. As an alternative protocol, the susceptibility to H_2O_2, diamide, and the crop fungicide fludioxonil was investigated in 96-well plate assays containing 200 μl of liquid MM supplemented with xylose 0.06% and different concentrations of the agents mentioned above.

For the genetic analysis of double and single mutants, 10-fold dilution series (1×10^5–1×10^2) of the conidia were spotted on Petri dishes containing MM supplemented with different xylose concentrations and CASP. The plates were incubated at 30°C, 37°C, or 48°C for 48 h and analyzed.

Luciferase Activity Assay

Luminescence quantification of the relevant strains was performed as described elsewhere (Rocha et al., 2016), with minor modifications. For the luciferase activity assay during HS, 2×10^5 conidia of each strain were cultured in white, clear bottomed 96-well plates (Greiner Bio-one) containing 200 μl of MM supplemented with yeast extract 0.006% and grown at 30°C for 12 h for initial biofilm formation. Next, luciferin (0.5 mM) was added to each well and the plates were read initially at 30°C and incubated at 37°C or 48°C for 2 h. Luminescence readings were taken at 2-min intervals. For the cell wall stress assay, the same procedures were followed except that the plates were cultured at 37°C for 5 h. Subsequently, 2 μg/ml of CASP were added to each well along with luciferin 0.5 mM. The plates were incubated at 37°C for 4 h, and readings were recorded at 2-min intervals. All the luciferase activity experiments were read in Luminescence mode on the SpectraMax M5 (Molecular Devices). Normalization was made by the number of conidia. Mean ± SEM are shown in the graphs.

RNA Extraction and RT-qPCR Procedures

To evaluate the *hsfA* expression in the conditional *xylP::hsfA* mutant, 1×10^8 conidia of the wild-type and *xylP::hsfA* strains were grown for 24 h at 37°C in 50 ml of liquid MM supplemented with xylose 1% and transferred to fresh MM or MM without

glucose supplemented with different concentrations of xylose (0.06, 0.2, 1, and 5%) for additional 4 h of growth. HS stress induction was achieved by incubating 1×10^8 conidia of the wild-type strain in MM for 24 h at 30°C. Subsequently, mycelia were transferred to fresh pre-heated MM (48°C) for 2, 5, 10, 15, 30, 60, and 120 min of incubation at 48°C. The control was left at 30°C. Cell wall stress was achieved by incubating 2×10^7 conidia of the wild-type strain in YG for 16 h at 37°C. Subsequently, the samples were subjected to CASP or CR exposure for 60 or 30 min, respectively. Mycelia from each culture condition were collected via vacuum filtration, frozen in liquid nitrogen, and stored at −80°C until used for RNA extractions.

The total RNA was extracted with Trizol reagent (Thermo Scientific) according to the manufacturer's protocol. RNA was processed as described previously (Rocha et al., 2015). DNAse-treated total RNA from each strain was reverse-transcribed with High-Capacity cDNA Reverse Transcription kit (Thermo Scientific) as described elsewhere (Rocha et al., 2015). RT-qPCR was conducted with Power Sybr Green PCR Master Mix (Thermo Scientific). The primers for the individual genes were designed using Primer Express 3.0 software (Life Technologies) and are listed in **Supplementary Table 3**. RT-qPCR was performed in duplicate from three independent biological samples in a StepOne Plus Real-time PCR System (Thermo Scientific). The fold change in mRNA abundance was calculated using $2^{-\Delta\Delta Ct}$ equation, and all the values were normalized to the expression of β-tubulin (*tubA*).

RNA-Sequencing

To induce heat stress, 1×10^8 conidia from wild-type and *xylP::hsfA* strains were incubated in 50 ml of liquid MM supplemented with xylose 1% for 24 h at 30°C. Subsequently, mycelia were washed twice with MM and incubated for 4 h at 30°C in MM for *hsfA* repression (Baldin et al., 2015). HS was induced by transferring the mycelia to fresh pre-heated MM for 15 and 60 min at 48°C. The control was left at 30°C. Mycelium from each time point for both pre- and post-stress exposure was collected via vacuum filtration, immediately frozen in liquid nitrogen, and stored at −80°C until used for RNA extraction.

Total RNA was extracted using Trizol reagent, treated with DNase I (Qiagen) and purified using the RNeasy kit (Qiagen), according to the manufacturer's instructions. RNA from each treatment was quantified using NanoDrop (Thermo Scientific) and analyzed on an Agilent 2100 Bioanalyzer system to assess RNA integrity (RIN = 9.0–9.5). Sample preparation and library construction were performed as described previously (Alves de Castro et al., 2016) using Illumina TruSeq stranded mRNA sample preparation kit. Libraries were quantified on Step One Plus equipment (Applied Biosystems) and sequenced (2×100 bp) on a HiSeq 2500 instrument. Short reads were submitted to the NCBI's Short Read Archive under the Bioproject PRJNA690780. Obtained fastq files were quality checked with FastQC[1] and cleaned with Trimmomatic (Bolger et al., 2014). Ribosomal RNA was removed using SortMeRNA (Kopylova et al., 2012), and high-quality reads were mapped to the *A. fumigatus* Af293 genome sequence using Tophat2 (Kim et al., 2013) in strand-specific mode. The saturation of sequencing effort was assessed by counting the number of detected exon–exon junctions at different subsampling levels of the total high-quality reads, using RSeQC (Wang et al., 2012). All samples achieved saturation of known exon–exon junctions. To assess transcript abundance, exonic reads were counted in a strand-specific way using the Rsubread library (Liao et al., 2013) from the Bioconductor suite (Huber et al., 2015). Calling of differentially expressed genes was carried out in EdgeR (Robinson et al., 2010), controlling for an FDR of 0.01. The fold changes and the statistical significances of all genes for each comparison are shown in **Supplementary Table 4**. Gene ontology (GO) enrichment analysis was performed using the KOBAS tool kobas.cbi.pku.edu.cn (Xie et al., 2011). Cluster analysis of the differently expressed genes was performed using hierarchical clustering in Multiple Experiment Viewer (MeV) software[2].

RESULTS

Heat Stress Affects the Structure of *A. fumigatus* Cell Wall

Our previous results indicated that the *A. fumigatus* CWI pathway mutants are less tolerant to HS and PkcA signaling is required for early adaptation to HS (Rocha et al., 2020b). To gain insights about the early and prolonged effects of HS on the cell wall, we further analyzed the cell wall organization in the wild-type strain before and after HS at 48°C using TEM (**Figure 1A**). We observed a remarkable increase in the thickness of the fungus cell wall after HS exposure. Surprisingly, this increase is noticeable as early as after 5 min of exposure to high temperature resulting in a 27% increase in the cell wall thickness. Consistently, this increase is more evident after 10–15 min (60% increase) and 60 min (75% increase) of HS (**Figure 1B**). These results suggest that the sudden increase in temperature triggers the cell wall remodeling, indicating that this structure is highly dynamic and responsive to fluctuations in the surrounding temperature, potentially underlying a survival mechanism to counteract HS represented by the dramatic expansion of the cell wall.

The *hsfA* Gene Is Essential for Thermotolerance and Required for Cell Wall Stress Resistance in *A. fumigatus*

The dramatic and quick changes in the cell wall architecture observed above when cells are challenged with HS prompted us to look for the impact of known regulators of thermoadaptation on the CWI of *A. fumigatus*. We have previously shown that the CWI pathway is activated when the cells are exposed to elevated temperatures and that the molecular chaperone Hsp90 interacts with the main components of this signaling pathway, assisting both the adaptation to HS and cell wall stress (Rocha et al., 2020b). Since, in eukaryotes, the *HSP90* gene expression is tightly governed by the transcription factor

[1] http://www.bioinformatics.babraham.ac.uk/projects/fastqc/

[2] http://mev.tm4.org/

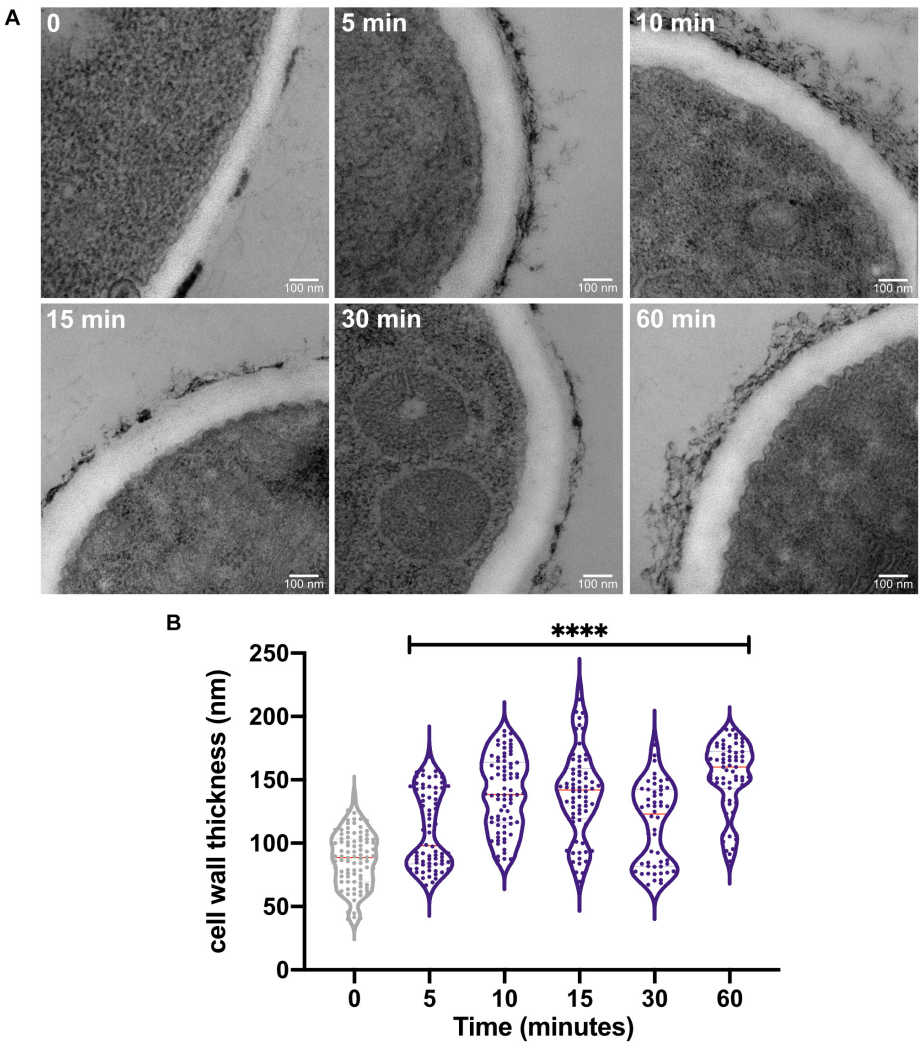

FIGURE 1 | The heat shock stress causes an increase in the cell wall thickness of *A. fumigatus*. **(A)** The *A. fumigatus* wild-type strain was statically grown in complete liquid media for 36 h at 30°C, heat-shocked at 48°C for the indicated times, and prepared for transmission electron microscopy analysis. **(B)** Cell wall thickness measurement of the germlings shown in violin plot of 50 sections of different germlings. Dashed lines indicate the quartiles and red lines indicate the median for each point. ****$p \leq 0.0001$ (one-way ANOVA and Dunnett's multiple comparisons test).

Hsf1 and this protein is one of the most important regulators of the HS response (Leach et al., 2016; Schopf et al., 2017), we searched for the *hsf1* homolog in *A. fumigatus*. A BLASTp search of the *A. fumigatus* A1163 genome database using *S. cerevisiae* and *C. albicans HSF1* as queries revealed a single open reading frame with significant similarity. The potential homolog, Afu5g01900 (hereafter named *hsfA*), shares 30% identity and 51% similarity (e-value 5e–26) with the ScHsf1 and 27% identity and 46% similarity (e-value 9e–29) with the CaHsf1. Furthermore, HsfA shows significant identity with Hsf1 of *A. nidulans* and *Aspergillus niger* (70% identity and 79% similarity, e-value 0.0; and 74% identity and 83% similarity, e-value 0.0, respectively). The HsfA region with the highest identity comprises the HSF-type DNA-binding domain of both yeast and human proteins (Veri et al., 2018), from residues 150 to 252 (2.8e-28; Pfam 00447).

As a first approach to study the role of HsfA in *A. fumigatus*, we analyzed the expression of *hsfA* in the *A. fumigatus* wild-type strain during HS and cell wall stress. We also assessed the mRNA levels of the *hsp90* gene, which is one of the most significant transcriptional targets of Hsf1 in eukaryotes (Erkine et al., 1999; Leach et al., 2016; Prodromou, 2016). We found that both *hsfA* and *hsp90* mRNA accumulation were rapidly induced in response to HS (**Figure 2A**), with *hsfA* reaching maximum expression after 15 min and *hsp90* after 30 min post-HS treatment compared to the control condition (30°C). After reaching the peak, *hsfA* mRNA levels decrease over time while high *hsp90* expression levels are sustained post-60 min of HS. These results are consistent with the role of *hsfA* as a transcription factor potentially upregulated when Hsp90-mediated *hsfA* inhibition is relieved upon HS, culminating with subsequent HsfA-mediated enhanced transcription of HSP, including Hsp90. When cells

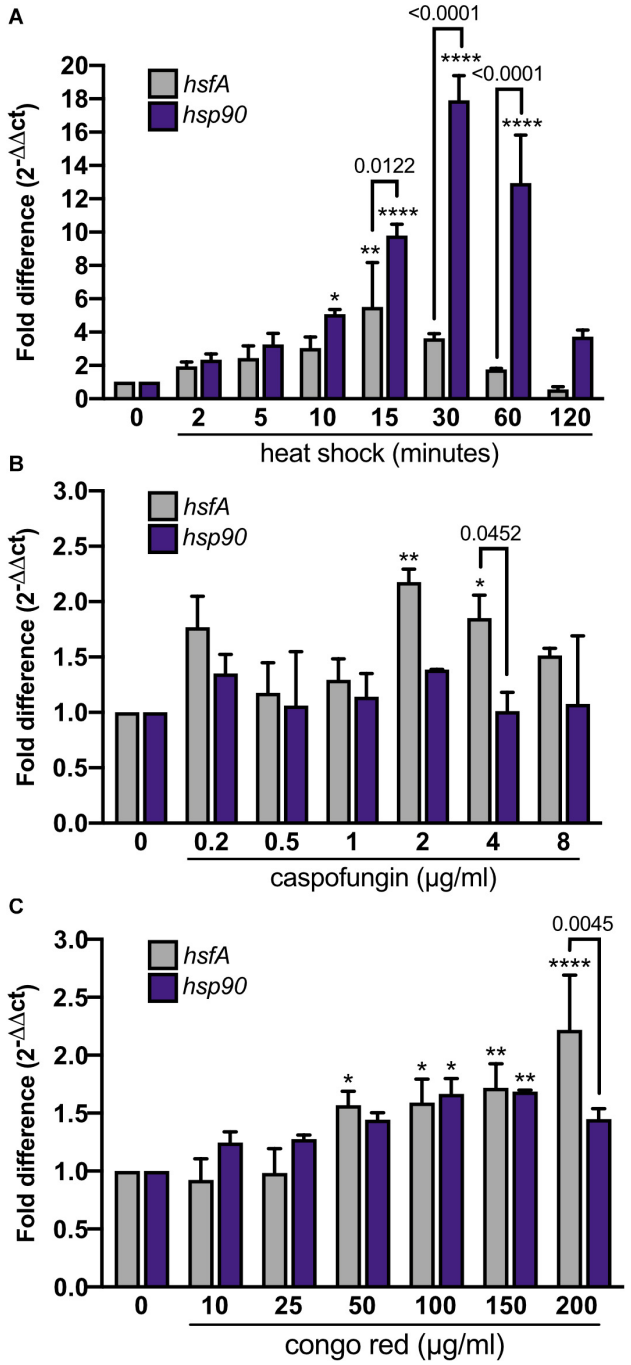

FIGURE 2 | *hsfA* and *hsp90* expression respond to heat shock and cell wall stress. Expression of *hsfA* and *hsp90* was investigated by RT-qPCR. **(A)** The wild-type strain was grown in MM for 24 h at 30°C and heat-shocked for the indicated time points (min) at 48°C. The wild-type strain was grown in YG for 16 h at 37°C, and cell wall stress was achieved using increasing caspofungin concentrations for 60 min **(B)** or congo red for 30 min **(C)**. The fold difference of each gene represents the normalized total mRNA in relation to the same gene in the control condition. Mean ± SD ($n = 3$) are shown. Significant differences were observed by using two-way ANOVA followed by Sidak's posttest. *$p < 0.05$, **$p < 0.01$, and ****$p < 0.0001$ indicate significant differences from comparisons to the same gene at the control condition. Differences between the genes are indicated by the bars.

were challenged with cell wall stress induced by the addition of increasing concentrations of CASP, *hsfA* mRNA levels were significantly increased in the presence of 2 μg/ml and 4 μg/ml of the drug compared to the non-treated control condition (**Figure 2B**). Curiously, the *hsp90* accumulation under these conditions did not significantly change in comparison to the non-treated control. A similar expression profile for both genes was observed when different CR (congo red) concentrations were employed (**Figure 2C**), where an increase in *hsfA* mRNA abundance was detected at CR concentration ranging from 50 μg/ml to 200 μg/ml. These results indicate that *hsfA* is required to cope with the cell wall stress, but without a dramatic increase in mRNA *hsp90* abundance, suggesting a different regulatory mechanism for this TF in the presence of cell wall damage compared to temperature stress.

To further explore the role of *hsfA* in the *A. fumigatus* HS and cell wall stress response, we next attempted to generate an *hsfA* null mutant. Various deletion strategies and constructions were not successful, and after repeated attempts, no positive transformants were obtained (data not shown), suggesting that under standard laboratory conditions, *hsfA* is essential for viability in *A. fumigatus*, as observed for other fungal species, such as *S. cerevisiae* and *C. albicans* (Wiederrecht et al., 1988; Nicholls et al., 2009). Subsequently, we decided to generate a conditional *xylP::hsfA* mutant, in which the *hsfA* gene is under the control of the *P. chrysogenum xylP* promoter (Zadra et al., 2000). The substitution cassette contained the *pyrG* gene as the prototrophy marker, fused to the *xylP* promoter containing the first 467 bp of the native *hsfA* promoter (**Supplementary Figure 1A**). Diagnostic PCR and Southern blot analysis confirmed a single integration event in the conditional mutant (**Supplementary Figures 1B,C**).

To validate the conditional expression of *hsfA* in this mutant, the mRNA abundance of *hsfA* was determined by RT-qPCR, both in the presence of glucose 1% (MM) for repression and in MM supplemented with increasing concentrations of xylose for *xylP* promoter induction (**Figure 3A**). The *hsfA* expression levels in the conditional lethal mutant increased in a xylose concentration-dependent manner (up to 5%), while in the wild-type strain, it remained constant. The results showed that at low xylose concentration (0.06%) *hsfA* mRNA abundance in the *xylP::hsfA* mutant was similar to that recorded for the wild-type strain. Consistently, *hsfA* expression was significantly suppressed in the absence of xylose.

In order to evaluate if *hsfA* repression causes any changes in the germination and structure of *A. fumigatus* hyphae such as lysis, which could be consistent with cell wall defects, an optical microscopy experiment was conducted in which both the wild-type and the *xylP::hsfA* strains were cultivated in MM containing different concentrations of xylose for 12 h at 37°C. As expected, the absence of xylose completely inhibited growth of the conditional mutant without noticeably affecting germination of the conidia (**Figure 3B**). In contrast, the *xylP::hsfA* mutant started germination with an increase in xylose concentration, achieving a comparable wild-type growth with 0.06 to 0.1% of xylose in the medium. These results indicate that HsfA

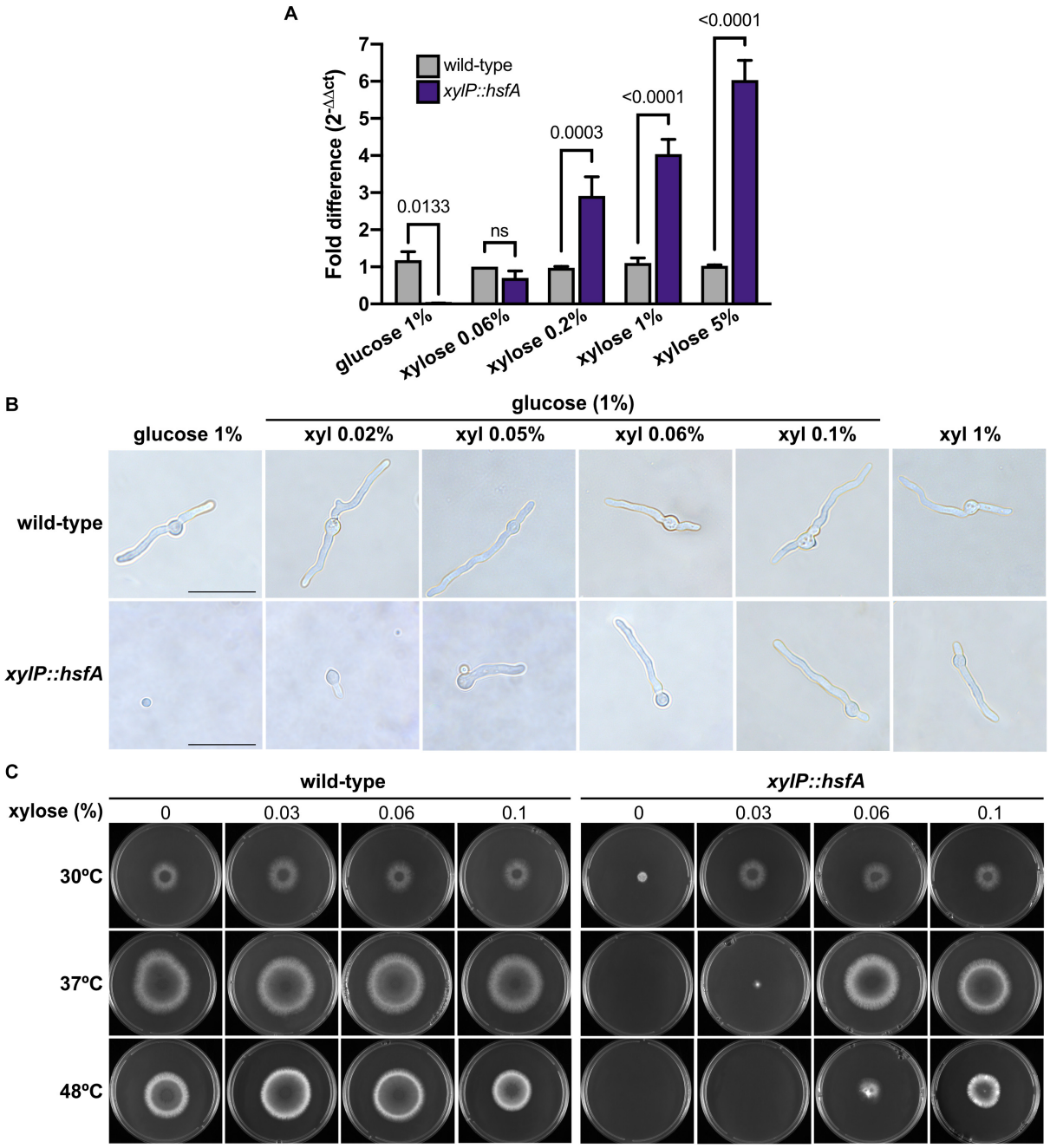

FIGURE 3 | *hsfA* is essential for vegetative growth and thermotolerance. **(A)** *hsfA* expression in the wild-type and conditional lethal *xylP::hsfA* strain. The strains were grown for 24 h at 37°C in liquid MM supplemented with xylose 1% and transferred to fresh MM or MM lacking glucose supplemented with different xylose concentrations for 4 h. The fold difference of each condition represents the normalized mRNA abundance in comparison to the wild-type strain. Mean ± SD (n = 3) are shown. Statistics are indicated by the bars and p values are depicted (ns: non-significant; two-way ANOVA and Sidak's multiple comparison test). **(B)** *hsfA* is required for *A. fumigatus* germination. The wild-type and *xylP::hsfA* strains were cultivated for 12 h at 37°C in glass-bottom dishes containing 2 ml of MM (glucose 1%) supplemented with increasing concentrations of xylose (xyl), or in xylose 1% as the sole carbon source. Magnification 100×; bar = 10 μm. **(C)** Radial growth of the wild-type and *xylP::hsfA* strains under repressive (glucose) or inducing conditions (xylose). A total of 1 × 10^4 conidia of wild-type and *xylP::hsfA* strains were inoculated into the center of solid MM plates supplemented with the indicated concentrations of xylose and incubated at 30°C, 37°C, or 48°C for 72 h.

is essential for *A. fumigatus* viability. Except for germination inhibition at low xylose concentrations, no change in the mutant hyphae morphology was observed. For comparison, in a medium lacking glucose and supplemented with xylose 1% as the sole carbon source, the conditional mutant grew normally, without the emergence of any hyphae structural alteration (**Figure 3B**).

Because thermotolerance is a key feature for the *A. fumigatus* biology (Bhabhra and Askew, 2005) and HsfA may be a major regulator of this attribute, we initially attempted to understand the role played by *hsfA* in ensuring thermotolerance. The wild-type and the *xylP::hsfA* strains were cultured in MM supplemented with varying xylose concentrations at different temperatures (**Figure 3C**). Although under basal condition (30°C), the *xylP::hsfA* strain under repressive condition showed decreased radial growth compared to the wild-type strain, growth was comparable to that of the wild-type strain when a small concentration of xylose was added to the medium (0.03%). However, at 37°C, the conditional mutant could not grow under repressive conditions, further suggesting the crucial role of *hsfA* for thermoadaptation of the fungus. The radial growth of the mutant was equivalent to the wild-type strain in the presence of at least 0.06% xylose. For this reason, this concentration of xylose was chosen for the next phenotypic assays below. The *xylP::hsfA* mutant susceptibility was even higher at 48°C since it could only grow properly when more than 0.1% of xylose was added to the medium (**Figure 3C**). Altogether, these results suggest that the cell viability is highly dependent on *hsfA* upon temperature increase.

As our qPCR analysis hinted at the importance of *hsfA* as an adjunctive transcription factor required to cope with cell wall stress, we next investigated the relevance of *hsfA* for cell wall maintenance by evaluating the susceptibility of the conditional lethal mutant when grown in low *hsfA* expression level conditions (0.06% xylose, **Figure 3**). We observed differences in the conditional mutant susceptibility profile compared to the wild-type strain in the presence of cell wall stressing agents. Among the drugs tested, the highest growth inhibition was recorded for CASP, CAF, and CR treatments (**Figure 4A**). For these experiments, small increments in the amount of xylose added to the culture media caused recovery of the lethal phenotype, thus making it difficult to determine a xylose concentration to balance viability of the mutant and repression of *hsfA* to assess susceptibility to these cell wall stressors. Thus, we suggest that the narrow range of xylose concentration that results in a dramatic difference in growth (for instance, compare xylose concentration of 0.03 and 0.06% in **Figure 3C**) can partially explain the subtle cell wall phenotypes we present here.

Nevertheless, the results shown in **Figure 4A** point to a role of *hsfA* in cell wall homeostasis. In line with this evidence, when the *xylP::hsfA* conditional lethal mutant was grown under repressive conditions (MM) and analyzed by TEM, we observed a significant cell wall thickening (15%) at non-HS basal condition (30°C), which was fully recovered when 0.06% xylose was added to the culture medium (**Figures 4B,C**), further suggesting that *hsfA* plays a crucial role controlling the expression of cell wall-related genes. As expected, the cell wall thickness of the wild-type strain increased during the HS and during cell wall stress caused by CASP. In contrast, the cell wall thickening of the *xylP::hsfA* conditional mutant was similar to the wild-type strain under the two stress conditions, although significantly different from the control condition (1% glucose, 30°C), where the cell wall is constitutively thicker. These results suggest that *hsfA* is required for typical cell wall architecture under basal conditions, while *hsfA* loss of function retains the ability to remodel the cell wall ultrastructure when challenged with CASP and HS.

In addition to temperature stress tolerance, Hsf1 in yeast is also induced by oxidative stress, ethanol exposure, and glucose starvation (Liu and Thiele, 1996; Hahn and Thiele, 2004; Hashikawa et al., 2007). Consistently, the *xylP::hsfA* strain showed increased sensitivity to all oxidative stress compounds tested (menadione, hydrogen peroxide, and diamide) in comparison to the wild-type strain, except for paraquat (**Supplementary Figure 2**). The conditional mutant was also more susceptible to the crop fungicide fludioxonil (**Supplementary Figure 2B**). In contrast, there were no growth differences between the conditional mutant and the wild-type strain in the presence of osmotic stress caused by high concentrations of sorbitol (data not shown). These results suggest a role for *hsfA* in oxidative stress detoxification in *A. fumigatus*.

HsfA Genetically Interacts With the MAPKs *mpkA* and *sakA*

Previous reports suggested that *A. fumigatus* cell wall undergoes continuous remodeling in response to environmental stimuli or stress conditions (Rocha et al., 2020a). Under these circumstances, the biosynthesis and reinforcement of the cell wall rely on the concerted actions of the CWI pathway and the High Osmolarity Glycerol (HOG) pathway since both cascades have overlapping functions to promote adaptation to cell wall-targeting and temperature stresses (Altwasser et al., 2015; Rocha et al., 2015, 2020b; Bruder Nascimento et al., 2016). Also, the MAPK cascades associated with these circuits crosstalk with the Hsf1 transcription factor through the action of the Hsp90 in *S. cerevisiae* and *C. albicans* (Lamoth et al., 2012; Leach et al., 2012a). As *hsfA* repression caused cell wall phenotypes, we asked whether this transcription factor genetically interacts with the apical kinase (*pkcA*) and the MAPK (*mpkA*) of the CWI pathway and the MAPK of the HOG pathway (*sakA*). Accordingly, double conditional mutants of *xylP::hsfA* with $pkcA^{G579R}$ allele and Δ*mpkA*, or Δ*sakA* were constructed (**Supplementary Figures 1D–I**).

Phenotypic tests with these double mutants were conducted under low xylose concentration to titrate out the expression of *hsfA* and score genetic interactions when *hsfA* is limiting inside the cell, since the recovery of *hsfA* expression occurs in largely low xylose concentration, as mentioned above (**Figure 3**). We observed that *mpkA* and *sakA* genetically interact with *hsfA* upon growth at 37°C and 48°C since the respective double conditional mutants grew less at lower xylose concentrations than the parental strains (**Figure 5A**). The same results were observed during cell wall stress caused by CASP (**Figure 5B**), CR, and CFW (**Supplementary Figures 3A,B**), as well as in the presence of SDS (**Supplementary Figure 3C**). Consistently, when the xylose concentration is increased to 0.1–0.5%, growth of the double conditional mutant

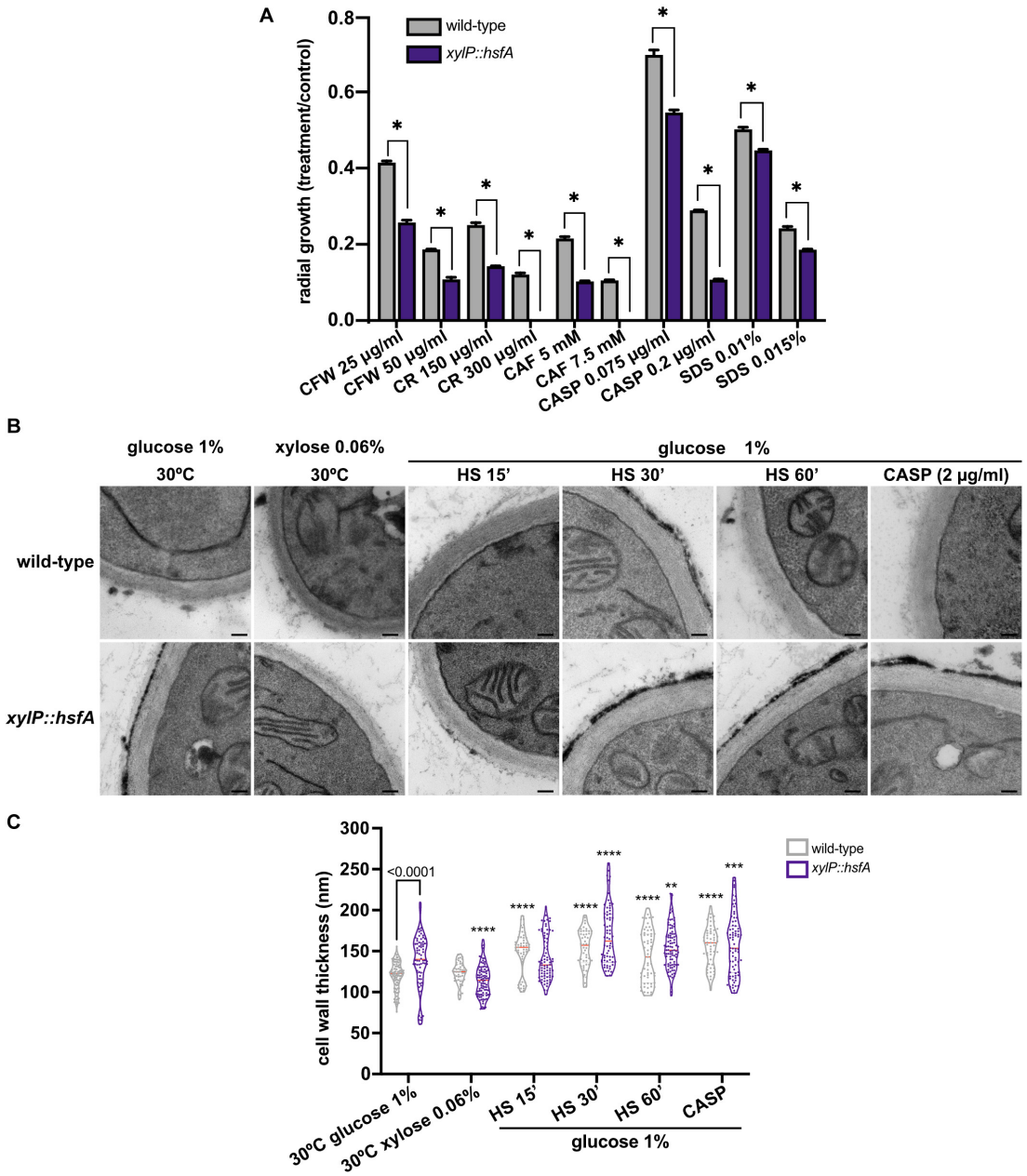

FIGURE 4 | The *xylP::hsfA* mutant is more susceptible to cell wall stress. **(A)** A total of 1×10^4 conidia of the wild-type and *xylP::hsfA* strains were inoculated onto solid MM supplemented with 0.06% xylose (low *hsfA* expression conditions) and varying concentrations of calcofluor white (CFW), congo red (CR), caffeine (CAF), caspofungin (CASP), and sodium dodecil sulfate (SDS). The plates were incubated at 37°C for 72 h and the ratio of radial growth of treated to the control condition was calculated. The results were expressed as mean ± SD, $n = 3$. *$p \leq 0.0001$ (two-way ANOVA and Sidak's posttest). **(B)** HsfA depletion increases cell wall thickness in *A. fumigatus*. The wild-type and *xylP::hsfA* strains were grown in liquid MM supplemented with 1% xylose for 36 h at 30°C and further incubated in MM (repression) or MM lacking glucose supplemented with xylose 0.06% (induction) for 4 h at 30°C. Next, the repressed samples were heat-shocked at 48°C for 15, 30, and 60 min or treated with 2 µg/ml of CASP for 60 min, and prepared for transmission electron microscopy analysis. Black bars: 100 nm. **(C)** Cell wall thickness measurement of the germlings shown in violin plot of 50 sections of different germlings. Dashed lines indicate the quartiles and red lines indicate the median for each condition. Significant differences were observed by using two-way ANOVA followed by Sidak's posttest. **$p < 0.01$, ***$p < 0.001$, and ****$p < 0.0001$ indicate significant differences from comparisons to the same strain at the control (30°C, glucose 1%) condition. Differences between the strains in the same growth condition are indicated by the bars.

is completely rescued, indicating that restoration of *hsfA* expression to wild-type levels is sufficient to fully recover the phenotype in the absence of either *mpkA* or *sakA*. These results also point out that *mpkA* and *sakA* are not essential for *hsfA* activation during thermoadaptation and cell wall stress.

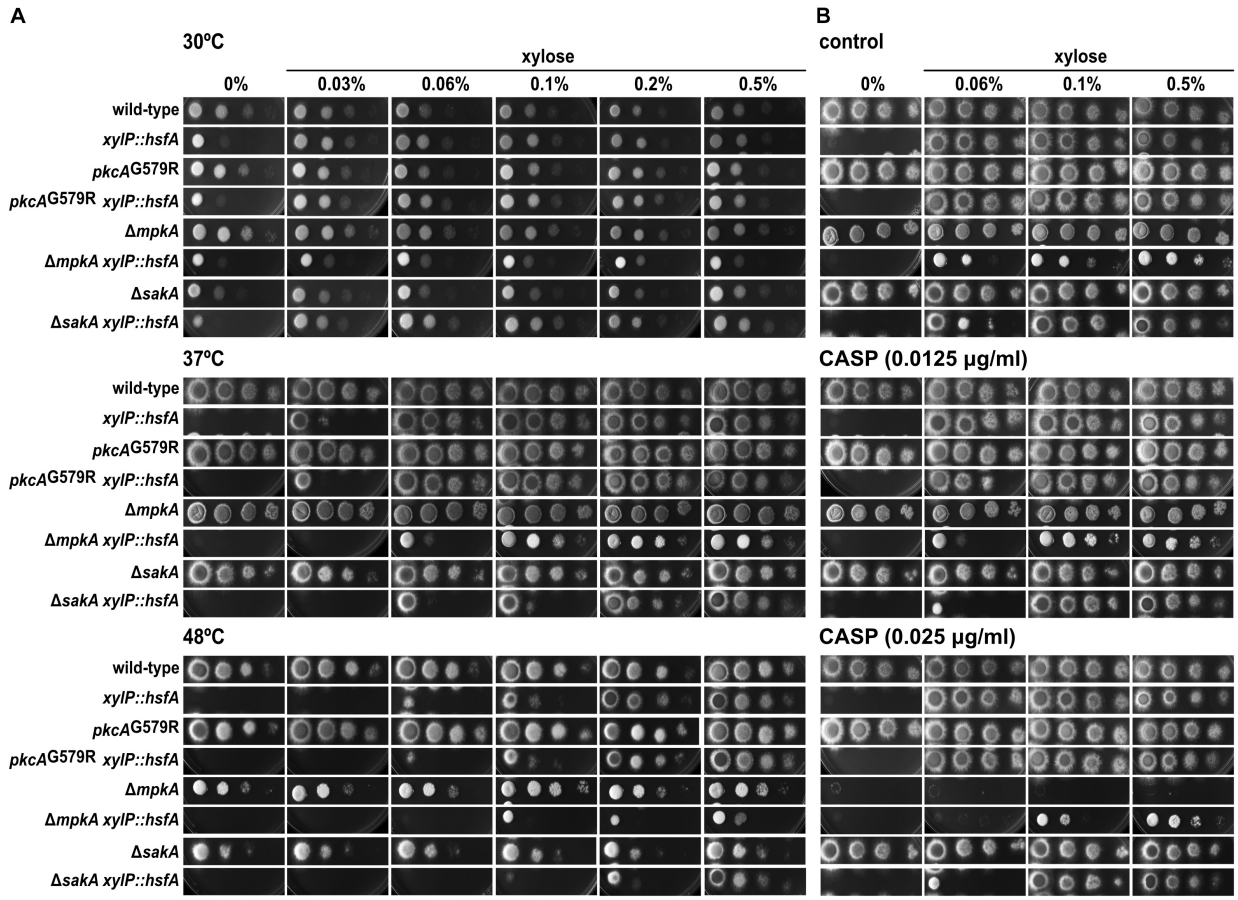

FIGURE 5 | *hsfA* genetically interacts with *mpkA* and *sakA* during temperature and cell wall stresses. Tenfold dilution series of conidia from the wild-type, *xylP::hsfA*, $pkcA^{G579R}$, $pkcA^{G579R}$ *xylP::hsfA*, Δ*mpkA*, Δ*mpkA xylP::hsfA*, Δ*sakA*, and Δ*sakA xylP::hsfA* strains was inoculated into solid MM containing different concentrations of xylose. **(A)** Plates were incubated at 30°C, 37°C, or 48°C for 48 h. **(B)** 0.0125 μg/ml and 0.025 μg/ml of caspofungin (CASP) were used to induce cell wall stress and the plates were incubated at 37°C for 48 h.

HsfA and Hsp90 Act Together to Endure Cell Wall Stress and HS via the CWI Pathway

Given the above reported synthetically sick genetic interactions between *hsfA* and the MAPKs of the CWI and HOG pathways, we used the luciferase (*luc*) reporter gene to investigate differences in HsfA protein expression during HS and cell wall stress induced by CASP. The rationale behind this experiment was to examine a role of these MAPKs in regulating posttranscriptional levels of HsfA. Hence, single and double mutants containing HsfA protein controlled by its native promoter and C-terminally fused to the luciferase protein were constructed (**Supplementary Figures 1J–P**). All the reporter strains, with the exception of Δ*sakA hsfA::luc*, showed no growth defects compared to the parental strains, indicating that the replaced alleles are fully functional (**Supplementary Figure 4**). Since the viability and growth of several Δ*sakA hsfA::luc* transformation mutants were impaired under HS conditions compared to the parental strains (data not shown), the evaluation of the *hsfA* expression was not possible in this mutant.

The luciferase activity was recorded after exposing the germlings of the reporter strains to HS and CASP. We observed that HsfA protein expression was rapidly induced after 15 min of HS at both 37°C (**Figure 6A**) and 48°C (**Figure 6B**) in the biofilm of all strains. These results are consistent with the peak in mRNA abundance recorded under the same conditions for the wild-type strain (**Figure 2A**), thus validating our HsfA reporter strain. However, the luciferase signal was more intense in the strains carrying the $pkcA^{G579R}$ and Δ*mpkA* mutations at both temperatures. In these genetic backgrounds, sustained high HsfA levels were recorded at 37°C up to 120 min of HS. Although, at 48°C, the same HsfA expression peak was detected after 15 min, the luciferase signal returned to wild-type levels after the 30 min of HS adaptation. These results highlight the importance of *hsfA* and the CWI pathway in the thermoadaptation of *A. fumigatus* to the mammalian host environment.

The expression of HsfA was also significantly induced by CASP treatment after 60 min of drug exposure (**Figures 6C,D**), similarly to the mRNA *hsfA* levels recorded under the same conditions in the wild-type strain (**Figure 2B**). Interestingly, the

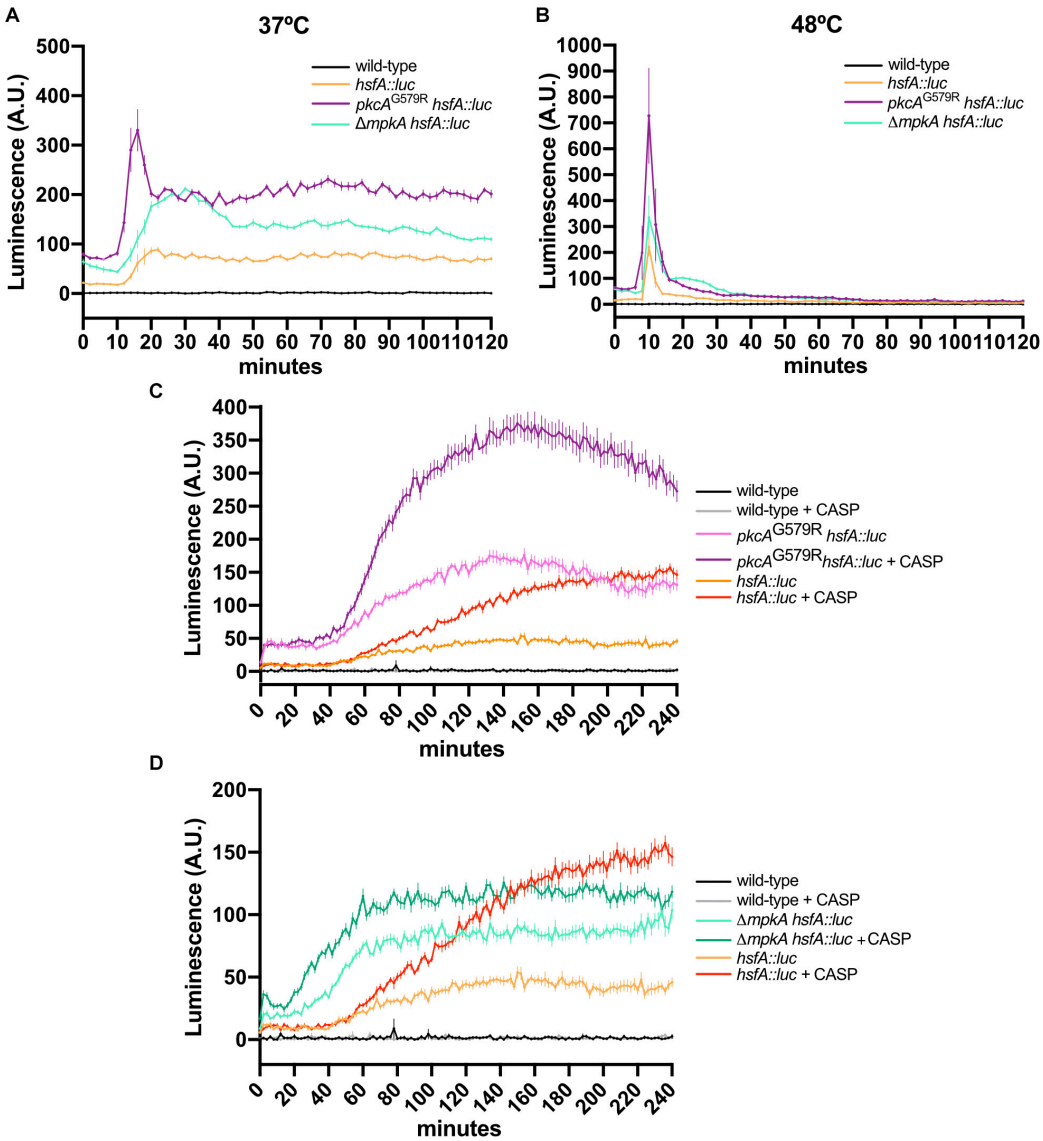

FIGURE 6 | The loss of function of CWI regulators increases HsfA expression in *A. fumigatus* biofilms under HS and cell wall stress. **(A,B)** Luciferase activity assay of the *hsfA::luc*, *pkcA*^{G579R} *hsfA::luc*, and Δ*mpkA hsfA::luc* strains during the HS at 37°C **(A)** and 48°C **(B)**. **(C,D)** Luciferase activity assay of the *pkcA*^{G579R} *hsfA::luc* **(D)** and Δ*mpkA hsfA::luc* strains during cell wall stress caused by CASP. The wild-type strain without luciferase gene was used as the negative control in all experiments. Mean ± SEM ($n \geq 8$) are shown. The results were normalized by the number of conidia (2×10^5 per assay) and are expressed as luminescence (arbitrary units). CASP: caspofungin (2 μg/ml).

HsfA high levels were maintained up to 240 min of treatment. Again, we observed a positive synergistic effect in the HsfA expression when the *pkcA*^{G579R} mutant allele was combined with the CASP exposure (**Figure 6C**). The same synergistic effect was also observed in the combination of CASP and the Δ*mpkA* mutant (**Figure 6D**). We also conclude that *pkcA* and *mpkA* are not required for HsfA expression, and the loss of function of these kinases enhances the accumulation of HsfA possibly via undescribed compensatory mechanisms to retain the CWI and thermotolerance.

Given the *hsp90* levels are critical for the HsfA transcription and to probe further into the potential mechanisms underlying the enhanced HsfA expression in the CWI pathway mutants, we assessed the activity of the *hsp90* promoter (*hsp90P*) under the same conditions we used above to trace the HsfA protein accumulation. We constructed CWI pathway mutants in which the *hsp90P* was fused to the luciferase gene to generate relevant reporter strains (**Supplementary Figures 1Q–W**). For these experiments, we also included the deletion strain of the CWI pathway-associated transcription factor RlmA. As expected, *hsp90P* activity was rapidly upregulated during HS in the *hsp90P::luc* strain at 37°C (**Figure 7A**) and 48°C (**Figure 7B**), peaking at 15–20 min post-HS. At 37°C, there were no significant differences in the

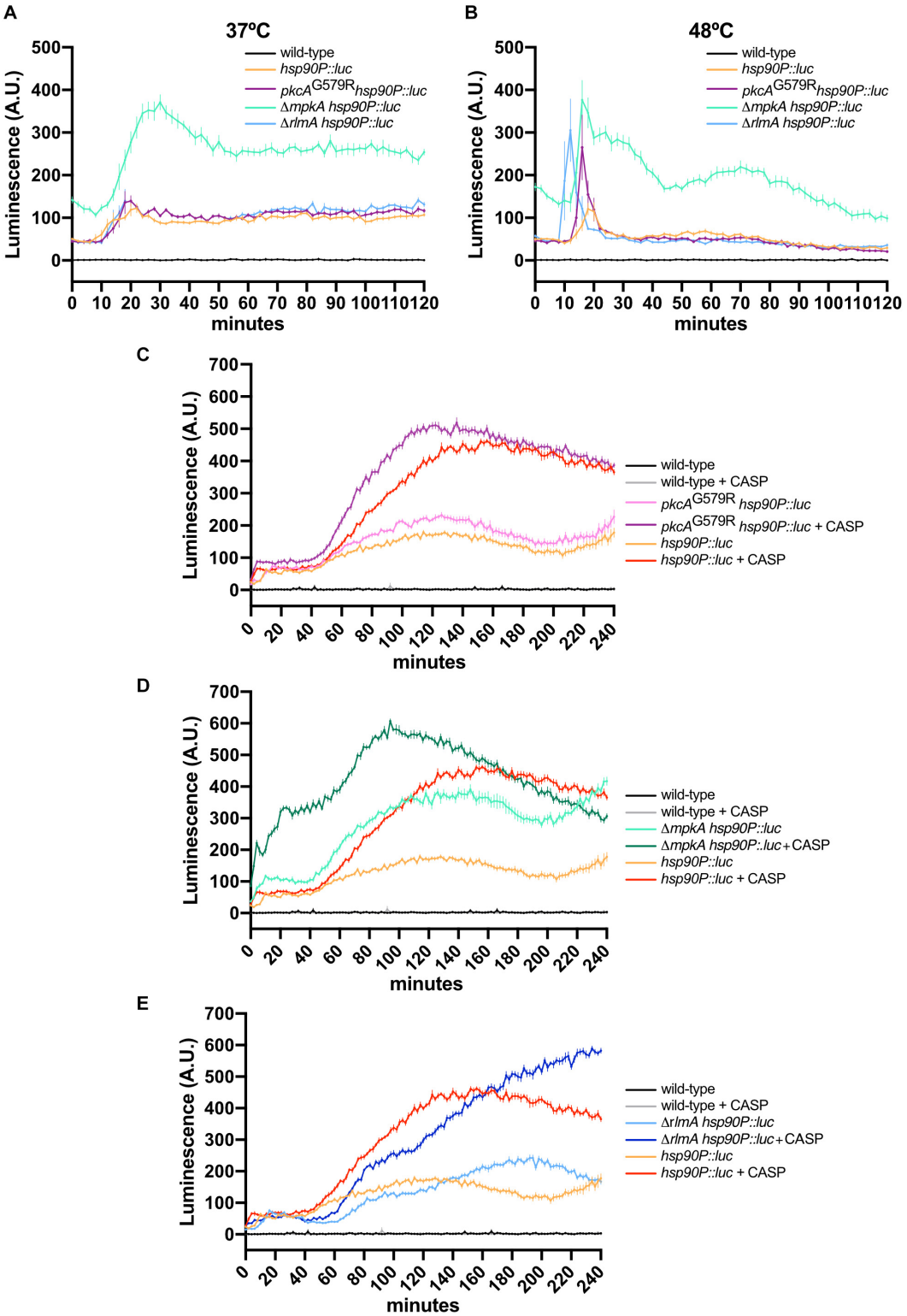

FIGURE 7 | The loss of function of CWI regulators increases *hsp90* expression in *A. fumigatus* biofilms under HS and cell wall stress. **(A,B)** Luciferase activity assay of the *hsp90P::luc*, *pkcA*^{G579R} *hsp90P::luc*, Δ*mpkA hsp90P::luc*, and Δ*rlmA hsp90P::luc* strains during the HS at 37°C **(A)** and 48°C **(B)**. **(C–E)** Luciferase activity assay of the *pkcA*^{G579R} *hsp90P::luc* **(C)**, Δ*mpkA hsp90P::luc* **(D)**, and Δ*rlmA hsp90P::luc* **(E)** strains during cell wall stress caused by CASP. The wild-type strain without luciferase gene was used as the negative control in all experiments. Mean ± SEM ($n \geq 8$) are shown. The results were normalized by the number of conidia (2×10^5 per assay) and are expressed as luminescence (arbitrary units). CASP: caspofungin (2 μg/ml).

luminescence signal between the wild-type, *pkcA*^{G579R}, and Δ*rlmA* backgrounds.

In contrast, the *mpkA* deletion strongly induced the *hsp90P* throughout the experiment, even under basal conditions (time point 0). At 48°C, a peak of *hsp90P* activity occurred earlier in all mutant strains compared to the wild-type reporter, and this effect was more evident in the Δ*rlmA* deletion background. Similar to the results scored at 37°C, the higher induction of *hsp90P* occurred in the *mpkA* deletion strain. Altogether, these data (**Figures 6**, **7**) confirm our previous results that the HS response in the *A. fumigatus* biofilm is dysregulated when the CWI pathway is impaired (Rocha et al., 2020b) and reveal that *pkcA* and *mpkA* are also the primary sensors for the compensatory activation of both *hsfA* and *hsp90* expression.

Finally, *hsp90P* activity was also highly induced during the cell wall stress caused by CASP (**Figure 7**). Interestingly, this effect was similar for the *pkcA*^{G579R} and Δ*mpkA* mutants, which peaked after 100–120 min post-CASP treatment. However, the luminescence signal was higher in the Δ*mpkA* strain under basal conditions. In contrast, the luciferase signal increased later in the Δ*rlmA* strain and was kept at high levels after the signal of the *hsp90P* activity decreased in the other CWI pathway mutants (**Figures 7C,D**). Collectively, the luciferase assays indicate that the expression of HsfA and Hsp90 is connected, and both jointly work in response to HS and cell wall stress. Additionally, the results suggest a direct HsfA role in governing the expression of genes involved in the cell adaptation to these stressing conditions as noted by the compensatory increase in the HsfA expression in the CWI pathway mutants.

HsfA Repression Modulates the Expression of Genes Related to Cell Wall Homeostasis and HS Response

In order to assess HsfA-dependent gene expression targets during HS, the wild-type and *xylP::hsfA* transcriptomes were investigated during HS exposure for 15 and 60 min at 48°C, after *xylP::hsfA* was repressed in MM lacking xylose, as described in the *Materials and Methods* section. The first time point (15 min) corresponds to the peak in *hsfA* expression at mRNA and protein levels (**Figures 2A**, **6B**). The exposure of *A. fumigatus* for 60 min causes an overall 20% reduction of the metabolic activity of mature wild-type *A. fumigatus* biofilm (Rocha et al., 2020b) and does not cause loss of viability of the *xylP::hsfA* conditional lethal mutant when shifted to repressive conditions. Thus, these two time points allow us to identify early and late genes induced by HS.

HS elicited rapid modulation of gene expression since 1,362 genes were upregulated ($\log_2$FC $\geq$ 1.0) while 1,499 genes were downregulated ($\log_2$FC $\leq$ −1.0) in the wild-type strain post-15 min. After 60 min of HS, these numbers increased to 1,384 and 1,549, respectively (**Figures 8A,B**). In the *xylP::hsfA* strain under repression, 1,375 genes were upregulated ($\log_2$FC $\geq$ 1.0) while 1,729 genes were downregulated ($\log_2$FC $\leq$ −1.0) post-15 min of HS. After 60 min HS, these numbers decreased to 1,136 and 1,474, respectively (**Figures 8A,B**).

Intriguingly, the *xylP::hsfA* mutant showed a GO enrichment similar to the wild-type strain after 15 min of HS. Both strains demonstrated a transcriptional upregulation of genes involved in the cellular response to heat, protein folding, and refolding (**Figures 8C,D**), which are expected biological processes activated in response to temperature increase (Albrecht et al., 2010). Some of these genes were also differentially expressed at the protein level under HS, such as the chaperones Hsp90 (Afu5g04170), Hsp30 (Afu3g14540), Hsp70 (Afu1g07440), Hsp60 (Afu2g09290), Hsp78 (Afu1g11180), Hsp88 (Afu1g12610), Ssc70 (Afu2g09960), and Sti1 (Afu7g01860), as previously reported (Albrecht et al., 2010). The early HS response also caused significant upregulation of genes involved in glucan biosynthetic process and cell wall organization or biogenesis in both strains (**Figures 8C,D**), including the CWI pathway transcription factor *rlmA* (Afu3g08520); the catalytic subunit of the β-1,3-glucan synthase *fksA* (Afu6g12400); the β-1,3-glucanosyltransferases *gelA* (Afu2g01170) and *gel7* (Afu6g12410); the chitin synthases *chsE* (Afu2g13440), *chsF* (Afu8g05630), and *csmB* (Afu2g13430); and the MAPK kinase of the HOG signaling pathway *pbs2* (Afu1g15950). These results support the cell wall remodeling observed during HS (**Figure 1**). In contrast, only the wild-type strain showed enrichment of genes involved in trehalose biosynthesis (**Figure 8C**), suggesting the participation of HsfA in this process. At the same time, protein ubiquitination and the response to endoplasmic reticulum stress were processes enriched only in the repressed *xylP::hsfA* mutant (**Figure 8D**). Among the downregulated genes post-15 min of HS, there was an enrichment of ribosome biogenesis and translation processes in both the wild-type and mutant strains (**Figures 8C,D**), suggesting an abrogation of protein synthesis to sustain thermoadaptation. The GO analysis of downregulated genes also showed enrichment in the category involved in the ergosterol biosynthetic process and unsaturated fatty acid biosynthetic process in the wild-type strain (**Figure 8C**). These findings reflect the cellular balance to overcome increased membrane fluidity caused by temperature increase and suggest that HsfA has a role in lipid homeostasis and the balance in the content of saturated/unsaturated fatty acids ratio elicited by the HS.

After 60 min of HS, the upregulated genes in both strains were enriched for different metabolic processes, such as DNA repair, RNA biosynthetic process, and transcription, while the downregulated genes were involved in ribosome assembly and translation (**Figures 8C,D**). The profile of genes modulated after prolonged HS exposure excluded the categories involved in cell wall metabolism. Interestingly, only the wild-type strain retained an enrichment of upregulated genes involved in response to HS after 60 min, supporting the evidence of a late *hsfA* role during the HS. Again, the lipid and ergosterol biosynthetic processes were also found downregulated only in the wild-type strain. The iron assimilation and cellular response to iron ion starvation categories were also downregulated exclusively in the wild type (**Figure 8C**), which is in agreement with previous studies that have shown a relationship between Hsf1 and the cellular iron pool in *C. albicans* (Nair et al., 2017, 2018).

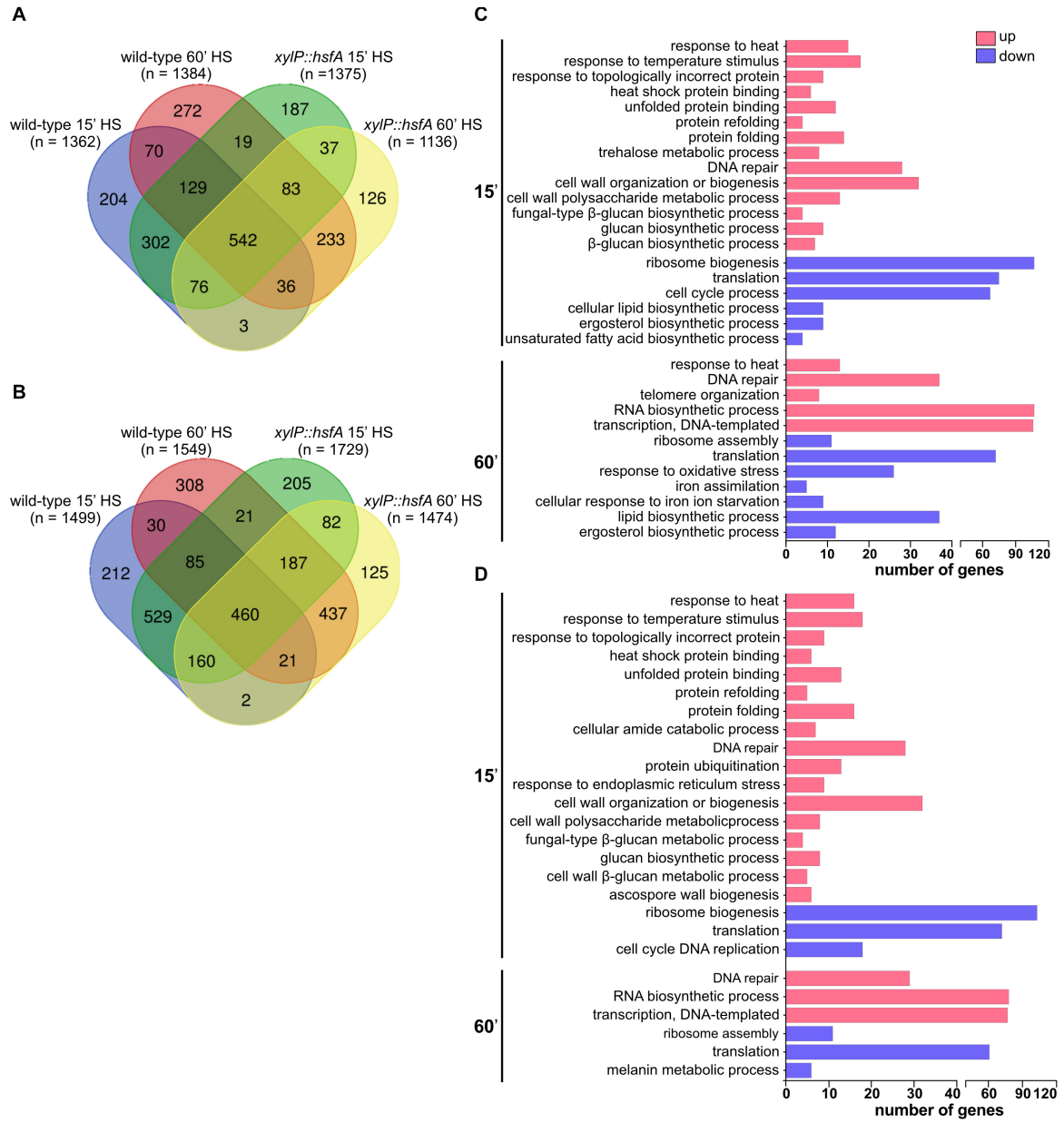

FIGURE 8 | Global transcriptional response of the wild-type and *xylP::hsfA* strains to HS. Venn diagram depicting the number of upregulated ($log_2FC \geq 1.0$) **(A)** and downregulated ($log_2FC \leq -1.0$) **(B)** genes in the wild type and *xylP::hsfA* strains post-15 min and 60 min of HS. **(C)** Selected Biological Process Gene Ontology terms enriched from significantly differently expressed genes ($log_2FC \geq 1.0$ or $log_2FC \leq -1.0$) in the wild-type strain during HS (15 min and 60 min time points), in comparison to control condition (30°C). **(D)** Selected Biological Process Gene Ontology terms enriched from significantly differently expressed genes ($log_2FC \geq 1.0$ or $log_2FC \leq -1.0$) in the *xylP::hsfA* strain during HS compared to control condition (30°C). For the full Biological Process Gene Ontology terms list, refer to **Supplementary Table 5**.

Subsequently, to identify genes whose expression was directly influenced by *hsfA*, we compared the *xylP::hsfA* mutant grown on repressive conditions with the wild-type strain, and we observe that several genes are modulated either at the non-HS control condition (30°C) or during temperature stress (**Figures 9A,B**). Some of them were constitutively repressed or induced in the mutant strain, including the *hsfA* gene, which is repressed throughout the experiment, thus validating our experimental conditions (**Supplementary Figure 5**). Notably, four genes of the pyripyropene biosynthetic gene cluster (*pyr4*, *pyr5*, *pyr6*, and *pyr9*) were highly induced in the mutant strain. Consistently, other genes belonging to this secondary metabolite cluster, such as *pyr1* (Afu6g13920), *pyr3* (Afu6g13940), and *pyr8* (Afu6g14000), were upregulated both in the non-HS and at the 60-min time point (**Supplementary Table 4**). These data suggest that HsfA has a role in the biosynthesis of this meroterpenoid.

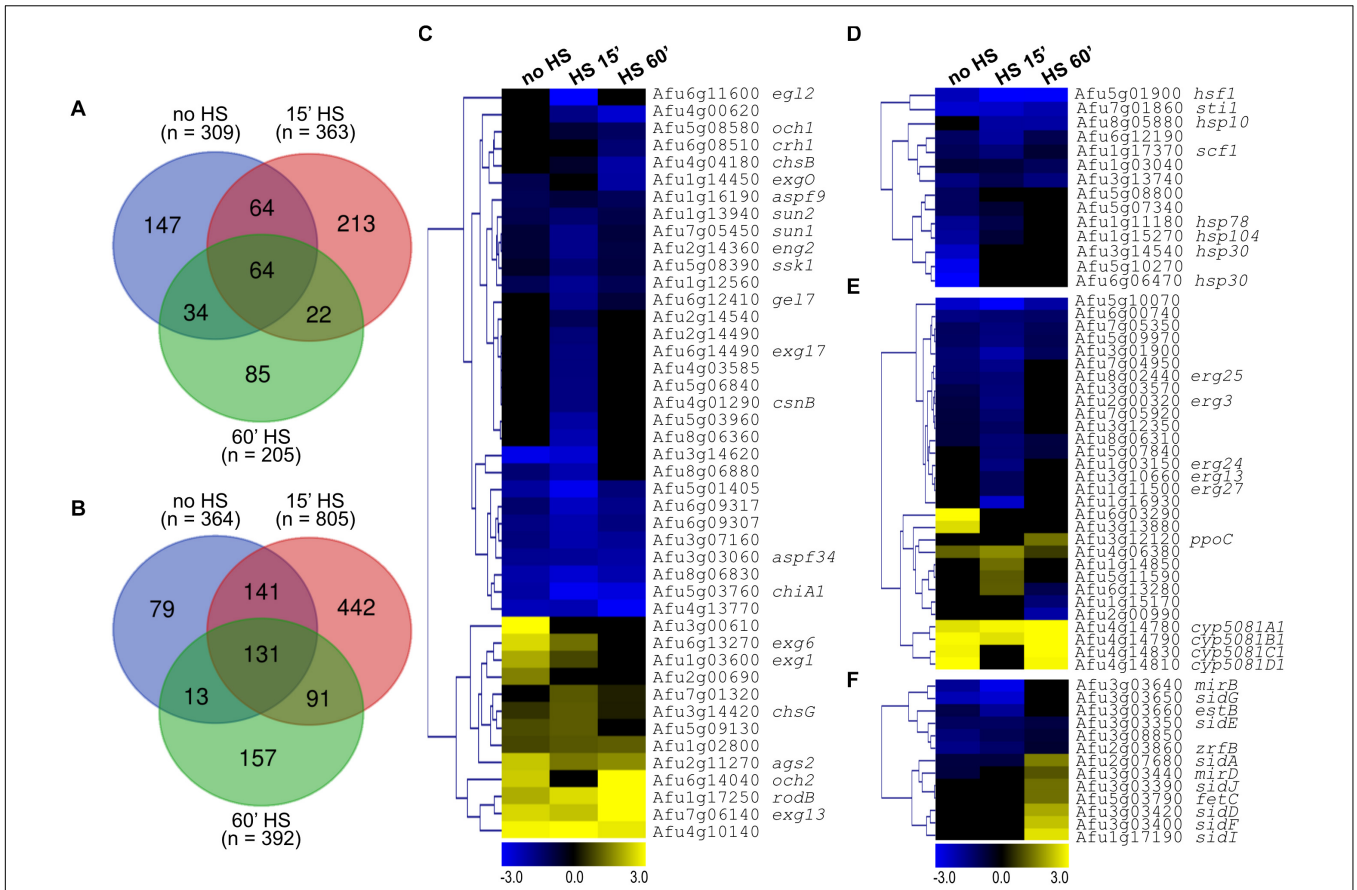

FIGURE 9 | *hsfA* repression impacts the expression of genes related to HS, cell wall, lipid, and iron metabolism. Venn diagrams comparing the genes upregulated ($log_2FC \geq 1.0$) **(A)** and downregulated ($log_2FC \leq -1.0$) **(B)** in the *xylP::hsfA* mutant strain relative to the wild-type strain at no HS condition and post-15 min or 60 min of HS. **(C–F)** Hierarchical clustering analysis showing selections of differently expressed genes ($log_2FC \geq 1.0$ or $log_2FC \leq -1.0$). The heat maps are divided by processes and categories of interest: cell wall biosynthesis and organization **(C)**; heat shock response, chaperone activity, and protein folding **(D)**; lipid metabolism **(E)**; and iron metabolism **(F)**. All the heat maps were created in the Multiple Experiment Viewer (MeV) platform, using hierarchical clustering and Euclidean Distance with average linkage clustering.

Focusing on the genes with participation on the cell wall organization, we observed few genes involved in the biosynthesis of cell wall, such as the α-1,3-glucan synthase *ags2* (Afu2g11270) and the chitin synthase *chsG* (Afu3g14420), which were upregulated, and β-1,3-glucanosyltransferase *gel7* (Afu6g12410) and the chitin synthase *chsB* (Afu4g04180), which were downregulated in at least one time point. In contrast, a number of genes involved in the remodeling of the cell wall were identified including the β-1,3-exoglucanases *exg1* (Afu1g03600) and *exg6* (Afu6g13270), the glycosyl hydrolase Afu4g13770, the chitinases *chiA1* (Afu5g03760), Afu5g03960 and Afu5g06840, and the glucanases *eg12* (Afu6g11600), *aspf9* (Afu1g16190), *exgO* (Afu1g14450), Afu1g12560, Afu8g06830, Afu2g14490, and Afu8g06360 (**Figure 9C**). Noteworthy, the more evident alterations in the mRNA abundance of most of these cell wall-related genes were a noticeable repression post-15 min of HS, when the expression of HsfA reaches its peak (**Figures 2A**, **6B**), suggesting that *hsfA* has a role in the transcriptional activation of such genes and is important for cell wall metabolism during thermoadaptation.

As expected, many HSPs, such as *sti1* (Afu7g01860), *hsp10* (Afu8g05880), *scf1* (Afu1g17370), *hsp78* (Afu1g11180), *hsp104* (Afu1g15270), *hsp30/42* (Afu3g14540), *hsp20/26* (Afu5g10270) and *hsp30* (Afu6g06470), were repressed in the mutant strain in comparison to the wild type (**Figure 9D**), also indicating that they are putative HsfA transcriptional targets. In addition, several genes related to lipid metabolism, mainly those involved in ergosterol and fatty acids biosynthesis, were downregulated, especially at no HS condition and post-15 min of HS (**Figure 9E**), pointing to a rearrangement of the cellular plasma membrane to increase its fluidity in response to thermal insult (Leach and Cowen, 2014). Finally, siderophore metabolic genes were also considerably modulated and divided into two groups: one containing downregulated genes at basal condition and post-15 min of HS, and another comprising upregulated genes post-60 min of HS (**Figure 9F**). This last group coincides with the repression of the GO terms related to iron metabolism in the wild-type strain at that time point (**Figure 8C**). Independent RT-qPCR experiments validated the RNA-seq results for the six selected genes that represent the GO categories shown in

Figure 9. We investigated the mRNA levels of *hsfA*, *hsp30*, *ags2*, *chsG*, *ppoC*, and *sidA* and presented the results as the ratio *xylP::hsfA*/wild-type (**Supplementary Figure 6**).

Collectively, our RNA-seq results strongly suggest that temperature stress causes major changes in the *A. fumigatus* transcriptome, and the transcription factor HsfA is a key regulator in the modulation of a significant number of these genes, being especially important for the response to HS, cell wall remodeling, plasma membrane homeostasis, and iron metabolism.

Given that thermotolerance and CWI are reciprocally controlled, and multiple transcription factors are intertwined to regulate these two polygenic biological processes, we analyzed our dataset to identify transcription factors differentially expressed in the wild-type and the *xylP::hsfA* strains exposed to HS. We concentrated our analysis in the transcription factors that presented differential expression values ($\log_2$FC $\geq$ 1.0 or $\log_2$FC ≤ -1.0) in at least one time point by comparing in this analysis the wild-type versus the *xylP::hsfA*. This search identified many transcription factors, including several of them uncharacterized (**Supplementary Figure 7**).

The putative transcription factors encoded by the genes Afu17060, Afu1g17150, Afu1g15370, Afu4g06420, and Afu4g07090 (*znfA*) were upregulated only in the mutant strain in at least one time point of HS, suggesting that they may play a role similar to that of HsfA during the HS response when *hsfA* is repressed. Concomitantly, Afu2g03020, Afu5g01662, Afu6g01840, Afu7g01820, and Afu1g01340 were genes upregulated only in the wild-type strain (**Supplementary Figure 7**), indicating that these genes may be direct or indirect regulated by HsfA. Afu7g06590, Afu3g06940, Afu8g05010 (*zpfA*), Afu1g11290, Afu5g00435, Afu5g10040, and Afu1g03210 (*flbD*) were among the downregulated genes only in the *xylP::hsfA* mutant strain in at least one time point of HS (**Supplementary Figure 7**). RgdA (Afu3g13920) is a transcriptional factor important for conidiation and cell wall architecture (Jun et al., 2020). Interestingly, in our analysis, this gene was considerably upregulated after 60 min of HS only in the wild-type strain, suggesting a possible target of HsfA regulatory network. Moreover, the gene encoding the transcription factor RttA (Afu7g04740) was also recently identified as playing a role in adaptation to the azole tebuconazole (Toyotome et al., 2020), and here it was downregulated in the wild-type strain post-60 min of HS. Altogether, the transcriptome analysis of transcription factors revealed probable additional regulators of the *A. fumigatus* HS response.

DISCUSSION

Although endothermy is a mammalian protective mechanism against fungal infections (Robert and Casadevall, 2009; Bergman and Casadevall, 2010), thermophilic fungi such as *A. fumigatus* can overcome this obstacle, indicating that thermotolerance in this fungus may be related to the expression of stress response genes that support its persistence inside the host. However, the cellular consequences of *A. fumigatus* adaptation to heat, the impact on the cell wall organization, and the participation of the signaling pathways that coordinate these two events are not fully understood.

Recently, we demonstrated that in addition to the regulation of cell wall biosynthesis and maintenance, the CWI pathway activity is modulated during early regulation of *A. fumigatus* thermotolerance and showed that Hsp90 is necessary for this crosstalk by interacting with the mains players of the CWI signaling cascade (Rocha et al., 2020b). Hsp90 is fundamental for the eukaryotic HS response by promoting the folding and assembly of newly synthesized proteins (Taipale et al., 2010). Since the conserved transcription factor Hsf1 controls *HSP90* transcription (Sarge et al., 1993; Eastmond and Nelson, 2006; Nicholls et al., 2009; Leach et al., 2016), here we identified and characterized the putative *A. fumigatus HSF1* homolog and assigned its function in thermotolerance and the associate cell wall stress response, which we hypothesize is a key fungal response mechanism to heat (**Figure 10**). We revealed that HsfA is an essential transcription factor necessary for thermotolerance and vegetative growth, as observed in other fungi (Wiederrecht et al., 1988; Thompson et al., 2008; Nicholls et al., 2009; Yang et al., 2017).

Here, we provide strong evidence that an outcome of the heat stress is the exacerbated thickening of the cell wall in *A. fumigatus* (**Figures 1**, **4**) accompanied by the induction of genes involved in cell wall biogenesis and remodeling (**Figure 8**). These results suggest that the cell wall expansion is necessary to sustain thermoadaptation without loss of viability. Increased cell wall thickness has also been recently reported in *C. albicans* biofilm hyphae during mild heat stress (Ikezaki et al., 2019). However, our results reveal that such modifications in cell wall architecture are very rapidly sensed by the cells since we detect a thickening of this structure as early as after 5 min of HS exposure (**Figure 1**). However, we should also consider that this rearrangement process in the cell wall observed at the initial times, such as after 5 min of HS, can be an event not exclusively directed by the activity of the CWI pathway or the transcriptional activity of HsfA. For instance, it could also be related to physical changes in the cell surface, such as increased Brownian movement of water molecules or expansion of proteins and polysaccharides in the cell wall. Additional experimentation is required to address this hypothesis. Nevertheless, these data point out that the morphological alterations of the cell wall during HS potentially result in modifications in the synthesis or exposure of specific sugars on the cell surface, e.g., α-glucan, β-glucan, chitin, mannoproteins, or galactosaminogalactan (**Figure 10**). Since the invading conidia germinate and eventually proliferate at high-temperature conditions inside the host, compared to the environmental niche, such cell wall adaptation may also exist during the initial steps of fungal infection and can be a determinant for immune recognition. However, the consequences of these alterations for the immune recognition of the fungus still need rigorous investigation. In *C. albicans*, repression of *HSP90* expression in a *tetO-HSP90* conditional mutant leads to increased detection of chitin by CFW fluorescence binding assay (Leach et al., 2012a; Nair et al., 2017).

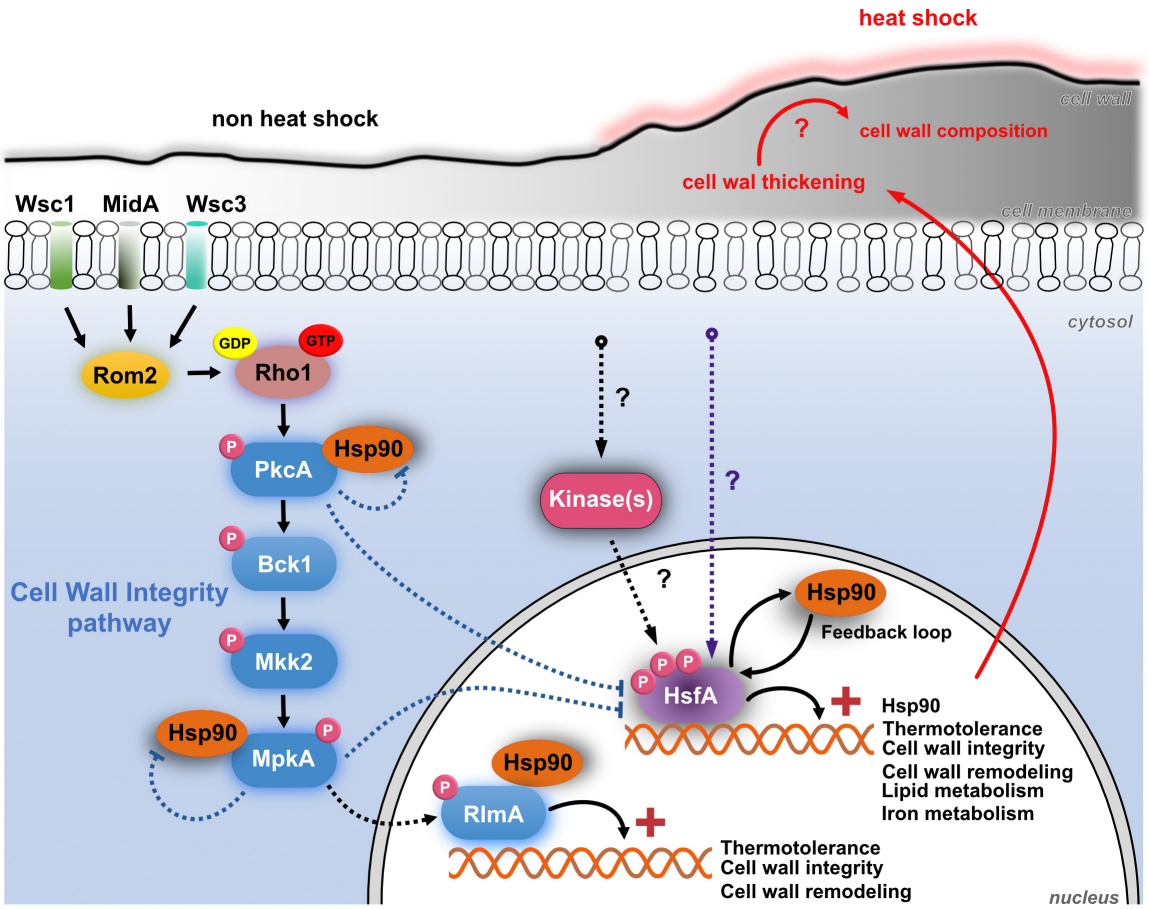

FIGURE 10 | The crosstalk between HsfA-Hsp90 and CWI pathway in *A. fumigatus* during HS. The CWI pathway is activated during early adaptation to HS, possibly via MidA mechanosensor located at the cell membrane. This signal funnels into Rom2, a guanine nucleotide exchange factor, and the small Rho GTPAse Rho1, leading to the activation of PkcA and the CWI pathway. These events culminate with the phosphorylation of the MAP kinase MpkA, which, in turn, phosphorylates the transcription factor RlmA, thus activating the transcription of genes (+) important for thermotolerance, cell wall integrity, and remodeling. The CWI pathway proteins PkcA, MpkA, and RlmA are constitutive Hsp90 clients. A direct consequence of the HS is the thickening of the cell wall after 5 min of temperature increase, which may have consequences to the remodeling of the cell wall and exposure of carbohydrate to the cell surface. However, these consequences remain to be investigated (red question marks). Also, the cellular plasma membrane becomes more fluid in response to thermal insult. Although not necessary for HsfA activation, PkcA and MpkA negatively regulate the expression of HsfA and Hsp90, both during the HS (dashed blue arrows) and upon cell wall stress induced by caspofungin (not shown in the Figure; see text for details). The resulting increase in protein abundance of HsfA and Hsp90 in the *pkcA* and *mpkA* mutants possibly occurs via undescribed compensatory mechanisms accompanied by the activation of additional signaling cascades to retain the CWI and thermotolerance (purple dashed line). In the face of heat stress, mRNA abundance of HsfA increases and triggers the expression of genes related to thermotolerance, cell wall integrity, cell wall remodeling, lipid, and iron metabolism. One of its transcriptional targets, Hsp90, is also induced to deal with HS and assist the stabilization of client proteins. After about 15–30 min of HS, the HsfA levels decrease, possibly due to the action of Hsp90 in the regulatory feedback loop. This regulatory mechanism comprises the Hsf1/Hsp90 protein–protein interaction (not investigated here), which is reversed during the HS, when Hsp90 protein levels increase and decouple from Hsf1 to assist the folding of client proteins. The activity of Hsf1 remains until Hsp90 again binds to Hsf1, negatively regulating Hsf1 (see text for details). Hyperphosphorylation (not investigated here) is another regulatory event that modulates the transcriptional activity of HsfA orthologs in other fungal pathogens. The protein(s) kinase(s) responsible for HsfA phosphorylation are still unknown in *A. fumigatus*. This diagram is based on data from this article and the references (Dichtl et al., 2012; Leach et al., 2012b; Rocha et al., 2020a,b).

Likewise, depletion of Hsp90 in *A. fumigatus* caused increased sensitivity to cell wall stress (Lamoth et al., 2012).

Interestingly, our data demonstrate that the ability of the cell wall to be remodeled during the heat stress or CASP treatment was maintained in the *xylP::hsfA* mutant, indicating that this process is not entirely dependent on this transcription factor, even though the conditional lethal mutant *xylP::hsfA* is sensitive to cell wall-damaging agents, including CASP. However, under the non-HS condition (30°C), the repression of *hsfA* instantly causes a thickening of the cell wall (**Figure 4**), similar to the *C. albicans HSF1* (Nair et al., 2017) and *HSP90* conditional mutants (Leach et al., 2012a). In our case, we show that the cell wall thickening in the *xylP::hsfA* mutant is completely rescued if *hsfA* expression is restored by low xylose concentration, again reinforcing the crosstalk between resistance to heat and the cell wall structure. Despite the subtle increase in *hsfA* expression recorded in a wild-type strain challenged with CASP and CR (**Figure 2**), a peak in *hsfA* mRNA abundance occurred after

15 min of HS, coinciding with the higher thickening of the cell wall and the HS response establish by the concomitant increase in *hsp90* expression (**Figures 2**, **7**). Similar patterns of gene expression are observed for other transcription factors, which are regulated posttranscriptionally and undergo minimal transcriptional changes. In this case, the intracellular pools of these transcription factors are likely present at all times in order to respond to stress quickly. A similar scenario may be the case for HsfA in the presence of cell wall stress. Whether posttranscriptional regulation of HsfA instead of transcriptional activation is a key event to deal with cell wall stress would require additional experiments, including investigation of the phosphorylation status and the activity of HsfA in response to cell wall-damaging agents. In line with this idea, very slight changes in xylose concentration can rescue the conditional lethal phenotype of *xylP::hsfA* mutant, suggesting that low levels of *hsfA* provide a survival benefit (**Figures 3**, **5**).

Concomitantly to the dramatic changes in the cell wall structure, we observed increased expression of *hsp90* in response to *hsfA* upregulation, followed by a subsequent drop in *hsfA* mRNA accumulation (**Figures 2**, **6**, **7**), suggesting that the expected feedback loop between HsfA and Hsp90 described in *C. albicans* also occurs in *A. fumigatus* (Nicholls et al., 2009; Leach et al., 2012a, 2016). Consistently, the protein levels of Hsp90 remain high up to 240 min post-HS (Rocha et al., 2020b). In addition, HsfA was also shown to be important in controlling the expression of genes encoding HSPs (**Figure 9**) and enzymes involved in trehalose biosynthesis (**Figure 8** and **Supplementary Table 4**), which together make up part of the canonical HS response (Takahashi et al., 2017). However, the genes encoding chaperones such as *hsp60*, *hsp70*, and *hsp90*, although modulated by HS, were not significantly impacted by the repression of *hsfA* (**Supplementary Table 4**), differently from what was observed in *C. albicans* (Nicholls et al., 2009; Leach et al., 2016). Possibly, the small increase in *hsfA* mRNA levels recorded in our RNA-seq samples under repressive conditions (1.5-fold; 15 min HS, **Supplementary Table 4**) could have elicited upregulation of these HSPs in the *xylP::hsfA* conditional mutant. The hypothesis that other transcription factors may be acting should also be considered, and **Supplementary Figure 7** shows some possible candidates, such as *znfA*, which was more expressed in depleted *hsfA* cells and recently identified as important for the regulation of the CASP paradoxical effect (Valero et al., 2020). Noteworthy, human transcription factors involved in the immune response, such as STAT1, STAT3, NF-IL6, and NF-kB, can induce *HSP90* expression, either synergistically or antagonistically to HSF1 [reviewed in Prodromou (2016)].

Our present study results indicate that the thickening of the cell wall is a consequence of HS, and the mechanisms by which HsfA participates in this event are intertwined with the main signaling pathways that control cell integrity, including the CWI and HOG pathways. We found synthetically sick genetic interaction between *hsfA* and *mpkA* or *sakA* both under temperature and cell wall stresses, but not with the hypomorphic allele $pkcA^{G579R}$ (Rocha et al., 2015), suggesting that these MAPKs act upstream *hsfA* in response to these stressors.

However, our luciferase assays indicate that PkcA and MpkA are not crucial for HsfA activation since the expression of HsfA and *hsp90P* activity were boosted during the HS and CASP treatment in the CWI pathway mutant backgrounds (**Figures 6**, **7**). We argue that functional impairment of any CWI pathway component is sufficient to increase HsfA expression to likely activate downstream targets, and some of them could be shared with the CWI pathway. To this end, another observation of our study is that the HsfA signal was more intense in the $pkcA^{G579R}$ background at both stress conditions. In contrast, the activity of *hsp90P* was more intense in the Δ*mpkA* only in the HS, given the signals recorded in the $pkcA^{G579R}$ and Δ*mpkA* strains were comparable in the presence of CASP. These observations again point to the crucial role of PkcA in the early adaptation to HS as described previously (Rocha et al., 2020b). Supporting this idea, overexpression of $Pkc1^{PkcA}$, but not the MAPKs $Mpk1^{MpkA}$, $Mkk1^{Mkk1}$, and $Bck1^{Bck1}$ in *S. cerevisiae*, can suppress the $Hsf1^{HsfA}$ defects in response to heat stress, meaning that the signaling emerging from Pkc1 and not Pkc1-regulated MAPK cascade was necessary for *HSF1* suppression (Imazu and Sakurai, 2005). Although a collection of kinases that phosphorylate and modulate the ScHsf1 activity (reviewed in Veri et al., 2018) is known, the enzymes that phosphorylate HsfA during the HS or cell wall stress are still unknown, thus requiring further experimentation (**Figure 10**).

Noteworthy, our RNA-seq indicates that HsfA is also important for the plasma membrane homeostasis in the face of a temperature upshift (**Figures 8**, **9**). Since the fungal plasma membrane adapts to temperature changes [reviewed in Fabri et al. (2020)], our data suggested that HsfA has a repressive role in the biosynthesis of ergosterol and lipids in general, especially the unsaturated fatty acids, indicating that this transcription factor may regulate the chemical and consequently physical changes of the plasma membrane during HS. Not surprisingly, a molecular link between fatty acid synthesis and the HS response governed by Hsf1 in *C. albicans* was described previously (Leach and Cowen, 2014) and is an open field of investigation in *A. fumigatus*.

In summary, we characterized the essential HSF HsfA and demonstrated its contribution to cell wall maintenance. We observed a crosstalk between HsfA-Hsp90 and CWI and provided evidence that the kinases PkcA and MpkA are not essential for the HsfA activation during the cell wall and heat stresses. Additionally, we identified genes modulated by HsfA, including those related to HS response, cell wall biogenesis, lipid metabolism, and iron homeostasis. Our results reinforce the concept that cell wall adaptation contributes to the thermotolerance of *A. fumigatus* via an integrated mechanism encompassing HS response and the regulation of the CWI signaling pathways in fungi.

DATA AVAILABILITY STATEMENT

The datasets presented in this study can be found in online repositories. The names of the repository/repositories and accession number(s) can be found in the article/**Supplementary Material**.

AUTHOR CONTRIBUTIONS

IM planned and designed research. JF, MR, CF, and LR performed research. IM, AC, GG, LR, and MD contributed reagents/analytic tools. IM, JF, AC, LR, GG, CF, and MD analyzed and validated the data. GP conducted RNA-seq analyses. JF and IM wrote the original draft of the manuscript. All authors discussed the data, and edited and approved the manuscript.

FUNDING

This study was supported by Fundação de Amparo à Pesquisa do Estado de São Paulo (FAPESP grant numbers: 2015/17541-0, 2016/07870-9, and 2017/19694-3) and Conselho Nacional de Desenvolvimento Científico e Tecnológico (CNPq grant number 462383/2014-8) to IM. This work was also supported by NIH grants AI136934 and AI125770, and by Merit Grant I01BX002924 from the Veterans Affairs Program to MD. The funding body had no role in designing the study or in collecting, analyzing, and interpreting the data, or in writing the manuscript.

ACKNOWLEDGMENTS

We thank Fundação de Amparo à Pesquisa do Estado de São Paulo (FAPESP) and Conselho Nacional de Desenvolvimento Científico e Tecnológico (CNPq) for financial support. We are indebted to Dr. Vito Valiante for providing the pYES-hph-pXyl devR vector and the Δ*mpkA* and Δ*sakA* strains and to Dr. Matthias Brock for providing the pUC57 plasmid containing the luciferase gene. We are grateful to Magda Regina Ometto Patricio for technical assistance (FAPESP 2019/00967-5). We also thank Douglas Antonio Alvaredo Paixão and Brazilian Bioethanol Science and Technology Laboratory CNPEM/MCTIC NGS Sequencing Facility for generating the sequencing data described here. JF was awarded a FAPESP Research Internships Abroad (BEPE) fellowship (2018/22755-7).

SUPPLEMENTARY MATERIAL

The Supplementary Material for this article can be found online at: https://www.frontiersin.org/articles/10.3389/fmicb.2021.656548/full#supplementary-material

REFERENCES

Albrecht, D., Guthke, R., Brakhage, A. A., and Kniemeyer, O. (2010). Integrative analysis of the heat shock response in *Aspergillus fumigatus*. *BMC Genomics* 11:32. doi: 10.1186/1471-2164-11-32

Altwasser, R., Baldin, C., Weber, J., Guthke, R., Kniemeyer, O., Brakhage, A. A., et al. (2015). Network Modeling Reveals Cross Talk of MAP Kinases during Adaptation to Caspofungin Stress in *Aspergillus fumigatus*. *PLoS One* 10:e0136932. doi: 10.1371/journal.pone.0136932

Alves de Castro, P., Dos Reis, T. F., Dolan, S. K., Oliveira Manfiolli, A., Brown, N. A., et al. (2016). The *Aspergillus fumigatus* SchA(SCH9) kinase modulates SakA(HOG1) MAP kinase activity and it is essential for virulence. *Mol. Microbiol.* 102, 642–671. doi: 10.1111/mmi.13484

Araujo, R., and Rodrigues, A. G. (2004). Variability of germinative potential among pathogenic species of *Aspergillus*. *J. Clin. Microbiol.* 42, 4335–4337. doi: 10.1128/JCM.42.9.4335-4337.2004

Baldin, C., Valiante, V., Kruger, T., Schafferer, L., Haas, H., Kniemeyer, O., et al. (2015). Comparative proteomics of a tor inducible *Aspergillus fumigatus* mutant reveals involvement of the Tor kinase in iron regulation. *Proteomics* 15, 2230–2243. doi: 10.1002/pmic.201400584

Benedict, K., Jackson, B. R., Chiller, T., and Beer, K. D. (2019). Estimation of Direct Healthcare Costs of Fungal Diseases in the United States. *Clin. Infect. Dis.* 68, 1791–1797. doi: 10.1093/cid/ciy776

Bergman, A., and Casadevall, A. (2010). Mammalian endothermy optimally restricts fungi and metabolic costs. *MBio* 1:10. doi: 10.1128/mBio.00212-10

Bhabhra, R., and Askew, D. S. (2005). Thermotolerance and virulence of *Aspergillus fumigatus*: role of the fungal nucleolus. *Med. Mycol.* 43(Suppl. 1), S87–S93. doi: 10.1080/13693780400029486

Bolger, A. M., Lohse, M., and Usadel, B. (2014). Trimmomatic: a flexible trimmer for Illumina sequence data. *Bioinformatics* 30, 2114–2120. doi: 10.1093/bioinformatics/btu170

Brown, A. J., Leach, M. D., and Nicholls, S. (2010). The relevance of heat shock regulation in fungal pathogens of humans. *Virulence* 1, 330–332. doi: 10.4161/viru.1.4.12364

Brown, G. D., Denning, D. W., Gow, N. A., Levitz, S. M., Netea, M. G., and White, T. C. (2012). Hidden killers: human fungal infections. *Sci. Transl. Med.* 4:165rv113. doi: 10.1126/scitranslmed.3004404

Bruder Nascimento, A. C., Dos Reis, T. F., de Castro, P. A., Hori, J. I., Bom, V. L., de Assis, L. J., et al. (2016). Mitogen activated protein kinases SakA(HOG1) and MpkC collaborate for *Aspergillus fumigatus* virulence. *Mol. Microbiol.* 100, 841–859. doi: 10.1111/mmi.13354

Casadevall, A., Kontoyiannis, D. P., and Robert, V. (2019). On the Emergence of *Candida auris*: Climate Change, Azoles, Swamps, and Birds. *MBio* 10:19. doi: 10.1128/mBio.01397-19

Chatterjee, S., and Tatu, U. (2017). Heat shock protein 90 localizes to the surface and augments virulence factors of *Cryptococcus neoformans*. *PLoS Negl. Trop. Dis.* 11:e0005836. doi: 10.1371/journal.pntd.0005836

Chaveroche, M. K., Ghigo, J. M., and d'Enfert, C. (2000). A rapid method for efficient gene replacement in the filamentous fungus *Aspergillus nidulans*. *Nucleic Acids Res.* 28:E97.

Cowen, L. E. (2009). Hsp90 orchestrates stress response signaling governing fungal drug resistance. *PLoS Pathog.* 5:e1000471. doi: 10.1371/journal.ppat.1000471

Dichtl, K., Helmschrott, C., Dirr, F., and Wagener, J. (2012). Deciphering cell wall integrity signalling in *Aspergillus fumigatus*: identification and functional characterization of cell wall stress sensors and relevant Rho GTPases. *Mol. Microbiol.* 83, 506–519. doi: 10.1111/j.1365-2958.2011.07946.x

Eastmond, D. L., and Nelson, H. C. (2006). Genome-wide analysis reveals new roles for the activation domains of the *Saccharomyces cerevisiae* heat shock transcription factor (Hsf1) during the transient heat shock response. *J. Biol. Chem.* 281, 32909–32921. doi: 10.1074/jbc.M602454200

Erkine, A. M., Magrogan, S. F., Sekinger, E. A., and Gross, D. S. (1999). Cooperative binding of heat shock factor to the yeast HSP82 promoter in vivo and in vitro. *Mol. Cell Biol.* 19, 1627–1639. doi: 10.1128/mcb.19.3.1627

Fabri, J., de Sa, N. P., Malavazi, I., and Del Poeta, M. (2020). The dynamics and role of sphingolipids in eukaryotic organisms upon thermal adaptation. *Prog. Lipid Res.* 80:101063. doi: 10.1016/j.plipres.2020.101063

Fuchs, B. B., and Mylonakis, E. (2009). Our paths might cross: the role of the fungal cell wall integrity pathway in stress response and cross talk with other stress response pathways. *Eukaryot Cell* 8, 1616–1625. doi: 10.1128/EC.00193-09

Garcia-Solache, M. A., and Casadevall, A. (2010). Global warming will bring new fungal diseases for mammals. *MBio* 1:10. doi: 10.1128/mBio.00061-10

Gomez-Pastor, R., Burchfiel, E. T., and Thiele, D. J. (2018). Regulation of heat shock transcription factors and their roles in physiology and disease. *Nat. Rev. Mol. Cell Biol.* 19, 4–19. doi: 10.1038/nrm.2017.73

Haas, D., Lesch, S., Buzina, W., Galler, H., Gutschi, A. M., Habib, J., et al. (2016). Culturable fungi in potting soils and compost. *Med. Mycol.* 54, 825–834. doi: 10.1093/mmy/myw047

Hahn, J. S., and Thiele, D. J. (2004). Activation of the *Saccharomyces cerevisiae* heat shock transcription factor under glucose starvation conditions by Snf1 protein kinase. *J. Biol. Chem.* 279, 5169–5176. doi: 10.1074/jbc.M311005200

Hartl, F. U. (1996). Molecular chaperones in cellular protein folding. *Nature* 381, 571–579. doi: 10.1038/381571a0

Hashikawa, N., and Sakurai, H. (2004). Phosphorylation of the yeast heat shock transcription factor is implicated in gene-specific activation dependent on the architecture of the heat shock element. *Mol. Cell Biol.* 24, 3648–3659. doi: 10.1128/mcb.24.9.3648-3659.2004

Hashikawa, N., Yamamoto, N., and Sakurai, H. (2007). Different mechanisms are involved in the transcriptional activation by yeast heat shock transcription factor through two different types of heat shock elements. *J. Biol. Chem.* 282, 10333–10340. doi: 10.1074/jbc.M609708200

Huber, W., Carey, V. J., Gentleman, R., Anders, S., Carlson, M., Carvalho, B. S., et al. (2015). Orchestrating high-throughput genomic analysis with Bioconductor. *Nat. Methods* 12, 115–121. doi: 10.1038/nmeth.3252

Ikezaki, S., Cho, T., Nagao, J. I., Tasaki, S., Yamaguchi, M., Arita-Morioka, K. I., et al. (2019). Mild Heat Stress Affects on the Cell Wall Structure in *Candida albicans* Biofilm. *Med. Mycol. J.* 60, 29–37. doi: 10.3314/mmj.19-00001

Imazu, H., and Sakurai, H. (2005). *Saccharomyces cerevisiae* heat shock transcription factor regulates cell wall remodeling in response to heat shock. *Eukaryot. Cell* 4, 1050–1056. doi: 10.1128/EC.4.6.1050-1056.2005

Jacobsen, I. D., Luttich, A., Kurzai, O., Hube, B., and Brock, M. (2014). In vivo imaging of disseminated murine *Candida albicans* infection reveals unexpected host sites of fungal persistence during antifungal therapy. *J. Antimicrob. Chemother.* 69, 2785–2796. doi: 10.1093/jac/dku198

Jun, S. C., Choi, Y. H., Lee, M. W., Yu, J. H., and Shin, K. S. (2020). The Putative APSES Transcription Factor RgdA Governs Growth, Development, Toxigenesis, and Virulence in *Aspergillus fumigatus*. *mSphere* 5:20. doi: 10.1128/mSphere.00998-20

Kamada, Y., Jung, U. S., Piotrowski, J., and Levin, D. E. (1995). The protein kinase C-activated MAP kinase pathway of *Saccharomyces cerevisiae* mediates a novel aspect of the heat shock response. *Genes Dev.* 9, 1559–1571. doi: 10.1101/gad.9.13.1559

Kijima, T., Prince, T. L., Tigue, M. L., Yim, K. H., Schwartz, H., Beebe, K., et al. (2018). HSP90 inhibitors disrupt a transient HSP90-HSF1 interaction and identify a noncanonical model of HSP90-mediated HSF1 regulation. *Sci. Rep.* 8:6976. doi: 10.1038/s41598-018-25404-w

Kim, D., Pertea, G., Trapnell, C., Pimentel, H., Kelley, R., and Salzberg, S. L. (2013). TopHat2: accurate alignment of transcriptomes in the presence of insertions, deletions and gene fusions. *Genome Biol.* 14:R36. doi: 10.1186/gb-2013-14-4-r36

Kopylova, E., Noe, L., and Touzet, H. (2012). SortMeRNA: fast and accurate filtering of ribosomal RNAs in metatranscriptomic data. *Bioinformatics* 28, 3211–3217. doi: 10.1093/bioinformatics/bts611

Krakowiak, J., Zheng, X., Patel, N., Feder, Z. A., Anandhakumar, J., Valerius, K., et al. (2018). Hsf1 and Hsp70 constitute a two-component feedback loop that regulates the yeast heat shock response. *Elife* 7:31668. doi: 10.7554/eLife.31668

LaFayette, S. L., Collins, C., Zaas, A. K., Schell, W. A., Betancourt-Quiroz, M., Gunatilaka, A. A., et al. (2010). PKC signaling regulates drug resistance of the fungal pathogen *Candida albicans* via circuitry comprised of Mkc1, calcineurin, and Hsp90. *PLoS Pathog.* 6:e1001069. doi: 10.1371/journal.ppat.1001069

Lamoth, F., Juvvadi, P. R., Fortwendel, J. R., and Steinbach, W. J. (2012). Heat shock protein 90 is required for conidiation and cell wall integrity in *Aspergillus fumigatus*. *Eukaryot. Cell* 11, 1324–1332. doi: 10.1128/EC.00032-12

Lamoth, F., Juvvadi, P. R., Gehrke, C., and Steinbach, W. J. (2013). In vitro activity of calcineurin and heat shock protein 90 Inhibitors against *Aspergillus fumigatus* azole- and echinocandin-resistant strains. *Antimicrob. Agents Chemother.* 57, 1035–1039. doi: 10.1128/AAC.01857-12

Lamoth, F., Juvvadi, P. R., Soderblom, E. J., Moseley, M. A., and Steinbach, W. J. (2015). Hsp70 and the Cochaperone StiA (Hop) Orchestrate Hsp90-Mediated Caspofungin Tolerance in *Aspergillus fumigatus*. *Antimicrob. Agents Chemother.* 59, 4727–4733. doi: 10.1128/AAC.00946-15

Leach, M. D., and Cowen, L. E. (2013). Surviving the heat of the moment: a fungal pathogens perspective. *PLoS Pathog.* 9:e1003163. doi: 10.1371/journal.ppat.1003163

Leach, M. D., and Cowen, L. E. (2014). Membrane fluidity and temperature sensing are coupled via circuitry comprised of Ole1, Rsp5, and Hsf1 in *Candida albicans*. *Eukaryot. Cell* 13, 1077–1084. doi: 10.1128/EC.00138-14

Leach, M. D., Budge, S., Walker, L., Munro, C., Cowen, L. E., and Brown, A. J. (2012a). Hsp90 orchestrates transcriptional regulation by Hsf1 and cell wall remodelling by MAPK signalling during thermal adaptation in a pathogenic yeast. *PLoS Pathog.* 8:e1003069. doi: 10.1371/journal.ppat.1003069

Leach, M. D., Farrer, R. A., Tan, K., Miao, Z., Walker, L. A., Cuomo, C. A., et al. (2016). Hsf1 and Hsp90 orchestrate temperature-dependent global transcriptional remodelling and chromatin architecture in *Candida albicans*. *Nat. Commun.* 7:11704. doi: 10.1038/ncomms11704

Leach, M. D., Klipp, E., Cowen, L. E., and Brown, A. J. (2012b). Fungal Hsp90: a biological transistor that tunes cellular outputs to thermal inputs. *Nat. Rev. Microbiol.* 10, 693–704. doi: 10.1038/nrmicro2875

Liao, Y., Smyth, G. K., and Shi, W. (2013). The Subread aligner: fast, accurate and scalable read mapping by seed-and-vote. *Nucleic Acids Res.* 41:e108. doi: 10.1093/nar/gkt214

Liu, X. D., and Thiele, D. J. (1996). Oxidative stress induced heat shock factor phosphorylation and HSF-dependent activation of yeast metallothionein gene transcription. *Genes Dev.* 10, 592–603.

Malavazi, I., and Goldman, G. H. (2012). Gene disruption in *Aspergillus fumigatus* using a PCR-based strategy and in vivo recombination in yeast. *Methods Mol. Biol.* 845, 99–118. doi: 10.1007/978-1-61779-539-8_7

Munshi, M. A., Gardin, J. M., Singh, A., Luberto, C., Rieger, R., Bouklas, T., et al. (2018). The Role of Ceramide Synthases in the Pathogenicity of *Cryptococcus neoformans*. *Cell Rep.* 22, 1392–1400. doi: 10.1016/j.celrep.2018.01.035

Nair, R., Khandelwal, N. K., Shariq, M., Redhu, A. K., Gaur, N. A., Shaikh, S., et al. (2018). Identification of genome-wide binding sites of heat shock factor 1, Hsf1, under basal conditions in the human pathogenic yeast, *Candida albicans*. *AMB Express* 8:116. doi: 10.1186/s13568-018-0647-7

Nair, R., Shariq, M., Dhamgaye, S., Mukhopadhyay, C. K., Shaikh, S., and Prasad, R. (2017). Non-heat shock responsive roles of HSF1 in *Candida albicans* are essential under iron deprivation and drug defense. *Biochim. Biophys. Acta Mol. Cell Res.* 1864, 345–354. doi: 10.1016/j.bbamcr.2016.11.021

Nicholls, S., Leach, M. D., Priest, C. L., and Brown, A. J. (2009). Role of the heat shock transcription factor, Hsf1, in a major fungal pathogen that is obligately associated with warm-blooded animals. *Mol. Microbiol.* 74, 844–861. doi: 10.1111/j.1365-2958.2009.06883.x

Nicholls, S., MacCallum, D. M., Kaffarnik, F. A., Selway, L., Peck, S. C., and Brown, A. J. (2011). Activation of the heat shock transcription factor Hsf1 is essential for the full virulence of the fungal pathogen *Candida albicans*. *Fungal Genet. Biol.* 48, 297–305. doi: 10.1016/j.fgb.2010.08.010

Parsell, D. A., and Lindquist, S. (1993). The function of heat-shock proteins in stress tolerance: degradation and reactivation of damaged proteins. *Annu. Rev. Genet.* 27, 437–496. doi: 10.1146/annurev.ge.27.120193.002253

Prodromou, C. (2016). Mechanisms of Hsp90 regulation. *Biochem. J.* 473, 2439–2452. doi: 10.1042/BCJ20160005

Robert, V. A., and Casadevall, A. (2009). Vertebrate endothermy restricts most fungi as potential pathogens. *J. Infect. Dis.* 200, 1623–1626. doi: 10.1086/644642

Robinson, M. D., McCarthy, D. J., and Smyth, G. K. (2010). edgeR: a Bioconductor package for differential expression analysis of digital gene expression data. *Bioinformatics* 26, 139–140. doi: 10.1093/bioinformatics/btp616

Rocha, M. C., Fabri, J. H., Franco, de Godoy, K., Alves, de Castro, P., et al. (2016). *Aspergillus fumigatus* MADS-Box Transcription Factor rlmA Is Required for Regulation of the Cell Wall Integrity and Virulence. *G3* 6, 2983–3002. doi: 10.1534/g3.116.031112

Rocha, M. C., Fabri, J., Simoes, I. T., Silva-Rocha, R., Hagiwara, D., da Cunha, A. F., et al. (2020a). The Cell Wall Integrity Pathway Contributes to the Early Stages of *Aspergillus fumigatus* Asexual Development. *Appl. Environ. Microbiol.* 86:19. doi: 10.1128/AEM.02347-19

Rocha, M. C., Godoy, K. F., de Castro, P. A., Hori, J. I., Bom, V. L., Brown, N. A., et al. (2015). The *Aspergillus fumigatus* pkcA G579R Mutant Is Defective in the Activation of the Cell Wall Integrity Pathway but Is Dispensable for Virulence in a Neutropenic Mouse Infection Model. *PLoS One* 10:e0135195. doi: 10.1371/journal.pone.0135195

Rocha, M. C., Minari, K., Fabri, J., Kerkaert, J. D., Gava, L. M., da Cunha, A. F., et al. (2020b). *Aspergillus fumigatus* Hsp90 interacts with the main components

of the cell wall integrity pathway and cooperates in heat shock and cell wall stress adaptation. *Cell Microbiol.* 23:e13273. doi: 10.1111/cmi.13273

Sarge, K. D., Murphy, S. P., and Morimoto, R. I. (1993). Activation of heat shock gene transcription by heat shock factor 1 involves oligomerization, acquisition of DNA-binding activity, and nuclear localization and can occur in the absence of stress. *Mol. Cell Biol.* 13, 1392–1407. doi: 10.1128/mcb.13.3.1392

Schopf, F. H., Biebl, M. M., and Buchner, J. (2017). The HSP90 chaperone machinery. *Nat. Rev. Mol. Cell Biol.* 18, 345–360. doi: 10.1038/nrm.2017.20

Sorger, P. K., and Nelson, H. C. (1989). Trimerization of a yeast transcriptional activator via a coiled-coil motif. *Cell* 59, 807–813.

Sorger, P. K., and Pelham, H. R. (1988). Yeast heat shock factor is an essential DNA-binding protein that exhibits temperature-dependent phosphorylation. *Cell* 54, 855–864.

Sueiro-Olivares, M., Fernandez-Molina, J. V., Abad-Diaz-de-Cerio, A., Gorospe, E., Pascual, E., Guruceaga, X., et al. (2015). *Aspergillus fumigatus* transcriptome response to a higher temperature during the earliest steps of germination monitored using a new customized expression microarray. *Microbiology* 161(Pt 3), 490–502. doi: 10.1099/mic.0.000021

Taipale, M., Jarosz, D. F., and Lindquist, S. (2010). HSP90 at the hub of protein homeostasis: emerging mechanistic insights. *Nat. Rev. Mol. Cell Biol.* 11, 515–528. doi: 10.1038/nrm2918

Takahashi, H., Kusuya, Y., Hagiwara, D., Takahashi-Nakaguchi, A., Sakai, K., and Gonoi, T. (2017). Global gene expression reveals stress-responsive genes in *Aspergillus fumigatus* mycelia. *BMC Genomics* 18:942. doi: 10.1186/s12864-017-4316-z

Thompson, S., Croft, N. J., Sotiriou, A., Piggins, H. D., and Crosthwaite, S. K. (2008). *Neurospora crassa* heat shock factor 1 Is an essential gene; a second heat shock factor-like gene, hsf2, is required for asexual spore formation. *Eukaryot. Cell* 7, 1573–1581. doi: 10.1128/EC.00427-07

Toyotome, T., Onishi, K., Sato, M., Kusuya, Y., Hagiwara, D., Watanabe, A., et al. (2020). Identification of novel mutations contributing to azole tolerance of *Aspergillus fumigatus* through in vitro exposure to tebuconazole. Preprint. doi: 10.1101/2020.07.20.213256

Truman, A. W., Millson, S. H., Nuttall, J. M., Mollapour, M., Prodromou, C., and Piper, P. W. (2007). In the yeast heat shock response, Hsf1-directed induction of Hsp90 facilitates the activation of the Slt2 (Mpk1) mitogen-activated protein kinase required for cell integrity. *Eukaryot. Cell* 6, 744–752. doi: 10.1128/EC.00009-07

Valero, C., Colabardini, A. C., Chiaratto, J., Pardeshi, L., de Castro, P. A., Ferreira Filho, J. A., et al. (2020). *Aspergillus fumigatus* Transcription Factors Involved in the Caspofungin Paradoxical Effect. *mBio* 11:20. doi: 10.1128/mBio.00816-20

Valiante, V., Jain, R., Heinekamp, T., and Brakhage, A. A. (2009). The MpkA MAP kinase module regulates cell wall integrity signaling and pyomelanin formation in *Aspergillus fumigatus*. *Fungal Genet. Biol.* 46, 909–918. doi: 10.1016/j.fgb.2009.08.005

Valiante, V., Macheleidt, J., Foge, M., and Brakhage, A. A. (2015). The *Aspergillus fumigatus* cell wall integrity signaling pathway: drug target, compensatory pathways, and virulence. *Front. Microbiol.* 6:325. doi: 10.3389/fmicb.2015.00325

van Paassen, J., Russcher, A., In 't Veld-van Wingerden, A. W., Verweij, P. E., and Kuijper, E. J. (2016). Emerging aspergillosis by azole-resistant *Aspergillus fumigatus* at an intensive care unit in the Netherlands, 2010 to 2013. *Euro Surveill.* 21:30300. doi: 10.2807/1560-7917.ES.2016.21.30.30300

Veri, A. O., Robbins, N., and Cowen, L. E. (2018). Regulation of the heat shock transcription factor Hsf1 in fungi: implications for temperature-dependent virulence traits. *FEMS Yeast Res.* 18:foy041. doi: 10.1093/femsyr/foy041

Wang, L., Wang, S., and Li, W. (2012). RSeQC: quality control of RNA-seq experiments. *Bioinformatics* 28, 2184–2185. doi: 10.1093/bioinformatics/bts356

Wiederrecht, G., Seto, D., and Parker, C. S. (1988). Isolation of the gene encoding the *S. cerevisiae* heat shock transcription factor. *Cell* 54, 841–853.

Xie, C., Mao, X., Huang, J., Ding, Y., Wu, J., Dong, S., et al. (2011). KOBAS 2.0: a web server for annotation and identification of enriched pathways and diseases. *Nucleic Acids Res.* 39, W316–W322. doi: 10.1093/nar/gkr483

Yamamoto, A., Mizukami, Y., and Sakurai, H. (2005). Identification of a novel class of target genes and a novel type of binding sequence of heat shock transcription factor in *Saccharomyces cerevisiae*. *J. Biol. Chem.* 280, 11911–11919. doi: 10.1074/jbc.M411256200

Yang, D. H., Jung, K. W., Bang, S., Lee, J. W., Song, M. H., Floyd-Averette, A., et al. (2017). Rewiring of Signaling Networks Modulating Thermotolerance in the Human Pathogen *Cryptococcus neoformans*. *Genetics* 205, 201–219. doi: 10.1534/genetics.116.190595

Zadra, I., Abt, B., Parson, W., and Haas, H. (2000). xylP promoter-based expression system and its use for antisense downregulation of the *Penicillium chrysogenum* nitrogen regulator NRE. *Appl. Environ. Microbiol.* 66, 4810–4816. doi: 10.1128/aem.66.11.4810-4816.2000

Conflict of Interest: MD is a Co-Founder and Chief Scientific Officer (CSO) of MicroRid Technologies Inc.

The remaining authors declare that the research was conducted in the absence of any commercial or financial relationships that could be construed as a potential conflict of interest.

frontiers in Cellular and Infection Microbiology

MINI REVIEW
published: 21 April 2021
doi: 10.3389/fcimb.2021.657502

Cryptococcal Virulence in Humans: Learning From Translational Studies With Clinical Isolates

*Herdson Renney de Sousa[1], Stefânia de Frazão[2], Getúlio Pereira de Oliveira Júnior[3], Patrícia Albuquerque[1,2,4] and André Moraes Nicola[1,5]**

[1] Microbiology, Immunology and Biotechnology Laboratory, Faculty of Medicine, University of Brasília, Brasília, Brazil, [2] Laboratory of Molecular Biology of Pathogenic Fungi, Department of Cell Biology, Institute of Biological Sciences, University of Brasília, Brasília, Brazil, [3] Division of Allergy and Inflammation, Department of Medicine, Beth Israel Deaconess Medical Center, Harvard Medical School, Boston, MA, United States, [4] Faculty of Ceilândia, University of Brasília, Brasília, Brazil, [5] Graduate Program in Genomic Sciences and Biotechnology, Catholic University of Brasília, Brasília, Brazil

OPEN ACCESS

Edited by:
Lívia Kmetzsch, Federal University of Rio Grande do Sul, Brazil

Reviewed by:
Luna Sobrino Joffe, Stony Brook University, United States
Emma Camacho, Johns Hopkins University, United States

***Correspondence:**
André Moraes Nicola
andre.nicola@gmail.com

Specialty section:
This article was submitted to Fungal Pathogenesis, a section of the journal Frontiers in Cellular and Infection Microbiology

Received: *25 January 2021*
Accepted: *31 March 2021*
Published: *21 April 2021*

Citation:
de Sousa HR, Frazão Sd, Oliveira Júnior GPd, Albuquerque P and Nicola AM (2021) Cryptococcal Virulence in Humans: Learning From Translational Studies With Clinical Isolates. Front. Cell. Infect. Microbiol. 11:657502. doi: 10.3389/fcimb.2021.657502

Cryptococcosis, an invasive mycosis caused by *Cryptococcus* spp, kills between 20% and 70% of the patients who develop it. There are no vaccines for prevention, and treatment is based on a limited number of antifungals. Studying fungal virulence and how the host responds to infection could lead to new therapies, improving outcomes for patients. The biggest challenge, however, is that experimental cryptococcosis models do not completely recapitulate human disease, while human experiments are limited due to ethical reasons. To overcome this challenge, one of the approaches used by researchers and clinicians is to: 1) collect cryptococcal clinical isolates and associated patient data; 2) study the set of isolates in the laboratory (virulence and host-pathogen interaction variables, molecular markers); 3) correlate the laboratory and patient data to understand the roles fungal attributes play in the human disease. Here we review studies that have shed light on the cryptococcosis pathophysiology using these approaches, with a special focus on human disease. Isolates that more effectively evade macrophage responses, that secrete more laccase, melanize faster and have larger capsules in the cerebrospinal fluid are associated with poorer patient outcomes. Additionally, molecular studies have also shown that cryptococcal clades vary in virulence, with clinical impact. Limitations of those studies include the use of a small number of isolates or retrospectively collected clinical data. The fact that they resulted in very important information is a reflection of the impact this strategy has in understanding cryptococcosis and calls for international collaboration that could boost our knowledge.

Keywords: cryptococcosis, *Cryptococcus neoformans*, *Cryptococcus gattii*, meningitis, virulence

INTRODUCTION

The genus *Cryptococcus* is one of the deadliest among those that cause systemic mycoses in humans (Bongomin et al., 2017). Pathogenic species are part of the *C. neoformans* and *C. gattii* complexes, but the genus includes many other species that are rarely or never pathogenic to humans and animals (Enoch et al., 2017; Kwon-Chung et al., 2017). These encapsulated yeasts are normally

found in the soil and trees. How these environmental microbes have evolved complex virulence factors that allow them to survive and multiply in the human host is an important question that has been the target of research for decades. Beyond being interesting from an evolutionary point of view, cryptococcal virulence and its interaction with the human host are also clinically critical.

A global epidemiology study estimated that each year the disease kills 181,100 out of 223,100 individuals it affects (Rajasingham et al., 2017). Mortality rate estimates in this study were of up to 70% in low-income countries; however, even in optimal settings in high-income countries in North America and Europe, the estimated mortality rates range around 20% - 30%. One of the reasons for that is the limited arsenal of antifungals to treat the disease, with basically just three drugs: amphotericin B, flucytosine and fluconazole. Amphotericin B can be cheap (US$ 3.80 per dose) but very toxic in its deoxycholate formulation (Bicanic et al., 2005), whereas lipidic formulations are safer (Faustino and Pinheiro, 2020) but very expensive (US$ 443 per dose for the liposomal and US$ 506 per dose for the lipid complex formulations, all prices in Brazil for the year 2016) (Borba et al., 2018). Flucytosine improves the efficacy of amphotericin therapy, but is toxic and not available in most countries, whereas fluconazole is ineffective as monotherapy (Lu et al., 2019). As exemplified by tetanus, diphtheria and several other infectious diseases, virulence factors are frequent therapeutic and prophylactic targets. Studying the host response is also very important, because it could lead to host-directed therapies that would be very important in a disease in which immunocompromise is the major risk factor. Thus, research on virulence and host-pathogen interaction has great potential in decreasing the disease burden of cryptococcosis.

An important problem, however, is that it is very difficult to study virulence and host-pathogen interaction in human beings. A key experiment in determining a microbe's virulence attributes is to impair functionality of the genes that encode them and compare the outcomes of experimental infection with the original strain and the mutants. On the host side, a frequent approach to test hypotheses involves infecting genetically modified animals and comparing the outcome with wild-type animals. However, neither approach is feasible in humans. Experiments like these have been done extensively in animal models, but they do not always recapitulate human diseases. For example, mice succumb to cryptococcal infection (Goldman et al., 1996; Carroll et al., 2007) and commonly used immortalized macrophages have weak *in vitro* fungicidal activity (Pan et al., 2009). In contrast, an intact immune response in healthy human beings effectively deals with the fungus in most individuals as evidenced by the fact that most people are infected with *Cryptococcus* spp. during their early life (Goldman et al., 2001) but the incidence of cryptococcosis in the HIV uninfected is a few cases per million people per year (Chen et al., 2000; Mirza et al., 2003).

One strategy that researchers have used to obtain information about virulence and host-pathogen interaction in humans starts with collecting clinical isolates together with information from the patients from whom each isolate was obtained. The microorganisms are then studied in the laboratory, where virulence attributes and host-pathogen interaction variables are systematically measured. The laboratory measurements are then correlated with patient data, revealing how virulence attributes are associated with the outcome of the disease (**Figure 1**). Additionally, many groups have used biochemical, serological or more recently molecular tools such as multi-locus sequence typing (MLST) or genome sequencing to phylogenetically classify clinical isolate collections, and then correlated this information with patient data as well. This approach has been used extensively to study other pathogens, resulting for example in important insight on the virulence of *Candida albicans* (Rajendran et al., 2016), *Mycobacterium tuberculosis* (Lan et al., 2003) and *Plasmodium falciparum* (Bernabeu et al., 2016). In this paper, we review some of the knowledge we have acquired on human cryptococcosis using these strategies and discuss both existing limitations and what could be done to further progress in this area.

Virulence and Host-Pathogen Interaction in Humans

The pathogenesis of pulmonary cryptococcosis or cryptococcal meningitis depends on the host immune status and is influenced by several fungal virulence factors (Bicanic and Harrison, 2004). The most studied *Cryptococcus* virulence factors are the polysaccharide capsule (Ngamskulrungroj et al., 2011; Robertson et al., 2014), the ability to produce melanin (Ngamskulrungroj et al., 2011; Renney de Sousa et al., 2020), thermotolerance (Johnston et al., 2016) and the production enzymes such as laccase (Frazão et al., 2020), urease (Shi et al., 2010) and phospholipases (Santangelo et al., 2004).

The capsule was the focus of a study made by Robertson and colleagues with *Cryptococcus* spp. isolates from HIV-infected Ugandan adults as part of a clinical trial (Robertson et al., 2014). They measured the capsule thickness and capsular polysaccharide shedding both *ex vivo*, in the patients' cerebrospinal fluid (CSF), and *in vitro*, after culture in the laboratory. There was no correlation between the two sets of measurements, an indication that the complex environment inside the human host is not fully reproduced in the laboratory. Interestingly, the authors found that isolates with larger *ex vivo* capsules were found in patients with higher CSF cryptococcal antigen titers, less intense central nervous system (CNS) inflammation and higher intracranial pressure. Beyond the capsule, other morphologic aspects of the *Cryptococcus* spp. cell affect patient outcomes (Fernandes et al., 2018). *C. neoformans* and *C. tetragattii* isolates from Botswana were cultivated *in vitro* and observed microscopically, with multiple morphologies such as giant cells, micro cells and shed capsule fragments. Higher pleomorphism, with a more diverse mix of cell shapes and sizes, was associated with increased risk of death.

The important role of the CNS environment for disease outcome was also highlighted by a second study from the same group (Sabiiti et al., 2014). This study, performed with clinical

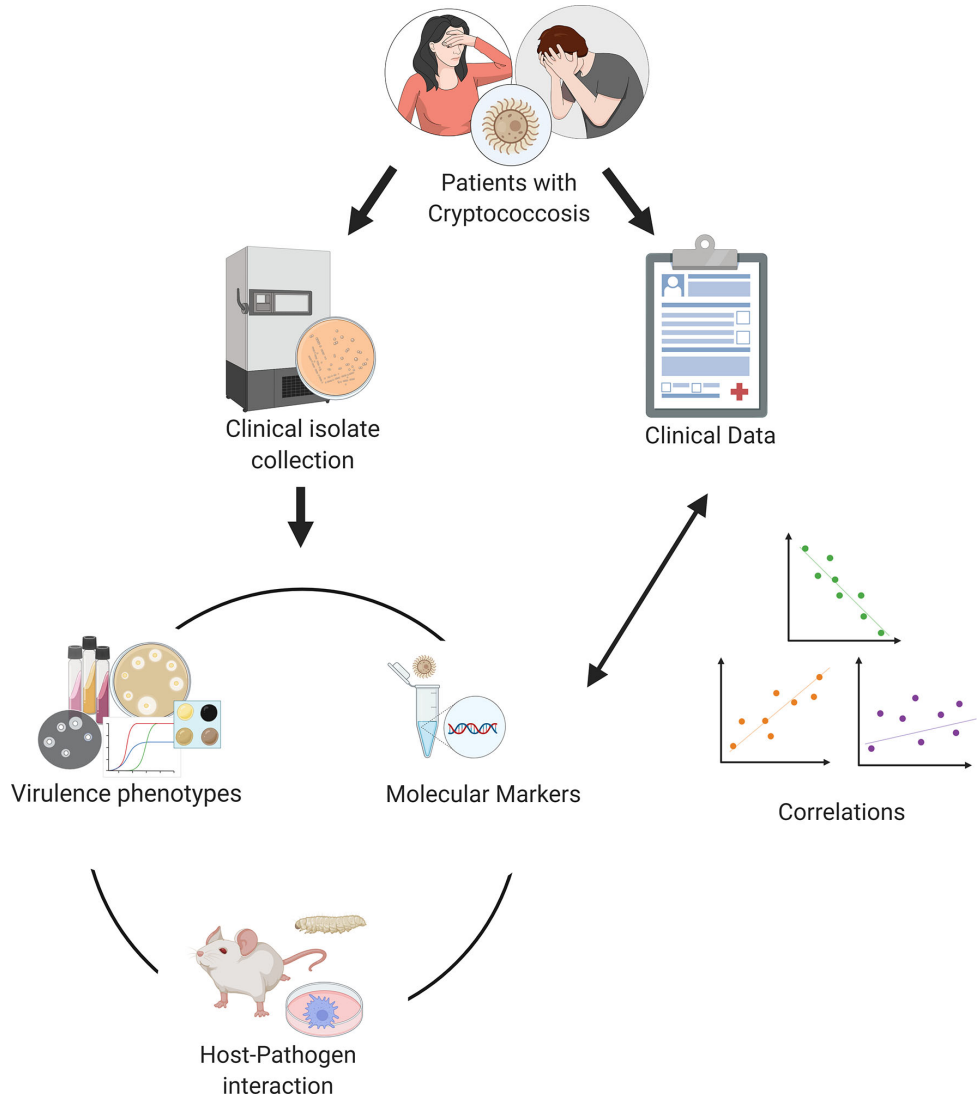

FIGURE 1 | Experimental strategy of translational studies in cryptococcosis. Individual research groups collect patient data and clinical isolates. Information about the isolates is then collected experimentally in the laboratory and finally correlated with clinical data. Figure generated using Biorender.com.

isolates obtained during five clinical trials in Thailand and South Africa, focused on the fungal interaction with macrophages and on melanin and the enzyme that synthesizes this pigment, laccase. The authors found that some isolates were more efficiently phagocytosed by macrophages than others, and that those with higher *in vitro* uptake by macrophages were isolated from patients with higher CSF fungal burden and higher risk of death. The high-uptake strains were also hypocapsular and had higher laccase activity than the low-uptake strains. Surprisingly, uptake by macrophages correlated positively with laccase activity but not with total melanin produced by each isolate. This observation hinted at melanin-independent activities for laccase, a hypothesis that was proven by *in vitro* exposure of the clinical isolates to CSF. The fluid was toxic to fungi, but strains with increased laccase activity were able to survive better.

Melanin-independent roles for laccase were also central in two recent studies we conducted with Brazilian *Cryptococcus* spp. Isolates. In one of them, we measured the non-lytic exocytosis of a small set of *C. neoformans* isolates (Frazão et al., 2020). This is a process in which macrophages expel *Cryptococcus* spp. cells without harm to either cell (Alvarez and Casadevall, 2006; Ma et al., 2006), and its mechanism is not fully understood. We found that isolates that melanized faster were expelled more frequently. Further experiments showed that what affected the non-lytic exocytosis was actually laccase, not melanin, because pre-melanizing cells did not alter the rates but knocking out laccase did. In another study, at the moment of writing still at the preprint stage (Renney de Sousa et al., 2020), we measured

multiple virulence attributes of *C. neoformans* and *C. deuterogattii* isolates, especially the capsule and laccase/melanin. As previously reported (Robertson et al., 2014; Fernandes et al., 2018), we did not observe any correlations between *in vitro* capsule phenotypes and clinical outcomes; we also observed that secreted laccase activity negatively correlates with survival in both cryptococcosis patients and *Galleria mellonella* animal models, in line with previous observations as well (Sabiiti et al., 2014). However, we did observe an important role for melanization rate in survival of both *G. mellonella* and humans, irrespective of laccase secretion. The risk of death was positively associated with how fast each isolate melanized.

The interaction between *C. neoformans* and murine macrophages was the focus of a study made with clinical isolates obtained in a French prospective study (Alanio et al., 2011). Alanio and collaborators observed great variation in the phagocytosis and intracellular proliferation of fungi inside infected macrophages. Isolates that more effectively evaded phagocytosis (low phagocytic index) and had lower intracellular proliferation rates were associated with a higher risk of therapeutic failure, determined as lack of CSF sterilization at 2 weeks. Isolates that were more efficiently phagocytosed but proliferated more efficiently inside macrophages were obtained from patients with a higher risk of death. These findings confirmed that the *Cryptococcus*-macrophage interaction, which in studies with mice and other animal models is crucial for disease outcome, is also important in infected humans. Another study with clinical isolates also found clinical outcomes that parallel those of mouse models (Mukaremera et al., 2019). Using an inhalation infection model, the authors show a strong association between the mortality rates in humans and mice. They have also found that survival in both hosts is dependent on the burden of fungal cells in affected tissues and on each isolate's growth speed and resistance to stresses.

Genotypic Diversity

For many years, *C. neoformans* was considered a unique species with four serotypes based on differences in capsule antigenicity. Further characterization of those serotypes revealed epidemiological, biochemical, and genetic differences among them that lead to their subdivision into four varieties: *C. neoformans* var. *grubii* (serotype A), *C. neoformans* var. *gattii* (serotypes B and C) and *C. neoformans* var. *neoformans* (serotype D). Genetics and molecular biology advances during the last two decades resulted in more precise phylogenetic characterization of the different varieties leading first to their separation into two species with different molecular types (*C. neoformans* VNI, VNII, VNB, VNIII and VNIV and *C. gattii* VGI, VGII, VGIII and VGIV) and later in seven different species (Kwon-Chung and Varma, 2006; Lin and Heitman, 2006; Hagen et al., 2015). Species in the *C. neoformans* complex are usually opportunistic, causing mostly meningoencephalitis in immunocompromised individuals. In contrast, those in the *C. gattii* complex are more frequently primary pathogens and are associated with pneumonia in addition to meningoencephalitis (Galanis and MacDougall, 2010).

Most genetic studies with clinical isolates focus on the geographic distribution of the different molecular types, with only a few presenting correlations with clinical data. Most of these are focused on the *C. neoformans* complex, especially the most common VNI (*C. neoformans strictu sensu*) molecular type, the most frequent cause of cryptococcosis worldwide. Wiesner and collaborators found a significant association between the genotype and phenotype of clinical strains of *C. neoformans* VNI and severity of cryptococcal meningitis (Wiesner et al., 2012). Multilocus sequencing typing (MLST) of their isolates resulted in four clonal clusters and three nonredundant evolutionary groups which presented significant differences in patient mortality. The isolates obtained from patients with higher mortality also presented increased capsular polysaccharide shedding and induced a more pronounced Th2 response *ex vivo*. Similarly, other studies have shown that specific subgroups within the *C. neoformans* VNI clade are associated with more or less severe disease:

- A specific sequence type named ST5 is associated with the development of lymphadenopathy and higher blood lymphocyte counts in patients, as well as with worse disability outcomes in people who were cured (Day et al., 2017).
- Among HIV-positive patients from five countries in Asia and Africa, three VNI subclades were found. Individuals infected with isolates from the VNIa-93 subclade, commonly reported in Uganda and Malawi, had lower mortality than those infected with the VNIa-4 and VNIa-5 subclades (Ashton et al., 2019).

As for other clades within the *C. neoformans* complex, two other studies have correlated molecular and clinical data. Using isolates from HIV-positive patients in South Africa, Beale and colleagues found that the VNB lineage was linked to worse patient survival (Beale et al., 2015). They also found an association between the fungal genotype and virulence phenotypes in isolates from the VNII lineage, which had increased laccase activity and *ex vivo* survival on CSF, fungal phenotypes that were previously associated with poorer disease outcomes (Sabiiti et al., 2014). The second report was from the French Cryptococcosis Study Group, who characterized *C. neoformans* isolates from the hybrid AD serotype (Desnos-Ollivier et al., 2015). Their data showed that patients infected with AD hybrids had lower fungal dissemination, less frequent lung involvement and more frequent CSF sterilization after treatment compared to patients infected with either serotype A or D.

Most of what has been learned about human cryptococcosis with this strategy of correlating molecular and patient data has been done with multi-locus sequence typing. The most recent studies, however, have begun to use whole genome sequencing, which is far more robust and results in richer, more detailed data. Gerstein and collaborators have used whole genome sequence typing to characterize a set of clinical isolates (Gerstein et al., 2019). Their work, however,

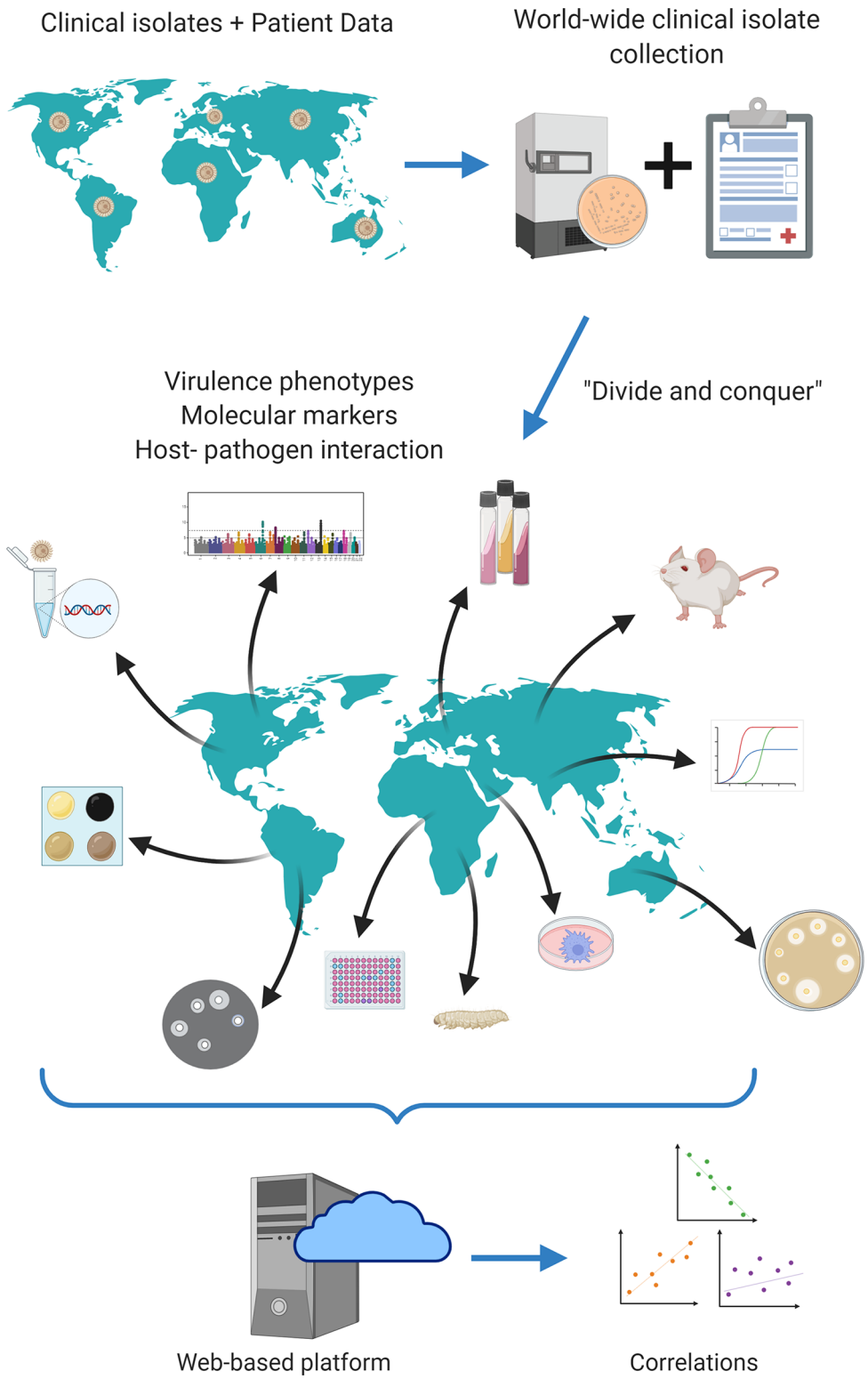

FIGURE 2 | Proposed strategy of translational studies in cryptococcosis as an international collaboration. *Cryptococcus* spp. clinical isolates from all over the world would be gathered in a single biobank; all associated clinical data would equally be gathered in a single open database. Each laboratory would receive all isolates available in the biobank and would be responsible for measuring one or a few virulence factors according to its expertise. All data would finally be combined and analyzed together, increasing statistical power. Figure generated using Biorender.com.

highlights a new tool that can greatly enhance how much information we get from this type of study: genome-wide association studies. The authors identified hundreds of polymorphisms in the genome sequences and correlated those with clinical data, as well as with laboratory information on virulence and host-pathogen interaction. This strategy resulted in 40 *C. neoformans* genes associated with human disease, many of them with unknown functions. Knockout strains were available for 17 of these, and mouse models proved that 35% were indeed less virulent than the wild-type *C. neoformans*. We believe this powerful new approach will result in very important information in the next few years.

THE WAY FORWARD – MULTINATIONAL COLLABORATION

The selected studies we reviewed above have brought important insights on *Cryptococcus* spp. virulence and the host response in cryptococcosis. They have, however, important limitations. One of these limitations is intrinsic to the experimental strategy itself: correlation does not imply causation. Experiments like these are thus often followed up with additional experiments to confirm hypotheses raised by the correlations with clinical data. Other important limitations are:

- Most of the papers we reviewed were made with dozens or a few hundred isolates that originated from a single geographic region. The small number of isolates tested means that the studies are powered to discover only strong correlations, whereas the similar origin from all isolates reduces the breadth of the diverse genetic landscape being probed.
- Most often different studies are made with different sets of clinical isolates that were collected by different researchers, hindering reproducibility. It is difficult to distribute and share pathogenic isolates and clinical data with other researchers who could count on existing datasets.
- Microbiology techniques and molecular characterization methodologies vary between research groups, as do strategies used to diagnose and treat the disease. The quality of the clinical data collected also varies a lot, with a tendency for more uniform and complete data when the strains originate from clinical trials in comparison with less precise information gathered retrospectively from patient charts in observational studies.
- The same virulence attributes are measured differently by each research group. For example, Robertson et al. measured the cryptococcal capsule sizes from clinical isolates directly out of the CSF (Robertson et al., 2014), whereas we (Frazão et al., 2020; Renney de Sousa et al., 2020) and others (Fernandes et al., 2018) have measured it in isolates grown *in vitro* in different media.
- Different groups correlate virulence and host-pathogen interaction information with different aspects of the patient outcome. Alanio et al. for example, made correlations with therapeutic efficacy, measured by CSF sterilization after two weeks, and death after three months of diagnosis (Alanio et al., 2011). On the other hand, Robertson et al. (2014) correlated their data with intracranial pressure, fungal clearing and CSF inflammation whereas Sabiiti et al. (Sabiiti et al., 2014) used CSF fungal burden and 10-week survival.

The fact that very important information regarding the pathogenesis of cryptococcosis has been obtained from these studies despite the many limitations means that much more can be understood about the disease with this strategy. Overcoming these limitations, however, would probably require a different approach than what has already been used. Problems with low statistical power and genetic variety can be solved by creating collections with hundreds to thousands of isolates from different regions of the planet (**Figure 2**). Ideally, these isolates would be molecularly characterized with the gold standard (full genome sequencing) and both fungi and associated clinical, molecular, virulence and host-pathogen data would be deposited in publicly available repositories, to allow other researchers to build upon existing knowledge.

This would probably only be possible through worldwide collaborative work between clinicians and basic scientists working on Genomics, Microbiology and Immunology. Such collaboration could also decrease the heterogeneity of patient variables to be collected and the choice of laboratory techniques and data analysis strategies, which could be agreed upon prospectively. This is a complex and laborious proposition, but one that could result in advances that lead to improved outcomes for people dying from cryptococcosis.

AUTHOR CONTRIBUTIONS

HS, SF, GO, PA, and AN wrote different sections of the manuscript. AN revised, wrote, and prepared the manuscript. PA and HS prepared the figures. All authors contributed to the article and approved the submitted version.

FUNDING

AN was funded by FAP-DF awards 0193.001048/2015-0193.001561/2017 and the CNPq grant 437484/2018-1. PA was funded by FAP-DF grants 193.000.192/2014 and 193.001.003/2015 and CNPq grant 461230/2014-3.

ACKNOWLEDGMENTS

The authors would like to thank Drs. Hugo Costa Paes and Arturo Casadevall for revising the manuscript and providing critical insights.

REFERENCES

Alanio, A., Desnos-Ollivier, M., and Dromer, F. (2011). Dynamics of *Cryptococcus neoformans*-macrophage interactions reveal that fungal background influences outcome during cryptococcal meningoencephalitis in humans. *mBio* 2 (4), e00158–11. doi: 10.1128/mBio.00158-11

Alvarez, M., and Casadevall, A. (2006). Phagosome extrusion and host-cell survival after *Cryptococcus neoformans* phagocytosis by macrophages. *Curr. Biol.* 16 (21), 2161–2165. doi: 10.1016/j.cub.2006.09.061

Ashton, P. M., Thanh, L. T., Trieu, P. H., Van Anh, D., Trinh, N. M., Beardsley, J., et al. (2019). Three phylogenetic groups have driven the recent population expansion of *Cryptococcus neoformans*. *Nat. Commun.* 10 (1), 1–10. doi: 10.1038/s41467-019-10092-5

Beale, M. A., Sabiiti, W., Robertson, E. J., Fuentes-Cabrejo, K. M., O'Hanlon, S. J., Jarvis, J. N., et al. (2015). Genotypic diversity is associated with clinical outcome and phenotype in cryptococcal meningitis across Southern Africa. *PloS Neglect Trop. Dis* 9 (6), e0003847. doi: 10.1371/journal.pntd.0003847

Bernabeu, M., Danziger, S. A., Avril, M., Vaz, M., Babar, P. H., Brazier, A. J., et al. (2016). Severe adult malaria is associated with specific PfEMP1 adhesion types and high parasite biomass. *Proc. Natl. Acad. Sci. U.S.A.* 113 (23), E3270–E3279. doi: 10.1073/pnas.1524294113

Bicanic, T., and Harrison, T. S. (2004). Cryptococcal meningitis. *Br. Med. Bull* 72 (1), 99–118. doi: 10.1093/bmb/ldh043

Bicanic, T., Wood, R., Bekker, L. G., Darder, M., Meintjes, G., and Harrison, T. S. (2005). Antiretroviral roll-out, antifungal roll-back: access to treatment for cryptococcal meningitis. *Lancet Infect. Dis.* 5, 530–531. doi: 10.1016/S1473-3099(05)70197-3

Bongomin, F., Gago, S., Oladele, R. O., and Denning, D. W. (2017). Global and multi-national prevalence of fungal diseases—estimate precision. *J. Fungi.* 3, e57. doi: 10.3390/jof3040057

Borba, H. H. L., Steimbach, L. M., Riveros, B. S., Tonin, F. S., Ferreira, V. L., Bagatim, B. A., et al. (2018). Cost-effectiveness of amphotericin B formulations in the treatment of systemic fungal infections. *Mycoses* 61 (10), 754–763. doi: 10.1111/myc.12801

Carroll, S. F., Guillot, L., and Qureshi, S. T. (2007). Mammalian model hosts of cryptococcal infection. *Comp. Med.*, 9–17.

Chen, S., Sorrell, T., Nimmo, G., Speed, B., Currie, B., Ellis, D., et al. (2000). Epidemiology and host- and variety-Dependent characteristics of Infection due to *Cryptococcus neoformans* in Australia and New Zealand. *Clin. Infect. Dis* 31 (2), 499–508. doi: 10.1086/313992

Day, J. N., Qihui, S., Thanh, L. T., Trieu, P. H., Van, A. D., Thu, N. H., et al. (2017). Comparative genomics of *Cryptococcus neoformans* var. *grubii* associated with meningitis in HIV infected and uninfected patients in Vietnam. *PloS Neglect Trop. Dis* 11 (6), e0005628. doi: 10.1371/journal.pntd.0005628

Desnos-Ollivier, M., Patel, S., Raoux-Barbot, D., Heitman, J., and Dromer, F. (2015). Cryptococcosis serotypes impact outcome and provide evidence of *Cryptococcus neoformans* speciation. *mBio* 6 (3), e00311–15. doi: 10.1128/mBio.00311-15

Enoch, D. A., Yang, H., Aliyu, S. H., and Micallef, C. (2017). "The changing epidemiology of invasive fungal infections," in *Methods in Molecular Biology: Methods and Protocols*. Ed. T. Lion (New York: Springer Science+Business Media), 17–65. doi: 10.1007/978-1-4939-6515-1_2

Faustino, C., and Pinheiro, L. (2020). Lipid systems for the delivery of amphotericin B in antifungal therapy. *Pharmaceutics* 12 (1), 29. doi: 10.3390/pharmaceutics12010029

Fernandes, K. E., Brockway, A., Haverkamp, M., Carter, D. A., Cuomo, C. A., van Ogtrop, F., et al. (2018). Phenotypic variability correlates with clinical outcome in *Cryptococcus* isolates obtained from Botswanan HIV/AIDS patients. *mBio* 9 (5), 1–16. doi: 10.1128/mBio.02016-18

de Oliveira Frazão, S., de Sousa, H. R., da Silva, L. G., dos Santos Folha, J., de Melo Gorgonha, K. C., de Oliveira, G. P. Jr, et al. (2020). Laccase affects the rate of *Cryptococcus neoformans* nonlytic exocytosis from macrophages. *mBio* 11 (5), 1–6. doi: 10.1128/mBio.02085-20

Galanis, E., and MacDougall, L. (2010). Epidemiology of *Cryptococcus gattii*, British Columbia, Canada 1999-2007. *Emerg Infect. Dis.* 16 (2), 251–257. doi: 10.3201/eid1602.090900

Gerstein, A. C., Jackson, K. M., McDonald, T. R., Wang, Y., Lueck, B. D., Bohjanen, S., et al. (2019). Identification of pathogen genomic differences that impact human immune response and disease during *Cryptococcus neoformans* infection. *mBio* 10 (4), e01440–19. doi: 10.1128/mBio.01440-19

Goldman, D. L., Casadevall, A., Cho, Y., and Lee, S. C. (1996). *Cryptococcus neoformans* meningitis in the rat. *Lab. Invest.* 75 (6), 759–770.

Goldman, D. L., Khine, H., Abadi, J., Lindenberg, D. J., La, P., Niang, R., et al. (2001). Serologic evidence for *Cryptococcus neoformans* infection in early childhood. *Pediatrics* 107 (5), e66–e66. doi: 10.1542/peds.107.5.e66

Hagen, F., Khayhan, K., Theelen, B., Kolecka, A., Polacheck, I., Sionov, E., et al. (2015). Recognition of seven species in the *Cryptococcus gattii/Cryptococcus neoformans* species complex. *Fungal Genet. Biol.* 78, 16–48. doi: 10.1016/j.fgb.2015.02.009

Johnston, S. A., Voelz, K., and May, R. C. (2016). *Cryptococcus neoformans* thermotolerance to avian Body temperature is sufficient for extracellular growth but not intracellular survival in macrophages. *Sci. Rep.* 6 (October 2015), 1–9. doi: 10.1038/srep20977

Kwon-Chung, K. J., and Varma, A. (2006). Do major species concepts support one, two or more species within *Cryptococcus neoformans*? *FEMS Yeast Res.* 6 (4), 574–587. doi: 10.1111/j.1567-1364.2006.00088.x

Kwon-Chung, K. J., Bennett, J. E., Wickes, B. L., Meyer, W., Cuomo, C. A., Wollenburg, K. R., et al. (2017). The case for adopting the "species complex" nomenclature for the etiologic agents of cryptococcosis. *mSphere* 2 (1), 1–7. doi: 10.1128/msphere.00357-16

Lan, N. T. N., Lien, H. T. K., Tung, L. B., Borgdorff, M. W., Kremer, K., and Van Soolingen, D. (2003). *Mycobacterium tuberculosis* Beijing Genotype and Risk for Treatment Failure and Relapse, Vietnam. *Emerg. Infect. Dis.* 9, 1633–1635. doi: 10.3201/eid0912.030169

Lin, X., and Heitman, J. (2006). The biology of the *Cryptococcus neoformans* species complex. *Annu. Rev. Microbiol.* 60 (1), 69–105. doi: 10.1146/annurev.micro.60.080805.142102

Lu, R., Hollingsworth, C., Qiu, J., Wang, A., Hughes, E., Xin, X., et al. (2019). Efficacy of oral encochleated amphotericin B in a mouse model of cryptococcal meningoencephalitis. *mBio* 10 (3), e00724–19. doi: 10.1128/mBio.00724-19

Ma, H., Croudace, J. E., Lammas, D. A., and May, R. C. (2006). Expulsion of live pathogenic yeast by macrophages. *Curr. Biol.* 16 (21), 2156–2160. doi: 10.1016/j.cub.2006.09.032

Mirza, S. A., Phelan, M., Rimland, D., Graviss, E., Hamill, R., Brandt, M. E., et al. (2003). The changing epidemiology of cryptococcosis: an update from population-based active surveillance in 2 large metropolitan areas 1992-2000. *Clin. Infect. Dis.* 36 (6), 789–794. doi: 10.1086/368091

Mukaremera, L., McDonald, T. R., Nielsen, J. N., Molenaar, C. J., Akampurira, A., Schutz, C., et al. (2019). The mouse inhalation model of *Cryptococcus neoformans* infection recapitulates strain virulence in humans and shows that closely related strains can possess differential virulence. *Infect. Immun.* 87 (5), e00046–19. doi: 10.1128/IAI.00046-19

Ngamskulrungroj, P., Price, J., Sorrell, T., Perfect, J. R., and Meyer, W. (2011). *Cryptococcus gattii* virulence composite: Candidate genes revealed by microarray analysis of high and less virulent Vancouver Island outbreak strains. *PloS One* 6 (1), 16076. doi: 10.1371/journal.pone.0016076

Pan, C., Kumar, C., Bohl, S., Klingmueller, U., and Mann, M. (2009). Comparative proteomic phenotyping of cell lines and primary cells to assess preservation of cell type-specific functions. *Mol. Cell. Proteomics* 8 (3), 443–450. doi: 10.1074/mcp.M800258-MCP200

Rajasingham, R., Smith, R. M., Park, B. J., Jarvis, J. N., Govender, N. P., Chiller, T. M., et al. (2017). Global burden of disease of HIV-associated cryptococcal meningitis: an updated analysis. *Lancet Infect. Dis.* 17 (8), 873–881. doi: 10.1016/S1473-3099(17)30243-8

Rajendran, R., Sherry, L., Nile, C. J., Sherriff, A., Johnson, E. M., Hanson, M. F., et al. (2016). Biofilm formation is a risk factor for mortality in patients with *Candida albicans* bloodstream infection-Scotland 2012-2013. *Clin. Microbiol. Infect.* 22 (1), 87–93. doi: 10.1016/j.cmi.2015.09.018

Renney de Sousa, H., Oliveira Júnior, G. P., de Frazão, S., de Gorgonha, O., de M., K. C., Rosa, C. P., et al. (2020). Faster *Cryptococcus* melanization increases virulence in experimental and human cryptococcosis. *bioRxiv.*, 1–46. doi: 10.1101/2020.07.29.222794

Robertson, E. J., Najjuka, G., Rolfes, M. A., Akampurira, A., Jain, N., Anantharanjit, J., et al. (2014). *Cryptococcus neoformans* ex vivo capsule size is associated with intracranial pressure and host immune response in hiv-associated cryptococcal meningitis. *J. Infect. Dis.* 209 (1), 74–82. doi: 10.1093/infdis/jit435

Sabiiti, W., Robertson, E., Beale, M. A., Johnston, S. A., Brouwer, A. E., Loyse, A., et al. (2014). Efficient phagocytosis and laccase activity affect the outcome of HIV-associated cryptococcosis. *J. Clin. Invest.* 124 (5), 2000–2008. doi: 10.1172/JCI72950

Santangelo, R., Zoellner, H., Sorrell, T., Wilson, C., Donald, C., Djordjevic, J., et al. (2004). Role of extracellular phospholipases and mononuclear phagocytes in dissemination of cryptococcosis in a murine model. *Infect. Immun.* 72 (4), 2229–2239. doi: 10.1128/IAI.72.4.2229-2239.2004

Shi, M., Li, S. S., Zheng, C., Jones, G. J., Kim, K. S., Zhou, H., et al. (2010). Real-time imaging of trapping and urease-dependent transmigration of *Cryptococcus neoformans* in mouse brain. *J. Clin. Invest.* 120 (5), 1683–1693. doi: 10.1172/JCI41963

Wiesner, D. L., Moskalenko, O., Corcoran, J. M., Mcdonald, T., Rolfes, M. A., Meya, D. B., et al. (2012). Cryptococcal genotype influences immunologic response and human clinical outcome after meningitis. *mBio* 3 (5), e00196–12. doi: 10.1128/mBio.00196-12

Conflict of Interest : The authors declare that the research was conducted in the absence of any commercial or financial relationships that could be construed as a potential conflict of interest.

frontiers in Microbiology

ORIGINAL RESEARCH
published: 27 April 2021
doi: 10.3389/fmicb.2021.641258

Silver(I) and Copper(II) Complexes of 1,10-Phenanthroline-5,6-Dione Against *Phialophora verrucosa*: A Focus on the Interaction With Human Macrophages and *Galleria mellonella* Larvae

*Marcela Q. Granato[1], Thaís P. Mello[2], Renata S. Nascimento[3], Marcos D. Pereira[3], Thabatta L. S. A. Rosa[4], Maria C. V. Pessolani[4], Malachy McCann[5], Michael Devereux[6], Marta H. Branquinha[2], André L. S. Santos[2,3] and Lucimar F. Kneipp[1]**

[1]Laboratório de Taxonomia, Bioquímica e Bioprospecção de Fungos (LTBBF), Instituto Oswaldo Cruz (IOC), Fundação Oswaldo Cruz (FIOCRUZ), Rio de Janeiro, Brazil, [2]Laboratório de Estudos Avançados de Microrganismos Emergentes e Resistentes (LEAMER), Instituto de Microbiologia Paulo de Góes, Universidade Federal do Rio de Janeiro (UFRJ), Rio de Janeiro, Brazil, [3]Laboratório de Citotoxicidade e Genotoxicidade (LaCiGen), Instituto de Química, UFRJ, Rio de Janeiro, Brazil, [4]Laboratório de Microbiologia Celular, IOC/FIOCRUZ, Rio de Janeiro, Brazil, [5]Department of Chemistry, Maynooth University, National University of Ireland, Maynooth, Ireland, [6]Center for Biomimetic and Therapeutic Research, Focas Research Institute, Technological University Dublin, Dublin, Ireland

Phialophora verrucosa is a dematiaceous fungus that causes mainly chromoblastomycosis, but also disseminated infections such as phaeohyphomycosis and mycetoma. These diseases are extremely hard to treat and often refractory to current antifungal therapies. In this work, we have evaluated the effect of 1,10-phenanthroline-5,6-dione (phendione) and its metal-based complexes, [Ag (phendione)$_2$]ClO$_4$ and [Cu(phendione)$_3$](ClO$_4$)$_2$.4H$_2$O, against *P. verrucosa*, focusing on (i) conidial viability when combined with amphotericin B (AmB); (ii) biofilm formation and disarticulation events; (iii) *in vitro* interaction with human macrophages; and (iv) *in vivo* infection of *Galleria mellonella* larvae. The combination of AmB with each of the test compounds promoted the additive inhibition of *P. verrucosa* growth, as judged by the checkerboard assay. During the biofilm formation process over polystyrene surface, sub-minimum inhibitory concentrations (MIC) of phendione and its silver(I) and copper(II) complexes were able to reduce biomass and extracellular matrix production. Moreover, a mature biofilm treated with high concentrations of the test compounds diminished biofilm viability in a concentration-dependent manner. Pre-treatment of conidial cells with the test compounds did not alter the percentage of infected THP-1 macrophages; however, [Ag(phendione)$_2$]ClO$_4$ caused a significant reduction in the number of intracellular fungal cells compared to the untreated system. In addition, the killing process was significantly enhanced by post-treatment of infected macrophages with the

OPEN ACCESS

Edited by:
Ruoyu Li,
Peking University First Hospital, China

Reviewed by:
Erin E. McClelland,
Independent Researcher,
Murfreesboro, TN, United States
Marta Palusinska-Szysz,
Marie Curie-Sklodowska University, Poland

***Correspondence:**
Lucimar F. Kneipp
lucimar@ioc.fiocruz.br

Specialty section:
This article was submitted to Microbial Physiology and Metabolism, a section of the journal Frontiers in Microbiology

Received: *13 December 2020*
Accepted: *31 March 2021*
Published: *27 April 2021*

Citation:
Granato MQ, Mello TP, Nascimento RS, Pereira MD, Rosa TLSA, Pessolani MCV, McCann M, Devereux M, Branquinha MH, Santos ALS and Kneipp LF (2021) Silver(I) and Copper(II) Complexes of 1,10-Phenanthroline-5,6-Dione Against Phialophora verrucosa: A Focus on the Interaction With Human Macrophages and Galleria mellonella Larvae. Front. Microbiol. 12:641258. doi: 10.3389/fmicb.2021.641258

test compounds. *P. verrucosa* induced a typically cell density-dependent effect on *G. mellonella* larvae death after 7 days of infection. Interestingly, exposure to the silver(I) complex protected the larvae from *P. verrucosa* infection. Collectively, the results corroborate the promising therapeutic potential of phendione-based drugs against fungal infections, including those caused by *P. verrucosa*.

Keywords: 1,10-phenanthroline-5,6-dione, chromoblastomycosis, dematiaceous fungi, antifungal activity, cellular interaction

INTRODUCTION

Phialophora verrucosa is a well-known chromoblastomycosis etiological agent that may also cause other cutaneous and subcutaneous diseases as well as disseminated infections, such as phaeohyphomycosis and mycetoma (Turiansky et al., 1995; Tong et al., 2013; Queiroz-Telles et al., 2017). *P. verrucosa* has been observed in patients suffering with distinct illnesses, including keratitis, endophthalmitis, sinusitis, osteomyelitis, and endocarditis (Lundstrom et al., 1997; Hofmann et al., 2005; Campos-Herrero et al., 2012). Infections caused by this melanized filamentous fungus can affect both immunocompetent and immunosuppressed individuals (Lundstrom et al., 1997; Qiu et al., 2019). To date, there is no gold standard therapy for these incapacitating and neglected diseases. Overall, the infections caused by *P. verrucosa* tend to chronicity and hinder treatments, leading to recurrence and resistance to available conventional therapies (Li et al., 2014; Brito and Bittencourt, 2018). This scenario has emphasized the necessity for the development of new drugs against *P. verrucosa* infections, to be administered either alone or in combination with established antifungal agents.

Metal-based drugs have attracted enormous attention due to their pharmacological effects, which includes anticancer, anti-inflammatory, antioxidant, and antimicrobial activities (Mjos and Orvig, 2014; Anthony et al., 2020). In fact, inorganic medicinal chemistry has advanced in recent years, providing an alternative therapeutic approach to the purely organic antimicrobial agents (Lemire et al., 2013; Viganor et al., 2017; Claudel et al., 2020). Several studies have shown that 1,10-phenanthroline (phen) and its derivatives, as ligands coordinated to transition metals, exhibit potent antifungal activity against *Candida albicans* and non-*albicans Candida* species, such as *C. tropicalis*, *C. krusei*, *C. glabrata*, and *C. haemulonii* (Geraghty et al., 2000; McCann et al., 2000, 2012; Coyle et al., 2003; Hoffman et al., 2015; Gandra et al., 2017, 2020). In a previous study, we showed that 1,10-phenanthroline-5,6-dione (phendione) and its silver(I) and copper(II) complexes, $[Ag(phendione)_2]ClO_4$ and $[Cu(phendione)_3](ClO_4)_2.4H_2O$ (henceforth represented as their biologically active cations $[Ag(phendione)_2]^+$ and $[Cu(phendione)_3]^{2+}$), affected crucial physiological events of *P. verrucosa* (Granato et al., 2017). These three agents inhibited fungal proliferation, presenting minimum inhibitory concentration [MIC; mg/L (μM)] values of 2.5 (12.0), 2.5 (4.0), and 5.0 (5.0), respectively. Moreover, the compounds affected filamentation, sterol production, and the metallo-type peptidase activity of *P. verrucosa* (Granato et al., 2017).

Cytotoxicity assays revealed that phendione, $[Ag(phendione)_2]^+$, and $[Cu(phendione)_3]^{2+}$ were well tolerated *in vitro* by several mammalian tumor and non-tumor lines and also macrophages, and *in vivo* by Swiss mice and *Galleria mellonella* larvae (McCann et al., 2012; Gandra et al., 2020). This insect larva is a good and alternative *in vivo* experimental model due to the similarities exhibited with respect to the innate immune system of mammals, its ease of manipulation, low cost, and ethical acceptance (Jemel et al., 2020). Thus, *G. mellonella* larvae are widely used to assess the toxicity, efficacy, and safety of conventional antifungal agents and potential new drugs (Kavanagh and Sheehan, 2018; Maurer et al., 2019; Treviño-Rangel et al., 2019; Jemel et al., 2020).

The antimicrobial efficacy of phendione and its metal-based complexes has been shown against planktonic cells and also biofilm-growing cells (Viganor et al., 2016; Gandra et al., 2017; Ventura et al., 2020). Several studies have highlighted the biofilm relevance in the fungal pathogenesis, contextualizing the real issue of this structure formation in the medical settings (Vila and Rozental, 2016; Santos et al., 2018; Wall et al., 2019). This complex microbial community, which is adhered to a surface, is surrounded by an extracellular matrix that gives its cells several advantages, such as increased virulence, immune system, and environmental stress protection as well as resistance to antimicrobial agents (Costa-Orlandi et al., 2017; Santos et al., 2018). The biofilm extracellular matrix is formed mainly by polysaccharides, but also contains proteins, lipids, and DNA. This matrix is one of the most relevant structures of the biofilm and is directly associated with antimicrobial resistance (Ramage et al., 2012; Santos et al., 2018). In recent years, the capability of filamentous fungi (e.g., *Aspergillus fumigatus*, *Paracoccidioides brasiliensis*, *Scedosporium* spp., and *Exophiala dermatitidis*) to form a biofilm has been well documented (Kaur and Singh, 2014; Sardi et al., 2015; Mello et al., 2016; Kirchhoff et al., 2017). The ability of *P. verrucosa* to establish a biofilm on a polystyrene surface was previously investigated by our research group, and it was found that biofilm-growing *P. verrucosa* cells were more resistant to the action of conventional antifungal drugs than their planktonic counterparts (unpublished data).

The present study was designed to investigate the effects of phendione, $[Ag(phendione)_2]^+$, and $[Cu(phendione)_3]^{2+}$ on *P. verrucosa*, focusing on (i) the combination of these test agents with the classical antifungal drug, amphotericin B, (ii) biofilm formation and disarticulation, (iii) the *in vitro* interaction with human macrophages; and (iv) *in vivo* infection using *G. mellonella* larvae as a model.

MATERIALS AND METHODS

Fungal Growth Conditions

P. verrucosa (strain FMC.2214 isolated from a human patient with chromoblastomycosis and used in our previous work; Granato et al., 2017) was maintained in Sabouraud dextrose agar (SDA) medium with mineral oil at 4°C. For all assays, fungal cells were cultivated for 7 days under constant agitation (130 rpm) at 26°C in 100 ml of Czapek-Dox broth medium (BD-Difco, United States). Conidia were obtained by gauze filtering followed by centrifugation at 4,000 × *g* for 10 min. The fungal cells were then washed three times with saline solution (0.85% NaCl), and the number of conidia cells was estimated using a Neubauer chamber (Granato et al., 2015).

Test Compounds

Phendione was purchased from Sigma-Aldrich. $[Ag(phendione)_2]^+$ and $[Cu(phendione)_3]^{2+}$ were prepared by reacting phendione with the appropriate metal perchlorate salts in accordance with procedures previously published by McCann et al. (2004). For all of the experiments, the compounds were dissolved in dimethyl sulfoxide (DMSO; Sigma-Aldrich).

Combinatory Effects of Phendione and Its Metal Complexes With Amphotericin B on *P. verrucosa* Viability

The drug combinations were assessed using the checkerboard microdilution method as described by Chudzik et al. (2019). Briefly, initial concentrations equivalent to 8 × MIC of amphotericin B (AmB, MIC = 6.25 mg/L) were serially diluted in a cross fashion mode against 4 × MIC of each compound (phendione, $[Ag(phendione)_2]^+$, and $[Cu(phendione)_3]^{2+}$) in 96-well plates containing Roswell Park Memorial Institute (RPMI) 1640 medium (Sigma-Aldrich). Thus, the final concentrations range from 0.09 to 50 mg/L for AmB, 0.039 to 20 mg/L for $[Cu(phendione)_3]^{2+}$, and 0.019 to 10 mg/L for both phendione and $[Ag(phendione)_2]^+$. The inoculation and culture conditions followed the Clinical and Laboratory Standards Institute (CLSI, 2008) standard document M38-A2 for filamentous fungi with some minor modifications (Granato et al., 2017). Minimum inhibitory concentration values were established when the combination of AmB and each test compound inhibited 100% of the fungal growth as evidenced by visual inspection and the resazurin staining assay (Liu et al., 2007). The interaction type of two-drug combination was defined according to the fractional inhibitory concentration index (FICI) from the following formula: FICI = FICA + FICB, where FICA and FICB = MIC of drug A or B in combination divided by the MIC of drug A or B alone. Synergism was established when FICI value ≤ 0.5; additivity FICI > 0.5 to < 2.0; indifference FICI $\geq$ 2.0 to <4.0; and antagonism FICI $\geq$ 4.0 (Chudzik et al., 2019).

Effects of Phendione and Its Metal Complexes on *P. verrucosa* Biofilms

In this set of experiments, phendione, $[Ag(phendione)_2]^+$ and $[Cu(phendione)_3]^{2+}$ were tested on *P. verrucosa* biofilm using the broth microdilution assay in accordance with the document M38-A2 CLSI (2008) and Mello et al. (2016). Firstly, the compounds were examined for their ability to modulate biofilm formation. Conidia (1×10^6 cells) were placed in flat-bottom 96-well polystyrene microtiter plates containing RPMI medium supplemented or not with each test compound at concentrations varying from MIC to ⅛ × MIC values. After 72 h, non-adhered fungal cells were removed and the plates containing adhered biofilm-growing cells were subjected to colorimetric assays designed to measure the following biofilm parameters: biomass, viability, and extracellular matrix. The biomass quantification was evaluated after biofilm fixation with methanol (at 99%), followed by staining for 20 min with 0.3% crystal violet solution and the absorbance read at 590 nm. The determination of metabolic activity was conducted in non-fixed biofilms by the addition of 100 µl of a solution containing 2,3-bis (2-methoxy-4-nitro-5-sulfophenyl)-5-[(phenylamino) carbonyl]-2H-tetrazolium hydroxide (XTT, 0.04 mg) and menadione (0.0005 mg) into the plate wells, followed by incubation in the dark at 37°C for 4 h, and finally an absorbance reading at 490 nm. The assessment of the extracellular matrix was carried out using non-fixed biofilms, by staining with 0.1% safranin solution and the absorbance read at 530 nm (Mello et al., 2016). In order to investigate the effect of phendione and its metal complexes on mature biofilms, *P. verrucosa* conidia (1×10^6 cells) were added to 96-well polystyrene microplates and incubated for 72 h. Then, different concentrations of the test compounds, ranging from MIC to 64 × MIC values, were added to the plates and these were incubated for an additional 48 h. The biofilm MIC_{90} value ($bMIC_{90}$) was determined by considering the lowest concentration of each test compound capable of causing a 90% reduction in biofilm viability (Romera et al., 2019). System controls were prepared with non-treated cells in RPMI medium supplemented or not with DMSO, and RPMI medium containing DMSO or not. All dyes and reagents used for the colorimetric assays were obtained from Sigma-Aldrich. The absorbance measurements were performed using a microplate reader (SpectraMax M3, Molecular Devices, United States). Biofilm formation was observed using an inverted microscope (Nikon TS100-F, Tokyo, Japan) with a ×40 objective lens.

Effects of Phendione and Its Metal Complexes on *P. verrucosa*-Macrophage Interaction

Cell Culture and Stimulation

Human monocytic leukemia THP-1 cells (ATCC TIB-202) were cultured in 25 cm^3 culture flasks containing RPMI 1640 medium and 10% fetal bovine serum (Sigma-Aldrich) at 37°C in a 5% CO_2 atmosphere. For experimental assays, 1×10^6 cells were added to each well of a 24-well cell culture plate and cultivated in the same conditions as detailed above, with the addition of phorbol myristate acetate (PMA, 80 nM, Sigma-Aldrich) to promote the differentiation of monocytic cells into macrophages. After 24 h, the THP-1 cells were washed three times with RPMI and incubated in fresh medium without

PMA for an additional 24 h to allow for cell recovery. The differentiation of THP-1 monocytes into macrophages was confirmed by observing the cells adhesion capacity to culture plates and alteration of their morphology to a flat, amoeboid, and spreading shape using inverted microscope Nikon (Batista-Silva et al., 2016).

Fungi-Host Cells Interaction: Pre-treatment Assay

Conidia (2×10^6 cells) were treated with each test compound at concentrations varying from ¼ × MIC to 2 × MIC values, and after 20 h at 35°C, the fungal viability was assessed using the XTT assay (Mowat et al., 2007). For the interaction assay, *P. verrucosa* conidia were treated for 20 h with a non-cytotoxic concentration of each test compound, washed, and incubated for 30 min with the fluorescent dye PKH26 (2 μM; Sigma-Aldrich). After that, 250 μl of fetal bovine serum were added to interrupt the reaction, and the conidial cells were then washed and re-suspended in RPMI medium and incubated with macrophages in a 10:1 ratio (fungi:macrophage) for 3 h in a 5% CO_2 atmosphere at 37°C. The interaction systems were washed three times with sterile phosphate-buffered saline, pH 7.2 (PBS) and then with 2 mM PBS-EDTA buffer for their transference to cytometry tubes (Ersland et al., 2010). The interaction was monitored by flow cytometry (BD FACSAria) using Flowjo software. Results were represented as percentage of infected macrophages, which indicates the percentage of macrophage infected with fluorescent-labeled conidial cells. Systems consisting of non-treated conidia (control) and unlabeled conidia were also examined. The fluorescence values were adjusted after subtracting the non-specific fluorescence values of unlabeled cells (autofluorescence). In parallel, macrophages infected with either untreated or treated conidial cells were lysed with sterile cold water, and the suspensions were plated onto SDA medium to count the number of colony forming units (CFU; Palmeira et al., 2008).

Fungi-Host Cells Interaction: Post-treatment (Killing) Assay

In this set of experiments, the effect of the test compounds on macrophage viability was initially investigated. THP-1 macrophages (1×10^6) were incubated in a 96-well cell culture plate for 20 h in the absence (control) or in the presence of each test compound at a concentration varying from 0.03 to 5 mg/L. Then, the viability of macrophages was assessed after addition of 3-(4,5-dimethylthiazol-2-yl)-2,5-diphenyl tetrazolium bromide (MTT, Sigma-Aldrich) at 0.5 mg/ml and incubation for 3 h at 37°C as described by Mosmann (1983). Subsequently, in order to investigate the killing capability of THP-1 macrophages against *P. verrucosa*, viable conidia were washed in PBS and transferred to a 24-well plate containing macrophages at 10:1 ratio (fungi:macrophage) and incubated for 1 h at 37°C. Non-adhered conidia were removed and the interaction systems were incubated for 20 h with RPMI medium supplemented or not (control) with a non-cytotoxic concentration of test compound. The cultures were washed with PBS, lysed with sterile cold water and the suspensions then plated onto SDA medium for establishing the CFU number (Palmeira et al., 2008).

Effect of $[Ag(phendione)_2]^+$ on *G. mellonella* Larvae Infected With *P. verrucosa*

G. mellonella Larvae

The larvae of *G. mellonella* were reared in the insectary of the Department of Biochemistry of the Institute of Chemistry at UFRJ in plastic boxes at 21°C in the dark. Healthy larvae from the last instar with similar size (15–20 mm) and weight (0.2 g), and without alterations in their color, were chosen for the experiments. In order to determine the *in vivo* cytotoxicity and the antifungal activity of each test compound, 10 larvae were used in each experimental system (McCann et al., 2012; Fernandes et al., 2017).

Larval Survival Assay

Firstly, the non-toxic concentrations of $[Ag(phendione)_2]^+$ and the appropriate fungal cellular density were determined as described by McCann et al. (2012). Briefly, the compound (10 μl) was administered by injection through the last left proleg directly into the larvae haemocoel, using a Hamilton syringe, resulting in the final concentrations of either 5 or 10 μg compound/larva. Simultaneously, *P. verrucosa* conidia were suspended in PBS and adjusted to final densities equal to 1×10^4, 1×10^5, 1×10^6, 4×10^6, or 1×10^7 and inoculated as described above into each group of *G. mellonella* larvae. Then, the larvae were incubated at 37°C for 7 days and survival monitored every 24 h. Larvae mortality was assessed by lack of movement in response to mechanical stimulus. Larvae inoculated with 10 μl of PBS or DMSO were used as control systems. Infected larvae images were obtained after 1 h of incubation. For antifungal assessment, each *G. mellonella* larvae group was infected with *P. verrucosa* conidia, at a concentration presenting an intermediate rate of larvae mortality, and after 2 h a non-cytotoxic concentration of the test compound was injected. After that, the experimental protocol and the survival rate determination were performed as detailed above.

Statistical Analysis

The experiments were performed in triplicate in three independent experimental sets. The graphics and data were constructed and analyzed statistically by means of the ANOVA-test. Survival curves of *G. mellonella* larvae experiments were constructed using the method of Kaplan-Meier and compared using the Log-Rank (Mantel-Cox) test. All statistical analyses were performed with GraphPad Prism 5.0 software. Values of $p = 0.05$ or less were assumed as significant.

RESULTS AND DISCUSSION

Combinatory Effects of Phendione and Its Metal Complexes With Amphotericin B on *P. verrucosa* Viability

Using the checkerboard assay, we firstly investigated the effects of AmB combined with each of the test compounds (**Table 1**).

TABLE 1 | Effects of phendione and its metal complexes combined with amphotericin B on *Phialophora verrucosa* growth.

	MIC mg/L (μM)			
Agents	**Alone**	**Combined**	**FIC**	**FICI**
AmB	6.2 (6.8)	3.1 (3.4)	0.5	1.0
Phendione	2.5 (12.0)	1.2 (6.0)	0.5	
AmB	6.2 (6.8)	3.1 (3.4)	0.5	1.0
$[Ag(phendione)_2]^+$	2.5 (4.0)	1.2 (2.0)	0.5	
AmB	6.2 (6.8)	1.5 (3.4)	0.2	0.7
$[Cu(phendione)_3]^{2+}$	5.0 (5.0)	2.5 (2.5)	0.5	

The type of interaction was determined by calculating the fractional inhibitory concentration (FIC) index (FICI) as described by Chudzik et al. (2019) and detailed in Material and Methods. Minimum inhibitory concentration (MIC) was defined as the lowest concentration capable of inhibiting 100% of fungal growth. AmB, amphotericin B.

The combinations, AmB-$[Cu(phendione)_3]^{2+}$ and AmB-$[Ag(phendione)_2]^+$, were both additive (FICI = 0.7 and 1.0, respectively). Although none of the drug combinations displayed synergism (FICI $\leq$ 0.5) in the present case, such an effect has been observed in previous studies involving combinations of the metal-phendione complexes with classical antifungal drugs. Eshwika et al. (2004) showed that *C. albicans* treated with non-cytotoxic concentrations of $[Ag(phendione)_2]^+$ became more susceptible to miconazole and AmB. In a later study on *C. albicans*, the combination of AmB with copper(II) ions (AmB-Cu(II) complex) was again found to be more effective than AmB alone (Gagoś et al., 2011; Chudzik et al., 2013). It has been suggested that drug combinations with an additive effect may enhance pharmaceutical efficacy and reduce toxicity when each compound targets distinct stages of the same biological pathway (Spitzer et al., 2017). Importantly, the combination of benzothioureas with caspofungin has been shown to function in an additive manner regarding anti-cryptococcal activity, even though caspofungin on its own is ineffective against *Cryptococcus* species (Hartland et al., 2016; Spitzer et al., 2017). Overall, metal-based drugs have different modes of action conventional organic antifungal agents, thus combination therapy could potentiate the effect as well as possibly minimizing both resistance and toxicity.

Effects of Phendione and Its Metal Complexes on *P. verrucosa* Biofilms

The effectiveness of the phendione-based drugs to inhibit *P. verrucosa* conidial growth was previously described by our research group, with the following order: $[Cu(phendione)_3]^{2+}$ > $[Ag(phendione)_2]^+$ > phendione (Granato et al., 2017). Herein, we evaluated the effects of the test compounds upon biofilm formation by *P. verrucosa* on a polystyrene substrate. The fungal cells (1×10^6) incubated with sub-MIC concentrations preserved their metabolic viability along the process of biofilm formation, as shown by the XTT assay (**Figure 1A**). However, the biofilm biomass was affected by the incubation with the test compounds, showing a significant reduction when treated with phendione and $[Cu(phendione)_3]^{2+}$ at both ¼ × and ⅛ × MIC values, as well as with $[Ag(phendione)_2]^+$ at ½ × MIC value (**Figure 1B**). The extracellular matrix production was also affected by $[Ag(phendione)_2]^+$ at both ½ × and ¼ × MIC values, and by phendione at ¼ × MIC (**Figure 1C**).

The test compounds were also evaluated regarding their ability to disturb a mature biofilm formed by *P. verrucosa*. Phendione, $[Ag(phendione)_2]^+$, and $[Cu(phendione)_3]^{2+}$ inhibited fungal viability by approximately 90% ($bMIC_{90}$) when treated with concentrations [mg/L (μM)] of 20 (96), 80 (128), and 20 (20), respectively (**Figures 1D–F**). Moreover, biofilm cells were more resistant to the test compounds, since their $bMIC_{90}$ values were higher than those observed for the planktonic counterparts (Granato et al., 2017), increasing by about 4-, 8-, and 32-fold to $[Cu(phendione)_3]^{2+}$, phendione, and $[Ag(phendione)_2]^+$, respectively. Previous studies had shown that the biofilm of the *C. haemulonii* species complex was also disturbed by phen- and phendione-containing compounds, including copper(II) and silver(I) complexes (Gandra et al., 2017). In contrast to *P. verrucosa*, silver(I) chelates (16 mg/L, 25.5 μM) had a lower geometric mean of the bMIC values than their copper(II) counterparts (27.4 mg/L, 28.4 μM) for the *C. haemulonii* species complex. However, in comparison to the metal complexes containing perchlorate counter anions, the most active were manganese(II), silver(I), and copper(II) phen chelates containing coordinated dicarboxylate anions, which presented $bMIC_{50}$ values below 10 μM for these opportunistic yeasts (Gandra et al., 2017).

Effects of Phendione and Its Metal Complexes on the Interaction Between *P. verrucosa* and Human Macrophages

Firstly, *P. verrucosa* conidial (2×10^6) viability was assessed after treatment with different concentrations of the test compounds. The XTT assay showed that only the highest concentration (2 × MIC) affected fungal viability after 20 h (**Figure 2A**). The pre-treatment of *P. verrucosa* conidia with the MIC value of each compound did not significantly affect the percentage of infected macrophages (**Figure 2B**). However, the number of intracellular viable conidia was significantly diminished (around 60%) when the fungal cells were pre-treated with $[Ag(phendione)_2]^+$, as judged by the CFU assay (**Figure 2C**).

In order to investigate the killing capability of macrophages against *P. verrucosa* during the *in vitro* treatment, we firstly evaluated the effect of the test compounds on macrophage viability using the MTT assay. The results showed that phendione and its silver(I) complex were less toxic than the copper(II) complex, since around 90% of the macrophages remained viable

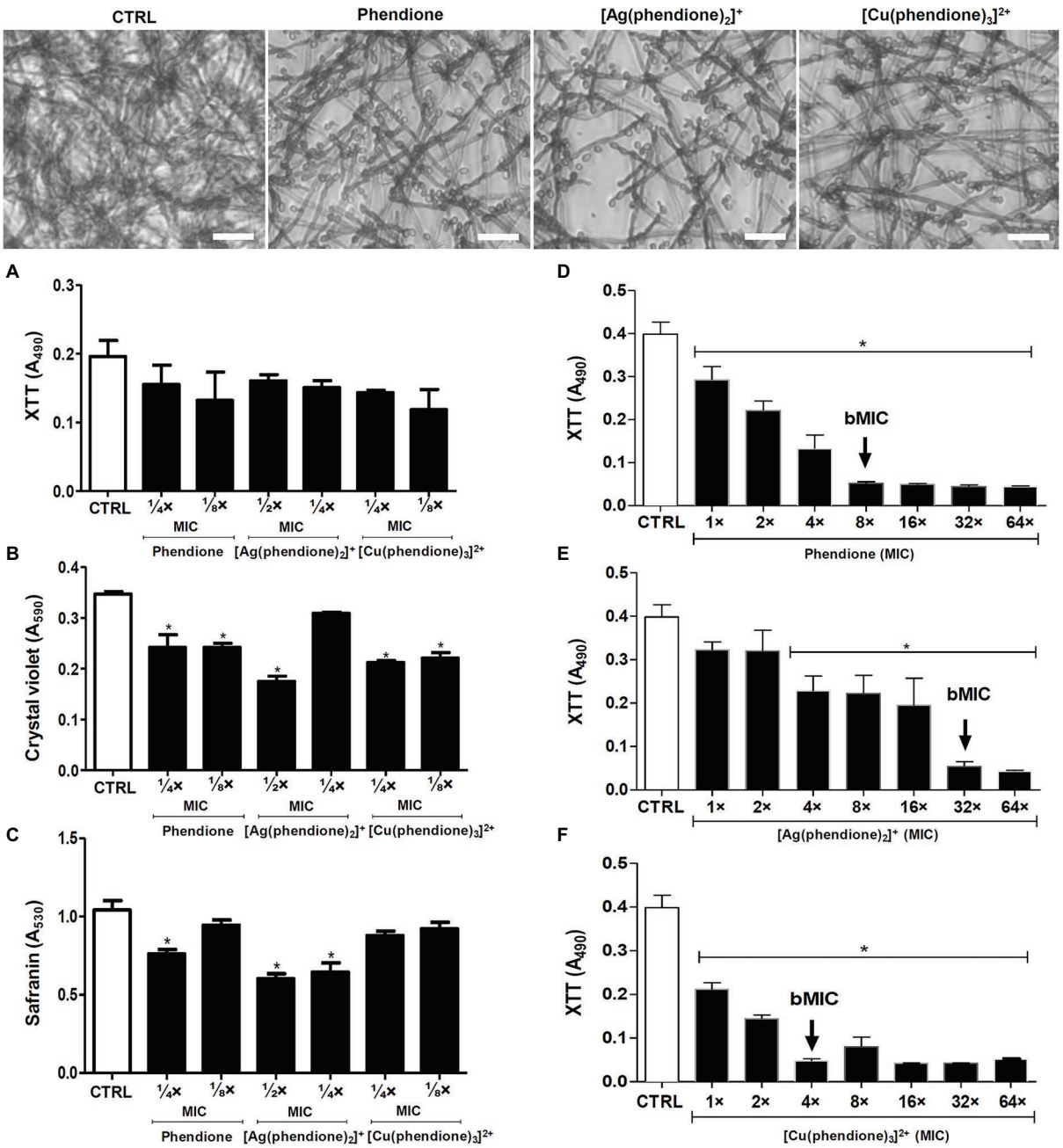

FIGURE 1 | Effects of phendione and its metal complexes on *P. verrucosa* biofilm formation and maturation. Conidia (1×10^6) were added to 96-well plates containing Roswell Park Memorial Institute (RPMI) medium supplemented with sub-MIC concentrations of each test compound. After incubation for 72 h at 37°C, **(A)** cell viability, **(B)** quantification of biomass, and **(C)** extracellular matrix were evaluated, as described in Material and Methods. The same conidia density **(D–F)** was placed to interact with polystyrene for 72 h in RPMI medium. Then, concentrations varying from MIC to 64 × MIC of each test compound were added and the plates incubated for additional 48 h. The MIC_{90} values of the biofilm ($bMIC_{90}$) were detected using the XTT reduction assay. Systems containing non-treated conidia were also prepared (CTRL, control). The eluent (dimethyl sulfoxide, DMSO) did not affect fungal growth (data not shown). The symbol (*) highlights the MIC values that caused a statistically significant reduction on each evaluated parameter in relation to the respective control ($p < 0.05$). Representative images of biomass (crystal violet-stained) formed by *P. verrucosa* non-treated (CTRL, control) and treated with phendione (¼ × MIC) and its silver(I) (½ × MIC) and copper(II) (¼ × MIC) complexes. Bar: 20 μm.

following treatment with 1.25 (6 μM), 1.25 (2 μM), and 0.31 mg/L (0.31 μM) concentrations, respectively (**Figure 3A**). Similarly, previous cytotoxicity studies showed that animal cell lineages were more tolerant toward $[Ag(phendione)_2]^+$. McCann et al. (2012) showed that $[Ag(phendione)_2]^+$ (IC_{50} > 10 mg/L; 15.9 μM) was less toxic than $[Cu(phendione)_3]^{2+}$

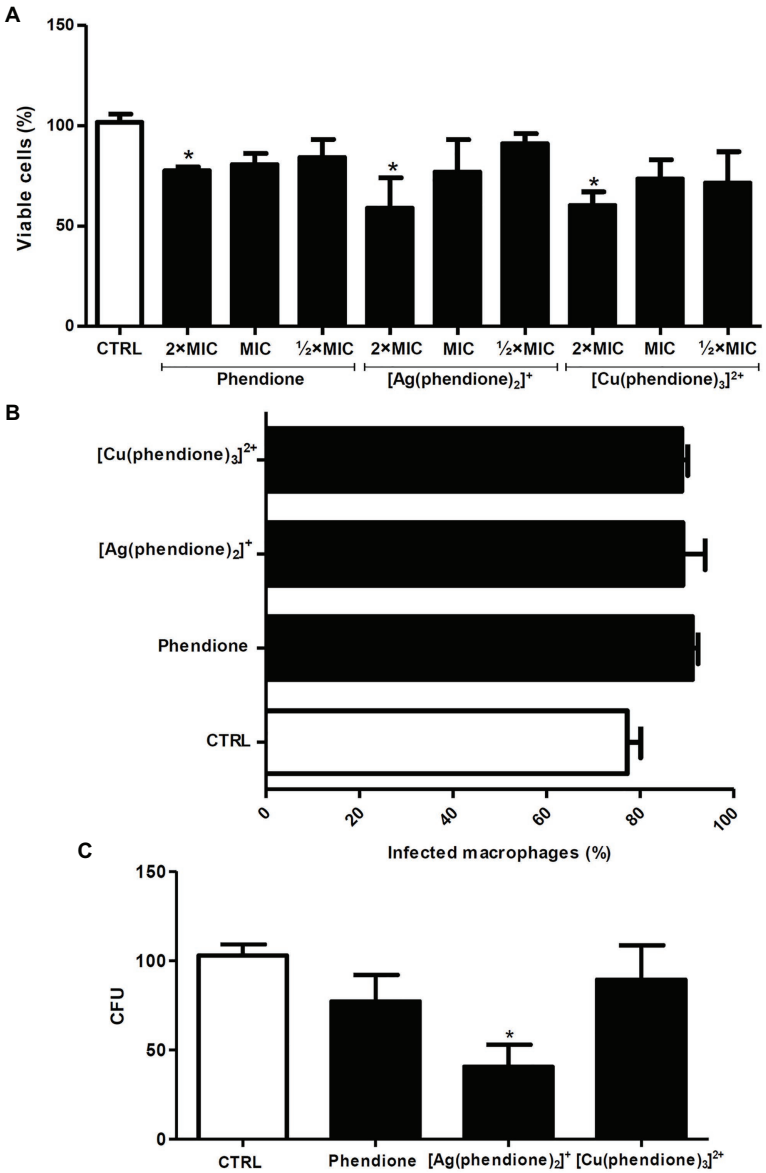

FIGURE 2 | Effects of phendione and its metal complexes on *P. verrucosa*-macrophage interaction. **(A)** Conidia (2×10^6) were treated for 20 h with each test compound in order to establish non-cytotoxic concentrations using the XTT assay. Then, the fungal cells **(B,C)** were treated with the MIC values of each compound, washed, and added to 24-well plates containing macrophages, in a 1:10 ratio (macrophage:fungi). After 3 h at 37°C, **(B)** the cells were transferred to tubes and subjected to flow cytometry to determine the number of infected macrophages, **(C)** the cells were washed, lysed with sterile cold water and the colony forming units (CFU) counted. Systems containing non-treated conidia were also prepared (CTRL, control). The eluent (DMSO) did not affect fungal growth (data not shown). For the flow cytometry assay, conidia were stained with PKH26. The values represent the mean SD of three independent experiments performed in triplicate. Asterisks indicate values of $p \leq 0.05$.

(IC_{50} = 6.1 mg/L; 6.3 μM) when murine macrophages (RAW 264.7 lineage) were assayed. In addition, Gandra et al. (2017) assessed the toxicity of the same compounds against A549, a lung epithelial cell lineage, and showed that the CC_{50} value was significantly larger for the silver(I) complex (3.76 mg/L) than its copper(II) analogue (0.68 mg/L). Herein, we showed that the infected macrophages, subsequently treated for 20 h with non-toxic concentrations of phendione [1.25 mg/L (6 μM)], $[Ag(phendione)_2]^+$ [1.25 mg/L (2 μM)], and $[Cu(phendione)_3]^{2+}$ [0.31 mg/L (0.31 μM)], were able to reduce the viability of intracellular conidial cells by approximately 65, 60, and 70%, respectively (**Figure 3B**).

The mechanism of action of metal complexes of phen and phendione has not yet been fully established. However, the impact of these compounds on fungal cells can be attributed to their ability to induce different cellular changes, such as disruption of the cell membrane, rupture of internal organelles, nuclear fragmentation, sequestration of essential metals, and

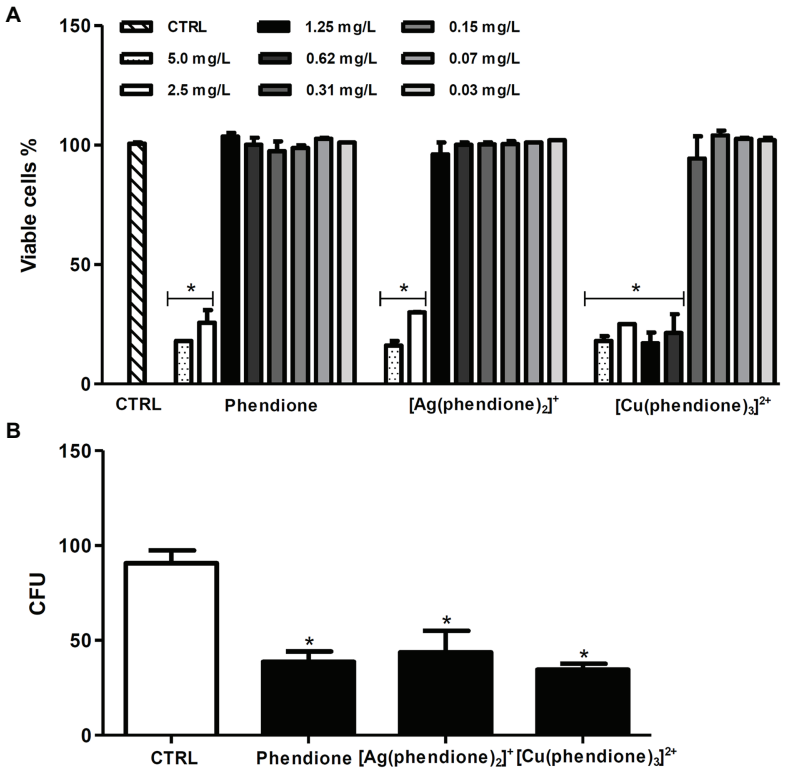

FIGURE 3 | Effects of phendione and its metal complexes on THP-1 viability and the ability of macrophages to kill *P. verrucosa* conidia. **(A)** Macrophages (1×10^6) were incubated in the absence (CTRL, control) or in the presence of phendione and its silver(I) and copper(II) complexes (0.03–5 mg/L) for 20 h. After treatment, macrophage viability was determined using the MTT assay. **(B)** THP-1 cells were infected with *P. verrucosa* conidia in a ratio of 1:10 (macrophage:fungi) for 1 h. Then, non-adherent fungi were removed and the microplates incubated for an additional 20 h with non-cytotoxic concentrations [mg/L (μM)] of phendione [1.25 (6)], $[Ag(phendione)_2]^+$ [1.25 (2)], and $[Cu(phendione)_3]^{2+}$ [0.31 (0.31)]. Then, macrophages were washed and lysed with sterile cold water, and the suspensions were plated onto sabouraud dextrose agar (SDA) medium to count the number of colony forming units (CFU). The values represent the mean SD of three independent experiments performed in triplicate. Asterisks indicate values of $p \leq 0.05$.

damage of the mitochondrial function (Coyle et al., 2003; McCann et al., 2012). In the previous study involving *P. verrucosa* conidia, we revealed some potential mechanisms of action of these test compounds (Granato et al., 2017). The phendione metal complexes were able to affect the production of fungal membrane ergosterol, thus possibly contributing to cell death. In addition, the complexes also inhibited the metallopeptidase activity of *P. verrucosa* conidia (Granato et al., 2017). Inhibition of this enzyme can prevent the fungal cells ability to access peptides and amino acids essential for their nutrition and thus restricting cell growth. From the current study, it is evident that addition of the test compounds improved the antifungal action of macrophages. The increase of compound-treated *P. verrucosa* susceptibility to macrophage killing could be related to an increase in the production of reactive oxygen species by these phagocytes since the respiratory burst is one of the most important mechanisms for the antimicrobial immunity of phagocytic cells (Herb and Schramm, 2021). Thus, the enhanced ability of macrophages to combat the fungal infection could be explained by the direct action of the test compounds on the intracellular conidia, and by the induction of intracellular macrophage mechanisms that mediate the antimicrobial immune responses, just as has previously been reported in regard to the anti-mycobacterial and antitumoral activities of phen- and phendione-based complexes (Kellett et al., 2011; McCarron et al., 2018). However, further studies are required in order to more fully understand the mechanisms involved in the anti- *P. verrucosa* activity of the test compounds.

Effects of $[Ag(Phendione)_2]^+$ on *G. mellonella* Infected With *P. verrucosa*

Although the copper(II) chelate was the most effective in disturbing a *P. verrucosa* mature biofilm, the silver(I) complex was less toxic toward THP-1 and it also affected the viability of conidial cells, at both pre- and post-treated proposals, in the *in vitro* interactions with macrophages. Thus, $[Ag(phendione)_2]^+$ was selected for the *in vivo G. mellonella* experiments. At dosages of 5 and 10 μg per larva, the silver(I) complex did not affect *G. mellonella* viability for a test period of up to 7 days (**Figure 4A**). This result corroborated the data obtained previously by McCann et al. (2012), who showed the low toxicity of phendione and its metal complexes for an exposure period of 72 h using the *G. mellonella* larvae as

an experimental model. Similarly, the test compounds were also well tolerated by Swiss mice, as previously reported by McCann et al. (2012). In that study, phendione, $[Ag(phendione)_2]^+$, and $[Cu(phendione)_3]^{2+}$, at dosages up to 45 mg/kg, were injected into mice and after 7 days no deaths were recorded. Interestingly, only $[Ag(phendione)_2]^+$, administered at a concentration of 150 mg/kg over the same time period, did not cause mortality, indicating that this complex was the least toxic. Thus, mice tolerance was in the order $[Ag(phendione)_2]^+$ > phendione > $[Cu(phendione)_3]^{2+}$ (McCann et al., 2012).

The survival of *G. mellonella* larvae following infection with *P. verrucosa* was also studied (**Figure 4A**). After inoculation of larvae with the lowest fungal densities (1×10^4 and 1×10^5), 80% survived up to the last day of monitoring. However, 1×10^6 conidia induced larvae death gradually until the fifth day, and at the end of the incubation period only 30% survived. Administering a cell density of 4×10^6 conidia caused a reduction of 50% of viable larvae by the third day and 100% mortality by the fifth day. In addition, it was found that injection of 1×10^7 conidia triggered 80% of larval death by the second day and 100% by the fourth day (**Figure 4A**). These experiments demonstrated that the mortality of *G. mellonella* infected with *P. verrucosa* was dependent upon the fungal inoculum density. It is well known that disease outcomes are influenced by the quantity of the infective particles.

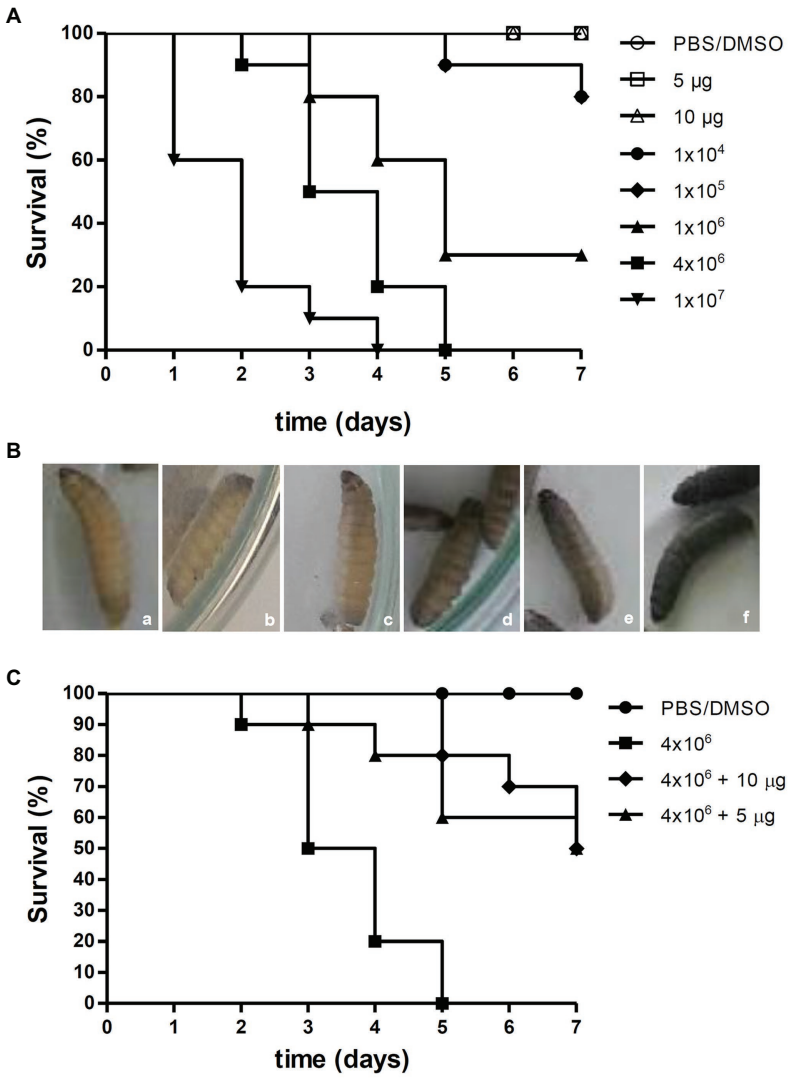

FIGURE 4 | Effects of $[Ag(phendione)_2]^+$ on *P. verrucosa* infection of *G. mellonella* larvae. **(A)** Different cell densities of *P. verrucosa* conidia and $[Ag(phendione)_2]^+$, at concentrations of 5 and 10 µg/larva, were injected in *G. mellonella* larvae and the survival rate determined over a total period of 7 days. **(B)** Representative images of *G. mellonella* larvae 1 h post injection with (a) PBS/DMSO and different densities of *P. verrucosa* conidia (b) 1×10^4, (c) 1×10^5, (d) 1×10^6, (e) 4×10^6, and (f) 1×10^7. **(C)** Each larva was infected with *P. verrucosa* conidia (4×10^6), and after a period of 2 h was treated with the silver(I) complex at a concentration of either 5 or 10 µg/larva. Injection with only the PBS/DMSO eluent represents the control. The survival rate (10 larvae/systems) was monitored over 7 days, and death was assessed by the lack of larval movement in response to a stimulus.

However, tests using the same invertebrate model infected with *Paracoccidioides lutzii* and *Histoplasma capsulatum* revealed that these fungi were lethal to the larvae and without any correlation with cellular density (Thomaz et al., 2013). With the current infection assay using *P. verrucosa*, it was observed that the melanization of the larvae increased in accordance with dispensed cell density. In fact, larvae inoculated with the highest *P. verrucosa* cell density (1×10^7) immediately became melanized, whereas with cell densities of 1×10^6 and 4×10^6, the pigmentation was observed only after 1 h (**Figure 4B**). Larvae melanization, when exposed to other fungi, has been well documented (Li et al., 2013; Thomaz et al., 2013; Gandra et al., 2020). Like *P. verrucosa*, other non-*albicans Candida* species induced early larvae melanization and its progression was dependent upon inoculum density (Silva et al., 2018). However, premature larvae melanization was not observed following infection with *Cryptococcus neoformans* (Trevijano-Contador et al., 2015). The *G. mellonella* model was also used for studying the virulence of other fungi that cause chromoblastomycosis and phaeohyphomycosis, such as *Fonsecaea* spp. and *Exophiala jeanselmei* (Vicente et al., 2017; Huang et al., 2018). Huang et al. (2018) showed that the increase in fungal inoculum resulted in greater larval mortality. In contrast to *P. verrucosa*, the authors observed that *F. monophora* (1×10^6 conidia/larva) infection induced *G. mellonella* melanization only on the second day post injection. *G. mellonella* larvae melanization process occurs in response to trauma or microbial cell invasion through the activation of phenoloxidase (Trevijano-Contador and Zaragoza, 2019). The insect enzymatic system can be activated during the immune response after recognition of specific components, such as β-glucans in the fungal cell wall (Pereira et al., 2018; Trevijano-Contador and Zaragoza, 2019).

Addition of $[Ag(phendione)_2]^+$ at two non-toxic concentrations (5 and 10 μg/larva) to *G. mellonella* larvae which were pre-infected with *P. verrucosa* (inoculum density of 4×10^6 conidia), resulted in an intermediate rate of larval mortality. The results showed that by the third day of incubation, 50% of untreated larvae had perished, while 90% of larvae treated with the same two concentrations of the silver(I) complex remained alive (**Figure 4C**). On the fifth day, 100% mortality was recorded for the untreated larvae. However, 80% of larvae survived after $[Ag(phendione)_2]^+$ treatment at 10 μg per larva. At the lower concentration of added $[Ag(phendione)_2]^+$ (5 μg per larva) there was a 60% survival rate, suggesting a dose-dependent effect. It was also found that, following treatment with $[Ag(phendione)_2]^+$, 50% of larvae survived until the last day of monitoring (**Figure 4C**), thus clearly demonstrating a protective effect by the silver(I) complex. In their study of *G. mellonella* infected with *Candida* spp., Rowan et al. (2009) found that the larvae survival rate was increased after treatment with the silver(I) complex, $[Ag_2(mal)(phen)_3]$ (mal H_2 = malonic acid). Gandra et al. (2020) showed that different phen and phendione metal complexes, including $[Ag(phendione)_2]^+$, were able to inhibit *C. haemulonii* proliferation in *G. mellonella* infected larvae. In that study, the manganese(II) phen chelate containing the 3,6,9-trioxaundecanedioate dianion was the most effective. The antifungal efficacy against other fungi, such as *Candida* spp., *Cryptococcus* spp., *Aspergillus* spp., and *Trichosporon* spp. has also been assessed using the *G. mellonella* model (Kavanagh and Sheehan, 2018; Jemel et al., 2020). Thus, our present work has demonstrated that the *G. mellonella in vivo* model can be employed successfully to evaluate the antifungal effectiveness of phendione complexes presenting *in vitro* anti-*P. verrucosa* activity.

CONCLUSION

The silver(I) phendione complex, $[Ag(phendione)_2]^+$, is capable of reducing the viability of *P. verrucosa* conidia following interaction with human macrophages *in vitro*, and also conferring protection, *in vivo*, to *G. mellonella* larvae infected with the fungus. Transition metal complexes represent a novel group of antifungal agents due to their multi-modal activity, low cost, ease of synthesis, and their relatively high tolerance in *in vitro* animal cells as well as in lower mammals and insects used routinely as *in vivo* experimental models. Further studies are ongoing in an effort to understand the mechanisms of action of these metal complexes against *P. verrucosa* and other fungi that also cause chromoblastomycosis and phaeohyphomycosis. This advancement will further inform and facilitate the development of more effective compounds with reduced toxicity and enhanced potency against the microbes responsible for these debilitating diseases.

DATA AVAILABILITY STATEMENT

All datasets generated for this study are included in the article/supplementary material.

AUTHOR CONTRIBUTIONS

MG, MDP, MCP, MM, MD, MB, AS, and LK conceived and designed the study and wrote and revised the paper. MG, TM, RN, and TR performed the experiments. All authors analyzed the data. MDP, MCP, MM, MD, MB, AS, and LK contributed the reagents, materials, and/or analysis tools. All authors contributed to the research, approved the final version of the manuscript, and agree to be accountable for all aspects of the work.

FUNDING

This study was supported by grants from the Brazilian agencies: Conselho Nacional de Desenvolvimento Científico e Tecnológico (CNPq), Fundação de Amparo à Pesquisa no Estado do Rio de Janeiro (FAPERJ), Coordenação de Aperfeiçoamento de Pessoal de Nível Superior (CAPES, financial code 001), and Fundação Oswaldo Cruz (FIOCRUZ).

REFERENCES

Anthony, E. J., Bolitho, E. M., Bridgewater, H. E., Carter, O. W., Donnelly, J. M., Imberti, C., et al. (2020). Metallodrugs are unique: opportunities and challenges of discovery and development. *Chem. Sci.* 11:12888. doi: 10.1039/D0SC04082G

Batista-Silva, L. R., Rodrigues, L. S., Vivarini, A. C., Costa, F. M. R., Mattos, K. A., Costa, M. R. S. N., et al. (2016). *Mycobacterium leprae*-induced insulin-like growth factor I attenuates antimicrobial mechanisms, promoting bacterial survival in macrophages. *Sci. Rep.* 6:27632. doi: 10.1038/srep27632

Brito, A. C., and Bittencourt, M. J. S. (2018). Chromoblastomycosis: an etiological, epidemiological, clinical, diagnostic, and treatment update. *An. Bras. Dermatol.* 93, 495–506. doi: 10.1590/abd1806-4841.20187321

Campos-Herrero, M. I., Tandón, L., Horcajada, I., and Medina-Rivero, F. (2012). Endophthalmitis caused by *Phialophora verrucosa*: A case report and literature review of *Phialophora* ocular infections. *Enferm. Infecc. Microbiol. Clin.* 30, 163–166. doi: 10.1016/j.eimc.2011.10.012

Chudzik, B., Bonio, K., Dabrowski, W., Pietrzak, D., Niewiadomy, A., Olender, A., et al. (2019). Synergistic antifungal interactions of amphotericin B with 4-(5-methyl-1,3,4-thiadiazole-2-yl) benzene-1,3-diol. *Sci. Rep.* 9:12945. doi: 10.1038/s41598-019-49425-1

Chudzik, B., Tracz, I. B., Czernel, G., Fiołka, M. J., Borsuk, G., and Gagoś, M. (2013). Amphotericin B-copper(II) complex as a potential agent with higher antifungal activity against *Candida albicans*. *Eur. J. Pharm. Sci.* 49, 850–857. doi: 10.1016/j.ejps.2013.06.007

Claudel, M., Schwarte, J. V., and Fromm, K. M. (2020). New antimicrobial strategies based on metal complexes. *Chemistry* 2, 849–899. doi: 10.3390/chemistry2040056

CLSI (2008). *Clinical Laboratory Standards Institute: Reference Method for Broth Dilution Antifungal Susceptibility Testing of Filamentous Fungi, 2nd Edn., Approved Standard M38-A2.* Wayne, PA: CLSI.

Costa-Orlandi, C. B., Sardi, J. C. O., Pitangui, N. S., Oliveira, H. C., Scorzoni, L., Galeane, M. C., et al. (2017). Fungal biofilms and polymicrobial diseases. *J. Fungi* 3:22. doi: 10.3390/jof3020022

Coyle, B., Kavanagh, K., McCann, M., Devereux, M., and Geraghty, M. (2003). Mode of anti-fungal activity of 1, 10-phenanthroline and its Cu(II), Mn(II) and Ag(I) complexes. *Biometals* 16, 321–329. doi: 10.1023/A:1020695923788

Ersland, K., Wüthrich, M., and Klein, B. S. (2010). Dynamic interplay among monocyte derived, dermal, and resident lymph node dendritic cells during the generation of vaccine immunity to fungi. *Cell Host Microbe* 7, 474–487. doi: 10.1016/j.chom.2010.05.010

Eshwika, A., Coyle, B., Devereux, M., McCann, M., and Kavanagh, K. (2004). Metal complexes of 1,10-phenanthroline-5,6-dione alter the susceptibility of the yeast *Candida albicans* to amphotericin B and miconazole. *Biometals* 17, 415–422. doi: 10.1023/B:BIOM.0000029438.97990.c6

Fernandes, C. M., Fonseca, F. L., Goldman, G. H., Pereira, M. D., and Kurtenbach, E. (2017). A reliable assay to evaluate the virulence of *Aspergillus nidulans* using the alternative animal model *Galleria mellonella* (Lepidoptera). *Bio-Protocol* 7:e2329. doi: 10.21769/BioProtoc.2329

Gagoś, M., Czernel, G., Kamiński, D. M., and Kostro, K. (2011). Spectroscopic studies of amphotericin B-Cu^{2+} complexes. *Biometals* 24:915. doi: 10.1007/s10534-011-9445-2

Gandra, R. M., McCarron, P., Fernandes, M. F., Ramos, L. S., Mello, T. P., Aor, A. C., et al. (2017). Antifungal potential of copper(II), manganese(II) and silver(I) 1,10-phenanthroline chelates against multidrug-resistant fungal species forming the *Candida haemulonii* complex: impact on the planktonic and biofilm lifestyles. *Front. Microbiol.* 8:1257. doi: 10.3389/fmicb.2017.01257

Gandra, R. M., McCarron, P., Viganor, L., Fernandes, M. F., Kavanagh, K., McCann, M., et al. (2020). *In vivo* activity of copper(II), manganese(II), and silver(I) 1,10-phenanthroline chelates against *Candida haemulonii* using the *Galleria mellonella* model. *Front. Microbiol.* 11:470. doi: 10.3389/fmicb.2020.00470

Geraghty, M., Cronin, J. F., Devereux, M., and McCann, M. (2000). Synthesis and antimicrobial activity of copper (II) and manganese (II) α,ω-dicarboxylate complexes. *Biometals* 13, 1–8. doi: 10.1023/A:1009271221684

Granato, M. Q., Gonçalves, D. S., Seabra, S. H., McCann, M., Devereux, M., Santos, A. L. S., et al. (2017). 1,10-phenanthroline-5,6-dione-based compounds are effective in disturbing crucial physiological events of *Phialophora verrucosa*. *Front. Microbiol.* 8:76. doi: 10.3389/fmicb.2017.00076

Granato, M. Q., Massapust, P. A., Rozental, S., Alviano, C. S., Santos, A. L. S., and Kneipp, L. F. (2015). 1,10-phenanthroline inhibits the metallopeptidase secreted by *Phialophora verrucosa* and modulates its growth, morphology and differentiation. *Mycopathologia* 179, 231–242. doi: 10.1007/s11046-014-9832-7

Hartland, K., Pu, J., Palmer, M., Dandapani, S., Moquist, P. N., Munoz, B., et al. (2016). Highthroughput screen in identifies a novel molecular scaffold that inhibits cell wall integrity pathway signaling. *ACS Infect. Dis.* 2, 93–102. doi: 10.1021/acsinfecdis.5b00111

Herb, M., and Schramm, M. (2021). Functions of ROS in macrophages and antimicrobial immunity. *Antioxidants* 10:313. doi: 10.3390/antiox10020313

Hoffman, A. E., Miles, L., Greenfield, T. J., Shoen, C., DeStefano, M., Cynamon, M., et al. (2015). Clinical isolates of *Candida albicans*, *Candida tropicalis*, and *Candida krusei* have different susceptibilities to Co(II) and Cu(II) complexes of 1,10-phenanthroline. *Biometals* 28, 415–423. doi: 10.1007/s10534-015-9825-0

Hofmann, H., Choi, S. M., Wilsmann-Theis, D., Horré, R., de Hoog, G. S., and Bieber, T. (2005). Invasive chromoblastomycosis and sinusitis due to *Phialophora verrucosa* in a child from northern Africa. *Mycoses* 48, 456–461. doi: 10.1111/j.1439-0507.2005.01150.x

Huang, X., Liu, Y., Xi, L., Zeng, K., and Mylonakis, E. (2018). *Galleria mellonella* as a model invertebrate host for the study of muriform cells of dematiaceous fungi. *Future Microbiol.* 13, 1021–1028. doi: 10.2217/fmb-2018-0036

Jemel, S., Guillot, J., Kallel, K., Botterel, F., and Dannaoui, E. (2020). *Galleria mellonella* for the evaluation of antifungal efficacy against medically important fungi, a narrative review. *Microorganisms* 8:390. doi: 10.3390/microorganisms8030390

Kaur, S., and Singh, S. (2014). Biofilm formation by *Aspergillus fumigatus*. *Med. Mycol.* 52, 2–9. doi: 10.3109/13693786.2013.819592

Kavanagh, K., and Sheehan, G. (2018). The use of *Galleria mellonella* larvae to identify novel antimicrobial agents against fungal species of medical interest. *J. Fungi* 4:E113. doi: 10.3390/jof4030113

Kellett, A., O'Connor, M., McCann, M., Howe, O., Casey, A., McCarron, P., et al. (2011). Water-soluble bis(1,10-phenanthroline) octanedioate Cu^{2+} and Mn^{2+} complexes with unprecedented nano and picomolar *in vitro* cytotoxicity: promising leads for chemotherapeutic drug development. *Med. Chem. Commun.* 2, 579–584. doi: 10.1039/c0md00266f

Kirchhoff, L., Olsowski, M., Zilmans, K., Dittmer, S., Haase, G., Sedlacek, L., et al. (2017). Biofilm formation of the black yeast-like fungus *Exophiala dermatitidis* and its susceptibility to antiinfective agents. *Sci. Rep.* 7:42886. doi: 10.1038/srep42886

Lemire, J., Harrison, J., and Turner, R. (2013). Antimicrobial activity of metals: mechanisms, molecular targets and applications. *Nat. Rev. Microbiol.* 11, 371–384. doi: 10.1038/nrmicro3028

Li, D.-D., Deng, L., Hu, G.-H., Zhao, L. X., Hu, D.-D., Jiang, Y.-Y., et al. (2013). Using *Galleria mellonella-Candida albicans* infection model to evaluate antifungal agents. *Biol. Pharm. Bull.* 36, 1482–1487. doi: 10.1248/bpb.b13-00270

Li, Y., Wan, Z., and Li, R. (2014). *In vitro* activities of nine antifungal drugs and their combinations against *Phialophora verrucosa*. *Antimicrob. Agents Chemother.* 58, 5609–5612. doi: 10.1128/AAC.02875-14

Liu, M., Seidel, V., Katerere, D. R., and Gray, A. I. (2007). Colorimetric broth microdilution method for the antifungal screening of plant extracts against yeasts. *Methods* 42, 325–329. doi: 10.1016/j.ymeth.2007.02.013

Lundstrom, T. S., Fairfax, M. R., Dugan, M. C., Vazquez, J. A., Chandrasekar, P. H., Abella, E., et al. (1997). *Phialophora verrucosa* infection in a BMT patient. *Bone Marrow Transplant.* 20, 789–791. doi: 10.1038/sj.bmt.1700969

Maurer, E., Hörtnagl, C., Lackner, M., Grässle, D., Naschberger, V., Moser, P., et al. (2019). *Galleria mellonella* as a model system to study virulence potential of mucormycetes and evaluation of antifungal treatment. *Med. Mycol.* 57, 351–362. doi: 10.1093/mmy/myy042

McCann, M., Coyle, B., McKay, S., McCormack, P., Kavanagh, K., Devereux, M., et al. (2004). Synthesis and X-ray crystal structure of $[Ag(phendio)_2]ClO_4$ (phendio = 1,10-phenanthroline-5,6-dione) and its effects on fungal and mammalian cells. *Biometals* 17, 635–645. doi: 10.1007/s10534-004-1229-5

McCann, M., Geraghty, M., Devereux, M., O'Shea, D., Mason, J., and O'Sullivan, L. (2000). Insights into the mode of action of the anti-*Candida* activity of 1,10-phenanthroline and its metal chelates. *Met. Based Drugs* 7, 185–193. doi: 10.1155/MBD.2000.185

McCann, M., Santos, A. L. S., Silva, B. A., Romanos, M. T. V., Pyrrho, A. S., Devereux, M., et al. (2012). *In vitro* and *in vivo* studies into the biological

activities of 1,10-phenanthroline, 1,10-phenanthroline-5, 6-dione and its copper(II) and silver(I) complexes. *Toxicol. Res.* 1, 47–54. doi: 10.1039/c2tx00010e

McCarron, P., McCann, M., Devereux, M., Kavanagh, K., Skerry, C., Karakousis, P. C., et al. (2018). Unprecedented *in vitro* antitubercular activitiy of manganese(II) complexes containing 1,10-phenanthroline and dicarboxylate ligands: increased activity, superior selectivity, and lower toxicity in comparison to their copper(II) analogs. *Front. Microbiol.* 9:1432. doi: 10.3389/fmicb.2018.01432

Mello, T. P., Aor, A. C., Gonçalves, D. S., Seabra, S. H., Branquinha, M. H., and Santos, A. L. S. (2016). Assessment of biofilm formation by *Scedosporium apiospermum*, *S. aurantiacum*, *S. minutisporum* and *Lomentospora prolificans*. *Biofouling* 32, 737–749. doi: 10.1080/08927014.2016.1192610

Mjos, K. D., and Orvig, C. (2014). Metallodrugs in medicinal inorganic. *Chem. Rev.* 114, 4540–4563. doi: 10.1021/cr400460s

Mosmann, T. (1983). Rapid colorimetric assay for cellular growth and survival: application to proliferation and cytotoxicity assays. *J. Immunol. Methods* 65, 55–63. doi: 10.1016/0022-1759(83)90303-4

Mowat, E., Butcher, J., Lang, S., Williams, C., and Ramage, G. (2007). Development of a simple model for studying the effects of antifungal agents on multicellular communities of *Aspergillus fumigatus*. *J. Med. Microbiol.* 56, 1205–1212. doi: 10.1099/jmm.0.47247-0

Palmeira, V. F., Kneipp, L. F., Rozental, S., Alviano, C. S., and Santos, A. L. S. (2008). Beneficial effects of HIV peptidase inhibitors on *Fonsecaea pedrosoi*: promising compounds to arrest key fungal biological processes and virulence. *PLoS One* 3:e3382. doi: 10.1371/journal.pone.0003382

Pereira, T. C., Barros, P. P., Fugisaki, L. R. O., Rossoni, R. D., Ribeiro, F. C., Menezes, R. T., et al. (2018). Recent advances in the use of *Galleria mellonella* model to study immune responses against human pathogens. *J. Fungi* 4:128. doi: 10.3390/jof4040128

Qiu, Y., Zhang, J., Tang, Y., Zhong, X., and Deng, J. (2019). Case report: fever- pneumonia- lymphadenectasis- osteolytic- subcutaneous nodule: disseminated chromoblastomycosis caused by *Phialophora*. *J. Infect. Chemother.* 25, 1031–1036. doi: 10.1016/j.jiac.2019.05.002

Queiroz-Telles, F., de Hoog, S., Santos, D. W. C. L., Salgado, C. G., Vicente, V. A., Bonifaz, A., et al. (2017). Chromoblastomycosis. *Clin. Microbiol. Rev.* 30, 233–276. doi: 10.1128/CMR.00032-16

Ramage, G., Rajendran, R., Sherry, L., and Williams, C. (2012). Fungal biofilm resistance. *Int. J. Microbiol.* 2012:528521. doi: 10.1155/2012/528521

Romera, D., Aguilera-Correa, J. J., Gadea, I., Vinuela-Sandoval, L., Garcia-Rodriguez, J., and Esteban, J. (2019). *Candida auris*: a comparison between planktonic and biofilm susceptibility to antifungal drugs. *J. Med. Microbiol.* 68, 1353–1358. doi: 10.1099/jmm.0.001036

Rowan, R., Moran, C., McCann, M., and Kavanagh, K. (2009). Use of *Galleria mellonella* larvae to evaluate the *in vivo* anti-fungal activity of $[Ag_2(mal)(phen)_3]$. *Biometals* 22, 461–467. doi: 10.1007/s10534-008-9182-3

Santos, A. L. S., Galdino, A. C. M., Mello, T. P., Ramos, L. S., Branquinha, M. H., Bolognese, A. M., et al. (2018). What are the advantages of living in a community? A microbial biofilm perspective! *Mem. Inst. Oswaldo Cruz* 113:e180212. doi: 10.1590/0074-02760180212

Sardi, J. C. O., Pitangui, N. S., Voltan, A. R., Braz, J. D., Machado, M. P., Fusco-Almeida, A. M., et al. (2015). *In vitro Paracoccidioides brasiliensis* biofilm and gene expression of adhesins and hydrolytic enzymes. *Virulence* 6, 642–651. doi: 10.1080/21505594.2015.1031437

Silva, L. N., Campos-Silva, R., Ramos, L. S., Trentin, D. S., Macedo, A. J., Branquinha, M. H., et al. (2018). Virulence of *Candida haemulonii* complex in *Galleria mellonella* and efficacy of classical antifungal drugs: A comparative study with other clinically relevant non-albicans *Candida* species. *FEMS Yeast Res.* 18:foy082. doi: 10.1093/femsyr/foy082

Spitzer, M., Robbins, N., and Wright, G. D. (2017). Combinatorial strategies for combating invasive fungal infections. *Virulence* 8, 169–185. doi: 10.1080/21505594.2016.1196300

Thomaz, L., García-Rodas, R., Guimarães, A. J., Taborda, C. P., Zaragoza, O., and Nosanchuk, J. D. (2013). *Galleria mellonella* as a model host to study *Paracoccidioides lutzii* and *Histoplasma capsulatum*. *Virulence* 4, 139–146. doi: 10.4161/viru.23047

Tong, Z., Chen, S. C., Chen, L., Dong, B., Li, R., Hu, Z., et al. (2013). Generalized subcutaneous phaeohyphomycosis caused by *Phialophora verrucosa*: report of a case and review of literature. *Mycopathologia* 175, 301–306. doi: 10.1007/s11046-013-9626-3

Trevijano-Contador, N., Herrero-Fernández, I., García-Barbazán, I., Scorzoni, L., Rueda, C., Rossi, S. A., et al. (2015). *Cryptococcus neoformans* induces antimicrobial responses and behaves as a facultative intracellular pathogen in the non mammalian model *Galleria mellonella*. *Virulence* 6, 66–74. doi: 10.4161/21505594.2014.986412

Trevijano-Contador, N., and Zaragoza, O. (2019). Immune response of *Galleria mellonella* against human fungal pathogens. *J. Fungi* 5:3. doi: 10.3390/jof5010003

Treviño-Rangel, R. J., Villanueva-Lozano, H., Méndez-Galomo, K. S., Solís-Villegas, E. M., Becerril-García, M. A., Montoya, A. M., et al. (2019). *In vivo* evaluation of the antifungal activity of sertraline against *Aspergillus fumigatus*. *J. Antimicrob. Chemother.* 74, 663–666. doi: 10.1093/jac/dky455

Turiansky, G. W., Benson, P. M., Sperling, L. C., Sau, P., Salkin, I. F., McGinnis, M. R., et al. (1995). *Phialophora verrucosa*: a new cause of mycetoma. *J. Am. Acad. Dermatol.* 32, 311–315. doi: 10.1016/0190-9622(95)90393-3

Ventura, R. F., Galdino, A. C. M., Viganor, L., Schuenck, R. P., Devereux, M., McCann, M., et al. (2020). Antimicrobial action of 1,10-phenanthroline-based compounds on carbapenemase-producing *Acinetobacter baumannii* clinical strains: efficacy against planktonic- and biofilm-growing cells. *Braz. J. Microbiol.* 51, 1703–1710. doi: 10.1007/s42770-020-00351-9

Vicente, V. A., Weiss, V. A., Bombassaro, A., Moreno, L. F., Costa, F. F., Raittz, R. T., et al. (2017). Comparative genomics of sibling species of *Fonsecaea* associated with human chromoblastomycosis. *Front. Microbiol.* 8:1924. doi: 10.3389/fmicb.2017.01924

Viganor, L., Galdino, A. C. M., Nunes, A. P. F., Santos, K. R. N., Branquinha, M. H., Devereux, M., et al. (2016). Anti-*Pseudomonas aeruginosa* activity of 1,10-phenanthroline-based drugs against both planktonic- and biofilm-growing cells. *J. Antimicrob. Chemother.* 71, 128–134. doi: 10.1093/jac/dkv292

Viganor, L., Howe, O., McCarron, P., McCann, M., and Devereux, M. (2017). The antibacterial activity of metal complexes containing 1,10-phenanthroline: potential as alternative therapeutics in the era of antibiotic resistance. *Curr. Top. Med. Chem.* 17, 1280–1302. doi: 10.2174/1568026616666161003143333

Vila, T. V. M., and Rozental, S. (2016). "Biofilm Formation as a Pathogenicity Factor of Medically Important Fungi," in *Fungal Pathogenicity*. ed. S. Sultan (London: InTech), 978–953.

Wall, G., Montelongo-Jauregui, D., Bonifacio, B. V., Lopez-Ribot, J. L., and Uppuluri, P. (2019). *Candida albicans* biofilm growth and dispersal: contributions to pathogenesis. *Curr. Opin. Microbiol.* 52, 1–6. doi: 10.1016/j.mib.2019.04.001

Conflict of Interest: The authors declare that the research was conducted in the absence of any commercial or financial relationships that could be construed as a potential conflict of interest.

frontiers in Microbiology

ORIGINAL RESEARCH
published: 08 June 2021
doi: 10.3389/fmicb.2021.654855

Transcriptome Dynamics Underlying Chlamydospore Formation in *Trichoderma virens* GV29-8

Xinhong Peng†, Beilei Wu†, Shuaihu Zhang, Mei Li and Xiliang Jiang**

Institute of Plant Protection, Chinese Academy of Agricultural Sciences, Beijing, China

Trichoderma spp. are widely used biocontrol agents which are antagonistic to a variety of plant pathogens. Chlamydospores are a type of propagules produced by many fungi that have thick walls and are highly resistant to adverse environmental conditions. Chlamydospore preparations of *Trichoderma* spp. can withstand various storage conditions, have a longer shelf life than conidial preparations and have better application potential. However, large-scale production of chlamydospores has proven difficult. To understand the molecular mechanisms governing chlamydospore formation (CF) in *Trichoderma* fungi, we performed a comprehensive analysis of transcriptome dynamics during CF across 8 different developmental time points, which were divided into 4 stages according to PCA analysis: the mycelium growth stage (S1), early and middle stage of CF (S2), flourishing stage of CF (S3), and late stage of CF and mycelia initial autolysis (S4). 2864, 3206, and 3630 DEGs were screened from S2 vs S1, S3 vs S2, and S4 vs S3, respectively. We then identified the pathways and genes that play important roles in each stage of CF by GO, KEGG, STC and WGCNA analysis. The results showed that DEGs in the S2 vs S1 were mainly enriched in organonitrogen compound metabolism, those in S3 vs S2 were mainly involved in secondary metabolite, cell cycle, and N-glycan biosynthesis, and DEGs in S4 vs S3 were mainly involved in lipid, glycogen, and chitin metabolic processes. We speculated that mycelial assimilation and absorption of exogenous nitrogen in the early growth stage (S1), resulted in subsequent nitrogen deficiency (S2). At the same time, secondary metabolites and active oxygen free radicals released during mycelial growth produced an adverse growth environment. The resulting nitrogen-deficient and toxin enriched medium may stimulate cell differentiation by initiating cell cycle regulation to induce morphological transformation of mycelia into chlamydospores. High expression of genes relating to glycogen, lipid, mannan, and chitin synthetic metabolic pathways during the flourishing (S3) and late stages (S4) of CF may be conducive to energy storage and cell wall construction in chlamydospores. For further verifying the functions of the amino sugar and nucleotide sugar metabolism (tre00520) pathway in the CF of *T. virens* GV29-8 strain, the chitin synthase gene (TRIVIDRAFT_90152), one key gene of the pathway, was deleted and resulted in the dysplasia of mycelia and an incapability to form normal chlamydospores, which illustrated the pathway affecting the CF of *T. virens* GV29-8 strain. Our results provide a new perspective for understanding the genetics of biochemical pathways involved in CF of *Trichoderma* spp.

Keywords: *Trichoderma virens*, chlamydospores, transcriptome, GO enrichment, KEGG enrichment, STC analysis, WGCNA analysis

OPEN ACCESS

Edited by:
Lívia Kmetzsch, Federal University of Rio Grande do Sul, Brazil

Reviewed by:
Lisa Kappel, University of Applied Sciences Wien, Austria
Sergio Casas-Flores, Instituto Potosino de Investigación Científica y Tecnológica (IPICYT), Mexico

****Correspondence:***
Mei Li
limei@caas.cn
Xiliang Jiang
jiangxiliang@caas.cn

†These authors share first authorship

Specialty section:
This article was submitted to Microbial Physiology and Metabolism, a section of the journal Frontiers in Microbiology

Received: *17 January 2021*
Accepted: *03 May 2021*
Published: *08 June 2021*

Citation:
Peng X, Wu B, Zhang S, Li M and Jiang X (2021) Transcriptome Dynamics Underlying Chlamydospore Formation in Trichoderma virens GV29-8. Front. Microbiol. 12:654855. doi: 10.3389/fmicb.2021.654855

INTRODUCTION

Fungi in the genus *Trichoderma* are widely applied bio-control agents which are inhibitory to a variety of plant pathogens (Harman, 2006; Steindorff et al., 2014; Vos et al., 2015; Kim and Vujanovic, 2016; Deng et al., 2018). Currently, commercially available *Trichoderma* formulations primarily use conidiospore preparations, which can experience reductions in viability under nonoptimal storage conditions. Chlamydospores are a type of large, spherical, thick-walled spore produced by numerous fungi, including *Trichoderma* spp., under adverse environmental conditions (Hsu, 1973; Griffin, 1976; Ment et al., 2010; Agustí-Brisach and Armengol, 2012; Li et al., 2012; Navarathna et al., 2016; Sun et al., 2019; Yuan et al., 2019). Due to these properties, chlamydospore-based bio-control preparations could offer a longer shelf-life and higher bio-control capabilities against plant diseases than conidiospore-based preparations (Mishra et al., 2012; Zhang et al., 2017; Yuan et al., 2019). However, their application is limited by the difficulty of producing large numbers of chlamydospores. Research thus far has mainly focused on optimizing culture conditions to promote chlamydospore formation (CF) by *Trichoderma* (Zou et al., 2006; Mishra et al., 2012; Zhang et al., 2015; Li et al., 2016), but few molecular mechanisms underlying CF in *Trichoderma* have been explored (Yang et al., 2015; Yuan et al., 2019). Therefore, a comprehensive understanding of the molecular mechanisms regulating CF in *Trichoderma* could benefit the development of *Trichoderma* chlamydospore preparations.

CF involves multiple, complicated biological processes and pathways. High-resolution transcriptome sequencing technology has been utilized in single-celled eukaryotes, such as the yeast *Candida albicans*, providing insights into the molecular pathways and networks, along with their interactions, that are involved in various aspects of CF (Sonneborn et al., 1999; Alonso-Monge et al., 2003; Nobile et al., 2004; Eisman et al., 2006; Palige et al., 2013; Böttcher et al., 2016; Giosa et al., 2017). It was reported that the TOR, cAMP and MAPK signal pathways are very important for inducing CF in *C. albicans* (Alonso-Monge et al., 2003; Nobile et al., 2004; Staib and Morschhäuser, 2005; Böttcher et al., 2016). Other studies have shown that chitinase, chitin synthase, glucanase, and glycosyltransferase genes, as well as genes involved in amino sugar and nucleotide sugar metabolism, starch and sucrose metabolic pathways were speculated to be involved in CF in *T. harzianum* (Yang et al., 2015; Yuan et al., 2019). However, little other research has been performed to dissect the molecular mechanisms underlying CF in *Trichoderma* spp. To understand such mechanisms, we used RNA-seq to determine the transcriptomics of CF in *T. virens* GV29-8 at different developmental stages, hoping to reveal transcriptome-based dynamics of CF, and identify key determining factors of CF in *T. virens*. The transcript modules of co-expressed genes at different stages of CF and the series test of cluster (STC) analysis of differential time points during gene expression were performed to identify candidate genes and pathways that might determine CF. Furthermore, we created a knockout mutant of those genes to verify their functions in CF. This study provides insights into the molecular mechanisms underlying CF in *T. virens*.

MATERIALS AND METHODS

Strain Culture and Sampling

The *T. virens* strain GV29-8 was used (Baek and Kenerley, 1998; Kubicek et al., 2011; Morán-Diez et al., 2015). It was purchased from the fungal genetics stock center (FGSC 10586, United States) and stored as conidial suspensions in 20% glycerol at -80 ℃. The strain was inoculated onto a PDA plate, activated at 28°C for 3 days, then transferred to a fresh PDA plate and cultured at 28°C for 7 days. Conidia were harvested and adjusted to 1×10^7 conidia mL^{-1} with sterile distilled water, 3 mL of which was added into 120 mL of chlamydospore inducing medium (glucose 1%, cornmeal 1%, yeast extract powder 0.5%, corn steep powder 1% and inductive agent 5%) in 500 mL Erlenmeyer flasks, and incubated at 28℃ on a rotary shaker (180 rpm) in the dark for 3 days. Glucose was obtained from Beijing Chemical Works, yeast extract powder from Thermo Fisher Oxoid, cornmeal from Xinghua Yufeng Food Co., Ltd., and corn steep powder was supplied by Shandong Weiduofeng Biotechnology Co. Ltd. Inductive agent was explored by our lab.

Chlamydospore formation was observed using a microscope (Olympus BX53, Tokyo, Japan) every one to two hours, over the course of 3 days. Eight sampling time points were selected; samples were collected with 3 biological replicates at 20, 24, 26, 28, 32, 38, 45, and 56 h, represented by the labels TVS1, TVS2, TVS3, TVS4, TVS5, TVS6, TVS7, and TVS8, respectively. Samples were harvested by filtration and washed 3 times with sterile water. Residual water was removed using sterile filter paper. Samples were frozen in liquid nitrogen and used for transcriptome sequencing.

Construction of cDNA Libraries and Transcriptome Sequencing

We commissioned Nuohe Zhiyuan Technology Co., Ltd., to conduct transcriptome sequencing using the Illumina NovaSeq 6000 platform. Total RNAs from each sample were extracted with Trizol reagent, using the manufacturer's protocol. RNA concentration and quality were assessed using agarose gel electrophoresis, Nanodrop, Qubit 2.0 and the Agilent 2100 Bioanalyzer. After total RNA was extracted and quality tested, RNA-seq libraries were constructed using the NEBNext UltraTM RNA Library Prep Kit for Illumina (NEB). Briefly, after mRNA fragmentation, random primers were used for first-strand cDNA synthesis through M-MuLV reverse transcriptase system, before synthesis of second-strand cDNA, to obtain double-stranded cDNA. End-repair and addition of adenines to the 3′terminus of the double-stranded cDNA was performed, followed by ligation of sequencing adapters. Ligated products were purified and subjected to PCR amplification; PCR products were again purified with AMPure XP beads, to produce the final library preparation. The Agilent Bioanalyzer 2100 system was used

for quality control of the libraries prior to loading on the machine for sequencing.

Gene Annotation and Quantitative Analysis of Expression Levels

Clean reads were obtained by removing adapter sequences and filtering out low quality and poly-N containing reads (Chao et al., 2019). Next, clean reads were mapped onto the *T. virens* GV29-8 genome[1]. Gene expression levels were expressed as fragments per kilobase of transcript per million fragments mapped (FPKM), i.e., the number of matches for every kilobase of transcript per million fragments. Correlation among biological replicates was determined via the Pearson correlation coefficient, PCA, and phylogenetic analysis, which were performed using the R software package.

Analysis of Differentially Expressed Genes

Differentially expressed genes (DEGs) between samples were identified using Deseq2 software, in which the fold-change was the ratio of the expression levels between two samples: i.e., $\log_2{}^{(FC)}$ was $\log_2{}^{(fold-change)} = \log_2{}^{(SampleA/SampleB)}$. Here, we set the p-value < 0.05 and $|\log_2{}^{(FC)}| > 0$ as significant differences.

GO Functional Classification and KEGG Pathway Enrichment Analysis of DEGs During CF in *T. virens* GV29-8

Gene ontology (GO) and Kyoto encyclopedia of genes and genomes (KEGG) pathway enrichment analyses for DEGs were performed using the Clusterprofiler software. The GO terms exhibiting a corrected (after adjusting with false discovery rate) p-value < 0.05 were considered significantly enriched. We used *T. reesei* as a reference for the KEGG pathway significant enrichment analysis with a p-value<0.05, because there was no information of *T. virens* in the KEGG database.

STC and WGCNA Analysis During CF in *T. virens* GV29-8

Series test of cluster analysis was conducted based on Pearson correlations of gene expression profiles. To find trends in characteristics of gene expression and consolidate genes with the same characteristics into one trend, to produce the most representative gene group involved in CF. STC was implemented entirely in Java. Portions of the STC interface were implemented using the third-party library, the Java Piccolo toolkit from the University of Maryland (Bederson et al., 2004). STC also makes use of external Gene Ontology and gene annotation files. We specified a tab delimited gene expression data file as input to STC. Following the input phase, the STC clustering algorithm is executed and a new window will appear displaying the clustering results.

The weighted correlation network (WGCNA) analysis package in R (version 3.5.0) was used to construct a co-expression network for the filtered genes. After sample clustering, scale independence and mean connectivity analysis of modules with different power values was performed to determine the soft threshold of module analysis. The power value was set from 1 to 30, and values of scale independence and mean connectivity were generated according to these power values. The power value was determined when the scale independence value was 0.8. A hierarchical clustering dendrogram of the TOM matrix was constructed by the average distance with a minimum size threshold of 30 and the merge cut height of 0.25 to classify similar genes expression profiles into different gene modules. A cluster dendrogram among modules and an eigengene adjacency heatmap between modules were generated. Co-expression networks were visualized using the igraph package in R, which was also used to determine the betweenness of modules. Module-trait relationships were calculated according to the correlation between modules and traits, modules that were significantly correlated with individual traits ($P < 0.05$) were identified, and genes in significant modules were exported for further analysis.

Validation of Transcriptome Data Using Reverse Transcription Quantitative PCR (RT-qPCR)

cDNA was synthesized from 1 μg of total RNA extracted using Trizol reagent, and 2 ul of cDNA was subsequently used as template for RT-qPCR. Gene-specific primers were designed using Primer 5 (v3.0) software (**Supplementary Table 1**). The product annotations are listed in **Supplementary Table 1**. The RT-qPCR reaction was performed on a 7500 Real-Time PCR System (Applied Biosystems, United States) using TB Green® Premix ExTaq™ (TaKaRa, China) according to the manufacturer's instructions. The amplification conditions were 95°C for 30 s, followed by 40 cycles of 95°C for 5 s and 60°C for 34 s. Three biological replicates and at least 3 technical replicates were used for each sample. Normalization of transcript levels for each gene was done against transcript levels of the internal control gene glyceraldehyde-3-phosphate dehydrogenase (*GAPDH*), and fold changes were calculated using the $2^{-\Delta\Delta Ct}$ method (Livak and Schmittgen, 2001). RT-qPCR results were compared with the RNA-Seq data to detect the correlation of each gene expression.

Analysis of Glycogen, Lipid, and Chitin Contents During CF in *T. virens* GV 29-8

Samples were collected across 8 time points (TVS1, TVS2, TVS3, TVS4, TVS5, TVS6, TVS7, and TVS8), using 3 biological replicates per sample. Samples were observed using a microscope (Olympus BX53, Tokyo, Japan) with bright-field optics, or appropriate filter sets for fluorescent visualization. A solution containing 60 mg mL^{-1} KI and 10 mg mL^{-1} I_2 in distilled water was used for glycogen detection and observed in the bright-field optics (Seong et al., 2008). Nile Red solution (Sigma, N-3013) (0.01 mg mL^{-1} in acetone) was used for lipid detection (Son et al., 2012). A filter (excitation 543; emission 598) was applied for visualization of lipids. Chitin staining was performed

[1]https://www.ncbi.nlm.nih.gov/genome/?term=GCA_000170995.2

by adding 2 μL of calcofluor white stock solution (10 mg mL^{-1}, Sigma, 18909) to 20 μL of mycelia and chlamydospore samples placed on glass slides. which were then incubated for 15 min at 4°C, after which mycelia and chlamydospores were observed using a filter (excitation 355, emission 445) (Yu et al., 2008).

Effect of Chitin Synthase Gene (TRIVIDRAFT_90152) Knockout on CF in *T. virens* GV29-8

To verify the contribution of the chitin synthase gene (*Chs*) (TRIVIDRAFT_90152) to CF in *T. virens* GV29-8, the *Chs* deletion mutant strain, *Chs*Δ, was generated using the split-PCR strategy (Catlett et al., 2003). The primers used are listed in **Supplementary Table 26**. The hygromycin resistance gene (*hyg*), which was amplified from the plasmid pKH-KO, conferred hygromycin resistance on the fungus. The protoplast transformation was used to generate the *Chs*Δ by transforming two fragments containing homologous region sequences of the *Chs* gene and partial hygromycin gene fragment into the protoplasts of wild-type *T. virens* GV29-8 (Aragona and Valente, 2015; Li et al., 2017). The genotypes of *Chs*Δ mutants were confirmed by amplifying internal fragment of *Chs* (no PCR product generated), and the *hyg* fragment (PCR product was 719 bp in size). Southern hybridization was performed using a DIG High prime DNA labeling and detection starter kit II (Roche, Germany) according to the manufacturer's protocol. The *Chs* (407bp) gene fragment was amplified as the probe. The primers of the probe are listed in **Supplementary Table 26**. DNAs of wild-type *T. virens* GV29-8 and *Chs*Δ mutant strains were digested by BamHI/NotI.

The wild-type *T. virens* GV29-8 and mutant *Chs*Δ strain were each inoculated onto the center of PDA plates and cultured for 7 days at 28℃. Conidia of wild-type *T. virens* GV29-8 and *Chs*Δ strain were harvested and adjusted to 1×10^6 conidia mL^{-1} with sterile distilled water, 3 mL of which was added into 120 mL of chlamydospore inducing medium and incubated at 28°C on a rotary shaker (180 rpm), and chlamydospore formation of each culture was observed by microscopy 4 days after inoculation. To determine the chitin content of chlamydospores and mycelia in wild-type *T. virens* GV29-8 and *Chs*Δ strain, calcofluor white staining was performed as previously described (Yu et al., 2008). Oil red O staining solution was used to determine lipid content (Shin et al., 2011).

Statistical Analysis

Individual means and standard deviation of the mean were calculated using the data from independent samples in Microsoft Excel 2007 (Microsoft, United States). IBM SPSS statistics software (SPSS 17.0, United States) was used for correlation coefficient analysis. The correlation coefficient (r) between RNA-Seq and RT-qPCR was calculated using a two-tailed p-value with a confidence interval of 95%.

RESULTS

Global Transcriptome Analysis of CF in *T. virens* GV29-8

Eight morphologically significant time point samples (TVS1, TVS2, TVS3, TVS4, TVS5, TVS6, TVS7, and TVS8) that represented significant events during CF were selected for transcriptome sequencing (**Figure 1**). The TVS1, TVS2 and TVS3 time point samples were collected during the mycelium growth stage. TVS4 and TVS5 samples were collected during the early stage of CF; chlamydospores were initially observed in TVS4 and became more obvious in TVS5. TVS6 and TVS7 samples were collected during the middle and flourishing stages of CF, respectively. About half of the mycelium tips produced chlamydospores in TVS6. All mycelium tips and parts of the mycelium interior produced chlamydospores in TVS7. Mycelia autolysis occurred during TVS8, at which point the mycelia had become vacuolated (**Figure 1h**).

We performed RNA-seq experiments using total RNA extracted from samples across the 8 selected time points. More than 688 million high quality reads (average 28 million reads from each sample) and 206.08 G of clean bases (average 8.59 G of data for each sample) were generated from different samples. Mapping to the *T. virens* GV29-8 genome (GenBank assembly accession: *GCA_000170995.2*), the alignment rate (total map) reached 79.34% ∼ 85.96%, among which sequences with unique alignment positions along the reference sequence reached over 79.07% (**Table 1**).

A total of 19,737 genes were obtained from RNA-seq experiments of 24 samples. Among them, 7332 were novel genes predicted by stringtie software (Pertea et al., 2015). About 63.61% (12555/19737) of these genes were found to be expressed in at least one of the 24 samples (**Supplementary Table 2**). The number of expressed genes in different samples varied from 57.21% to 58.81%. About 0.56% - 0.88% of genes exhibited very high expression levels (FPKM > 1000) in different samples. The number of genes showing high (500 < FPKM ≤ 1000), moderate (10 < FPKM ≤ 500), low (0 < FPKM ≤ 10) and no (FPKM = 0) expression was similar in all samples (**Supplementary Table 3**). These analyses demonstrated sufficient coverage of the transcriptome during CF in *T. virens* GV29-8.

Global Comparison of Transcriptomes Revealed Relationships Between Samples During CF

We performed correlation coefficient and principal component analyses (PCA) based on Pearson correlation coefficient analysis of average FPKM values for all expressed genes in all samples (**Figures 2A,B**). According to correlation coefficient analysis, we used the longest distance method to construct the phylogenetic tree for the samples (**Figure 2C**; Murtagh and Legendre, 2014). The Pearson correlation coefficients between biological replicates varied from 0.93 to 0.98, demonstrating the high quality of the replicates (**Figure 2A**). PCA analysis showed that the 8 sampling time points could be clearly assigned into 4 stages,

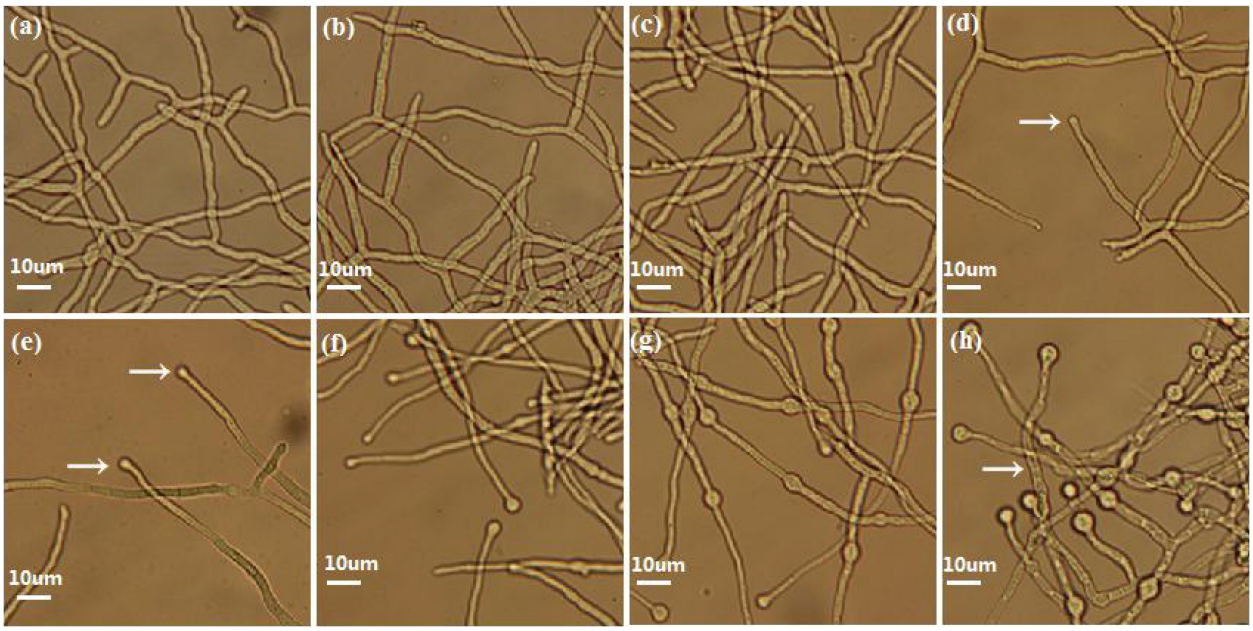

FIGURE 1 | Phenotype of CF at different stages in *Trichoderma virens* GV29-8. No chlamydospores were produced in TVS1 (20 h), TVS2 (24 h) and TVS3 (26 h) as shown in pictures **(a)**, **(b)**, and **(c)**, respectively. **(d)** Chlamydospores production in mycelium tips began at TVS4 (28 h) (arrow). **(e)** Chlamydospores began to appear on the tips of a small number of mycelia in TVS5 (32 h) (arrow). **(f)** About half of the mycelium tips produced chlamydospores in TVS6 (38 h). **(g)** Almost all mycelium tips produced chlamydospores and a lot of internal chlamydospore production was also observed in TVS7 (45 h). **(h)** Mycelia began autolysis in TVS8 (56 h) (arrow). Scale bars = 10 μm.

TABLE 1 | Statistical analysis of sequencing results.

Sample	Raw reads	clean reads	Clean bases	Q20(%)	Q30(%)	total_reads	total_map (%)	unique_map (%)
TVS1_1	29417905	28921539	8.68G	97.73	93.68	57843078	49722058(85.96%)	49494155(85.57%)
TVS1_2	24816348	24317521	7.3G	97.03	92.2	48635042	41416437(85.16%)	41214532(84.74%)
TVS1_3	28808008	28215691	8.46G	97.13	92.41	56431382	47589649(84.33%)	47343663(83.9%)
TVS2_1	32787554	32288499	9.69G	97.17	92.48	64576998	54731573(84.75%)	54530206(84.44%)
TVS2_2	35585217	35013599	10.5G	97.19	92.56	70027198	58382659(83.37%)	58153313(83.04%)
TVS2_3	23229622	22870748	6.86G	96.7	91.45	45741496	38116549(83.33%)	37960918(82.99%)
TVS3_1	29495711	28581672	8.57G	97.3	92.83	57163344	46864148(81.98%)	46647373(81.6%)
TVS3_2	34168038	33519114	10.06G	97.24	92.65	67038228	55014001(82.06%)	54761803(81.69%)
TVS3_3	29082289	28641615	8.59G	97.74	93.72	57283230	47892671(83.61%)	47640072(83.17%)
TVS4_1	33371573	32170556	9.65G	96.91	91.99	64341112	52134998(81.03%)	51872009(80.62%)
TVS4_2	35623406	35011956	10.5G	97.12	92.4	70023912	57308188(81.84%)	57037980(81.46%)
TVS4_3	29058932	28280180	8.48G	96.72	91.53	56560360	46165285(81.62%)	45954745(81.25%)
TVS5_1	29231630	28686006	8.61G	97.54	93.29	57372012	46176229(80.49%)	45993516(80.17%)
TVS5_2	25794278	25394091	7.62G	97.01	92.14	50788182	40679800(80.1%)	40541740(79.83%)
TVS5_3	32493581	31550095	9.47G	97.13	92.46	63100190	50060893(79.34%)	49890603(79.07%)
TVS6_1	29930540	29346925	8.8G	97.21	92.58	58693850	47151572(80.33%)	46997999(80.07%)
TVS6_2	24223306	23792470	7.14G	97.15	92.43	47584940	38399674(80.7%)	38272844(80.43%)
TVS6_3	26809341	26292374	7.89G	97.19	92.5	52584748	43263917(82.27%)	43120911(82.0%)
TVS7_1	25685031	24880361	7.46G	96.6	91.5	49760722	40204719(80.8%)	40038671(80.46%)
TVS7_2	28874746	28232481	8.47G	96.29	90.95	56464962	45889190(81.27%)	45689173(80.92%)
TVS7_3	23380694	22383763	6.72G	97.2	92.65	44767526	36817462(82.24%)	36670967(81.91%)
TVS8_1	27453135	26750600	8.03G	96.2	90.85	53501200	43833110(81.93%)	43613489(81.52%)
TVS8_2	34022559	33069479	9.92G	96.88	92.18	66138958	54932687(83.06%)	54679524(82.67%)
TVS8_3	30945699	28689151	8.61G	96.86	92.1	57378302	47310837(82.45%)	47174743(82.22%)

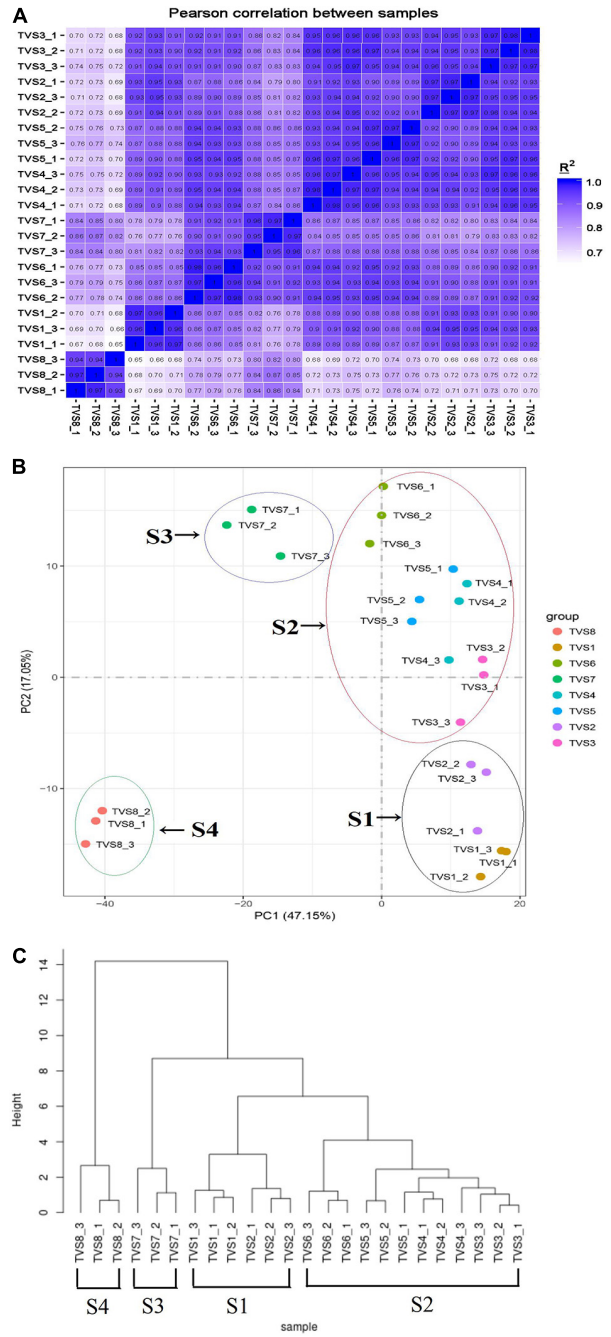

FIGURE 2 | Correlation between the transcriptomes of different samples during CF of *T. virens* GV29-8. **(A)** Pearson correlation coefficient analysis of RNA-seq data from 8 sampling time points of *T. virens* GV29-8. **(B)** Principal component analysis (PCA) plot showing clustering of transcriptomes of different *T. virens* GV29-8 samples. The samples in black, red, purple and green circles represent S1, S2, S3, and S4 samples, respectively. **(C)** Phylogenetic analysis of sample correlation coefficients.

referred to as S1, S2, S3 and S4 (**Figure 2B**). TVS1 and TVS2, shown by microscopic observation to be in the mycelial growth stage, were grouped into S1. TVS3, TVS4, TVS5 and TVS6 were assigned to group S2. TVS3 represented the transition stage from mycelium to chlamydospore, although microscopic observation showed TVS3 to be in the mycelial growth stage and TVS4 was the first time point at which CF could be observed. PCA results indicated that TVS3 was closer to TVS4. Generally speaking, while gene expression takes precedence over phenotype, it is possible that the genes related to CF were already being expressed in TVS3. About half of the mycelium tips had produced chlamydospores in TVS6. Therefore, samples of TVS3-TVS6 were divided into S2, and represented as the early and middle stages of CF. Samples at TVS7 and TVS8 were separated from each other and other time points. All mycelium tips and parts of the mycelium interior produced chlamydospores in TVS7. Mycelia autolysis was observed during TVS8. Therefore, TVS7 and TVS8 were classified into S3 and S4, respectively. S3 represents the flourishing stage, and S4 was the late stage of CF and initial mycelia autolysis. The results of phylogenetic analysis of sample correlation coefficients were consistent with those of the PCA analysis. This indicated that expression patterns in the mycelium growth stage (S1), early and middle stage of CF (S2), flourishing stage of CF (S3) and late stage of CF and mycelia initial autolysis (S4) were strikingly different from one another.

Differential Gene Expression During CF

According to PCA analysis, we divided the 8 sampling time points into 4 groups. A total of 6462 DEGs were obtained by comparison with adjacent stages (**Supplementary Table 4**). There were 2864, 3206 and 3630 DEGs screened from S2 vs S1, S3 vs S2 and S4 vs S3, respectively (**Figure 3A**). The largest number of up-regulated (1961) and down-regulated (1669) DEGs were contained in S4 vs S3 (**Figures 3B,C**). Reference genome annotation indicated that S2 vs S1, S3 vs S2, and S4 vs S3 contained 1689, 1761, and 2166 hypothetical protein genes and 500, 645, and 573 novel genes lacking annotation information, respectively. In order to better understand the function of these genes, NR, NT, Ko, Swiss, Pfam, GO and KOG database annotations were added in this study (**Supplementary Table 4**). Gene annotations showed that DEGs in S2 vs S1 were mainly related to metabolic and oxidation-reduction processes. In S3 vs S2, DEGs associated with oxidation-reduction, transcription, and transport processes dominated. In S4 vs S3, DEGs related to oxidation-reduction, transcription, and transport process were still activity (**Supplementary Table 4**).

Differentially expressed genes analysis for the 8 sampling time points was also performed by comparing adjacent time points (**Figures 3D,E** and **Supplementary Table 5**). 1588, 980, 648, 822, 1474, 1838 and 3630 DEGs were included in TVS2 vs TVS1, TVS3 vs TVS2, TVS4 vs TVS3, TVS5 vs TVS4, TVS6 vs TVS5, TVS7 vs TVS6 and TVS8 vs TVS7, respectively. There were 14 DEGs shared by the 7 comparisons. The greatest number of stage-specific DEGs were found in the TVS8 vs TVS7 (1615) comparison, while only 33 DEGs were unique to that of TVS4 vs TVS3 (**Figure 3D** and **Supplementary Table 5**). The largest number of up-regulated (1961) and down-regulated (1669) DEGs were identified in TVS8 vs TVS7 (**Figure 3E** and **Supplementary Table 5**).

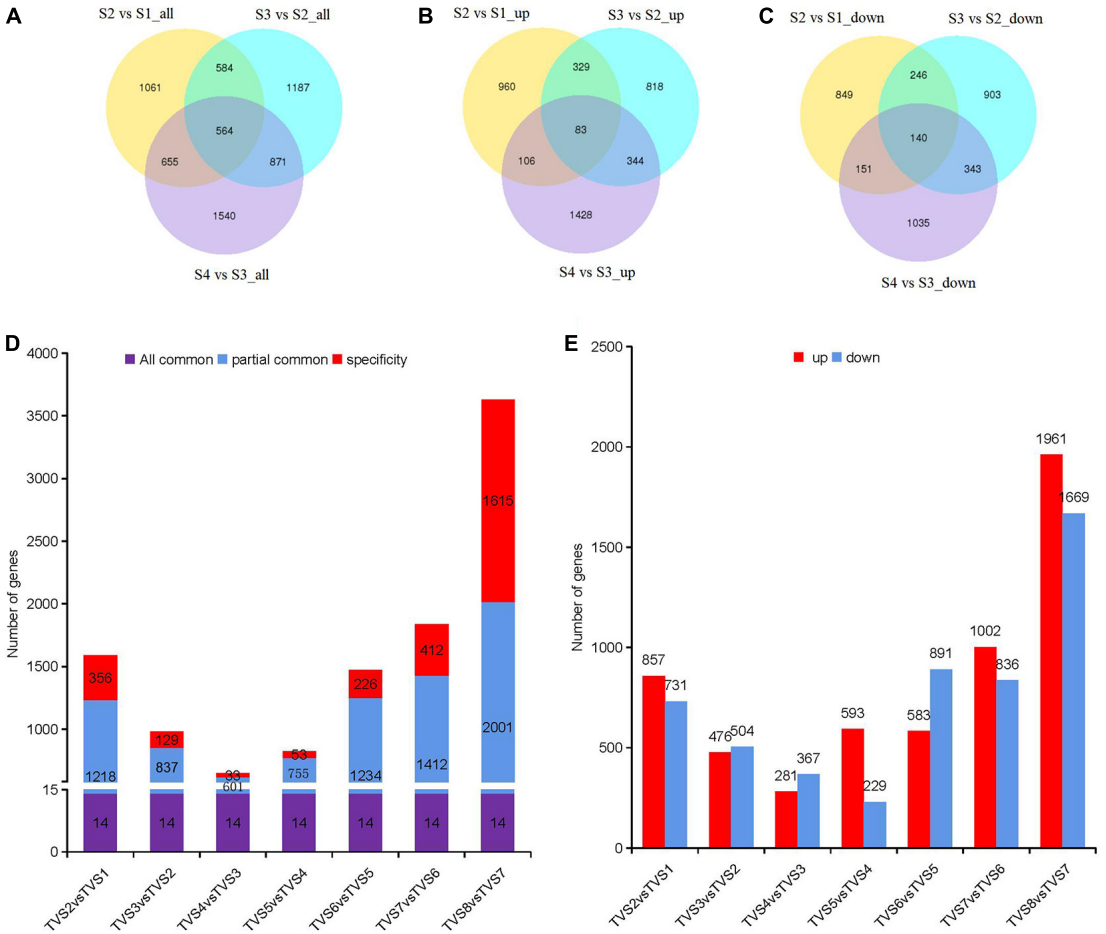

FIGURE 3 | DEGs analysis among samples of adjacent stages and time points. Diagrams comparing shared and specific DEGs between adjacent developmental stages and sampling time points of CF. Venn diagrams of S2 vs S1, S3 vs S2 and S4 vs S3. **(A)** All DEGs. **(B)** Up-regulated DEGs. **(C)** Down-regulated DEGs. The non-overlapping regions represent DEGs unique to each comparison; Overlapping regions represent DEGs shared by two or more combinations. The number in the circle represents the number of DEGs. **(D)** Diagrams comparing shared and specific DEGs among samples of adjacent time points. The number of DEGs are indicated in the center of histograms. "All common" represents the DEGs that were shared by all comparisons. "Partially common" refers to DEGs that were shared by two or more comparisons. "Specific" refers to DEGs that were unique to a specific comparison. **(E)** Up-regulated and down-regulated DEG distribution between adjacent time points. The number of DEGs are indicated above the histograms.

Functional Classification of DEGs

All DEGs were classified into biological process (BP), cellular component (CC) and molecular function (MF) categories by comparison between samples from 4 adjacent stages (**Supplementary Figure 1** and **Supplementary Table 6**). In S2 vs S1, organonitrogen compound metabolic (GO:1901564) was the most significantly enriched GO term in BP. 144 DEGs were down-regulated, while only 12 DEGs belonging to this term were up-regulated (**Supplementary Table 7**). Among them, 96 down-regulated DEGs were linked to organonitrogen compound biosynthetic processes, half of which were ribosomal proteins (e.g., ribosomal protein S2, TRIVIDRAFT_74494). Other down-regulated DEGs mainly corresponded with amino acid metabolism (e.g., aspartate-tRNA ligase, TRIVIDRAFT_79308; glutamine synthetase, TRIVIDRAFT_77167). Combined with microscopic observation of S1 and S2 (**Figure 1**), we speculated that organonitrogen compound metabolism might participate in induction of CF. It was reported that the oligopeptide transporter gene, *PTR2*, was significantly up-regulated under chlamydospore-inducing conditions in *C. albicans* (Palige et al., 2013). In this study, two *PTR2* genes (TRIVIDRAFT_50243 and TRIVIDRAFT_79497) were also differentially expressed during CF (**Supplementary Table 2**). In S3 vs S2, tetrapyrrole binding (GO:0046906) and heme binding (GO:0020037) were the most significantly enriched GO terms in MF. A total of 52 DEGs were recognized in these two GO terms. Among them, 16 and 36 DEGs were up-regulated and down-regulated, respectively. Most of the DEGs were cytochrome P450 family and antioxidants genes. For the up-regulated DEGs, 9 of them were P450 family genes. Some of these were homologous to genes involved in the synthesis of toxic secondary metabolites produced during fungal growth (e.g., O-methylsterigmatocystin oxidoreductase, TRIVIDRAFT_90820; versicolorin B desaturase, TRIVIDRAFT_212112), others were linked to the functions

of detoxification and antioxidant activities (e.g., benzoate 4-monooxygenase, TRIVIDRAFT_47284; protein lutein deficient 5, TRIVIDRAFT_160585). Except for cytochrome P450 genes, the other up-regulated DGEs were mostly associated with antioxidant activity associated with ROS elimination (e.g., catalase, TRIVIDRAFT_38844/TRIVIDRAFT_45138). *Nox1* is a NADPH oxidase (Noxs) gene that produces ROS, regulates cell differentiation, and affects asexual spore formation in *T. atroviride* (Hernández-Oñate et al., 2012). In this study, *Nox1* (TRIVIDRAFT_32702) was differentially expressed during

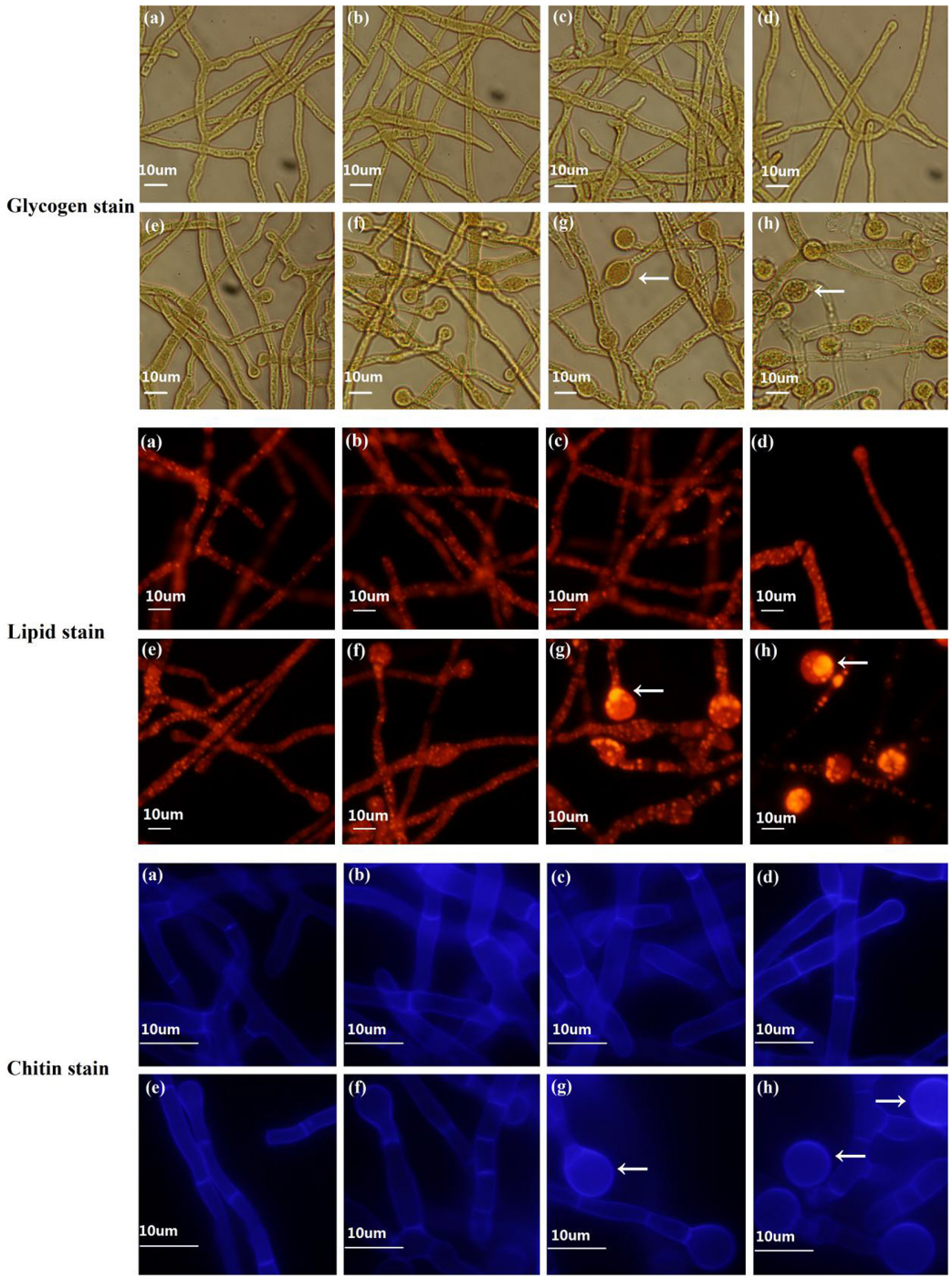

FIGURE 4 | Fluorescence staining to determine dynamic changes in chlamydospore components in *T. virens* GV29-8. Glycogen, lipid, and chitin components were stained with KI and I_2, nile red and calcofluor white, respectively. **(a–h)** represent the samples of TVS1, TVS2, TVS3, TVS4, TVS5, TVS6, TVS7, and TVS8 of *T. virens* GV29-8, respectively. Scale bar = 10 μm.

CF (**Supplementary Table 2**). For the down-regulated DEGs, 29 were P450 family genes, most of which were involved in the synthesis of toxic secondary metabolites (e.g., trichodiene oxygenase, TRIVIDRAFT_74291; abscisic acid 8′-hydroxylase, TRIVIDRAFT_216144/TRIVIDRAFT_230790; beta-amyrin 11-oxidase, TRIVIDRAFT_53690/TRIVIDRAFT_53375/TRIVIDRAFT_151337). Considering in S3 vs S2, DEGs were significantly enriched in secondary metabolic processes such as tetrapyrrole binding and heme binding, we speculated that secondary metabolic processes might further promote CF. During later stages (S4 vs S3), all significantly enriched GO terms were assigned into the BP category. Lipid metabolic process (GO:0006629) was the most significantly enriched GO term, in which 54 DEGs were enriched. These DEGs were mainly involved in phospholipid (e.g., ethanolaminephosphotransferase, novel.10349), glycerolipid (e.g., patatin-like phospholipase, TRIVIDRAFT_74421) and fatty acid (e.g., Sphingolipid C4-hydroxylase sur2, TRIVIDRAFT_43350) metabolic processes. It has been reported that mature chlamydospores contain a large number of fat droplets in *C. albicans* (Miller et al., 1974). In this study, Nile red staining showed that a large number of lipid droplets were formed during the late stages of CF (S3 and S4) (**Figure 4**), and genes related to fatty acid metabolism were indeed differentially expressed (**Supplementary Table 23**), including genes encoding acetyl-CoA C-acetyltransferase (TRIVIDRAFT_169943), enoyl-CoA hydratase (TRIVIDRAFT_87842), acetyl-CoA carboxylase (TRIVIDRAFT_78374), fatty acid synthase subunit beta, fungi type (TRIVIDRAFT_171412), fatty acid elongase 3 (TRIVIDRAFT_82162) and acetyl-CoA acyltransferase 1 (TRIVIDRAFT_80821). Genes related to lipid metabolism were differentially expressed in S4 and S3, suggesting that they might be associated with the CF.

Gene ontology analysis was also performed for the DEGs obtained from the comparisons between the 8 adjacent sampling time points (**Supplementary Figure 2** and **Supplementary Tables 8, 9**). In TVS2 vs TVS1, the most significantly enriched GO term was protein metabolic process (GO:0019538) in BP. Small molecule metabolic process (GO:0044281) and organic acid metabolic process (GO:0006082) were the most significantly enriched GO terms in BP of TVS4 vs TVS3, and TVS6 vs TVS5, respectively. The most significantly enriched GO term in BP in TVS8 vs TVS7 was lipid metabolic process (GO:0006629). For the CC category, significantly enriched terms were similar in TVS3 vs TVS2, TVS4 vs TVS3, TVS5 vs TVS4 and TVS7 vs TVS6, comprised mainly of the integral component of membrane (GO:0016021) and intrinsic component of membrane (GO:0031224) categories. The MF category differed greatly across time point comparisons. The number of GO terms in the MF category was highest in TVS5 vs TVS4. Among these, purine ribonucleoside triphosphate binding (GO:0035639) was the most significantly represented GO term. Oxidoreductase activity, acting on CH-OH group of donors (GO:0016614) was significantly enriched in TVS7 vs TVS6.

The DEGs obtained by comparison across the 4 adjacent sampling stages were mapped to the KEGG database and tested for enrichment to further explore their functions (**Supplementary Figure 3** and **Supplementary Table 10**). The ribosome (tre03010) pathway category was the most significantly enriched pathway in S2 vs S1. The DEGs in the ribosomal pathway were all ribosomal protein genes (e.g., ribosomal protein S2, TRIVIDRAFT_74494) and down regulated at S2. The metabolic pathway (tre01100) category was the most significantly enriched pathway in S3 vs S2 and S4 vs S3. The oxidative phosphorylation pathway (tre00190) always runs throughout the entire CF process, and all DEGs in this pathway were down-regulated. Additionally, the protein processing in endoplasmic reticulum (tre04141), tryptophan metabolism (tre00380) and N-glycan biosynthesis (tre00510) categories were also significantly enriched in S3 vs S2. There were 14 DEGs included in the N-glycan biosynthesis pathway. Among them, 10 were up-regulated and involved in mannan synthesis, including dolichyldiphosphatase (TRIVIDRAFT_25816), oligosaccharyltransferase complex subunit (TRIVIDRAFT_111960 and TRIVIDRAFT_121404), and dolichol-phosphate mannosyltransferase (TRIVIDRAFT_84289). 3 down-regulated DEGs (e.g., mannosyl-oligosaccharide alpha-1,2-mannosidase, TRIVIDRAFT_193426/TRIVIDRAFT_54636/TRIVIDRAFT_86342) were involved in mannose degradation (**Supplementary Tables 11, 22**). Mannan is a common fungal cell wall component (Henry et al., 2016). Since DEGs related to the N-glycan biosynthesis pathway were significantly differentially expressed in S3 vs S2, we speculated that N-glycan biosynthesis might be involved in cell wall biosynthesis in chlamydospores.

KEGG enrichment analysis was also performed on DEGs obtained by comparison of across the 8 adjacent time points (**Supplementary Figure 4** and **Supplementary Table 12**). The ribosome (tre03010) pathway was the most significantly enriched in TVS2 vs TVS1. The metabolic pathway (tre01100), with a *p*-value of nearly 0, was significantly enriched in TVS3 vs TVS2, TVS4 vs TVS3, TVS7 vs TVS6 and TVS8 vs TVS7. Glyoxylate and dicarboxylate metabolism (tre00630) was the next most enriched pathway in TVS3 vs TVS2. N-Glycan biosynthesis (tre00510) and various types of N-glycan biosynthesis (tre00513) were included in TVS7 vs TVS6. In TVS8 vs TVS7, the pentose phosphate pathway (tre00030), oxidative phosphorylation (tre00190) and ribosome biogenesis in eukaryotes (tre03008) categories were significantly enriched. The most abundant pathway for the TVS5 vs TVS4 and TVS6 vs TVS5 was cell cycle-yeast (tre04111). A total of 16 DEGs were contained in the cell cycle-yeast pathway, including genes encoding DNA replication licensing factor (TRIVIDRAFT_79120), structural maintenance of chromosome protein (TRIVIDRAFT_90905), and *CDC4* (TRIVIDRAFT_56502) (**Supplementary Tables 13, 21**). It was reported that *CDC10* or *CDC11* gene mutations lead to morphological defects of chlamydospores in *C. albicans* (Martin et al., 2005). In this study, CDC family genes (e.g., *CDC10,* TRIVIDRAFT_87191; CDC42; CDC48, TRIVIDRAFT_216898/TRIVIDRAFT_76254/TRIVIDRAFT_211309/TRIVIDRAFT_184509) were also differentially expressed during different CF stages. We deduced that the cell cycle pathway may be involved in regulating the mycelium to chlamydospore transformation. Fructose and mannose metabolism (tre00051) and the pentose

phosphate pathway (tre00030) were also significantly enriched in TVS5 vs TVS4. For TVS6 vs TVS5, the meiosis-yeast (tre04113), nucleotide excision repair (tre03420) and DNA replication (tre03030) categories were significantly enriched (**Supplementary Table 13**).

Clustering of Gene Expression Profiles Across the Eight Sampling Time Points

A total of 5699 DEGs were obtained from 7 comparisons according to a p-value < 0.05 and $|\log_2^{(FC)}| > 0$. Using STC analysis, 3581 DEGs were grouped into 50 clusters, which represent 62.8% of all DEGs (**Supplementary Figure 5**). Next, significance analysis of the DEG expression trends and fitting curves in the 50 clusters were performed. The results showed that DEG expression trends and fitting curves in 7 clusters (K1∼K7) were within the acceptable range ($p < 0.05$), while the remaining 43 clusters did not meet the significance standard (**Figure 5** and **Supplementary Table 14**). Expression patterns of DEGs in the K1 cluster decreased from TVS1 to TVS8. However, DEGs in the K2 cluster showed an opposite expression pattern to those in the K1 cluster. Other DEGs from the K3, K4, K5, K6, and K7 clusters were predominantly expressed at one or more of the 8 time points.

To better understand the functions of identified DEGs in different clusters, GO analysis was performed for each of the clusters (**Figure 6** and **Supplementary Table 15**). The most enriched GO terms were found in the K1 cluster, which is consistent with this cluster having the most DEGs. Predominantly expressed DEGs in the K1 and K7 clusters had similar functional classifications, including organonitrogen compound biosynthetic process (GO:1901566), peptide biosynthetic process (GO:0043043), and the amide biosynthetic process (GO:0043604) categories. Furthermore, transferase activity and oxidoreductase activity metabolic processes were also significantly enriched in the K1 cluster.

Construction of Gene Co-expression Networks

Weighted gene co-expression network analysis can comprehensively reveal the relationships between gene expression and phenotype in the successive developmental stages (Langfelder and Horvath, 2008). Co-expression networks were constructed based on the previously reported methods (Guo et al., 2016; Riquelme Medina and Lubovac-Pilav, 2016). Each tree branch constitutes a module, and each leaf in the branch represents one gene, as shown in the hierarchical clustering tree (**Figure 7A**). For further analysis, we divided the tree from the resulting dendrogram into isolate modules. Ultimately, 14 modules (colored pink, dark red, sky blue, gray 60, dark turquoise, green, saddle brown, magenta, orange, white, light cyan, black, purple, and gray) were identified during the different CF stages. Genes in grey could not be assigned to any module, and bore no relative significance (**Figure 7**, **Supplementary Tables 16, 17**). The Pearson correlation algorithm was used to calculate the correlation coefficients and p-values of module characteristic genes and traits (**Figure 7B**). Genes which showed the most connectedness with other genes were identified as hub genes, as indicated by their high ImConn value (Eigengene connectivity). Correlation networks of different modules were constructed (**Supplementary Figure 6**). Each node represents a gene and the connecting lines (edges) between genes represent co-expression correlations (Langfelder and Horvath, 2008). WGCNA analysis showed that the pink (124) module genes exhibited high positive correlations with S1 (**Figure 7B**). Genes encoding ribosomal proteins comprised a large proportion of the pink module, including ribosomal protein S2 (TRIVIDRAFT_74494) and ribosomal protein L11 (TRIVIDRAFT_78230) (**Supplementary Tables 16–18**). KEGG enrichment analysis of genes in the pink module showed significant enrichment in the ribosome pathway (tre03010) (**Supplementary Tables 19, 20**). However, magenta (244) module genes exhibited high negative correlation with S1 (**Figure 7B**). Genes in the magenta module were mainly related to metabolic processes, including propionyl-CoA synthase (TRIVIDRAFT_55262) and L-threo-3-deoxy-hexylosonate aldolase (TRIVIDRAFT_215195) (**Supplementary Tables 16–18**). Magenta module genes were significantly enriched in the pentose and glucuronate interconversions (tre00040) and valine, leucine, and isoleucine degradation (tre00280) pathways (**Supplementary Tables 19, 20**). Orange module genes (59) were positively associated with S2 (**Figure 7B**). Genes related to oxidation-reduction (e.g., Sordaria macrospora k-hell, TRIVIDRAFT_46447) and transmembrane transport (e.g., major facilitator superfamily transporter, TRIVIDRAFT_43674) processes were included in the orange module (**Supplementary Tables 16–18**). KEGG enrichment analysis showed that genes in the orange module were mainly enriched in phenylalanine metabolism (tre00360), glutathione metabolism (tre00480), tryptophan metabolism (tre00380) and biosynthesis of secondary metabolites (tre01110) pathways (**Supplementary Tables 19, 20**). Black (976) and purple (169) modules exhibited high positive correlation with S4 (**Figure 7B**). Genes in the black module were mainly involved in metabolic, oxidation-reduction, and transport processes, including chitin synthase (TRIVIDRAFT_77496) and fatty acid synthase subunit beta fungi type (TRIVIDRAFT_171412) (**Supplementary Tables 16–18**). KEGG enrichment analysis showed that genes in these modules were all enriched in fatty acid metabolism (tre01212), biosynthesis of unsaturated fatty acids (tre01040), amino sugar and nucleotide sugar metabolism (tre00520), and starch and sucrose metabolism (tre00500) (**Supplementary Tables 19, 20**). Dark red (319) and green (685) modules genes were negatively correlated with S4 (**Figure 7B**). In these two modules, metabolic and oxidation-reduction genes were dominant. Enoyl-CoA hydratase (TRIVIDRAFT_87842), glucan endo-1,3-beta-D-glucosidase (TRIVIDRAFT_111476), glucanase (TRIVIDRAFT_89797) and phosphoglucomutase (TRIVIDRAFT_87728) were included (**Supplementary Table 16, 17**). The fatty acid degradation (tre00071) pathway was enriched in the dark red and green modules (**Supplementary Tables 19, 20**).

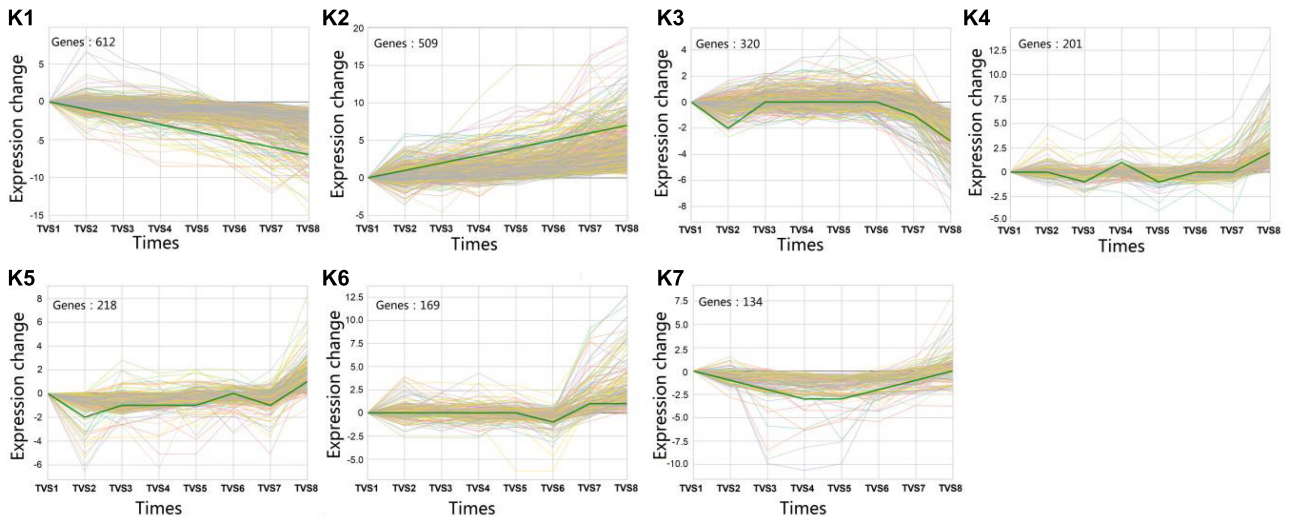

FIGURE 5 | Series test of cluster (STC) analysis of DEGs between adjacent time points. STC analysis showing gene expression profiles. Seven clusters (K1-K7) were identified based on expression levels in 8 time points (TVS1, TVS2, TVS3, TVS4, TVS5, TVS6, TVS7, and TVS8).

Contents of Glycogen, Lipid, and Chitin Changes During CF in *T. virens* GV29-8

The dynamic changes of the components of CF were measured by staining. Microscopic observation showed that glycogen and lipid accumulation was noticeable in the interior of the mycelia at TVS1, TVS2 and TVS3, and chitin also accumulated in the cell wall and diaphragm of the mycelia at the same time. Chlamydospores were first observed at TVS4, a small amount of glycogen and lipids had accumulated in the center of chlamydospores, and chitin had accumulated in the chlamydospore cell wall by this time. After that, more glycogen and lipid in the cytoplasm and chitin in the chlamydospore cell wall and diaphragm had accumulated with the enlargement of chlamydospores. Glycogen, lipid and chitin accumulation was highest at S3 and S4 (**Figure 4**).

The Chitin Synthase Gene (TRIVIDRAFT_90152) Is Essential for CF

It was reported that the amino sugar metabolism pathway was involved in CF of *Fusarium oxysporum* f. sp. *cubense* (FOC) (Ding et al., 2019). In the study, a large number of DEGs were enriched in the amino sugar and nucleotide sugar metabolism (tre00520) pathway. Among them, chitin synthase genes (*Chs*) TRIVIDRAFT_90152 had a large variation. Chitin synthases catalyze the formation of β-(1,4)-glycosidic bonds between GlcNAC residues to form the unbranched polysaccharide chitin, which is the major component of cell walls in most filamentous fungi (Liu et al., 2013). The chitin synthase genes (*Chs*) TRIVIDRAFT_90152 was significantly up-regulated by 5-fold from S1 to S4, and especially from S3 to S4 (**Supplementary Table 25**), which may promote the accumulation of chitin and contribute to the thickening of chlamydospore cell walls. In this study, chitin synthase gene (TRIVIDRAFT_90152) knockout mutant strains were constructed by using the split-PCR strategy (**Supplementary Figure 7a**). For mutant strains 1, 9 and 21, the PCR analysis confirmed the existence of the *hyg* sequence and the absence of the *Chs* sequence (**Supplementary Figure 7b**). Southern hybridization showed a single copy of the *Chs* sequence in wild-type *T. virens* GV29-8, and absence of the *Chs* sequence in the mutant strains (**Supplementary Figure 7c**). The results showed that the chitin synthase gene (TRIVIDRAFT_90152) of those 3 mutants (*Chs*Δ*1*, *Chs*Δ*9* and *Chs*Δ*21*) were successfully knocked out and selected for subsequent experiments.

The *Chs*Δ deletion mutants exhibited reduced mycelial growth, and produced significantly less mycelia than the wild-type *T. virens* GV29-8 on PDA medium (**Supplementary Figure 7d**). Sporulation structure of chlamydospore and mycelium morphology of wild-type *T. virens* GV29-8 and the chitin synthase gene (TRIVIDRAFT_90152) deletion mutant *Chs*Δ were observed by microscope; significant differences between the wild-type and *Chs*Δ mutant were observed. The results showed that chlamydospore formation was normal in the wild-type strain, while no chlamydospores were observed in the *Chs*Δ mutant, in which the mycelium was abnormally curved and twisted (**Figure 8A**). Fluorescence white staining showed that the chitin content in the *Chs*Δ mutant was significantly reduced and the chitin distribution was uniform in the mycelium cell wall (**Figure 8B**). Red oil O staining showed that no lipids accumulated in the *Chs*Δ mutant, which was a distinct structural feature of chlamydospores (**Figure 8C**). The results implied that the *Chs* gene plays a key role in CF. It is inferred that amino sugar and nucleotide sugar metabolism (tre00520) pathway affects the CF of *T. virens* GV29-8 strain.

Validation of RNA-Seq-Based Gene Expression

To validate the gene expression profiles obtained by RNA-Seq, reverse transcription quantitative PCR (RT-qPCR) was

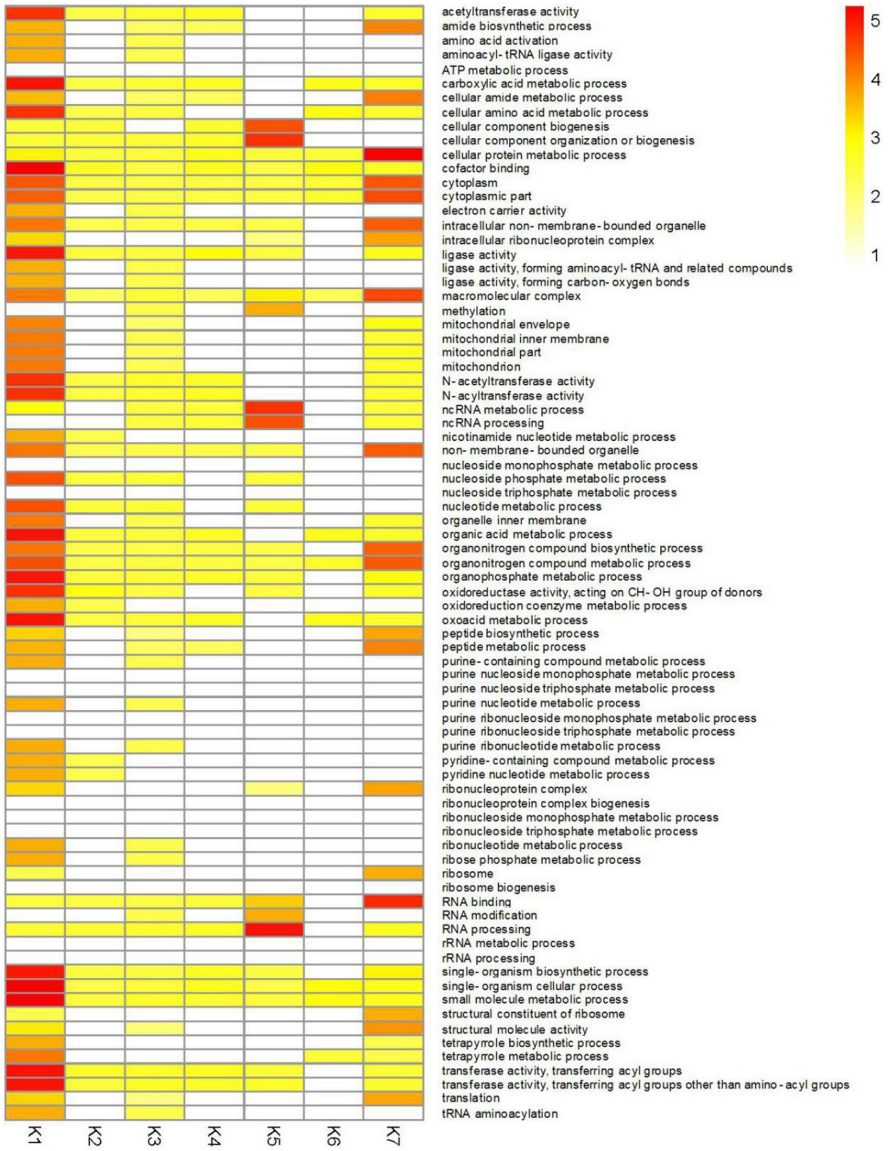

FIGURE 6 | GO enrichment analysis of DEGs in different clusters of CF in *T. virens* GV29-8. Gene Ontology enrichment among the 7 clusters. Yellow to red: significant enrichment ($P < 0.05$). White, non-significant.

performed for 15 genes potentially related to CF. Correlation coefficients were calculated between the RNA-seq and RT-qPCR data for these 15 genes. The expression patterns of these genes determined by RT-qPCR were consistent with the RNA-Seq data (**Figure 9**), indicating the reliability and accuracy of the RNA-seq data.

DISCUSSION

Chlamydospore formation is a complex process regulated by many pathways. In this study, transcriptome sequencing was conducted for 8 developmental time points during the CF of *T. Virens* Gv29-8. Through transcriptomic data analysis, we found that organonitrogen deficiency, stress response and cell cycle regulation may be the main factors inducing CF. Additionally, large amounts of glycogen, lipids, chitin and mannose accumulated during the late stage of CF.

Pairwise comparisons were made for S1, S2, S3 and S4 stages. The S1 and S2 stages had the greatest differences in transcript and morphological changes during the process of developmental differentiation. DEGs were mostly significantly enriched in genes involved in organonitrogen compound metabolic processes (GO:1901564) and the ribosome pathway (tre03010) (**Supplementary Figures 1, 3** and **Supplementary Tables 6, 10**). The majority of DEGs in the organonitrogen compound metabolic process and ribosome pathways were ribosomal protein genes, which were down-regulated in S2

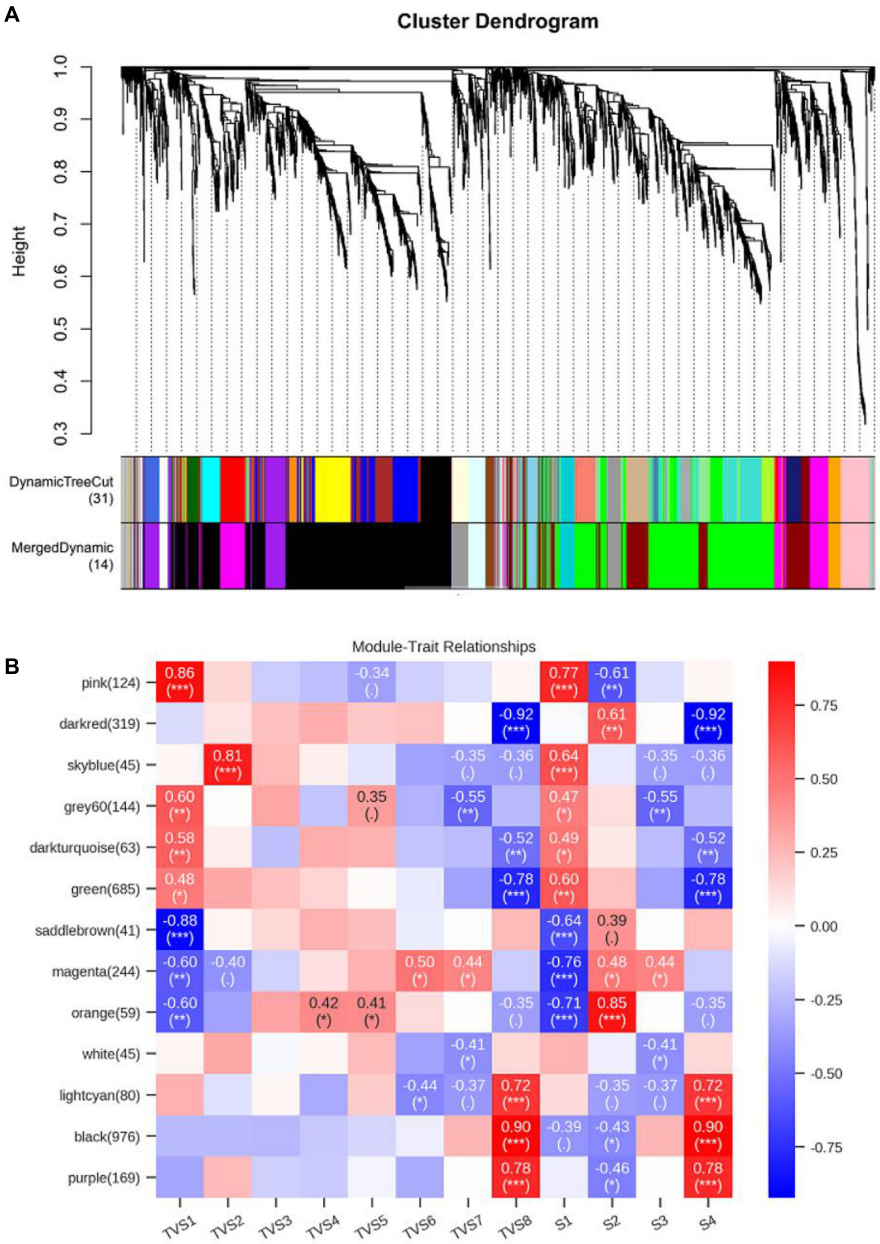

FIGURE 7 | Weighted gene co-expression network analysis (WGCNA) of genes in different CF stages of *T. virens* GV29-8. **(A)** Cluster dendrogram of genes based on expression levels during the 8 sampling time points and 4 developmental stages. Each branch represents a gene and each color below represents a gene co-expression module. The dynamic tree cut indicates the modules were divided based on the gene clustering results. The merged dynamic cut indicates the modules were divided by combining modules with similar expression patterns. **(B)** Heatmap of gene expression patterns during the 8 sampling time points and 4 developmental stages. The expression patterns of 13 modules are shown by the heatmap. Each column represents a developmental stage. The module name is shown to the left side of each cell. The number of genes in each module is indicated in parentheses. Numbers in the table report the correlations of the corresponding module genes and stages, with the *p*-values (*) printed below the correlations in parentheses. Each column corresponds to a specific stage. The scale bar on the right indicates the range of possible correlations from positive (red) to negative (blue).

(**Supplementary Tables 7, 11**). This suggests that organic nitrogen metabolism might be inhibited, protein biosynthesis was slowed down overall, and that nitrogen in the culture medium was relatively scarce in S2. In yeast, a poor nitrogen source (e.g., aminobutyric acid and urea) was only used when an abundant nitrogen source was scarce (Ramos et al., 1985; Marzluf, 1997; Palavecino et al., 2015). The 4-aminobutyrate transaminase (TRIVIDRAFT_57634) encoded by *GatA* catalyzed the conversion of aminobutyric acid into glutamic acid (Arst, 1976; Bailey et al., 1979), which was up-regulated from the latter of S1 (TVS2) to S4 in our study (**Supplementary Table 2**). This also indicates that available nitrogen may be scarce in the medium

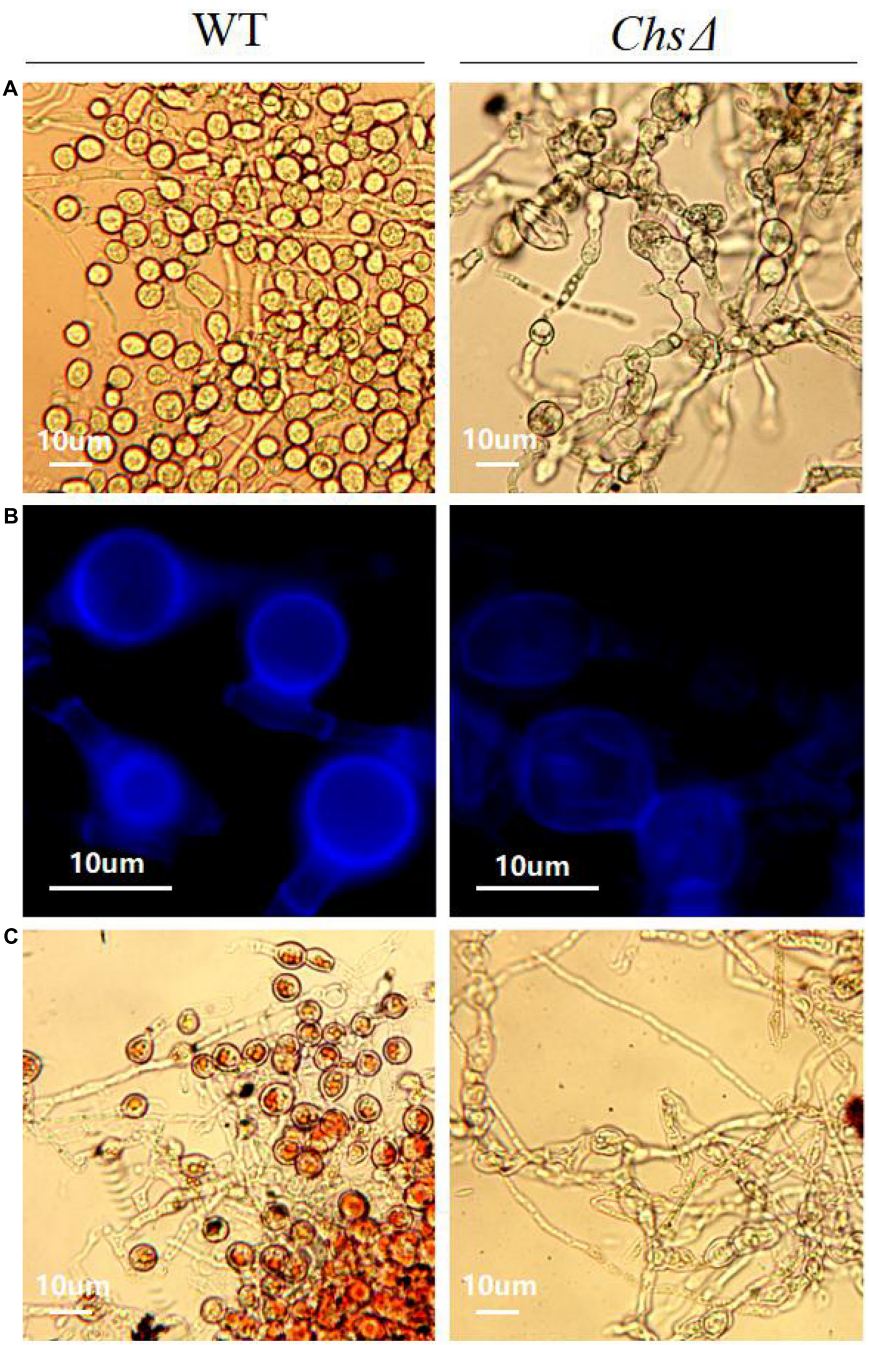

FIGURE 8 | Effect of chitin synthase gene (TRIVIDRAFT_90152) deletion on CF in *T. virens* GV29-8. **(A)** The chlamydospores formed by the wild-type *T. virens* GV29-8 and chitin synthase gene (TRIVIDRAFT_90152) deletion mutant (*Chs*Δ). **(B)** Chitin staining of wild-type and *Chs*Δ mutant strains. **(C)** Oil red O staining of wild type and *Chs*Δ mutant strains.

after the later stage of S1. The nitrogen source was an important factor affecting CF: even adding a small amount of peptone (0.2%) as an organic nitrogen source can strongly inhibit CF of *C. albicans* in culture (Böttcher et al., 2016). The nitrogen source mainly regulates CF via the TOR signaling pathway (Böttcher et al., 2016). Tor1 kinase is a highly conserved complex that senses the availability of nitrogen and other nutrients. Under conditions of sufficient nutrient availability, the activity of Tor1 is enhanced, which can drive the signal cascade that promotes cell proliferation (Kamada et al., 2004). Under nitrogen-poor conditions, it facilitates nuclear entry of the GATA factors, Gat1 and Gln3, to mediate expression of nitrogen catabolite repressed (NCR) genes (Beck and Hall, 1999; Cardenas et al., 1999). Mutations in either the *gat1* or *gln3* gene could inhibit CF

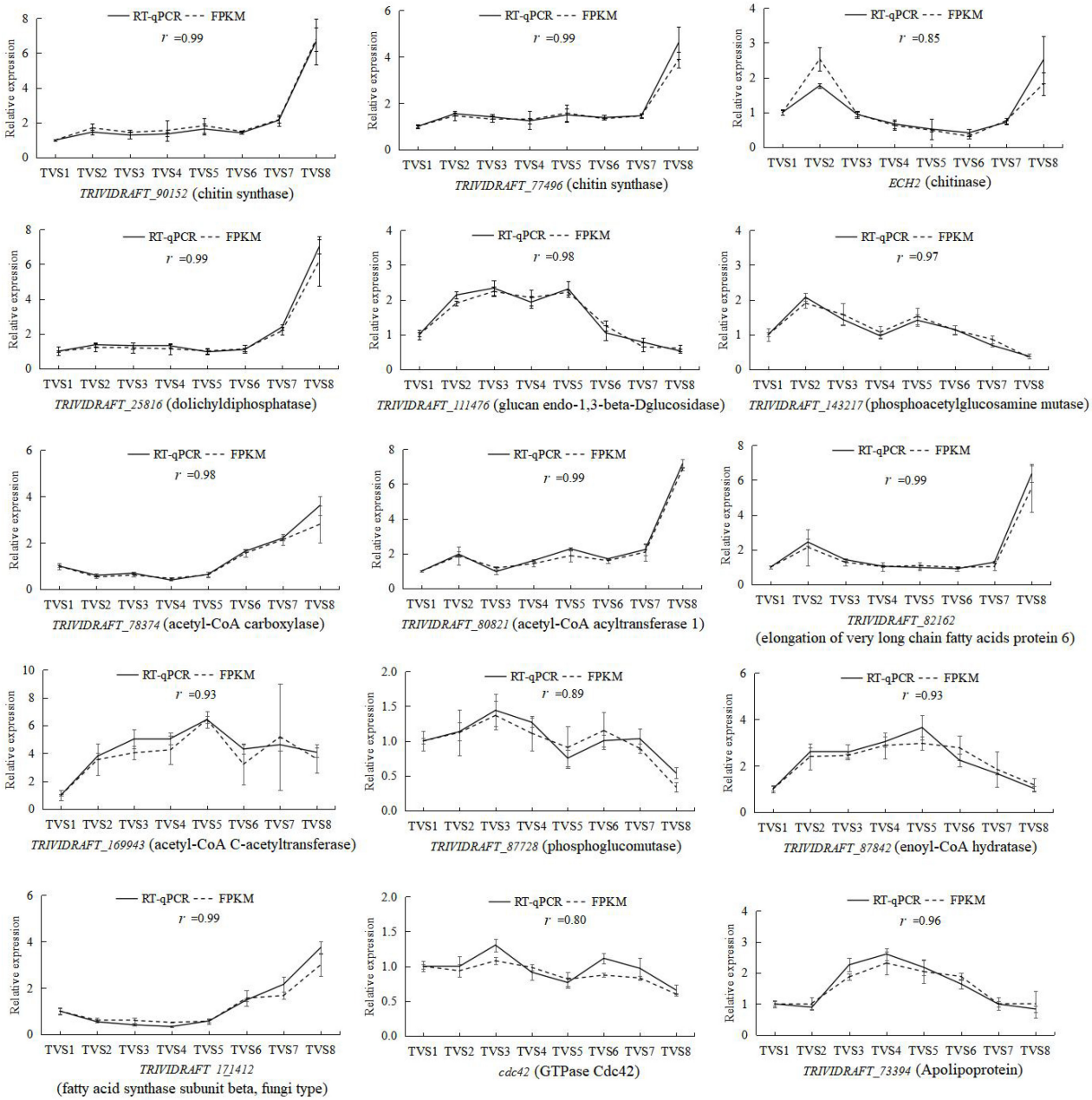

FIGURE 9 | RT-qPCR determination of the expression levels of 15 selected DEGs during CF in *T. virens* GV29-8. The vertical axis represents the relative expression levels of DEGs across 8 sampling time points. The horizontal axis indicates the sampling time. Error bars represent the standard deviation of three independent replicates for each tested gene. The value *r* represents the correlation between RT-qPCR and RNA-seq data.

(Böttcher et al., 2016). In our study, the seryl-tRNA synthetase encoding gene (TRIVIDRAFT_172396) which is involved in positive regulation of the TOR signaling pathway, and the nitrogen metabolism repressor gene (TRIVIDRAFT_176019), were down-regulated from S2 to S4 (**Supplementary Table 2**). The results showed that the availability of an abundant nitrogen source in the medium was reduced, thus the strain might be entering a nitrogen starvation state by S2 and subsequent stages. *PTR2* is a nitrogen starvation response gene, and a conserved high affinity transporter shown to physically interact with the nutrient-sensing *Tor1* and *Tor2* complexes in *Saccharomyces cerevisiae* (Aronova et al., 2007). Palige et al. (2013) showed that expression of the nitrogen starvation response gene *PTR2* was significantly up-regulated during the induction of CF in *C. albicans*. In our study, two *PTR2* genes, TRIVIDRAFT_50243 and TRIVIDRAFT_79497, were up-regulated and highly expressed in TVS2-TVS5 and TVS6-TVS8, respectively (**Supplementary Table 2**). Phenotypic results

showed that chlamydospores initially formed on the tips of the mycelia at the early stage of S2. Subsequently, a large number of chlamydospores formed in the interior of mycelia at the later stages of S2-S4 (**Figure 1**). These two genes might play an important role in CF, and up-regulation of them at different periods might be related to regulation of different stages of CF. In summary, the strains made extensive use of the supplied nitrogen source in the early vegetative growth stage, leading to organic nitrogen deficiency in the late stage of S1, and the strains might induce CF by regulating differential expression of nitrogen utilization regulators.

The GO analysis showed that DEGs were most significantly enriched for tetrapyrrole binding (GO:0046906) and heme binding (GO:0020037) in S3 vs S2 (**Supplementary Figure 1** and **Supplementary Table 6**). The DEGs in these 2 terms were mainly the cytochrome P450 family and antioxidant genes. Most of the P450 genes were homologous to genes required for synthesizing toxic secondary metabolites during the growth of fungi; others were linked to the function of detoxification and antioxidant (**Supplementary Table 7**). The results showed that not only nutrient deficiency, but also secondary metabolism and stress responses, may induce CF. Sclerotia, like chlamydospores, are also dormancy structures produced by many fungi. Studies showed that genes linked to secondary metabolite production also control sclerotia production (Jirjis and Moore, 1976; Willetts and Bullock, 1992; Kües, 2000; Georgiou et al., 2006; Bayram and Braus, 2012; Calvo and Cary, 2015; Song, 2018; Shu et al., 2019). For example, different members of the velvet protein family interact with each other and the non-velvet protein *LaeA*. *LaeA* is a methyltransferase-domain protein that functions as a regulator of secondary metabolism and sclerotial morphogenesis (Bayram and Braus, 2012; Calvo and Cary, 2015). Moreover, Mukherjee and Kenerley (2010) reported that the *Velvet1* gene mutation resulted in increased chlamydospore production under conditions of nutritional stress in *T. virens*. In this study, 2 new genes (novel.11798 and novel.972) were annotated as velvet factors and differentially expressed during CF (**Supplementary Table 2**). The P450 genes O-methylsterigmatocystin oxidoreductase and versicolorin B desaturase are mainly involved in the synthesis of aflatoxins in fungi. Aflatoxin is a highly toxic polyketone-derived secondary metabolite which can poison fungal cells. It was reported that the genes involved in aflatoxin synthesis are co-regulated with sclerotia formation in *Aspergillus flavus* (Chang et al., 2002; Duran et al., 2007; Cary et al., 2012; Calvo and Cary, 2015). Microsclerotia are another type of dormancy structure of many fungi, so we speculate the up-regulation of the O-methylsterigmatocystin oxidoreductase and versicolorin B desaturase genes might lead to the accumulation of aflatoxins and affect CF in *Trichoderma* (**Supplementary Table 7**). Benzoate 4-monooxygenase is a benzoate detoxification enzyme (Podobnik et al., 2008). Benzoic acid interferes with the permeability of microbial cells, inhibits the absorption of amino acids by the cell membrane and the activity of the cellular respiratory enzyme system, and hinders the condensation reaction of acetyl-COA to affect normal life activities of cells (Kresnowati et al., 2008). Up-regulated expression of the benzoate 4-monooxygenase gene could accelerate the catalytic conversion of benzoic acid to p-hydroxybenzoic acid in S3 (**Supplementary Table 7**), reducing harm to cells. It has been reported that a gene encoding the lutein deficient 5 protein was involved in biosynthesis of lutein in plants (Fiore et al., 2006; Kim and DellaPenna, 2006; Kim et al., 2009). In this study, TRIVIDRAFT_160585 was annotated as a protein lutein deficient 5 homologous gene, which was up-regulated from S2 to S4 (**Supplementary Table 7**), possibly accelerated biosynthesis of lutein. Lutein exhibits strong anti-oxidant capabilities and can reduce the damage of reactive oxygen species (ROS) to cells (Picot et al., 2013). ROS are formed in during normal life activities of cells; excessive ROS accumulation can directly or indirectly damage cellular components (e.g., DNA, proteins and lipids), and lead to cell death (Jamieson, 1998; Ruhland and Reniere, 2019). *Nox1* is a NADPH oxidase (Noxs) family gene that participates in the production of ROS, which can regulate cell differentiation and affect the formation of asexual spores in *T. atroviride* (Hernández-Oñate et al., 2012). In our study, up-regulation of the *Nox1* gene might promote the production of ROS in S2 stage (**Supplementary Table 2**). The expression levels of ROS scavenging genes were relatively lower during S1 and S2, which might lead to the accumulation of ROS, placing the strain under an environment of oxidative stress, further promoting the transformation of mycelia into chlamydospores. Conversely, to survive, genes encoding catalase were up-regulated at S3 and S4 to eliminate ROS and alleviate damage to cells caused by oxidative stress (**Supplementary Table 7**). Most of the down-regulated DEGs were P450 family genes and involved in the synthesis of toxic secondary metabolites (**Supplementary Table 7**). Trichodiene oxygenase, is involved in the synthesis of trichodermin, a highly effective antifungal substance (Takahashi-Ando et al., 2008; Malmierca et al., 2012). TRIVIDRAFT_74291 was annotated as homologous genes of the Trichodiene oxygenase gene, in this study. In plants, abscisic acid 8′-hydroxylase takes part in the synthesis of abscisic acid (Saito et al., 2004; Kushiro et al., 2004; Umezawa et al., 2006). In our study, TRIVIDRAFT_230790 and TRIVIDRAFT_216144 were annotated as being homologous with the abscisic acid 8′-hydroxylase gene and might be involved in the formation of abscisic acid (**Supplementary Table 7**). Excessive accumulation of abscisic acid may promote transformation of mycelia into dormant spores. Beta-amyrin 11-oxidase is the precursor substance used to synthesize glycyrrhizin in plants (Seki et al., 2008). TRIVIDRAFT_53690, TRIVIDRAFT_53375 and TRIVIDRAFT_151337 were annotated as homologous genes of the beta-amyrin 11-oxidase gene (**Supplementary Table 7**). By comparing the expression levels of these genes at the S1, S2, S3 and S4, we found that most of the DEGs involved in toxic secondary substance synthesis were highly expressed during S1 and S2, and lowly expressed during S3 and S4. DEGs encoding detoxifying enzyme and free radical scavenging enzymes were highly expressed during S3 and S4 (**Supplementary Table 7**). This suggests that the rapid growth of mycelia under abundant nutrient conditions would be accompanied by the accumulation of toxic and harmful secondary metabolites. When large amounts of harmful substances accumulated, strains will produce detoxifying and

free radical scavenging enzymes to alleviate adverse stress. Alternatively, fungi can change their developmental strategies in favor of long-term survival by producing resistant propagules. Therefore, we hold the opinion that both nutrient decline in the media, and non-nutrient factors such as environmental conditions and secondary stress factors caused by metabolism, are involved in fungi CF.

Cell differentiation might be a vital factor in regulating the transformation of mycelia into chlamydospores. KEGG enrichment analysis showed that cell cycle-yeast (tre04111) genes were significantly enriched in TVS5 vs TVS4 and TVS6 vs TVS5 (**Supplementary Figures 4, 8** and **Supplementary Tables 12, 13**). DEGs in this pathway were involved in different phases of cell differentiation. It has been reported that the formation of chlamydospores is regulated by different cell cycle genes in *C. albicans*, and deletion of the *CDC10* or *CDC11* genes lead to morphological defects in chlamydospores (Martin et al., 2005). The *CDC10* gene was highly expressed during S1 and S2, then significantly down-regulated in S3 and S4 (**Supplementary Table 2**). Higher expression of the *CDC10* gene in the first two stages may positively regulate CF. Additionally, the *CDC4* gene was also significantly up-regulated, 5.66-fold, from S2 (TVS4) to S4 (TVS8) (**Supplementary Table 21**). Other CDC family genes (CDC42 and CDC48) were also differentially expressed during different stages (**Supplementary Table 2**). Microsclerotia are a type of dormant structure, which is considered to originate from polar hyphae in fungi (Biles et al., 1992; Colotelo, 1974; Jackson and Jaronski, 2009; Yin et al., 2012). Inhibition of Rho/Rac/CDC42 family GTPases have been noted to significantly reduce polarized hyphal growth and microsclerotia production (Jiang et al., 2014; Song et al., 2016). Similarly, we deduced that the GTPase *CDC42* gene was highly expressed in S1∼S3 and might be related to CF. According to the above data, we hypothesize that DEGs in cell cycle pathways may be involved in regulating CF.

N-glycan biosynthesis pathway (tre00510) genes, which are involved in both anabolism and catabolism of mannan, were also significantly enriched in S3 vs S2 (**Supplementary Figures 3, 9** and **Supplementary Tables 10, 11**). Mannan is a primary component of cell walls in *C. albicans*, and deletion of the α-1,6-mannosyltransferase gene can affect cell wall integrity (Pérez-García et al., 2016). Damage to the mannose synthesis pathway prevents CF in *C. albicans* (Whelan et al., 1990). This suggests that the N-glycan biosynthesis pathway may be related to cell wall construction of chlamydospores in *Trichoderma*. There were 14 DEGs in the N-glycan biosynthesis pathway, 10 of which are involved in mannan synthesis and up-regulated at S3 (**Supplementary Figure 9** and **Supplementary Tables 11, 22**). For example, dolichyldiphosphatase catalyzes dolichyl diphosphate into dolichol phosphate, the first step of the N-glycan synthesis reaction (Janik et al., 2019). The gene encoding dolichyldiphosphatase was significantly up-regulated at S3. Three DEGs encoding mannosyl-oligosaccharide alpha-1,2-mannosidase, which is involved in mannose degradation, were all down regulated at S3 (**Supplementary Figure 9** and **Supplementary Tables 11, 22**). It could be inferred that up-regulation of mannan anabolism genes and down-regulation of catabolism genes could lead to mannan accumulation during S3, which might affect chlamydospore cell wall formation.

We found that lipid metabolism genes were significantly enriched in S4 vs S3, and DEGs in this category were mainly correlated with fat, phospholipid, and sterol metabolism (**Supplementary Figure 1** and **Supplementary Table 7**). It has been reported that the mature chlamydospore center of *C. albicans* contains a large number of fat droplets (Miller et al., 1974). The main components of fats are glycerol and fatty acids. In our study, DEGs in all 3 comparisons (S2 vs S1, S3 vs S2 and S4 vs S3) appeared to be enriched for pathways related to fatty acid metabolism (including fatty acid metabolism (tre01212), fatty acid degradation (tre00071) and biosynthesis of unsaturated fatty acids (tre01040), and the number and expression level of DEGs changed at different stages (**Supplementary Table 10**). A total of 20 DEGs were enriched in these 3 pathways. Among them, 6 genes were involved in the fatty acid degradation pathway, and the others were all related to fatty acid synthesis (**Supplementary Figure 10** and **Supplementary Table 23**). By analyzing the gene expression levels of these 20 DEGs in S1∼S4, we found that DEGs involved in the fatty acid degradation pathway were highly expressed in S1 and S2, then decreased in S3 and S4. For example, the genes encoding acetyl-CoA C-acetyltransferase and enoyl-CoA hydratase were up-regulated 2.9 and 6.4-fold from S1 to S2, respectively, and then significantly down-regulated in S3 and S4. The expression of acetyl-CoA C-acetyltransferase gene was down-regulated 15-fold from S2 to S4. In contrast, most DEGs in the fatty acid synthesis pathway maintained lower expression levels from S1 to the middle stages of S2 (TVS1∼TVS5), then were significantly up-regulated from late S2 to S4 (TVS6 ∼ TVS8). For example, the acetyl-CoA carboxylase gene increased 5.96-fold from the early stage of S2 (TVS4) to S4 (TVS8). Acetyl-CoA carboxylase is a rate-limiting enzyme of fatty acid synthesis, which can catalyze acetyl-CoA into malonyl-CoA (Wakil et al., 1958; Davis et al., 2000; Tong, 2013); up-regulated expression of this gene during CF (S2∼S4/TVS4∼TVS8) may accelerate the accumulation of fatty acids. The gene *Fas1*, encoding the fatty acid synthase subunit beta was up-regulated 5.8-fold from the late stage of S2 (TVS5) to S4. Fatty acid synthetase catalyzes the formation of long-chain fatty acids from acetyl-CoA, malonyl-CoA and NADPH (Kuziora et al., 1983; Nguyen et al., 2009). *FAS1* mutations reduced lipid deposition in conidia of *Magnaporthe oryzae* (Sangappillai and Nadarajah, 2020). Additionally, genes encoding fatty acid elongase 3 and acetyl-CoA acyltransferase 1 are involved in fatty acid synthesis and were significantly up-regulated at S4 (**Supplementary Figure 10** and **Supplementary Table 23**). This indicated that fatty acid degradation may provide energy for basic life functions during the mycelium growth and early CF stages. Biosynthesis of fatty acid pathway genes were significantly up-regulated at the later stage of CF, which could promote fat accumulation in chlamydospores. Nile red staining results also confirmed that a large number of lipid droplets formed in the late stage (S3 and S4) of CF (**Figure 4**). Chlamydospores are propagules produced under unfavorable conditions, and

the accumulation of lipids could provide energy for spore germination once more favorable environmental conditions are re-established.

To obtain a comprehensive understanding of which genes contribute to different the developmental stages of CF, WGCNA was performed on samples from the 8 time points and 4 stages (**Figure 7**; **Supplementary Tables 16, 17**). Genes with similar expression patterns likely had similar functions, so they were grouped into the same module. Pearson correlation coefficients were used to judge the relationship between different modules and phenotypes at different development stages. Our results show that the pink and magenta modules were highly positively and negatively correlated with S1, respectively (**Figure 7**). The genes in the pink module were significantly enriched in the ribosome (tre03010) pathway (**Supplementary Table 19**), which was consistent with the results of previous KEGG enrichment analyses at S1 (**Supplementary Figure 3** and Supplementary **Table 10**). Genes in magenta are mainly enriched in the pentose and glucuronate interconversions (tre00040) and valine, leucine, and isoleucine degradation (tre00280) pathways (**Supplementary Table 19**). Pentose and glucuronate interconversions is one of the primary pathways involved in carbohydrate utilization in fungal strain (Cui et al., 2020). These results show that the strain absorbed nutrients in the medium and synthesized various substances to meet its own growth needs at S1, and as nutrients became depleted in the late growth stage, nutrient assimilation was reduced. The orange module showed high positive correlation with S2 (**Figure 7**), in which glutathione metabolism (tre00480), phenylalanine metabolism (tre00360) and tryptophan metabolism (tre00380) related genes were enriched (**Supplementary Table 19**). The products of these pathways have confirmed roles in antioxidant, antifungal and antibacterial activity (Allen et al., 1960; Haile and Dekebo, 2013). These results and previous GO analysis of DEGs in S3 vs S2 were consistent with each other (**Supplementary Figure 1** and **Supplementary Table 6**). We speculate that the culture environment became hostile at S2, stimulating the fungal strain to produce resistant substances and dormancy structures in favor of survival. Black, purple, and light cyan modules showed high positive correlation with S4, while dark red and green modules showed high negative correlation (**Figure 7**). Genes in black and purple modules were enriched in the fatty acid metabolism (tre01212) and biosynthesis of unsaturated fatty acids (tre01040) pathways. Conversely, genes in the dark red and green modules were enriched in fatty acid metabolism (tre01212) and fatty acid degradation (tre00071) pathways (**Supplementary Table 19**). This suggests that fatty acid synthesis was dominant at S4 and may contribute to accumulation of fatty acids, which is consistent with the results of GO and KEGG enrichment analyses in S4 vs S3. Additionally, starch and sucrose metabolism (tre00500) and amino sugar and nucleotide sugar metabolism (tre00520) pathways were also enriched in these 4 modules (**Supplementary Table 19**). Starch and sucrose metabolic pathways were mainly related to anabolism and catabolism of glycogen. In *Coprinopsis cinerea*, glycogen served as a carbon storage molecule, and was actively transformed between monomeric and polymeric forms during morphogenesis (Jirjis and Moore, 1976). The gene encoding glucan endo-1,3-beta-D-glucosidase is relevant to the process of glycogen decomposition, which transforms Udp-glucose into D-glucose. The gene was significantly up-regulated at S1 and S2, then declined sharply at S3 and S4, after which it remained at a relatively low expression level (**Supplementary Figure 11** and **Supplementary Table 24**). Phosphoglucomutase mediates the conversion of α-D-Glucose 6-phosphate and α-D-Glucose 1-phosphate, which is involved in glycogen decomposition (Ray and Roscelli, 1964; Mesak and Dahl, 2000). Similarly, the gene expression level was also significantly reduced at S4 (**Supplementary Figure 11** and **Supplementary Table 24**). The down-regulation of glucan endo-1,3-beta-D-glucosidase and phosphoglucomutase genes may be conducive to glycogen accumulation at S3 and S4, which is consistent with the results of I_2 and KI staining which showed a large amount of glycogen accumulated in chlamydospores at S3 and S4 (**Figure 4**). Therefore, mycelia growth accompanied a gradual decrease in nutrient availability in the medium at the early stage of CF (S1 and S2), leading to nutritional stress, after which glycogen decomposition increased to alleviate the nutritional stress. However, this did not prevent CF, due to regulation of nutrient consumption, stress caused by secondary metabolites, and induction of the cell cycle. A sharp decrease in glycogen decomposition at the later stage of CF may be conducive to glycogen accumulation in chlamydospores, which provided energy for germination under more favorable conditions. Previous studies showed that large amounts of glycogen accumulated in the cytoplasm of chlamydospores to store energy (Son et al., 2012). Chitin and glucan are the main components of the cell wall in fungal chlamydospores (Roncero et al., 2016). Chlamydospores have a large cell volume and thick cell walls. Therefore, large amounts of glucan and chitin might be synthesized during the formation of mature chlamydospores. Excluding genes related to glycogen metabolism, expression of genes encoding glucanase and alpha, alpha-trehalase (TRIVIDRAFT_42275) also sharply declined at S4 (**Supplementary Tables 19, 24**), resulting in accumulation of glucan and trehalose and thickening of chlamydospore cell walls, which helps fungal cells overcome osmotic stress. Fungi, through acetylation, convert glucose into N-acetyl-D-glucosamine (GlcNAC) and synthesize chitin by chitin synthase. Chitin synthases and deacetylase might play a key role in the construction of chlamydospore cell walls. There were 12 genes involved in amino sugar and nucleotide sugar metabolism, contained in the black, purple, dark red, and green modules, which correlated with S4 (**Figure 7** and **Supplementary Figure 12**; **Supplementary Tables 19, 25**). It was reported that GlcNAC inhibited CF of *Fusarium oxysporum* f. sp. *cubense* (Ding et al., 2019). Chitinase (*Ech2*), involved in the amino sugar and nucleotide sugar metabolism pathway, could break down chitin into GlcNAC (Tzelepis et al., 2012). In our study, the Chitinase (*Ech2*) gene was significantly down-regulated and maintained a low expression level from S1 to S2, then experienced a slow increase until S3 and S4 (**Supplementary Table 25**). This suggests that low expression of *Ech2* at S2 might reduce the accumulation of GlcNAC and promote the formation of chlamydospores. Increased expression of the *Ech2* gene during S3

and S4 (**Supplementary Table 25**), may play a role in the aging of mycelia and cell-wall degradation, releasing the internal nutrients and providing nutrients and energy for CF when medium nutrients become lacking. Additionally, the chitin synthase genes (TRIVIDRAFT_77496 and TRIVIDRAFT_90152) was significantly up-regulated (3.1 and 5-fold) from S1 to S4, especially from S3 to S4 (**Supplementary Table 25**), which may promote the accumulation of chitin and contribute to the thickening of chlamydospore cell walls. In our study, deletion of the chitin synthase gene TRIVIDRAFT_90152 blocked chitin biosynthesis of the cell wall, resulting in mycelium dysplasia and an inability to form normal chlamydospores in *T. virens* GV29-8 (**Figure 8**). This indicated that the chitin synthase gene (TRIVIDRAFT_90152) plays an important role in cell wall formation of mycelia and was necessary for CF. The amino acid sugar and nucleotide sugar metabolism (tre00520) pathway affects the CF of *T. virens* GV29-8 strain.

In conclusion, CF is a complex biological process that acts via multiple integrated signal transduction pathways. In the early stage, fungal strains were mainly engaging in assimilation and absorption of nutrients in the medium for mycelium growth. When nutrients in the medium were depleted to a certain threshold, the stress stimulated the fungal strain to induce chlamydospore formation. Simultaneously, the organism's own life activities led to changes in the culture environment conditions and the production of secondary metabolites and ROS, which further stimulated chlamydospore production. Pathway associated with the cell cycle were differentially expressed to regulate cell differentiation of the fungal strain. Finally, through the synergistic action of multiple pathways and genes, necessary components of chlamydospore structure, such as glycogen, lipids, and thickened cell walls, were synthesized to guarantee the formation of chlamydospores. Our results provide insights into the key pathways and hub genes involved in CF, from a transcriptomic perspective. Further verification through deletion of these genes is needed to clarify their functions in CF. This is the first detailed developmental transcriptomic study of CF in *T. virens* GV29-8. which will aid in further understanding of the mechanisms underlying CF in fungi and provides a foundation for improving the production and utilization of chlamydospore containing agents.

DATA AVAILABILITY STATEMENT

The original contributions presented in the study are publicly available. This data can be found here: NCBI repository, https://www.ncbi.nlm.nih.gov/assembly/GCA_000170995.2.

AUTHOR CONTRIBUTIONS

XP and BW contributed the experiment and writing for the manuscript. SZ did the experiment. ML and XJ contributed the design of the experiments and writing for the manuscript. All authors contributed to the article and approved the submitted version.

FUNDING

This work was supported by the National key research and development plan (Chemical fertilizer and pesticide reducing efficiency synergistic technology research and development): New technology and product development of Trichoderma efficient fermentation (2019YFD1002000-2); Beijing National Science Foundation (6192022); Survey of basic resources of science and technology: A comprehensive survey of biodiversity in the Mongolian Plateau (2019FY102004); Demonstration of comprehensive prevention and control technology of non-point source pollution in main vegetable producing areas of Huanghuaihai (2018YFD0800401).

SUPPLEMENTARY MATERIAL

The Supplementary Material for this article can be found online at: https://www.frontiersin.org/articles/10.3389/fmicb.2021.654855/full#supplementary-material

Supplementary Figure 1 | Gene ontology (GO) functional classification of DEGs among samples of adjacent stages. **(a)**, **(b)**, and **(c)** represent functional classification of DEGs between S2 vs S1, S3 vs S2, and S4 vs S3, respectively. The bars represent significantly enriched GO terms ($p < 0.05$), and the numbers beside terms indicate the number of DEGs for each term. The numbers in the centers of red and blue bars represent the number of up-regulated and down-regulated DEGs in the term, respectively. Because the picture is too big, we split it into 2 parts to display it more clearly.

Supplementary Figure 2 | GO functional classification of DEGs between adjacent sampling time points. **(a), (b), (c), (d), (e), (f)** and **(g)** represent GO functional classification of DEGs between TVS2 vs TVS1, TVS3 vs TVS2, TVS4 vs TVS3, TVS5 vs TVS4, TVS6 vs TVS5, TVS7 vs TVS6 and TVS8 vs TVS7, respectively. The bars represented significantly enriched GO terms ($p < 0.05$), and the number beside each term indicates the number of DEGs in the term. The numbers in the centers of the red and blue bars represent the number of up-regulated and down-regulated DEGs in the term, respectively. Because the picture is too big, we split it into 2 parts to display it more clearly.

Supplementary Figure 3 | Kyoto encyclopedia of genes and genomes (KEGG) functional classification of DEGs between adjacent stages. The bars represent significantly enriched KEGG pathways ($p < 0.05$), and the number beside the term indicates the number of DEGs included in the pathway. The numbers in the centers of red and blue bars represents up-regulated and down-regulated DEGs, respectively.

Supplementary Figure 4 | KEGG functional classification of DEGs among samples of adjacent time points. The bars represent significantly enriched KEGG pathways ($p < 0.05$), and the number beside the term indicates the number of DEGs included in the pathway. The numbers in the centers of red and blue bars represents up-regulated and down-regulated DEGs, respectively.

Supplementary Figure 5 | Summary Plot of all DEGs STC classification. black_Hub_network. dark red_Hub_network. darkturquoise_Hub_network. green_Hub_network. grey60_Hub_network. light cyan_Hub_network. magenta_Hub_network. orange_Hub_network. pink_Hub_network. purple_Hub_network. saddle brown_Hub_network. sky blue_Hub_network. white_Hub_network.

Supplementary Figure 6 | Protein-protein interaction (PPI) network of genes in the black, dark red, dark turquoise, green, grey60, light cyan, magenta, orange, pink, purple, saddle brown, sky blue and white modules.

Supplementary Figure 7 | Construction of chitin synthase gene (TRIVIDRAFT_90152) deletion mutants and the effect on phenotypes of the *T. virens* GV29-8. **(a)** Chitin synthase gene (TRIVIDRAFT_90152) deleting strategy.

The *Chs* gene of *T.virens* GV29-8 was knocked out by split-PCR strategy. The split-marker cassettes were developed using fusion PCR, and involved two rounds of PCR. First round PCR: the upstream and downstream homologous fragments of *Chs* were amplified using primers upF/upR and downF/downR with the genome DNA of *T.virens* GV29-8 as template, respectively. Fragment of the hygromycin gene was amplified with the plasmid pKH-KO as template, and *hyg*F/*hyg*R as primer. Second round PCR: the upstream homologous fragment of *Chs* gene and the *hyg* gene fragment from the first round of PCR products were simultaneously used as templates, and the final fragment (1) was amplified by using the primer up2F/*hyg*2R, which contained the upstream homologous region of the *Chs* gene and two thirds of the hygromycin gene fragment. Similarly, the downstream homologous region of the *Chs* gene and two thirds of the hygromycin gene fragment was amplified (2). There were 554 bp *hyg* gene overlap region between (1) and (2) in the center of *hyg*. **(b)** PCR identification of *Chs* and *hyg* genes in *Chs*Δ*1*, *Chs*Δ*9*, *Chs*Δ*21* and WT. M was a 250-bp ladder. PCR templates were genomic DNA of *Chs*Δ*1*, *Chs*Δ*9*, *Chs*Δ*21* and wild-type GV29-8 respectively. **(c)** Southern hybridization analysis. Probe: *Chs*, DNAs of wild-type GV29-8, *Chs*Δ*1*, *Chs*Δ*9*, and *Chs*Δ*21* were digested by BamHI/NotI. (d) Phenotypes of the wild-type *T. virens* GV29-8 and *Chs*Δ mutant strains.

Supplementary Figure 8 | Cell cycle-yeast pathway (tre04111). DEGs in cell cycle-yeast pathway: Apc/c: anaphase-promoting complex subunit 8 (25794716); CDC45: cell division control protein 45 (25786744); MCM: DNA replication licensing factor MCM3 (25797744/25797702/25797864); CDC7: cell division control protein 7 (25795105); Pom1: dual specificity tyrosine-phosphorylation-regulated kinase (25791399); Met30: F-box and WD-40 domain protein MET30 (25795627); Smc2: structural maintenance of chromosome 2 (25797454); Smc4: structural maintenance of chromosome 4 (25798962); Mcm2: DNA replication licensing factor MCM2 (25797864); Mcm6: DNA replication licensing factor MCM6 (25797744); Mcm7: DNA replication licensing factor MCM7 (25797702); Orc1: origin recognition complex subunit 1 (25793997); Orc6: origin recognition complex subunit 6 (25787414); Mcm4: DNA replication licensing factor MCM4 (25798055). The green box represents a specific gene or enzyme in *Trichoderma Reesei* and does not indicate up-regulation or down-regulation of the gene.

Supplementary Figure 9 | N-Glycan biosynthesis pathway (tre00510). DEGs in N-Glycan biosynthesis pathway: 3.6.1.43: dolichyldiphosphatase (25792540); DMP1: dolichol-phosphate mannosyltransferase (25798517); ALG5: dolichyl-phosphate beta-glucosyltransferase (25795393); OST: oligosaccharyltransferase complex subunit alpha (25786852/25787193/25798795); MAN1: mannosyl-oligosaccharide alpha-1,2-mannosidase (25798667/25789754/25795445); STT: dolichyl-diphosphooligosaccharide-protein glycosyltransferase (25797749); ALG1: beta-1,4-mannosyltransferase (25795163); GCS1: mannosyl-oligosaccharide glucosidase (25793447); DPM3: dolichol-phosphate mannosyltransferase subunit 3 (25799030), beta-1,4-N-acetylglucosaminyltransferase (25793326). The green box represents a specific gene or enzyme in *Trichoderma Reesei* and does not indicate up-regulation or down-regulation of the gene. DEGs in fatty acid degradation pathway: 4.2.1.17: enoyl-CoA hydratase (25798760); 2.3.1.9: acetyl-CoA C-acetyltransferase (25788734/25797542); 5.3.3.8: Delta3-Delta2-enoyl-CoA isomerase (25795747); 1.1.1.1: alcohol dehydrogenase, propanol-preferring (25793381); 1.3.8.7: acyl-CoA dehydrogenase (25788983). DEGs in biosynthesis of unsaturated fatty acid pathway: ① 2.3.1.199: fatty acid elongase 3 (25798319/25794969);②1.1.1.62/1.1.1.330: 17 beta-estradiol 17-dehydrogenase/very-long-chain 3-oxoacyl-CoA reductase (25797972/25798045/ 25792427); ③ 4.2.1.134: very-long-chain (3R)-3-hydroxyacyl-CoA dehydratase (25796723); ④ 1.3.1.93: very-long-chain enoyl-CoA reductase (25792467); ⑤ 2.3.1.16: acetyl-CoA acyltransferase 1 (25798206/25786723). DEGs in fatty acid biosynthesis pathway: 6.4.1.2: acetyl-CoA carboxylase (25798001); 2.3.1.86: fatty acid synthase subunit beta, fungi type (25788772); 2.3.1.179: 3-oxoacyl-[acyl-carrier-protein] synthase II (25798380); 1.1.1.100: 3-oxoacyl-[acyl-carrier protein] reductase (25792427); 6.2.1.3: long-chain acyl-CoA synthetase (25798208).

Supplementary Figure 10 | Fatty acid metabolic pathway(fatty acid degradation(tre00071), biosynthesis of unsaturated fatty acid (tre01040) and fatty acid biosynthesis pathway (tre00061)). The green box represents a specific gene or enzyme in *Trichoderma Reesei* and does not indicate up-regulation or down-regulation of the gene.

Supplementary Figure 11 | Starch and sucrose metabolism pathway (tre00500). DEGs in starch and sucrose metabolism pathway: 3.2.1.39: glucan endo-1,3-beta-D-glucosidase (25786810); 3.2.1.21: beta-glucosidase (25797680); 3.2.1.28: alpha,alpha-trehalase (25794082); 5.4.2.2: phosphoglucomutase (25798750). The green box represents a specific gene or enzyme in *Trichoderma Reesei* and does not indicate up-regulation or down-regulation of the gene.

Supplementary Figure 12 | Amino sugar and nucleotide sugar metabolism (tre00520). DEGs in Amino sugar and nucleotide sugar metabolism pathway: 3.2.1.14: chitinase (25795194/25786774/25786843); 3.2.1.52: beta-N-acetylhexosaminidase (25786802); 5.4.2.3: phosphoacetylglucosamine mutase (25787876); 3.2.1.165: exo-1,4-beta-D-glucosaminidase (25794739); 2.4.1.16: chitin synthase (25798917/25797926/25797171); 2.3.1.4: glucosamine-phosphate N-acetyltransferase (25797997); 5.4.2.2: phosphoglucomutase (25798750). The green box represents a specific gene or enzyme in *Trichoderma Reesei* and does not indicate up-regulation or down-regulation of the gene.

REFERENCES

Agustí-Brisach, C., and Armengol, J. (2012). Effects of temperature, pH and water potential on mycelial growth, sporulation and chlamydospore production in culture of *cylindrocarpon* spp. associated with black foot of grapevines. *Phytopathol. Mediterr.* 51, 37–50. doi: 10.1080/00103624.2012.675394

Allen, G. R., Baker, B. R., Dornbush, A. C., Joseph, J. P., Kissman, H. M., and Weiss, M. J. (1960). The preparation of various esters of certain L-Phenylalanine derivatives and their antifungal and antibacterial activity. *J. Med. Pharm. Chem.* 2, 391–413. doi: 10.1021/jm50011a004

Alonso-Monge, R., Navarro-Garcia, F., Roman, E., Negredo, A. I., Eisman, B., Nombela, C., et al. (2003). The hog1 mitogen-activated protein kinase is essential in the oxidative stress response and chlamydospore formation in candida albicans. *Eukaryot. Cell* 2, 351–361. doi: 10.1128/ec.2.2.351-361.2003

Aragona, M., and Valente, M. T. (2015). Genetic transformation of the tomato pathogen *Pyrenochaeta lycopersici* allowed gene knockout using a split-marker approach. *Curr. Genet.* 61, 211–220. doi: 10.1007/s00294-014-0461-y

Aronova, S., Wedaman, K., Anderson, S., Yates, J., and Powers, T. (2007). Probing the membrane environment of the TOR kinases reveals functional interactions between TORC1, actin, and membrane trafficking in *Saccharomyces cerevisiae*. *Mol. Biol. Cell* 18, 2779–2794. doi: 10.1091/mbc.e07-03-0274

Arst, H. N. (1976). Integrator gene in *Aspergillus nidulans*. *Nature* 262, 231–234. doi: 10.1038/262231a0

Baek, J. M., and Kenerley, C. M. (1998). The arg2 gene of *Trichoderma virens*: cloning and development of a homologous transformation system. *Fungal Genet. Biol.* 23, 34–44. doi: 10.1006/fgbi.1997.1025

Bailey, C. R., Penfold, H. A., and Arst, H. N. (1979). Cis-dominant regulatory mutations affecting the expression of GABA permease in *Aspergillus nidulans*. *Mol. Gen. Genet.* 169, 79–83. doi: 10.1007/BF00267548

Bayram, O., and Braus, G. H. (2012). Coordination of secondary metabolism and development in fungi: the velvet family of regulatory proteins. *FEMS Microbiol. Rev.* 36, 1–24. doi: 10.1111/j.1574-6976.2011.00285.x

Beck, T., and Hall, M. N. (1999). The TOR signalling pathway controls nuclear localization of nutrient-regulated transcription factors. *Nature* 402, 689–692. doi: 10.1038/45287

Bederson, B. B., Grosjean, J., and Meyer, J. (2004). Toolkit design for interactive structured graphics. *IEEE T. Softw. Eng.* 30, 535–546. doi: 10.1109/TSE.2004.44

Biles, C. L., Holland, M., Ulloa-Godinez, M., Clason, D., and Corgan, J. (1992). Pyrenochaeta terrestris microsclerotia production and pigmentation on onion roots. *HortScience* 27, 1213–1216. doi: 10.1016/0304-4238(92)90035-B

Böttcher, B., Pöllath, C., Staib, P., Hube, B., and Brunke, S. (2016). Candida species rewired hyphae developmental programs for chlamydospore formation. *Front. Microbiol.* 7:1697. doi: 10.3389/fmicb.2016.01697

Calvo, A. M., and Cary, J. W. (2015). Association of fungal secondary metabolism and sclerotial biology. *Front. Microbiol.* 6:62. doi: 10.3389/fmicb.2015.00062

Cardenas, M. E., Cutler, N. S., Lorenz, M. C., Di Como, C. J., and Heitman, J. (1999). The TOR signaling cascade regulates gene expression in response to nutrients. *Genes Dev.* 13, 3271–3279. doi: 10.1101/gad.13.24.3271

Cary, J. W., Harris-Coward, P. Y., Ehrlich, K. C., Mack, B. M., Kale, S. P., Larey, C., et al. (2012). NsdC and NsdD affect *Aspergillus flavus* morphogenesis and aflatoxin production. *Eukaryot. Cell* 11, 1104–1111. doi: 10.1128/EC.00069-12

Catlett, N. L., Lee, B., Yoder, O. C., and Turgeon, B. G. (2003). Split-marker recombination for efficient targeted deletion of fungal genes. *Fung. Genet. Rep.* 50, 0. doi: 10.4148/1941-4765.1150

Chang, P. K., Bennett, J. W., and Cotty, P. J. (2002). Association of aflatoxin biosynthesis and sclerotial development in *Aspergillus parasiticus*. *Mycopathologia* 153, 41–48. doi: 10.1023/a:1015211915310

Chao, Q., Gao, Z. F., Zhang, D., Zhao, B. G., Dong, F. Q., Fu, C. X., et al. (2019). The developmental dynamics of the *Populus stem transcriptome*. *Plant Biotechnol. J.* 17, 206–219. doi: 10.1111/pbi.12958

Colotelo, N. (1974). A scanning electron microscope study of developing sclerotia of sclerotinia sclerotiorum. *Can. J. Bot.* 52, 1127–1130. doi: 10.1139/b74-143

Cui, K., Zhao, Y., He, L., Ding, J., Li, B., Mu, W., et al. (2020). Comparison of transcriptome profiles of the fungus *Botrytis cinerea* and insect pest Bradysia odoriphaga in response to benzothiazole. *Front. Microbiol.* 11:1043. doi: 10.3389/fmicb.2020.01043

Davis, M. S., Solbiati, J., and Cronan, J. E. (2000). Overproduction of acetyl-coa carboxylase activity increases the rate of fatty acid biosynthesis in *escherichia coli*. *J. Biol. Chem.* 275, 28593–28598. doi: 10.1074/jbc.M004756200

Deng, J. J., Huang, W. Q., Li, Z. W., Lu, D. L., Zhang, Y., and Luo, X. C. (2018). Biocontrol activity of recombinant aspartic protease from *Trichoderma harzianum* against pathogenic fungi. *Enzyme Microb. Technol.* 112, 35–42. doi: 10.1016/j.enzmictec.2018.02.002

Ding, Z. J., Qi, Y. X., Zeng, F. Y., Peng, J., Xie, Y. X., and Zhang, X. (2019). Amino sugar metabolism pathway involved in chlamydospore formation of fusarium oxysporum f. sp. cubense. *Mycosystema* 38, 485–493. doi: 10.13346/j.mycosystema.180279

Duran, R. M., Cary, J. W., and Calvo, A. M. (2007). Production of cyclopiazonic acid, aflatrem, and aflatoxin by *Aspergillus flavus* is regulated by veA, a gene necessary for sclerotial formation. *Appl. Microbiol. Biotechnol.* 73, 1158–1168. doi: 10.1007/s00253-006-0581-5

Eisman, B., Alonso-Monge, R., Román, E., Arana, D., Nombela, C., and Pla, J. (2006). The Cek1 and Hog1 mitogen-activated protein kinases play complementary roles in cell wall biogenesis and chlamydospore formation in the fungal pathogen *Candida albicans*. *Eukaryot. Cell* 5, 347–358. doi: 10.1128/EC.5.2.347-358.2006

Fiore, A., Dall'osto, L., Fraser, P. D., Bassi, R., and Giuliano, G. (2006). Elucidation of the beta-carotene hydroxylation pathway in *Arabidopsis thaliana*. *FEBS Lett.* 580, 4718–4722. doi: 10.1016/j.febslet.2006.07.055

Georgiou, C. D., Patsoukis, N., Papapostolou, I., and Zervoudakis, G. (2006). Sclerotial metamorphosis in filamentous fungi is induced by oxidative stress. *Integr. Comp. Biol.* 46, 691–712. doi: 10.1093/icb/icj034

Giosa, D., Felice, M. R., Lawrence, T. J., Gulati, M., Scordino, F., Giuffrè, L., et al. (2017). Whole RNA-sequencing and transcriptome assembly of candida albicans and candida africana under chlamydospore-inducing conditions. *Genome Biol. Evol.* 9, 1971–1977. doi: 10.1093/gbe/evx143

Griffin, G. J. (1976). Roles of low pH, carbon and inorganic nitrogen source use in chlamydospore formation by *Fusarium solani*. *Can. J. Microbiol.* 22, 1381–1389. doi: 10.1139/m76-202

Guo, L., Zhao, G., Xu, J. R., Kistler, H. C., Gao, L., and Ma, L. J. (2016). Compartmentalized gene regulatory network of the pathogenic fungus *Fusarium graminearum*. *New Phytol.* 211, 527–541. doi: 10.1111/nph.13912

Haile, K., and Dekebo, A. (2013). Chemical composition and antimicrobial activity of haramaya propolis (Bee Glue), ethiopia. *Int. J. Pharmaceut. Sci. Res.* 4, 734–740. doi: 10.13040/IJPSR.0975-8232.4(2).734-40

Harman, G. E. (2006). Overview of mechanisms and uses of *Trichoderma* spp. *Phytopathology* 96, 190–194. doi: 10.1094/PHYTO-96-0190

Henry, C., Fontaine, T., Heddergott, C., Robinet, P., Aimanianda, V., Beau, R., et al. (2016). Biosynthesis of cell wall mannan in the conidium and the mycelium of *Aspergillus fumigatus*. *Cell Microbiol.* 18, 1881–1891. doi: 10.1111/cmi.12665

Hernández-Oñate, M. A., Esquivel-Naranjo, E. U., Mendoza-Mendoza, A., Stewart, A., and Herrera-Estrella, A. H. (2012). An injury-response mechanism conserved across kingdoms determines entry of the fungus *Trichoderma atroviride* into development. *Proc. Natl. Acad. Sci. U.S.A.* 109, 14918–14923. doi: 10.1073/pnas.1209396109

Hsu, S. C. (1973). Chlamydospore formation in fusarium in sterile salt solutions. *Phytopathology* 63:597. doi: 10.1094/Phyto-63-597

Jackson, M. A., and Jaronski, S. T. (2009). Production of microsclerotia of the fungal entomopathogen Metarhizium anisopliae and their potential for use as a biocontrol agent for soil-inhabiting insects. *Mycol. Res.* 113, 842–850. doi: 10.1016/j.mycres.2009.03.004

Jamieson, D. J. (1998). Oxidative stress responses of the yeast *Saccharomyces cerevisiae*. *Yeast* 14, 1511–1527. doi: 10.1002/(SICI)1097-0061(199812)14:16<1511::AID-YEA356>3.0.CO;2-S

Janik, A., Niewiadomska, M., Perlińska-Lenart, U., Lenart, J., Kołakowski, D., Skorupińska-Tudek, K., et al. (2019). Inhibition of dephosphorylation of dolichyl diphosphate alters the synthesis of dolichol and hinders protein N-Glycosylation and morphological transitions in *Candida albicans*. *Int. J. Mol. Sci.* 20:5067. doi: 10.3390/ijms20205067

Jiang, S. S., Yin, Y. P., Song, Z. Y., Zhou, G. L., and Wang, Z. K. (2014). RacA and Cdc42 regulate polarized growth and microsclerotium formation in the dimorphic fungus *Nomuraea rileyi*. *Res. Microbiol.* 165, 233–242. doi: 10.1016/j.resmic.2014.03.003

Jirjis, R. I., and Moore, D. (1976). Involvement of glycogen in morphogenesis of coprinus cinereus. *J. Gen. Microbiol.* 95, 348–352. doi: 10.1099/00221287-95-2-348

Kamada, Y., Sekito, T., and Ohsumi, Y. (2004). Autophagy in yeast: a TOR mediated response to nutrient starvation. *Curr. Top. Microbiol. Immunol.* 279, 73–84. doi: 10.1007/978-3-642-18930-2_5

Kim, J., and DellaPenna, D. (2006). Defining the primary route for lutein synthesis in plants: the role of Arabidopsis carotenoid beta-ring hydroxylase CYP97A3. *Proc. Natl. Acad. Sci. U.S.A.* 103, 3474–3479. doi: 10.1073/pnas

Kim, J., Smith, J. J., Tian, L., and Dellapenna, D. (2009). The evolution and function of carotenoid hydroxylases in Arabidopsis. *Plant Cell Physiol.* 50, 463–479. doi: 10.1093/pcp/pcp005

Kim, S. H., and Vujanovic, V. (2016). Relationship between mycoparasites lifestyles and biocontrol behaviors against *Fusarium* spp. and mycotoxins production. *Appl. Microbiol. Biot.* 100, 5257–5272. doi: 10.1007/s00253-016-7539-z

Kresnowati, M. T., van Winden, W. A., Gulik, W. M., and Heijnen, J. J. (2008). Energetic and metabolic transient response of Saccharomyces cerevisiae to benzoic acid. *FEBS J.* 275, 5527–5541. doi: 10.1111/j.1742-4658.2008.06667.x

Kubicek, C. P., Herrera-Estrella, A., Seidl-Seiboth, V., Martinez, D. A., Druzhinina, I. S., Thon, M., et al. (2011). Comparative genome sequence analysis underscores mycoparasitism as the ancestral life style of Trichoderma. *Genome Biol.* 12:R40. doi: 10.1186/gb-2011-12-4-r40

Kües, U. (2000). Life history and developmental processes in the basidiomycete *Coprinus cinereus*. *Microbiol. Mol. Biol. R* 64, 316–353. doi: 10.1128/mmbr.64.2.316-353.2000

Kushiro, T., Okamoto, M., Nakabayashi, K., Yamagishi, K., Kitamura, S., Asami, T., et al. (2004). The Arabidopsis cytochrome P450 CYP707A encodes ABA 8'-hydroxylases: key enzymes in ABA catabolism. *EMBO J.* 23, 1647–1656. doi: 10.1038/sj.emboj.7600121

Kuziora, M. A., Chalmers, J. H. Jr., Douglas, M. G., Hitzeman, R. A., Mattick, J. S., and Wakil, S. J. (1983). Molecular cloning of fatty acid synthetase genes from Saccharomyces cerevisiae. *J. Biol. Chem.* 258, 11648–11653. doi: 10.1016/S0021-9258(17)44277-3

Langfelder, P., and Horvath, S. (2008). WGCNA: an R package for weighted correlation network analysis. *BMC Bioinform.* 9:559. doi: 10.1186/1471-2105-9-559

Li, D., Tang, Y., Lin, J., and Cai, W. (2017). Methods for genetic transformation of filamentous fungi. *Microb. Cell Fact.* 16:168. doi: 10.1186/s12934-017-0785-7

Li, L., Ma, M., Huang, R., Qu, Q., Li, G., Zhou, J., et al. (2012). Induction of chlamydospore formation in fusarium by cyclic lipopeptide antibiotics from *Bacillus subtilis* C2. *J. Chem. Ecol.* 38, 966–974. doi: 10.1007/s10886-012-0171-1

Li, Y. Q., Song, K., Li, Y. C., and Chen, J. (2016). Statistical culture-based strategies to enhance chlamydospore production by *Trichoderma harzianum* SH2303 in liquid fermentation. *J. Zhejiang Univ. Sci. B* 17, 619–627. doi: 10.1631/jzus.B1500226

Liu, H., Zheng, Z., Wang, P., Gong, G., Wang, L., and Zhao, G. (2013). Morphological changes induced by class III chitin synthase gene silencing could enhance penicillin production of *Penicillium chrysogenum*. *Appl. Microbiol. Biot.* 97, 3363–3372. doi: 10.1007/s00253-012-4581-3

Livak, K. J., and Schmittgen, T. D. (2001). Analysis of relative gene expression data using real-time quantitative PCR and the 2(-Delta C(T)) method. *Methods* 25, 402–408. doi: 10.1006/meth.2001.1262

Malmierca, M. G., Cardoza, R. E., Alexander, N. J., McCormick, S. P., Hermosa, R., Monte, E., et al. (2012). Involvement of *Trichoderma trichothecenes* in the biocontrol activity and induction of plant defense-related genes. *Appl. Environ. Microb.* 78, 4856–4868. doi: 10.1128/AEM.00385-12

Martin, S. W., Douglas, L. M., and Konopka, J. B. (2005). Cell cycle dynamics and quorum sensing in *Candida albicans* chlamydospores are distinct from budding and hyphal growth. *Eukaryot. Cell* 4, 1191–1202. doi: 10.1128/EC.4.7.1191-1202.2005

Marzluf, G. A. (1997). Genetic regulation of nitrogen metabolism in the fungi. *Microbiol. Mol. Biol. R* 61, 17–32. doi: 10.1042/CS20110631

Ment, D., Gindin, G., Glazer, I., Perl, S., Elad, D., and Samish, M. (2010). The effect of temperature and relative humidity on the formation of Metarhizium anisopliae chlamydospores in tick eggs. *Fungal Biol.* 114, 49–56. doi: 10.1016/j.mycres.2009.10.005

Mesak, L. R., and Dahl, M. K. (2000). Purification and enzymatic characterization of pgcm: a beta-phosphoglucomutase and glucose-1-phosphate phosphodismutase of bacillus subtilis. *Arch. Microbiol.* 174, 256–264. doi: 10.1007/s002030000200

Miller, S. E., Spurlock, B. O., and Michaels, G. E. (1974). Electron microscopy of young *Candida albicans* chlamydospores. *J. Bacteriol.* 119, 992–999. doi: 10.1128/JB.119.3.992-999.1974

Mishra, D. S., Prajapati, C. R., Gupta, A. K., and Sharma, S. D. (2012). Relative bio-efficacy and shelf-life of mycelial fragments, conidia and chlamydospores of *Trichoderma harzianum*. *Int. J. Plant Res.* 25, 225–232. doi: 10.1111/j.1469-8137.2012.04124.x

Morán-Diez, M. E., Trushina, N., Lamdan, N. L., Rosenfelder, L., Mukherjee, P. K., Kenerley, C. M., et al. (2015). Host-specific transcriptomic pattern of *Trichoderma virens* during interaction with maize or tomato roots. *BMC Genomics* 16:8. doi: 10.1186/s12864-014-1208-3

Mukherjee, P. K., and Kenerley, C. M. (2010). Regulation of morphogenesis and biocontrol properties in *Trichoderma virens* by a VELVET protein. *Vel1. Appl. Environ. Microbiol.* 76, 2345–2352. doi: 10.1128/AEM.02391-09

Murtagh, F., and Legendre, P. (2014). Ward's hierarchical agglomerative clustering method: which algorithms implement ward's criterion? *J. Classif.* 31, 274–295. doi: 10.1007/s00357-014-9161-z

Navarathna, D. H., Pathirana, R. U., Lionakis, M. S., Nickerson, K. W., and Roberts, D. D. (2016). Candida albicans ISW2 regulates chlamydospore suspensor cell formation and virulence in vivo in a mouse model of disseminated candidiasis. *PLoS One* 11:e0164449. doi: 10.1371/journal.pone.0164449

Nguyen, L. N., Trofa, D., and Nosanchuk, J. D. (2009). Fatty acid synthase impacts the pathobiology of *Candida parapsilosis* in vitro and during mammalian infection. *PLoS One* 4:e8421. doi: 10.1371/journal.pone.0008421

Nobile, C. J., Bruno, V. M., Richard, M. L., Davis, D. A., and Mitchell, A. P. (2004). Genetic control of chlamydospore formation in candida albicans. *Microbiology* 149, 3629–3637. doi: 10.1099/mic.0.26640-0

Palavecino, M. D., Correa-García, S. R., and Bermúdez-Moretti, M. (2015). Genes of different catabolic pathways are coordinately regulated by Dal81 in Saccharomyces cerevisiae. *J. Amino Acids* 2015:484702. doi: 10.1155/2015/484702

Palige, K., Linde, J., Martin, R., Böttcher, B., Citiulo, F., Sullivan, D. J., et al. (2013). Global transcriptome sequencing identifies chlamydospore specific markers in *Candida albicans* and *Candida dubliniensis*. *PLoS One* 8:e61940. doi: 10.1371/journal.pone.0061940

Pérez-García, L. A., Csonka, K., Flores-Carreón, A., Estrada-Mata, E., Mellado-Mojica, E., Németh, T., et al. (2016). Role of protein glycosylation in *Candida parapsilosis* cell wall integrity and host interaction. *Front. Microbiol.* 7:306. doi: 10.3389/fmicb.2016.00306

Pertea, M., Pertea, G. M., Antonescu, C. M., Chang, T. C., Mendell, J. T., and Salzberg, S. L. (2015). StringTie enables improved reconstruction of a transcriptome from RNA-seq reads. *Nat. Biotechnol.* 33, 290–295. doi: 10.1038/nbt.3122

Picot, A., Atanasova-Pénichon, V., Pons, S., Marchegay, G., Barreau, C., Pinson-Gadais, L., et al. (2013). Maize kernel antioxidants and their potential involvement in *Fusarium* ear rot resistance. *J. Agric. Food Chem.* 61, 3389–3395. doi: 10.1021/jf4006033

Podobnik, B., Stojan, J., Lah, L., Krasevec, N., Seliskar, M., Rizner, T. L., et al. (2008). CYP53A15 of *Cochliobolus lunatus*, a target for natural antifungal compounds. *J. Med Chem.* 51, 3480–3486. doi: 10.1021/jm800030e

Ramos, F., Guezzar, M., Grenson, M., and Wiame, J. M. (1985). Mutations affecting the enzymes involved in the utilization of 4-aminobutyric acid as nitrogen source by the yeast *Saccharomyces cerevisiae*. *Eur. J. Biochem.* 149, 401–404. doi: 10.1111/j.1432-1033.1985.tb08939.x

Ray, W. J. Jr., and Roscelli, G. A. (1964). A kinetic study of the phosphoglucomutase pathway. *J. Biol. Chem.* 239, 1228–1236. doi: 10.1016/S0168-9525(01)02409-X

Riquelme Medina, I., and Lubovac-Pilav, Z. (2016). Gene co-expression network analysis for identifying modules and functionally enriched pathways in type 1 diabetes. *PLoS One* 11:e0156006. doi: 10.1371/journal.pone

Roncero, C., Sanchez-Diaz, A., and Valdivieso, M. H. (2016). "9 Chitin synthesis and fungal cell morphogenesis," in *Biochemistry and Molecular Biology*, ed H. Dirk (Berlin: Springer International Publishing), 167–190.

Ruhland, B. R., and Reniere, M. L. (2019). Sense and sensor ability: redox-responsive regulators in *Listeria monocytogenes*. *Curr. Opin. Microbiol.* 47, 20–25. doi: 10.1016/j.mib.2018.10.006

Saito, S., Hirai, N., Matsumoto, C., Ohigashi, H., Ohta, D., Sakata, K., et al. (2004). Arabidopsis CYP707As encode (+)-abscisic acid 8'-hydroxylase, a key enzyme in the oxidative catabolism of abscisic acid. *Plant Physiol.* 134, 1439–1449. doi: 10.1104/pp.103.037614

Sangappillai, V., and Nadarajah, K. (2020). Fatty acid synthase beta dehydratase in the lipid biosynthesis pathway is required for conidiogenesis, pigmentation and appressorium formation in magnaporthe oryzae S6. *Int. J. Mol. Sci.* 21:7224. doi: 10.3390/ijms21197224

Seki, H., Ohyama, K., Sawai, S., Mizutani, M., Ohnishi, T., Sudo, H., et al. (2008). Licorice beta-amyrin 11-oxidase, a cytochrome P450 with a key role in the biosynthesis of the triterpene sweetener glycyrrhizin. *Proc. Natl. Acad. Sci. U.S.A.* 105, 14204–14209. doi: 10.1073/pnas.0803876105

Seong, K. Y., Zhao, X., Xu, J. R., Güldener, U., and Kistler, H. C. (2008). Conidial germination in the filamentous fungus *Fusarium graminearum*. *Fungal Genet. Biol.* 45, 389–399. doi: 10.1016/j.fgb.2007.09.002

Shin, H. Y., Lee, J. Y., Kim, E. J., and Kim, S. W. (2011). Rapid quantification of lipids in *Acremonium chrysogenum* using Oil red O. *Curr. Microbiol.* 62, 1023–1027. doi: 10.1007/s00284-010-9818-8

Shu, C., Zhao, M., Anderson, J. P., Garg, G., Singh, K. B., Zheng, W., et al. (2019). Transcriptome analysis reveals molecular mechanisms of sclerotial development in the rice sheath blight pathogen *Rhizoctonia solani* AG1-IA. *Funct. Integr. Genomic* 19, 743–758. doi: 10.1007/s10142-019-00677-0

Son, H., Min, K., Lee, J., Choi, G. J., Kim, J. C., and Lee, Y. W. (2012). Differential roles of pyruvate decarboxylase in aerial and embedded mycelia of the ascomycete *Gibberella zeae*. *FEMS Microbiol. Lett.* 329, 123–130. doi: 10.1111/ j.1574-6968.2012.02511.x

Song, Z. (2018). Fungal microsclerotia development: essential prerequisites, influencing factors, and molecular mechanism. *Appl. Microbiol. Biot.* 102, 9873–9880. doi: 10.1007/s00253-018-9400-z

Song, Z. Y., Jiang, W., Yin, Y. P., and Wang, Z. K. (2016). Polarity proteins Mrcdc24 and Mrbem1 required for hypha growth and microsclerotia formation in *Metarhizium rileyi*. *Biocontrol Sci. Technol.* 26, 1–29. doi: 10.1080/09583157

Sonneborn, A., Bockmühl, D. P., and Ernst, J. F. (1999). Chlamydospore formation in *Candida albicans* requires the Efg1p morphogenetic regulator. *Infect. Immun.* 67, 5514–5517. doi: 10.1128/IAI.67.10.5514-5517.1999

Staib, P., and Morschhäuser, J. (2005). Differential expression of the NRG1 repressor controls species-specific regulation of chlamydospore development in *Candida albicans* and *Candida dubliniensis*. *Mol. Microbiol.* 55, 637–652. doi: 10.1111/j.1365-2958.2004.04414.x

Steindorff, A. S., Ramada, M. H., Coelho, A. S., Miller, R. N., Pappas, G. J. Jr., Ulhoa, C. J., et al. (2014). Identification of mycoparasitism-related genes against the phytopathogen Sclerotinia sclerotiorum through transcriptome and expression profile analysis in *Trichoderma harzianum*. *BMC Genomics* 15:204. doi: 10.1186/1471-2164-15-204

Sun, Z. B., Zhang, J., Sun, M. H., and Li, S. D. (2019). Identification of genes related to chlamydospore formation in Clonostachys rosea 67-1. *MicrobiologyOpen* 8:e00624. doi: 10.1002/mbo3.624

Takahashi-Ando, N., Ochiai, N., Tokai, T., Ohsato, S., Nishiuchi, T., Yoshida, M., et al. (2008). A screening system for inhibitors of trichothecene biosynthesis: hydroxylation of trichodiene as a target. *Biotechnol. Lett.* 30, 1055–1059. doi: 10.1007/s10529-008-9649-x

Tong, L. (2013). Structure and function of biotin-dependent carboxylases. *Cell. Mol. Life Sci.* 70, 863–891. doi: 10.1007/s00018-012-1096-0

Tzelepis, G. D., Melin, P., Jensen, D. F., Stenlid, J., and Karlsson, M. (2012). Functional analysis of glycoside hydrolase family 18 and 20 genes in neurospora crassa. *Fungal Genet. Biol.* 49, 717–730. doi: 10.1016/j.fgb.2012

Umezawa, T., Okamoto, M., Kushiro, T., Nambara, E., Oono, Y., Seki, M., et al. (2006). CYP707A3, a major ABA 8'-hydroxylase involved in dehydration and rehydration response in *Arabidopsis thaliana*. *Plant J.* 46, 171–182. doi: 10.1111/j.1365-313X.2006.02683.x

Vos, C. M., De Cremer, K., Cammue, B. P., and De Coninck, B. (2015). The toolbox of *Trichoderma* spp. in the biocontrol of *Botrytis cinerea* disease. *Mol. Plant Pathol.* 16, 400–412. doi: 10.1111/mpp.12189

Wakil, S. J., Titchener, E. B., and Gibson, D. M. (1958). Evidence for the participation of biotin in the enzymic synthesis of fatty acids. *Biochim. Biophys. Acta* 29, 225–226. doi: 10.1016/0006-3002(58)90177-x

Whelan, W. L., Delga, J. M., Wadsworth, E., Walsh, T. J., Kwon-Chung, K. J., Calderone, R., et al. (1990). Isolation and characterization of cell surface mutants of *Candida albicans*. *Infect. Immun.* 58, 1552–1557. doi: 10.1128/IAI.58.6.1552-1557.1990

Willetts, H. J., and Bullock, S. (1992). Developmental biology of sclerotia. *Mycol. Res.* 96, 801–816. doi: 10.1016/S0953-7562(09)81027-7

Yang, X. Y., Li, M., Zhang, L., Pang, L., Sun, Q., and Jiang, X. L. (2015). Transcriptome analysis of *Trichoderma harzianum* TH-33 in chlamydospore formation. *Chinese J. Biol. Control* 31, 85–95. doi: 10.16409/j.cnki.2095-039x.2015.01.013

Yin, Y. P., Huang, S., Song, Z. Y., and Wang, Z. K. (2012). Microsclerotia artificial inductions of Nomuraea rileyi CQNr01. *Sci. Agric. Sin.* 45, 4801–4807. doi: 10.3864/j.issn.0578-1752.2012.23.006

Yu, H. Y., Seo, J. A., Kim, J. E., Han, K. H., Shim, W. B., Yun, S. H., et al. (2008). Functional analyses of heterotrimeric G protein G alpha and G beta subunits in *Gibberella zeae*. *Microbiology* 154, 392–401. doi: 10.1099/mic.0.2007/012260-0

Yuan, M., Huang, Y., Jia, Z., Ge, W., Zhang, L., Zhao, Q., et al. (2019). Whole RNA-sequencing and gene expression analysis of *Trichoderma harzianum* Tr-92 under chlamydospore-producing condition. *Genes Genom.* 41, 689–699. doi: 10.1007/s13258-019-00812-y

Zhang, J. J., Huang, Y. L., Hong, M., Jia, Z. H., Shi, Y. M., and Song, S. S. (2015). Optimization of liquid fermentation conditions for production of Trichoderma Tr-92 chlamydospores. *Plant Protect.* 41, 25–29. doi: 10.1002/pip.2543

Zhang, J. J., Xu, W., Huang, Y. L., Huang, Y. Y., and Jia, Z. H. (2017). Storage ability and application effect of Trichoderma Tr-92 chlamydospores wettable powder. *J. Plant Protect.* 44, 495–500. doi: 10.13802/j.cnki.zwbhxb.2017

Zou, Y., Wen, C. J., Tang, G. Q., and Li, N. (2006). Effects of several factors on the chlamydospores production of Trichoderma aureoviride T-33. *Microbiology* 33, 43–47. doi: 10.1016/S1872-2032(06)60050-4

Conflict of Interest: The authors declare that the research was conducted in the absence of any commercial or financial relationships that could be construed as a potential conflict of interest.

frontiers in Microbiology

ORIGINAL RESEARCH
published: 11 June 2021
doi: 10.3389/fmicb.2021.640931

Comparative Proteomic Analysis of *Histoplasma capsulatum* Yeast and Mycelium Reveals Differential Metabolic Shifts and Cell Wall Remodeling Processes in the Different Morphotypes

*Marcos Abreu Almeida[1], Lilian Cristiane Baeza[2], Rodrigo Almeida-Paes[1], Alexandre Melo Bailão[3], Clayton Luiz Borges[3], Allan Jefferson Guimarães[4], Célia Maria Almeida Soares[3] and Rosely Maria Zancopé-Oliveira[1]**

[1] Instituto Nacional de Infectologia Evandro Chagas, Fundação Oswaldo Cruz, Rio de Janeiro, Brazil, [2] Centro de Ciências Médicas e Farmacêuticas, Universidade Estadual do Oeste do Paraná, Cascavel, Brazil, [3] Instituto de Ciências Biológicas, Universidade Federal de Goiás, Goiânia, Brazil, [4] Departamento de Microbiologia e Parasitologia, Universidade Federal Fluminense, Niterói, Brazil

OPEN ACCESS

Edited by:
Hui Wu,
East China University of Science and Technology, China

Reviewed by:
Rosana Puccia,
Federal University of São Paulo, Brazil
Yinhua Lu,
Shanghai Normal University, China

***Correspondence:**
Rosely Maria Zancopé-Oliveira
rosely.zancope@ini.fiocruz.br

Specialty section:
This article was submitted to Microbial Physiology and Metabolism, a section of the journal Frontiers in Microbiology

Received: *12 December 2020*
Accepted: *10 May 2021*
Published: *11 June 2021*

Citation:
Almeida MA, Baeza LC, Almeida-Paes R, Bailão AM, Borges CL, Guimarães AJ, Soares CMA and Zancopé-Oliveira RM (2021) Comparative Proteomic Analysis of Histoplasma capsulatum Yeast and Mycelium Reveals Differential Metabolic Shifts and Cell Wall Remodeling Processes in the Different Morphotypes. Front. Microbiol. 12:640931. doi: 10.3389/fmicb.2021.640931

Histoplasma capsulatum is a thermally dimorphic fungus distributed worldwide, but with the highest incidence in the Americas within specific geographic areas, such as the Mississippi River Valley and regions in Latin America. This fungus is the etiologic agent of histoplasmosis, an important life-threatening systemic mycosis. Dimorphism is an important feature for fungal survival in different environments and is related to the virulence of *H. capsulatum*, and essential to the establishment of infection. Proteomic profiles have made important contributions to the knowledge of metabolism and pathogenicity in several biological models. However, *H. capsulatum* proteome studies have been underexplored. In the present study, we report the first proteomic comparison between the mycelium and the yeast cells of *H. capsulatum*. Liquid chromatography coupled to mass spectrometry was used to evaluate the proteomic profile of the two phases of *H. capsulatum* growth, mycelium, and yeast. In summary, 214 and 225 proteins were only detected/or preferentially abundant in mycelium or yeast cells, respectively. In mycelium, enzymes related to the glycolytic pathway and to the alcoholic fermentation occurred in greater abundance, suggesting a higher use of anaerobic pathways for energy production. In yeast cells, proteins related to the tricarboxylic acid cycle and response to temperature stress were in high abundance. Proteins related to oxidative stress response or involved with cell wall metabolism were identified with differential abundance in both conditions. Proteomic data validation was performed by enzymatic activity determination, Western blot assays, or immunofluorescence microscopy. These experiments corroborated, directly or indirectly, the abundance of isocitrate lyase, 2-methylcitrate synthase, catalase B, and mannosyl-oligosaccharide-1,2-alpha-mannosidase in the mycelium and heat shock protein (HSP) 30, HSP60, glucosamine-fructose-6-phosphate aminotransferase,

glucosamine-6-phosphate deaminase, and *N*-acetylglucosamine-phosphate mutase in yeast cells. The proteomic profile-associated functional classification analyses of proteins provided new and interesting information regarding the differences in metabolism between the two distinct growth forms of *H. capsulatum*.

Keywords: *Histoplasma capsulatum,* dimorphism, yeast, mycelium, proteomic analysis, fungal biology

INTRODUCTION

The thermally dimorphic fungus *Histoplasma capsulatum* is the etiological agent of histoplasmosis, an important systemic mycosis with a worldwide distribution that is endemic to areas of the United States of America, especially in the Ohio and Mississippi River Valleys, and most Latin American countries (Armstrong et al., 2018; Sahaza et al., 2020). Histoplasmosis causes a wide spectrum of clinical forms, from an asymptomatic, self-limited illness to a progressive disseminated and often fatal disease. The prognosis of infection depends fundamentally on three factors: the host immune response, the inhaled fungal inoculum, and the specific virulence characteristics of the infecting strain (Deepe and Buesing, 2012). *Histoplasma capsulatum* grows as a hyphal form in the environment at room temperature. Infection is initiated upon host inhalation of fungal propagules (conidia and/or hyphal fragments), which are then taken up by macrophages and other phagocytic cells. Once inside the mammalian host, the filamentous phase quickly differentiates into the yeast form, which can evade phagocytic killing and is able to replicate in phagosome milieu (Woods, 2003).

The morphological shift of *H. capsulatum* from mycelium to yeast cells, or vice versa, can also be reproduced *in vitro* by switching the fungal growth temperature from 25 to 37°C or the other direction (Maresca et al., 1994). *Histoplasma* differentiation into yeast-like cells is required for virulence, since *Histoplasma* strains genetically or chemically prevented from transitioning into yeasts are attenuated (Medoff et al., 1986; Nguyen and Sil, 2008). Several genes have been reported to play roles in phase transition regulation, such as the hybrid histidine kinase (Drk1) and four transcriptional regulators (Ryp1, Ryp2, Ryp3, and Ryp4) (Nemecek et al., 2006; Nguyen and Sil, 2008; Webster and Sil, 2008; Beyhan et al., 2013). Edwards et al. (2013) proposed that many genes specifically expressed by the yeast phase worked as virulence factors and greatly contributed to *Histoplasma* pathogenesis. Nonetheless, studies on the characterizations of several biological aspects of *H. capsulatum* continue to be applied to mycelium and/or yeast cells grown in the laboratory in order to identify genes and their products connected to virulence and explore their role during pathogenesis (Edwards and Rappleye, 2011; Mihu and Nosanchuk, 2012; Woods, 2016).

There are several *H. capsulatum* cell surface components identified that are related to virulence/pathogenicity: α-1,3-glucan synthase (Edwards et al., 2011), Yps3 (Bohse and Woods, 2007), Hsp60 (Habich et al., 2006), Histone-2B (Nosanchuk et al., 2003), and melanin (Nosanchuk et al., 2002). Additionally, iron acquisition by *H. capsulatum* (Hwang et al., 2008; Hilty et al., 2011) and several fungal secretory proteins (Deepe and Gibbons, 2001; Guimarães et al., 2008; Edwards and Rappleye, 2011) are also associated with pathogenesis.

Fungal cell walls are dynamic and essential structures for cell viability, morphogenesis, and pathogenesis. The cell wall composition greatly influences the fungus' ecology, and this composition is highly regulated in response to environmental conditions and imposed stress conditions (Gow et al., 2017). Glucose, mannose, and galactose are the most abundant monosaccharides found in the *H. capsulatum* cell wall under both morphologies. The saccharide concentrations vary according to the culture medium composition, environmental conditions, and the extraction method used (Domer et al., 1967; Kanetsuna et al., 1974). Glucans are glucose polymers that have a glycoside bond that differs in mycelium and yeast cells. The α- and β-glucans present in the cell walls of these morphological forms have different biological roles. While β-1,3-glucan is an antigenic molecule and can be recognized by innate immunity cell through dectin-1 and is involved in the modulation of the host immune response (Gorocica et al., 2009), the α-1,3-glucan present on yeasts can inhibit the recognition of the fungal cell and facilitate fungal immune escape (Rappleye et al., 2007).

Despite the importance of morphology transition in *H. capsulatum*, there is a lack of proteomic quantitative comparisons between mycelium and yeast cells of this fungus. Thus, in this present study, proteomic strategies were used in order to identify molecular differences between the two *H. capsulatum* morphologies. We believe that the obtained data will be helpful in the determination of metabolic and molecular aspects preferentially used by mycelial and yeast cells, and the data provide new information that is helpful for understanding facets of the morphological transition.

MATERIALS AND METHODS

Microorganism and Culture Conditions

Histoplasma capsulatum G217B (ATCC 26032) was used throughout this study. The cells were cultured in Ham's F12 medium supplemented with cystine (8.4 mg/L), HEPES (6 g/L), glutamic acid (1 g/L), and glucose (18.2 g/L), pH 7.5, at 36°C and 25°C, to yield yeast and mycelial phases, respectively.

Preparation of Protein Extracts

Cultures were carried out in 50 ml of Ham's F12 medium, with an initial density of 1×10^8cells/ml, under agitation (150x rpm), at 36°C (72 h) or 25°C (96 h), for the yeast and mycelial phases, respectively. After the incubation times, cells were harvested by centrifugation at 10,000 × *g* for 15 min at

4°C, followed by three washes with phosphate-buffered saline (PBS; 1.4 mM KH_2PO_4, 8 mM Na_2HPO_4, 140 mM NaCl, 2.7 mM KCl; pH 7.2). Then, the cells were suspended in extraction buffer (20 mM Tris-HCl pH 8.8; 2 mM $CaCl_2$) containing a mixture of nuclease and protease inhibitors (GE Healthcare, Uppsala, Sweden). This mixture was distributed in tubes containing an equal volume of cell pellet and glass beads (0.5 mm, BioSpec Products), and the suspension was processed in a bead beater (BioSpec, Bartlesville, OK, United States) apparatus with five cycles of 30 s, with intervals of 1 min on ice. The supernatant was collected by centrifugation at 10,000 × *g* for 15 min at 4°C, and the protein concentrations were determined by Bradford assay using bovine serum albumin (BSA, Sigma-Aldrich Steinheim, Germany) as a standard (Bradford, 1976). The profile of the protein extracts (20 μg) obtained was evaluated by sodium dodecyl sulfate-polyacrylamide gel electrophoresis (SDS-PAGE) on 12% polyacrylamide gels (Laemmli, 1970).

Digestion of Protein Extracts for Mass Spectrometry

Protein enzymatic digestion was processed according to the protocol described by Murad et al. (2011). Of the protein from each sample, 150 μg was added to 50 mM ammonium bicarbonate buffer, pH 8.5, and RapiGESTTM SF (0.2% v/v) (Waters, Milford, MA, United States), and incubated at 80°C for 15 min. Disulfide bonds were reduced by incubation with 100 mM dithiothreitol (DTT) (GE Healthcare, Piscataway, NJ, United States) at 60°C for 30 min, and then alkylation was performed by incubation with 300 mM iodoacetamide (GE Healthcare, Piscataway, NJ, United States) at room temperature in the dark for 30 min. Trypsin digestion was performed overnight at 37°C through the addition of 30 μl of a 0.05 -μg/μl trypsin solution (Promega, Madison, WI, United States). Digestion was stopped with the addition of 30 μl of 5% trifluoroacetic acid (v/v), followed by incubation at 37°C for 90 min. The samples were centrifuged, and supernatants were dried in a speed vacuum. The peptides were suspended in a solution containing 20 mM ammonium formate and 150 fmol/μl of Rabbit Phosphorylase B (PHB; Waters, Manchester, United Kingdom) as an internal standard.

Proteomic Analysis by NanoUPLC-MS^E

The tryptic peptides were separated by Ultra Performance Liquid Chromatography according to Pigosso et al. (2017). Peptides from each sample (1,660 ng) were injected to the nanoACQUITYTM UPLC system (Waters, Manchester, United Kingdom). The first dimension chromatography included a 5-μm NanoEaseTM BEH130 C18, 300 μm × 50 mm column (Waters, Milford, MA, United States). The bound peptides were separated into five fractions eluting at 11.4, 14.7, 17.4, 25.7, and 50% (v/v) acetonitrile/0.1% (v/v) formic acid gradient with a flow rate of 2,000 μl/min. In-line, eluted fractions were trapped in 5-μm Symmetry C18, 180 μm × 20 mm column (Waters, Milford, MA, United States). Second, dimension chromatography was carried out with a 1.7-μm NanoEaseTM BEH130 C18, 100 μm × 100 mm analytical column (Waters, Milford, MA, United States). All analyses were performed with nanoelectrospray ionization in the positive ion mode nanoESI(+) with a NanoLockSpray source. The double charged [(M + 2H)2 + = 785.8426] precursor ion [Glu]1-Fibrinopeptide B (GluFib) (Sigma, St. Louis, United States) at 200 fmol/μl solution was delivered through the reference sprayer of the NanoLockSpray source, and the MS/MS fragment ions of GluFib were used to obtain the final instrument calibration. Data-independent scanning (MSE) experiments were performed with a SynaptTM G1 HDMSTM System mass spectrometer (Waters, Manchester, United Kingdom) with a hybrid quadrupole/time-of-flight. The radiofrequency applied to the quadrupole mass analyzer was adjusted, such that the ions from m/z 50 to 2,000 were efficiently transmitted. Moreover, the spectrometer was automatically programmed to switch between low collision energy MS (3 eV) and elevated collision energies MS^E (12–40 eV). The transfer collision cell was adjusted to 1 eV with a scan time of 1.0 s, both in low and high energies, to give a minimum of 10 points for both conditions above 10% of peak capacity. The time-of-flight (TOF) analyzer was operated in mode "V" reflection. Runs were performed in triplicates for each sample.

Raw Data Processing and Analysis

Raw files were analyzed together using the ProteinLynx Global Server software version 3.0.2 (PLGS) (Waters, Manchester, United Kingdom). The protein identifications and quantitative packaging were generated using specific algorithms (Silva et al., 2005, 2006), and search was performed against an *H. capsulatum*-specific database[1]. The ProteinLynx Global server v.3.0.2 (PLGS) with Expression E informatics v.3.0.2 was used for proper spectral processing, database searching conditions, and quantitative comparisons. The mathematic model used to calculate the ratios is part of the expression algorithm inside the PLGS from Waters Corporation (Geromanos et al., 2009). The identified proteins are organized by the expression algorithm into a statistically significant list corresponding to induced and reduced regulation ratios between yeast and mycelium phases. The software shows the expression analysis statistics as the induced proteins with a probability of upregulation of 0.95 or more and also the reduced proteins with a probability of 0.05 or less. A value of 1.00 indicates that the cluster is definitely upregulated; a value of 0.00 indicates that the cluster is definitively downregulated. PLGS uses the following strategy to peptide identification: first, only completely cleaved tryptic peptides are used for identification (PepFrag1). The second pass of the database algorithm (PepFrag2) is designed to identify peptide modifications and non-specific cleavage products to proteins that were positively identified in the first pass. The parameters for protein identification were as follows: (i) the detection of at least two fragment ions per peptide, (ii) five fragments per protein, (iii) the determination of at least one peptide per protein, (iv) maximum protein mass (600 kDa), (v) one missed cleavage site was allowed for trypsin, (vi) carbamidomethylation of cysteine was a fixed modification, (vii) methionine oxidation and phosphoryl STY as a variable modification, (viii) and a maximum 4% false-positive discovery

[1]http://www.ncbi.nlm.nih.gov/bioproject/20041

rate, in at least two out of three technical replicate injections. Correct and reversed sequences databases were used to estimate false-positive rates (FPR). Proteins identified with low accuracy were excluded; on the other hand, proteins with one or more peptides were admitted, in at least two replicates. For the analysis of protein quantification levels, the observed intensity measurements were normalized with a protein that showed a variance coefficient of 0.05 and that was detected in all replicates (accession number: HCAG_07031). A 50%-fold change (Baeza et al., 2017) was used as a cutoff to determine the differentially abundant proteins in the yeast and mycelial forms of the fungus. The mass spectrometry proteomics data have been deposited in the PRIDE partner repository for the ProteomeXchange Consortium with the data set identifier: PXD022623. Proteins were functionally classified using Uniprot[2] and KEGG[3] databases. The annotation of non-characterized proteins was performed by homology from proteins present in the NCBI[4]. Experiment dynamic range, the peptide parts per million error (ppm) and peptide detection type using the softwares such as MassPivot v1.0.1. and Spotfire v8.0. Microsoft Excel 2013 (Microsoft, United States) was also used for table manipulations. Heat maps generated by the MultiExperiment Viewer software V.4.9[5]. Thereafter, the proteomic data were further validated through the experiments described below.

Ethanol Quantification Assay

Protein extracts were obtained from 0.5 g of normalized dry weight cells from each morphology as described above. The ethanol concentrations in extracts were determined using an enzymatic detection kit according to the manufacturer's instructions (UV-test for ethanol, RBiopharm, Darmstadt, Germany). The ethanol quantification was performed in triplicate.

Western Blot Analysis

Proteins from yeast and mycelial phases of *H. capsulatum* were separated by SDS-PAGE, as described above, and transferred to 0.2-μm nitrocellulose membranes (Bio-Rad, Germany). The membranes were blocked at room temperature for 1 h PBS containing 5% (w/v) non-fat skim milk and supplemented with 0.2% Tween 20 (pH 7.2) (T-PBS). Then, the membranes were washed three times with T-PBS (5 min per wash). Next, the membranes were incubated overnight at 4°C with antibodies diluted in T-PBS: polyclonal antibody anti-HSP30 [1/500 (v/v)] (protein molecular mass 27.6 kDa), monoclonal antibody (mAb) anti-HSP60 [1/1,000 (v/v)] (protein molecular mass 61.8 kDa), or mAb anti-catalase [1/100 (v/v)] (protein molecular mass 57.3 kDa). A commercial polyclonal antibody (Abcam Plc, Cambridge, United Kingdom) anti-β-tubulin [1.0 mg/ml] [1/5,000 (v/v)] (molecular mass of 55.0 kDa), was used as a loading control. This step was followed by three washes of 5 min in T-PBS. The membranes were incubated with the appropriate conjugated secondary antibody, either a horseradish-peroxidase conjugated anti-rabbit IgG (Jackson ImmunoResearch, United States) or anti-mouse IgG (Jackson ImmunoResearch, United States), at 0.16 μg/ml. Finally, the Western blots were developed with SuperSignal West Dura Chemiluminescent substrate (Pierce, Rockford, IL, United States). The X-ray films were exposed and developed according to the manufacturer's instructions (Kodak, Rochester, NY, United States).

[2]https://www.uniprot.org/proteomes/

[3]https://www.genome.jp/kegg/pathway.html

[4]https://www.ncbi.nlm.nih.gov/

[5]mev.tm4.org/

Isocitrate Lyase Activity

In this assay, 50 μg of protein extracts from mycelial and yeast cells were used. The isocitrate lyase activity was determined by measuring the glyoxylate formation as its phenylhydrazone derivative as described (Ebel et al., 2006). The product formation was followed by measuring the absorbance at 324 nm using an extinction coefficient of 16.8 mM^{-1} cm^{-1} in a reaction mixture containing 2 mM threo-D,L-isocitrate (Sigma Aldrich), 2 mM $MgCl_2$, 10 mM phenylhydrazine HCl (Sigma Aldrich), 2 mM dithiothreitol, and 50 mM potassium phosphate at pH 7.0. Specific activity was determined as the amount of enzyme required to form 1 μmol of glyoxylate-phenylhydrazone per min per mg of total protein. Enzyme activity was performed in three biologically independent replicates.

Methylcitrate Synthase Activity Measurement

The determination of methylcitrate synthase activity is based on the nitrothiophenolate (2-mercapto-5-nitrobenzoate dianion) formation during the reaction of 5,5'-ditiobis-(2-nitrobenzoate) (DTNB) with CoASH, which is released during the condensation of oxaloacetate with propionyl-CoA, as described (Brock and Buckel, 2004). A standard curve of DTT (Dithiothreitol), using concentrations ranging from 1 to 25 mM, was used as a control, as it exerted an analogous function to the CoASH group during reaction with 1 mM DTNB. The reaction final volume was adjusted to 150 μl with 50 mM Tris-HCl pH 8.0 and spectrophotometric measurements performed at 412 nm. For the assay, 5 μg of either crude protein extract was used, 1 mM DTNB, 0.2 mM propionyl-CoA, and the final reaction volume adjusted to 150 μl with Tris-HCl pH 8.0 at 50 mM. The assay was started by the addition of 1 mM oxaloacetate and monitored at 412 nm. The experiment was performed in triplicate. One unit of activity (U) was defined as the release of 1 μmol CoASH per milligram of protein per minute per ml.

Immunofluorescence Microscopy

Differences in the cell wall constitutions of both phases of *H. capsulatum* were evaluated by determining the binding profiles of lectins such as concanavalin A (ConA) against mannosylated residues, wheat germ agglutinin (WGA) to chitoligomers, and Dectin-Fc against β-1,3-glucan by fluorescence microscopy. Uvitex 2B fluorescent dye was used for determining total chitin in fungal cell walls. Briefly, after the cultivation of yeast and mycelial phase cells of *H. capsulatum* as described previously, cells were washed three times in PBS, and 10^6 cells were fixed

with 4% paraformaldehyde overnight at –20°C. After, the cells were blocked with 1% BSA in PBS for 1 h. Then the analyses were carried out in two different systems: (i) Cells were incubated with Con A-FITC at a final concentration of 10 μg/ml and WGA-Alexa 546 at a final concentration of 1 μg/ml for 1 h, in an orbital shaker, in the dark at room temperature. (ii) Cells were incubated with Dectin-Fc at a final concentration of 5 μg/ml and WGA-Alexa 546 at a final concentration of 1 μg/ml for 1 h, under shaking, in the dark, at room temperature. A subsequent incubation with 2 μg/ml of goat anti-mouse IgG-Alexa 488 for 1 h was performed. Chitin in the cell wall was visualized by incubating the cells with a 5-mg/ml solution of Uvitex 2B in PBS for 15 min, at room temperature. Cells were washed three times with PBS between incubations. The samples were visualized using a fluorescence microscope (Carl Zeiss MicroImaging, Inc.), with a magnification of 100X. The fluorescence intensity of Images was analyzed by Image J (NIH, Bethesda, MD, United States) and edited with Adobe Photoshop C5S (Adobe Systems Software). A minimum of 100 cells were measured and total intensities compared between yeast and mycelium phases.

Statistical Analyses

Statistical analyzes were performed using the GraphPad Prism 7.0. The Student's *t*-test was employed, and $p \leq 0.05$ was considered significant.

RESULTS

Protein Extracts

The electrophoretic profiles of the proteins extracts from the yeast and mycelium forms of *H. capsulatum* were qualitatively evaluated through SDS-PAGE. For both samples, proteins displayed molecular weights above 30 kDa (**Supplementary Figure 1**).

Evaluation of the Proteomic Data

From the analyses of the mycelium and yeast extracts by the nanoUPLC-MS^E, 54 and 57% of the peptides were obtained upon the first step of protein fragmentation, respectively, whereas 10% occurred in the second step for both. Totals of 14 and 13% of the total peptides were identified by the lost trypsin cleavage, respectively, whereas the fragmentation rate that occurred at the ionization source was 12% for both conditions (**Supplementary Figure 2**). False-positive rates were 0.77 and 1.12%, respectively. These data represented good quality, since identifications by PepFrag 1 and 2 correspond to more than 50%, whereas in source fragmentation and lost cleavages, the comprised values were lower than 20% each. Most of the peptides generated by the two samples (>90%) were detected within a 10-ppm error (**Supplementary Figure 3**). The dynamic range of peptide detection analysis (**Supplementary Figure 4**) indicated distribution of three orders of magnitude, and demonstrating high and low abundance proteins levels. The dynamic detection range data for both samples are in accordance with the literature, as the sigmoid pattern curve and the spiked standard of rabbit phosphorylase B (PHB) were displayed in a similar way within the two samples.

Differentially Abundant Proteins on Mycelial and Yeast *H. capsulatum* Morphologies

Proteins (387) were identified in the mycelial form extracts (**Supplementary Table 1**) in comparison with 440 proteins in the yeast form (**Supplementary Table 2**). Proteins (280) were commonly present in extracts of both morphologies of *H. capsulatum* (**Figure 1A**). Two hundred fourteen were more abundant in mycelium, and 335 were more abundant in *H. capsulatum* yeast cells ($p < 0.05$). The exclusively detected or differentially abundant proteins within each extract were categorized and grouped in accordance with the Functional Catalog (FunCat2), accessed in the MIPS database (Ruepp et al., 2004). The functional classification of proteins within both extracts is described in **Supplementary Tables 3**, **4**. Proteins related to metabolism are the most abundant in both yeast (21.3%) and mycelium (48.2%) forms. In the yeast phase, the next most prevalent protein types belonged to protein fate and degradation (13.2%), transcription (12.0%), and protein synthesis (11.4%) categories. For the mycelial morphotype after metabolism, the most common proteins belonged to energy (13.6%) and protein fate and degradation (7.3%) categories. Less than 20% of the analyzed proteins were not classified or had unknown functions (**Figure 1B**).

Glycolysis and Fermentation Are Favored Pathways in Mycelial *H. capsulatum* Cells

Glycolysis enzymes, such as hexokinase (HCAG_03661) and fructose-1,6-bisphosphate aldolase (HCAG_08789), were detected exclusively in mycelium. Besides detection in both morphologies, glucose-6-phosphate isomerase (HCAG_08202) and pyruvate kinase (HCAG_07781) were more abundant in the mycelium (**Supplementary Table 3**). Notably, the enzyme glycogen phosphorylase (HCAG_08447), which digests glycogen and provides glucose for glycolysis, accumulated in mycelium. Besides the detection of the fermentation enzyme alcohol dehydrogenases in both morphologies, six of them were exclusive at the mycelial extracts (HCAG_05959, HCAG_00576, HCAG_01578, HCAG_02317, HCAG_05083, and HCAG_06397), whereas only HCAG_08561 was more abundant in yeast. The comparison of abundance levels of enzymes related to glycolysis and fermentation in the mycelium and yeast forms of *H. capsulatum* are presented in **Figure 2A**.

In order to validate whether, in fact, fermentation occurs preferably in *H. capsulatum* mycelia, the capacity for ethanol production of both extracts was compared. Upon incubations, ethanol concentrations were determined to be almost five times higher in the mycelial extract than in the yeast extract ($p = 0.0006$), confirming the higher capacity of *H. capsulatum* mycelial cells to obtain energy through fermentative metabolism than yeasts (**Figure 2B**).

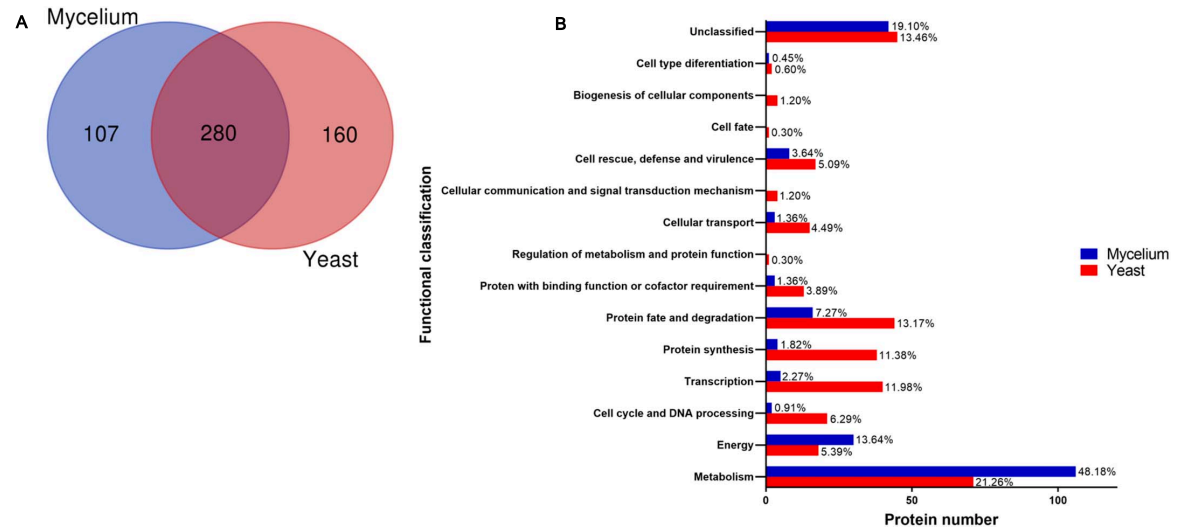

FIGURE 1 | Proteome profile of *Histoplasma capsulatum* mycelium and yeast forms. **(A)** Venn diagram presenting the total number of proteins identified in extracts from both *H. capsulatum* morphologies (http://bioinformatics.psb.ugent.be/webtools/Venn/); **(B)** Functional classification of *H. capsulatum* proteins obtained by NanoUPLC-MS^{E} analysis identified with preferential abundance in mycelium and yeast forms. The biological processes of the differentially expressed proteins in the isolates were obtained using the Uniprot (http://www.uniprot.org) and KEGG: Kyoto Encyclopedia of Genes and Genomes (www.genome.jp/kegg).

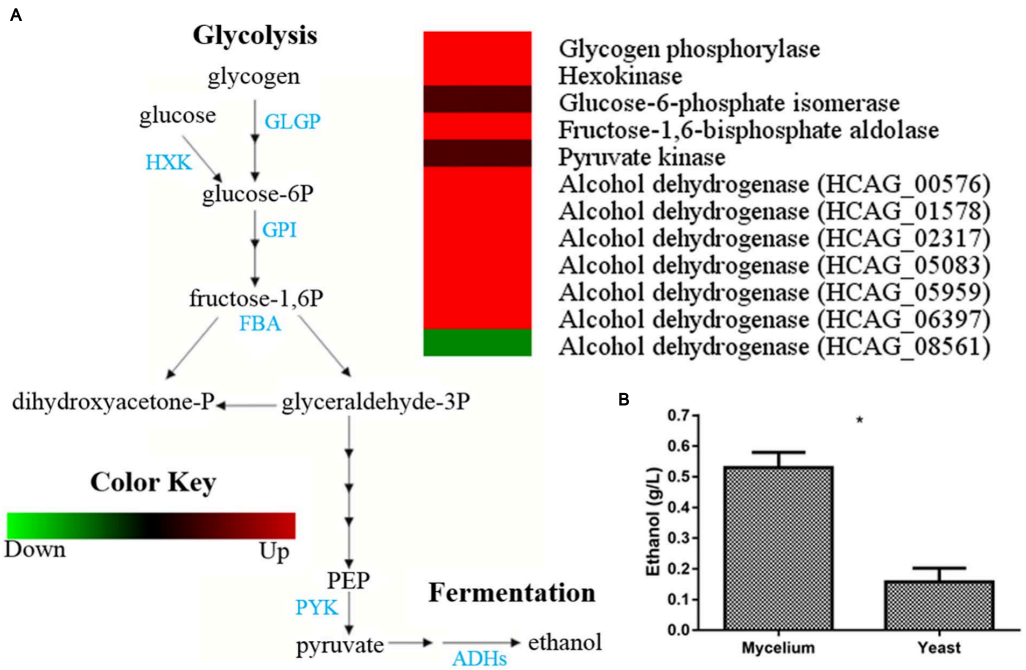

FIGURE 2 | Comparison of protein profiles related to glycolysis and fermentation in *H. capsulatum* mycelium and yeast forms. A 50%-fold change was used as a cutoff to determine the differentially abundant proteins in the fungus yeast and mycelial forms. The Multi Experiment Viewer software V.4.9 was used to group and compare the abundance data. **(A)** The diagram representing the glycolytic and fermentation metabolic pathways represents differentially abundant proteins in the mycelium and yeast phases. Changes in the abundance levels in the mycelium compared with the yeast are represented in the heat map. Experimental triplicate mean values are presented for the lowest abundance (green) and the *H. capsulatum* proteins highest abundance (red) in the mycelium form. Black indicates that no significant difference was observed. GLGP, glycogen phosphorylase; HXK, hexokinase; GPI, glucose-6-phosphate isomerase; FBA, fructose-1,6-bisphosphate aldolase; PYK, pyruvate kinase; ADHs, alcohol dehydrogenases. **(B)** Ethanol quantification assay. The ethanol concentration (g/L) was determined in *H. capsulatum* yeast and mycelial phase cells, upon growth in Hams F12 media for 72 h (36°C) and 96 h (25°C), respectively. The cells were disrupted in the bead beater, and the ethanol compound was quantified using an enzymatic detection kit (UV-test for ethanol, RBiopharm, Darmstadt, Germany). Data are expressed as the mean ± standard deviation of biological triplicates in independent experiments. *$p < 0.05$.

Pentose Phosphate Pathway and Stress Response Are Different in Mycelial and Yeast *H. capsulatum* Cells

Mass spectrometry detection of proteins suggests a preferential use of the pentose phosphate pathway by *H. capsulatum* mycelia (**Figure 3A**, left panel). The enzymes glucose-6-phosphate 1-dehydrogenase (HCAG_04329), 6-phosphogluconolactonase (HCAG_04762), and 6-phosphogluconate dehydrogenase (HCAG_05884) were more abundant in this morphology, indicating NADPH generation by mycelium. Since NADPH oxidases generate oxygen free radicals, we further evaluated the proteins involved in the oxidative stress response. Enzymes related to detoxification and response to oxidative stress were differentially expressed in either morphologies of *H. capsulatum*, as depicted in **Figure 3A** (right panel). Two superoxide dismutase (SODs, HCAG_00642, and HCAG_01543) and a catalase A (HCAG_05109) were identified exclusively in the mycelium proteome. In contrast, a catalase B (HCAG_08064), which was identified in both phases, was preferentially expressed in the mycelium form. A cytochrome *c* peroxidase (HCAG_08658) and thioredoxin reductase (HCAG_07019) were exclusively found in yeasts. Two other cytochrome *c* peroxidases (HCAG_07098 and HCAG_09319) were also detected in both phases, but more abundant in the yeast proteome. Other proteins related to the stress response were also differentially abundant in mycelial or yeast cells of *H. capsulatum* (**Figure 3B**). All heat shock proteins (HSPs) were exclusive or more abundant in yeast cells. The expression of catalase B, HSP60, and HSP30 in distinct phase extracts were further evaluated using a Western blot approach (**Figures 3C–E**, respectively), which demonstrated expression levels in agreement with the proteomic data. **Figure 3F** shows the β-tubulin control, with similar expression in both morphotypes.

Beta-Oxidation, Methylcitrate, and Glyoxylate Cycles Occur Preferentially in *H. capsulatum* Mycelia

Pathways involved in lipid utilization, such as beta-oxidation, methylcitrate, and glyoxylate cycles were more abundant in the *H. capsulatum* mycelial form, as demonstrated by proteomics (**Figure 4A**). The enzymes acetyl-CoA C-acyltransferase (HCAG_00780), enoyl-CoA hydratase (HCAG_02218), and acyl-CoA dehydrogenase (HCAG_08510) were identified exclusively in mycelia, and a second acyl-CoA dehydrogenase (HCAG_09978) was also more abundant in this form, indicating preferably lipid degradation and generation of acetyl-CoA and propionyl-CoA by this morphology. Regarding the glyoxalate cycle, the enzymatic activity of its key enzyme, an isocitrate lyase (HCAG_10962), was evaluated in both protein extracts, and a twofold increase ($p = 0.0002$) was detected in the mycelia (**Figure 4B**). A similar scenario was observed for enzymes related to the methylcitrate cycle, such as the methylcitrate synthase (HCAG_05090), an enzyme that catalyzes a key step of the pathway and, therefore, regulates cycle speed, whose activity was four times higher in the mycelial extract ($p = 0.0001$) (**Figure 4C**).

Amino Acid Metabolism Is Active and Distinct in *H. capsulatum* Mycelia and Yeast Phases

The main products generated by the amino acid group degradation and their fate on the tricarboxylic acid (TCA) cycle, as well as a heat map of the enzyme abundance levels in the mycelium extract, in comparison with the yeast extract are displayed in **Figure 5**. Seventy-two proteins in this category presented differential abundance among the two fungal morphologies. In general, proteins involved on the amino acid degradation that generate pyruvate precursors, such as alanine transaminase (HCAG_05679) and alanine-glyoxylate aminotransferase (HCAG_10952), were more abundant in yeast cells. Additionally, enzymes involved in the generation of oxaloacetate from aspartate, as the aspartyl transferases HCAG_03751, HCAG_06102, and HCAG_08678, and arginase (HCAG_00035), which generates α-ketoglutarate from arginine, were also more abundant in yeasts. In contrast, mycelial samples had a greater abundance of enzymes producing fumarate from tyrosine and phenylalanine, such as fumarylacetoacetase hydrolase (HCAG_02120) and homogentisate 1,2-dioxygenase (HCAG_05721), and those involved in the conversion of succinyl-CoA from branched amino acids, such as 2-oxoisovalerate dehydrogenase (HCAG_05761), methylmalonate-semialdehyde dehydrogenase (HCAG_06059), and branched-chain amino acid aminotransferase (HCAG_03302).

Tricarboxylic Acid Cycle and Oxidative Phosphorylation Are More Active in *H. capsulatum* Yeast Cells

Most TCA cycle enzymes were more abundant in the *H. capsulatum* yeast phase (**Figure 6**). A pyruvate dehydrogenase (HCAG_04294), which promotes the conversion of pyruvate into acetyl-CoA for the initiation of the TCA cycle, and aconitate hydratase (HCAG_05531) were exclusively found in the yeast proteome. Additionally, four other enzymes belonging to the TCA cycle were more abundant in the yeast form: alpha-ketoglutarate dehydrogenase (HCAG_01535), isocitrate dehydrogenase (HCAG_04093), succinate dehydrogenase (HCAG_06317), and succinyl-CoA ligase (HCAG_07697). In contrast, only two enzymes were predominant in mycelium: fumarate reductase (HCAG_03323) and isocitrate dehydrogenase (HCAG_04358). As for oxidative phosphorylation, proteins associated with the electron membrane transport and respiration were more abundant in yeast than the mycelial proteome (**Supplementary Tables 3**, **4**).

Differential Abundance of Enzymes Involved in the Cell Wall Synthesis Dictates Compositional Differences Between Mycelium and Yeast

Enzymes involved in the synthesis and/or degradation of *H. capsulatum* cell with differential abundance in mycelium

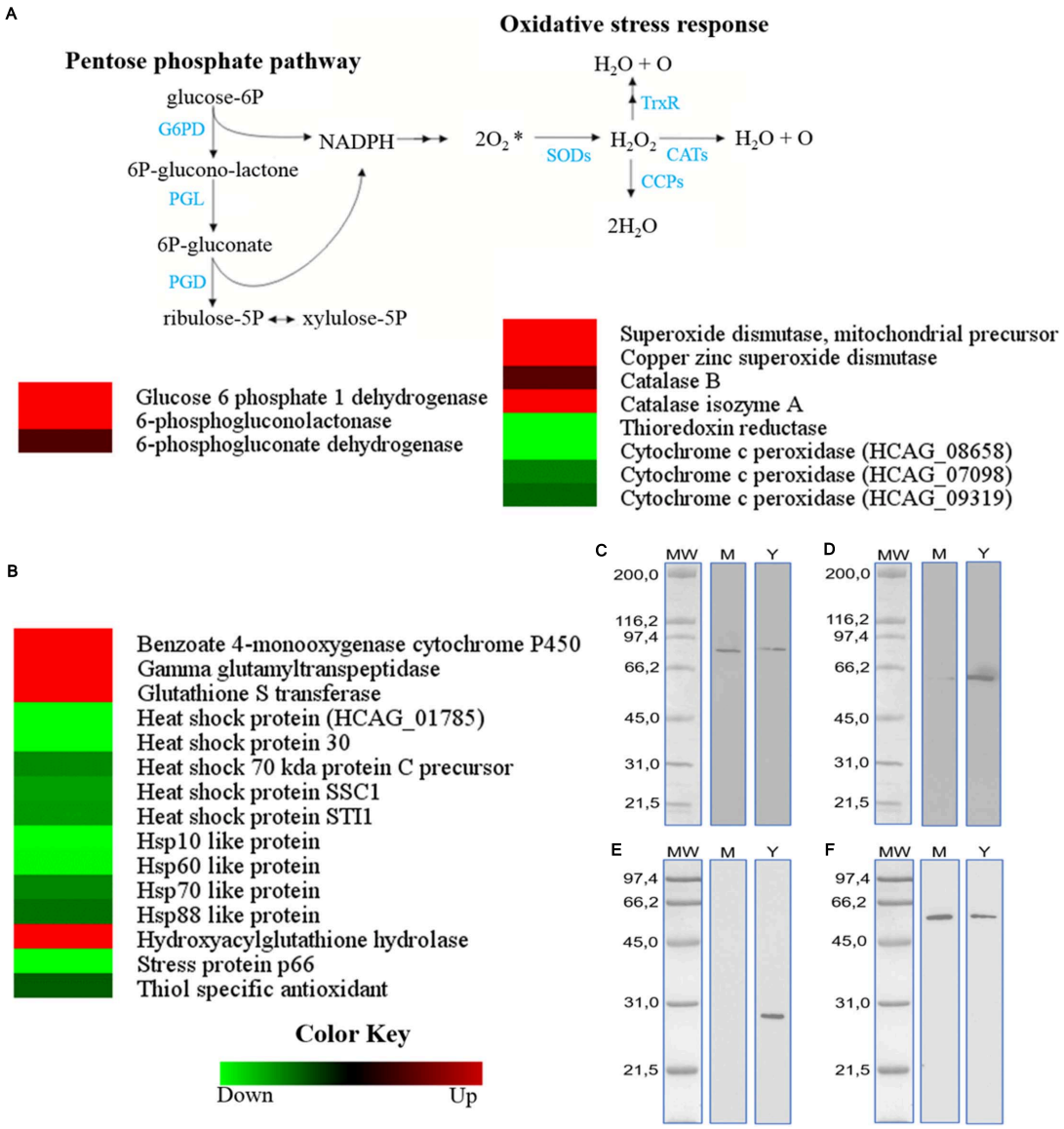

FIGURE 3 | Comparison of protein profiles related to pentose phosphate pathway and stress response in *H. capsulatum* mycelium and yeast forms. Dataset comparisons were carried out as cited in the **Figure 2** legend. **(A)** The diagram representing the pentose phosphate and oxidative stress response pathways represents differentially abundant proteins in the mycelium and yeast phases. **(B)** Comparison of protein profiles related to the stress response in mycelium and yeast forms of *H. capsulatum*. Changes in the abundance levels in the mycelium compared with the yeast are represented in the heat map. Experimental triplicate mean values are presented for the lowest (green) and the highest (red) abundance of *H. capsulatum* proteins in the mycelium form. Black indicates that no significant difference was observed. G6PD, glucose 6 phosphate 1 dehydrogenase; PGL, 6-phosphogluconolactonase; PGD, 6-phosphogluconate dehydrogenase; SODs, superoxide dismutases; TRxR, thioredoxin reductase; CATs, catalases; C, cytochrome *c* peroxidases. Confirmatory Western blot analysis of selected proteins detected in the *H. capsulatum* proteomic analyses. Protein extracts are shown after the reaction with antibodies against the following proteins: **(C)** catalase; **(D)** HSP60; **(E)** HSP30; **(F)** β-tubulin, as a loading control. The blots were incubated with goat anti-mouse IgG polyclonal or goat anti-rabbit IgG polyclonal antibodies coupled to peroxidase and developed with SuperSignal West Dura Chemiluminescent substrate (Pierce, Rockford, IL, United States). The X-ray films were developed using Kodak imaging films according to the manufacturer's instructions.

and yeast are shown in **Figure 7**. The enzymes glycan 1,3-beta glucosidase (HCAG_01828) and 1,3-beta glucanosyltransferase (HCAG_07210), which catalyze the conversion of β-1,3-glucan to glucose and the linkage of distinct β-1,3-glucan and polysaccharide fiber elongation, respectively, were identified exclusively in the yeast proteome. The high expression of both could lead to a rapid turnover and remodeling on the *H. capsulatum* cell wall.

Enzymes related to chitin production in *H. capsulatum,* such as glucosamine-fructose-6-phosphate aminotransferase (HCAG_04088), glucosamine-6-phosphate deaminase (HCAG_08152) and *N*-acetylglucosamine-phosphate mutase

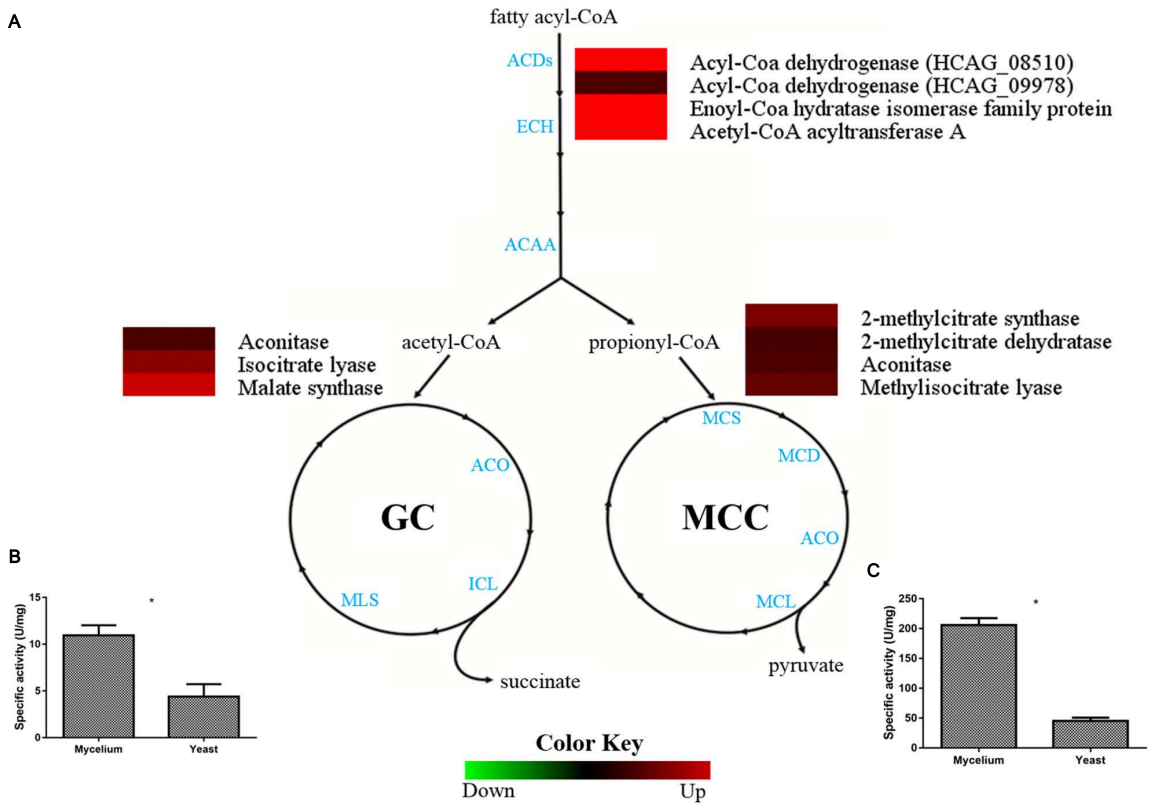

FIGURE 4 | Comparison of protein profiles related to beta-oxidation, methylcitrate, and glyoxylate cycles in *H. capsulatum* mycelium and yeast forms. Dataset comparisons were carried out as cited in the **Figure 2** legend. **(A)** The diagram representing the metabolic pathways of beta-oxidation, methylcitrate, and glyoxylate cycles represents differentially abundant proteins in the mycelium and yeast phases. Changes in the abundance levels in the mycelium compared with the yeast are represented in the heat map. Experimental triplicate mean values are presented for the lowest (green) and the highest (red) abundance of *H. capsulatum* proteins in the mycelium form. Black indicates that no significant difference was observed. ACDs, Acyl-Coa dehydrogenases; ECH, enoyl-Coa hydratase; ACAA, Acetyl-CoA acyltransferase; ACO, aconitase; ICL, isocitrate lyase; MLS, malate synthase; MCS, 2-methylcitrate synthase; MCD, 2-methylcitrate dehydratase; MCL, methylisocitrate lyase; **(B)** Isocitrate lyase (ICL) activity was determined by measuring glyoxylate formation as its phenylhydrazone derivative under the two conditions. The specific activity of ICL was determined as the amount of enzyme required to form 1 μmol of glyoxylate-phenylhydrazone per minute, per mg of total protein, and represented as U·mg-1. Errors bars represent standard deviation from three biological replicates. *$p < 0.05$. **(C)** Methylcitrate synthase measurement was determined in *H. capsulatum* yeast and mycelial phase cells, upon growth in Hams F12 media for 72 h (36°C) and 96°h (25°C), respectively. Activity was determined by nitrothiophenolate (2-mercapto-5-nitrobenzoate dianion) formation during the 5,5'-Dithiobis (2-nitrobenzoic acid) (DTNB) reaction with Coenzyme A, released during the condensation of oxaloacetate with propionyl-CoA.

(HCAG_00064), were also more abundant in the yeast form. In contrast, the enzyme nucleoside-diphosphate-sugar epimerase, which catalyzes the conversion of UDP-*N*-acetylgalactosamine into UDP-*N*-acetyl-D-glucosamine, was preferentially abundant in the mycelium phase, indicating the use of this substrate in the synthesis of chitin by this morphology. Enzymes related to mannose metabolism, such as mannosyl-oligosaccharide 1,2-alpha-mannosidase (HCAG_08449), and galactose metabolism, UDP-glucose 4-epimerase (HCAG_09614), were also more abundant in the *H. capsulatum* mycelium.

To validate the above findings, fluorescence microscopy targeting cell wall structures was performed with mycelium and yeast forms, and fluorescence levels were compared (**Figure 8**). Concanavalin A, which interacts with mannose residues, bound more intensely to the mycelial phase cell wall, displaying higher fluorescence intensity ($P < 0.0001$). WGA, a lectin with affinity for chitin oligomers, showed better binding to and higher fluorescence intensity with *H. capsulatum* yeast ($P < 0.0001$). Dectin-1-Fc, which recognizes β-1,3-glucan structures, did not produce statistically significant differences in binding when comparing mycelium and yeast fluorescence levels ($P = 0.7725$). Uvitex 2B was used to detect total cell wall chitin and delineate the cell wall dimensions, and fluorescence levels showed no difference when comparing both morphologies ($P = 0.0549$).

The enzyme tyrosinase (HCAG_04336), an enzyme directly related to the production of melanin, which is another important component of the *H. capsulatum* cell wall, was more abundant in the *H. capsulatum* mycelium form.

DISCUSSION

Dimorphism is one of the factors associated with fungal pathogenicity (Gauthier, 2017). The knowledge on the proteomic

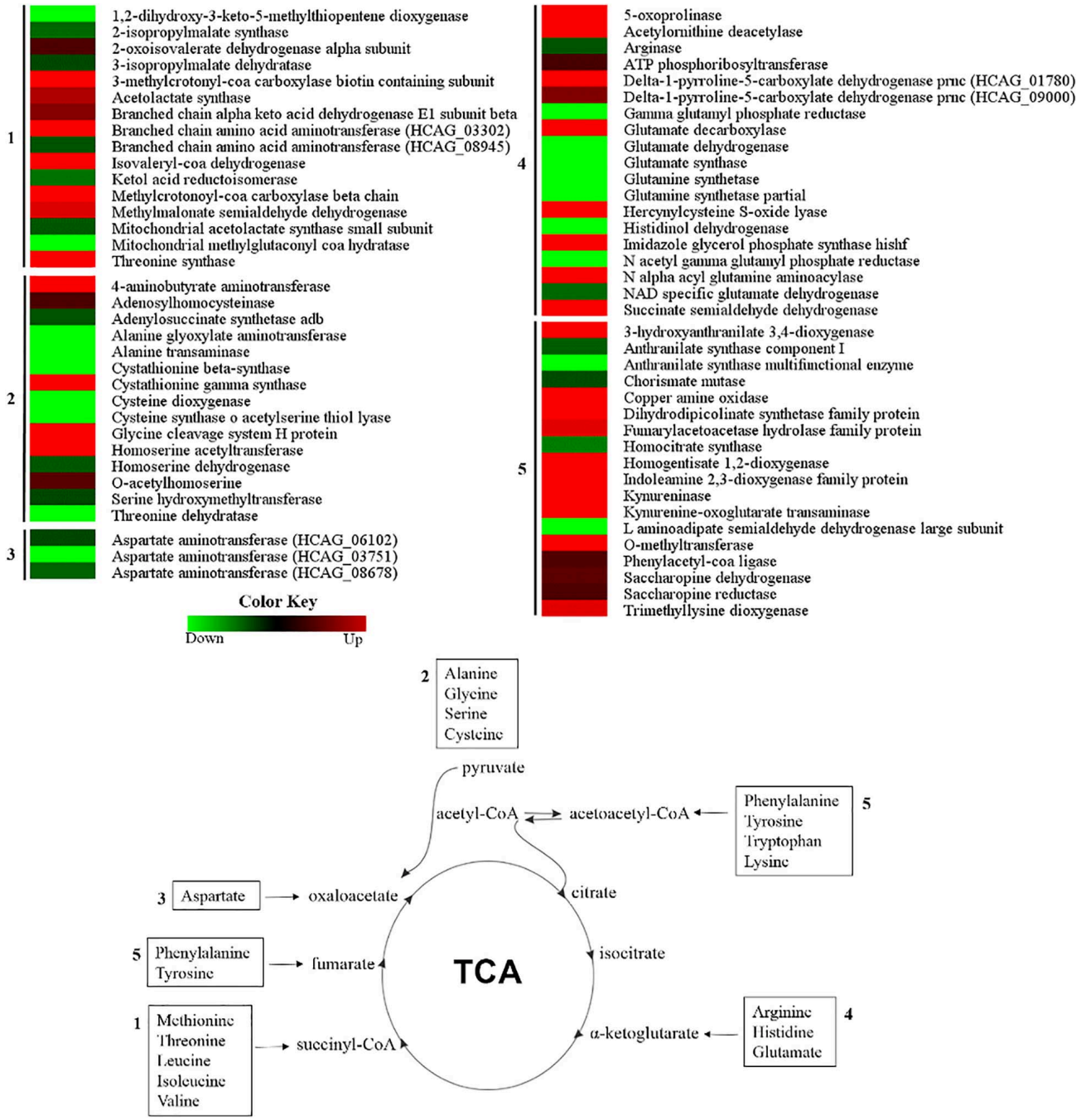

FIGURE 5 | Comparison of protein profiles related to amino acid metabolism in *H. capsulatum* mycelium and yeast forms. Dataset comparisons were carried out as cited in the **Figure 2** legend. Changes in the abundance levels in the mycelium compared with the yeast are represented in the heat map. Experimental triplicate mean values are presented for the lowest (green) and the highest (red) abundance of *H. capsulatum* proteins in the mycelium form. Black indicates that no significant difference was observed.

profile of both saprotrophic and parasitic forms of *H. capsulatum* is a way to understand its metabolism and to potentially reveal new strategies to be applied in the histoplasmosis management. This is the first study that has compared the proteomic profiles of the two morphologies of *H. capsulatum*. It demonstrates that proteins specifically expressed or differentially abundant in either phase are involved in distinct pathways, suggesting a metabolic change during dimorphism.

In our model, glycolysis and pyruvate generation occurs preferentially in mycelium, since pyruvate kinase was more abundant, and hexokinase was identified exclusively in the mycelial phase. An increase in enzymes involved in glycogen

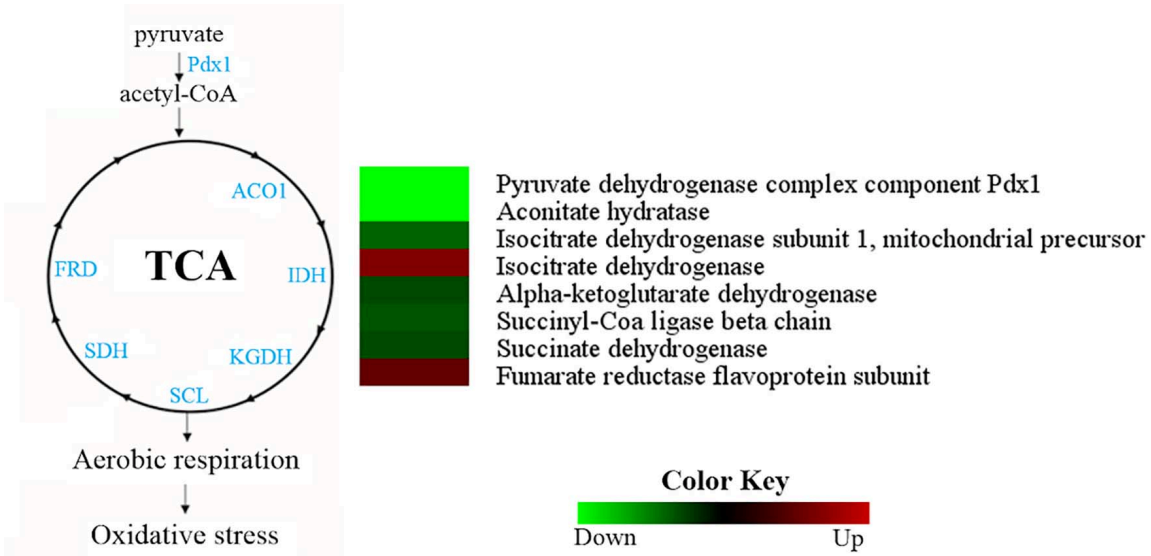

FIGURE 6 | Comparison of protein profiles related to tricarboxylic acid (TCA) cycle and oxidative phosphorylation in *H. capsulatum* mycelium and yeast forms. Dataset comparisons were carried out as cited in the **Figure 2** legend. The diagram representing the metabolic pathways of TCA cycle and oxidative phosphorylation represents differentially abundant proteins in the mycelium and yeast phases. Changes in the abundance levels in the mycelium compared with the yeast are represented in the heat map. Experimental triplicate mean values are presented for the lowest (green) and the highest (red) abundance of *H. capsulatum* proteins in the mycelium form. Black indicates that no significant difference was observed. Pdx1, pyruvate dehydrogenase; ACO1, aconitate hydratase; IDH, isocitrate dehydrogenase; KGDH, alpha-ketoglutarate dehydrogenase; SCL, succinyl-Coa ligase; SDH, succinate dehydrogenase; FRD, fumarate reductase.

metabolism, such as glycogen phosphorylase and glucose-6-phosphate isomerase, was detected in mycelium, which could explain a glucose supply to the glycolytic pathway. As a result, there is an increase in glucose-6-phosphate (G6P) and fructose-6-phosphate (F6P) derivatives, which could be used in other metabolic pathways. The pentose phosphate pathway is linked to glycolysis at G6P and glyceraldehyde 3-phosphate (G3P) levels. The G6P resultin from hexokinase or glycogen phosphorylase activities can be used in the pentose phosphate pathway, since the first enzyme in the pathway (glucose-6-phosphate 1-dehydrogenase) was also detected only in mycelium, as well as 6-phosphogluconolactonase. Consequently, the pentose phosphate pathway in this morphological phase of *H. capsulatum* was also increased, unlike in *Candida albicans* and *Paracoccidioides lutzii* models, in which these pathways were increased in yeast cells (Monteoliva et al., 2011; Rezende et al., 2011).

In the comparative *H. capsulatum* proteome, some alcohol dehydrogenases were exclusively identified in mycelium suggesting that *H. capsulatum* mycelium is capable of utilizing glucose anaerobic metabolism. Higher ethanol concentrations in mycelium confirmed that the alcoholic fermentation occurs preferably in the *H. capsulatum* mycelial phase, which is similar to processes in *Paracoccidioides brasiliensis* (Vaz, 2014) and *C. albicans* (Monteoliva et al., 2011). These studies differ from the *P. lutzii* proteome, where alcoholic fermentation occurs preferentially in the yeast form (Rezende et al., 2011).

In fungi, HSPs respond to various stimuli, such as pH changes, oxidative stress, and increased temperatures (Burnie et al., 2006). Their adaptive expression in fungi indicates their importance in dimorphic pathogens (Cleare et al., 2017). Nine HSPs were identified in this study, all with greater abundance in or exclusive to the yeast form. HSP60 has been described as the main cell recognition ligand between *H. capsulatum* and CD11b/CD18 (CR3) in host macrophages (Long et al., 2003), highlighting its importance in fungal pathogenesis. Its protective role was also demonstrated through three different mouse strains in which vaccination with HSP60 provided protection against an intravenous lethal challenge with *H. capsulatum* yeasts (Gómez et al., 1991) and in a pulmonary histoplasmosis model (Gómez et al., 1995). Its importance as a target for passive immunotherapies was also described (Guimarães et al., 2009). *H. capsulatum* HSP60 interacts with other proteins, acts on dimorphism, heat stress, and pathogenesis of the fungus, as demonstrated by an analysis of the physical interaction network with this chaperone, which showed a possible involvement of this protein in the unfolding and protein translocation pathways (Guimarães et al., 2011a). Translocation of stress can also be performed with other chaperones' help, such as HSP70. Similarities reported in the study by Guimarães et al. (2011a) are observed in studies that investigated the interactions between chaperones and other proteins in the *S. cerevisiae* model (Gong et al., 2009; Tapley et al., 2009, 2010). Both species showed HSP60 interaction with chaperonins HSP82 (HCAG_04686), SSA4 (HCAG_05805, HSP 70 kDa precursor), and SSE1 (HCAG_00783, HSP88 type protein). In addition, they also demonstrated another interaction in *S. cerevisiae* with a peptidyl-prolyl *cis-trans* isomerase (HCAG_08833). In our analysis, all the five proteins mentioned above were also more abundant in *H. capsulatum* yeast cells.

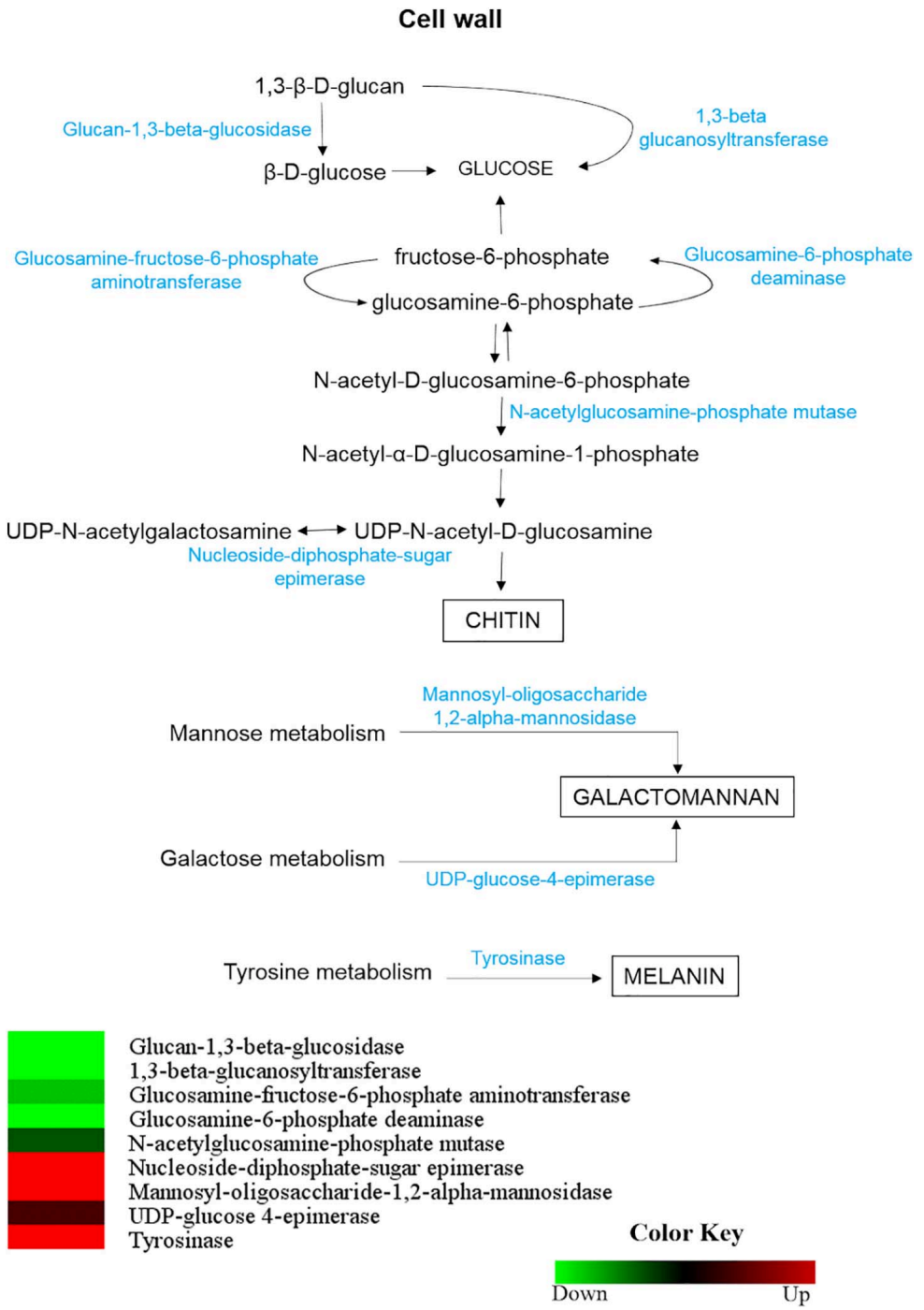

FIGURE 7 | Comparison of protein profiles related to the metabolism of compounds present in the *H. capsulatum* mycelium and yeast forms the cell wall. Dataset comparisons were carried out as cited in the **Figure 2** legend. Changes in the abundance levels in the mycelium compared with the yeast are represented in the heat map. Experimental triplicate mean values are presented for the lowest (green) and the highest (red) abundance of *H. capsulatum* proteins in the mycelium form. Black indicates that no significant difference was observed.

Some proteins involved in oxidative stress protection, such as superoxide dismutases, were uniquely identified in the *H. capsulatum* mycelium form. A cytosolic copper–zinc superoxide dismutase was also identified with greater abundance in the *Paracoccidioides* spp. mycelium (Tamayo et al., 2016). Catalases were also identified in the *H. capsulatum* proteome; catalase A was uniquely identified in mycelium and catalase B with greater abundance in the same morphotype. Our findings

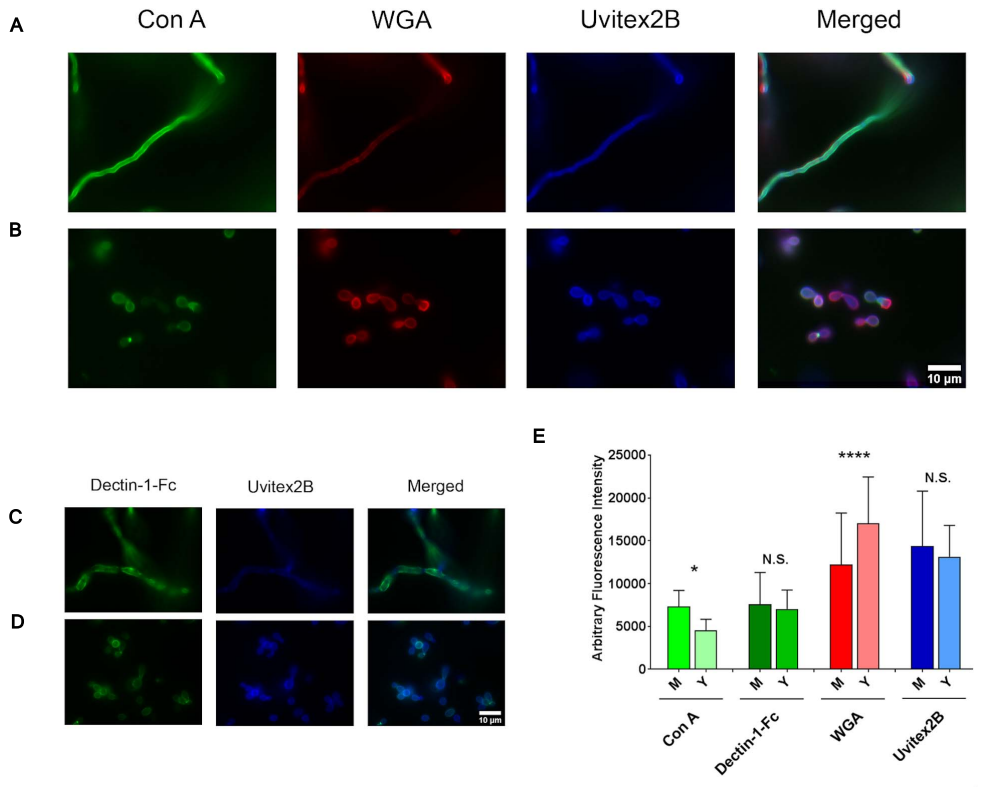

FIGURE 8 | *Histoplasma capsulatum* cell wall composition from mycelium and yeast cells. Immunofluorescence microscopy showing the labeling pattern of *H. capsulatum* mycelium **(A**,**C)** and yeast cells **(B**,**D)** by Con A–FITC, WGA-Fc (Alexa 546), Uvitex 2B, and Dectin-Fc. **(E)** Arbitrary fluorescence intensity of markers presented in previous panels. N. S., not significant; $^{*}p < 0.05$; $^{****}p < 0.0001$.

corroborate with the data of Johnson et al. (2002) that described the higher abundance of catalase A in the mycelium and catalase B expression in both morphologies (Guimarães et al., 2008).

Fatty acid catabolism is important for virulence and survival of pathogens (Muñoz-Elías et al., 2006). The comparative *H. capsulatum* proteomics results suggest that beta-oxidation, and the glyoxylate and methylcitrate cycles are preferentially induced in the mycelium, which is different from what occurs in the genus *Paracoccidioides* (Rezende et al., 2011; Vaz, 2014). In *Aspergillus fumigatus*, the methylcitrate synthase gene deletion led to virulence attenuation (Brock and Buckel, 2004), and in *Paracoccidioides* spp., the ability to metabolize propionyl-CoA is related to virulence (Santos et al., 2020). Further studies will be necessary to assess its role on *H. capsulatum*.

Amino acid catabolism, with the substrates produced for the TCA cycle, is an aspect of the *H. capsulatum* metabolism that differs between the two fungal morphologies. According to our proteomic data, both morphologies can differentially use amino acids as an energy source. Our results demonstrated a high number of enzymes related to the metabolism of alanine, arginine, aspartate, phenylalanine, isoleucine, leucine, tyrosine, tryptophan, and valine. This finding was unusual, since similar patterns were not observed in other fungal proteomes (Monteoliva et al., 2011; Rezende et al., 2011; Vaz, 2014). A hypothesis that would explain this observation is the differences in culture medium used for fungal growth, as we utilized Nutrient Mixture Ham's F12. This medium contains the 20 essential amino acids, in concentrations ranging from 0.01 to 1 mM. The higher abundance of proteins related to protein fate and degradation in the fungus yeast form (**Supplementary Tables 3**, **4**) suggests that amino acids are used as an energy source during parasitism. Other hypotheses for this observation include the differences in protein turnover or the need for new proteins in the mycelial *H. capsulatum* cells relative to yeasts.

Cysteine dioxygenase appears to play an important role in *H. capsulatum* dimorphism, a process where redox control and cysteine levels are crucial (Kumar et al., 1983). In the work by Kumar et al. (1983), this protein was purified from the cytosolic fraction of yeast cells and was present only in this *H. capsulatum* morphology, an observation our data confirmed. Interestingly, two other enzymes involved in cysteine metabolism have been detected only in the yeast phase, cystathionine beta-synthase and cysteine synthase *O*-acetylserine (thiol)-liase, suggesting a role of this amino acid in yeast maintenance.

The *H. capsulatum* yeast form seems to preferentially obtain pyruvate, oxaloacetate, and alpha-ketoglutarate for the TCA cycle by the degradation of the amino acids alanine, aspartate, and arginine, respectively. In our model, the key enzymes of the TCA cycle were more abundant in yeast cells, as occurs in *P. brasiliensis*

(Vaz, 2014) and *Tallaromyces marneffei* (Pasricha et al., 2017). This is in agreement with a lower fermentative metabolism observed through ethanol dosage in *H. capsulatum* yeasts. In mycelium, the TCA cycle seems to be driven by the phenylalanine and tyrosine degradation in acetoacetyl-CoA and fumarate, tryptophan, and leucine in acetyl-CoA, and leucine, isoleucine, and valine to succinyl-CoA. In *C. albicans,* hyphal growth is associated with a decrease in the TCA cycle and an increase in ethanol production (Monteoliva et al., 2011). Since hyphae are one of the *C. albicans* parasitic structures, the fermentative metabolism occurs preferentially into the host during mycelial growth, as opposed to what probably occurs with *H. capsulatum* where the yeast phase predominates.

Histoplasma capsulatum cell wall composition changes during morphogenesis, which has biological implications (Guimarães et al., 2011b). Previous studies comparing *H. capsulatum* yeast and mycelium report that the yeast cell walls contain more chitin (Domer et al., 1967; Kanetsuna, 1981), which is in agreement with the WGA interaction results herein presented (Liedke et al., 2017). Moreover, enzymes related to chitin biosynthesis presented lower abundance in mycelium. The results also suggest that *H. capsulatum* mycelial cell walls present more mannose, since an enzyme related to the mannose metabolism was uniquely detected in this condition. These findings are corroborated with the microscopy data, which showed greater mycelial fluorescence after ConA incubation. This is also in agreement with previous studies that quantified mannose in the mycelium and yeast cell walls of *H. capsulatum* and *H. farciminosum*, and both had higher amounts of mannose in the mycelium (Domer et al., 1967; San-Blas and Carbonell, 1974).

Melanin protects *H. capsulatum* against several harsh conditions (Guimarães et al., 2011b). *H. capsulatum* produces melanin in both morphologies: mycelium melanizes under regular culture conditions, while the yeast form requires medium supplementation with phenolic compounds for *in vitro* melanization (Nosanchuk et al., 2002). We hypothesize that tyrosinase was not detected in the yeast proteome because the culture medium used in this study was not supplemented with phenolic compounds. Hwang et al. (2003) identified a differential expression of tyrosinase, a regulator of melanin production in mycelium. This enzyme was also detected in the mycelium proteome herein described, which would support conidial melanization (Nosanchuk et al., 2002).

Pyomelanin is a water-soluble pigment produced from the homogentisate excess obtained during L-tyrosine catabolism, which is oxidized to benzoquinone acetate and then polymerized. In *H. capsulatum*, only yeasts produce pyomelanin after growth in the presence of L-tyrosine (Almeida-Paes et al., 2018). The absence of pyomelanin in the mycelium phase observed in our previous study could be explained by our current results as this phase preferentially express two enzymes (homogentisate 1,2 dioxigenase and fumarylacetoacetate hydrolase) that participate in the homogentisate degradation, the pyomelanin precursor.

The protein disulfide isomerase was identified with preferential abundance in *H. capsulatum* yeast cells. This protein was identified during the dimorphism of *P. lutzii* and *Ustilago maydis* (Böhmer et al., 2007; Rezende et al., 2011). This protein could also be associated with the *H. capsulatum* dimorphic transition. Another hypothetical role for this enzyme is the interaction with YPS3, a protein located in the *H. capsulatum* cell wall that has homology with the BAD1 adhesin of *B. dermatitidis* (Bohse and Woods, 2005).

CONCLUSION

Considering the proteomic differences found in the two *H. capsulatum* morphologies, we can conclude that abundant proteins in the mycelial form without human homologs, such as saccharopine dehydrogenase (HCAG_01145) or the Y20 protein (HCAG_04745), may be future targets for the development of new prophylactic approaches to combat the development of histoplasmosis by inhibiting the dimorphic transition to the pathogenic yeast phase. Similarly, the preferential pathways in yeast cells, such as cell wall remodeling, and enzymes from amino acid metabolism not present in mammalian cells, such as anthranilate synthase (HCAG_05224 and HCAG_00748), chorismate mutase (HCAG_00290), and histidinol dehydrogenase (HCAG_02357), may be candidates as targets for the development of new antifungal drugs. Additionally, proteins present in the yeast form can be used to develop diagnostics, particularly through antibody-based methodologies (Almeida et al., 2020). In sum, our findings reveal that proteomic analyses of the dimorphic pathogen can provide important insights into disease pathogenesis and lead to potential targets that can change future clinical practice.

DATA AVAILABILITY STATEMENT

The datasets presented in this study can be found in online repositories. The names of the repository/repositories and accession number(s) can be found below: https://www.ebi.ac.uk/pride/archive/, PXD022623.

AUTHOR CONTRIBUTIONS

MA and LB performed the experiments. MA, LB, RA-P, AB, CB, and AG designed the experiments, analyzed and interpreted the data, and wrote the manuscript. CS and RZ-O participated in the study design, data analysis, and revised the manuscript. All authors have contributed intellectually during the writing process, and have read and approved the final manuscript.

FUNDING

This work was supported by grants from Conselho Nacional de Desenvolvimento Científico e Tecnológico (CNPq), Fundação de Amparo à Pesquisa do Estado do Rio de Janeiro (FAPERJ), and Fundação de Amparo à Pesquisa do Estado de Goiás (FAPEG), grant numbers 302796/2017-7, E-26/202.527/2019, and 10267000022, respectively. This work was part of the INCT program of Strategies of Host Pathogen Interaction.

ACKNOWLEDGMENTS

The authors thank Dr. Joshua Nosanchuk for his editorial assistance. This study is partially supported by the Coordination for the Improvement of Higher Education Personnel (Coordenação de Aperfeiçoamento de Pessoal de Nível Superior CAPES) Finance Code 001.

SUPPLEMENTARY MATERIAL

The Supplementary Material for this article can be found online at: https://www.frontiersin.org/articles/10.3389/fmicb.2021.640931/full#supplementary-material

Supplementary Figure 1 | SDS-PAGE (12% acrylamide) in Coomassie blue staining. MM, molecular mass; Y, yeast; M, mycelium. Numbers on the left correspond to the molecular mass pattern.

Supplementary Figure 2 | Peptide detection type of *H. capsulatum* mycelia and yeast forms. PepFrag1 and Pepfrag2 – percentage of peptides compared to the *H. capsulatum* database in ProteinLynx Global Server version 2.4; VarMod, variable modifications; InSource, fragmentation occurred at the ionization source; MissedCleavage, missed cleavage performed by trypsin; and Neutral loss H_2O and NH_3 correspond to water and ammonia precursor losses. **(A,B)** Corresponds to yeast and mycelium forms, respectively.

Supplementary Figure 3 | Experiment parts per million (ppm) error at the peptide level. The graphs indicate the identified peptides number in ppm. A total of 91.8 and 91.4% identified peptides were detected with an error of less than 10 ppm in yeast **(A)** and mycelium **(B)** forms.

Supplementary Figure 4 | Detection dynamic range of proteomic analysis. Graphs for yeast **(A)** and mycelium **(B)** were generated, presenting proteins identified in a regular way (red), reverse (blue), and the rabbit phosphorylase B was the external standard (yellow).

Supplementary Table 1 | Identified proteins from *Histoplasma capsulatum* in mycelium.

Supplementary Table 2 | Identified proteins from *Histoplasma capsulatum* in yeast cells.

Supplementary Table 3 | Identified proteins from *Histoplasma capsulatum* up-regulated in mycelium compared to yeast cells.

Supplementary Table 4 | Identified proteins from *Histoplasma capsulatum* up-regulated in yeast cells compared to mycelium.

REFERENCES

Almeida, M. A., Almeida-Paes, R., Guimarães, A. J., Valente, R. H., Soares, C. M. A., and Zancopé-Oliveira, R. M. (2020). Immunoproteomics reveals pathogen's antigens involved in *Homo sapiens-Histoplasma capsulatum* interaction and specific linear B-cell epitopes in histoplasmosis. *Front. Cell. Infect. Microbiol.* 29:591121. doi: 10.3389/fcimb.2020.591121

Almeida-Paes, R., Almeida-Silva, F., Pinto, G. C. M., Almeida, M. A., Muniz, M. M., Pizzini, C. V., et al. (2018). L-tyrosine induces the production of a pyomelanin-like pigment by the parasitic yeast-form of *Histoplasma capsulatum*. *Med. Mycol.* 56, 506–509. doi: 10.1093/mmy/myx068

Armstrong, P. A., Jackson, B. R., Haselow, D., Fields, V., Ireland, M., Austin, C., et al. (2018). Multistate epidemiology of histoplasmosis, United States, 2011-2014. *Emerg. Infect. Dis.* 24, 425–431. doi: 10.3201/eid2403.171258

Baeza, L. C., da Mata, F. R., Pigosso, L. L., Pereira, M., de Souza, G. H. M. F., Coelho, A. S. G., et al. (2017). Differential metabolism of a two-carbon substrate by members of the *Paracoccidioides* Genus. *Front. Microbiol.* 8:2308. doi: 10.3389/fmicb.2017.02308

Beyhan, S., Gutierrez, M., Voorhies, M., and Sil, A. (2013). A temperature-responsive network links cell shape and virulence traits in a primary fungal pathogen. *PLoS Biol.* 11:e1001614. doi: 10.1371/journal.pbio.1001614

Böhmer, M., Colby, T., Böhmer, C., Bräutigam, A., Schmidt, J., and Bölker, M. (2007). Proteomic analysis of dimorphic transition in the phytopathogenic fungus *Ustilago maydis*. *Proteomics* 7, 675–685. doi: 10.1002/pmic.200600900

Bohse, M. L., and Woods, J. P. (2005). Surface localization of the Yps3p protein of *Histoplasma capsulatum*. *Eukaryot. Cell* 4, 685–693. doi: 10.1128/EC.4.4.685-693.2005

Bohse, M. L., and Woods, J. P. (2007). Expression and interstrain variability of the YPS3 gene of *Histoplasma capsulatum*. *Eukaryot. Cell* 6, 609–615. doi: 10.1128/EC.00010-07

Bradford, M. M. (1976). A rapid and sensitive method for the quantitation of microgram quantities of protein utilizing the principle of protein-dye binding. *Anal. Biochem.* 72, 248–254. doi: 10.1016/0003-2697(76)90527-3

Brock, M., and Buckel, W. (2004). On the mechanism of action of the antifungal agent propionate. *Eur. J. Biochem.* 271, 3227–3241. doi: 10.1111/j.1432-1033.2004.04255.x

Burnie, J. P., Carter, T. L., Hodgetts, S. J., and Matthews, R. C. (2006). Fungal heat-shock proteins in human disease. *FEMS Microbiol. Rev.* 30, 53–88. doi: 10.1111/j.1574-6976.2005.00001.x

Cleare, L. G., Zamith-Miranda, D., and Nosanchuk, J. D. (2017). Heat shock proteins in *Histoplasma* and *Paracoccidioides*. *Clin. Vacc. Immunol.* 24:e00221-17. doi: 10.1128/CVI.00221-17

Deepe, G. S., and Buesing, W. R. (2012). Deciphering the pathways of death of *Histoplasma capsulatum*-infected macrophages: implications for the immunopathogenesis of early infection. *J. Immunol.* 188, 334–344. doi: 10.4049/jimmunol.1102175

Deepe, G. S., and Gibbons, R. (2001). Protective efficacy of H antigen from *Histoplasma capsulatum* in a murine model of pulmonary histoplasmosis. *Infect. Immun.* 69, 3128–3134. doi: 10.1128/IAI.69.5.3128-3134.2001

Domer, J. E., Hamilton, J. G., and Harkin, J. C. (1967). Comparative study of the cell walls of the yeastlike and mycelial phases of *Histoplasma capsulatum*. *J. Bacteriol.* 94, 466–474. doi: 10.1128/jb.94.2.466-474.1967

Ebel, F., Schwienbacher, M., Beyer, J., Heesemann, J., Brakhage, A. A., and Brock, M. (2006). Analysis of the regulation, expression, and localisation of the isocitrate lyase from *Aspergillus fumigatus*, a potential target for antifungal drug development. *Fungal Genet. Biol.* 43, 476–489. doi: 10.1016/j.fgb.2006.01.015

Edwards, J. A., Alore, E. A., and Rappleye, C. A. (2011). The yeast-phase virulence requirement for α-glucan synthase differs among *Histoplasma capsulatum* chemotypes. *Eukaryot. Cell* 10, 87–97. doi: 10.1128/EC.00214-10

Edwards, J. A., Chen, C., Kemski, M. M., Hu, J., Mitchell, T. K., and Rappleye, C. A. (2013). *Histoplasma* yeast and mycelial transcriptomes reveal pathogenic-phase and lineage-specific gene expression profiles. *BMC Genomics* 14:695. doi: 10.1186/1471-2164-14-695

Edwards, J. A., and Rappleye, C. A. (2011). *Histoplasma* mechanisms of pathogenesis - one portfolio doesn't fit all. *FEMS Microbiol. Lett.* 324, 1–9. doi: 10.1111/j.1574-6968.2011.02363.x

Gauthier, G. M. (2017). Fungal dimorphism and virulence: molecular mechanisms for temperature adaptation, immune evasion, and in vivo survival. *Mediat. Inflamm.* 2017:8491383. doi: 10.1155/2017/8491383

Geromanos, S. J., Vissers, J. P., Silva, J. C., Dorschel, C. A., Li, G. Z., Gorenstein, M. V., et al. (2009). The detection, correlation, and comparison of peptide precursor and product ions from data independent LC-MS with data dependant LC-MS/MS. *Proteomics* 9, 1683–1695. doi: 10.1002/pmic.200800562

Gómez, F. J., Allendoerfer, R., and Deepe, G. S. (1995). Vaccination with recombinant heat shock protein 60 from *Histoplasma capsulatum* protects mice against pulmonary histoplasmosis. *Infect. Immun.* 63, 2587–2595. doi: 10.1128/iai.63.7.2587-2595.1995

Gómez, F. J., Gomez, A. M., and Deepe, G. S. (1991). Protective efficacy of a 62-kilodalton antigen, HIS-62, from the cell wall and cell membrane of *Histoplasma capsulatum* yeast cells. *Infect. Immun.* 59, 4459–4464. doi: 10.1128/iai.59.12.4459-4464.1991

Gong, Y., Kakihara, Y., Krogan, N., Greenblatt, J., Emili, A., Zhang, Z., et al. (2009). An atlas of chaperone-protein interactions in *Saccharomyces cerevisiae*:

implications to protein folding pathways in the cell. *Mol. Syst. Biol.* 5:275. doi: 10.1038/msb.2009.26

Gorocica, P., Taylor, M. L., Alvarado-Vásquez, N., Pérez-Torres, A., Lascurain, R., and Zenteno, E. (2009). The interaction between *Histoplasma capsulatum* cell wall carbohydrates and host components: relevance in the immunomodulatory role of histoplasmosis. *Mem. Inst. Oswaldo Cruz* 104, 492–496. doi: 10.1590/s0074-02762009000300016

Gow, N. A. R., Latge, J. P., and Munro, C. A. (2017). The fungal cell wall: structure, biosynthesis, and function. *Microbiol. Spectr.* 5, 267–292. doi: 10.1128/microbiolspec.FUNK-0035-2016

Guimarães, A. J., de Cerqueira, M. D., and Nosanchuk, J. D. (2011a). Surface architecture of *Histoplasma capsulatum*. *Front. Microbiol.* 2:225. doi: 10.3389/fmicb.2011.00225

Guimarães, A. J., Frases, S., Gomez, F. J., Zancopé-Oliveira, R. M., and Nosanchuk, J. D. (2009). Monoclonal antibodies to heat shock protein 60 alter the pathogenesis of *Histoplasma capsulatum*. *Infect. Immun.* 77, 1357–1367. doi: 10.1128/IAI.01443-08

Guimarães, A. J., Hamilton, A. J., Guedes, H. L. M., Nosanchuk, J. D., and Zancopé-Oliveira, R. M. (2008). Biological function and molecular mapping of M antigen in yeast phase of *Histoplasma capsulatum*. *PLoS One* 3:e3449. doi: 10.1371/journal.pone.0003449

Guimarães, A. J., Nakayasu, E. S., Sobreira, T. J., Cordero, R. J., Nimrichter, L., Almeida, I. C., et al. (2011b). *Histoplasma capsulatum* heat-shock 60 orchestrates the adaptation of the fungus to temperature stress. *PLoS One* 6:e14660. doi: 10.1371/journal.pone.0014660

Habich, C., Kempe, K., Gomez, F. J., Lillicrap, M., Gaston, H., Van der Zee, R., et al. (2006). Heat shock protein 60: identification of specific epitopes for binding to primary macrophages. *FEBS Lett.* 580, 115–120. doi: 10.1016/j.febslet.2005.11.060

Hilty, J., Smulian, A. G., and Newman, S. L. (2011). *Histoplasma capsulatum* utilizes siderophores for intracellular iron acquisition in macrophages. *Med. Mycol.* 49, 633–642. doi: 10.3109/13693786.2011.558930

Hwang, L., Hocking-Murray, D., Bahrami, A. K., Andersson, M., Rine, J., and Sil, A. (2003). Identifying phase-specific genes in the fungal pathogen *Histoplasma capsulatum* using a genomic shotgun microarray. *Mol. Biol. Cell* 14, 2314–2326. doi: 10.1091/mbc.E03-01-0027

Hwang, L. H., Mayfield, J. A., Rine, J., and Sil, A. (2008). *Histoplasma* requires SID1, a member of an iron-regulated siderophore gene cluster, for host colonization. *PLoS Pathog.* 4:e1000044. doi: 10.1371/journal.ppat.1000044

Johnson, C. H., Klotz, M. G., York, J. L., Kruft, V., and McEwen, J. E. (2002). Redundancy, phylogeny and differential expression of *Histoplasma capsulatum* catalases. *Microbiology* 148, 1129–1142. doi: 10.1099/00221287-148-4-1129

Kanetsuna, F. (1981). Ultrastructural studies on the dimorphism of *Paracoccidioides brasiliensis*, *Blastomyces dermatitidis* and *Histoplasma capsulatum*. *Sabouraudia* 19, 275–286. doi: 10.1080/00362178185380451

Kanetsuna, F., Carbonell, L. M., Gil, F., and Azuma, I. (1974). Chemical and ultrastructural studies on the cell walls of the yeast like and mycelial forms of *Histoplasma capsulatum*. *Mycopathol. Mycol. Appl.* 54, 1–13. doi: 10.1007/bf02055967

Kumar, V., Maresca, B., Sacco, M., Goewert, R., Kobayashi, G. S., and Medoff, G. (1983). Purification and characterization of a cysteine dioxygenase from the yeast phase of *Histoplasma capsulatum*. *Biochemistry* 22, 762–768. doi: 10.1021/bi00273a009

Laemmli, U. K. (1970). Cleavage of structural proteins during the assembly of the head of bacteriophage T4. *Nature* 227, 680–685. doi: 10.1038/227680a0

Liedke, S. C., Miranda, D. Z., Gomes, K. X., Gonçalves, J. L. S., Frases, S., Nosanchuk, J. D., et al. (2017). Characterization of the antifungal functions of a WGA-Fc (IgG2a) fusion protein binding to cell wall chitin oligomers. *Sci. Rep.* 7:12187. doi: 10.1038/s41598-017-12540-y

Long, K. H., Gomez, F. J., Morris, R. E., and Newman, S. L. (2003). Identification of heat shock protein 60 as the ligand on *Histoplasma capsulatum* that mediates binding to CD18 receptors on human macrophages. *J. Immunol.* 170, 487–494. doi: 10.4049/jimmunol.170.1.487

Maresca, B., Carratù, L., and Kobayashi, G. S. (1994). Morphological transition in the human fungal pathogen *Histoplasma capsulatum*. *Trends Microbiol.* 2, 110–114. doi: 10.1016/0966-842x(94)90596-7

Medoff, G., Maresca, B., Lambowitz, A. M., Kobayashi, G., Painter, A., Sacco, M., et al. (1986). Correlation between pathogenicity and temperature sensitivity in different strains of *Histoplasma capsulatum*. *J. Clin. Invest.* 78, 1638–1647. doi: 10.1172/JCI112757

Mihu, M. R., and Nosanchuk, J. D. (2012). *Histoplasma* virulence and host responses. *Int. J. Microbiol.* 2012:268123. doi: 10.1155/2012/268123

Monteoliva, L., Martinez-Lopez, R., Pitarch, A., Hernaez, M. L., Serna, A., Nombela, C., et al. (2011). Quantitative proteome and acidic subproteome profiling of *Candida albicans* yeast-to-hypha transition. *J. Proteome Res.* 10, 502–517. doi: 10.1021/pr100710g

Muñoz-Elías, E. J., Upton, A. M., Cherian, J., and McKinney, J. D. (2006). Role of the methylcitrate cycle in *Mycobacterium tuberculosis* metabolism, intracellular growth, and virulence. *Mol. Microbiol.* 60, 1109–1122. doi: 10.1111/j.1365-2958.2006.05155.x

Murad, A. M., Souza, G. H., Garcia, J. S., and Rech, E. L. (2011). Detection and expression analysis of recombinant proteins in plant-derived complex mixtures using nanoUPLC-MS(E). *J. Sep. Sci.* 34, 2618–2630. doi: 10.1002/jssc.201100238

Nemecek, J. C., Wüthrich, M., and Klein, B. S. (2006). Global control of dimorphism and virulence in fungi. *Science* 312, 583–588. doi: 10.1126/science.1124105

Nguyen, V. Q., and Sil, A. (2008). Temperature-induced switch to the pathogenic yeast form of *Histoplasma capsulatum* requires Ryp1, a conserved transcriptional regulator. *Proc. Natl. Acad. Sci. U.S.A.* 105, 4880–4885. doi: 10.1073/pnas.0710448105

Nosanchuk, J. D., Gómez, B. L., Youngchim, S., Díez, S., Aisen, P., Zancopé-Oliveira, R. M., et al. (2002). *Histoplasma capsulatum* synthesizes melanin-like pigments in vitro and during mammalian infection. *Infect. Immun.* 70, 5124–5131. doi: 10.1128/iai.70.9.5124-5131.2002

Nosanchuk, J. D., Steenbergen, J. N., Shi, L., Deepe, G. S., and Casadevall, A. (2003). Antibodies to a cell surface histone-like protein protect against *Histoplasma capsulatum*. *J. Clin. Invest.* 112, 1164–1175. doi: 10.1172/JCI19361

Pasricha, S., MacRae, J. I., Chua, H. H., Chambers, J., Boyce, K. J., McConville, M. J., et al. (2017). Extensive metabolic remodeling differentiates non-pathogenic and pathogenic growth forms of the dimorphic pathogen. *Front. Cell. Infect. Microbiol.* 7:368. doi: 10.3389/fcimb.2017.00368

Pigosso, L. L., Baeza, L. C., Tomazett, M. V., Faleiro, M. B. R., Moura, V. M. B. D., Bailão, A. M., et al. (2017). *Paracoccidioides brasiliensis* presents metabolic reprogramming and secretes a serine proteinase during murine infection. *Virulence* 8, 1417–1434. doi: 10.1080/21505594.2017.1355660

Rappleye, C. A., Eissenberg, L. G., and Goldman, W. E. (2007). Histoplasma capsulatum alpha-(1,3)-glucan blocks innate immune recognition by the beta-glucan receptor. *Proc. Natl. Acad. Sci. U.S.A.* 104, 1366–1370. doi: 10.1073/pnas.0609848104

Rezende, T. C., Borges, C. L., Magalhães, A. D., Sousa, M. V., Ricart, C. A., Bailão, A. M., et al. (2011). A quantitative view of the morphological phases of *Paracoccidioides brasiliensis* using proteomics. *J. Proteomics* 75, 572–587. doi: 10.1016/j.jprot.2011.08.020

Ruepp, A., Zollner, A., Maier, D., Albermann, K., Hani, J., Mokrejs, M., et al. (2004). The FunCat, a functional annotation scheme for systematic classification of proteins from whole genomes. *Nucleic Acids Res.* 32, 5539–5545. doi: 10.1093/nar/gkh894

Sahaza, J. H., Rodríguez-Arellanez, G., Canteros, C. E., Reyes-Montes, M. D. R., and Taylor, M. L. (2020). Thermotolerance of *Histoplasma capsulatum* at 40°C predominates among clinical isolates from different Latin American regions. *Braz. J. Infect. Dis.* 24, 44–50. doi: 10.1016/j.bjid.2019.12.007

San-Blas, G., and Carbonell, L. M. (1974). Chemical and ultrastructural studies on the cell walls of the yeast like and mycelial forms of *Histoplasma farciminosum*. *J. Bacteriol.* 119, 602–611. doi: 10.1128/jb.119.2.602-611.1974

Santos, L. P. A., Assunção, L. D. P., Lima, P. S., Tristão, G. B., Brock, M., Borges, C. L., et al. (2020). Propionate metabolism in a human pathogenic fungus: proteomic and biochemical analyses. *IMA Fungus* 11:9. doi: 10.1186/s43008-020-00029-9

Silva, J. C., Denny, R., Dorschel, C. A., Gorenstein, M., Kass, I. J., Li, G. Z., et al. (2005). Quantitative proteomic analysis by accurate mass retention time pairs. *Anal. Chem.* 77, 2187–2200. doi: 10.1021/ac048455k

Silva, J. C., Gorenstein, M. V., Li, G. Z., Vissers, J. P., and Geromanos, S. J. (2006). Absolute quantification of proteins by LCMSE: a virtue of parallel MS acquisition. *Mol. Cell. Proteomics* 5, 144–156. doi: 10.1074/mcp.M500230-MCP200

Tamayo, D., Muñoz, J. F., Lopez, Á, Urán, M., Herrera, J., Borges, C. L., et al. (2016). Identification and analysis of the role of superoxide dismutases isoforms in the pathogenesis of *Paracoccidioides* spp. *PLoS Negl. Trop. Dis.* 10:e0004481. doi: 10.1371/journal.pntd.0004481

Tapley, T. L., Franzmann, T. M., Chakraborty, S., Jakob, U., and Bardwell, J. C. (2010). Protein refolding by pH-triggered chaperone binding and release. *Proc. Natl. Acad. Sci. U.S.A.* 107, 1071–1076. doi: 10.1073/pnas.0911610107

Tapley, T. L., Körner, J. L., Barge, M. T., Hupfeld, J., Schauerte, J. A., Gafni, A., et al. (2009). Structural plasticity of an acid-activated chaperone allows promiscuous substrate binding. *Proc. Natl. Acad. Sci. U.S.A.* 106, 5557–5562. doi: 10.1073/pnas.0811811106

Vaz, A. F. (2014). *Análise Proteômica Comparativa do Processo de Diferenciação Celular Do Fungo Patogênico Paracoccidioides Brasiliensis*. Master's thesis. Goiânia, GO: Universidade Federal de Goiás.

Webster, R. H., and Sil, A. (2008). Conserved factors Ryp2 and Ryp3 control cell morphology and infectious spore formation in the fungal pathogen *Histoplasma capsulatum*. *Proc. Natl. Acad. Sci. U.S.A.* 105, 14573–14578. doi: 10.1073/pnas.0806221105

Woods, J. P. (2003). Knocking on the right door and making a comfortable home: *Histoplasma capsulatum* intracellular pathogenesis. *Curr. Opin. Microbiol.* 6, 327–331. doi: 10.1016/s1369-5274(03)00080-8

Woods, J. P. (2016). Revisiting old friends: developments in understanding *Histoplasma capsulatum* pathogenesis. *J. Microbiol.* 54, 265–276. doi: 10.1007/s12275-016-6044-5

Conflict of Interest: The authors declare that the research was conducted in the absence of any commercial or financial relationships that could be construed as a potential conflict of interest.

frontiers in Microbiology

ORIGINAL RESEARCH
published: 02 July 2021
doi: 10.3389/fmicb.2021.630753

Lower Funneling Pathways in *Scedosporium* Species

*Wilfried Poirier, Kevin Ravenel, Jean-Philippe Bouchara and Sandrine Giraud**

UNIV Angers, UNIV Brest, Groupe d'Etude des Interactions Hôte-Pathogène (GEIHP), SFR ICAT, Angers, France

Lignin, a natural polyaromatic macromolecule, represents an essential component of the lignocellulose biomass. Due to its complexity, the natural degradation of this molecule by microorganisms still remains largely misunderstood. Extracellular oxidative degradation is followed by intracellular metabolic degradation of conserved aromatic intermediate compounds (protocatechuate, catechol, hydroxyquinol, and gentisic acid) that are used as carbon and energy sources. The lower funneling pathways are characterized by the opening of the aromatic ring of these molecules through dioxygenases, leading to degradation products that finally enter into the tricarboxylic acid (TCA) cycle. In order to better understand the adaptation mechanisms of *Scedosporium* species to their environment, these specific catabolism pathways were studied. Genes encoding ring-cleaving dioxygenases were identified in *Scedosporium* genomes by sequence homology, and a bioinformatic analysis of the organization of the corresponding gene clusters was performed. In addition, these predictions were confirmed by evaluation of the expression level of the genes of the gentisic acid cluster. When the fungus was cultivated in the presence of lignin or gentisic acid as sole carbon source, experiments revealed that the genes of the gentisic acid cluster were markedly overexpressed in the two *Scedosporium* species analyzed (*Scedosporium apiospermum* and *Scedosporium aurantiacum*). Only the gene encoding a membrane transporter was not overexpressed in the gentisic acid-containing medium. Together, these data suggest the involvement of the lower funneling pathways in *Scedosporium* adaptation to their environment.

Keywords: lignin degradation, central aromatic molecules, *Scedosporium*, gene cluster, catechol, hydroxyquinol, gentisate

OPEN ACCESS

Edited by:
Allan J. Guimaraes, Fluminense Federal University, Brazil

Reviewed by:
Willem JH Van Berkel, Wageningen University and Research, Netherlands
Marta Helena Branquinha, Federal University of Rio de Janeiro, Brazil

****Correspondence:***
Sandrine Giraud
sandrine.giraud@univ-angers.fr

Specialty section:
This article was submitted to Microbial Physiology and Metabolism, a section of the journal Frontiers in Microbiology

Received: *18 November 2020*
Accepted: *10 June 2021*
Published: *02 July 2021*

Citation:
Poirier W, Ravenel K, Bouchara J-P and Giraud S (2021) Lower Funneling Pathways in Scedosporium Species. Front. Microbiol. 12:630753. doi: 10.3389/fmicb.2021.630753

INTRODUCTION

Environmental contamination by xenobiotics is now a worldwide phenomenon with frequent serious effects on human and animal health. A large number of fungi characterized as opportunistic pathogens, such as *Exophiala*, *Cladophialophora*, *Aspergillus*, or *Scedosporium* species, are found in human-made environments and exhibit degrading abilities toward aliphatic and aromatic hydrocarbons (Prenafeta-Boldú et al., 2006; Blasi et al., 2016). Interestingly, it has been established for several pathogenic microorganisms also associated with polluted environments that there is a link between their capacity to degrade aromatic pollutants and their virulence. For example, in the bacteria *Acinetobacter baumannii*, the *paaI* and *paaY* genes involved in the catabolism

of phenylacetic acid play a role in virulence (Cerqueira et al., 2014). These two genes, as well as six other genes involved in the catabolism of aromatic compounds, are necessary for the multiplication of the bacteria in the *Galleria mellonella* model (Gebhardt et al., 2015). Similarly, in *Escherichia coli*, two clusters of genes involved in the degradation of aromatic compounds (Liu et al., 2015) were not detected in the genome of the non-pathogenic strain PCN061 compared to the genome of the strain PCN031 which is pathogenic for piglets. Regarding fungi, a link between pathogenicity and capacity to degrade the aromatic compounds has been investigated only in *Fusarium oxysporum*, and it was demonstrated that the degradation of aromatic compounds by the β-ketoadipate pathway is essential for virulence of this phytopathogenic fungus (Michielse et al., 2012). Considering the low susceptibility to current antifungal drugs of most of the above-mentioned life-threatening fungal pathogens, a better understanding of their adaptative mechanisms to polluted environments could allow to identify interesting metabolic pathways as targets for the development of more potent antifungals.

Lignocellulolytic fungi that are capable to degrade lignin, a polymer of phenylpropanoid units, have received a particular attention during the past two decades since they are also able to efficiently break down synthetic estrogens, polychlorobiphenyl, or emerging micropollutants, such as nanoparticles (Cajthaml, 2015). Recent works evidence that they use a similar enzymatic arsenal to degrade lignin, lignocellulose components, and organic pollutants, such as aromatic hydrocarbons (Korniłłowicz-Kowalska and Rybczyńska, 2015). Lignin degradation by fungi firstly involves extracellular steps leading to various phenolic breakdown products, which are then degraded intracellularly. It may be summarized into two successive processes: (1) formation of a dihydroxylated aromatic ring and (2) ring fission and subsequent reactions channeling to the tricarboxylic acid cycle, through oxaloacetate, fumarate, and pyruvate (Harwood and Parales, 1996). Extracellular oxidative degradation of lignin produces an heterogeneous mixture of aromatic monomers (Bugg et al., 2011) that are further catabolized through the microbial "funneling pathway," including upper and lower pathways (for a detailed description of the pathways, see Lubbers et al., 2019). In the upper pathways, these aromatic molecules are catabolized into seven main aromatic compounds: hydroxyquinol (benzene-1,2,4-triol), catechol (benzene-1,2-diol), protocatechuate (3,4-dihydroxybenzoic acid), gentisic acid (2,5-dihydroxybenzoic acid), hydroxyquinone (benzene-1,4-diol), gallic acid (3,4,5-trihydroxybenzoic acid), and pyrogallol (benzene-1,2,3-triol; Harwood and Parales, 1996; Johnson and Beckham, 2015; Wang et al., 2017; Lubbers et al., 2019). These compounds serve as substrates in the lower funneling pathways where they undergo a critical ring-opening step which is catalyzed by ring cleavage dioxygenases. While these enzymes have been well studied in bacteria, their fungal counterparts are poorly characterized. To date, four main pathways have been in some extent described in fungi; specific dioxygenases opening the aromatic ring in hydroxyquinone, gallic acid, and pyrogallol have not been yet identified. However, in *Candida parapsilosis*, an alternative pathway was described for hydroxyquinone degradation *via* a hydroxylation step of this molecule by a phenol-2-monooxygenase (Eppink et al., 2000). While gentisic acid undergoes an extradiol (or *meta*)-ring cleavage, hydroxyquinol, catechol, and protocatechuate are converted to 3-oxoadipate/ß-ketoadipate (in a pathway with the same name) through an intradiol or *ortho*-pattern (Harwood and Parales, 1996; Bugg et al., 2011; Lubbers et al., 2019). Finally, genes involved in these lower pathways are usually organized in clusters in the fungal genomes (Greene et al., 2014; Gluck-Thaler et al., 2018).

Scedosporium species are soil saprophyte filamentous fungi that may cause in humans a wide variety of infections affecting both immunocompetent and immunocompromised individuals (Cortez et al., 2008). They notably rank second among the filamentous fungi colonizing the lungs of patients with cystic fibrosis (Cimon et al., 2000; Pihet et al., 2009). These fungi are thermotolerant and halophilic and have the ability to survive at very low oxygen pressure and to tolerate high osmotic pressure (Guarro et al., 2006; Cortez et al., 2008). They are mainly found in human-made environments, such as wastewater effluents from sewage treatment plants, urban playgrounds as well as on roadsides, and petrol stations (de Hoog et al., 1994; Kaltseis et al., 2009; Rougeron et al., 2015). Their common occurrence in polluted environments could be related to their ability to grow on gaseous n-alkanes and to use cyclic or aromatic pollutants as carbon and energy sources (April et al., 1998; Claußen and Schmidt, 1998, 1999; Prenafeta-Boldú et al., 2006; Rougeron et al., 2018), using the funneling pathways involved in lignin degradation. Therefore, this work was aimed to characterize *in silico* the lower funneling pathways implemented by the main *Scedosporium* species to degrade lignin and its major degradation intermediates and to validate experimentally part of these bioinformatic results.

MATERIALS AND METHODS

Genome Mining and Phylogenetic Analysis

A literature review was performed to identify reference protein sequences of dioxygenases (notably on KEGG enzyme and UniProt sites). Ortholog protein sequences in the whole genome sequence of the reference strain *Scedosporium apiospermum* Institute of Hygiene and Epidemiology-Mycology (IHEM) 14462 were then searched through tBLASTn analyzes.[1] Only results with an value of $E < 1E^{-6}$ on at least 40% of the query sequence were considered.

The Mega X software (Kumar et al., 2018; Stecher et al., 2020) was used for the phylogenetic study. An alignment was created using ClustalW, and phylogenetic tree was constructed by the maximum likelihood method (Jones et al., 1992).

Scedosporium protein sequences were also aligned with bacterial functionally characterized dioxygenases using ClustalW in Geneious software (Kearse et al., 2012).

[1]https://blast.ncbi.nlm.nih.gov/Blast.cgi

Strains

Experiments were conducted on two of the major species within the *Scedosporium* genus: *S. apiospermum* which has been largely studied in our laboratory and commonly occurs in Europe (Kaltseis et al., 2009; Rougeron et al., 2015, 2018), and *Scedosporium aurantiacum* which predominates in Australia (Harun et al., 2010; Rougeron et al., 2018). For each species, three strains were investigated, including both clinical strains deposited at Sciensano (Brussels, Belgium) in the IHEM section culture collection that are publicly available, and clinical or environmental strains that are preserved in our culture collection at Angers University, therefore designated UA: *S. apiospermum* IHEM 14462, IHEM 23580, UA 110350824, and *S. aurantiacum* IHEM 23578, UA 100353192–01, and UA 110344103. The whole genome of all strains of this panel has been sequenced and assembled by our group, but it was annotated only for the reference strain *S. apiospermum* IHEM 14462 (whole genome sequence available in the GenBank database under the accession number JOWA00000000.1; Vandeputte et al., 2014).

All isolates were preserved in our laboratory by freeze-drying. For the experiments, strains were maintained by weekly passages on YPDA plates (containing in g per liter: yeast extract, 5; peptone, 10; dextrose, 20; agar, 20; and chloramphenicol, 0.5) with incubation at 37°C.

Growth Studies

Growth studies were carried out in triplicate on a synthetic agar-based medium derived from the Scedo-Select III selective culture medium (Pham et al., 2015) and containing in g per liter: carbon source, 0.9; ammonium sulfate, 5; potassium dihydrogenophosphate, 1.25; magnesium sulfate, 0.625; agar, 20; and chloramphenicol, 0.5. A unique carbon source was used in all experiments, either glucose for control conditions, kraft lignin (Sigma-Aldrich), or gentisic acid (Sigma). Inoculation was performed by a central pricking, and growth was evaluated by measuring the diameter of the colonies every day for 10 days. Results were compared with those obtained on YPDA medium.

RNA Isolation and Reverse Transcription

For RNA extraction, isolates were first grown on potato dextrose agar (Conda, Madrid, Spain) plates at 37°C for 7 days to induce sporulation. Conidia were harvested by aseptically scraping the plates in water and filtrating through Miracloth® mesh filter (Merck, Darmstadt, Germany) to remove the hyphae. Conidia were then enumerated by hemocytometer counts, and 2.10^7 conidia were inoculated in 50 ml of YEPD liquid medium (containing in g per liter: yeast extract, 5; peptone, 10; dextrose, 20; and chloramphenicol, 0.5). After a 24-h incubation at 37°C with agitation (120 rpm), nascent germ tubes were collected on 11-µm nylon filter, inoculated in 50 ml of derived Scedo-Select III media (containing the same components that the agar-based one except agar) with the appropriate carbon source and incubated with agitation (120 rpm) at 37°C during 4 h. Fungal cells were then collected by filtration through Miracloth® mesh filter, and the fungal material was ground in liquid nitrogen with a mortar and pestle. Total RNAs were extracted using the NucleoSpin® RNA plant kit (Macherey-Nagel, Düren, Germany), according to the manufacturer's instructions. RNA samples were then treated with 2 U of RNase-free DNase I (Ambion™ Life Technologies, Carlsbad, 168 CA), following the manufacturer's recommendations. RNA quantity and quality were evaluated by the Qubit assay and electrophoretic analysis. Complementary DNA (cDNA) was synthetized from 500 ng total RNA using High Capacity cDNA Reverse Transcription kit (Applied Biosystems) and random primers, according to the protocol supplied by the manufacturer. After a 10-fold dilution, cDNA samples were used as template for real-time quantitative PCR (qPCR).

Real-Time Quantitative PCR

Each PCR reaction was performed in a final volume of 12.5 µl containing FAST SYBR®Green PCR Master Mix (Applied Biosystems, Foster City, CA), 200 nM of each primer (Integrated DNA Technologies Inc., Leuven, Belgium), and 2 µl of diluted cDNA. Primers used for qPCR experiments and PCR efficiencies are compiled in **Supplementary Table S1**. qPCR reactions were carried out on StepOnePlus™ thermocycler (Applied Biosystems) with the following amplification program: 95°C for 20 s, 40 cycles of 95°C for 3 s, and 60°C for 30 s. Melting curve analysis (95°C for 15 s and stepwise annealing from 60 to 95 with 0.3°C increments) was performed immediately after the amplification. For each gene, fold changes relative to standard condition (i.e., in the presence of glucose as carbon source) were calculated with the ΔΔCt method (Livak and Schmittgen, 2001; Pfaffl, 2001). Two reference genes were selected based on their stable expression whatever the culture conditions and the species considered (validated by an ANOVA statistical test). For each point, three biological replicates and two technical replicates were performed, and a variation in expression of a given gene was considered significant if the Log2 fold change ± standard deviation was >1 or <−1.

RESULTS

Bioinformatic Analyses

Some specific properties of *Scedosporium* species, especially their common occurrence in polluted environments, their ability to grow using lignin as sole carbon source, and their capacity to use aromatic pollutants as carbon and energy sources (April et al., 1998; Claußen and Schmidt, 1998, 1999; Prenafeta-Boldú et al., 2006; Rougeron et al., 2018), suggest the existence of metabolic pathways allowing ring opening of the aromatic compounds that are identical to the lower funneling pathways in the degradation of lignin. Ring-cleaving dioxygenases play a critical role and determine the diversity of lower pathways. Genes reported in the literature as encoding such dioxygenases in fungi were used to screen the genome of the reference strain *S. apiospermum* IHEM 14462 by tBLASTn analyses. Sixteen putative genes were identified. A phylogenetic analysis

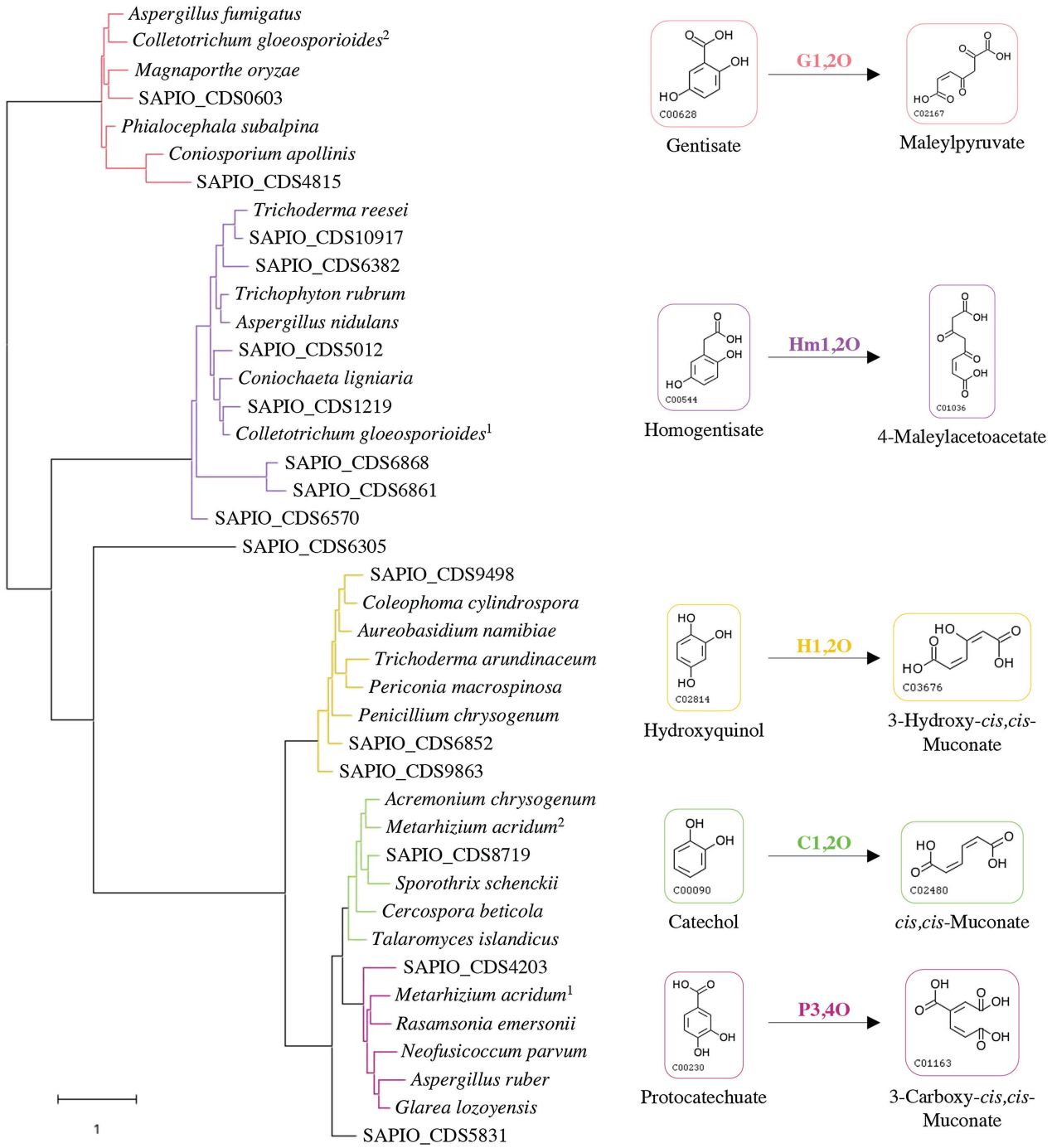

FIGURE 1 | Classification of *Scedosporium* candidate genes among fungal reference sequences of dioxygenases. The evolution history was inferred by using maximum likelihood method and JTT matrix-based model. The tree with the highest log likelihood (−25371.88) is shown. Each color corresponds to a specific dioxygenase: gentisate 1,2-dioxygenase (G1,2O) in red; homogentisate 1,2-dioxygenase (Hm1,2O) in purple; hydroxyquinol 1,2-dioxygenase (H1,2O) in yellow; catechol 1,2-dioxygenase (C1,2O) in green; and protocatechuate 3,4-dioxygenase (P3,4O) in pink. *Scedosporium apiospermum* genes are identified by their accession numbers in the GenBank database, and reference protein sequences used with the corresponding UniProt IDs are the following: *Aspergillus fumigatus* (Q4W9H3); *Colletotrichum gloeosporioides* ([1]: T0JZC0/[2]: T0K095); *Magnaporthe oryzae* (Q2KEQ4); *Phialocephala subalpina* (A0A1L7XPN4); *Coniosporium apollinis* (R7YTB2); *Trichoderma reesei* (G0RIN3); *Trichophyton rubrum* (A0A087PFF1); *Aspergillus nidulans* (Q00667); *Coniochaeta ligniaria* (A0A1J7IAU0); *Coleophoma cylindrospora* (A0A3D8S1I0); *Aureobasidium namibiae* (A0A074WM13); *Trichoderma arundinaceum* (A0A395NVW6); *Periconia macrospinosa* (A0A2V1E4S4); *Penicillium chrysogenum* (B6HA25); *Acremonium chrysogenum* (A0A086T400); *Metarhizium acridum* ([1]: E9DYI0/[2]: E9DYX5); *Sporothrix schenckii* (U7PWF0); *Cercospora beticola* (A0A2S6C3P1); *Talaromyces islandicus* (A0A0U1LSH3); *Rasamsonia emersonii* (A0A0F4YLZ4); *Neofusicoccum parvum* (R1EJ65); *Aspergillus ruber* (A0A017S957); and *Glarea lozoyensis* (S3D670).

was carried out to discriminate these enzymes and promote a putative functional association dioxygenase/lower pathway (**Figure 1**). The coding sequence SAPIO_CDS6305 did not well-align with the other *Scedosporium* coding sequences or the fungal homologues, thus constituting alone a branch of the tree. Two *Scedosporium* proteins were shown to share significant sequence homologies with gentisate 1,2-dioxygenases, and seven with homogentisate 1,2-dioxygenases. Finally, six sequences clustered with intradiol dioxygenases: Three grouped with genes encoding hydroxyquinol 1,2-dioxygenases, one with catechol 1,2-dioxygenase, one with protocatechuate 3,4-dioxygenase, and the last one appeared within intradiol dioxygenases but separated from the three other branches. These results suggest that *S. apiospermum* is able to catabolize the main aromatic intermediates derived from lignin degradation (i.e., gentisic acid, hydroxyquinol, protocatechuate, and catechol), as well as homogentisic acid. However, this last compound is mainly reported in phenylalanine and tyrosine catabolism (Pérez-Pantoja et al., 2008; Perez-Cuesta et al., 2020) as well as in pyomelanin biosynthesis (Mäkelä et al., 2015) and does not seem to be related to lignin degradation, explaining that it was not further investigated here.

In order to further characterize the putative *Scedosporium* dioxygenases, a second alignment was performed with bacterial functionally characterized ring-cleaving dioxygenases (i.e., intradiol dioxygenases for SAPIO_CDS9498, SAPIO_CDS6852, SAPIO_CDS9863, SAPIO_CDS5831, SAPIO_CDS8719, and SAPIO_CDS4203, on the one hand, and gentisate 1,2-dioxygenases for SAPIO_CDS0603 and SAPIO_CDS4815, on the other hand). In both cases, a good alignment was observed and multiple conserved residues within the active-sites were shown, as predicted by the CDD (Marchler-Bauer et al., 2015) and CATH (Sillitoe et al., 2021) databases. The conserved residues responsible for active-site nonheme ferric iron coordination and activity in dioxygenases were also conserved in the *Scedosporium* protein sequences: the 4 residues, Tyr(Y)-186, Tyr(Y)-221, His(H)-245, and His(H)-247, within intradiol dioxygenases (**Figure 2**) and the 3 residues, His(H)-132, His(H)-134, and His(H)-173, within gentisate 1,2-dioxygenases (**Figure 3**).

Identification within the sequences of the putative dioxygenases involved in the lower funneling pathway was carried out by the analysis of the genomic environment of each dioxygenase gene in *S. apiospermum* and *S. aurantiacum* (**Figure 4**), based on the gene cluster organization described in several ascomycetes by Martins and his colleagues (Martins et al., 2019). In fungi, the protocatechuate pathway is initiated by the intradiol cleavage of protocatechuate that forms 3-carboxy-cis,cis-muconate. This product is then converted into 3-carboxymuconolactone and 3-oxoadipate. In *Aspergillus nidulans*, three genes were assigned to this pathway: an intradiol dioxygenase, a 3-carboxy-*cis,cis*-muconate cyclase and a 3-carboxymuconolactone hydrolase. In *Scedosporium* genome, SAPIO_CDS4203 is the only gene identified as encoding a protocatechuate 3,4-dioxygenase. Moreover, orthologs of the two other essential genes involved in protocatechuate catabolism in *A. nidulans* were identified in *S. apiospermum* genome, located on distinct scaffolds SAPIO_CDS4774/SAPIO_CDS8203 for the 3-carboxy-*cis,cis*-muconate cyclase and SAPIO_CDS10656 for the 3-carb oxymuconolactone hydrolase. As previously reported in *A. nidulans* (Martins et al., 2015), genes involved in the intradiol cleavage of protocatechuate were not clustered in *Scedosporium* genome. Conversely, the catechol 1,2-dioxygenase SAPIO_CDS8719 was localized within a cluster of five genes (SAPIO_CDS8717 to SAPIO_CDS8721) involved in phenol or catechol catabolism (**Figure 4A**), which comprises (1) a fungal transcription factor (SAPIO_CDS8717); (2) a phenol 2-monooxygenase (SAPIO_CDS8718), structurally related to 4-hydroxybenzoate 3-hydroxylase from the ortho-hydroxylases clade (Westphal et al., 2021) which suggests its involvement in conversion of *p*-hydroxybenzoic acid molecules (**Supplementary Figure S1**); (3) a muconate cycloisomerase (SAPIO_CDS8720), the second key enzyme of this degradation pathway (Martins et al., 2019); and (4) a membrane transporter belonging to the major facilitator superfamily (MFS; SAPIO_CDS8721). In *A. nidulans*, two additional genes encoding a muconolactone isomerase (AN4061) and a 3-oxoadipate-enol lactonase (AN4531) have been reported as essential for the degradation of catechol (Martins et al., 2019). Interestingly, orthologs of these genes, SAPIO_CDS6464 and SAPIO_CDS6465, respectively, were identified in another scaffold (scaffold 103) of the S. apiospermum genome (**Figure 4B**), clustered with a MFS gene (SAPIO_CDS6466) and genes encoding for proteins involved in the early stages of formaldehyde detoxification (SAPIO_CDS6463 and SAPIO_CDS6467). Moreover, many aromatic compounds are channeled to the hydroxyquinol pathway (such as *p*-hydroxybenzoic and vanillic acids). This is a very short pathway, comprising only one specific dioxygenase and a maleylacetate reductase. In *S. apiospermum* genome, these genes are adjacent in scaffold 141 (SAPIO_CDS9497 and SAPIO_CDS9498 encoding a maleylacetate reductase and the dioxygenase, respectively) followed by genes encoding a CoA-transferase (SAPIO_CDS9499) and a cytochrome P450 (SAPIO_CDS9500; **Figure 4C**). Finally, the gentisic acid derives from 3-hydroxybenzoic acid and *p*-hydroxybenzoic and salicylic acids. The cluster organization of the gentisic acid pathway in *Scedosporium* genome was previously reported (Rougeron et al., 2018; Martins et al., 2019), but the fine composition of this cluster diverges between the two studies: The former included two supplemental genes within the cluster (i.e., a gene encoding a quinone oxidoreductase – SAPIO_CDS0606 – and a not annotated sequence encoding a Zn(II)2Cys6 transcription factor). As a gene encoding Zn(II)2Cys6 transcription factor is commonly observed in fungal gentisic acid pathway (Martins et al., 2019), the not annotated sequence encoding this protein was conserved (unidentified CDS). Conversely, the gene encoding the quinone oxidoreductase (SAPIO_CDS0606) was excluded from the gene cluster. Consequently, we define here that the gentisic acid pathway comprised six genes encoding: an MFS (SAPIO_CDS0601), a cytochrome P450 (SAPIO_CDS0602), the specific dioxygenase (SAPIO_CDS0603), a monooxygenase (SAPIO_CDS0604), a fumaryl

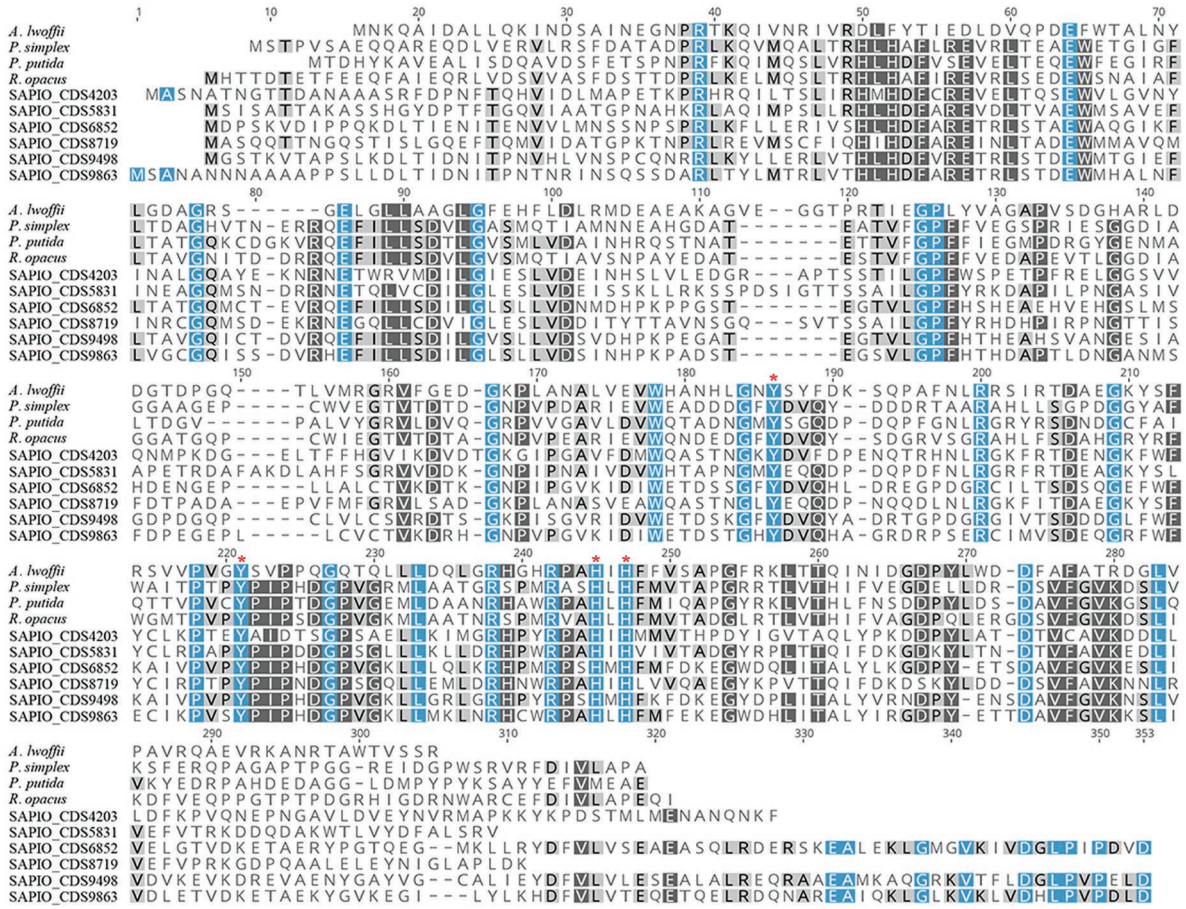

FIGURE 2 | Multiple-sequence alignment of amino acid sequences of *S. apiospermum* intradiol proteins with characterized bacterial dioxygenases of the *ß*-ketoadipate pathway. *S. apiospermum* proteins are identified by their accession numbers in the GenBank database. The bacterial reference protein sequences used, with the corresponding UniProt IDs, are the following: *A. lwoffii* (O33950) from *Acinetobacter lwoffii*; *P. simplex* (Q5PXQ6) from *Pimelobacter simplex*; *P. putida* (C6FI44) from *Pseudomonas putida*; and *R. opacus* (Q6F4M7) from *Rhodococcus opacus* (Semana and Powlowski, 2019).

acetoacetate hydrolase (SAPIO_CDS0605), and the Zn(II)2Cys6 transcription factor (unidentified CDS; **Figure 4D**). The monooxygenase gene that was structurally related to 4-hydroxybenzoate 1-hydroxylases from the decarboxylating hydroxylases clade (Westphal et al., 2021) suggesting an involvement in conversion of *p*-hydroxybenzoic acid molecules (**Supplementary Figure S1**) was shorter in *S. aurantiacum,* one of the three FAD fingerprints being missing (**Supplementary Figure S2**). Similar gene organization was found in *S. aurantiacum* genome except for the hydroxyquinol pathway, since we did not find any orthologs of these corresponding genes.

Based on these *in silico* analysis, we identify the most probable ring-cleaving dioxygenases involved in the lower funneling pathways among 16 candidate genes.

Validation of the Gentisic Acid Cluster

In order to validate our bioinformatic results, we focus on the gentisic acid pathway. Growth of the two *Scedosporium* species (*i.e.*, *S. apiospermum* and *S. aurantiacum*) was investigated on synthetic agar-based media containing lignin or gentisic acid as the sole carbon source, or glucose for control conditions. **Figure 5** illustrates the results obtained after 10 days of incubation for carbon source and a representative strain of each species. Even if growth was reduced compared to YPDA conditions, all isolates were able to use lignin or gentisic acid as carbon and energy source.

In order to follow the relative expression of the genes of the gentisic acid pathway according to the ΔΔCt method, two reference genes were validated in our experimental conditions. Thus, actin and *β*-tubulin genes were used to standardize the expression of the target genes (**Figure 6**). In both media, a similar pattern was observed for *S. apiospermum* and *S. aurantiacum*. In gentisic acid-containing medium, apart from the MFS gene SAPIO_CDS0601, all the genes of this cluster showed a marked overexpression compared to growth control conditions. In lignin-containing medium, all the genes were overexpressed. However, discrepancies between the two species were observed in the gene expression levels. All the genes were strongly overexpressed

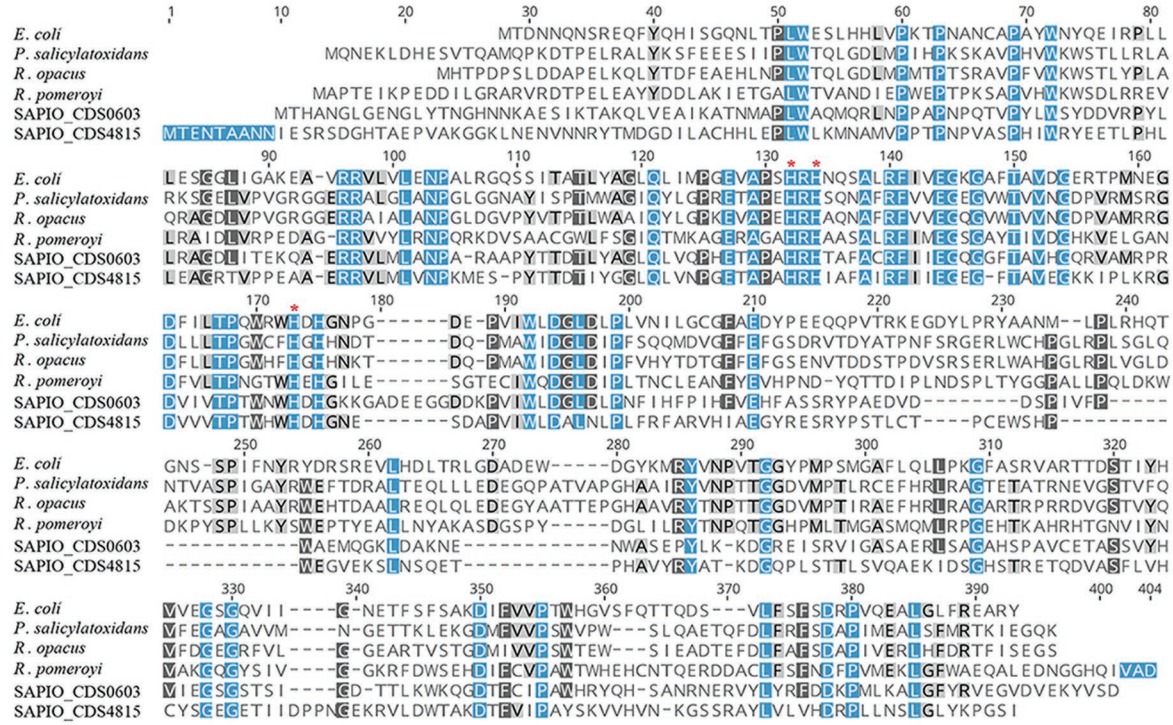

FIGURE 3 | Multiple-sequence alignment of amino acid sequences of *S. apiospermum* dioxygenases with characterized bacterial gentisate 1,2 -dioxygenases. *S. apiospermum* proteins are identified by their accession numbers in the GenBank database. The bacterial reference protein sequences used, with the corresponding UniProt IDs, are the following: *Escherichia coli* (Q8X655) from *E. coli* O157:H7; *P. salicylatoxidans* (Q67FT0) from *Pseudaminobacter salicylatoxidans*; *R. opacus* (Q0PES5) from *Rhodococcus opacus*; and *R. pomeroyi* (Q5LLB1) from *Ruegeria pomeroyi* (Buongiorno and Straganz, 2013; Eppinger et al., 2015).

in *S. aurantiacum* (between 27-fold increase for SAPIO_CDS0601 and 161-fold increase for SAPIO_CDS0602), whereas a 8-fold increase only was seen for *S. apiospermum* in the expression of SAPIO_CDS0601, SAPIO_CDS0602, and SAPIO_CDS0604. Only the gentisate 1,2-dioxygenase SAPIO_CDS0603 and the fumaryl pyruvate hydrolase SAPIO_CDS0605 were markedly overexpressed (136- and 37-fold increase, respectively; **Figure 7**). These results demonstrated that expression of the genes of this cluster was induced by the presence in the medium of gentisic acid but also of lignin.

DISCUSSION

Although it is well established that the ecology of *Scedosporium* species is associated with human activities, there is still controversy regarding the natural habitat of these fungi. Nevertheless, there is now an increasing body of evidence that these soil fungi have lignocellulolytic properties. Several strains of the genus *Scedosporium* were recovered from submerged woods in estuarian (Kirk, 1967) or marine coasts (Azevedo et al., 2011), and an enrichment procedure was developed for the recovery of these fungi from liquid samples using wooden blocks which showed abundant development of ascomata on the wood support (Kirk, 1967). Likewise, several strains have been reported from forest soils or wood (de Hoog et al., 1994; Gilgado et al., 2005), but also from xylophagous insects, including Amazonian *Nasutermites* sp. termite workers (Nirma et al., 2013), Chinese bark beetles (Wu et al., 2014), and larvae of some wood-feeding Coleoptera collected in tropical forests of Costa Rica (Rojas-Jiménez and Hernández, 2015). Besides, these last strains also showed capacity to degrade the main structural components of wood, i.e., cellulose, lignin, β-D-xylan, β-D-cellobiose, and β-D-glucan (Rojas-Jiménez and Hernández, 2015). Finally, in two recently published metagenomic studies aimed to investigate the effects of copper-based fungicides used for wood protection (Lasota et al., 2018), or to analyze the fungal community structure and its association with the cause of decay on the wooden pillars of an ancient archway in Beijing (China; Ma et al., 2020), the genus *Scedosporium* was revealed among the main fungal operational taxonomic units identified. Moreover, *Scedosporium* species are able to grow using lignin as a carbon source, and the semi-selective medium we developed in the laboratory for *Scedosporium* isolation relies on the ability of the fungus to use 4-hydroxybenzoate as a carbon source. The bioinformatic part of this study confirmed that the *Scedosporium* genome comprises all the genes required for the main lower funneling pathways involved in the catabolism of aromatic intermediates derived from lignin degradation: the three branches of the 3-oxoadipate pathway (catechol, hydroxyquinol, and protocatechuate branches) and the gentisic acid pathway. Apart from the protocatechuate branch of the 3-oxoadipate pathway,

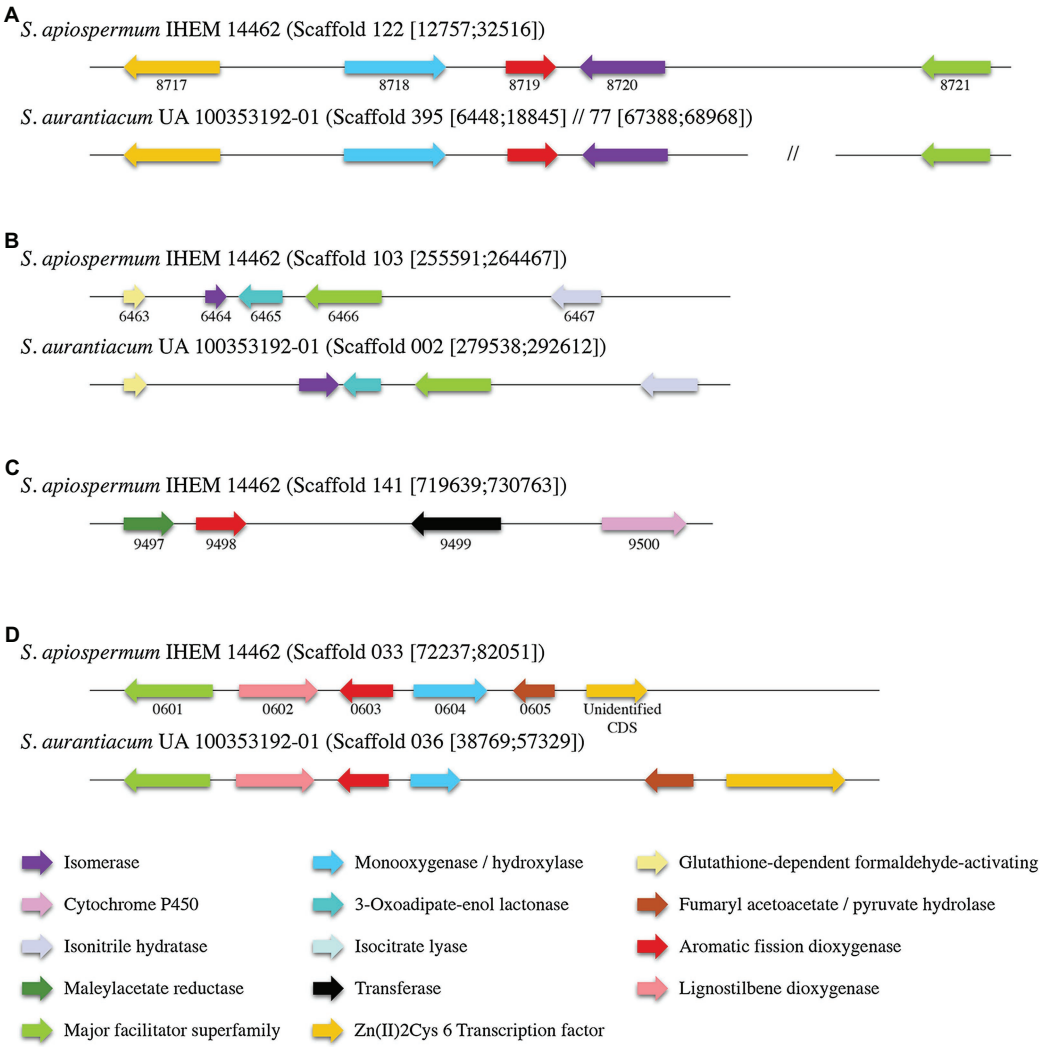

FIGURE 4 | Organization of the gene clusters of the main lower funneling pathways in *Scedosporium* species **(A)**: gene cluster of the catechol degradation pathway; **(B)**: Secondary cluster associated to catechol degradation; **(C)**: gene cluster of the hydroxyquinol degradation pathway; and **(D)**: gene cluster of the gentisic acid degradation pathway. Each color corresponds to a specific enzyme. *S. apiospermum* genes are identified by their CDS accession numbers in the GenBank database.

all these genes are organized in clusters. Considering the protocatechuate degradation, orthologs of three essential genes encoding a protocatechuate 3,4-dioxygenase, a 3-carboxy-*cis,cis*-muconatecyclase and a hydrolase with a decarboxylase activity were identified as described in *A. nidulans*, suggesting functionality of the pathway. Likewise, our experiments validated the functional character of the gentisic acid pathway and its activation when *Scedosporium* is cultivated in the presence of lignin. Further experiments are required to validate the other lower pathways. Moreover, biochemical analyses are required to evidence lignin degradation and to characterize the involvement of these funneling pathways in this degradation.

Interestingly, these central metabolites derived from lignin are also the result of the degradation of many other aromatic molecules, such as certain environmental pollutants and some plant defense toxins (flavonoids and stilbenes; Naoumkina et al., 2010; Enguita and Leitão, 2013; Wang et al., 2013; Greene et al., 2014). Therefore, the presence of all the genes of the lower funneling pathways in the genome of *Scedosporium* species may partly explain, for example, their ability to degrade *p*-cresol (Claußen and Schmidt, 1998, 1999) and their bleaching properties (Tigini et al., 2014). *Scedosporium* abundance in human-made or polluted environments correlated to the identification of these lower pathways within their genome suggests that *Scedosporium* species are active elements of ecological recycling and may play an important role in agriculture. Although the opportunist pathogen character may impede the use of *Scedosporium* in bioremediation, the enzymatic arsenal of these fungi could be of industrial interest.

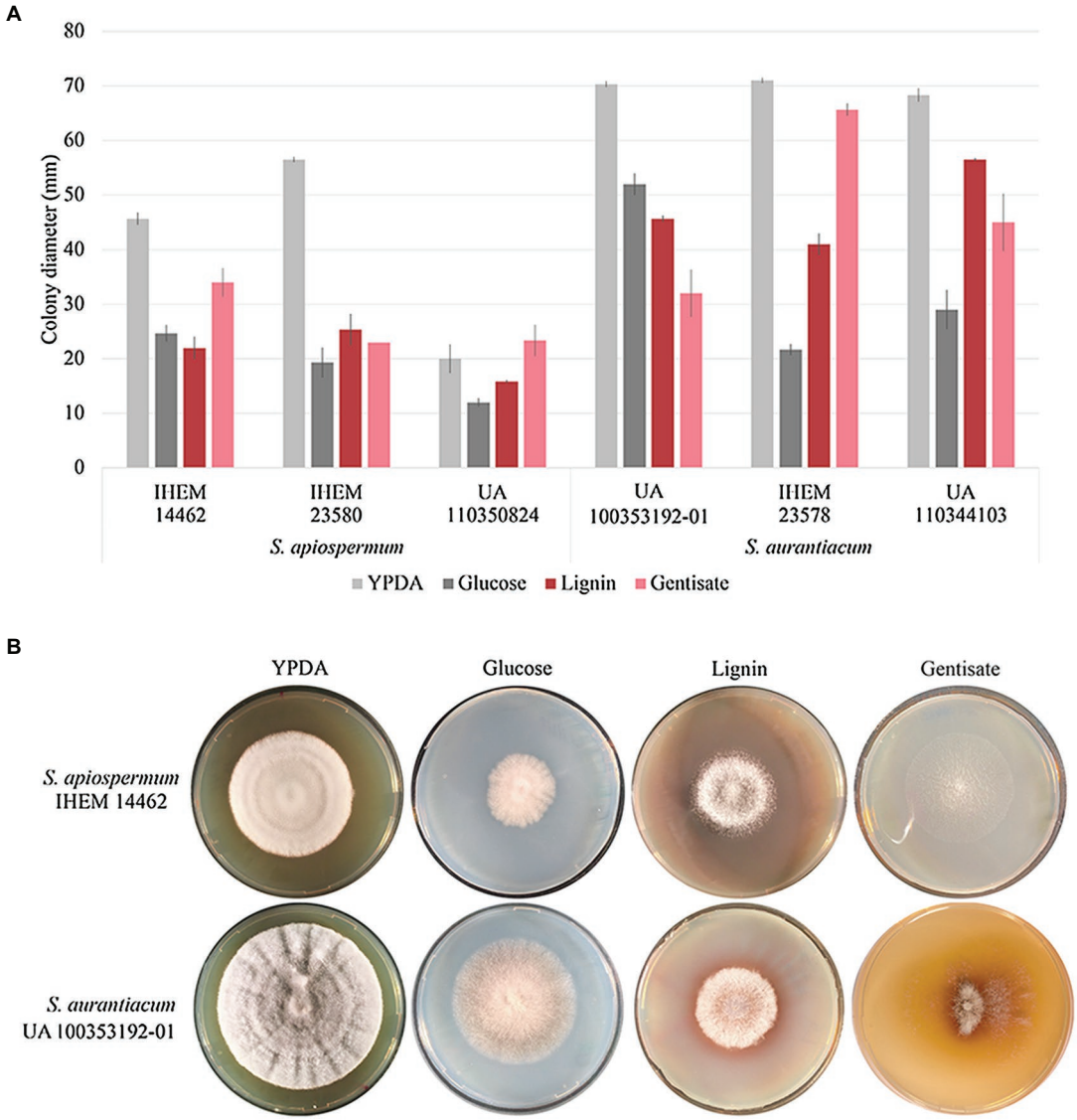

FIGURE 5 | Influence of the carbon source on growth of *Scedosporium* isolates. Clinical (deposited at Sciensano in Brussels, Belgium, and designated by IHEM for Institute of Hygiene and Epidemiology-Mycology section culture collection) as well as clinical or environmental (preserved in our culture collection at the University of Angers and designated UA) strains of *S. apiospermum* and *S. aurantiacum* were cultivated in triplicate on YPDA or lignin or gentisic acid-containing agar-based media for 10 days at 37°C. **(A)**: The growth was evaluated by measuring the diameter of the colonies. Bars indicate the standard deviation of the mean. **(B)**: Aspect of the colony at day 10.

Moreover, a link between aromatic hydrocarbon catabolism and pathogenicity for human and animals has been suggested. Adaptation of *Scedosporium* species to extreme environments, as well as their thermotolerance and their melanized spores, may predispose these fungi toward pathogenesis favoring their survival in growth factor and nutrient-limited microenvironment encountered in the host tissues. Recently, it was demonstrated that the exposure to an aromatic chlorinated compound and its degradation induce an increased pathogenic potential of fungal communities, which in turn may increase the dispersal of airborne opportunistic pathogens (Martins et al., 2018). As already mentioned, a link between pathogeny and degradation of aromatic compounds has been suggested, but regarding fungi, it was actually demonstrated only for phytopathogenic ones. The ability of these fungi to metabolize antifungal defense components of the plant host appears as an important virulence factor. For example, *Sclerotinia sclerotiorum* metabolizes salicylate, a key defense-signaling molecule (Penn and Daniel, 2013), and the virulence of *Botrytis cinerea* on grape is correlated at least in part with its ability to metabolize stilbene-type phytoalexins (Sbaghi et al., 1996). Involvement of these lower funneling pathways in the pathogenesis of *Scedosporium* species should be further analyzed (pathway silencing by dioxygenase invalidation and analysis

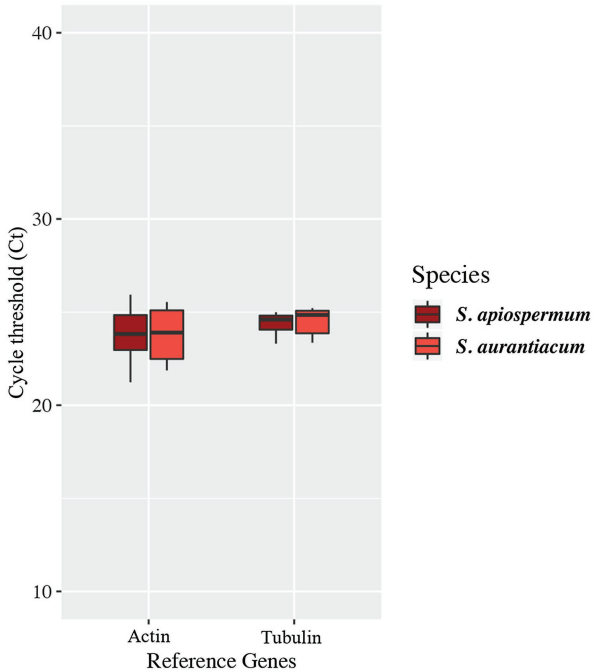

FIGURE 6 | Variations of expression of reference genes in the different culture conditions studied. Central lines in each box indicate the median, and the lower and upper rims represent the first and third quartiles. The whiskers extend to the lowest and highest datum within 1.5-fold the interquartile range from the lower or upper quartile.

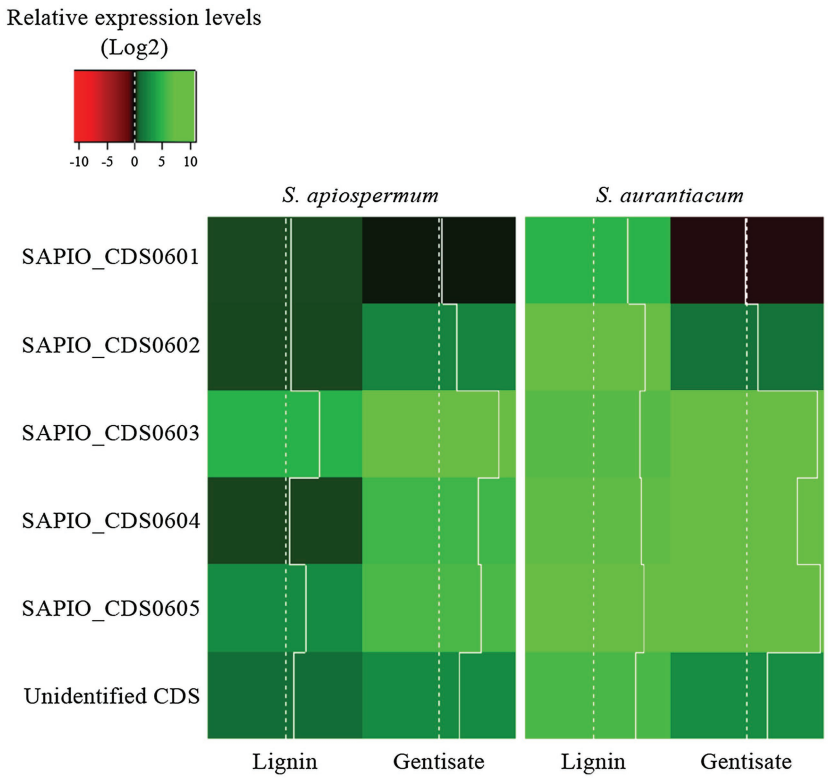

FIGURE 7 | Relative expression levels (Log2) of genes of the gentisic acid degradation pathway in the fungus grown in the presence of lignin or gentisic acid. *S. apiospermum* or *S. aurantiacum* strains were cultivated in a lignin- or gentisic acid-containing liquid culture medium for 4 h at 37°C, and the expression level of the genes (designated by their GenBank accession number for *S. apiospermum*, or their orthologs in *S. aurantiacum* genome) was evaluated by quantitative PCR after reverse transcription. For each species, results correspond to an average of real-time qPCR analysis performed on three different isolates.

of virulence of deficient mutants in mouse model) in order to identify new therapeutic targets for drug design.

DATA AVAILABILITY STATEMENT

Publicly available datasets were analyzed in this study. This data can be found here: JOWA01000000 for *Scedosporium apiospermum* genome and JUDQ01 for *Scedosporium aurantiacum* genome.

AUTHOR CONTRIBUTIONS

WP performed the experiments of the initial manuscript and data analysis, and wrote the first draft. KR participated to the revision work. J-PB provided the funding for research and reviewed the manuscript. SG managed the study and wrote the final manuscript. All authors contributed to the article and approved the submitted version.

FUNDING

During this work, WP benefited from a doctoral contract funded by the University of Angers (France), which was gratefully acknowledged.

SUPPLEMENTARY MATERIAL

The Supplementary Material for this article can be found online at: https://www.frontiersin.org/articles/10.3389/fmicb.2021.630753/full#supplementary-material.

REFERENCES

April, T. M., Abbott, S. P., Foght, J. M., and Currah, R. S. (1998). Degradation of hydrocarbons in crude oil by the ascomycete *Pseudallescheria boydii* (Microascaceae). *Can. J. Microbiol.* 44, 270–278. doi: 10.1139/w97-152

Azevedo, E., Caeirao, M. F., Rebelo, R., and Barata, M. (2011). Biodiversity and characterization of marine mycota from Portuguese waters. *Anim. Biodivers. Conserv.* 34, 205–215.

Blasi, B., Poyntner, C., Rudavsky, T., Prenafeta-Boldú, F. X., Hoog, S.de, Tafer, H., et al. (2016). Pathogenic yet environmentally friendly? Black fungal candidates for bioremediation of pollutants. *Geomicrobiol J.* 33, 308–317. doi:10.1080/01490451.2015.1052118.

Bugg, T. D., Ahmad, M., Hardiman, E. M., and Singh, R. (2011). The emerging role for bacteria in lignin degradation and bio-product formation. *Curr. Opin. Biotechnol.* 22, 394–400. doi: 10.1016/j.copbio.2010.10.009

Buongiorno, D., and Straganz, G. D. (2013). Structure and function of atypically coordinated enzymatic mononuclear non-heme-Fe(II) centers. *Coord. Chem. Rev.* 257, 541–563. doi: 10.1016/j.ccr.2012.04.028

Cajthaml, T. (2015). Biodegradation of endocrine-disrupting compounds by ligninolytic fungi: mechanisms involved in the degradation. *Environ. Microbiol.* 17, 4822–4834. doi: 10.1111/1462-2920.12460

Cerqueira, G. M., Kostoulias, X., Khoo, C., Aibinu, I., Qu, Y., Traven, A., et al. (2014). A global virulence regulator in *Acinetobacter baumannii* and its control of the phenylacetic acid catabolic pathway. *J. Infect. Dis.* 210, 46–55. doi: 10.1093/infdis/jiu024

Cimon, B., Carrère, J., Vinatier, J. F., Chazalette, J. P., Chabasse, D., and Bouchara, J. P. (2000). Clinical significance of *Scedosporium apiospermum* in patients with cystic fibrosis. *Eur. J. Clin. Microbiol.* 19, 53–56. doi: 10.1007/s100960050011

Claußen, M., and Schmidt, S. (1998). Biodegradation of phenol and *p*-cresol by the hyphomycete *Scedosporium apiospermum*. *Res. Microbiol.* 149, 399–406. doi: 10.1016/S0923-2508(98)80322-7

Claußen, M., and Schmidt, S. (1999). Biodegradation of phenylbenzoate and some of its derivatives by *Scedosporium apiospermum*. *Res. Microbiol.* 150, 413–420. doi: 10.1016/s0923-2508(99)80077-1

Cortez, K. J., Roilides, E., Quiroz-Telles, F., Meletiadis, J., Antachopoulos, C., Knudsen, T., et al. (2008). Infections caused by *Scedosporium* spp. *Clin. Microbiol. Rev.* 21, 157–197. doi: 10.1128/CMR.00039-07

de Hoog, G. S., Marvin-Sikkema, F. D., Lahpoor, G. A., Gottschall, J. C., Prins, R. A., and Guého, E. (1994). Ecology and physiology of the emerging opportunistic fungi *Pseudallescheria boydii* and *Scedosporium prolificans*. *Mycoses* 37, 71–78. doi: 10.1111/j.1439-0507.1994.tb00780.x

Enguita, F. J., and Leitão, A. L. (2013). Hydroquinone: environmental pollution, toxicity, and microbial answers. *Biomed. Res. Int.* 2013:542168. doi: 10.1155/2013/542168

Eppinger, E., Ferraroni, M., Bürger, S., Steimer, L., Peng, G., Briganti, F., et al. (2015). Function of different amino acid residues in the reaction mechanism of gentisate 1, 2-dioxygenases deduced from the analysis of mutants of the salicylate 1, 2-dioxygenase from *Pseudaminobacter salicylatoxidans*. *Biochim. Biophys. Acta* 1854, 1425–1437. doi: 10.1016/j.bbapap.2015.06.005

Eppink, M. H. M., Cammaart, E., van Wassenaar, D., Middelhoven, W. J., and van Berkel, W. J. H. (2000). Purification and properties of hydroquinone hydroxylase, a FAD-dependent monooxygenase involved in the catabolism of 4-hydroxybenzoate in *Candida parapsilosis* CB604. *Eur. J. Biochem.* 267, 6832–6840. doi: 10.1046/j.1432-1033.2000.01783.x

Gebhardt, M. J., Gallagher, L. A., Jacobson, R. K., Usacheva, E. A., Peterson, L. R., Zurawski, D. V., et al. (2015). Joint transcriptional control of virulence and resistance to antibiotic and environmental stress in *Acinetobacter baumannii*. *mBio* 6:e01660-15. doi: 10.1128/mBio.01660-15

Gilgado, F., Cano, J., Gené, J., and Guarro, J. (2005). Molecular phylogeny of the *Pseudallescheria boydii* species complex: proposal of two new species. *J. Clin. Microbiol.* 43, 4930–4942. doi: 10.1128/JCM.43.10.4930-4942.2005

Gluck-Thaler, E., Vijayakumar, V., and Slot, J. C. (2018). Fungal adaptation to plant defenses through convergent assembly of metabolic modules. *Mol. Ecol.* 27, 5120–5136. doi: 10.1111/mec.14943

Greene, G. H., McGary, K. L., Rokas, A., and Slot, J. C. (2014). Ecology drives the distribution of specialized tyrosine metabolism modules in fungi. *Genome Biol. Evol.* 6, 121–132. doi: 10.1093/gbe/evt208

Guarro, J., Kantarcioglu, A. S., Horré, R., Rodriguez-Tudela, J. L., Cuenca Estrella, M., Berenguer, J., et al. (2006). *Scedosporium apiospermum*: changing clinical spectrum of a therapy-refractory opportunist. *Med. Mycol.* 44, 295–327. doi: 10.1080/13693780600752507

Harun, A., Gilgado, F., Chen, S. C., and Meyer, W. (2010). Abundance of *Pseudallescheria/Scedosporium* species in the Australian urban environment suggests a possible source for scedosporiosis including the colonization of airways in cystic fibrosis. *Med. Mycol.* 48(Suppl. 1), S70–S76. doi: 10.3109/13693786.2010.515254

Harwood, C. S., and Parales, R. E. (1996). The *β*-ketoadipate pathway and the biology of self-identity. *Annu. Rev. Microbiol.* 50, 553–590. doi: 10.1146/annurev.micro.50.1.553

Johnson, C. W., and Beckham, G. T. (2015). Aromatic catabolic pathway selection for optimal production of pyruvate and lactate from lignin. *Metab. Eng.* 28, 240–247. doi: 10.1016/j.ymben.2015.01.005

Jones, D. T., Taylor, W. R., and Thornton, J. M. (1992). The rapid generation of mutation data matrices from protein sequences. *Bioinformatics* 8, 275–282. doi: 10.1093/bioinformatics/8.3.275

Kaltseis, J., Rainer, J., and De Hoog, G. S. (2009). Ecology of *Pseudallescheria* and *Scedosporium* species in human-dominated and natural environments and their distribution in clinical samples. *Med. Mycol.* 47, 398–405. doi: 10.1080/13693780802585317

Kearse, M., Moir, R., Wilson, A., Stones-Havas, S., Cheung, M., Sturrock, S., et al. (2012). Geneious basic: an integrated and extendable desktop software

platform for the organization and analysis of sequence data. *Bioinformatics* 28, 1647–1649. doi: 10.1093/bioinformatics/bts199

Kirk, P. W. (1967). A comparison of saline tolerance and sporulation in marine and clinical isolates of *Allescheria boydii* shear. *Mycopathol. Mycol. Appl.* 33, 65–75. doi: 10.1007/BF02049792

Korniłowicz-Kowalska, T., and Rybczyńska, K. (2015). Screening of microscopic fungi and their enzyme activities for decolorization and biotransformation of some aromatic compounds. *Int. J. Environ. Sci. Technol.* 12, 2673–2686. doi: 10.1007/s13762-014-0656-2

Kumar, S., Stecher, G., Li, M., Knyaz, C., and Tamura, K. (2018). MEGA X: molecular evolutionary genetics analysis across computing platforms. *Mol. Biol. Evol.* 35, 1547–1549. doi: 10.1093/molbev/msy096

Lasota, S., Stephan, I., Horn, M. A., Otto, W., and Noll, M. (2018). Copper in wood preservatives delayed wood decomposition and shifted soil fungal but not bacterial community composition. *Appl. Environ. Microbiol.* 85:e02391-18. doi: 10.1128/AEM.02391-18

Liu, C., Zheng, H., Yang, M., Xu, Z., Wang, X., Wei, L., et al. (2015). Genome analysis and in vivo virulence of porcine extraintestinal pathogenic *Escherichia coli* strain PCN033. *BMC Genomics* 16:717. doi: 10.1186/s12864-015-1890-9

Livak, K. J., and Schmittgen, T. D. (2001). Analysis of relative gene expression data using real-time quantitative PCR and the $2-\Delta\Delta CT$ method. *Methods* 25, 402–408. doi: 10.1006/meth.2001.1262

Lubbers, R. J. M., Dilokpimol, A., Visser, J., Mäkelä, M. R., Hildén, K. S., and de Vries, R. P. (2019). A comparison between the homocyclic aromatic metabolic pathways from plant-derived compounds by bacteria and fungi. *Biotechnol. Adv.* 37:107396. doi: 10.1016/j.biotechadv.2019.05.002

Ma, X., Zhang, B., and Liu, B. (2020). Analysis of fungal diversity of the rotten wooden pillars of a historic building. *Res. Square* [Preprint]. doi: 10.21203/rs.2.23473/v1

Mäkelä, M. R., Marinović, M., Nousiainen, P., Liwanag, A. J. M., Benoit, I., Sipilä, J., et al. (2015). Aromatic metabolism of filamentous fungi in relation to the presence of aromatic compounds in plant biomass. A*dv. Appl. Microbiol.* 91, 63–137. doi: 10.1016/bs.aambs.2014.12.001

Marchler-Bauer, A., Derbyshire, M. K., Gonzales, N. R., Lu, S., Chitsaz, F., Geer, L. Y., et al. (2015). CDD: NCBI's conserved domain database. *Nucleic Acids Res.* 43, D222–D226. doi: 10.1093/nar/gku1221

Martins, T. M., Hartmann, D. O., Planchon, S., Martins, I., Renaut, J., and Silva Pereira, C. (2015). The old 3-oxoadipate pathway revisited: new insights in the catabolism of aromatics in the saprophytic fungus *Aspergillus nidulans*. *Fungal Genet. Biol.* 74, 32–44. doi: 10.1016/j.fgb.2014.11.002

Martins, T. M., Martins, C., and Silva Pereira, C. (2019). Multiple degrees of separation in the central pathways of the catabolism of aromatic compounds in fungi belonging to the Dikarya sub-kingdom. *Adv. Microb. Physiol.* 75, 177–203. doi: 10.1016/bs.ampbs.2019.07.003

Martins, C., Varela, A., Leclercq, C. C., Núñez, O., Větrovský, T., Renaut, J., et al. (2018). Specialisation events of fungal metacommunities exposed to a persistent organic pollutant are suggestive of augmented pathogenic potential. *Microbiome* 6:208. doi: 10.1186/s40168-018-0589-y

Michielse, C. B., Reijnen, L., Olivain, C., Alabouvette, C., and Rep, M. (2012). Degradation of aromatic compounds through the β-ketoadipate pathway is required for pathogenicity of the tomato wilt pathogen *Fusarium oxysporum* f. sp. *lycopersici*: β-Ketoadipate pathway is required for pathogenicity. *Mol. Plant Pathol.* 13, 1089–1100. doi: 10.1111/j.1364-3703.2012.00818.x

Naoumkina, M. A., Zhao, Q., Gallego-Giraldo, L., Dai, X., Zhao, P. X., and Dixon, R. A. (2010). Genome-wide analysis of phenylpropanoid defence pathways. *Mol. Plant Pathol.* 11, 829–846. doi: 10.1111/j.1364-3703.2010.00648.x

Nirma, C., Eparvier, V., and Stien, D. (2013). Antifungal agents from *Pseudallescheria boydii* SNB-CN73 isolated from a *Nasutitermes* sp. termite. *J. Nat. Prod.* 76, 988–991. doi: 10.1021/np4001703

Penn, C. D., and Daniel, S. L. (2013). Salicylate degradation by the fungal plant pathogen *Sclerotinia sclerotiorum*. *Curr. Microbiol.* 67, 218–225. doi: 10.1007/s00284-013-0349-y

Perez-Cuesta, U., Aparicio-Fernandez, L., Guruceaga, X., Martin-Souto, L., Abad-Diaz-de-Cerio, A., Antoran, A., et al. (2020). Melanin and pyomelanin in *Aspergillus fumigatus*: from its genetics to host interaction. *Int. Microbiol.* 23, 55–63. doi: 10.1007/s10123-019-00078-0

Pérez-Pantoja, D., De la Iglesia, R., Pieper, D. H., and González, B. (2008). Metabolic reconstruction of aromatic compounds degradation from the genome of the amazing pollutant-degrading bacterium *Cupriavidus necator* JMP134. *FEMS Microbiol. Rev.* 32, 736–794. doi: 10.1111/j.1574-6976.2008.00122.x

Pfaffl, M. W. (2001). A new mathematical model for relative quantification in real-time RT–PCR. *Nucleic Acids Res.* 29:e45. doi: 10.1093/nar/29.9.e45

Pham, T., Giraud, S., Schuliar, G., Rougeron, A., and Bouchara, J.-P. (2015). Scedo-select III: a new semi-selective culture medium for detection of the *Scedosporium apiospermum* species complex. *Med. Mycol.* 53, 512–519. doi: 10.1093/mmy/myv015

Pihet, M., Carrere, J., Cimon, B., Chabasse, D., Delhaes, L., Symoens, F., et al. (2009). Occurrence and relevance of filamentous fungi in respiratory secretions of patients with cystic fibrosis – a review. *Med. Mycol.* 47, 387–397. doi: 10.1080/13693780802609604

Prenafeta-Boldú, F. X., Summerbell, R., and Sybren de Hoog, G. (2006). Fungi growing on aromatic hydrocarbons: biotechnology's unexpected encounter with biohazard? *FEMS Microbiol. Revue* 30, 109–130. doi: 10.1111/j.1574-6976.2005.00007.x

Rojas-Jiménez, K., and Hernández, M. (2015). Isolation of fungi and bacteria associated with the guts of tropical wood-feeding coleoptera and determination of their lignocellulolytic activities. *Int. J. Microbiol.* 2015:285018. doi: 10.1155/2015/285018

Rougeron, A., Giraud, S., Alastruey-Izquierdo, A., Cano-Lira, J., Rainer, J., et al. (2018). Ecology of *Scedosporium* species: present knowledge and future research. *Mycopathologia* 183, 185–200. doi: 10.1007/s11046-017-0200-2

Rougeron, A., Schuliar, G., Leto, J., Sitterlé, E., Landry, D., Bougnoux, M.-E., et al. (2015). Human-impacted areas of France are environmental reservoirs of the *Pseudallescheria boydii/Scedosporium apiospermum* species complex. *Environ. Microbiol.* 17, 1039–1048. doi: 10.1111/1462-2920.12472

Sbaghi, M., Jeandet, P., Bessis, R., and Leroux, P. (1996). Degradation of stilbene-type phytoalexins in relation to the pathogenicity of *Botrytis cinerea* to grapevines. *Plant Pathol.* 45, 139–144. doi: 10.1046/j.1365-3059.1996.d01-101.x

Semana, P., and Powlowski, J. (2019). Four aromatic intradiol ring cleavage dioxygenases from *Aspergillus niger*. *Appl. Environ. Microbiol.* 85:e01786-19. doi: 10.1128/AEM.01786-19

Sillitoe, I., Bordin, N., Dawson, N., Waman, V. P., Ashford, P., Scholes, H. M., et al. (2021). CATH: increased structural coverage of functional space. *Nucleic Acids Res.* 49, D266–D273. doi: 10.1093/nar/gkaa1079

Stecher, G., Tamura, K., and Kumar, S. (2020). Molecular evolutionary genetics analysis (MEGA) for macOS. *Mol. Biol. Evol.* 37, 1237–1239. doi: 10.1093/molbev/msz312

Tigini, V., Prigione, V., and Varese, G. C. (2014). Mycological and ecotoxicological characterisation of landfill leachate before and after traditional treatments. *Sci. Total Environ.* 487, 335–341. doi: 10.1016/j.scitotenv.2014.04.026

Vandeputte, P., Ghamrawi, S., Rechenmann, M., Iltis, A., Giraud, S., Fleury, M., et al. (2014). Draft genome sequence of the pathogenic fungus *Scedosporium apiospermum*. *Genome Announc.* 2:e00988-14. doi: 10.1128/genomeA.00988-14

Wang, H., Chen, H., Hao, G., Yang, B., Feng, Y., Wang, Y., et al. (2013). Role of the phenylalanine-hydroxylating system in aromatic substance degradation and lipid metabolism in the oleaginous fungus *Mortierella alpina*. *Appl. Environ. Microbiol.* 79, 3225–3233. doi: 10.1128/AEM.00238-13

Wang, W., Zhang, C., Sun, X., Su, S., Li, Q., and Linhardt, R. J. (2017). Efficient, environmentally-friendly and specific valorization of lignin: promising role of non-radical lignolytic enzymes. *World J. Microbiol. Biotechnol.* 33:125. doi: 10.1007/s11274-017-2286-6

Westphal, A. H., Tischler, D., and van Berkel, W. J. H. (2021). Natural diversity of FAD-dependent 4-hydroxybenzoate hydroxylases. *Arch. Biochem. Biophys.* 702:108820. doi: 10.1016/j.abb.2021.108820

Wu, Q., Jiang, N., Bo Han, W., Ning Mei, Y., Ming Ge, H., Kai Guo, Z., et al. (2014). Antibacterial epipolythiodioxopiperazine and unprecedented sesquiterpene from *Pseudallescheria boydii*, a beetle (coleoptera)-associated fungus. *Org. Biomol. Chem.* 12, 9405–9412. doi: 10.1039/C4OB01494D

Conflict of Interest: The authors declare that the research was conducted in the absence of any commercial or financial relationships that could be construed as a potential conflict of interest.

frontiers in Microbiology

REVIEW
published: 06 January 2022
doi: 10.3389/fmicb.2021.708550

Long-Reads-Based Metagenomics in Clinical Diagnosis With a Special Focus on Fungal Infections

*Minh Thuy Vi Hoang[1,2], Laszlo Irinyi[1,2,3], Yiheng Hu[4], Benjamin Schwessinger[4] and Wieland Meyer[1,2,3,5]**

[1]*Molecular Mycology Research Laboratory, Centre for Infectious Diseases and Microbiology, Faculty of Medicine and Health, Sydney Medical School, Westmead Clinical School, The University of Sydney, Sydney, NSW, Australia,* [2]*Westmead Institute for Medical Research, Westmead, NSW, Australia,* [3]*Sydney Infectious Disease Institute, The University of Sydney, Sydney, NSW, Australia,* [4]*Research School of Biology, Australia National University, Canberra, ACT, Australia,* [5]*Westmead Hospital (Research and Education Network), Westmead, NSW, Australia*

OPEN ACCESS

Edited by:
Marcos Dias Pereira, Federal University of Rio de Janeiro, Brazil

Reviewed by:
Leho Tedersoo, Tartu University Hospital, Estonia
Sandip Paul, JIS Institute of Advanced Studies and Research, India

***Correspondence:**
Wieland Meyer
wieland.meyer@sydney.edu.au;
wieland.meyer@curtin.edu.au

Specialty section:
This article was submitted to Microbial Physiology and Metabolism, a section of the journal Frontiers in Microbiology

Received: *12 May 2021*
Accepted: *03 December 2021*
Published: *06 January 2022*

Citation:
Hoang MTV, Irinyi L, Hu Y, Schwessinger B and Meyer W (2022) Long-Reads-Based Metagenomics in Clinical Diagnosis With a Special Focus on Fungal Infections. Front. Microbiol. 12:708550. doi: 10.3389/fmicb.2021.708550

Identification of the causative infectious agent is essential in the management of infectious diseases, with the ideal diagnostic method being rapid, accurate, and informative, while remaining cost-effective. Traditional diagnostic techniques rely on culturing and cell propagation to isolate and identify the causative pathogen. These techniques are limited by the ability and the time required to grow or propagate an agent *in vitro* and the facts that identification based on morphological traits are non-specific, insensitive, and reliant on technical expertise. The evolution of next-generation sequencing has revolutionized genomic studies to generate more data at a cheaper cost. These are divided into short- and long-read sequencing technologies, depending on the length of reads generated during sequencing runs. Long-read sequencing also called third-generation sequencing emerged commercially through the instruments released by Pacific Biosciences and Oxford Nanopore Technologies, although relying on different sequencing chemistries, with the first one being more accurate both platforms can generate ultra-long sequence reads. Long-read sequencing is capable of entirely spanning previously established genomic identification regions or potentially small whole genomes, drastically improving the accuracy of the identification of pathogens directly from clinical samples. Long-read sequencing may also provide additional important clinical information, such as antimicrobial resistance profiles and epidemiological data from a single sequencing run. While initial applications of long-read sequencing in clinical diagnosis showed that it could be a promising diagnostic technique, it also has highlighted the need for further optimization. In this review, we show the potential long-read sequencing has in clinical diagnosis of fungal infections and discuss the pros and cons of its implementation.

Keywords: pathogenic fungi, long-read sequencing, metagenomics, identification, diagnosis, mycoses

INTRODUCTION

Rapid and accurate diagnosis of pathogens is essential in the management of infectious disease and is the ultimate goal for clinical microbiology laboratories. Successful diagnosis ensures effective treatment, with patient outcome improved the faster the pathogen is identified (Perfect, 2013). The ideal diagnostic test would be capable of reliably identifying any potential pathogen, provide additional information, such as the antimicrobial resistance profile, and offer the potential for further epidemiological analysis, while remaining cost-effective (Wickes and Wiederhold, 2018). The current available identification techniques for fungal pathogens are unable to meet all these criteria. The main drawback of the wide range of traditional identification techniques is that they rely in general on the *in vitro* growth of the causative pathogen before its diagnosis (Irinyi et al., 2016).

Sequence-based metagenomics is a powerful culture independent tool for the identification of mixed microbial communities, regardless of the ability of member organisms to be grown *in vitro* (Miller and Chiu, 2018). Recently, developed long-read sequencing technologies generate sequencing reads far longer than previous sequencing technologies and are capable of addressing the shortcomings of conventional identification, inaccurate, time consuming, requires specific expertise, and short-read based metagenomics, which is unable to detect all pathogens when based on short DNA fragments (Tedersoo et al., 2021).

This review explores previous and potential use of long-read sequencing in the clinical diagnosis, focusing on fungal infections.

NON-SEQUENCING-BASED IDENTIFICATION TECHNIQUES

Many identification techniques have been developed and are currently used in clinical diagnosis, public health, animal welfare, plant protection, quarantine implications, and many other industrial fields (**Figure 1**). These conventional diagnostic tools vary in their success depending on the type of sample. However, despite advancements in molecular identification techniques of pathogens, these traditional methods still are an important component of routine diagnosis.

Morphology

Morphology-based methods rely on the identification of phenotypic features of the pathogens at the macroscopic or microscopic level. Physical characteristics can be observed within patient samples through tissue staining. However, growth on media is often required for diagnosis (Guarner and Brandt, 2011; Austin, 2017). Fungal pathogens may be identified based upon simple characteristics, such as the color, size, and smell of the isolates. Often, these do not allow for complete diagnosis, as these features may be shared among many species. More in-depth observations are required, including the analysis of the complexity of morphology, the presence of sexual reproductive structures, the effect on surrounding media, and the effect of different staining techniques (Kurtzman et al., 2011; Schelenz et al., 2015).

Biochemical Methods

Commercial diagnostic tests based on characteristic biochemical profiles produced by fungi are available for diagnostic use. These tests provide a positive or negative result for metabolic, enzymatic, or fermentation products produced by specific fungal species and so are suitable for confirmatory testing after a suspected pathogen has been found through more broad range methods (Chen et al., 2014; Lackner et al., 2014; Schelenz et al., 2015; Wagner et al., 2017).

Serology

Serology-based tests identify the presence of antigens and antibodies within patient serum indicating current and previous infections (Im et al., 2019). Serological tests for fungal infections include testing for the presence of Galactomannan antigen for cases of invasive Aspergillosis (Pfeiffer et al., 2006; de Heer et al., 2019) and (1–3)-β-d-glucan (BDG) antigen testing for diagnosis of Candidemia and *Pneumocystis jirovecii* Pneumonia (Karageorgopoulos et al., 2011; White et al., 2017).

Targeted PCR Amplification

Targeted amplification of DNA regions using species-specific primers by PCR has been widely employed for the identification of fungal pathogens (Kidd et al., 2019). A wide array of primers targeting the ITS1/2 region of the rDNA gene cluster has been designed for specific fungal species, including the prominent pathogenic fungal species *Candida*, *Aspergillus*, and *Fusarium* (Carvalho et al., 2007; Springer and Loffler, 2017). Additional regions have also been targeted by species-specific primers, e.g., the D1/D2 region of the large ribosomal subunit (LSU) of the rDNA gene cluster is used for the identification of *Candida* species (Mannarelli and Kurtzman, 1998) and for *P. jirovecii* (Tia et al., 2012). The latest targeted amplification-based identification method is the T2Candida Panel (T2 Biosystems), which is a new diagnostic tool for rapid, sensitive, and specific detection of invasive candidiasis from whole blood without culturing or nucleic acid extraction (Neely et al., 2013). It relies on PCR amplification and T2 Magnetic Resonance which enables nanoparticle-mediated rapid detection of candidemia with a sensitivity of one colony forming unit (CFU)/ml of whole blood (Mylonakis et al., 2015; Clancy et al., 2018). The use of species-specific PCR is limited in fungal diagnostics, as it is reliant on prior suspicion of the fungal pathogen to select the correct PCR target, primers, and amplification conditions (Wickes and Wiederhold, 2018).

Matrix-Assisted Laser Desorption/Ionization Time of Flight Mass Spectrometry

Matrix-assisted laser desorption/ionization time of flight mass spectrometry (MALDI-TOF MS) is a high-throughput, reliable technology used to identify and analyze large biomolecules

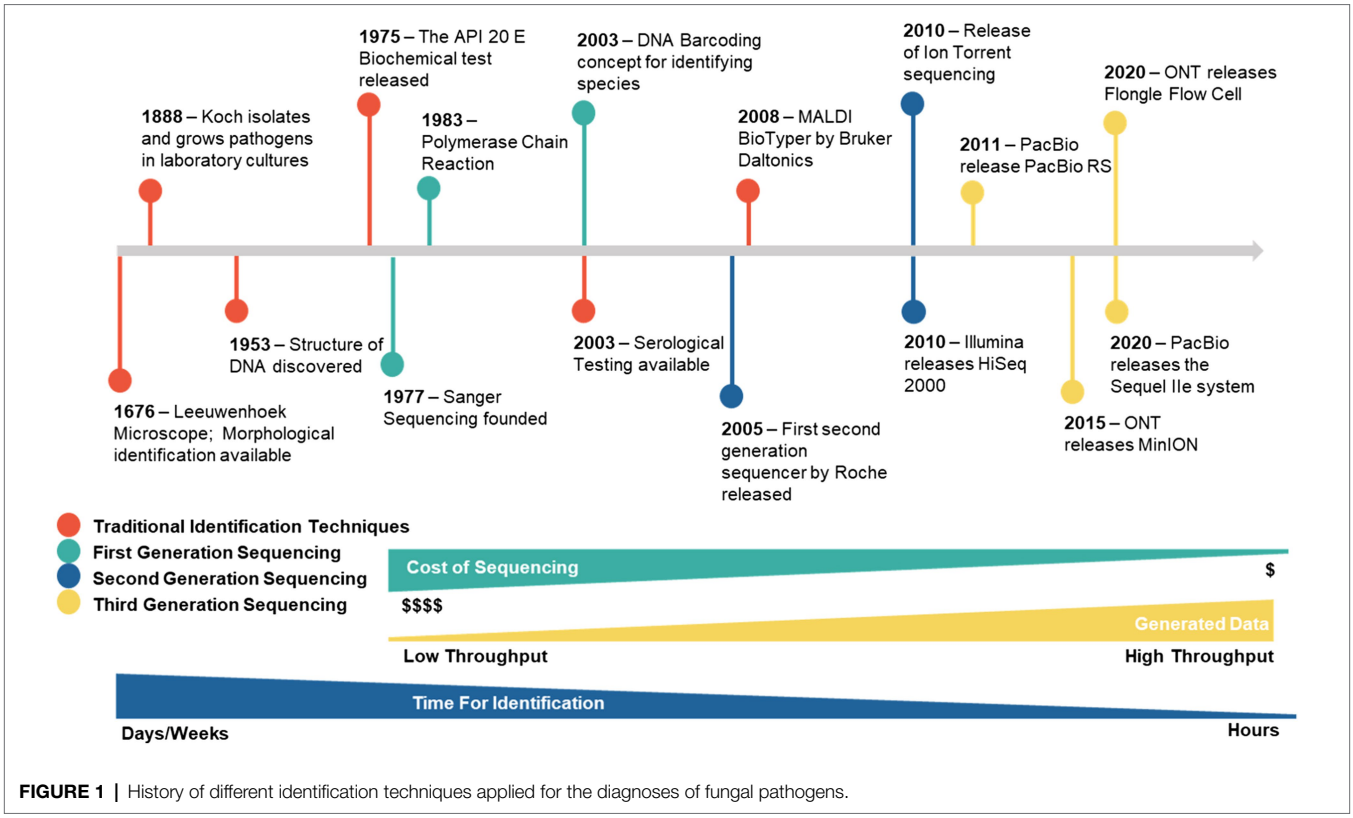

FIGURE 1 | History of different identification techniques applied for the diagnoses of fungal pathogens.

(Fenselau and Demirev, 2001; Clark et al., 2013). Starting material for MALDI-TOF can be found within sterile patient samples with high microbial load; however, this is not commonly possible and so prior pathogen growth is required. The processed material is then suspended in a crystalline matrix, vaporized, and ionized by a laser. Charged particles are then separated in a high voltage field, and the time of flight of the particles is measured and recorded as mass spectrum. Organism identification is obtained *via* the comparison of the obtained mass spectra with a reference database, which is currently the limiting factor (Angeletti, 2017).

Traditional identification techniques largely rely on prior growth of pathogens before testing may commence. This puts a strain on diagnosis as some fungal species may require up to 4 weeks before discriminatory features can be observed (Irinyi et al., 2016). Closely related species and species complexes, which may have different responses to antifungals, are unable to be reliably identified as characteristic phenotypic traits are not displayed and can only be genetically distinguished, such as in the genera *Fusarium*, *Aspergillus*, and *Scedosporium* (Goldstein et al., 2015; De Hoog et al., 2019). Traditional identification methods have been shown to be more insensitive than more advanced techniques, as results are highly subjective and error prone, leading to potential misidentifications (**Table 1**; Irinyi et al., 2016; Gustafson et al., 2019). Additionally, a number of fungal species, such as *P. jirovecii*, cannot be cultured under laboratory conditions and so culture-based methods are inappropriate for the identification (White et al., 2017). MALDI-TOF most closely meets the criteria for an ideal diagnostic test; however, it remains reliant on culturing and still lacks an exhaustive curated database. Although MALDI-TOF has been demonstrated to be more cost-efficient than traditional culturing techniques, the initial instrument cost limits widespread use in smaller diagnostic laboratories (Patel et al., 2017).

Overall, non-sequencing-based identification techniques are inadequate as the gold standard diagnostic technique for fungal infections.

SEQUENCING-BASED IDENTIFICATION TECHNIQUES

The advancement in the understanding of the genetic information of microorganisms has been fundamental for the development of molecular diagnosis techniques of pathogenic fungi. These techniques include PCR – restriction fragment length polymorphism analysis (Dendis et al., 2003), random amplified polymorphic DNA analysis (Brandt et al., 1998; Mobasherizadeh et al., 2016), hybridization with genus/species specific DNA or RNA probes (Sandhu et al., 1995; Lindsley et al., 2001), PCR-fingerprinting (Lieckfeldt et al., 1993), species-specific PCR assays (Martin et al., 2000; Kulik et al., 2004), real-time PCR (Klingspor and Jalal, 2006), and increasingly DNA sequencing (Pryce et al., 2003; Romanelli et al., 2010). DNA sequencing introduced by Sanger et al. (1977) dominated the sequencing technology for 20 years, being recognized as first-generation sequencing. When applied to the identification of

TABLE 1 | Features of diagnostic tests available for fungal infections.

	Diagnostic test	Available since	Culture dependency	Need for single culture	Test turnaround time without culture time	Accuracy	Curated database needed	Expertise	Cost	Portability	Resolution power	Potential for virulence and drug resistance detection	Generated clinical information
Non-sequence-based	Morphology	1676	Yes	Yes	Long	Low	No	High	Low	No	Medium	No	Low
	Biochemical	1975	Yes	Yes	Long	Low	Yes	Low	Medium	No	Medium	No	Low
	Serological	2003	Yes	No	Short	Low	No	Low	Low	No	None	No	Low
	Targeted PCR amplification (T2Candida panel)	2013	No	No	Short	High	No	Low	Low	No	High	No	Low
	MALDI-TOF	2008	Yes	Yes	Short	High	Yes	Low	Low	No	High	No	Low
Sequence-based	PCR based assays	1977	Yes	No	Medium	High	No	Medium	Low	No	High	No	Medium
	Sanger sequencing/DNA barcoding	1977	Yes	Yes	Medium	High	Yes	Medium	Medium	No	High	No	Medium
	Whole genome sequencing	2005	Yes	Yes	Long	High	Yes	High	High	No	High	Yes	Very high
	Long-read metagenomics/ Metabarcoding	2015	No	No	Short	High	Yes	Medium	Low	Yes	High	Yes	Very high

microorganisms, it relies on the analysis of pathogen-specific genome regions for comparison to reference sequence databases.

DNA barcoding is one of the most promising and efficient sequencing-based methods enabling rapid identification of species and recognition of cryptic species. The concept was first proposed by Hebert et al. (2003). DNA barcodes are standardized, easily amplified, universal, short DNA sequences (500–800 bp), which show a high divergence at the species level. These allow for the rapid identification of an organism though comparison of the generated genetic barcode to a reference collection of DNA barcodes from well-identified species. Two barcoding regions have been established for use in the identification of pathogenic fungi. The primary fungal DNA barcoding region is the internal transcribed spacer region (ITS1/2; Schoch et al., 2012) and the secondary fungal DNA barcoding region is the *translational elongation factor 1α* (Stielow et al., 2015). DNA barcoding using Sanger sequencing has major inherent limitations, including: (1) the requirement of a single fungal organism in the sample, (2) high target amplicon yield to avoid biases and errors (Polz and Cavanaugh, 1998), and (3) intra-individual variability (heteroplasmy). Especially, the high intra-genomic diversity of the ITS1/2 region in fungi cannot be simultaneously detected from one sample using Sanger sequencing alone, as samples with multiple amplicons will appear as mixed peaks in the sequencing chromatograms (O'Donnell and Cigelnik, 1997). The high intra-genomic diversity was only able to be detected after cloning (Jumpponen, 2003; Simon and Weiss, 2008) and the application of Next-Generation Sequencing (NGS) technologies (Ganley and Kobayashi, 2007; Colabella et al., 2021).

Sequencing technologies have recently rapidly advanced. The early NGS technologies were classified as second-generation sequencing technologies and achieved increased sequencing throughput after the amplification of thousands of DNA templates and the simultaneous sequencing of the resulting DNA fragments, saving time, and decreasing costs (Heather and Chain, 2016; Ravi et al., 2018). The most prominent short-read sequencing technology is those produced by Illumina. While Sanger sequencing suffered from low throughput, it did produce long-reads (up to 1,000 bp) with high accuracy. Short-read NGS technologies focused on achieving high throughput while sacrificing read length (100–600 bp; van Dijk et al., 2014; Illumina, 2021). The high throughput of NGS allowed for in-depth sequencing, recovering more data and thus more species from complex samples (Shokralla et al., 2014).

> *The introduction of sequence-based identification methods improved the speed and accuracy of fungal diagnostics and the rapid advancements of sequencing technologies enables the identification of fungi in complex samples.*

METABARCODING AND METAGENOMICS

Metabarcoding/metagenomic sequencing is a method in which nucleic acid (DNA or RNA) of all organisms in a sample is extracted and sequenced using NGS techniques. The generated

sequences are then used to identify organisms present in the sample. It was first mentioned in 1998 (Handelsman et al., 1998), when it was applied for the culture independent analysis of a complex and diverse ("meta") community of microorganisms.

There are two main approaches which can be used to characterize the microbiome of a specific sample: (i) **targeted amplicon sequencing (metabarcoding)** and (ii) **shotgun metagenomics**. While the amplicon sequencing is based on the amplification of well-characterized genetic regions, shotgun metagenomics attempts to sequence the entire genetic content in a sample. The detailed differences between the two approaches have been previously discussed elsewhere (Forbes et al., 2017).

Targeted amplicon sequencing (metabarcoding) enables the direct identification of multiple species simultaneously from any environmental or clinical sample without culturing. It has been extensively used in microbiome studies and its biggest advantage over shotgun sequencing is the low amount of microbial DNA needed for identification and targeted enrichment of the sequence of interest. It is based on the amplification of specific taxonomic genetic regions (barcodes), such as the 16S ribosomal RNA (rRNA) gene cluster for bacteria (Riesenfeld et al., 2004; Janda and Abbott, 2007) or the internal transcribed spacer region (ITS1/2; Nilsson et al., 2009; Schoch et al., 2012) for fungi, by universal degenerated primers in a PCR reaction. These barcodes are ubiquitous in varying copy numbers, can be easily amplified, and have two fundamental characteristics: high taxonomic coverage and high resolution (Schoch et al., 2012). This approach combines the concept of DNA barcoding (Hebert et al., 2003) and the application of high-throughput sequencing technology (metabarcoding). The generated barcodes are then computationally clustered by sequence similarity into operational taxonomic units (OTUs) and queried against a reference database, such as UNITE[1] (Koljalg et al., 2005), BOLD[2] (Ratnasingham and Hebert, 2007), RefSeq[3] (Schoch et al., 2014), and the ISHAM Barcoding Database[4] (Irinyi et al., 2015; Meyer et al., 2019). The targeted approach only sequences the amplified barcodes and not the whole genome. Due to the smaller size of the generated data, the computational analyses are less complex and faster. However, amplicon-based sequencing has PCR biases due to its inability to amplify all microorganisms across multiple taxa and it does not provide any additional characterization beyond taxonomic information.

Short-read sequencing has been widely used in metabarcoding studies; however, it only targets short barcodes, such the ITS1 or ITS2 region for fungi, as second-generation sequencer read lengths (500–600 bp for paired and reads) are unable to span the full length of the established barcodes, the entire ITS1/2 region (Edouard et al., 2018; Hamad et al., 2018; Tsang et al., 2021). In addition, short-reads are unable to resolve repeated sequences that are longer than the reads generated by short-read NGS and as such these may lead to misassembles and gaps (Salzberg and Yorke, 2005; Treangen and Salzberg, 2011; Teng et al., 2017). Furthermore, even the short-reads lend themselves to identifying single-nucleotide variants and short indels accurately, longer structural variations are more challenging to resolve, as the variation is different within the ITS1 or ITS2 regions (**Figure 2**), leading to different discriminatory powers (van Dijk et al., 2018). As a result, in some species, the ITS1 or the ITS2 alone cannot resolve all species, which will only be possible using the combined ITS1/2 region (Irinyi et al., 2016). Longer sequencing reads would eliminate these issues and so drove the development of long-read NGS, see below.

In contrast, **shotgun metagenomic** sequencing allows for a higher resolution, as it sequences most parts of the genomes of every organism present in the sample. This feature enables the technology not only to identify the organism, but also to characterize their extended profiles, such as antimicrobial resistance, genetic subtypes, and virulence. It involves extraction of nucleic acid (DNA or RNA) from primary specimens (e.g., soil samples, water samples, blood, feces, bronchoalveolar lavage (BAL), and sputum, tissue), fragmentation of the obtained DNA or RNA extracts, library preparation, in-depth sequencing, and subsequent data analysis. Shotgun metagenomics is significantly more expensive (depending on the sequencing depth) and computationally more extensive than amplicon sequencing. Another challenge is the overwhelming amount of host or background DNA compared to the microbial DNA. Many methods have been developed for enriching microbial DNA to combat this for both environmental and clinical samples, see below. Additionally, in cases of non-sterile patient samples or co-infections, genomic material from multiple microbial species may prove difficult to assign correctly to the particular species present (Bharti and Grimm, 2021).

The application of shotgun metagenomics to diagnostics eliminates the need for culturing as identification would be made directly from patient samples (e.g., tissue, blood, feces, BAL, and sputum). As previously discussed, culturing greatly limits the detection of causative pathogens, as not all pathogens can be grown in a laboratory setting and it also greatly delays the timing of accurate identification (Garrido-Cardenas and Manzano-Agugliaro, 2017). In addition, metagenomics eliminates any sequencing bias that may occur as a result of PCR amplification (Wang et al., 2015). Comparing to amplicon sequencing, shotgun metagenomics also allows for better estimation of the relative abundance of microbes in samples based on the number of reads generated (Laudadio et al., 2018). Most importantly, shotgun metagenomics data contain additional genomic information from the patient samples, potentially informing not only on pathogen identities, but also underlying host factors. Previously established antimicrobial markers may also be identified from metagenomic data and as such can be used to guide targeted treatment, leading to the reduction of inappropriate use of antimicrobials and a subsequent reduction in the development of antimicrobial resistance. Additionally, further genomic information can be generated, to be used for epidemiological studies and outbreak tracing *via* the utilization of multi-locus sequence typing data generated as part of the metagenomics dataset (Couto et al., 2018).

[1]https://unite.ut.ee/
[2]https://www.boldsystems.org/
[3]https://www.ncbi.nlm.nih.gov/refseq/
[4]https://its.mycologylab.org/

The quantity and quality of data generated from metagenomic studies is reliant upon the NGS technology used and as such the advantages and disadvantages must be considered. The characteristics of the main technologies used for the identification of fungal pathogens are summarized in ***Table 1****.*

LONG-READ SEQUENCING TECHNOLOGIES

Third-generation sequencing technologies are characterized by the generation of ultra-long-reads and offer a number of advantages over short-read sequencing. Long-read sequencing routinely generates reads over 10 kb (Pollard et al., 2018; Mantere et al., 2019). Currently, commercial long-read sequencing is supported by two companies, Pacific Biosciences and Oxford Nanopore Technologies.

Pacific Biosciences

Pacific Biosciences (PacBio) released the first commercial long-read sequencer in 2011 and continue to maintain and release improved sequencing instruments (Ardui et al., 2018; Tedersoo et al., 2021). The basis of Pacific Biosciences sequencers is known as single molecule real-time sequencing (SMRT), which takes place in single use SMRT Cells. These contain multiple Zero-mode waveguiders (ZMWs) that hold an immobilized polymerase. Double-stranded DNA (dsDNA) is prepared for sequencing by forming SMRT bells by adding hairpin adaptors to both ends of the dsDNA template (Eid et al., 2009). Each SMRT bell is diffused into one ZMW and nucleotides with identifying fluorescent labels are added to the ZMW alongside reagents required for PCR. From there, the immobilized polymerase binds to the hairpin adaptor of the SMRT bells and begins replication. As a nucleotide is added to the complementary strand, fluorescence at a characteristic wavelength is emitted and the sequence of fluorescence pulses is recorded into a movie. The wavelengths emitted are then converted into a nucleotide sequence called a continuous long-read. After the polymerase completes replication of one DNA strand, it continues to sequence the opposite adapter and second strand. As a result, it is possible to generate multiple passes of the same template depending on the lifetime of the polymerase. Upon sequencing completion and conversion to continuous long-reads, subreads are formed by identifying and cleaving the adaptor region sequences. Multiple computationally merged subreads of the same template DNA strand are called circular consensus sequences or HiFi reads, and the more subreads, the higher the accuracy, currently reaching up to Q30–50 for consensus HiFi (Rhoads and Au, 2015; Tedersoo et al., 2021).

PacBio currently have three sequencers on the market, the Sequel System, the Sequel II system, and the Sequel IIe system, released in October 2020 (Pacific Biosciences, 2020). The newer iterations Sequel II and Sequel IIe boast a new SMRT Cell, dubbed the SMRT Cell 8 M, containing 8 million ZMWs capable of running for 30 h and generating up to 4,000,000 reads with over 99% (Q20+) accuracy (Wenger et al., 2019; Pacific Biosciences, 2021a). The Sequel IIe improves upon the Sequel II by upgrading the software and data analysis function through data processing capability on the instrument and cloud facilitation leading to potentially 70% reduction in secondary analysis time and 90% reduction in file transfer and data storage (Pacific Biosciences, 2020).

SMRT sequencers initially reported low read accuracy of 85–87%, when at the same time, short-read sequencers from Illumina had read accuracy >99% (Chin et al., 2013; Ardui et al., 2018). Errors in sequencing through insertions and deletions were more common in SMRT sequencing. However, improvements in sequencing chemistry and polishing methods increased the read accuracy of SMRT sequencing to 99.8% (Ardui et al., 2018; Tedersoo et al., 2018; Wenger et al., 2019). This allowed its use in direct sequencing studies rather than only be used to scaffold short-read Illumina reads (Parker et al., 2017; Teng et al., 2017; De Maio et al., 2019). The increased throughput of SMRT sequencers has made adequate coverage with multiplexed samples achievable (Armanhi et al., 2016; Pacific Biosciences, 2021b). The current SMRT Cell 8 M supports the simultaneous sequencing of 348 samples when using the largest barcoding kit PacBio currently offers, and the sequencing depth can achieve reference quality for *de novo* assemblies for genomes up to 2GB of a single sample and full length 16S region sequences for 192 samples for strain level identification (Pacific Biosciences, 2021b).

Disadvantages of PacBio instruments are, that they require a high initial investment cost, limiting widespread use. The throughput of Illumina sequencers remains higher than PacBio, as PacBio sequencers are limited by the number of ZMWs available in the SMRT Cells. Not all ZMWs are guaranteed to successfully sequence, as there maybe more than one DNA fragment being present in a ZMW, and there maybe issues with the polymerase binding. The nature of SMRT bells results in a trade-off between read length and read quality as longer DNA inserts are sequenced less often and hence the generated consensus sequence is of lower quality (Tedersoo et al., 2018). Further, the library preparation for the Sequel II Instrument is estimated to be 1 day, far longer than needed for the Oxford Nanopore Technology library preparation kits (see below), which may not be suitable for time sensitive diagnostic applications.

Overall, Pacific Biosciences has successfully created sequencing instruments capable of generating high accuracy ultra-long-reads.

Oxford Nanopore Technologies

The idea of nanopore-based technologies originated from the Coulter counter and ion channels (Cornell et al., 1997). The single molecule sequencing using biological nanopores was first proposed in 1995 and published in 1998 (Church et al., 1998). Kasianowicz et al. (1996) than described the detection of ssDNA passing through an α-hemolysin nanopore (2.6 nm in diameter; Kasianowicz et al., 1996). Oxford Nanopore Technologies (ONT) officially launched the concept of MinION™ in 2012 as a new generation nucleic acid sequencing technology based on nanopores, free from florescence labels and amplification requirements. It became commercially available in 2015 (Eisenstein, 2012; Deamer

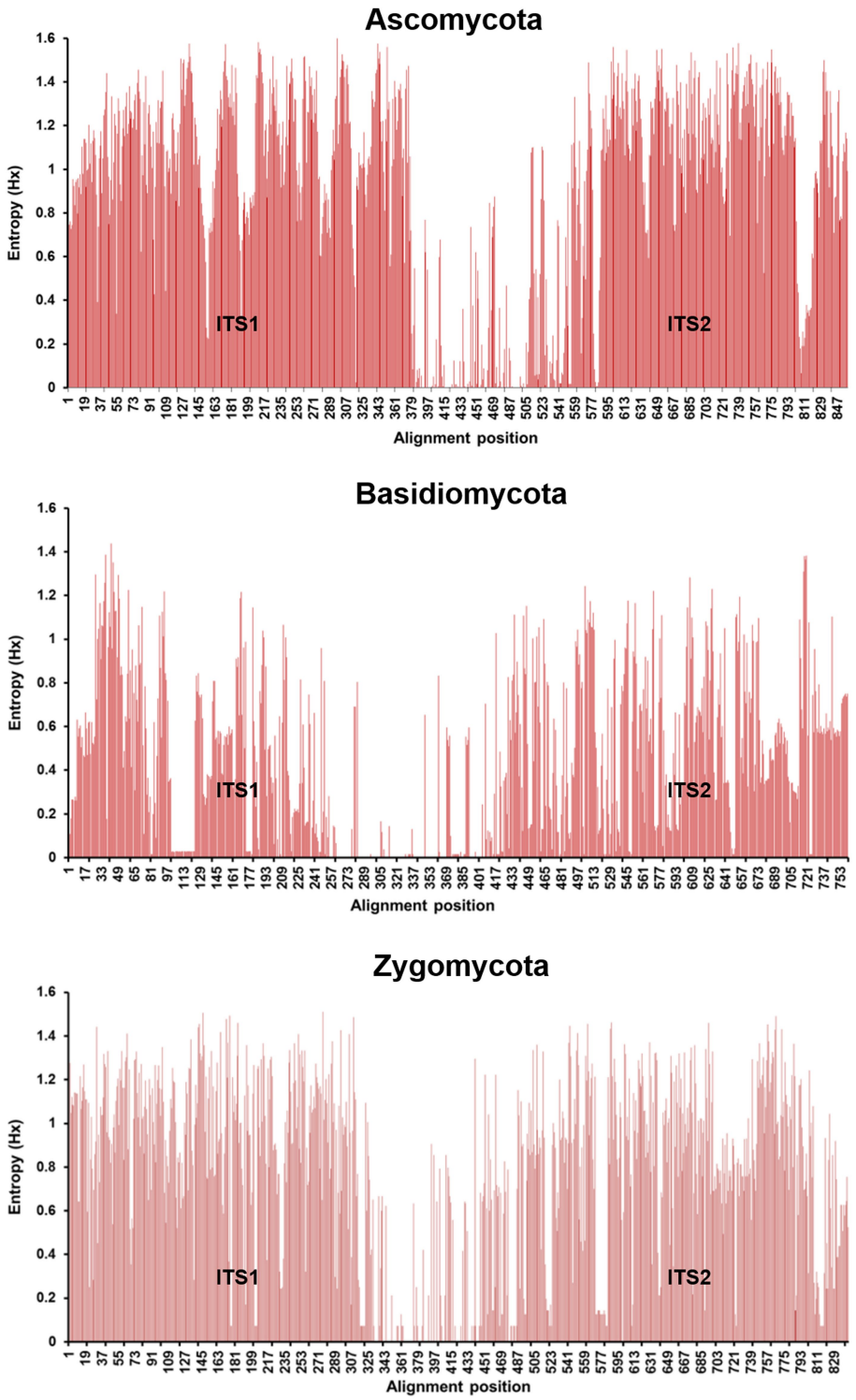

FIGURE 2 | Nucleotide entropy plots showing the variations in the ITS1/2 region for Ascomycota, Basidiomycota, and Zygomycota. The higher the bar is the greater the variation at that position in the nucleotide sequence. The variation of ITS1/2 is higher than that of the ITS1 or ITS2 regions alone and so indicates higher discriminatory power for identification. Entropy values were calculated using BioEdit 7.0.

et al., 2016). The MinION™ is a palm sized portable single molecule sequencing device capable of generating high-throughput, ultra-long sequence reads in real-time at relatively low cost.

The sequencing chemistry of ONT's sequencers has undergone rapid development with the latest flow cell released at the time of writing being the R10.4. However, the basis of nanopore

sequencing remains consistent, relying on biological nanopores embedded in solid state membranes within disposable flow cells (Leggett and Clark, 2017). Different sequencing library preparation methods are available depending on the intended use and data requirements. However, in all library preparation methods, a leader adapter and motor protein are ligated to the end of dsDNA fragments. This library is then loaded into the flow cells and the motor protein functions to unzip dsDNA and process the DNA strand throughout the pore at a specific speed. After one strand is processed, the pore is available to sequence the next available strand. Nucleotides are processed through the biological pores in groups of four called k-mers and as these travel through the pore, a change in an ionic current across the membrane occurs. These changes are then recorded as signal traces and during base calling, are converted to nucleotide sequences (Jain et al., 2016).

ONT's MinION flow cell contains 4x512 nanopore channels, each containing one nanopore, with 512 channels being accessed at a given time. These are run on both the MinION, which supports one flow cell at a time, and the GridION, which supports five flow cells. The PromethION is ONT's production-scale sequencer and provides 3,000 nanopore channels for each flow cell (Oxford Nanopore Technologies, 2021). All instruments can be run until the flow cells no longer have any pores available for sequencing and can be stopped when the intended sequencing depth is achieved. Additionally, the Flongle is a MinION adapter that enables the use of Flongle flow cells that contain 126 nanopore channels at a reduced cost (Oxford Nanopore Technologies, 2019).

The primary appeal of ONT sequencers over other current sequencing technologies is that read length is mostly dependent on sample DNA length, besides high DNA quantity and purity. It has been previously demonstrated to generate read lengths of over 2 million base pairs (Payne et al., 2019). ONT sequencers also offer reduced initial investment costs for sequencers when considering the MinION and the Flongle adapter although library preparation costs remain high (Tedersoo et al., 2021). Per sample sequencing costs depend on multiplexing, sequencing coverage, and re-use of flow cells after washing with a DNase. This makes sequencing available to a wider range of small routine laboratories when other sequencers may only be available for large laboratories or sequencing center. The availability of higher throughput instruments allows nanopore sequencing to be scaled to many different purposes. Multiplexing kits of up to 96 samples are available to further scale projects down if less in-depth sequencing is needed or a lower cost-per sample is necessary. ONT sequencers are highly suited for use in unconventional settings, as field library preparation kits are available that reduce library preparation time to 10 min with limited laboratory equipment. The sequencers are portable as the MinION and Flongle adapters are palm sized, allowing sequencing to be done outside the laboratory, such as at disease outbreak hotspots, war zones or for real-time environmental monitoring. This has previously been demonstrated through its use in space and resource poor settings (Quick et al., 2016; Castro-Wallace et al., 2017). The major drawback of nanopore sequencing has been the low read accuracy being reported with 90% with the R9.4 flow cell and earlier models (Lu et al., 2016). The introduction of new flow cells has led to strong improvements, with average accuracies of 87–98% being commonly reported (Loit et al., 2019; Logsdon et al., 2020). The highest accuracy ever reported after bioinformatics polishing, which might be computation-intensive and may take weeks, stands at >99% (Ashikawa et al., 2018; Morrison et al., 2020). In addition, new bioinformatic tools to improve the accuracy of nanopore reads are now readily available (Loman et al., 2015; Koren et al., 2017; Salmela et al., 2017; Xiao et al., 2017; Hu et al., 2021). As sequencing quality and length depends on the quality of the applied DNA/RNA samples a major drawback is that impurities within the loaded library may block pores and render them unable to sequence.

Overall, nanopore sequencing is by now a broadly accessible long-read sequencing platform with read length limited only by the DNA input making it a fundamentally different approach for sequencing.

HOW CAN LONG-READ SEQUENCING BE APPLIED TO CLINICAL DIAGNOSIS

As long-read sequencing platforms have the potential to accurately identify pathogenic species and simultaneously provide additional genomic information impacting patient outcome, we are focusing the remaining part of the review on the ONT and PacBio platforms for their use in clinical diagnostics.

The read length of SMRT sequencers has advanced to where it is comparable to those generated by ONT although read length is determined by input DNA for both sequencers. When using these directly on patient samples without prior amplification, as in metagenomics, long-reads provide genetic information spanning the whole informative regions of pathogen genomes. For example, DNA barcoding regions, which are between 500 and 800 bp, cannot be covered by short-read sequencing read lengths but are now being able to be fully sequenced by the long-read sequencing instruments. It would also be possible to sequence antimicrobial genes present in the genomes of resistant microbes, informing treatment strategies to improve patient outcome. Long-reads may also allow accurate sequencing of loci important in surveillance or strain typing. In samples where pathogen material is low in abundance, a prior amplification step of important genetic regions would ensure the sequencing of these important target regions although potentially missing other information.

The application of metagenomics to clinical diagnosis requires reliable and highly accurate sequencing and both ONT and PacBio have advertised over 99% per read accuracy for their latest sequencing chemistries. For PacBio, this has been reflected in many recent studies, e.g., Wenger et al., 2019. The accuracy of ONT depends on the type of sequencing chemistry and base-calling algorithms used. The accuracy of ONT technologies has been significantly improving and high accuracy levels are targeted to be achieved in the near future. Although nanopore sequencing may not yet be suitable for

applications, such as single-nucleotide variant identification or genotyping, which requires high coverage to exclude false positives, however, the accuracy required for pathogen identification can already be achieved (Greig et al., 2019; Feng et al., 2021).

Sequencing requirements of diagnostic laboratories cannot be guaranteed to be constant and so this may result in different throughput requirements. As such, investments into high-throughput sequencing instruments, such as the PacBio instruments, are not suitable for routine diagnostic laboratories. However, an alternative may be the implementation of core diagnostic centers that service multiple smaller laboratories and the multiplexing of samples, which would provide an effective way to reduce the cost-per sample. However, this would result in waiting for an adequate number of samples to be pooled for sequencing, which is contradicting the fact that fast diagnosis being the most important facture for the best patient outcome. As such, the smaller scale sequencing offered by ONT with the Flongle flow cells allows for sequencing of individual samples when needed, which is more suitable for general routine laboratories. Additionally, the initial capital investment in sequencing instruments, such as the ones produced by PacBio, may not be feasible for smaller diagnostic laboratories, which only could be overcome by pooling resources into larger diagnostic centers. The smaller scale ONT sequencers are generally affordable, making them more suitable in low throughput settings, such as it is the case in the diagnostic setting for mycoses.

The proposed workflow of the use of long-read sequencers in clinical diagnosis illustrates the need for timely identification (**Figure 3**). The time from sample collection to identification must be as rapid as possible and so the selection of a sequencer and its sample preparation and sequencing time must be considered. PacBio sequencing reports library preparation time of 1 day, while the slowest ONT library preparation kit, the direct cDNA Sequencing Kit, has an estimated preparation time of 270 min. The shortest library preparation option for ONT sequencing is the Field Sequencing Kit (SQK-LRK001) and the Rapid Sequencing Kit (SQK-RAD004), which have a preparation time of only 10 min although these kits produce a lower throughput (Kafetzopoulou et al., 2018). There are also further efforts to reduce turnaround time by reducing sample preparation and sequencing times (Loit et al., 2019). Further sample preparation may be added, which increases preparation times, such as a prior amplification step and sample multiplexing. Both PacBio (Sequel IIe) and ONT provide the option for real-time sequencing, thus eliminating the need to wait for the sequencing to be completed before base-calling can occur. This allows for a substantial reduction of the time from sample collection to pathogen identification to less than 24 h, enabling a faster introduction of the correct treatment, and improving patient outcome.

Before long-read sequencing can be applied to routine diagnostic testing, further work is required to determine the accuracy, specificity, and precision, of long-read sequencers in a clinical setting. The limit of detection must also be determined before it can be reliably implemented. In addition, adequate DNA isolation, library preparation, and loading according to standardized procedures performed by trained personnel are required to take full advantage of long-read technologies for routine diagnostics laboratories.

Long-read sequencers have many features that make them an attractive alternative for the use in clinical diagnosis of infectious disease agents.

LONG-READ SEQUENCING APPLIED TO INFECTIOUS DISEASE INVESTIGATIONS

The application of long-read sequencers to bacterial and viral species identification within a clinical setting is more advanced than that for fungal infections. The general smaller size of bacterial and viral genomes enables to use whole-genome

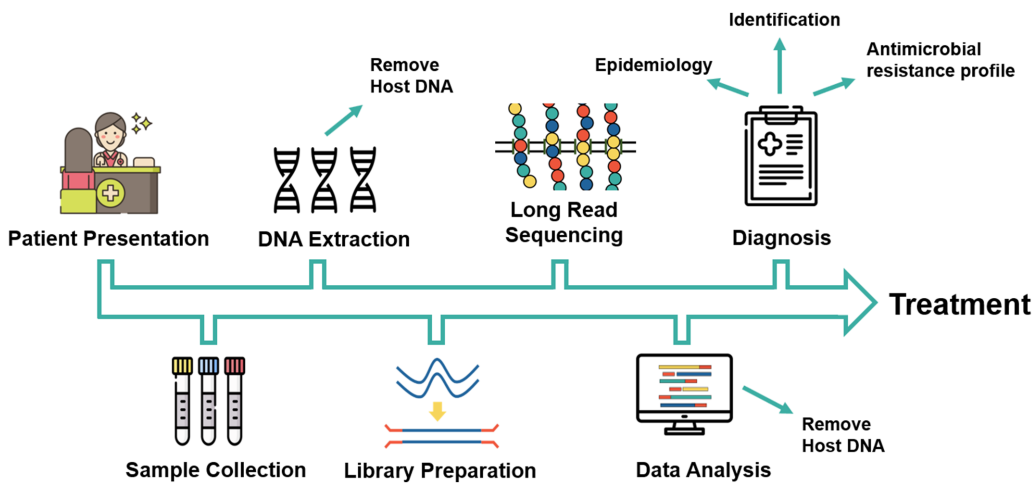

FIGURE 3 | Proposed workflow for long-read-based sequencing in clinical diagnosis of fungal diseases. Icons made by https://www.flaticon.com/authors/freepik.

sequencing studies instead of or in parallel with metagenomics studies, with both employing shotgun sequencing methods without prior amplification. As such, whole-genome sequencing studies will be discussed below alongside metagenomics and metabarcoding studies using long-read sequencers.

Bacterial Infections

The ability of PacBio to identify bacteria using the full length 16S region to the species level was demonstrated by the study by Earl et al. in which 100% of a mock community of 20 bacterial species was identified to the species level (Earl et al., 2018). This was then extended to apply sequencing of a mock community of 250 bacterial species, of which over 90% were accurately identified to the species level. Finally, it was successfully applied to characterize the microbiome of six sinonasal sites of 12 subjects (Earl et al., 2018). The use of PacBio in identification of bacterial species through sequencing of the full length 16S rRNA gene was further demonstrated through generation of microbiome profiles for vaginal samples and sputum samples from patients with cystic fibrosis (Hahn et al., 2016; Wagner et al., 2016). PacBio long-reads have also been used in the generation of whole-genome reference sequences of clinical samples indicating its potential use for future metagenomic studies to identify pathogenic bacteria (Kanamori et al., 2016; El-Rami et al., 2019).

Metagenomics and metabarcoding studies using nanopore sequencers for bacterial samples have been widely used in clinical and research settings. Rapid and accurate diagnosis of a *Capnocytophaga canimorsus* infection in a 62-year-old female patient using metagenomic nanopore sequencing has been reported (Bialasiewicz et al., 2019). This study demonstrated a positive identification was achieved by nanopore sequencing within 19 h, whereas conventional diagnostic techniques required 6.5 days to achieve the same. This short turnaround time from beginning of the sample preparation to pathogen identification is reflected in other studies, estimating a 6–8-h turnaround time (Schmidt et al., 2017; Charalampous et al., 2019; Gargis et al., 2019; Greig et al., 2019), and even using as little as 30 min of sequencing (Sakai et al., 2019; Taxt et al., 2020). Gu et al. (2021) also found a turnaround time of 6 h for nanopore sequencing compared to 24 h to Illumina sequencing. The study also demonstrated accurate identification of pathogenic bacterial species from a variety of clinical samples using metagenomic nanopore and Illumina sequencing. These samples also ranged from culture and PCR negative to PCR positive. In cases where NGS was unable to identify the causative pathogen, the cause was likely due to low pathogen titer or high levels of host background (Gu et al., 2021). An appeal of the use of metagenomics in clinical diagnostics is the potential for additional genomic information, such as antimicrobial resistance coding genes, to be obtained during sequencing. This has been achieved in studies for common bacterial pathogens, such as *Echerichia coli*, *Klebsiella pneumoniae*, *Mycobacterium tuberculosis,* and *Staphylococcus aureus* (Schmidt et al., 2017; Votintseva et al., 2017; Cheng et al., 2018; Charalampous et al., 2019; Gonzalez-Escalona et al., 2019; Taxt et al., 2020). Metagenomic sequencing of clinical bacterial samples has also revealed accurate epidemiological information that can be used for surveillance and outbreak tracing (Votintseva et al., 2017; Gorrie et al., 2018; Imai et al., 2020). ONT sequencers have also been used in metabarcoding studies involving the full length 16S rRNA gene to characterize complex mock communities and identify causative pathogens of clinical samples (Kai et al., 2019; Moon et al., 2019; Nakagawa et al., 2019; Winand et al., 2019).

Many published studies applying long-read sequencing to the identification of pathogenic bacterial species in clinical samples strongly suggest its potential incorporation into routine bacterial diagnosis and encouraging its potential application in fungal diagnoses.

Viral Infections

PacBio sequencing has been used for whole-genome sequencing of a variety of human pathogenic viruses. A limitation of sequencing of viral genomes from clinical samples is the low viral load within cells. As such, reaching the required coverage to ensure an accurate consensus is a challenge. The small size of viral genomes lends themselves to overcome this issue through the amplification of the viral genome, which has been successfully used in whole-genome sequencing studies using PacBio, where the read lengths are able to span the whole amplicon length (Ocwieja et al., 2012; Dilernia et al., 2015; Bull et al., 2016; Nakano et al., 2017). PacBio sequencing has been demonstrated to be capable of the identification of viral pathogens from clinical samples but has not yet been used in routine viral diagnosis due to the high costs associated (Ho et al., 2017; Li et al., 2020). Identification of norovirus from patient samples has been performed to simulate diagnosis during an outbreak and demonstrated PacBio achieved sequencing of the entire viral pathogen, Norovirus GII, with high coverage of 99.11%; however, this was greatly limited by the long turnaround time (66 h; Li et al., 2020). PacBio reads have also been utilized in sequencing SARS-CoV-2 from patient samples to study the evolution and progression of disease and inform antiviral treatment (Ko et al., 2021). PacBio has additionally been used to achieve deep sequencing of genomic regions of viruses that are unable to be resolved using short-read sequencers (Bergfors et al., 2016; Huang et al., 2016; Ho et al., 2017; Lui et al., 2019; Takeda et al., 2019; Yamashita et al., 2020). Although these studies do not aim to identify the pathogens, the regions targeted for deep sequencing inform on resistance to antiviral treatments.

ONT has been widely used for the identification of viral pathogens in disease diagnostics and surveillance. Like the PacBio studies, nanopore sequencing of viral genomes often first involves either the amplification of the full genome or the generation of overlapping pooled amplicons that span the entirety of the genome (Quick et al., 2017; Deng et al., 2020). Nanopore sequencing has been demonstrated to be a useful tool for the identification of major pathogens during outbreaks, such as for the Ebola epidemic in West Africa from 2014 to 2016 and to generate additional genomic information on geographic, climate, and demographic factors (Hoenen et al., 2016; Quick et al., 2016; Dudas et al., 2017). Nanopore sequencing

has also been used in the recent COVID-19 pandemic, e.g., for a prospective study of the complex transmission within healthcare settings through the generation of 747 SARS-CoV-2 genomes from PCR-positive diagnostic samples within 24 h of sample collection (Meredith et al., 2020). Epidemiological information of the spread of a variant of SARS-CoV-2 was generated using nanopore sequencing to inform on further action needed to control its spread (Washington et al., 2021). ONT sequencers have additionally been used for whole-genome sequencing during the Zika virus epidemic (Faria et al., 2017), Yellow fever virus epidemic (Faria et al., 2018), and the Lassa fever outbreak in Nigeria (Kafetzopoulou et al., 2019). Whole-genome sequencing from clinical samples has also been demonstrated for human metapneumovirus (Xu et al., 2020), Chikungunya and Dengue viruses (Kafetzopoulou et al., 2018), Influenza (Lewandowski et al., 2019), and Hepatitis C virus (Greninger et al., 2015).

Long-read sequencing technologies have demonstrated their ability to be used to diagnose viral infections in the clinical setting and have a proven track record for analysis of samples during epidemics and a pandemic to produce valuable public health information.

Fungal Infections

The application of long-read sequencing to fungal identification in a clinical setting is currently limited.

Whole genomes of major fungal pathogens have been generated with the use of long-read sequencers often in combination with short-read sequencing, so called as hybrid assemblies (Cuomo et al., 2017; Luo et al., 2017; Vale-Silva et al., 2017; Panthee et al., 2018; Rhodes et al., 2018; Morand et al., 2019; Schultzhaus et al., 2019; Pchelin et al., 2020). The use of whole-genome sequencing in clinical practice is not yet feasible, as the cost and data processing requirements are currently too high for routine use.

In clinical applications, PacBio sequencers have been used to characterize the fungal composition of fecal samples from 14 healthy individuals (Motooka et al., 2017). The study identified multiple fungal species present within the healthy gut mycobiota and characterized two major mycobiota types. This study by Motooka et al. (2017) additionally found PacBio was able to accurately identify all 26 fungal species in a mock community through metabarcoding of the ITS1 region, where short-read sequencers could not. Additionally, PacBio most accurately estimated the abundance of species within the mock community. The predominant reason PacBio outperformed the short-read sequencers was the use of long-reads, ensuring complete and accurate coverage of the entire 300–800 bp long ITS1 region (Motooka et al., 2017). PacBio has also been used for metabarcoding analysis of environmental fungal samples using the shorter ITS2 minibarcode and the large ribosomal subunit (28S), which are often used by short-read barcode studies (Cline and Zak, 2015; Kyaschenko et al., 2017). Sequencing of the full length ITS1/2 DNA barcoding region by PacBio sequencers has been demonstrated on a wide variety of fungal species (James et al., 2016; Walder et al., 2017; Heeger et al., 2018; Tedersoo et al., 2018; Purahong et al., 2019; Tedersoo and Anslan, 2019). A comparison between PacBio and nanopore sequencers found PacBio to be more efficient in the metabarcoding of complex environmental fungal samples due to errors found in nanopore sequencing (Loit et al., 2019). Additionally, sample to identification time was reduced to 2.5 h through metagenomic nanopore sequencing of plant samples (Loit et al., 2019). These studies indicate the further potential for long-read PacBio sequencing to be used in metabarcoding to identify causative pathogens in clinical samples.

The use of ONT in metabarcoding and metagenomics is similarly limited; however, direct clinical use has been previously demonstrated (Irinyi et al., 2020; Gu et al., 2021). Three patient samples, positive for *P. jirovecii* infection, alongside three samples without infection underwent metagenomic sequencing using ONT's MinION flow cells (Irinyi et al., 2020). The resulting reads were assigned using two different analysis tools, ONT's own "What's in my pot" and nucleotide BLAST, and the resulting assignments were compared. Sequencing of all three positive patient samples produced *P. jirovecii* reads while surprisingly, *Pneumocystis* reads were detected in negative samples when using the "What's in my pot" analysis tool; however, this is attributed to issues applying the analysis tool to fungal identification. *Homo sapiens* sequences accounted for 70–95% of all reads besides one outlier (10%). Additionally, the sample sites were bronchiolar lavage and induced sputum samples which are non-sterile sites and so multiple other fungal species were identified alongside the known causative pathogen. Notably, *Paracoccidioides* spp. were identified within the sample. However, this indicates a clear false positive, as *Paracoccidioides* spp. are geographically restricted to the tropical areas of Latin America, which did not align with the patient's travel history. This indicated that fungal diagnosis solely based off metagenomic sequencing using ONT has currently a number of limiting factors, including the low host:pathogen ratio, lack of comprehensive reference sequence databases, and the lack of appropriate bioinformatic tool, which need to be overcome before it can be applied in a routine diagnostic setting (Irinyi et al., 2020).

Gu et al. (2021) evaluated the diagnostic accuracy and performance of nanopore and Illumina sequencing on clinical body fluid samples (Gu et al., 2021). This study sequenced 87 patient samples by both sequencing technologies to compare the sensitivity and specificity. For fungal pathogen detection, the sensitivity and specificity of nanopore sequencing were found to be 90.9 and 100%, respectively, for nanopore sequencing, compared to 90.6 and 89.0% for Illumina sequencing. Additionally, five patient samples with negative culturing and PCR testing results were analyzed using NGS and three samples were found to be positive for fungal pathogens. For two samples, NGS did not detect any pathogens. However, the fungal pathogens *Cryptococcus neoformans* and *Sporothrix schenkii* were identified in these samples through further testing, most likely due to low pathogen titers or high host background DNA in the sample. This study demonstrated that mNGS can be applied to infectious disease diagnosis and would be a valuable tool in the routine diagnostic

process (Gu et al., 2021). Even though this study achieved the identification of causative pathogens using ONT sequencing, it also highlighted again many issues currently associated with practical implementation into routine diagnostics, including the importance of the quality of the input DNA, the proportion of pathogen DNA to host DNA, and the lack of comprehensive reference databases (Gu et al., 2021). Furthermore,

Metabarcoding for the identification of fungal pathogens from clinical samples using nanopore sequencing has also been performed. The ITS1/2 region was amplified in a patient sample previously confirmed having a *Candia albicans* infection and the resulting amplicons were sequenced on the ONT MinION (Ashikawa et al., 2018). This resulted in 97.3% of the first 4,000 reads and 99.1% of reads generated after 48 h being assigned to *C. albicans*, confirming the previous diagnosis. Another study used metabarcoding by nanopore sequencing to identify 16 members of an artificial fungal community using the ITS1/2 region (Mafune et al., 2020). The ITS1/2 region was also used to identify 87% of the fungal species present in 43 respiratory samples and identified others not detected through routine testing (Chan et al., 2020). Metabarcoding of 1,312 clinical respiratory samples with the bacterial 16S gene and fungal ITS1/2 region identified pathogens in 51.5% of samples with a turnaround time of <24 h. Nanopore sequence alone identified 31% of samples, while 0.5% were identified with culture-based techniques only (Wang et al., 2020). Long amplicon nanopore sequencing of the full ITS region and the whole fungal operon successfully identified all members of a mock community and microbial cultures (D'Andreano et al., 2021). The full ITS region was also used to characterize the fungal microbiota of healthy and potentially infected clinical canine samples (D'Andreano et al., 2021). The fungal intergenic spacer region has also been demonstrated to identify members from the *Cryptococcus gattii* and *Cryptococcus neoformans* species complexes by multiplexing 24 strains on a single MinION flow cell. Sequencing errors in regions with homopolymers were observed. However, with the R10.3 flow cell, this error rate was reduced by 57% and the sequence identity increased to 99.83% (Morrison et al., 2020).

These preliminary studies indicate the potential for the application of ONT and PacBio sequencers to the clinical diagnosis of fungal infections if the above-mentioned limitations are overcome to develop a workflow for clinical diagnosis.

CURRENT ISSUES WITH LONG-READ SEQUENCING

Long-read sequencers have been demonstrated to effectively identify bacteria, viruses, and fungi, from clinical samples using both metagenomics and metabarcoding approaches. Although these studies have illustrated the potential for long-read sequencing in clinical diagnosis, a range of current challenges facing their implementation has also been highlighted.

DNA Extraction

Sequencing success depends on sample DNA quantity and quality. Pathogens are often present at low concentrations during infection and so high DNA concentrations are optimal to ensure adequate sequencing coverage of the causative pathogen for identification. Metagenomics and metabarcoding sequencing are aimed to represent everything within a sample and so ideally genomic material will be directly representative of what is present. As such, DNA extraction methods must be able to effectively lyse all cell types and preserve all genomic material.

For fungal pathogens, this presents a challenge, as fungal species have thick cell walls, containing polysaccharides and high content of lipids, that are difficult to lyse, which impedes the release of nucleic acids. As such fungal DNA extraction methods often involve a manual disruption step, such as bead bashing or crushing with liquid nitrogen to break open the fungal cell walls. This often leads to DNA shearing, greatly reducing the lengths of DNA fragments, defeating the purpose of long-read sequencing. A number of methods describing the extraction of DNA from fungal material for the use of nanopore and PacBio sequencing have reported to produce DNA fragments with an average fragment size above 35 kbp, although this has not yet been applied to clinical samples (Feehan et al., 2017; Schwessinger and Rathjen, 2017; Inglis et al., 2018). The development of better extraction methods is important to improve the application of long-read sequencers to accurate clinical diagnosis.

Ratio of Host to Pathogen DNA

A major problem in metagenomics analysis is the high amount of host (human) DNA in the sample, which may shadow the detection of pathogen DNA. One possible solution would be to increase the proportion of pathogen DNA in comparison with host DNA within the sample. This may be achieved through the depletion of human DNA in the clinical sample, which still is suboptimal even though there are several commercial kits and laboratory protocols for this purpose available (Marotz et al., 2018; Charalampous et al., 2019; Helmersen and Aamot, 2020; Heravi et al., 2020).

An alternative to this would be to increase the abundance of pathogen DNA, which can be achieved through amplification of important genomic regions, such as in metabarcoding studies, or amplification of overlapping DNA regions as done in viral whole-genome sequencing (Quick et al., 2017; Deng et al., 2020). An improved host to pathogen DNA ratio would greatly improve identification using long-read sequencing as it would enable higher coverage of the causative pathogen, leading to more accurate identification and the possibility of further genomic information. An increase in pathogen reads would also make long-read sequencing more cost-effective since more relevant data would be generated, possibly allowing for multiplexing of samples.

Another way to enrich pathogen DNA and deplete host DNA is the application of adaptive sequencing with nanopore sequencers. DNA molecules are selected for by identifying unwanted sequences and reversing the voltage across the membrane, thereby stopping

sequencing. Bioinformatic tools have been developed to implement adaptive sequencing for the selection of specific chromosomes and the depletion of bacterial genomes to enrich the remaining species in a metagenomic population (Kovaka et al., 2020; Payne et al., 2020). For diagnosis of mycoses, fungal DNA would ideally be selected for while human DNA is rejected; however, this is yet to be explored. The improvement of host to pathogen DNA ratio would greatly increase the amount of relevant data for clinical diagnosis and further work is required to implement these methods to routine diagnostics.

Lack of Reference Genomes

The major appeal of long-read sequencing in a shotgun approach is the vast genomic information that can be gained from the data generated. In metagenomic studies, genomic information from throughout the genome is generated; however, there is a lack of reference genomes for most of the pathogenic fungal species (**Figure 4**) and as such a proportion of data generated cannot be mapped to an appropriate reference genome either in FungiDB[5] (Basenko et al., 2018) and GenBank[6] (Sayers et al., 2020).

The basis for accurate genomic-based identification is the availability of high-quality, curated reference whole-genome databases. It has been demonstrated that inaccurate reference sequences have caused miss-mapping of the generated sequence reads leading to clear misidentification that potentially causes confusion surrounding diagnosis in clinical practice (Bialasiewicz et al., 2019; Irinyi et al., 2020). In addition, it is causing an unproductive strain on bioinformatic tools used and lengthening the time for identification. Diagnostic whole-genome database entries must have accurate sequences, metadata, and phylogenetic coverage to prevent false positive and negative identifications.

It is predicted that with the implementation of a reliable and accurate whole-genome reference database, the accuracy of fungal identification will dramatically improve (**Figure 5**). The principle is demonstrated through the developing taxonomy of the *Fusarium solani* species complex. A previous study examined four loci of these species and proposed the change in nomenclature of the *F. solani* species complex to be placed in the *Neocosmospora* genus (Sandoval-Denis et al., 2019). However, a recent study has analyzed 19 loci and has maintained that the members of the *F. solani* species complex should remain in the genus *Fusarium* (Geiser et al., 2020; O'Donnell et al., 2020). As such, the increased loci analyzed generated more data and provided more insight into the taxonomy of the *F. solani* species complex and if whole-genome data were available, the most accurate taxonomic information would be revealed, which if applied to all (pathogenic) fungal species

[5]https://fungidb.org/
[6]https://www.ncbi.nlm.nih.gov/genbank/

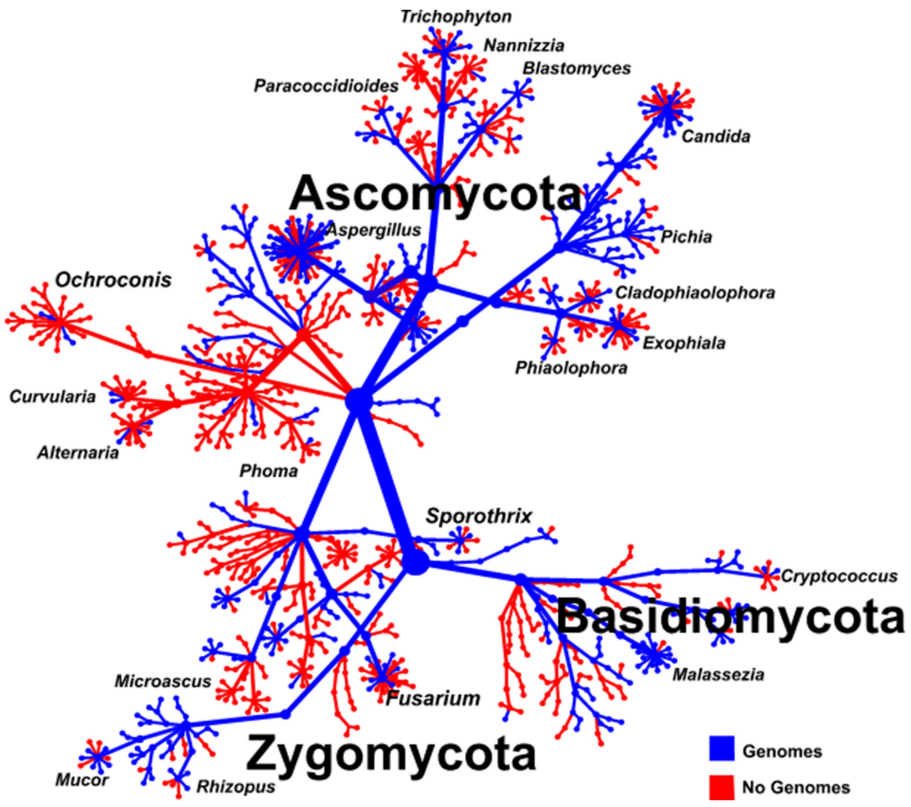

FIGURE 4 | Tree of the fungal Kingdom showing the major fungal classes and their human pathogenic species indicating species with (blue) and without (red) genomes.

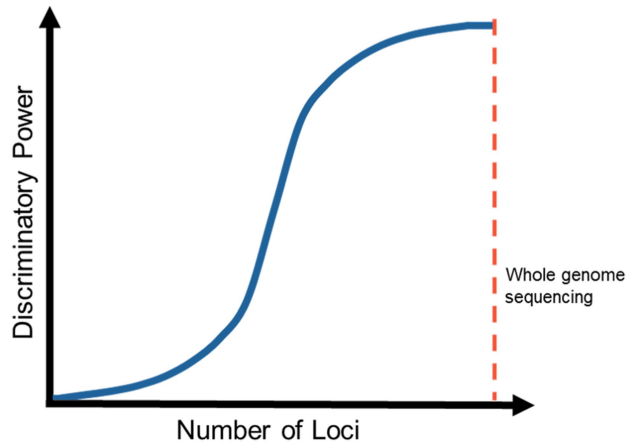

FIGURE 5 | Potential cumulative increase in discriminatory power with the addition of more loci or whole genomes being used for identification.

would greatly increase the discriminatory power of long-read sequencing in clinical diagnosis.

This highlights that global efforts are urgently needed to improve the relevant reference genome databases (FungiDB and GenBank) as well as the antifungal resistance database MARDy[7] (Nash et al., 2018), to be able to open up the full potential of the metagenomic data generated by long-read sequencers.

Bioinformatics

Currently, there is a wide variety of bioinformatics tools for the analysis of long-read sequences (Makalowski and Shabardina, 2020). Some such bioinformatics tools used for species identification in metagenomic studies are "What's In My Pot" (Juul et al., 2015), SUPRI real-time (Gu et al., 2021), MetaMaps (Dilthey et al., 2019), BugSeq (Fan et al., 2021), and NGSpeciesID (Vasiljevic et al., 2021).

For use in a clinical setting, a simple bioinformatics workflow would be necessary for practical implementation into routine diagnosis as it would be best to avoid requiring highly specialized personnel for analysis. A study comparing the ability of different bioinformatics tools to identify a wide array of pathogens from long-read sequencing dataset would be necessary to determine the most suitable bioinformatics tools.

Data interpretation is a major issue in metagenomics and metabarcoding analysis. Both methods generate large amounts of data and for the purpose of clinical diagnosis, the interpretation can be complex. When samples are taken from sterile sites, the expected sequencing results would consist of predominantly *Homo sapiens* reads and reads assigned the causative pathogen. However, if any contamination was to occur and reads were assigned to multiple microbes, this would complicate identification of the causative pathogen. This issue is magnified when patient samples are taken from non-sterile sites. Sequencing results will have reads assigned to multiple microbes and although it would be intuitive to assume the microbe with the highest abundance would be the causative pathogen, this is not always the case as has been observed in Irinyi et al. (2020). To overcome this, the application of machine-leaning algorithms helping to distinguish true pathogens from common colonizers or environmental contaminants may one of the ways forward. The large proportion of *H. sapiens* reads also complicates data interpretation as percentages of reads assigned to microorganisms is comparatively small. However, if bioinformatics tools were designed to remove host reads, microorganism abundance can be more easily compared and may further illuminate the causative pathogen.

[7]http://mardy.dide.ic.ac.uk/

THE FUTURE OF LONG-READ SEQUENCING AND FUNGAL DIAGNOSIS

The introduction of long-read sequencers from PacBio and ONT has allowed sequencing of genetic material in a way previously not possible. The first applications of long-read sequencing to identify agents of infectious disease has demonstrated its potential in clinical diagnosis.

The current state of DNA extraction technologies, the lack of comprehensive reference databases, and simple bioinformation pipelines requires further development before long-read sequencers can be implemented in routine diagnosis. Additionally, the identification of multiple microbes within a clinical specimen may not directly lead to a specific diagnosis, but in conjunction with the patient's presentation and further testing should seriously be considered as a way to achieve a fast and reliable diagnosis. Further advancements in the clinical diagnostic metagenomics workflow must be made to make its implementation in routine clinical diagnostic feasible. With the rapid decline of sequencing costs and the exponential improvement in sequencing capabilities, long-read sequencing is an important new technology which may eventually reduce the impact of pathogenic fungi on human health, by drastically reducing the turnaround time for diagnosis, supporting better treatment choices, reducing morbidity and mortality, and massively reduce associated healthcare costs, through its use in clinical diagnosis.

AUTHOR CONTRIBUTIONS

WM, LI, and BS conceived the review. WM coordinated and supervised the review. MH, LI, YH, BS, and WM wrote and corrected the manuscript. All authors contributed to the article and approved the submitted version.

FUNDING

This study was supported by a National Health and Medical Research Council of Australia (NH&MRC) grant (no. APP1121936) to WM.

REFERENCES

Angeletti, S. (2017). Matrix assisted laser desorption time of flight mass spectrometry (MALDI-TOF MS) in clinical microbiology. *J. Microbiol. Methods* 138, 20–29. doi: 10.1016/j.mimet.2016.09.003

Ardui, S., Ameur, A., Vermeesch, J. R., and Hestand, M. S. (2018). Single molecule real-time (SMRT) sequencing comes of age: applications and utilities for medical diagnostics. *Nucleic Acids Res.* 46, 2159–2168. doi: 10.1093/nar/gky066

Armanhi, J. S., de Souza, R. S., de Araujo, L. M., Okura, V. K., Mieczkowski, P., Imperial, J., et al. (2016). Multiplex amplicon sequencing for microbe identification in community-based culture collections. *Sci. Rep.* 6:29543. doi: 10.1038/srep29543

Ashikawa, S., Tarumoto, N., Imai, K., Sakai, J., Kodana, M., Kawamura, T., et al. (2018). Rapid identification of pathogens from positive blood culture bottles with the MinION nanopore sequencer. *J. Med. Microbiol.* 67, 1589–1595. doi: 10.1099/jmm.0.000855

Austin, B. (2017). The value of cultures to modern microbiology. *Antonie Van Leeuwenhoek* 110, 1247–1256. doi: 10.1007/s10482-017-0840-8

Basenko, E. Y., Pulman, J. A., Shanmugasundram, A., Harb, O. S., Crouch, K., Starns, D., et al. (2018). FungiDB: an integrated bioinformatic resource for fungi and oomycetes. *J. Fungi* 4, 1–28. doi: 10.3390/jof4010039

Bergfors, A., Leenheer, D. Bergqvist, A., Ameur, A., and Lennerstrand, J. (2016). Analysis of hepatitis C NS5A resistance associated polymorphisms using ultra deep single molecule real time (SMRT) sequencing. *Antivir. Res.* 126, 81–89. doi: 10.1016/j.antiviral.2015.12.005

Bharti, R., and Grimm, D. G. (2021). Current challenges and best-practice protocols for microbiome analysis. *Brief. Bioinform.* 22, 178–193. doi: 10.1093/bib/bbz155

Bialasiewicz, S., Duarte, T. P., Nguyen, S. H., Sukumaran, V., Stewart, A., Appleton, S., et al. (2019). Rapid diagnosis of *Capnocytophaga canimorsus* septic shock in an immunocompetent individual using real-time Nanopore sequencing: a case report. *BMC Infect. Dis.* 19:660. doi: 10.1186/s12879-019-4173-2

Brandt, M. E., Padhye, A. A., Mayer, L. W., and Holloway, B. P. (1998). Utility of random amplified polymorphic DNA PCR and TaqMan automated detection in molecular identification of *Aspergillus fumigatus*. *J. Clin. Microbiol.* 36, 2057–2062. doi: 10.1128/JCM.36.7.2057-2062.1998

Bull, R. A., Eltahla, A. A., Rodrigo, C., Koekkoek, S. M., Walker, M., Pirozyan, M. R., et al. (2016). A method for near full-length amplification and sequencing for six hepatitis C virus genotypes. *BMC Genomics* 17:247. doi: 10.1186/s12864-016-2575-8

Carvalho, A., Costa-De-Oliveira, S., Martins, M. L., Pina-Vaz, C., Rodrigues, A. G., Ludovico, P., et al. (2007). Multiplex PCR identification of eight clinically relevant *Candida* species. *Med. Mycol.* 45, 619–627. doi: 10.1080/13693780701501787

Castro-Wallace, S. L., Chiu, C. Y., John, K. K., Stahl, S. E., Rubins, K. H., McIntyre, A. B. R., et al. (2017). Nanopore DNA sequencing and genome assembly on the international space station. *Sci. Rep.* 7:18022. doi: 10.1038/s41598-017-18364-0

Chan, W. S., Au, C. H., Leung, S. M., Ho, D. N., Wong, E. Y. L., To, M. Y., et al. (2020). Potential utility of targeted nanopore sequencing for improving etiologic diagnosis of bacterial and fungal respiratory infection. *Diagn. Pathol.* 15:41. doi: 10.1186/s13000-020-00960-w

Charalampous, T., Kay, G. L., Richardson, H., Aydin, A., Baldan, R., Jeanes, C., et al. (2019). Nanopore metagenomics enables rapid clinical diagnosis of bacterial lower respiratory infection. *Nat. Biotechnol.* 37, 783–792. doi: 10.1038/s41587-019-0156-5

Chen, S. C.-A., Meyer, W., and Sorrell, T. C. (2014). *Cryptococcus gattii* infections. *Clin. Microbiol. Rev.* 27, 980–1024. doi: 10.1128/CMR.00126-13

Cheng, J., Hu, H., Kang, Y., Chen, W., Fang, W., Wang, K., et al. (2018). Identification of pathogens in culture-negative infective endocarditis cases by metagenomic analysis. *Ann. Clin. Microbiol. Antimicrob.* 17:43. doi: 10.1186/s12941-018-0294-5

Chin, C. S., Alexander, D. H., Marks, P., Klammer, A. A., Drake, J., Heiner, C., et al. (2013). Nonhybrid, finished microbial genome assemblies from long-read SMRT sequencing data. *Nat. Methods* 10, 563–569. doi: 10.1038/nmeth.2474

Church, G., Deamer, D.W., Branton, D., Baldarelli, R., and Kasianowicz, J. (1998). *Characterization of Individual Polymer Molecules Based on Monomer-Interface Interactions*. US Patent No. 5795782. Available at: https://patents.google.com/patent/US5795782A/en (Accessed 23 February 2016).

Clancy, C. J., Pappas, P. G., Vazquez, J., Judson, M. A., Kontoyiannis, D. P., Thompson, G. R. 3rd, et al. (2018). Detecting infections rapidly and easily for candidemia trial, part 2 (DIRECT2): a prospective, multicenter study of the T2Candida panel. *Clin. Infect. Dis.* 66, 1678–1686. doi: 10.1093/cid/cix1095

Clark, A. E., Kaleta, E. J., Arora, A., and Wolk, D. M. (2013). Matrix-assisted laser desorption ionization-time of flight mass spectrometry: a fundamental shift in the routine practice of clinical microbiology. *Clin. Microbiol. Rev.* 26, 547–603. doi: 10.1128/CMR.00072-12

Cline, L. C., and Zak, D. R. (2015). Initial colonization, community assembly and ecosystem function: fungal colonist traits and litter biochemistry mediate decay rate. *Mol. Ecol.* 24, 5045–5058. doi: 10.1111/mec.13361

Colabella, C., Casagrande Pierantoni, D., Corte, L., Roscini, L., Conti, A., Bassetti, M., et al. (2021). Single strain high-depth NGS reveals high rDNA (ITS-LSU) variability in the four prevalent pathogenic species of the genus *Candida*. *Microorganisms* 9:302. doi: 10.3390/microorganisms9020302

Cornell, B. A., Braach-Maksvytis, V. L. B., King, L. G., Osman, P. D. J., Raguse, B., Wieczorek, L., et al. (1997). A biosensor that uses ion-channel switches. *Nature* 387, 580–583. doi: 10.1038/42432

Couto, N., Schuele, L., Raangs, E. C., Machado, M. P., Mendes, C. I., Jesus, T. F., et al. (2018). Critical steps in clinical shotgun metagenomics for the concomitant detection and typing of microbial pathogens. *Sci. Rep.* 8:13767. doi: 10.1038/s41598-018-31873-w

Cuomo, C. A., Shea, T., Yang, B., Rao, R., and Forche, A. (2017). Whole genome sequence of the heterozygous clinical isolate Candida krusei 81-B-5. *G3* 7, 2883–2889. doi: 10.1534/g3.117.043547

D'Andreano, S., Cusco, A., and Francino, O. (2021). Rapid and real-time identification of fungi up to species level with long amplicon nanopore sequencing from clinical samples. *Biol. Methods Protoc.* 6:bpaa026. doi: 10.1093/biomethods/bpaa026

de Heer, K., Gerritsen, M. G., Visser, C. E., and Leeflang, M. M. (2019). Galactomannan detection in broncho-alveolar lavage fluid for invasive aspergillosis in immunocompromised patients. *Cochrane Database Syst. Rev.* 5:CD012399. doi: 10.1002/14651858.CD012399.pub2

De Hoog, G., Guarro, J., Gené, J., Ahmed, S., Al-Hatmi, A., Figueras, M., et al. (2019). *Atlas of Clinical Fungi 2019*. Reus: Utrecht, The Netherlands.

De Maio, N., Shaw, L. P., Hubbard, A., George, S., Sanderson, N. D., Swann, J., et al. (2019). Comparison of long-read sequencing technologies in the hybrid assembly of complex bacterial genomes. *Microb. Genom.* 5, 1–12. doi: 10.1099/mgen.0.000294

Deamer, D., Akeson, M., and Branton, D. (2016). Three decades of nanopore sequencing. *Nat. Biotechnol.* 34, 518–524. doi: 10.1038/nbt.3423

Dendis, M., Horvath, R., Michalek, J., Ruzicka, F., Grijalva, M., Bartos, M., et al. (2003). PCR-RFLP detection and species identification of fungal pathogens in patients with febrile neutropenia. *Clin. Microbiol. Infect.* 9, 1191–1202. doi: 10.1111/j.1469-0691.2003.00719.x

Deng, X., Achari, A., Federman, S., Yu, G., Somasekar, S., Bártolo, I., et al. (2020). Metagenomic sequencing with spiked primer enrichment for viral diagnostics and genomic surveillance. *Nat. Microbiol.* 5, 443–454. doi: 10.1038/s41564-019-0637-9

Dilernia, D. A., Chien, J.-T., Monaco, D. C., Brown, M. P., Ende, Z., Deymier, M. J., et al. (2015). Multiplexed highly-accurate DNA sequencing of closely-related HIV-1 variants using continuous long reads from single molecule, real-time sequencing. *Nucleic Acids Res.* 43:e129. doi: 10.1093/nar/gkv630

Dilthey, A. T., Jain, C., Koren, S., and Phillippy, A. M. (2019). Strain-level metagenomic assignment and compositional estimation for long reads with MetaMaps. *Nat. Commun.* 10:3066. doi: 10.1038/s41467-019-10934-2

Dudas, G., Carvalho, L. M., Bedford, T., Tatem, A. J., Baele, G., Faria, N. R., et al. (2017). Virus genomes reveal factors that spread and sustained the Ebola epidemic. *Nature* 544, 309–315. doi: 10.1038/nature22040

Earl, J. P., Adappa, N. D., Krol, J., Bhat, A. S., Balashov, S., Ehrlich, R. L., et al. (2018). Species-level bacterial community profiling of the healthy sinonasal microbiome using pacific biosciences sequencing of full-length 16S rRNA genes. *Microbiome* 6:190. doi: 10.1186/s40168-018-0569-2

Edouard, S., Million, M., Bachar, D., Dubourg, G., Michelle, C., Ninove, L., et al. (2018). The nasopharyngeal microbiota in patients with viral respiratory tract infections is enriched in bacterial pathogens. *Eur. J. Clin. Microbiol. Infect. Dis.* 37, 1725–1733. doi: 10.1007/s10096-018-3305-8

Eid, J., Fehr, A., Gray, J., Luong, K., Lyle, J., Otto, G., et al. (2009). Real-time DNA sequencing from single polymerase molecules. *Science* 323, 133–138. doi: 10.1126/science.1162986

Eisenstein, M. (2012). Oxford nanopore announcement sets sequencing sector abuzz. *Nat. Biotechnol.* 30, 295–296. doi: 10.1038/nbt0412-295

El-Rami, F. E., Zielke, R. A., Wi, T., Sikora, A. E., and Unemo, M. (2019). Quantitative proteomics of the 2016 WHO *Neisseria gonorrhoeae* reference strains surveys vaccine candidates and antimicrobial resistance determinants. *Mol. Cell. Proteomics* 18, 127–150. doi: 10.1074/mcp.RA118.001125

Fan, J., Huang, S., and Chorlton, S. D. (2021). BugSeq: a highly accurate cloud platform for long-read metagenomic analyses. *BMC Bioinform.* 22:160. doi: 10.1186/s12859-021-04089-5

Faria, N. R., Kraemer, M. U. G., Hill, S. C., Goes de Jesus, J., Aguiar, R. S., Iani, F. C. M., et al. (2018). Genomic and epidemiological monitoring of yellow fever virus transmission potential. *Science* 361, 894–899. doi: 10.1126/science.aat7115

Faria, N. R., Quick, J., Claro, I. M., Theze, J., de Jesus, J. G., Giovanetti, M., et al. (2017). Establishment and cryptic transmission of Zika virus in Brazil and the Americas. *Nature* 546, 406–410. doi: 10.1038/nature22401

Feehan, J. M., Scheibel, K. E., Bourras, S., Underwood, W., Keller, B., and Somerville, S. C. (2017). Purification of high molecular weight genomic DNA from powdery mildew for long-read sequencing. *J. Vis. Exp.* e55463, 1–8. doi: 10.3791/55463

Feng, Z., Clemente, J. C., Wong, B., and Schadt, E. E. (2021). Detecting and phasing minor single-nucleotide variants from long-read sequencing data. *Nat. Commun.* 12:3032. doi: 10.1038/s41467-021-23289-4

Fenselau, C., and Demirev, P. A. (2001). Characterization of intact microorganisms by MALDI mass spectrometry. *Mass Spectrom. Rev.* 20, 157–171. doi: 10.1002/mas.10004

Forbes, J. D., Knox, N. C., Ronholm, J., Pagotto, F., and Reimer, A. (2017). Metagenomics: the next culture-independent game changer. *Front. Microbiol.* 8:1069. doi: 10.3389/fmicb.2017.01069

Ganley, A. R., and Kobayashi, T. (2007). Highly efficient concerted evolution in the ribosomal DNA repeats: total rDNA repeat variation revealed by whole-genome shotgun sequence data. *Genome Res.* 17, 184–191. doi: 10.1101/gr.5457707

Gargis, A. S., Cherney, B., Conley, A. B., McLaughlin, H. P., and Sue, D. (2019). Rapid detection of genetic engineering, structural variation, and antimicrobial resistance markers in bacterial biothreat pathogens by nanopore sequencing. *Sci. Rep.* 9:13501. doi: 10.1038/s41598-019-49700-1

Garrido-Cardenas, J. A., and Manzano-Agugliaro, F. (2017). The metagenomics worldwide research. *Curr. Genet.* 63, 819–829. doi: 10.1007/s00294-017-0693-8

Geiser, D. M., Al-Hatmi, A., Aoki, T., Arie, T., Balmas, V., Barnes, I., et al. (2020). Phylogenomic analysis of a 55.1 kb 19-gene dataset resolves a monophyletic *Fusarium* that includes the *Fusarium solani* species complex. *Phytopathology* 111, 1064–1079. doi: 10.1094/PHYTO-08-20-0330-LE

Goldstein, E. J., Tyrrell, K. L., and Citron, D. M. (2015). *Lactobacillus* species: taxonomic complexity and controversial susceptibilities. *Clin. Infect. Dis.* 60(*Suppl. 2*), S98–S107. doi: 10.1093/cid/civ072

Gonzalez-Escalona, N., Allard, M. A., Brown, E. W., Sharma, S., and Hoffmann, M. (2019). Nanopore sequencing for fast determination of plasmids, phages, virulence markers, and antimicrobial resistance genes in Shiga toxin-producing *Escherichia coli*. *PLoS One* 14:e0220494. doi: 10.1371/journal.pone.0220494

Gorrie, C. L., Mirceta, M., Wick, R. R., Judd, L. M., Wyres, K. L., Thomson, N. R., et al. (2018). Antimicrobial-resistant *Klebsiella pneumoniae* carriage and infection in specialized geriatric care wards linked to acquisition in the referring hospital. *Clin. Infect. Dis.* 67, 161–170. doi: 10.1093/cid/ciy027

Greig, D. R., Jenkins, C., Gharbia, S., and Dallman, T. J. (2019). Comparison of single-nucleotide variants identified by illumina and oxford nanopore technologies in the context of a potential outbreak of Shiga toxin-producing *Escherichia coli*. *GigaScience* 8, 1–12. doi: 10.1093/gigascience/giz104

Greninger, A. L., Naccache, S. N., Federman, S., Yu, G., Mbala, P., Bres, V., et al. (2015). Rapid metagenomic identification of viral pathogens in clinical samples by real-time nanopore sequencing analysis. *Genome Med.* 7:99. doi: 10.1186/s13073-015-0220-9

Gu, W., Deng, X., Lee, M., Sucu, Y. D., Arevalo, S., Stryke, D., et al. (2021). Rapid pathogen detection by metagenomic next-generation sequencing of infected body fluids. *Nat. Med.* 27, 115–124. doi: 10.1038/s41591-020-1105-z

Guarner, J., and Brandt, M. E. (2011). Histopathologic diagnosis of fungal infections in the 21st century. *Clin. Microbiol. Rev.* 24, 247–280. doi: 10.1128/CMR.00053-10

Gustafson, E., Bakotic, W., Bennett, L., Page, L., and McCarthy, L. (2019). DNA-based detection for onychomycosis correlates better to histopathology than does fungal culture. *Dermatol. Online J.* 25, 1–9.

Hahn, A., Sanyal, A., Perez, G. F., Colberg-Poley, A. M., Campos, J., Rose, M. C., et al. (2016). Different next generation sequencing platforms produce different microbial profiles and diversity in cystic fibrosis sputum. *J. Microbiol. Methods* 130, 95–99. doi: 10.1016/j.mimet.2016.09.002

Hamad, I., Abou Abdallah, R., Ravaux, I., Mokhtari, S., Tissot-Dupont, H., Michelle, C., et al. (2018). Metabarcoding analysis of eukaryotic microbiota in the gut of HIV-infected patients. *PLoS One* 13:e0191913. doi: 10.1371/journal.pone.0191913

Handelsman, J., Rondon, M. R., Brady, S. F., Clardy, J., and Goodman, R. M. (1998). Molecular biological access to the chemistry of unknown soil microbes: a new frontier for natural products. *Chem. Biol.* 5, R245–R249. doi: 10.1016/S1074-5521(98)90108-9

Heather, J. M., and Chain, B. (2016). The sequence of sequencers: the history of sequencing DNA. *Genomics* 107, 1–8. doi: 10.1016/j.ygeno.2015.11.003

Hebert, P. D., Cywinska, A., Ball, S. L., and Dewaard, J. R. (2003). Biological identifications through DNA barcodes. *Proc. Biol. Sci.* 270, 313–321. doi: 10.1098/rspb.2002.2218

Heeger, F., Bourne, E. C., Baschien, C., Yurkov, A., Bunk, B., Sproer, C., et al. (2018). Long-read DNA metabarcoding of ribosomal RNA in the analysis of fungi from aquatic environments. *Mol. Ecol. Resour.* 18, 1500–1514. doi: 10.1111/1755-0998.12937

Helmersen, K., and Aamot, H. V. (2020). DNA extraction of microbial DNA directly from infected tissue: an optimized protocol for use in nanopore sequencing. *Sci. Rep.* 10:2985. doi: 10.1038/s41598-020-59957-6

Heravi, F. S., Zakrzewski, M., Vickery, K., and Hu, H. (2020). Host DNA depletion efficiency of microbiome DNA enrichment methods in infected tissue samples. *J. Microbiol. Methods* 170:105856. doi: 10.1016/j.mimet.2020.105856

Ho, C. K., Raghwani, J., Koekkoek, S., Liang, R. H., Van der Meer, J. T., Van Der Valk, M., et al. (2017). Characterization of hepatitis C virus (HCV) envelope diversification from acute to chronic infection within a sexually transmitted HCV cluster by using single-molecule, real-time sequencing. *J. Virol.* 91, 1–14. doi: 10.1128/JVI.02262-16

Hoenen, T., Groseth, A., Rosenke, K., Fischer, R. J., Hoenen, A., Judson, S. D., et al. (2016). Nanopore sequencing as a rapidly deployable Ebola outbreak tool. *Emerg. Infect. Dis.* 22:331. doi: 10.3201/eid2202.151796

Hu, K., Huang, N., Zou, Y., Liao, X., and Wang, J. (2021). MultiNanopolish: refined grouping method for reducing redundant calculations in nanopolish. *Bioinformatics* 37, 2757–2760. doi: 10.1093/bioinformatics/btab078

Huang, D. W., Raley, C., Jiang, M. K., Zheng, X., Liang, D., Rehman, M. T., et al. (2016). Towards better precision medicine: PacBio single-molecule long reads resolve the interpretation of HIV drug resistant mutation profiles at explicit quasispecies (haplotype) level. *J. Data Min. Genom. Proteom.* 7, 1–16. doi: 10.4172/2153-0602.1000182

Illumina (2021). Focused Power on the MiSeq System [Online]. Available: https://sapac.illumina.com/systems/sequencing-platforms/miseq.html (Accessed April 11, 2021).

Im, K., Mareninov, S., Diaz, M. F. P., and Yong, W. H. (2019). An introduction to performing immunofluorescence staining. *Methods Mol. Biol.* 1897, 299–311. doi: 10.1007/978-1-4939-8935-5_26

Imai, K., Nemoto, R., Kodana, M., Tarumoto, N., Sakai, J., Kawamura, T., et al. (2020). Rapid and accurate species identification of mitis group streptococci using the MinION nanopore sequencer. *Front. Cell. Infect. Microbiol.* 10:11. doi: 10.3389/fcimb.2020.00011

Inglis, P. W., Pappas, M. C. R., Resende, L. V., and Grattapaglia, D. (2018). Fast and inexpensive protocols for consistent extraction of high quality DNA and RNA from challenging plant and fungal samples for high-throughput SNP genotyping and sequencing applications. *PLoS One* 13:e0206085. doi: 10.1371/journal.pone.0206085

Irinyi, L., Hu, Y., Hoang, M. T. V., Pasic, L., Halliday, C., Jayawardena, M., et al. (2020). Long-read sequencing based clinical metagenomics for the detection and confirmation of *Pneumocystis jirovecii* directly from clinical specimens: a paradigm shift in mycological diagnostics. *Med. Mycol.* 58, 650–660. doi: 10.1093/mmy/myz109

Irinyi, L., Lackner, M., de Hoog, G. S., and Meyer, W. (2016). DNA barcoding of fungi causing infections in humans and animals. *Fungal Biol.* 120, 125–136. doi: 10.1016/j.funbio.2015.04.007

Irinyi, L., Serena, C., Garcia-Hermoso, D., Arabatzis, M., Desnos-Ollivier, M., Vu, D., et al. (2015). International Society of Human and Animal Mycology (ISHAM)-ITS reference DNA barcoding database—the quality controlled standard tool for routine identification of human and animal pathogenic fungi. *Med. Mycol.* 53, 313–337. doi: 10.1093/mmy/myv008

Jain, M., Olsen, H. E., Paten, B., and Akeson, M. (2016). The Oxford Nanopore MinION: delivery of nanopore sequencing to the genomics community. *Genome Biol.* 17:239. doi: 10.1186/s13059-016-1103-0

James, T. Y., Marino, J. A., Perfecto, I., and Vandermeer, J. (2016). Identification of putative coffee rust mycoparasites via single-molecule DNA sequencing of infected pustules. *J. Appl. Environ. Microbiol.* 82, 631–639. doi: 10.1128/AEM.02639-15

Janda, J. M., and Abbott, S. L. (2007). 16S rRNA gene sequencing for bacterial identification in the diagnostic laboratory: pluses, perils, and pitfalls. *J. Clin. Microbiol.* 45, 2761–2764. doi: 10.1128/JCM.01228-07

Jumpponen, A. (2003). Soil fungal community assembly in a primary successional glacier forefront ecosystem as inferred from rDNA sequence analyses. *New Phytol.* 158, 569–578. doi: 10.1046/j.1469-8137.2003.00767.x

Juul, S., Izquierdo, F., Hurst, A., Dai, X., Wright, A., Kulesha, E., et al. (2015). What's in my pot? Real-time species identification on the MinION™. bioRxiv. doi: 10.1101/030742

Kafetzopoulou, L. E., Efthymiadis, K., Lewandowski, K., Crook, A., Carter, D., Osborne, J., et al. (2018). Assessment of metagenomic Nanopore and Illumina sequencing for recovering whole genome sequences of chikungunya and dengue viruses directly from clinical samples. *Euro Surveill.* 23, 1–13. doi: 10.2807/1560-7917.ES.2018.23.50.1800228

Kafetzopoulou, L., Pullan, S., Lemey, P., Suchard, M., Ehichioya, D., Pahlmann, M., et al. (2019). Metagenomic sequencing at the epicenter of the Nigeria 2018 Lassa fever outbreak. *Science* 363, 74–77. doi: 10.1126/science.aau9343

Kai, S., Matsuo, Y., Nakagawa, S., Kryukov, K., Matsukawa, S., Tanaka, H., et al. (2019). Rapid bacterial identification by direct PCR amplification of 16S rRNA genes using the MinION™ nanopore sequencer. *FEBS Open Bio* 9, 548–557. doi: 10.1002/2211-5463.12590

Kanamori, H., Parobek, C. M., Weber, D. J., van Duin, D., Rutala, W. A., Cairns, B. A., et al. (2016). Next-generation sequencing and comparative analysis of sequential outbreaks caused by multidrug-resistant *Acinetobacter baumannii* at a large academic burn center. *Antimicrob. Agents Chemother.* 60, 1249–1257. doi: 10.1128/AAC.02014-15

Karageorgopoulos, D. E., Vouloumanou, E. K., Ntziora, F., Michalopoulos, A., Rafailidis, P. I., and Falagas, M. E. (2011). Beta-D-glucan assay for the diagnosis of invasive fungal infections: a meta-analysis. *Clin. Infect. Dis.* 52, 750–770. doi: 10.1093/cid/ciq206

Kasianowicz, J. J., Brandin, E., Branton, D., and Deamer, D. W. (1996). Characterization of individual polynucleotide molecules using a membrane channel. *Proc. Natl. Acad. Sci. U. S. A.* 93, 13770–13773. doi: 10.1073/pnas.93.24.13770

Kidd, S. E., Chen, S. C., Meyer, W., and Halliday, C. L. (2019). A new age in molecular diagnostics for invasive fungal disease: are we ready? *Front. Microbiol.* 10:2903. doi: 10.3389/fmicb.2019.02903

Klingspor, L., and Jalal, S. (2006). Molecular detection and identification of *Candida* and *Aspergillus* spp. from clinical samples using real-time PCR. *Clin. Microbiol. Infect.* 12, 745–753. doi: 10.1111/j.1469-0691.2006.01498.x

Ko, S. H., Bayat Mokhtari, E., Mudvari, P., Stein, S., Stringham, C. D., Wagner, D., et al. (2021). High-throughput, single-copy sequencing reveals SARS-CoV-2 spike variants coincident with mounting humoral immunity during acute COVID-19. *PLoS Pathog.* 17:e1009431. doi: 10.1371/journal.ppat.1009431

Koljalg, U., Larsson, K. H., Abarenkov, K., Nilsson, R. H., Alexander, I. J., Eberhardt, U., et al. (2005). UNITE: a database providing web-based methods for the molecular identification of ectomycorrhizal fungi. *New Phytol.* 166, 1063–1068. doi: 10.1111/j.1469-8137.2005.01376.x

Koren, S., Walenz, B. P., Berlin, K., Miller, J. R., Bergman, N. H., and Phillippy, A. M. (2017). Canu: scalable and accurate long-read assembly via adaptive k-mer weighting and repeat separation. *Genome Res.* 27, 722–736. doi: 10.1101/gr.215087.116

Kovaka, S., Fan, Y., Ni, B., Timp, W., and Schatz, M. C. (2020). Targeted nanopore sequencing by real-time mapping of raw electrical signal with UNCALLED. *Nat. Biotechnol.* 29, 431–441. doi: 10.1038/s41587-020-0731-9

Kulik, T., Fordoński, G., Pszczółkowska, A., Płodzień, K., and Łapiński, M. (2004). Development of PCR assay based on ITS2 rDNA polymorphism for the detection and differentiation of *Fusarium sporotrichioides*. *FEMS Microbiol. Lett.* 239, 181–186. doi: 10.1016/j.femsle.2004.08.037

Kurtzman, C., Fell, J. W., and Boekhout, T. (2011). *The Yeasts: A Taxonomic Study.* Amsterdam, Netherlands: Elsevier.

Kyaschenko, J., Clemmensen, K. E., Hagenbo, A., Karltun, E., and Lindahl, B. D. (2017). Shift in fungal communities and associated enzyme activities along an age gradient of managed Pinus sylvestris stands. *ISME J.* 11, 863–874. doi: 10.1038/ismej.2016.184

Lackner, M., de Hoog, G. S., Yang, L., Moreno, L. F., Ahmed, S. A., Andreas, F., et al. (2014). Proposed nomenclature for *Pseudallescheria*, *Scedosporium* and related genera. *Fungal Divers.* 67, 1–10. doi: 10.1007/s13225-014-0295-4

Laudadio, I., Fulci, V., Palone, F., Stronati, L., Cucchiara, S., and Carissimi, C. (2018). Quantitative assessment of shotgun metagenomics and 16S rDNA amplicon sequencing in the study of human gut microbiome. *OMICS* 22, 248–254. doi: 10.1089/omi.2018.0013

Leggett, R. M., and Clark, M. D. (2017). A world of opportunities with nanopore sequencing. *J. Exp. Bot.* 68, 5419–5429. doi: 10.1093/jxb/erx289

Lewandowski, K., Xu, Y., Pullan, S. T., Lumley, S. F., Foster, D., Sanderson, N., et al. (2019). Metagenomic nanopore sequencing of influenza virus direct from clinical respiratory samples. *J. Clin. Microbiol.* 58, 1–15. doi: 10.1128/JCM.00963-19

Li, Y., He, X. Z., Li, M. H., Li, B., Yang, M. J., Xie, Y., et al. (2020). Comparison of third-generation sequencing approaches to identify viral pathogens under public health emergency conditions. *Virus Genes* 56, 288–297. doi: 10.1007/s11262-020-01746-4

Lieckfeldt, E., Meyer, W., and Borner, T. (1993). Rapid identification and differentiation of yeasts by DNA and PCR fingerprinting. *J. Basic Microbiol.* 33, 413–425. doi: 10.1002/jobm.3620330609

Lindsley, M. D., Hurst, S. F., Iqbal, N. J., and Morrison, C. J. (2001). Rapid identification of dimorphic and yeast-like fungal pathogens using specific DNA probes. *J. Clin. Microbiol.* 39, 3505–3511. doi: 10.1128/JCM.39.10.3505-3511.2001

Logsdon, G. A., Vollger, M. R., and Eichler, E. E. (2020). Long-read human genome sequencing and its applications. *Nat. Rev. Genet.* 21, 597–614. doi: 10.1038/s41576-020-0236-x

Loit, K., Adamson, K., Bahram, M., Puusepp, R., Anslan, S., Kiiker, R., et al. (2019). Relative performance of MinION (Oxford Nanopore technologies) versus sequel (Pacific biosciences) third-generation sequencing instruments in identification of agricultural and Forest fungal pathogens. *J. Appl. Environ. Microbiol.* 85, 1–20. doi: 10.1128/AEM.01368-19

Loman, N. J., Quick, J., and Simpson, J. T. (2015). A complete bacterial genome assembled de novo using only nanopore sequencing data. *Nat. Methods* 12, 733–735. doi: 10.1038/nmeth.3444

Lu, H., Giordano, F., and Ning, Z. (2016). Oxford nanopore MinION sequencing and genome assembly. *Genom. Proteom. Bioinform.* 14, 265–279. doi: 10.1016/j.gpb.2016.05.004

Lui, W. Y., Yuen, C. K., Li, C., Wong, W. M., Lui, P. Y., Lin, C. H., et al. (2019). SMRT sequencing revealed the diversity and characteristics of defective interfering RNAs in influenza A (H7N9) virus infection. *Emerg. Microbes Infect.* 8, 662–674. doi: 10.1080/22221751.2019.1611346

Luo, R., Zimin, A., Workman, R., Fan, Y., Pertea, G., Grossman, N., et al. (2017). First draft genome sequence of the pathogenic fungus lomentospora prolificans (formerly scedosporium prolificans). *G3* 7, 3831–3836. doi: 10.1534/g3.117.300107

Mafune, K. K., Godfrey, B. J., Vogt, D. J., and Vogt, K. A. (2020). A rapid approach to profiling diverse fungal communities using the MinION nanopore sequencer. *BioTechniques* 68, 72–78. doi: 10.2144/btn-2019-0072

Makalowski, W., and Shabardina, V. (2020). Bioinformatics of nanopore sequencing. *J. Hum. Genet.* 65, 61–67. doi: 10.1038/s10038-019-0659-4

Mannarelli, B. M., and Kurtzman, C. P. (1998). Rapid identification of *Candida albicans* and other human pathogenic yeasts by using short oligonucleotides

in a PCR. *J. Clin. Microbiol.* 36, 1634–1641. doi: 10.1128/JCM.36.6.1634-1641.1998

Mantere, T., Kersten, S., and Hoischen, A. (2019). Long-read sequencing emerging in medical genetics. *Front. Genet.* 10:426. doi: 10.3389/fgene.2019.00426

Marotz, C. A., Sanders, J. G., Zuniga, C., Zaramela, L. S., Knight, R., and Zengler, K. (2018). Improving saliva shotgun metagenomics by chemical host DNA depletion. *Microbiome* 6:42. doi: 10.1186/s40168-018-0426-3

Martin, C., Roberts, D., van der Weide, M., Rossau, R., Jannes, G., Smith, T., et al. (2000). Development of a PCR-based line probe assay for identification of fungal pathogens. *J. Clin. Microbiol.* 38, 3735–3742. doi: 10.1128/JCM.38.10.3735-3742.2000

Meredith, L. W., Hamilton, W. L., Warne, B., Houldcroft, C. J., Hosmillo, M., Jahun, A. S., et al. (2020). Rapid implementation of SARS-CoV-2 sequencing to investigate cases of health-care associated COVID-19: a prospective genomic surveillance study. *Lancet Infect. Dis.* 20, 1263–1272. doi: 10.1016/S1473-3099(20)30562-4

Meyer, W., Irinyi, L., Hoang, M. T. V., Robert, V., Garcia-Hermoso, D., Desnos-Ollivier, M., et al. (2019). Database establishment for the secondary fungal DNA barcode *translational elongation factor 1α* (*TEF1α*). *Genome* 62, 160–169. doi: 10.1139/gen-2018-0083

Miller, S., and Chiu, C. (2018). "Metagenomic next-generation sequencing for pathogen detection and identification," in *Advanced Techniques in Diagnostic Microbiology: Volume 2: Applications*. eds. Y.-W. Tang and C. W. Stratton (Cham: Springer International Publishing), 617–632.

Mobasherizadeh, S., Shojaei, H., Havaei, S. A., Mostafavizadeh, K., Davoodabadi, F., Khorvash, F., et al. (2016). Application of the random amplified polymorphic DNA (RAPD) fingerprinting to analyze genetic variation in community associated-methicillin resistant *staphylococcus Aureus* (CA-MRSA) isolates in Iran. *Global J. Health Sci.* 8:53822. doi: 10.5539/gjhs.v8n8p185

Moon, J., Kim, N., Kim, T. J., Jun, J. S., Lee, H. S., Shin, H. R., et al. (2019). Rapid diagnosis of bacterial meningitis by nanopore 16S amplicon sequencing: a pilot study. *Int. J. Med. Microbiol.* 309:151338. doi: 10.1016/j.ijmm.2019.151338

Morand, S. C., Bertignac, M., Iltis, A., Kolder, I., Pirovano, W., Jourdain, R., et al. (2019). Complete genome sequence of *Malassezia restricta* CBS 7877, an opportunist pathogen involved in dandruff and seborrheic dermatitis. *Microbiol. Resour. Announc.* 8, 1–3. doi: 10.1128/MRA.01543-18

Morrison, G. A., Fu, J., Lee, G. C., Wiederhold, N. P., Canete-Gibas, C. F., Bunnik, E. M., et al. (2020). Nanopore sequencing of the fungal intergenic spacer sequence as a potential rapid diagnostic assay. *J. Clin. Microbiol.* 58, 1–16. doi: 10.1128/JCM.01972-20

Motooka, D., Fujimoto, K., Tanaka, R., Yaguchi, T., Gotoh, K., Maeda, Y., et al. (2017). Fungal ITS1 deep-sequencing strategies to reconstruct the composition of a 26-species community and evaluation of the gut mycobiota of healthy japanese individuals. *Front. Microbiol.* 8:238. doi: 10.3389/fmicb.2017.00238

Mylonakis, E., Clancy, C. J., Ostrosky-Zeichner, L., Garey, K. W., Alangaden, G. J., Vazquez, J. A., et al. (2015). T2 magnetic resonance assay for the rapid diagnosis of candidemia in whole blood: a clinical trial. *Clin. Infect. Dis.* 60, 892–899. doi: 10.1093/cid/ciu959

Nakagawa, S., Inoue, S., Kryukov, K., Yamagishi, J., Ohno, A., Hayashida, K., et al. (2019). Rapid sequencing-based diagnosis of infectious bacterial species from meningitis patients in Zambia. *Clin. Transl. Immunol.* 8:e01087. doi: 10.1002/cti2.1087

Nakano, K., Shiroma, A., Shimoji, M., Tamotsu, H., Ashimine, N., Ohki, S., et al. (2017). Advantages of genome sequencing by long-read sequencer using SMRT technology in medical area. *Hum. Cell* 30, 149–161. doi: 10.1007/s13577-017-0168-8

Nash, A., Sewell, T., Farrer, R. A., Abdolrasouli, A., Shelton, J. M. G., Fisher, M. C., et al. (2018). MARDy: mycology antifungal resistance database. *Bioinformatics* 34, 3233–3234. doi: 10.1093/bioinformatics/bty321

Neely, L. A., Audeh, M., Phung, N. A., Min, M., Suchocki, A., Plourde, D., et al. (2013). T2 magnetic resonance enables nanoparticle-mediated rapid detection of candidemia in whole blood. *Sci. Transl. Med.* 5:182ra154. doi: 10.1126/scitranslmed.3005377

Nilsson, R. H., Ryberg, M., Abarenkov, K., Sjökvist, E., and Kristiansson, E. (2009). The ITS region as a target for characterization of fungal communities using emerging sequencing technologies. *FEMS Microbiol. Lett.* 296, 97–101. doi: 10.1111/j.1574-6968.2009.01618.x

Ocwieja, K. E., Sherrill-Mix, S., Mukherjee, R., Custers-Allen, R., David, P., Brown, M., et al. (2012). Dynamic regulation of HIV-1 mRNA populations analyzed by single-molecule enrichment and long-read sequencing. *Nucleic Acids Res.* 40, 10345–10355. doi: 10.1093/nar/gks753

O'Donnell, K., Al-Hatmi, A. M. S., Aoki, T., Brankovics, B., Cano-Lira, J. F., Coleman, J. J., et al. (2020). No to neocosmospora: phylogenomic and practical reasons for continued inclusion of the *Fusarium solani* species complex in the genus *Fusarium*. *mSphere* 5, 1–7. doi: 10.1128/mSphere.00810-20

O'Donnell, K., and Cigelnik, E. (1997). Two divergent intragenomic rDNA ITS2 types within a monophyletic lineage of the fungus *Fusarium* are nonorthologous. *Mol. Phylogenet. Evol.* 7, 103–116. doi: 10.1006/mpev.1996.0376

Oxford Nanopore Technologies (2019). Oxford Nanopore launches Flongle, for Rapid, Smaller DNA/RNA Sequencing Tests in Any Environment [Online]. Available: https://nanoporetech.com/about-us/news/oxford-nanopore-launches-flongle-rapid-smaller-dnarna-sequencing-tests-any (Accessed October 28, 2021).

Oxford Nanopore Technologies (2021). Products [Online]. Available: https://nanoporetech.com/products (Accessed October 28, 2021).

Pacific Biosciences (2020). Pacific Biosciences Launches the Sequel IIe System to Accelerate Adoption of Highly Accurate HiFi Sequencing [Online]. Available: https://www.pacb.com/press_releases/pacific-biosciences-launches-the-sequel-iie-system-to-accelerate-adoption-of-highly-accurate-hifi-sequencing/ (Accessed October 28, 2021).

Pacific Biosciences (2021a). PacBio Sequel Systems [Online]. Available: https://www.pacb.com/products-and-services/sequel-system/ (Accessed October 28, 2021).

Pacific Biosciences (2021b). What Can You Do with One SMRT Cell? [Online]. Available: https://www.pacb.com/wp-content/uploads/Application-Brochure-What-Can-You-Do-with-One-SMRT-Cell.pdf (Accessed October 28, 2021).

Panthee, S., Hamamoto, H., Ishijima, S. A., Paudel, A., and Sekimizu, K. (2018). Utilization of hybrid assembly approach to determine the genome of an opportunistic pathogenic fungus, *Candida albicans* TIMM 1768. *Genome Biol. Evol.* 10, 2017–2022. doi: 10.1093/gbe/evy166

Parker, J., Helmstetter, A. J., Devey, D., Wilkinson, T., and Papadopulos, A. S. (2017). Field-based species identification of closely-related plants using real-time nanopore sequencing. *Sci. Rep.* 7, 1–8. doi: 10.1038/s41598-017-08461-5

Patel, T. S., Kaakeh, R., Nagel, J. L., Newton, D. W., and Stevenson, J. G. (2017). Cost analysis of implementing matrix-assisted laser desorption ionization-time of flight mass spectrometry plus real-time antimicrobial stewardship intervention for bloodstream infections. *J. Clin. Microbiol.* 55, 60–67. doi: 10.1128/JCM.01452-16

Payne, A., Holmes, N., Clarke, T., Munro, R., Debebe, B. J., and Loose, M. (2020). Readfish enables targeted nanopore sequencing of gigabase-sized genomes. *Nat. Biotechnol.* 35, 2193–2198. doi: 10.1038/s41587-020-00746-x

Payne, A., Holmes, N., Rakyan, V., and Loose, M. (2019). BulkVis: a graphical viewer for Oxford nanopore bulk FAST5 files. *Bioinformatics* 35, 2193–2198. doi: 10.1093/bioinformatics/bty841

Pchelin, I. M., Azarov, D. V., Churina, M. A., Ryabinin, I. A., Vibornova, I. V., Apalko, S. V., et al. (2020). Whole genome sequence of first *Candida auris* strain, isolated in Russia. *Med. Mycol.* 58, 414–416. doi: 10.1093/mmy/myz078

Perfect, J. R. (2013). Fungal diagnosis: how do we do it and can we do better? *Curr. Med. Res. Opin.* 29(Suppl 4), 3–11. doi: 10.1185/03007995.2012.761134

Pfeiffer, C. D., Fine, J. P., and Safdar, N. (2006). Diagnosis of invasive aspergillosis using a galactomannan assay: a meta-analysis. *Clin. Infect. Dis.* 42, 1417–1727. doi: 10.1086/503427

Pollard, M. O., Gurdasani, D., Mentzer, A. J., Porter, T., and Sandhu, M. S. (2018). Long reads: their purpose and place. *Hum. Mol. Genet.* 27, R234–R241. doi: 10.1093/hmg/ddy177

Polz, M. F., and Cavanaugh, C. M. (1998). Bias in template-to-product ratios in multitemplate PCR. *J. Appl. Environ. Microbiol.* 64, 3724–3730. doi: 10.1128/AEM.64.10.3724-3730.1998

Pryce, T. M., Fau, P. S., Kay, I. D., and Coombs, G. W. (2003). Rapid identification of fungi by sequencing the ITS1 and ITS2 regions using an automated capillary electrophoresis system. *Med. Mycol.* 41, 369–381. doi: 10.1080/13693780310001600435

Purahong, W., Mapook, A., Wu, Y. T., and Chen, C. T. (2019). Characterization of the *Castanopsis carlesii* deadwood mycobiome by PacBio sequencing of the full-length fungal nuclear ribosomal internal transcribed spacer (ITS). *Front. Microbiol.* 10:983. doi: 10.3389/fmicb.2019.00983

Quick, J., Grubaugh, N. D., Pullan, S. T., Claro, I. M., Smith, A. D., Gangavarapu, K., et al. (2017). Multiplex PCR method for MinION and illumina sequencing of Zika and other virus genomes directly from clinical samples. *Nat. Protoc.* 12, 1261–1276. doi: 10.1038/nprot.2017.066

Quick, J., Loman, N. J., Duraffour, S., Simpson, J. T., Severi, E., Cowley, L., et al. (2016). Real-time, portable genome sequencing for Ebola surveillance. *Nature* 530, 228–232. doi: 10.1038/nature16996

Ratnasingham, S., and Hebert, P. D. (2007). Bold: the barcode of life data system. *Mol. Ecol. Notes* 7, 355–364. doi: 10.1111/j.1471-8286.2007.01678.x

Ravi, R. K., Walton, K., and Khosroheidari, M. (2018). MiSeq: a next generation sequencing platform for genomic analysis. *Methods Mol. Biol.* 1706, 223–232. doi: 10.1007/978-1-4939-7471-9_12

Rhoads, A., and Au, K. F. (2015). PacBio sequencing and its applications. *Genom. Proteom. Bioinform.* 13, 278–289. doi: 10.1016/j.gpb.2015.08.002

Rhodes, J., Abdolrasouli, A., Farrer, R. A., Cuomo, C. A., Aanensen, D. M., Armstrong-James, D., et al. (2018). Genomic epidemiology of the UK outbreak of the emerging human fungal pathogen *Candida auris*. *Emerg. Infect. Dis.* 7:43. doi: 10.1038/s41426-018-0045-x

Riesenfeld, C. S., Schloss, P. D., and Handelsman, J. (2004). Metagenomics: genomic analysis of microbial communities. *Annu. Rev. Genet.* 38, 525–552. doi: 10.1146/annurev.genet.38.072902.091216

Romanelli, A. M., Sutton, D. A., Thompson, E. H., Rinaldi, M. G., and Wickes, B. L. (2010). Sequence-based identification of filamentous basidiomycetous fungi from clinical specimens: a cautionary note. *J. Clin. Microbiol.* 48, 741–752. doi: 10.1128/JCM.01948-09

Sakai, J., Tarumoto, N., Kodana, M., Ashikawa, S., Imai, K., Kawamura, T., et al. (2019). An identification protocol for ESBL-producing gram-negative bacteria bloodstream infections using a MinION nanopore sequencer. *J. Med. Microbiol.* 68, 1219–1226. doi: 10.1099/jmm.0.001024

Salmela, L., Walve, R., Rivals, E., and Ukkonen, E. (2017). Accurate self-correction of errors in long reads using de Bruijn graphs. *Bioinformatics* 33, 799–806. doi: 10.1093/bioinformatics/btw321

Salzberg, S. L., and Yorke, J. A. (2005). Beware of mis-assembled genomes. *Bioinformatics* 21, 4320–4321. doi: 10.1093/bioinformatics/bti769

Sandhu, G. S., Kline, B. C., Stockman, L., and Roberts, G. D. (1995). Molecular probes for diagnosis of fungal infections. *J. Clin. Microbiol.* 33, 2913–2919. doi: 10.1128/jcm.33.11.2913-2919.1995

Sandoval-Denis, M., Lombard, L., and Crous, P. W. (2019). Back to the roots: a reappraisal of *Neocosmospora*. *Persoonia* 43, 90–185. doi: 10.3767/persoonia.2019.43.04

Sanger, F., Nicklen, S., and Coulson, A. R. (1977). DNA sequencing with chain-terminating inhibitors. *Proc. Natl. Acad. Sci. U. S. A.* 74, 5463–5467. doi: 10.1073/pnas.74.12.5463

Sayers, E. W., Cavanaugh, M., Clark, K., Ostell, J., Pruitt, K. D., and Karsch-Mizrachi, I. (2020). GenBank. *Nucleic Acids Res.* 48, D84–D86. doi: 10.1093/nar/gkz956

Schelenz, S., Barnes, R. A., Barton, R. C., Cleverley, J. R., Lucas, S. B., Kibbler, C. C., et al. (2015). British society for medical mycology best practice recommendations for the diagnosis of serious fungal diseases. *Lancet Infect. Dis.* 15, 461–474. doi: 10.1016/S1473-3099(15)70006-X

Schmidt, K., Mwaigwisya, S., Crossman, L. C., Doumith, M., Munroe, D., Pires, C., et al. (2017). Identification of bacterial pathogens and antimicrobial resistance directly from clinical urines by nanopore-based metagenomic sequencing. *J. Antimicrob. Chemother.* 72, 104–114. doi: 10.1093/jac/dkw397

Schoch, C. L., Robbertse, B., Robert, V., Vu, D., Cardinali, G., Irinyi, L., et al. (2014). Finding needles in haystacks: linking scientific names, reference specimens and molecular data for fungi. *Database* 2014, 1–21. doi: 10.1093/database/bau061

Schoch, C. L., Seifert, K. A., Huhndorf, S., Robert, V., Spouge, J. L., Levesque, C. A., et al. (2012). Nuclear ribosomal internal transcribed spacer (ITS) region as a universal DNA barcode marker for fungi. *Proc. Natl. Acad. Sci. U. S. A.* 109, 6241–6246. doi: 10.1073/pnas.1117018109

Schultzhaus, Z., Cuomo, C. A., and Wang, Z. (2019). Genome sequence of the black yeast *Exophiala lecanii-corni*. *Microbiol. Resour. Announc.* 8, 1–2. doi: 10.1128/MRA.01709-18

Schwessinger, B., and Rathjen, J. P. (2017). Extraction of high molecular weight DNA from fungal rust spores for long read sequencing. *Methods Mol. Biol.* 1659, 49–57. doi: 10.1007/978-1-4939-7249-4_5

Shokralla, S., Gibson, J. F., Nikbakht, H., Janzen, D. H., Hallwachs, W., and Hajibabaei, M. (2014). Next-generation DNA barcoding: using next-generation sequencing to enhance and accelerate DNA barcode capture from single specimens. *Mol. Ecol. Resour.* 14, 892–901. doi: 10.1111/1755-0998.12236

Simon, U. K., and Weiss, M. (2008). Intragenomic variation of fungal ribosomal genes is higher than previously thought. *Mol. Biol. Evol.* 25, 2251–2254. doi: 10.1093/molbev/msn188

Springer, J., and Loffler, J. (2017). Genus- and species-specific PCR detection methods. *Methods Mol. Biol.* 1508, 267–279. doi: 10.1007/978-1-4939-6515-1_15

Stielow, J. B., Levesque, C. A., Seifert, K. A., Meyer, W., Irinyi, L., Smits, D., et al. (2015). One fungus, which genes? Development and assessment of universal primers for potential secondary fungal DNA barcodes. *Persoonia* 35:242. doi: 10.3767/003158515X689135

Takeda, H., Yamashita, T., Ueda, Y., and Sekine, A. (2019). Exploring the hepatitis C virus genome using single molecule real-time sequencing. *World J. Gastroenterol.* 25:4661. doi: 10.3748/wjg.v25.i32.4661

Taxt, A. M., Avershina, E., Frye, S. A., Naseer, U., and Ahmad, R. (2020). Rapid identification of pathogens, antibiotic resistance genes and plasmids in blood cultures by nanopore sequencing. *Sci. Rep.* 10:7622. doi: 10.1038/s41598-020-64616-x

Tedersoo, L., Albertsen, M., Anslan, S., and Callahan, B. (2021). Perspectives and benefits of high-throughput long-read sequencing in microbial ecology. *Appl. Environ. Microbiol.* 87:e0062621. doi: 10.1128/AEM.00626-21

Tedersoo, L., and Anslan, S. (2019). Towards PacBio-based pan-eukaryote metabarcoding using full-length ITS sequences. *Environ. Microbiol. Rep.* 11, 659–668. doi: 10.1111/1758-2229.12776

Tedersoo, L., Tooming-Klunderud, A., and Anslan, S. (2018). PacBio metabarcoding of fungi and other eukaryotes: errors, biases and perspectives. *New Phytol.* 217, 1370–1385. doi: 10.1111/nph.14776

Teng, J. L., Yeung, M. L., Chan, E., Jia, L., Lin, C. H., Huang, Y., et al. (2017). PacBio but not Illumina technology can achieve fast, accurate and complete closure of the high GC, complex *Burkholderia pseudomallei* two-chromosome genome. *Front. Microbiol.* 8:1448. doi: 10.3389/fmicb.2017.01448

Tia, T., Putaporntip, C., Kosuwin, R., Kongpolprom, N., Kawkitinarong, K., and Jongwutiwes, S. (2012). A highly sensitive novel PCR assay for detection of *Pneumocystis jirovecii* DNA in bronchoalveloar lavage specimens from immunocompromised patients. *Clin. Microbiol. Infect.* 18, 598–603. doi: 10.1111/j.1469-0691.2011.03656.x

Treangen, T. J., and Salzberg, S. L. (2011). Repetitive DNA and next-generation sequencing: computational challenges and solutions. *Nat. Rev. Genet.* 13, 36–46. doi: 10.1038/nrg3117

Tsang, C. C., Teng, J. L. L., Lau, S. K. P., and Woo, P. C. Y. (2021). Rapid genomic diagnosis of fungal infections in the age of next-generation sequencing. *J. Fungi* 7, 1–15. doi: 10.3390/jof7080636

Vale-Silva, L., Beaudoing, E., Tran, V. D. T., and Sanglard, D. (2017). Comparative genomics of two sequential *Candida glabrata* clinical isolates. *G3* 7, 2413–2426. doi: 10.1534/g3.117.042887

van Dijk, E. L., Auger, H., Jaszczyszyn, Y., and Thermes, C. (2014). Ten years of next-generation sequencing technology. *Trends Genet.* 30, 418–426. doi: 10.1016/j.tig.2014.07.001

van Dijk, E. L., Jaszczyszyn, Y., Naquin, D., and Thermes, C. (2018). The third revolution in sequencing technology. *Trends Genet.* 34, 666–681. doi: 10.1016/j.tig.2018.05.008

Vasiljevic, N., Lim, M., Humble, E., Seah, A., Kratzer, A., Morf, N. V., et al. (2021). Developmental validation of Oxford nanopore technology MinION sequence data and the NGSpeciesID bioinformatic pipeline for forensic genetic species identification. *Forensic Sci. Int. Genet.* 53:102493. doi: 10.1016/j.fsigen.2021.102493

Votintseva, A. A., Bradley, P., Pankhurst, L., Del Ojo Elias, C., Loose, M., Nilgiriwala, K., et al. (2017). Same-day diagnostic and surveillance data for tuberculosis via whole-genome sequencing of direct respiratory samples. *J. Clin. Microbiol.* 55, 1285–1298. doi: 10.1128/JCM.02483-16

Wagner, A., Chavez, V., Huang, R. S. P., Wahed, A., Actor, J. K., and Dasgupta, A. (2017). "Chapter 5: biochemical tests and staining techniques for microbial identification," in *Microbiology and Molecular Diagnosis in Pathology A Comprehensive Review for Board Preparation, Certification and Clinical Practice*. ed. T. Broderick and K. Padilla (Amsterdam, Netherlands: Elsevier), 61–73.

Wagner, J., Coupland, P., Browne, H. P., Lawley, T. D., Francis, S. C., and Parkhill, J. (2016). Evaluation of PacBio sequencing for full-length bacterial

16S rRNA gene classification. *BMC Microbiol.* 16:274. doi: 10.1186/s12866-016-0891-4

Walder, F., Schlaeppi, K., Wittwer, R., Held, A. Y., Vogelgsang, S., and van der Heijden, M. G. (2017). Community profiling of *Fusarium* in combination with other plant-associated fungi in different crop species using SMRT sequencing. *Front. Plant Sci.* 8:2019. doi: 10.3389/fpls.2017.02019

Wang, M., Fu, A., Hu, B., Shen, G., Liu, R., Zhao, W., et al. (2020). Same-day simultaneous diagnosis of bacterial and fungal infections in clinical practice by nanopore targeted sequencing. medRxiv. doi: 10.1101/2020.04.08.20057604

Wang, W. L., Xu, S. Y., Ren, Z. G., Tao, L., Jiang, J. W., and Zheng, S. S. (2015). Application of metagenomics in the human gut microbiome. *World J. Gastroenterol.* 21, 803–814. doi: 10.3748/wjg.v21.i3.803

Washington, N.L., Gangavarapu, K., Zeller, M., Bolze, A., Cirulli, E.T., Schiabor Barrett, K.M., et al. (2021). Genomic epidemiology identifies emergence and rapid transmission of SARS-CoV-2 B.1.1.7 in the United States. medRxiv. doi: 10.1101/2021.02.06.21251159

Wenger, A. M., Peluso, P., Rowell, W. J., Chang, P. C., Hall, R. J., Concepcion, G. T., et al. (2019). Accurate circular consensus long-read sequencing improves variant detection and assembly of a human genome. *Nat. Biotechnol.* 37, 1155–1162. doi: 10.1038/s41587-019-0217-9

White, P. L., Backx, M., and Barnes, R. A. (2017). Diagnosis and management of *Pneumocystis jirovecii* infection. *Expert Rev. Anti-Infect. Ther.* 15, 435–447. doi: 10.1080/14787210.2017.1305887

Wickes, B. L., and Wiederhold, N. P. (2018). Molecular diagnostics in medical mycology. *Nat. Commun.* 9:5135. doi: 10.1038/s41467-018-07556-5

Winand, R., Bogaerts, B., Hoffman, S., Lefevre, L., Delvoye, M., Braekel, J. V., et al. (2019). Targeting the 16s rRNA gene for bacterial identification in complex mixed samples: comparative evaluation of second (Illumina) and third (Oxford Nanopore technologies) generation sequencing technologies. *Int. J. Mol. Sci.* 21, 1–22. doi: 10.3390/ijms21010298

Xiao, C. L., Chen, Y., Xie, S. Q., Chen, K. N., Wang, Y., Han, Y., et al. (2017). MECAT: fast mapping, error correction, and de novo assembly for single-molecule sequencing reads. *Nat. Methods* 14, 1072–1074. doi: 10.1038/nmeth.4432

Xu, Y., Lewandowski, K., Jeffery, K., Downs, L. O., Foster, D., Sanderson, N. D., et al. (2020). Nanopore metagenomic sequencing to investigate nosocomial transmission of human metapneumovirus from a unique genetic group among haematology patients in the United Kingdom. *J. Inf. Secur.* 80, 571–577. doi: 10.1016/j.jinf.2020.02.003

Yamashita, T., Takeda, H., Takai, A., Arasawa, S., Nakamura, F., Mashimo, Y., et al. (2020). Single-molecular real-time deep sequencing reveals the dynamics of multi-drug resistant haplotypes and structural variations in the hepatitis C virus genome. *Sci. Rep.* 10:2651. doi: 10.1038/s41598-020-59397-2

Conflict of Interest: The authors declare that the research was conducted in the absence of any commercial or financial relationships that could be construed as a potential conflict of interest.

Publisher's Note: All claims expressed in this article are solely those of the authors and do not necessarily represent those of their affiliated organizations, or those of the publisher, the editors and the reviewers. Any product that may be evaluated in this article, or claim that may be made by its manufacturer, is not guaranteed or endorsed by the publisher.

Advantages of publishing in Frontiers

OPEN ACCESS
Articles are free to read for greatest visibility and readership

FAST PUBLICATION
Around 90 days from submission to decision

HIGH QUALITY PEER-REVIEW
Rigorous, collaborative, and constructive peer-review

TRANSPARENT PEER-REVIEW
Editors and reviewers acknowledged by name on published articles

Frontiers
Avenue du Tribunal-Fédéral 34
1005 Lausanne | Switzerland

Visit us: www.frontiersin.org
Contact us: frontiersin.org/about/contact

REPRODUCIBILITY OF RESEARCH
Support open data and methods to enhance research reproducibility

DIGITAL PUBLISHING
Articles designed for optimal readership across devices

FOLLOW US
@frontiersin

IMPACT METRICS
Advanced article metrics track visibility across digital media

EXTENSIVE PROMOTION
Marketing and promotion of impactful research

LOOP RESEARCH NETWORK
Our network increases your article's readership